STRONGLY NONLINEAR ACOUSTICS OF ONE-DIMENSIONAL GRANULAR SONIC VACUA

BY

JAYAPRAKASH KALKUNTE RAGHUNATH

DISSERTATION

Submitted in partial fulfillment of the requirements
for the degree of Doctor of Philosophy in Theoretical and Applied Mechanics
in the Graduate College of the
University of Illinois at Urbana-Champaign, 2013

Urbana, Illinois

Doctoral Committee:

Professor Alexander F. Vakakis, Chair
Professor Harry Dankowicz
Professor Martin Ostoja-Starzewski
Professor Lawrence A. Bergman

ABSTRACT

This research is concerned with the nonlinear dynamics and acoustics of one dimensional ordered granular media. In particular the considered granular systems are composed of discrete elastic spherical beads that mutually interact through strongly nonlinear Hertzian force interaction law. In this work we primarily consider the granular chains in the limit of zero pre-compression, thus leading to complete absence of linear acoustics and zero speed of sound (as defined in the classical sense), hence their characterization as 'sonic vacua'. Furthermore, we sparingly incorporate a dissipative mechanism between interacting neighboring beads. Due to the absence of cohesive interaction forces, the interaction between the beads is strongly nonlinear and non-smooth owing to possible bead separations and ensuing collisions. However, with the application of pre-compression the interaction between beads becomes weakly nonlinear and smooth and the granular media can no longer be considered as 'sonic vacua'. Hence, the dynamics and acoustics of these material systems are highly tunable with varying pre-compression.

The first part of the study is primarily focused on the oscillatory dynamics of finite dimensional homogeneous granular chains. We initiate the study by investigating the existence of nonlinear normal modes (NNMs) in these systems with fixed boundary conditions. The realized modes which have energy dependent frequency, when represented on frequency-energy plots (FEP) divide these plots into two mutually exclusive regions separated by the out of phase NNM which corresponds to the highest possible oscillation frequency. All the NNMs realized are situated in the region below the out-of-phase NNM, which is denoted as propagation band; the complementary region is then the attenuation band. When the chain is harmonically base excited, frequencies in the propagation band are spatially extended whereas those in the attenuation band are spatially localized wherein the beads experience constant

compression. The dynamics in the attenuation zone is weakly nonlinear and has been studied analytically. Furthermore, the existence of frequency bands has been experimentally verified. This happens to be the first exposition on the frequency band zones in homogeneous granular chains from both theoretical and experimental perspectives.

The second part of the study is concerned with periodic ordered diatomic (dimer) granular chains consisting of spherical beads of two types. Initially we consider the most simple dimer chain wherein each bead of type 1 is preceded and followed by a bead of type 2; such chains are denoted as 1:1 dimers and the dynamics of such chains is governed by a single parameter (ε) scaling the mass of the two types of beads. Due to the periodic variation of the masses, a propagating pulse loses energy in the form of radiating waves in its trail and thus the pulse attenuates in dimer chains with an arbitrary value of mass ratio. Interestingly, at certain discrete values of mass ratios, the energy leakage from the propagating pulse ceases and the pulse propagates without attenuation, thus such pulses are called solitary waves. At the particular mass ratios where solitary waves are realized, these waves form an important energy transfer mechanism and any arbitrary pulse eventually disintegrates into a train of solitary waves. This is the first exposition of the realization of solitary waves in 1:1 dimer granular chains. Moreover, we show that these chains support a countable infinity of solitary waves parameterized by energy. The contrasting (but more intuitive) effect of substantial energy radiation from the propagating pulse is also observed at a discrete set of mass ratios. This phenomenon is designated as resonance. A complete analytical formulation for these two phenomena is provided. Furthermore, these phenomena have been experimentally verified. The experimental results show good correspondence with the theoretical results thus validating the theoretically predicted existence of nonlinear resonances in granular media. This happens to be the first experimental investigation of the resonances in uncompressed dimer chains.

The spatial periodicity of traveling waves radiated in the trail of the propagating pulse (at arbitrary mass ratio) is found to depend only on the specific mass ratio of the dimer. The effect of the mass ratio on the realization of traveling waves, and in turn their significance to the resonance and pulse attenuation is studied by considering reduced order dimer chains composed of finite number of beads with periodic boundary conditions. Interesting bifurcations of the traveling waves have been discovered and correlation between the bifurcations and resonances is noted.

We further study the dynamics of a general class of $1{:}\,N$ ($N \geq 2$) dimer chains. The dynamics of these chains is governed by two non-dimensional parameters, the mass ratio (ε) and the stiffness ratio (α) scaling the respective properties of the two types of beads. We report on a countable infinity of traveling solitary waves and resonances and prove numerically and asymptotically their existence in the 1:2 dimer chain. These solitary waves studied in homogeneous and $1{:}\,1$ dimer chains possess symmetric velocity waveforms, In contrast, the traveling solitary waves velocity waveforms of the $1{:}\,2$ dimers of the heavy beads are symmetric, whereas those of the light beads are non-symmetric. Interestingly, we show that no such solitary waves or resonances can be realized in general $1{:}\,N$ granular dimers with $N > 2$.

The final part of this study is concerned with the nonlinear dynamics of granular containers. These are granular setups composed of different types of homogeneous chains positioned in alternating configurations. Depending on the properties of the different types of homogeneous granular chains of the container, the wave energy can be entrapped in an appropriately designed intermediate layer. The primary aim of this study is to apply the binary collision approximation (BCA) for the analytic estimation of the amplitude of the scattered pulses (solitary waves) in the granular container. In addition, we provide a numerical study showing the qualitatively different dynamics of these containers depending on the frequency and amplitude of an applied harmonic excitation.

ACKNOWLEDGEMENTS

I quote the great Albert Einstein, "Every day I remind myself that my inner and outer life are based on the labors of other men, living and dead, and that I must exert myself in order to give in the same measure as I have received and am still receiving." I believe in the great words from Rig Veda (I-89-i) "आ नो भद्राः कृतवो यन्तु विश्वतः" (Let noble thoughts come to us from every side). I sincerely acknowledge all the known and unknown people who have shared their knowledge, wisdom and have enriched my life and made me what I am.

First and foremost, I would like to thank my adviser Prof. Alexander F. Vakakis for giving me an opportunity to do my doctoral research on the exciting subject of granular media under his guidance. My admission at UIUC was due to the earnest efforts of my adviser and I am highly indebted to him. I hope I have lived up to his expectations. The current research involves concepts from different areas like nonlinear dynamics, wave propagation and experimental mechanics, and his vast experience in these areas shaped up my understanding of the subject. It was an extremely enriching research and learning experience for me under his aegis which I would cherish and remember all my life. I am extremely grateful for his careful guidance, needful advice and patience. He always believed 'devil is in the detail' and I used to think 'devil is in front of you who missed the detail'. Either it was writing papers or reports or posters, he was so keen on the nano detail that I inadvertently had neglected. He made sure things were just perfect. This research wouldn't have been so satisfying and complete without his creative inputs, mentoring and careful monitoring at every stage. I was really impressed with his teaching abilities. I had taken four graduate courses with him and found them to be impeccably well organized and extremely well delivered; it's an art that I would like to imbibe. A great teacher, a researcher with 'never say die' attitude and above all a very nice human being, thank you sir.

My friend Yuli Starosvetsky, I have learnt a lot of things from him during my doctoral studies. The most basic thing that I started appreciating is 'nothing is as obvious as it seems'. Every question made him inquisitive from the great Indian rope trick to preparing Indian masala chai. He showed a lot of patience in mentoring and answering my quirky questions. A great human being, an unrelenting researcher, grown up but still child at heart and an avid foodie. Yuli and Elina, thank you for spending your summer (2012) with us in India.

I thank all my fellow graduate and visiting students for such a nice, peaceful and cordial work environment. I thank the experimental support provided by undergraduate student Randi Potekin (MechSE, UIUC), graduate student Kevin Remick (MechSE, UIUC), Prof. Michael McFarland (Aerospace Engineering, UIUC), graduate student Joseph Lydon (Caltech) and Prof. Chiara Daraio (Caltech).

I would like to thank Prof. Vakakis, Prof. Harry Dankowicz (MechSE, UIUC), Prof. Martin Ostoja-Starzewski (MechSE, UIUC), Prof. Lawrence Bergman (Aerospace Engineering, UIUC) and Prof. Yuli Starosvetsky (Faculty of Mechanical Engineering, Technion, Israel) for being on my final thesis examination committee to scrutinize my research work.

I thank the research funding agency the Army Research Office for the Multidisciplinary University Research Initiative (ARO MURI) on Stress WAve Mitigation (SWAMI).

I wouldn't have been here without the uncompromising insistence of my parents (K. Raghunath and H. R. Sarojamma) and brothers (K. R. Krishna Prasad and K. R. Hari Prashanth) to pursue my doctoral studies in USA. They have been my moral support all my life and especially over the last five and half years when I was away from home. Finally, I thank my beloved wife Dr. K. J. Ranjani for making my life so beautiful. Thank you all for your patience and wait. I dedicate this thesis to my family.

TABLE OF CONTENTS

1 INTRODUCTION……... 1

1.1 Outline of the Thesis ……. 10

1.2 Literature Review……... 12

1.3 Figures……. 21

2 DYNAMICS OF HOMOGENEOUS GRANULAR CHAINS…… 22

2.1 Nonlinear Normal Modes (NNMs) and Frequency Bands of Homogeneous Granular Chains…….. 23

2.1.1 Introduction……. 23

2.1.2 Two-Bead Granular System…….. 25

2.1.3 Effect of Pre-Compression on the In-phase NNM of Two Bead System……... 35

2.1.4 Three-Bead Granular System...……. 37

2.1.5 Higher Dimensional Granular Systems……... 42

2.1.6 Intrinsic Dynamics of the Infinite Granular Chain: Propagation and Attenuation Bands (Zones)…….……... 45

2.1.7 Conclusions…….. 49

2.2 Forced Harmonic Responses of Homogeneous Granular Chains…….. 51

2.2.1 Study in the Frequency – Energy Domain…….. 52

2.2.1.1 Experimental Setup and Numerical Model…….. 55

2.2.1.2 Numerical Results……. 57

2.2.1.3 Experimental Results…… 59

2.2.2 Analytical study of the Dynamics in Attenuation Zone…….. 60

2.2.3 Conclusions…….. 66

2.3 Classification of NNMs in Finite Homogeneous Granular Chains…… 67

2.3.1 Introduction……. 68

2.3.2 Auxiliary and Vibro-Impact Models Based on the Concept of Effective particles…… 72
2.3.3 Classification of NNMs…….. 78
2.3.4 Theoretical Modeling of the Dynamics of Effective Particles….. 84
2.3.5 Application of Effective Particles to Study Primary Pulse Propagation in Layered Media…….. 88
2.3.6 Conclusions…….. 97
2.4 Figures……. 99
2.5 Tables……... 135
3 DYNAMICS OF DIATOMIC (DIMER) GRANULAR CHAINS……... 136
3.1 Dynamics of 1:1 Dimers…… 138
3.1.1 Introduction……. 138
3.1.2 Anti-resonances and Solitary Waves…… 140
3.1.2.1 Numerical Evidence of Solitary Waves in the Dimer….. 140
3.1.2.2 Analytical Study of Anti-Resonances in Dimers…….. 152
3.1.2.3 Conclusions…… 166
3.1.3 Resonances Leading to Pulse Attenuation in Dimers…… 168
3.1.3.1 Numerical Evidence of Pulse Attenuation and Resonances in Dimers……... 169
3.1.3.2 Beating Wave-packets following 1:1 Resonance…….. 179
3.1.3.3 Analytical Study of Nonlinear Resonances in Dimers.... 183
3.1.3.4 Binary Collision Approximation for 1:1 Resonance……. 185
3.1.3.5 Conclusions…… 188
3.1.4 Effect of Pre-compression on Resonances and Anti-resonances in Dimers…….. 189
3.1.5 Periodic Traveling Waves and Bifurcations…… 194
3.1.5.1 Excitation of Families of Traveling Waves in Semi-Infinite Dimer Chains…… 195

3.1.5.2 Dynamics of Periodic Traveling Waves in Dimer Chains…….. 198
3.1.5.3 Correlation of the Stability of Traveling Waves to the Dynamics of Finite Dimer Chains……... 208
3.1.5.4 Conclusions…… 211
3.1.6 Experimental Verification of Resonances and Anti-resonances in 1:1 Dimers…… 213
3.1.6.1 Experimental Fixture……. 214
3.1.6.2 Theoretical Modeling…… 216
3.1.6.3 Experimental Results…… 220
3.1.6.4 Conclusions…… 225
3.2 Dynamics of 1: N Dimers…… 227
3.2.1 Introduction……. 227
3.2.2 General Asymptotic Formulation for Primary Pulse Propagation in 1: N Dimer Chains…… 230
3.2.3 Anti-Resonances and Solitary Waves in 1:2 Dimer Chains…….. 237
3.2.3.1 Pulse Transmission in Finite 1:2 Dimer Chains…… 251
3.2.3.2 Conclusions…… 254
3.2.4 Resonances in 1:2 Dimer Chains……... 255
3.2.4.1 Conclusions…… 266
3.2.5 Resonances and Anti-resonances in General 1: N ($N > 2$) Dimer Chains……... 268
3.2.6 A Note on the Dynamics of 1: N Dimer Chains with Large Stiffness Ratios……. 277
3.2.7 Validity of the Asymptotic Approach for the General 1: N Dimer Chains……... 281
3.3 Figures……. 287
3.4 Tables……... 346

4 DYNAMICS OF GRANULAR CONTAINERS……. 351

4.1 Theoretical model……... 353

4.2 Numerical Simulations…….. 356

4.3 Excitation of Transient Breathers……. 359

4.4 Binary Collision Approximation…….. 361

4.5 Propagation and Attenuation Zones in Granular Containers……. 366

4.6 Conclusions……. 368

4.7 Figures……. 370

5 CONCLUSIONS AND DIRECTIONS FOR FUTURE RESEARCH……. 381

6 REFERENCES……... 389

1. INTRODUCTION

A granular system is defined as an assemblage of a finite number of granules (or particles or beads with typical characteristic length greater than 0.1 mm) of solid material, with particle distribution densities ranging from packed (e.g., as in the formation of pile of sand grains in a gravitational field or the compacted sand bags) to sparsely disperse (e.g., particles dispersed in a fluid or scattered interplanetary particles). Typical examples of granular materials are sand, gravel, food grains and salt. In the framework of the current research it is assumed that the grains obey the laws of classical physics, and thus preclude any relativistic or quantum mechanical effects. Further, we primarily deal with 'dry' granular materials, i.e., granular media where the interstitial space between granules is unfilled [1].

The study of the dynamics and acoustics of granular materials poses distinct challenges. It is well known that these media can exhibit the properties of all three states of matter, that is, solids, liquids and gases, under nearly identical environmental conditions. Similar to solids, granular materials under static condition can sustain shear stress and can form heaps. Interestingly enough, the angle of the heap (angle of the free surface of the heap with the horizontal plane) is dependent on the angle of repose (defined as the maximum slope at which the material is at rest [2, 3]). Granular particles beyond this repose angle surprisingly flow down under gravity like a liquid. In effect they can flow under gravity in similarity to liquids. A classic example of granular material in flow is a sand clock or hour glass with dry sand. But in contrast to liquids, granular materials are compressible [4], which is due to the vacant interstitial gaps between the particles. In essence, dry granular materials can be attributed with the properties of the three states of matter.

Different approaches to study the physics of granular materials at different time and length scales have been developed in the past. Generally speaking, they can be

categorized into two length scales: Microscopic and macroscopic. At a microscopic or particle scale, granular material can be regarded as a discrete system whose physical properties are discontinuous with respect to position. In this approach the analysis is based on the motion of individual particles and the properties of each particle and its interaction with other particles are considered individually. On the other hand, at a macroscopic or bulk scale, a granular material is regarded as a continuum system whose physical properties are continuous over the length scale considered. Then, a suitable constitutive relation is defined over the entire domain of interest and the granular medium can be studied in a continuum (or quasi-continuum) context. In this regard, continuum approximations are useful in describing the dynamics and acoustics of discrete systems with a very large number of degrees of freedom and have played an important role in the development of the field of granular media. In general, a continuum model is developed under certain assumptions/conditions. Thus it may not necessarily describe all possible solutions supported by the underlying discrete system, but only those that satisfy the assumptions made. The usefulness of a particular continuum model depends on the underlying assumptions and how close it can represent the dynamics of the discrete system (for studies of continuum approximations of the dynamics of discrete systems see the works by Andrianov et al. [5-7]).

In this work we will primarily focus on one dimensional granular chains with non-cohesive strongly nonlinear Hertzian interaction potential [8-10], under the assumption of weak pre-compression. The non-cohesive nature of the chain can lead to separation between the discrete particles, so continuum approximation fails to model such behavior. Furthermore, the phenomena we intend to study in this work are observable only in the discrete level of the system where continuum limit approximations are hardly applicable and seldom useful. Accordingly the continuum limit approximation is not invoked in the proceedings of this thesis, except when we employ results from previous works in the course of our asymptotic approximations.

The dynamics and acoustics of nonlinear lattices (i.e., arrays of discrete masses with nonlinear mutual interactions) have interested the researchers from different areas of research for quite a long time. Such study began with the celebrated work by Fermi, Pasta and Ulam about six decades back, who formulated the FPU problem [11]. The FPU lattice is a one-dimensional periodic system of masses that interact with their nearest neighbors through springs possessing linear and weak cubic terms; so the FPU lattice can be regarded as a linear lattice with weakly nonlinear perturbation. The main objective of the study [11] was to examine the equipartition of energy between the different vibration modes of the chain. Since the FPU lattice is nonlinear, interactions and energy exchanges between different nonlinear vibration modes [12] should be possible, in contrast to the corresponding linear chain (with no nonlinear perturbation) where vibration modes cannot interact (unless they are closely spaced [13, 14] thereby leading to beating phenomena). Furthermore, in an undamped linear system energy given to a certain mode stays localized in that mode (neglecting the dissipation), so if the system is started with initial conditions corresponding to a certain vibration mode, the system vibrates in that mode indefinitely. Hence, if this system is provided with random initial conditions, the ensuing motion can be decomposed into its corresponding modes and the energy in each mode can be ascertained due to the property of superposition. In contrast to this linear behavior, a nonlinear system can have energy leaking from one vibration mode and percolating to another; further, superposition is no longer valid and the frequency of each nonlinear vibration mode is energy dependent [12]. Owing to these distinctive features, Fermi, Pasta and Ulam anticipated that an initial energy distribution in the FPU lattice would be completely equipartitioned between all the modes of the system. Surprisingly enough, such energy equipartition was not observed; rather the energy remained in an initial nonlinear vibration mode and percolated only to a few nearby modes (although above a certain high energy input chaos ensues and this can lead to equipartition among the modes).

Further it was observed that the energy in each nonlinear mode varied periodically in time, and showed recurrence with no loss of energy to the higher modes. This seemingly unexpected revelation led to further investigation of the FPU lattice by Zabusky and Kruskal [15], and eventually the discrete FPU problem was considered in the continuum limit approximation and resulted in the well-known Kortweg de Vries (KdV) equation [16].

KdV is a nonlinear partial differential equation and it supports special localized wave solutions called solitons [15, 17]. The numerical experiments of Zabusky and Kruskal revealed stable nonlinear dispersive entities, to which they coined the name *solitons* [17-22]. These are highly localized packets of energy which propagate with constant velocity, without change in form and without distortion. A soliton can be defined as a propagating localized wave that does not break up or disperses upon collision with other such waves [23]. In essence, solitons exhibit particle-like behavior with certain momentum and they conserve energy as they propagate. On the other hand, one may rigorously define a *solitary wave* [17] propagating in a one-dimensional medium as a right-traveling (left-traveling) localized disturbance whose transition from its asymptotic state at the limit $\xi \to -\infty$ to its other asymptotic state at the limit $\xi \to +\infty$ is localized in terms of the independent variable ξ, where $\xi = x - ct$ ($\xi = x + ct$), with x and t being spatial and temporal independent variables, respectively, and c the speed of the traveling wave. In contrast to solitons, however, solitary waves do not remain undistorted after colliding with other solitary waves or boundaries.

Revisiting the discrete lattice and considering wave propagation in a linear lattice (disregarding the nonlinear interactions in the FPU chain), although the interaction between particles is linear, a propagating wave loses its initial spatial waveform as it travels due to *dispersion*. Hence, it is intuitive to expect a similar behavior in the nonlinearly perturbed chain (e.g., the FPU chain); this is indeed what happens in typical nonlinear chains, but under certain conditions and in certain types of

chains it is possible that the effect of dispersion is counterbalanced by the effect of the nonlinearity thus producing traveling waves that propagate with no distortion (either solitons or solitary waves). In addition, *discrete breathers* and *intrinsic localized modes (ILMs)* [24, 25] can be realized. Discrete breathers are time periodic, spatially localized solutions of the governing nonlinear partial differential equation (with no dissipation) [26] (in this context the FPU chain), whereas ILMs are stationary, spatially localized vibration modes [27-29].

In the context of ordered granular chains of spherical beads, a seemingly simple prototypical example is Newton's cradle [30, 31]. A Newton's cradle is quite an interesting toy to explain the basic laws of physics like conservation of momentum and energy [32]. These devices usually consist of an array (n balls, usually 5) of balls/spheres in mutual contact suspended through strings. If a certain number (N) of balls are displaced and allowed to impact the remaining ($n - N$) balls of the chain, it is observed that same number (N) of balls are displaced by the same magnitude on the other end of the chain and leaving the rest ($n - N$) of the balls stationary (of course neglecting the inevitable friction present in the setup). This expected behavior seems to be in complete accordance with the laws of classical physics as described in literature [32], but, in fact, very careful experiments reveal that this is not what actually happens [33, 34]. Rather, it is observed that few of the balls at the impacting end rebound, whereas the ball at the other end flies off with maximum positive velocity and other balls have decreasing positive velocities [35]. Therefore, unless the chain consists of only two balls, the previous two conservation laws are not sufficient to explain this behavior.

The required additional condition is *wave dispersion* which accounts for the aforementioned discrepancy. In the context of continuum system, dispersion is a property of the system by which the propagation speed of a signal is dependent on its wavenumber [36, 37]. But due to the discrete nature of the interacting balls in Newton's cradle, in this particular context dispersion can be considered as a measure of the

negative momentum or kinetic energy carried by the rebounding balls in comparison to the initial input momentum or kinetic energy, respectively. Let us consider only two balls (both of the same mass) in the chain, one being at rest and the second impacting the first with a unit velocity. Applying the momentum and energy conservation we obtain the well know result of first ball coming to rest and the second flying off with unit velocity. In fact this simplified system is dispersion free [33, 34, 38]. Further it should be noted that for a discrete chain (of equal masses and similar interaction stiffness) to be dispersion free, the discrete particles should be moving so that only two particles are in interaction at any instant of time (model of binary collisions [39]) . With such a scenario the first particle transfers all its momentum to the second, the second to the third and so on. Once the particle loses contact with its successive one, it comes to complete rest. If the particles are just in contact initially, the chain is bound to be dispersive. Due to the presence of dispersion, complete momentum transfer seldom happens. In fact the first few balls bounce back with a portion of the initial energy [35] [40]. Furthermore, dispersion is highly dependent on the interaction potential between particles [33]. For example consider an interaction force of the form $\tilde{F} = K\delta_+^r$, where k is the interaction stiffness (a function of material and the geometric properties of the interacting particles), δ is the compression between the particles, r is an exponent and subscript '+' indicates that the interaction force vanishes once the particles separate. It can be easily shown that the dispersion is weaker for the case of $r = 3$ as compared to the case when $r = 2$. For a chain with higher value of r, the momentum carried by the rebounding balls is comparatively lower than that in a chain with lower value of r. Furthermore, in any homogeneous chain with interaction force with $r > 1$, the applied impact takes the form of a stationary propagating pulse of constant amplitude as it propagates in the chain, and thus is in the form of a solitary wave [35, 41-43]. It is worth emphasizing that although dispersion is present in all these nonlinear chains, solitary waves are realized only in discrete chains with power law type contact force with

exponents $r > 1$ [43]. This is in fact due to the balancing of the dispersion and the nonlinearity [41, 42]. In the special case when $r = 1$ (linear force interaction), only dispersion exists so no solitary waves can be formed.

The interaction of the balls in the Newton's cradle experiment is governed by a force interaction law with $r = 1.5$, so in this case solitary waves are realized with wavenumber (spatial span) of about 6-7 balls [41, 44, 45]. In fact such a solitary wave has been termed as *compacton* owing to its compact support over the media where it propagates [46]. The existence of such solitary waves in Newton's cradle leads to the aforementioned deviations of predictions based solely on momentum and energy balance. Another interesting observation that came to light of late is the super-exponentially fast decay of these waves with regard to space-time [47]. The consideration of such fractional exponent for the interaction between the balls is not arbitrary, but has very profound theoretical basis based on the geometry of the interacting bodies.

Indeed, the interaction of two solids of arbitrary curvatures was first studied by Hertz [8, 9, 48, 49]. The proposed theory by Hertz predicts the geometry of the contact area and its evolution with increasing applied load. Furthermore, it also provides both the magnitude and distribution of surface tractions at the contact area in the interacting bodies. This theory of interaction was further applied to the collision of two elastic bodies with convex surfaces. The time of interaction between two colliding spherical particles and the underlying exponent of the interaction potential is of primary importance in our study. Few of the most important assumptions and observations made herein are of significance in our study, namely that:

a) The contacting surfaces are smooth, continuous, non-conforming and frictionless at both micro and macro scales; at the micro scale this implies that small surface aberrations/irregularities are completely absent or at least negligible, on the other

hand, at a macro scale it indicates that the surface profiles at the region of contact are smooth and are continuous at least up to their second derivatives;

b) When two curved bodies are brought into contact initially (i.e. under no load condition), the contact is over a point (as in two spheres in contact) or a line (as in two cylinders interacting with axes parallel); with the application of the load the elastic deformation evolves this point/line to an area and the load is distributed in the form of pressure over it;

c) The size of the contact area is small compared to the characteristic size of the interacting bodies;

d) The strains experienced are within the elastic limit, i.e. we preclude the permanent/plastic deformations;

e) Stress in the immediate vicinity of the contact is much higher than in the rest of the body; hence, the elastic deformation energy is stored exclusively in the near vicinity of the area of contact, and each body can be considered to behave as an elastic half space in the vicinity of the contact. Hence, it can be deduced that the material in the contact area can be considered as a spring (in which the total energy can be stored in the form of elastic potential energy) connecting two undeformable bodies (which can be attributed to the stored energy in the form of momentum); furthermore, the elastic and the inertial properties of the collision of two bodies can be spatially separated;

f) The time of interaction of the two bodies is found to be a function of the incoming velocity [50]; this interaction time should be much higher than the time required for the disturbance propagation inside the bulk of the material, so that time scale separation occurs between the dynamics of the body to body interaction and the wave acoustics within each body.

With these assumptions satisfied, the interaction of the balls as described in Newton's cradle experiment, or more generally the interaction of elastic bodies can be

approximated by a model where the colliding/interacting bodies are treated as discrete masses interacting through springs of appropriate force interaction law as predicted by the theory of Hertz. In our study we adhere to the above discussed assumptions and conditions and consider the spherical beads as point masses interacting through Hertzian interaction law.

From Hertz's theory it can be seen that the interaction of spherical bodies of arbitrary radii is governed by the relation $\tilde{F} = K\delta_+^r$ where $r = 1.5$. This has been experimentally proven in collision experiments [33, 34] and wave propagation experiments [51, 52]. Moreover, the validity of this interaction potential has been theoretically proven by Coste et al. [53]. For the case of two cylinders interacting along their axes, the interaction is along a line and we have $r = 1$ [8, 10]. However, it should be noted that for the phase of wave propagation, the interaction between cylinders cannot be modeled as discrete masses interacting via linear springs as the velocity of wave propagation is of the same order as the velocity of sound in the bulk material [35]. In Figure 1.1 (unless stated all units are non-dimensional) we present the comparison of force interaction law with three different exponents. As can be seen the slope is constant for the case of $r = 1$, whereas the slope of the curves for the case of $r = 1.5$ and $r = 2.5$ (realized for paraboidal solids [54]) is increasing with increasing deformation, indicating a hardening type nonlinear behavior. It is interesting to note that in both nonlinear cases the slope is zero at $\delta = 0$. In fact such a behavior leads to zero speed of sound propagation in this type of systems (i.e., complete absence of linear acoustics), and, hence, media with this type of interaction law have been aptly described as *sonic vacua* [42]. This definition is attributed only due to the zero slope of the force-displacement interaction law at $\delta = 0$. On the other hand, if there is an applied pre-compression (δ_0), the non-zero slope about $\delta_0 \neq 0$ defines the wave speed of the linearized acoustics. Moreover, we note that an additional form of strong nonlinearity in the interaction law stems from the fact that in the absence of compression the

interaction force is zero (cf. Fig. 1.1 for $\delta < 0$) so beads separate. The ensuing collisions between beads provide a second source of strong nonlinearity (in addition to the non linearizable force law for $\delta \geq 0$), which as we will show leads to interesting nonlinear dynamical phenomena and renders the analysis non-smooth.

The present work is solely devoted to the study of one dimensional ordered granular chains consisting of frictionless spherical balls (spheres/beads). Unless otherwise stated we consider only dry chains without incorporating any dissipative mechanisms and without any pre-compression. Furthermore, the considered granular chains are purely elastic (no plastic deformation considered) and non-cohesive (tension free). The Thesis has been broadly classified into a number of chapters.

1.1 Outline of the Thesis

We begin our study by considering the dynamics of homogeneous granular chains in Chapter 2. We particularly consider Nonlinear Normal Modes (NNMs) in finite granular chains constrained between rigid boundaries. The nonlinear nature of the system makes the dynamics energy dependent, and the most appropriate tool to study the NNMs is by depicting them in Frequency Energy Plots (FEP). The realized NNMs split the FEP into two zones, namely propagation and attenuation zones (PZs and AZs), which are studied numerically and experimentally. Although the considered system is strongly nonlinear, its dynamics in the AZ is weakly nonlinear and thus lends itself to analytical study. In contrast to a linear system wherein the number of normal modes is equal to the degrees of freedom (DOF), the number of NNMs in a nonlinear system can far exceed the DOF. Further, due to the non-cohesive nature of the granular chains the NNMs require appropriately tailored classification techniques. In Section 2.3 we consider the classification of NNMs in a finite granular chain. An interesting concept of

effective particles is introduced in Section 2.3.2 and its application to primary pulse propagation in layered granular chains is presented in 2.3.5.

In Chapter 3 we focus primarily on the dynamics of periodic diatomic (dimer) chains, i.e. chains consisting of two types of beads with type 2 beads placed periodically between beads of type 1. Section 3.1 is concerned with the propagatory dynamics of a $1:1$ dimer chain. A countable infinity of solitary waves has been discovered in $1:1$ dimer chains and the pertinent numerical and analytical study is presented in Section 3.1.2. In contrast to the un-attenuated propagation of solitary waves, specific conditions are devised when these dimers lead to substantial pulse attenuation. This phenomenon is attributed to a new type of nonlinear resonances, and their analytical and numerical study is presented in Section 3.1.3. The effect of pre-compression on the resonances and the solitary waves is an important consideration in designing practical systems incorporating dimer chains and Section 3.1.4 deals with this topic. Dimer chains not only support solitary waves but also periodic traveling waves of varying periodicities. The study of different types of traveling waves and their influence on the global dynamics of the dimers is carried out in Section 3.1.5. Finally in Section 3.1.6 the theoretically predicted resonances and anti-resonances are verified experimentally.

In Section 3.2 we consider propagatory dynamics in a general $1:N$ dimer chain. A generalized asymptotic model is formulated in Section 3.2.2. In Section 3.2.3 and 3.2.4 we consider the particular case of $1:2$ dimers and present the realization of anti-resonances (solitary waves) and resonances, respectively. Although further extension of the previous analysis of $1:1$ and $1:2$ dimer chains to general $1:N$ dimers seems straightforward, it is seldom so. In fact we prove that no exact solitary waves and resonances can be realized in a general $1:N$ dimer ($N > 2$), although approximate dynamics resembling this type of dynamics can be realized. This interesting revelation and the analytical reasoning are presented in Section 3.2.5. Further we consider a particular case of a dimer chain with very high stiffness ratio in Section 3.2.6. A special

asymptotic analysis is formulated for the study of dimers in Chapter 3 and this has been extensively utilized. Section 3.2.7 is concerned with the study of the validity of this asymptotic methodology and with its limitations in a more qualitative manner.

A brief introduction to an interesting system of granular containers is presented in Chapter 4. Section 4.1 provides the theoretical model of the granular wave containers, whereas Section 4.2 deals with the numerical simulation of granular containers with regard to their efficacy in containing the propagating pulses. Further the Section 4.3 dwells on the excitation of transient breathers when small mass intruders are placed in a homogeneous chain. Section 4.4 concerns the application of binary collision approximation in quantifying the amplitudes of scattered solitary waves in granular containers. The last section in this chapter explores the PZ, AZ and the transition region between these two zones realized in harmonically excited granular containers.

Finally, Chapter 5 provides a comprehensive overview of all the results presented in this Thesis and their potential application to practical metamaterials design. In addition, further development of the ideas and methodologies of the present work is discussed, together with suggestions for future work.

1.2 Literature Review

Granular media is a highly complex and distinct class of dynamical systems. The dynamics of this media is highly tunable [55], and depending on the applied pre-compression it can be either strongly or weakly nonlinear and smooth or non-smooth [42, 44]. Indeed, for strong pre-compression the dynamics of granular media is weakly nonlinear, whereas for no pre-compression the dynamics is strongly nonlinear (in fact not even linearizable) and bead separation is possible in the absence of external cohesive forces. Hence, the dynamics of granular chains with no (or sufficiently weak)

pre-compression is either smooth – when neighboring beads are in contact – or non-smooth due to bead separation accompanied by inter bead collisions.

Propagatory dynamics of homogeneous granular chains has been studied extensively both analytically and experimentally, notably in the works by Nesterenko [41, 42], Coste et al. [52], Daraio et al. [56], Sen et al. [44], Nesterenko et al. [51], Job et al. [57], Mackay et al. [58] and English et al. [59]. A pioneering breakthrough in the acoustics of one dimensional granular chain was the discovery of solitary waves [41] [42]. Continuum approximation was invoked to prove the existence of solitary waves in this medium. The theoretical foundation for the existence of solitary waves was provided by Friesecke et al. [43], Ji et al. [60] and [61]. Experimental verification of these waves was performed by Nesterenko et al. [51] and Coste et al. [52]. The continuum approximation solution to the solitary wave provided by Nesterenko was modified and improved by the works of Chatterjee [47], Sen et al. [44, 62] and Starosvetsky et al. [63]. Due to the nonintegrability of the governing equations of motion, the realized solitary wave is not a soliton [17]. Although solitary waves or solitons span infinite spatial domains in integrable systems [21, 22], solitary waves in homogeneous granular chain span (has compact support) a finite spatial domain, namely a span of about 6-7 beads [42, 44, 45, 51]. This was proven analytically and so these solitary waves were denoted as compactons [46].

Solitary waves provide the only mechanism for propagation of disturbances in homogeneous granular chains. Although such chains are dispersive, it is the balancing of the nonlinearity and the dispersion that leads to the formation of these solitary waves [42]. The absence of bead separation when a solitary wave propagates in a homogeneous granular chain enables the application of continuum approximation for their analytical treatment. Apart from solitary waves, homogeneous granular chains support periodic traveling waves [63], but these waves involve separations between beads and thus continuum approximation is no longer applicable for their analysis.

However, it is conjectured in [63] that these traveling waves asymptotically converge to the aforementioned solitary wave in the limit of large number of beads of the homogeneous chain.

The effect of a small mass intruder on the dynamics of a homogeneous granular chain has been studied [64-67], and it is shown that it leads to the excitation of discrete breathers. Further, the scattering of solitary waves at the interface of two homogeneous chains consisting of beads of different masses has been explored in other works [42, 68]. A solitary wave experiences complete transmission and disintegrates into a train of solitary waves at the interface of a chain composed of heavy beads to a chain composed of light beads, whereas there is partial transmission at the interface between a light and a heavy chain of beads. Such transitions has been taken into account in devising granular protectors or granular wave containers [69] composed of different types of homogeneous granular chains.

Although most current works have focused on granular chains without dissipation, any practical granular system would invariably contain dissipative mechanisms like dry friction and plasticity. The quantification and modeling of these damping mechanisms is of primary importance when designing practical granular systems. Modeling the dissipation with velocity dependent damping is very popular and (perhaps surprising!) successful [70-73].

The main emphasis of the current research has been on the propagatory dynamics of long homogeneous chains, and relatively little research has been devoted to studying the oscillatory dynamics of finite granular chains. By oscillatory dynamics we mean the time periodic motions or Nonlinear Normal Modes – NNMs that can be supported by finite granular chains. The discussion of NNMs in the literature has focused mainly on dynamical systems with smooth stiffness nonlinearities [12, 74-81], although some works on systems with non-smooth nonlinearities have also appeared [82-84]. These NNMs are defined as time-periodic oscillations of discrete or continuous

oscillators than can be either synchronous or asynchronous. The study of NNMs in granular chains poses its own distinct challenges, such as the strong nonlinearity of Hertzian interaction and the non-cohesiveness that leads to separation between beads. In such strongly nonlinear and possibly discontinuous systems, the definition of NNM will need to be modified [85] to include asynchronous but time periodic motions. It is well known that frequency zones (attenuation and propagation zones – AZs and PZs) exist in linear periodic systems [37, 86] where there is a characteristic speed of sound; however, one would expect that in sonic vacua like granular materials (with zero speed of sound) no such zones should exist. Yet, such frequency zones in homogeneous granular chains were studied theoretically and numerically in [85] and lately were confirmed in the experiments by Joseph et al. [87].

After substantial research on the homogeneous/monodisperse granular chains, heterogeneous/polydisperse granular chains have caught the attention of many researchers. Polydisperse systems typically support waves that radiate energy to the far field as they travel, and thus distort their initial waveforms due to continuous energy 'leakage'. In the context of one-dimensional granular media much emphasis has been given to periodic dimer systems [42, 88-92], i.e., systems composed of pairs of dissimilar beads, more often called 1:1 dimers. The dynamics of these systems has been studied both theoretically in the continuum approximation [93] and experimentally [89, 90, 93]. Although continuum approximation [94, 95] applied for granular diatomic chains [93] seems quite a logical extension of analogous studies in homogeneous granular chains, large periodic variations of system properties makes the continuum approximation inappropriate when bead separations are realized. Hence, we claim that to investigate the dynamics of granular dimer chains the discrete approach is more suitable, unless the granular chain is pre-compressed and bead separation is suppressed. In this context, frequency band gaps in pre-compressed dimer chains have been explored by Herbold et al. [91], whereas discrete breathers in these systems have been studied by Boechler et al.

[92]. Further to that, intrinsic energy localization by exciting breathers in dimer chains has been studied by Theocharis et al. [96]. All these previous studies are possible only due to the applied pre-compression that prevents bead separation. But no similar results exist, however, in the strongly nonlinear case, i.e. in the absence of pre-compression. Indeed, there has been no much progress in studying the dynamics of these systems analytically taking into account the discrete nature of the bead interactions; this perhaps is due to the complexity of the nonlinear dynamical interactions occurring in these media. The absence of pre-compression can reveal exciting new solutions, like families of solitary waves [97] which are analogs to those realized in homogeneous granular chains, and traveling waves [98, 99]. Further to that, resonance phenomena that lead to substantial attenuation of propagating pulses were explored [91]. The phenomena of resonances and anti-resonances have been experimentally verified by Potekin et al. [100].

Periodic dimer chains are a broad class of granular systems and $1:1$ dimers represent only a small sub-group. The dynamics of general $1:N$ dimer chains is more complicated and poses distinct challenges. Vibrational band gaps in $1:2$ dimers have been studied experimentally by Boechler et al. [101] but only in a pre-compressed state. Band gaps are those frequency regimes wherein pulse propagation in the medium is not possible. Due to the applied static pre-compression, the dimers considered in [101] exhibit linearized frequency spectra. Interestingly such spectra possess band gaps separated by pass bands. General $1:N$ dimers have not been considered in the limit of zero pre-compression in the literature. A particular case of $1:N$ and $N:1$ dimers has been studied by Porter et al. [90], considering stiff (steel) and soft (PTFE) beads and establishing the propagation of stationary shocks. In fact the theoretical study of $1:N$ dimer chains considered in this Thesis happens to be one of the first comprehensive studies in this regard. It has been shown that $1:2$ dimer chains can support a countable infinity of families of solitary waves and nonlinear resonances [102, 103], whereas

general $1:N$ $(N > 2)$ dimer chains cannot. Other classes of periodic granular systems have been considered in literature like trimers [90], wherein light and soft beads are periodically placed in a chain of heavy beads in the form $1:1:1$. The wave dynamics in this system is primarily governed by the heavy beads and propagation of stationary shocks has been observed.

Other classes of one dimensional granular systems considered are tapered/decorated granular chains [104-109] and randomly decorated chains [110]. Although a tapered chain might look quite complex due to monotonous decrease in particle size, a simple model of binary collision approximation (BCA) can predict the velocity response of its individual beads [104, 105]. Surprisingly enough, tapered chains act as effective shock protectors and attenuators [106-108]. Shock attenuation and energy transfer to higher frequencies [106, 109, 111] in tapered chains have been experimentally verified by Melo et al. [112]. The main intent of these types of granular setups is shock mitigation or shock isolation [107, 109].

In the previous cases of tapered chain or resonances in dimers [91, 103], the applied shock attenuates as it propagates through the granular chain. The other methodology evolved for the same application of shock protection/isolation is by entrapping/containing the shock energy in a certain spatial domain. Such granular systems evolved for shock protection are called granular wave containers or granular protectors [44, 69, 113]. These granular chains are designed in such a way that a considerable portion of the shock energy is mainly localized in a spatial domain, while leaking energy at a substantially lower rate in an intermittent fashion.

The application of granular media in blast protection is not new; in fact it dates back to the time of World War I. In the war field, though the troops are protected in the trenches, the shock due to the shelling and bomb explosions can be quite severe. In this regard sand bags have found a potential application. These sand bags form barricades for the trenches and absorb the artillery fire efficiently thus protecting the troops [114].

In a different scenario, sand bags have been effectively used to protect the world famous sculptures like the Venus de Milo statue in order to protect it from getting destroyed [115] during the time of World War II. Even to the present day, sand bags have been used by the military all over the world to protect troops and artillery in the war front [116-118]. Apart from the application of blast protection, sand bags have found their utility in erosion prevention and flood control. The high hydrodynamic pressure during floods can be detrimental to the engineering structures. These sand bags have been effectively deployed to counter the potential catastrophe due to the floods [119]. Sand bags have shown substantial efficacy in blast/shock protection. Although they have the drawback of mobility and labor intensive filling process, their applicability is inevitable in certain situations.

There has been a lot of interest recently in extending the knowledge gained in studying one dimensional chain to higher dimensional granular systems. One such study is with regard to branched granular structures [120] and splitting of solitary wave in such setups. Although this seems to be a two dimensional problem, due to the realization of solitary waves supported by different segments of homogeneous granular chains, a quasi-particle approach is evolved in studying the solitary wave propagation and their splitting at branch interfaces. Moreover, one and a half dimensional chains were proposed as extensions of one dimensional chain. These are discrete homogeneous granular chains coupled through weak links. Such chains represent a considerable reduction over two dimensional chains. Energy equipartition between parallel chains and energy localization and transfer phenomena have been studied in these systems [121, 122]. Studies of two dimensional systems have been primarily focused on wave propagation in square packing setups consisting of spherical beads [123, 124]. Interestingly, energy provided to a particular chain parallel to its axis remains in that chain and is seldom shared with neighboring chains. This is in fact due to the very small deformation of the beads and thus lateral deformation is negligibly small. In order to

transfer energy to neighboring chains, intruders are added in the interstitial space and the effect of small mass intruders (usually cylinders) on wave propagation in a two dimensional matrix of homogeneous beads was experimentally and numerically considered [123].

Much focus is devoted to the application of one dimensional granular media in practical engineering systems. One of the theoretical studies primarily concerns with the inclusion of granular chains as interfaces between one dimensional linear elastic continua [125]. Analytical and numerical studies indicate that NNMs of the granular chain are excited when the number of beads is small, whereas propagatory behavior and solitary waves are observed for larger number of beads in the granular chain. The excitation of solitary waves in homogeneous chains, their interactions with boundaries [126, 127] and the characteristics of the reflected pulses are taken into account in practical applications. Granular materials have found their use in non-destructive evaluation - NDE [128], in a system for orthopedics [129], in composite delamination [130], in monitoring of hydration of cement [131], in NDE of adhesive joints [132] and in highway infrastructure [133]. In all these applications, a strongly nonlinear solitary wave is created in the granular medium and is directed towards the intended test object. The test object is indirectly diagnosed by examining the form of the scattered pulse. Other potential applications include tunable vibration filters [91, 92] and acoustic switches and rectifiers [134]. An interesting application of granular chains concerns their interactions with elastic continua. It was shown recently that such interactions can lead to the creation of *sound bullets* in elastic half spaces. In principle, it is the constructive interference of the elastic waves at a point in the elastic half space causing such sound bullets; the source of these waves is a series of parallel uncoupled homogeneous granular chains with varying pre-compression that are in contact with the surface of the half space. Due to the tunability of the granular dynamics to pre-compression, solitary waves in these parallel granular chains possess different speeds

(depending on their amplitudes). Hence, at the points of contact of the granular chains with the elastic half space, sources of disturbances are formed that generate elastic waves with varying time-delays between them. Indeed, it is possible to focus acoustic energy at a single point in the elastic half-space due to positive interference of the emitted elastic waves, resulting in the formation of a high-intensity acoustic bullet. Experimental and numerical results are well presented in the work of Spadoni et al. [135] and the accompanying supporting information.

The granular chains (homogeneous and dimers) considered in this Thesis are in the strongly nonlinear limit of zero pre-compression, i.e., media possessing zero speed of sound (sonic vacua) [42]. In effect, the considered systems have no linearized dynamics whatsoever, in contrast to the majority of the above referenced works. Due to the absence of pre-compression, bead separation ensues and represents an added source of nonlinearity in addition to the strongly nonlinear Hertzian interaction. In fact there are no known and well established methods to comprehensively study such strongly nonlinear systems analytically. Although certain dynamical behaviors and responses of uncompressed granular chains can be analytically captured, we adhere to numerical simulations to analyze their complex dynamics. In the study of periodic diatomic chains a special asymptotic methodology is devised based of singular perturbation theory [136]. This methodology has paved way for the discovery of families of solitary waves realized in periodic dimer chains, unknown till now. This methodology is not without limitations, as it can be applied only to the regime of primary pulse propagation where bead separation cannot occur. Further to analytical and numerical studies, we have resorted to experiments in order to verify some of our theoretical findings like frequency bands in homogeneous granular chains and resonances and anti-resonances in periodic dimer chains. These experiments have verified our theoretical predictions.

1.3 Figures

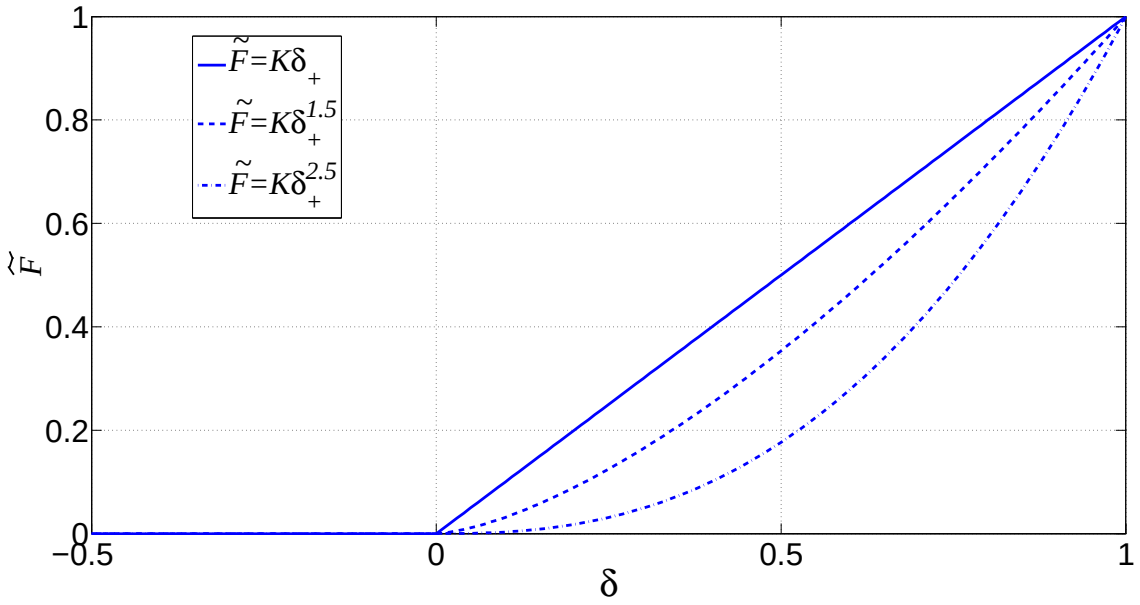

Figure 1.1 Comparison of elastic Hertzian force interaction law for non-cohesive elastic bodies with $K = 1$.

2. DYNAMICS OF HOMOGENEOUS GRANULAR CHAINS

The propagatory dynamics of homogeneous granular chains has been studied extensively both numerically and experimentally in the references cited in the previous chapter. The present study focuses on the oscillatory behavior of finite dimensional homogeneous granular chains. It is well known that normal vibration modes are the building blocks of the oscillatory dynamics of linear systems due to the applicability of the principle of superposition. One the other hand, nonlinear theory is deprived of such a general superposition principle (although special cases of nonlinear superposition do exist), but *nonlinear normal modes – NNMs* still play an important role in the forced and resonance dynamics of these systems. In their basic definition [77] NNMs were defined as time-periodic nonlinear oscillations of discrete or continuous dynamical systems where all coordinates (degrees-of-freedom) oscillate in-unison with the same frequency; further extensions of this definition have been considered to account for NNMs of systems with internal resonances [12].

We study time-periodic standing waves (NNMs) of finite granular chains composed of spherical granular beads in Hertzian contact, with fixed boundary conditions. Although these are homogeneous dynamical systems in the notation of Rosenberg [77, 79], we show that the discontinuous nature of the dynamics leads to interesting effects such as, separation between beads, NNMs that appear as traveling waves (these are characterized as *pseudo-waves*), and localization phenomena. In the limit of large number of beads we study band zones, i.e., pass and stop bands (or propagation and attenuation zones – PZs and AZs) in the frequency – energy plane (FEP) of these dynamical systems, and classify the essentially nonlinear responses that occur in these bands. This is the first instance of the realization of band zones in un-compressed homogeneous granular chains, characterized as sonic vacuum [42]. Moreover, we show how the topologies of these bands affect the forced dynamics of

these granular media subject to narrowband excitations. We note that these band zones have been experimentally verified. Although the propagatory type behavior is analytically un-tractable, the dynamics of these systems in AZs lends itself to linearized analysis. Moreover, the theory of band zones contributes towards the design of granular media as shock protectors, and passive mitigation of transmission of unwanted disturbances. The classification of NNMs according to the existing classification theories does not seem appropriate, so a new classification theory has been developed based on the concept of effective particles and balance of momentum.

2.1 Nonlinear Normal Modes (NNMs) and Frequency Bands of Homogeneous Granular Chains

2.1.1 Introduction

NNMs are defined as synchronous periodic particular solutions of the nonlinear equations of motion of dynamical systems, keeping in mind the fact that the superposition principle is no longer valid in the nonlinear case. With such a restricted definition, a nonlinear generalization of the concept of normal mode of linear vibration theory is possible, and beginning with the works of Lyapunov [74] several attempts were made in this direction. Lyapunov's theorem proves the existence of n synchronous periodic solutions (NNMs) in neighborhoods of stable equilibrium points of n degree-of-freedom (DOF) Hamiltonian systems whose linearized eigenfrequencies are not integrally related (so that no internal resonances between modes exist). The formulation and development of the theory of NNMs can be attributed to Rosenberg and his co-workers who developed general qualitative [75], and quantitative [76-79] techniques for analyzing NNMs in discrete conservative oscillators. Rosenberg considered n DOF

conservative oscillators and defined NNMs as *vibrations-in-unison*, i.e. synchronous time-periodic motions during which all coordinates of the system vibrate equiperiodically (in a synchronous fashion), reaching their maximum and minimum values at the same instant of time. In linearizable systems with weak nonlinearities it is intuitive that NNMs are particular periodic solutions, and that, as the nonlinearities tend to zero, approach in limit the classical normal modes of the corresponding linearized systems. On the contrary, essentially nonlinear systems do not show such a behavior, since the NNMs in these systems are not necessarily extensions of normal modes of linear systems. Thus the NNMs of these systems may exceed in number the degrees-of-freedom of the system, and, in addition, certain of the NNMs may not have any counterparts in linear theory. This is due to NNM bifurcations [12], which become exceedingly more complicated as the number of DOF of the systems increase and introduces new features such as nonlinear mode localization in the dynamics.

Our study of standing waves (NNMs) in one dimensional granular media will be structured as follows. We initiate our analysis by considering a two-bead system with fixed boundary conditions, and study NNMs by numerical Poincaré maps and analytical techniques in terms of hypergeometric functions [137]. We then extend our analysis to three-bead granular systems, and compute the corresponding NNMs by numerical methods. Further, we focus on higher (but finite-) dimensional) systems and consider exclusively two specific classes of NNMs, namely the in-phase and out-of-phase modes, since as we will show, these form the boundaries of the frequency – energy band within which all other NNMs are realized.

2.1.2 Two-Bead Granular System

The two-bead granular system considered is depicted in Figure 2.1. The system is *homogeneous* in the sense that the two spherical beads have identical geometric and material properties. Moreover, the beads are placed between rigid boundaries (fixed hemispheres of the same radius and material as the other beads) with no gaps existing between them or with the walls when they are in their trivial equilibrium positions. The system is considered without any pre-compression, and thus it exhibits strong (essential) stiffness nonlinearity and potentially non-smooth effects. Furthermore, no dissipative effects are yet considered in this study, but weak dissipative forces in the bead interactions will be considered later, in our computational study of the forced dynamics of high-dimensional granular media carried out in Section 2.2. Assuming Hertzian contact interaction between beads and between the end beads and the rigid boundaries which are effectively fixed hemispheres of the same material and radius as that of the moving beads, the kinetic ($\tilde{T}$) and potential energy ($\tilde{U}$) of the two-bead system are defined as follows,

$$\begin{aligned} \tilde{T} &= \frac{1}{2} m \left(\frac{d^2 u_1}{dt^2} + \frac{d^2 u_2}{dt^2} \right) \\ \tilde{U} &= \frac{2}{5} \frac{E(2R)^{1/2}}{3(1-\mu^2)} \left[(-u_1)_+^{5/2} + (u_2)_+^{5/2} + (u_1 - u_2)_+^{5/2} \right] \end{aligned} \tag{2.1}$$

where, u_i is the displacement of the $i-$th bead, R denotes the radius of the bead, E elastic modulus, μ Poisson's ratio, ρ mass density, and m mass of each bead; the (+) subscript in the expressions in (2.1) is used to emphasize that the bracketed term is non-zero only if the term inside the bracket is positive and zero otherwise. The equations of motion can be derived from Lagrange's equation as follows,

$$\frac{d^2u_1}{dt^2} = \Phi\left[(-u_1)_+^{3/2} - (u_1 - u_2)_+^{3/2}\right]$$
$$\frac{d^2u_2}{dt^2} = \Phi\left[-(u_2)_+^{3/2} + (u_1 - u_2)_+^{3/2}\right] \tag{2.2}$$

where $\Phi = E(2R)^{1/2}/[3m(1-\mu^2)]$. The non-smoothness due to the subscript (+) is introduced to mathematically model the possibility of separation between the beads in the absence of compressive forces and this considerably complicates the analysis.

The displacements are non-dimensionalized by means of the following normalizations,

$$x_i = \frac{u_i}{R},\ \tau = t\left[\frac{2}{3}\frac{E}{m(1-\mu^2)}\frac{R}{\sqrt{2}}\right]^{1/2} \tag{2.3}$$

So the equations of motion are placed in the following normalized form,

$$\ddot{x}_1 = (-x_1)_+^{3/2} - (x_1 - x_2)_+^{3/2}$$
$$\ddot{x}_2 = -(x_2)_+^{3/2} + (x_1 - x_2)_+^{3/2} \tag{2.4}$$

where $x_i = x_i(\tau)$ is in terms of the normalized time τ, and overdots denotes differentiation with respect to τ. System (2.4) will be employed in the following analysis. We re-emphasize at this point that the dynamics of system (2.4) is not only essentially nonlinear (as the stiffness terms do not possess any linear components), but, in addition, they are non-smooth. The loss of smoothness is due to the fact that the interaction force due to (compressive) Hertzian contact vanishes when the center distance between the two beads exceeds a length equal to twice the radius and due to

the non-cohesiveness of the interacting beads. From the above discussion of the subtle features of the system, it is certain that the system dynamics will be highly complex.

Since the system possesses two degrees-of-freedom (two-DOF) and is conservative, it is possible to analyze its global dynamics in terms of numerical Poincaré maps. Indeed, a NNM of this system is defined as a time-periodic oscillation where the bead oscillations possess identical frequencies but may not necessarily be synchronous due to possible bead separations. Moreover, whether the dynamics is smooth or non-smooth, a NNM should possibly be depicted as a (modal) curve in the configuration plane. System (2.4) possesses a four-dimensional phase space, but owing to energy conservation (since no dissipative effects considered),

$$h(x_1,\dot{x}_1,x_2,\dot{x}_2) \equiv (1/2)\left(\dot{x}_1^2+\dot{x}_2^2\right)+(2/5)\left[(-x_1)_+^{5/2}+(x_2)_+^{5/2}+(x_1-x_2)_+^{5/2}\right]=h \tag{2.5}$$

the dimensionality can be reduced by one, and the dynamics can be restricted to a three-dimensional isoenergetic manifold. Intersecting the isoenergetic flow by a two-dimensional cut section defined as, $S:\{x_2=0\}$, we obtain a two-dimensional Poincaré map $P:\Sigma\to\Sigma$, where the Poincaré section Σ is defined as, $\Sigma=\{x_2=0,\dot{x}_2>0\}\cap\{E(x_1,\dot{x}_1,x_2,\dot{x}_2)=h\}$, and depicts the global nonlinear dynamics of the system on the cut section that is now parameterized by $(x_1,\dot{x}_1)$. In Figure 2.2 (unless stated all units are non-dimensional) we depict the numerical Poincaré map at the energy level $h=0.0001$. Three types of periodic solutions are detected, namely an in-phase NNM, an out-of-phase NNM, together with numerous subharmonic orbits. We note that the out-of-phase NNM is a *synchronous* oscillation and lies on the $\dot{x}_1$ axis on the cut section, whereas the in-phase NNM is offset from that axis and is an *asynchronous* oscillation. Moreover, the two modes appear to be stable (since they are surrounded by closed

orbits in the Poincaré maps), and, hence, are physically realizable (i.e., they can be realized experimentally).

In Figure 2.3 we depict the in-phase NNM for the energy level $h = 0.0001$ (region A of the Poincaré plot of Figure 2.2). From the time series of Figure 2.3a, we note that the two beads pass through their equilibrium positions at different instants of time. Hence, such a mode does not conform to the classical definition of NNM as proposed by Rosenberg [77]; however, by extending the definition to account for non-synchronicity in the bead oscillation we may classify this time-periodic motion as in-phase NNM. It is interesting to note that this NNM exhibits bead separation.

The energy exchanges between beads for that NNM are of particular interest. Referring to Figure 2.3a, at point 1 the entire energy of the system is elastic due to the interaction of the second bead with the fixed right boundary, whereas the first bead is motionless but offset from its equilibrium position. As time progresses, at point 2 the beads start interacting with each other, and at that time instant the first bead collides with the second. Proceeding to point 3, the second bead loses contact with the boundary as it passes through its equilibrium position. Once the first bead passes through its equilibrium position at point 4, it starts interacting with the fixed left boundary and at that point the second bead has transferred almost all of its energy to the first bead and is about to get stationary. At point 5, the second bead loses all its energy, becomes stationary but offset from its equilibrium position, and the entire process repeats itself. It is interesting to note that from point 2 to 5, both beads remain in contact with each other, and, as explained previously, the second bead loses contact with the fixed right boundary whereas the first bead gains contact with the fixed left boundary. Beyond point 5, the first bead interacts with the boundary and subsequently loses contact with the second bead and the complete energy of the system is in the form of elastic potential energy due to the interaction of the first bead and the fixed left boundary (at point 6). Hence, complete exchange of energy between the two beads occurs, and the in-phase

NNM can be represented by the time-delayed relation $x_1(\tau) = -x_2(\tau - T/2)$, where T is the period of the in-phase NNM. The previous discussion highlights the complex and highly asymmetric oscillation of the granular system when it oscillates in this in-phase periodic motion.

The non-smooth character of the in-phase NNM can be inferred from the depiction of the dynamics in the projection of the phase plane (cf. Figure 2.3b), where a discontinuity in slope can be readily noted. This happens at the time instant when one of the beads loses contact with the fixed boundary and the other stands stationary. It follows that *non-smooth effects in the oscillation are associated with 'silent' periods of bead responses, i.e., with phases of the motion where a bead is stationary at an offset position from the zero equilibrium*. Moreover, the depiction of the modal curve in the configuration plane of Figure 2.3c confirms our earlier observation regarding the non-synchronicity of the bead oscillations since they cross their equilibrium points at different instants of time. Considering the motion of each bead, there are time instances where it *interacts simultaneously with both the other bead and the rigid boundary*; moreover, there are other time instances where the bead is stationary *not interacting with neither the other bead nor the wall*. This introduces asynchronicity in the NNM response.

Finally, a comparative study of the dynamics of the two-bead granular system to the dynamics of a two-DOF vibro-impacting system (corresponding to perfectly rigid beads and purely elastic collisions between them and the rigid boundaries cf. Figure 2.4c) is performed in Figure 2.4. Due to the Hertzian contact law, deformation of beads during collisions occurs, and as a result the time series is smooth. By contrast, in the vibro-impacting system bead deformation does not occur, and so there exist non-smooth transitions between different phases of the dynamics. Still, the vibro-impact in-phase NNM could be considered as a generating solution to develop asymptotic approximations for the in-phase NNM of the granular medium in the limit of small bead deformations. Although, the vibro impact response shown here is schematic, the

distance '*D*' (Figure 2.4c) can be estimated by matching the time period of the in-phase NNM in the two-bead granular system. It is worth noting that in the vibro-impacting system at any instant of time there is single bead to bead interaction (instead of simultaneous multiple bead interactions), and hence the dynamics is dispersion-free (ref. Chapter 1); furthermore, the interaction time is theoretically zero. In fact the in-phase NNM can be modeled using the concept of effective particle as a single particle accounting for the transfer of kinetic energy/momentum in the vibro-impacting system (this is elaborated in greater detail in Section 2.3.4).

Focusing now on the out-of-phase NNM (region B in the Poincaré map of Figure 2.2), in Figure 2.5a we depict the corresponding responses of the two beads. In this case neither of the two beads reaches a stationary position after separation, so no 'silent' regions exist, and the dynamics is completely smooth (in the sense that no non-smooth effects occur in the phase plot of Figure 2.5c). Indeed, the two beads oscillate in synchronicity and in out-of-phase fashion, and at the precise time instant when they lose contact with the fixed boundaries they get into contact and start interacting with each other; hence, at any given time a bead either interacts with the other bead or with the rigid boundary, *but not simultaneously with both and there is no 'free flight'*. This is in contrast to the in-phase NNM. Moreover, both beads cross their equilibrium positions at the same instant of time, so this mode conforms to Rosenberg's definition of NNM [77, 79]. It is worth mentioning that for higher dimensional systems the out-of-phase mode doesn't conform to Rosenberg's definition of NNM [77, 79]. In case of even number of beads, however, the pair of beads which are positioned symmetric about the center of mass of the chain would pass through their equilibrium points at the same instant of time.

Due to the fact that the out-of-phase NNM corresponds to synchronous and symmetric oscillations of the two beads, it can be explicitly analyzed. To this end, the oscillation is divided into two phases, in each of which the strongly nonlinear equations

of motion are decoupled and can be explicitly solved. In the first phase of the oscillation the total energy h of the granular system is partitioned equally between the two beads in the form of elastic potential energy due to their interactions with the fixed boundaries. Hence, in this phase each of the two beads remains in contact with its rigid boundary, being detached from each other. Consequently the mutual interaction terms in the equations of motion vanish and the equations of motion decouple completely,

$$\begin{aligned} \ddot{x}_1 &= (-x_1)_+^{3/2} \\ \ddot{x}_2 &= -(x_2)_+^{3/2} \end{aligned} \tag{2.6}$$

subject to the initial conditions $x_1(0) = -(5h/4)^{2/5}$, $\dot{x}_1(0) = 0$, $x_2(0) = (5h/4)^{2/5}$, and $\dot{x}_2(0) = 0$. Denoting $x_1(\tau) = -x_2(\tau) \equiv x(\tau)$, the solution of (2.6) is computed in explicit form as,

$$\tau = h^{-1/10}(5/4)^{2/5}\,{}_2F_1\left(\frac{1}{2},\frac{2}{5};\frac{7}{5};1\right) - \frac{x_2}{\sqrt{h}}\,{}_2F_1\left(\frac{1}{2},\frac{2}{5};\frac{7}{5};\frac{4x_2^{5/2}}{5h}\right) \tag{2.7}$$

where ${}_2F_1(\bullet,\bullet;\bullet;\bullet)$ is a Hypergeometric function defined as [137],

$${}_2F_1(a,b;c;z) = \frac{\Gamma(c)}{\Gamma(a)\Gamma(b)}\sum_{n=0}^{\infty}\left(\frac{\Gamma(a+n)\Gamma(b+n)}{\Gamma(c+n)}\right)\left(\frac{z^n}{n!}\right)$$

$${}_2F_1(a,b;c;1) = \frac{\Gamma(c)\Gamma(c-a-b)}{\Gamma(c-a)\Gamma(c-b)}$$

and $\Gamma(\cdot)$ is the Gamma function [137]. This solution is valid only until the two beads reach their respective equilibrium points and the first phase of the oscillation is completed.

At that time instant the second phase of the oscillation starts. As the beads pass through their equilibrium positions, they lose contact with the corresponding rigid boundaries and engage in mutual interaction. Again the equations of motion can be combined into a single one, which can be solved in closed form. To show this we consider again the equations of motion,

$$\begin{aligned} \ddot{x}_1 &= -(x_1 - x_2)_+^{3/2} \\ \ddot{x}_2 &= (x_1 - x_2)_+^{3/2} \end{aligned} \tag{2.8}$$

As can be noted, the terms accounting for the bead interactions with the boundaries are neglected beforehand. Furthermore, we introduce the relative displacement variable $\sigma = x_1 - x_2$. Then the equations of motion (2.8) can be combined to the following single equation,

$$\ddot{\sigma} = -2(\sigma)_+^{3/2} \tag{2.9}$$

this can be solved explicitly by quadratures. We note at this point that at the end of the first phase of the oscillation the total energy of the system *h* is in the form of pure kinetic energy, equally distributed between the two beads. Hence, at the beginning of the second phase of the oscillation both the beads have opposite velocities, which provide us with the necessary initial conditions in the form, $\sigma(0) = 0, \dot{\sigma}(0) = 2\sqrt{h}$. Hence, the following analytical solution for (2.9) is derived:

$$\tau = \frac{\sigma}{2\sqrt{h}}\, {}_2F_1\left(\frac{1}{2}, \frac{2}{5}; \frac{7}{5}; \frac{2\sigma^{5/2}}{5h}\right) \tag{2.10}$$

The time period of the out-of-phase NNM can then be evaluated from (2.10) as,

$$T = T(h) = h^{-1/10}\,{}_2F_1\left(\frac{1}{2},\frac{2}{5};\frac{7}{5};1\right)\left[2\left(\frac{5}{4}\right)^{2/5}+\left(\frac{5}{2}\right)^{2/5}\right] \approx 5.341\,h^{-0.1} \tag{2.11}$$

this provides an explicit expression for the dependence of the frequency $\omega = 2\pi/T$ of the out-of-phase NNM on the energy h. This analytical solution will be further utilized in our later discussion of the dynamics of the granular system in the frequency – energy plane.

The in-phase NNM corresponds to asynchronous and non-smooth oscillations of the two beads and it does not lend itself to a similar explicit solution. In fact, as many as five distinct phases of the dynamics exist for the in-phase NNM, of which only two (between point 1-2 and 5-6) can be analyzed explicitly (the other three phases correspond to concurrent interactions of the beads with each other and the rigid boundaries and are not amenable to direct analytic treatment). This prevents the decoupling of the nonlinear equations of motion and a closed form solution.

Focusing now on the subharmonic orbits of the two-bead system, we mention that there is a countable infinity of this type of motions (corresponding to the countable infinity of rational numbers). In Figures 2.6a, b we present two such representative subharmonic oscillations corresponding to $1:3$ and $2:3$ rational relations between the frequencies of the oscillations of the first and second beads, respectively. Both these orbits are stable but the domains of quasi-periodic ('regular') motions surrounding them are relatively small (cf. Figure 2.2). Moreover, as mentioned previously, due to the non-integrability of the dynamics of this system there exists a countable infinity of stable subharmonic orbits satisfying general $m:n$ rational frequency relationships, albeit with increasingly smaller domains of realization as the mutually prime integers m and n increase.

Due to the nonlinear nature of the two-bead granular system, the frequencies of its time-periodic motions are energy dependent [12, 76, 80, 81]. It follows that the aforementioned NNMs and subharmonic orbits can be better represented in a frequency – energy plot (FEP). As discussed in [138], by depicting the dynamics of a system in a FEP it is possible to study the influence of these modes on the forced and damped dynamics; moreover, it would be possible to better relate the dynamics of the two-bead granular system to the dynamics of higher dimensional granular systems that will be considered later. To depict the two NNMs in the FEP it is necessary to compute their analytic continuations for varying energy and derive the corresponding frequency-energy relationships. This can be performed immediately for the out-of-phase NNM by means of relation (2.11). Since no similar explicit relationship can be derived for the in-phase NNM, we formulate a numerical shooting method to study this NNM at higher energy ranges. The shooting method is applied by specifying initial displacements and zero initial velocities for the two beads, so that at $\tau = 0$ the entire energy is stored in the second bead due to its elastic compression by the right boundary (cf. Figure 2.7). It follows that at $\tau = 0$ the first bead is neither in contact with the boundary nor with the second bead. Hence, assuming that the total (conserved) energy of the system is equal to *h*, the initial conditions for the granular system is chosen as,

$$x_2(0) = (5h/2)^{2/5}, \quad x_1(0) = \alpha_1^{(2)}(5h/2)^{2/5}, \quad \dot{x}_2(0) = 0, \quad \dot{x}_1(0) = 0 \tag{2.12}$$

where $0 < \alpha_1^{(2)} < 1$ is a constant that determines the asymmetry in the initial conditions for the in-phase mode, and is computed by the numerical shooting method. This constant is computed as $\alpha_1^{(2)} \approx 0.5585$, and it is interesting to note that it remains fixed as the (conserved) energy level varies. This is due to the *homogeneous* nature of the system according to the definition of Rosenberg [77, 79]. To perform numerical

continuation for the subharmonic orbits at higher energy levels we utilized the numerical algorithm developed by Peeters et al. as discussed in [138].

In Figure 2.8 we present the different families of modes (NNMs and subharmonic orbits) of the two-bead system in the FEP. The frequency-energy curve of the out-of-phase NNM provides the upper limit of time-periodic orbits for this system, so no time-periodic oscillations can be realized in the upper region of the FEP, which is labeled as *'prohibited' band*. We note that the families of the two NNMs and subharmonic orbits are defined over the entire energy range and are represented by smooth curves that bifurcate from the origin of the FEP. This is in contrast to dynamical systems with essential but smooth stiffness nonlinearities, where subharmonic orbits appear as 'tongues' over finite energy intervals [138]. It will be of interest to study how the topological structure of the orbits on the FEP changes as we increase the number of beads, and in particular, how the 'prohibited' band changes as the number of beads tends to infinity and the granular chain becomes of infinite extent. These questions are discussed in the subsequent sections.

2.1.3 Effect of Pre-compression on the In-phase NNM of Two Bead System

As described in the previous chapter, the application of pre-compression on the granular chain introduces a linear component in the force interaction law and, hence, a linear component in the acoustics of the system. Thus the system can no longer be considered to be essentially nonlinear. The application of strong pre-compression may completely suppress the bead separation and render the dynamics weakly nonlinear, but with the application of an initial pulse of sufficiently high energy, the system can still exhibit strong nonlinearity. To demonstrate the effect of pre-compression on the dynamics we consider the two bead homogeneous chain of Section 2.1.2, but now with

uniform pre-compression. Then the non-dimensional energy of the pre-compressed system can be expressed in the form,

$$h = \frac{1}{2}\left(\dot{x}_1^2 + \dot{x}_2^2\right) + \frac{2}{5}\left[(\Delta - x_1)_+^{5/2} + (\Delta + x_2)_+^{5/2} + (\Delta + x_1 - x_2)_+^{5/2}\right] \tag{2.13}$$

and the corresponding equations of motion of the pre-compressed system are given by,

$$\begin{aligned} \ddot{x}_1 &= \left(\Delta - x_1\right)_+^{3/2} - \left(\Delta + x_1 - x_2\right)_+^{3/2} \\ \ddot{x}_2 &= \left(\Delta + x_1 - x_2\right)_+^{3/2} - \left(\Delta + x_2\right)_+^{3/2} \end{aligned} \tag{2.14}$$

where Δ is the non-dimensional applied pre-compression on the two bead chain. Clearly, we can still construct the Poincaré map of system (2.14) at a fixed energy level, similar to the case of two bead uncompressed chain. Again we realize two NNMs, namely, an in-phase and an out-of-phase one. The more interesting case of in-phase NNM is now considered and its evolution with the change in pre-compression is studied. To have a fair comparison we consider a constant energy of $h = 0.0001$ and vary the applied pre-compression from 0 to 0.023. The maximum pre-compression in the static condition of the system for certain energy h is given by $\Delta_{max} = (5h/6)^{2/5}$, and corresponds to $\Delta_{max} = 0.02335$ for $h = 0.0001$.

For zero pre-compression, i.e. $\Delta = 0$, we recover the previous uncompressed case and the corresponding in-phase NNM is shown in Figure 2.3. For pre-compression equaling $\Delta = 0.01$ and the corresponding in-phase NNM is shown in Figure 2.9a. As can be seen the amplitude of oscillations of the beads is higher than the applied pre-compression and furthermore, a zone of stationarity can be observed; this implies that the beads separate from one another, with one of the beads losing contact with the rigid boundary, and the other continuing to interact with the rigid boundary. The dynamics in this case is still strongly nonlinear. Increasing the pre-compression to $\Delta = 0.015$

(Figure 2.9b), we note that there is no zone of stationarity, and instead the beads remain always in mutual contact, but detach from the boundaries at certain periods during a cycle of oscillation. This can be ascertained by considering the relative displacements between beads. Further increasing the pre-compression renders the dynamics nearly linear and the in-phase NNM converges to the more recognizable in-phase NNM realized in two-DOF linear symmetric oscillators [12] wherein the two beads oscillate in-phase with almost same amplitude (cf. Figure 2.9c, d). From a different perspective, if we plot the response on the two-dimensional configuration plane, we observe that the modal lines for the in-phase NNMs for $\Delta = 0$ to 0.02 do not pass through the origin, and thus do not conform to Rosenberg's definition of isochronicity of the NNM. With further increase of the pre-compression to $\Delta = 0.023$, however, the modal line passes through the origin and thus it is a similar to isochronous NNMs [12] as predicted by Rosenberg (as can be seen in Figure 2.10a). It is clear then that the applied pre-compression eliminates the strongly nonlinear characteristics of the in-phase NNM.

2.1.4 Three-Bead Granular System

Considering the homogeneous three-bead granular system with rigid boundaries (similar to system in Figure 2.1), the governing normalized equations of motion are given by,

$$\begin{aligned} \ddot{x}_1 &= (-x_1)_+^{3/2} - (x_1 - x_2)_+^{3/2} \\ \ddot{x}_2 &= -(x_2 - x_3)_+^{3/2} + (x_1 - x_2)_+^{3/2} \\ \ddot{x}_3 &= -(x_3)_+^{3/2} + (x_2 - x_3)_+^{3/2} \end{aligned} \tag{2.15}$$

where the previous normalizations hold. In this case it is not feasible to compute Poincaré maps for studying the global dynamics since the dimensionality of the system is relatively high (it has a six-dimensional phase space). Nevertheless it is possible to numerically compute the NNMs and subharmonic orbits of this system using the methodology and computational techniques discussed in the previous section.

Since the in-phase NNM (labeled as 'NNM 1') plays an important role in the dynamics of the granular system we will examine this mode in detail. To compute this NNM we employ the shooting method by assuming zero initial velocities and non-zero initial displacements in the form,

$$x_3(0) = (5h/2)^{2/5},\ \ x_2(0) = \alpha_2^{(3)}(5h/2)^{2/5},\ \ x_1(0) = \alpha_1^{(3)}(5h/2)^{2/5} \tag{2.16}$$

where h is the (conserved) energy of the system, and, as previously, the coefficients $\alpha_{1,2}^{(3)}$ characterize the asymmetry in the initial spatial distribution of the in-phase NNM. These coefficients are computed as, $0 < (\alpha_1^{(3)} \approx 0.374) < (\alpha_2^{(3)} \approx 0.744) < 1$, and as for the two-bead system they are independent of the energy h. In Figures 2.11a-c we depict the in-phase NNM for this system; in similarity to the two-bead system, we infer that there are domains where the beads become motionless at offset (from the zero equilibrium) positions. In addition, non-smooth effects in the dynamics are clearly noted, and a high non-synchronicity between bead oscillations is deduced. The most important (and unique) features of this mode are the patterns of separation and loss of contact between beads and between the end beads and the fixed boundaries (which lead to the non-smooth effects depicted in Figures 2.11b, c). Indeed, the initial conditions required for the realization of the in-phase NNM are such that except for one of the beads, all other beads are detached from each other and the walls. It is this feature that prevents the study of this mode using a continuum approximation technique (this

holds also for the in-phase NNM of higher dimensional homogeneous granular chains with increased number of identical beads). Indeed we can state that *the in-phase NNM, which is the lowest frequency NNM, is the mode most affected and influenced by the discrete nature of the granular system*.

An even more peculiar feature of the in-phase NNM is that it resembles a traveling wave, since it appears to 'propagate' back and forth in the granular chain. This becomes more apparent in higher-dimensional granular media (cf. Section 2.1.5), but a first hint is provided by studying the velocity profiles depicted in Figure 2.12 for the three-bead system. In that plot we present the superposition of the velocity profiles of the central and end beads and show them on the same time scale. We note that the velocity profiles are in the form of single-hump 'pulses'; half of the velocity profiles of the end beads match exactly that of the central bead, whereas the other half is strongly influenced by the interaction of each end bead with the fixed boundaries. Moreover, there is a constant time delay between the transmission of velocity 'pulses' to the neighboring beads, so, in fact, *the in-phase NNM resembles a traveling wave*. This result will be generalized for higher dimensional systems where it will be shown that the velocity profiles of all beads except for the two end beads are identical but for a constant time shift. Hence, although the in-phase NNM is in actuality a time-periodic standing wave, the motion of each bead is followed by an extended period where it settles to an offset stationary position until the bead executes a motion in the reverse direction after a time interval equal to the half period of the NNM. Each bead (except for the end ones) executes an identical motion but for a constant time shift, so the in-phase NNM appears as a traveling wave. Based on these observations we will refer from here on the in-phase NNM as a *pseudo-wave*.

The second NNM (labeled as 'NNM 2') of the three-bead system corresponds to out-of-phase motion of the neighboring beads and is presented in Figure 2.13. Due to non-synchronicity of the oscillations of the three beads this mode is again in non-

conformance with the definition of NNM given by Rosenberg [77, 79], but, in similarity to the two-bead case, it represents the highest frequency NNM of the three-bead system, and as such, it forms the upper bound of the domain of periodic motions in the frequency – energy plane.

The third mode (labeled as 'NNM 3') of the three-bead system corresponds to lack of motion (stationarity) of the central bead (bead 2) for all times. As shown in Figure 2.14 the dynamics of the system can be partitioned into two phases. In the first phase the end beads share the energy of the system equally, which at $\tau = 0$ is purely elastic. At the end of the first phase the energy is completely transformed to kinetic and the two end beads have opposite velocities. Since the central bead is stationary, for this NNM it acts as a virtual fixed boundary. Hence, the dynamics of the system in the second phase is quite similar to the first one, and the equations of motion decouple throughout enabling us to solve for the bead responses in closed form. Omitting the details of the analysis we may express the period of this NNM as,

$$T = T(h) = 4h^{-1/10}\left(\frac{5}{4}\right)^{2/5}\,{}_2F_1\left(\frac{1}{2},\frac{2}{5};\frac{7}{5};1\right) \approx 6.436h^{-0.1} \tag{2.17}$$

where h denotes total conserved energy.

The last type of NNM (labeled NNM 4) supported by the three-bead system is localized, with one of the end beads interacting with the wall and oscillating with an amplitude that is much larger (about twice) than the corresponding amplitudes of the other two beads (cf. Figure 2.15). It is clear that due to the symmetry of the system this mode is degenerate as it may be realized in an alternative symmetric configuration where the motion is localized to the other end bead. It is interesting to note that this type of nonlinear localization occurs in the homogeneous granular system, and in complete absence of pre-compression. To our knowledge this is the first report of this

type of (strongly) localized motion in a single bead of a finite homogeneous granular system. We make the remark at this point that nonlinear localization in granular homogeneous media has been reported in previous works (e.g., [139, 140]) but only under sufficiently strong pre-compression and/or in the presence of disorder, so that no separation between beads would be possible; moreover, spatially periodic standing waves with recurring time-periodic localization (after a wavelength) have been reported in infinite granular chains with no pre-compression [63]. Surprisingly, no analogous localized NNM where the localization takes place in the central bead of the three bead system under consideration was found in this system.

In addition to the four NNMs (where all beads oscillate with the same frequency) the system supports a countable infinity of subharmonic orbits, in similarity to the two-bead system; in these periodic orbits the frequencies of the beads are related in rational ratios. The FEPs of the NNMs and some subharmonic orbits of the three-bead system are presented in Figure 2.16. From the above discussion, the number of NNMs in this system exceeds its degrees of freedom, and this is consistent with previous results concerning essentially nonlinear discrete oscillators [12]. The upper boundary that separates the region where time-periodic orbits are realized from the 'prohibited' band (where no NNMs can be realized) is formed again by the out-phase NNM 2 as in the case of two bead system, whereas the lowest frequency mode is the in-phase NNM 1, which, as discussed previously, is a pseudo-wave. Moreover, compared to the corresponding results of the two-bead system (cf. Figure 2.8) we note that *with increasing number of beads the upper boundary (corresponding to the out-of-phase NNM) moves toward higher frequencies, whereas the curve corresponding to the in-phase (pseudo-wave) NNM moves towards lower frequencies*. This trend will be confirmed in the next section where higher dimensional granular systems are considered. In the FEP of Figure 2.16 we depict also the frequency-energy curves of two subharmonic orbits, which occur within the complement of the 'prohibited' band. No time-periodic orbits (NNMs or

subharmonic orbits) can occur in the 'prohibited' band, similar to the case of the two-bead system.

2.1.5 Higher Dimensional Granular Systems

We now extend our analysis to homogeneous granular chains of higher dimensionality. Our main aim is to study the changes in the structure of the FEP as the number of beads increases, and, in particular, to identify regions in the frequency – energy plane where spatial transmission of disturbances (i.e., energy) is facilitated or prohibited by the intrinsic dynamics of the granular medium. This information is of practical significance when such media are designed as passive mitigators of shocks or other types of unwanted disturbances. Since the out-of-phase and in-phase NNMs represent the highest and lowest frequency NNMs of the granular medium, respectively, all other NNMs (localized or non-localized) are realized in the frequency – energy zone defined by these 'bounding' NNMs, irrespective of the dimensionality of the granular medium. Hence, in what follows we will only focus on these two NNMs and investigate how the topology of the band of realization of NNMs (and its complementary high-frequency 'prohibited' band) changes with increasing number of beads in the granular chain.

In Figure 2.17 we depict the in-phase and out-of-phase NNMs in the FEP for systems composed of two to seven beads. We note that as the number of beads increases the out-of-phase NNM makes a transition towards higher frequencies and quickly converges (accumulates) to a definite upper bounding curve, whereas the in-phase NNM makes a similar transition towards lower frequencies. No such quick convergence is noted for the in-phase NNM; rather, as the number of beads tends to infinity the in-phase NNM tends towards the zero frequency axis. This raises an interesting question concerning the physics of the dynamics of the infinite granular

system as the in-phase NNM approaches the zero-frequency limit. Namely, as discussed in the previous section due to bead separation the in-phase NNM resembles a traveling wave corresponding to a single-hump velocity disturbance propagating back and forth through the granular system (hence the previous characterization of this NNM as a pseudo-wave). Moreover, the 'silent' period for each bead response (corresponding to the time period where the bead remains motionless at an offset position) progressively increases with increasing dimensionality of the system. Following this argument one step further, one might deduce that in the limit of infinite number of beads the period of the NNM tends to infinity (and its frequency tends to zero as it approaches the energy axis in the FEP), so the in-phase mode should degenerate to a true traveling wave, similar (or may be identical) to the solitary wave studied by Nesterenko [41].

Motivated by the aforementioned observation, in Figure 2.18 we compare the velocity profile of the solitary wave studied by Nesterenko [41] to the single-hump velocity profiles of the in-phase NNMs of fixed-fixed three- to seven-bead granular systems. It is clear that *the velocity profiles of the in-phase NNMs do not converge to the profile of the solitary wave studied by Nesterenko* [41]. So, clearly *the in-phase NNM converges to a different limit as the dimensionality of the system tends to infinity*, and the obvious question at this point concerns the type of dynamics that this limit represents. The answer can be found by considering more closely the dynamics of the granular chain when it oscillates in the in-phase NNM. As discussed previously, for an $n-$bead granular system the initial conditions necessary for exciting the in-phase NNM can be expressed in terms of nonzero initial normalized displacements and zero initial velocities as follows,

$$\begin{aligned} x_1(0) = \alpha_1^{(n)}(5h/2)^{2/5} < x_2(0) = \alpha_2^{(n)}(5h/2)^{2/5} < \ldots \\ \ldots < x_{n-1}(0) = \alpha_{n-1}^{(n)}(5h/2)^{2/5} < x_n(0) = (5h/2)^{2/5} \end{aligned} \tag{2.18}$$

where h is the (conserved) energy of the system. This indicates that in order to realize the in-phase NNM it is necessary to compress the $n-$th bead at the right end of the granular system, and then allow for gaps (clearances) between the other beads, which monotonically decrease as the left end of the system is reached. In Figure 2.19 we depict the coefficients $\alpha_i^{(n)}, i = 1, \dots, n-1$ characterizing the asymmetry in the in-phase NNM deformation (in terms of the corresponding gaps) for systems with $\approx n = 2, \dots, 7$ beads, and note that as n increases the differences between these coefficients decrease. Moreover, the numerical results indicate that in the limit $n \to \infty$ these gaps tend to zero, which indicates that *the in-phase NNM cannot be realized in the limit of infinite granular chain*. We conclude that the limit of the infinite granular chain ($n \to \infty$) represents a singularity for the family of in-phase NNMs, which makes physical sense, since otherwise this family of NNMs (which are non-synchronous standing waves or pseudo-waves) would degenerate to an actual traveling wave; this would have been a clear inconsistency in terms of the dynamics. Hence, we conclude that *the pseudo-wave character and asymmetry of the in-phase NNM is a pure artifact of the finite dimensionality of the homogeneous granular chain, being more profound for smaller dimensionality*. We make the remark at this point (which will be corroborated by later results) that even though the asymmetry in-phase NNM is less profound as the dimensionality of the granular chain increases, this lowest frequency NNM can significantly influence the dynamics, acoustics and energy transfer of finite dimensional granular media.

To demonstrate more clearly the pseudo-wave character of the in-phase NNM, in Figure 2.20a we present the velocity profile over half the period of this mode for each of the beads of a seven-bead granular system with fixed-fixed boundary conditions for an energy of $h = 0.00012$, and compare it to the corresponding velocity profiles for seven beads for solitary wave propagation [42, 44]. Since theoretically the solitary wave can be

realized only in the infinite granular chain, the results of Figure 2.20b were computed for a chain with 100 beads and free-free boundary conditions; the magnitude of the impulse ($\dot{x}_1(0) \approx 0.019$) provided to the first bead was selected so that the velocity amplitude (≈ 0.01283) of the resulting solitary wave matches the velocity amplitude of the in-phase NNM of the seven-bead fixed-fixed granular system.

We note that, whereas the velocity profiles of all beads match exactly for the case of the solitary wave (cf. Figure 2.20b), the same holds only for the velocity profiles of the five central beads for the case of the in-phase NNM (cf. Figure 2.20a). For the end beads of the fixed-fixed granular system only half of their velocity profiles match those of the central beads, whereas the other half is strongly influenced by the interaction of these beads with the fixed boundary. Moreover, comparing the time delays of arrival of the pulse from the first bead to the last, we note that the solitary wave possesses a higher speed compared to the pseudo-wave in the fixed-fixed granular system. Furthermore, in Figure 2.20a the pseudo-wave is depicted for only one half of the period of the in-phase NNM (for the other half of the period the pseudo-wave is 'reflected' by the right rigid wall and it 'propagates' in the opposite direction – i.e., backwards – through the medium). A tabulation of these time delays for systems composed of three to seven beads is presented in Table 2.1, from which we infer that the pseudo-wave (i.e., the in-phase NNM) becomes slower compared to the solitary wave studied by Nesterenko with increasing number of beads.

2.1.6 Intrinsic Dynamics of the Infinite Granular Chain: Propagation and Attenuation Bands (Zones)

In the limit of infinite number of beads the frequency – energy plane is partitioned into two regions, namely a propagation band or zone (PB or PZ) and attenuation band or

zone (AB or AZ). The existence of this type of bands in linear [37, 86, 131, 141] and nonlinear [140, 142] periodic media has been well documented in the literature. Typically, in PBs traveling waves exist, and these represent the acoustic mechanism for spatial transfer of energy through the medium to the far field. On the contrary, in ABs near field motions with exponentially decaying envelopes are realized, so in these bands spatially localized waves are realized that cannot propagate energy to the far field; this is the mechanism for near-field confinement of acoustic disturbances. The boundaries separating the PBs and ABs are spatially extended time-periodic standing waves which can be regarded as NNMs of the corresponding infinite periodic media.

Similar types of time-periodic orbits are realized inside the PBs and ABs of infinite homogeneous granular medium with no pre-compression. The partitioning of the FEP of the infinite granular chain in terms of PBs and ABs is realized by the limiting (accumulating) curves of the in-phase and out-of-phase NNMs as depicted in Figure 2.17. As the number of beads tends to infinity the in-phase NNM tends towards the energy axis (i.e., the zero frequency limit), and the spacing between the frequency – energy curves of the NNMs and the countably infinite subharmonic orbits tends to zero, or alternately, the NNMs and subharmonic orbits become densely 'packed' in terms of frequency and energy inside the PB.

In the infinite limit the dynamics of the granular medium supports a continuum of families of traveling waves (each parameterized by energy) inside the PB. These motions were studied in [63], where it was shown that the infinite granular medium supports a countable infinity of families of stable traveling waves in the form of propagating multi-hump velocity pulses with arbitrary wavelengths; these families are parameterized by the 'silent' regions of zero velocity that separate successive maxima of the propagating velocity pulses. As these 'silent' regions increase, the corresponding wavelengths and periods of the traveling waves also increase and the frequencies of the waves decrease. In the limit of infinite 'silent' region the wave ceases to be periodic and

its frequency becomes zero; this asymptotic limit of single-hump solitary waves is the solitary wave studied by Nesterenko [41].

Different families of traveling waves were computed in [63] and their propagation properties were studied. It was found that these periodic waves are slower than the solitary wave studied by Nesterenko, with their speeds strongly depending on their amplitudes (energies). We wish to depict the frequency – energy curves of these families of traveling periodic waves in the FEP of the infinite granular chain. Now, each family of traveling waves corresponds to an infinite sequence of propagating velocity pulses separated by finite 'silent' regions (where no motion occurs). It follows, that in order to assign a finite energy measure ('quantum') to each family of traveling periodic waves we need to compute the corresponding energy density, i.e., the energy carried by each wave family over a single wavelength of the motion; moreover, the corresponding frequency follows directly from the time-periodic character of the waves. As the 'silent' region of the traveling wave increases, so does its period. It follows that with increasing 'silent' region the frequency of the wave decreases, until in the limit of infinite 'silent' region (corresponding to the solitary wave studied by Nesterenko) the energy axis is reached and the frequency of the wave is zero. In addition, it is interesting to note that for all traveling waves with finite 'silent' regions there occur separations between beads, whereas in the limit of infinite 'silent' region there are no separations between beads; it follows that in that limit a continuum approximation can be utilized to study the solitary wave (as performed by Nesterenko in [41]).

In Figure 2.21 we depict two of these families of traveling waves, which as discussed previously, are distinguished by the regions of zero velocity (the 'silent' regions) between successive maxima of velocity pulses. One family corresponds to traveling wave with three-bead periodicity (Figure 2.21b), whereas the second one to the four-bead periodicity (Figure 2.21c) [63]. Indeed, we confirm that these families of waves are realized inside the PB of the infinite granular medium. In the limit of infinite

'silent' region we obtain the single-hump solitary wave studied by Nesterenko which lies on the energy axis of the FEP (as it corresponds to infinite period or zero frequency).

In addition to these families of traveling periodic waves additional motions can occur inside the PB, including subharmonic motions, standing waves with recurring localization features (i.e., periodically spaced humps) and chaotic orbits. A family of such standing waves with three-bead periodicity [63] is shown in [85], with one of the beads oscillating in out-of-phase fashion and with higher amplitude compared to its neighboring beads. We conjecture that additional families of such standing waves occur inside the PB of the infinite granular medium, distinguished by the extent of bead-periodicity (spatial wavelength) of the standing wave, and type of localization characteristics. The standing wave separating the AB from the PB is the out–of-phase NNM of a two bead periodicity chain (it should be noted that no traveling waves can be realized in a two bead periodic chain). A brief discussion in this regard is presented in Section 3.1.5 where we discuss traveling waves in periodic dimer chains. We end our discussion of the dynamics inside the PB by noting that no similar standing waves (with or without localization characteristics) can occur in PBs of perfectly ordered linear periodic media, although standing waves with spatially localized slopes have been reported in ordered periodic media with smooth stiffness nonlinearities [143]. However, a full study of standing waves with localization features is beyond the aim of this work.

We now consider the dynamics of the infinite granular system inside the attenuation band (AB) of the FEP of Figure 2.21a. No spatially-periodic standing or traveling waves can occur for frequency – energy combinations in that band, so no spatial transfer of energy in the granular medium is possible for motions inside the AB. Rather, near-field motions occur inside the AB, corresponding to spatially periodic oscillations of the beads about different positive offset positions with spatially decaying envelopes; overall, the motion of the granular medium is a standing wave with decaying envelope, with each bead performing a time periodic oscillation about its own

(positive offset) equilibrium position. Examples of this type of near-field standing waves are provided in Section 2.2 where the influence of the propagation and attenuation bands on the forced response of the granular medium to narrowband excitation is studied. We note that the response of the granular medium inside the AB resembles the responses of unforced linear periodic media [86, 141, 144], which possess similar decaying standing waves (and even decaying 'complex' waves when more than one coupling coordinates between individual substructures exist [145]) in well-defined attenuation bands. This enables the analytical treatment of this type of attenuating standing waves in ABs of homogeneous granular media of infinite extent, as shown later.

2.1.7 Conclusions

New types of NNMs in granular media have been studied in this section. These media have the intriguing feature of 'sonic vacuum', that is, the characteristic velocity of sound in these media is zero due to the essentially nonlinear (non-linearizable) Hertzian contact interactions between neighboring beads. Moreover, non-smooth effects are added to the dynamics due to bead separation in the absence of sufficient compressive forces between them. Although the traditional terminology of NNMs is restricted to smooth dynamical systems, the essentially nonlinear and non-smooth features of the dynamics of granular media necessitates us to broaden the definition of NNMs to include time-periodic orbits that may not necessarily be synchronous. In the case of granular systems the non-synchronicity is caused due to bead separation, which can lead to 'silent' regions in the bead dynamics, whereby one or more beads become stationary for a finite period of time at an offset position from the zero equilibrium.

The most interesting of the NNMs of the homogeneous granular systems studied in this section is the in-phase NNM, which to the authors' knowledge has not been studied before in the scientific literature. This mode can be realized only when the initial state of the beads of the granular medium have prescribed gaps between them, i.e., for zero initial velocities, the initial bead displacements should be such that no bead is in touch with another bead or with the walls, except for one of the end beads. The in-phase NNM resembles a traveling wave propagating back and forth through the finite granular chain, and hence labeled as a pseudo-wave. In addition, it can only exist in the finite chain, since in the limit of infinite number of beads the gaps between beads (required for the excitation of this mode) tend to zero. On the contrary, the solitary wave studied by Nesterenko [41] does not involve bead separation, so it can be studied by an analysis based on continuum limit approximation of the strongly nonlinear equations of motion.

The significance of the in-phase (pseudo-wave) NNM and the out-of-phase NNM of the granular chain is that they form the boundaries of the band in the frequency-energy plane within which all other NNMs are realized. It follows that as the number of beads tends to infinity this region forms the propagation band (PB) in the frequency-energy plot (FEP), whereas the complementary region forms the attenuation band (AB). Motions inside the PB transfer energy through the medium and are spatially extended, whereas the corresponding motions inside the AB are near-field solutions.

In the next section we demonstrate the influence of the intrinsic dynamics of the *unforced* granular system on the *forced* dynamics of the same system forced by a narrowband excitation. It is expected that the partitioning of the FEP in terms of propagation and attenuation bands will significantly affect the capacity of the granular medium to transmit or attenuate disturbances through it. This, in turn, has clear implications on the capacity of the granular chain to act as passive mitigator of

unwanted disturbances. Further to that, we experimentally verify the existence of the band zones by considering a lower dimensional system of two beads.

2.2 Forced Harmonic Responses of Homogeneous Granular Chains

In the previous section we discussed about the dynamics of unforced systems and the NNMs that they support. These NNMs when depicted on the frequency-energy plane clearly split the plane into two zones which were denoted as the propagation band and the attenuation band. Although such bands are typical in linear or weakly nonlinear periodic media [37, 86, 141-144], their realization is not as intuitive in periodic 'sonic vacua' [42] i.e., in essentially nonlinear periodic media with complete lack of classical linear acoustics, such as the ordered granular media considered herein. In this section we show how the topology of the propagation and attenuation bands in the frequency-energy plot (FEP) affects the forced dynamics of the multi-dimensional granular chain. The influence of the intrinsic dynamics of the *unforced* chain on the *forced* dynamics is inferred from our discussion below that disturbances initiated inside the PB of the FEP can spatially transfer energy within the granular medium (through excitation of traveling waves), whereas motions initiated inside the AB are near-field solutions that cannot transfer energy through the medium.

First, we demonstrate this phenomenon numerically by considering a sufficiently long chain with harmonic base excitation and force the system in PB and AB. The second part of this section is devoted to the experimental verification of the existence of PBs and ABs in finite ordered granular media with fixed boundary conditions, forced by point harmonic excitations at their boundaries and provide its qualitative match with the corresponding numerical simulations. We find that the dynamics of these systems depend critically on the frequency and amplitude of the excitation. For fixed

forcing amplitude, at lower frequencies the responses are spatially extended, with the bead responses being strongly nonlinear and non-smooth, indicating PB behavior. On the contrary, at higher frequencies the dynamics is weakly nonlinear and smooth, in the form of spatially localized, compressed oscillations, indicating AB behavior. Although the propagatory dynamics of the PB cannot be analyzed analytically due to the strongly nonlinear characteristics and the bead separations therein, the dynamics inside the AB attains a compressed state and exhibits no bead separations. The final part of this study is concerned with the analytical study of the weakly nonlinear dynamics of the homogeneous granular chain in AB and shows how the pre-compressed dynamics becomes independent of the excitation frequency.

2.2.1 Study in the Frequency – Energy Domain

To numerically verify the theoretical predictions we excite a 50-bead granular chain by imposing a harmonic excitation of its left boundary in the form, $x_0(\tau) = B\sin(\beta\tau)$ where β is the circular frequency of the excitation in terms of the normalized time τ and B is the non-dimensional amplitude of excitation. Although this is a finite-dimensional medium, we expect that, with the exception of certain boundary effects, its intrinsic dynamics will be close to the dynamics of the corresponding infinite chain. In order to eliminate high-frequency components in the response of the chain that result due to the excitation of low-amplitude chaotic motions (resulting from the strong non-integrability of the granular chain – see the Poincaré map of Figure 2.2) we added weak viscous dissipative forces in the interactions between neighboring beads with viscous damping coefficients equal to $\xi = 0.01$. As shown below, these weak dissipative terms successfully dampen out high-frequency chaotic contributions to the dynamics and help us reveal coherent features generated by the intrinsic dynamics in the forced responses.

In Figure 2.22 we depict the forced response of the granular system for excitation parameters $B = 1.5$ and $\beta = 1$. This corresponds to dynamics that occur inside the PB of the infinite chain, and this is confirmed by the spatially extended dynamical response of the system. We note that the initial disturbance generated at the left boundary of the 50-bead chain is transmitted throughout the chain; in addition, the total energy in the system gradually builds up until it forms an oscillation about a mean energy level. Moreover, from the snapshots of the chain deformation at different time instants presented in Figure 2.22b, we infer that an initial disturbance travels from the left boundary through the chain and gets reflected from the right boundary. It follows that the forced dynamics of the chain is mainly caused by excitation of the spatially extended intrinsic motions, which, as discussed in the previous section, are densely 'packed' inside the PB of the FEP. Hence, we conclude that in this case, the intrinsic dynamics favor the transfer of disturbances through the chain.

A qualitatively different picture for the dynamics is inferred from the results of Figure 2.23 that depicts the forced response of the chain inside the AB of the FEP. In this case the excitation parameters are selected as for $B = 0.3$ and $\beta = 1$; so we keep the same frequency with the previous simulation by decrease the amplitude of the excitation, or equivalently the energy input in the system. Judging from the FEP of Figure 2.21, we make the theoretical prediction that by decreasing the energy input from a high to a sufficiently low level while keeping the frequency fixed, the dynamics should make a transition from the PB to the AB. Hence, the dynamics should change qualitatively, and the responses from spatially extended become spatially confined. This is confirmed by the numerical simulations presented in Figure 2.23, where we note that in this case no energy transmission occurs through the chain, but rather the input energy is confined in a region close to the left boundary where it is originally generated by the oscillating left rigid boundary. Moreover, from the transient responses of system presented in Figure 2.23a we note that after some initial transients the dynamics settles

into a pattern of a standing wave with a decaying envelope; it follows that the response of the system becomes increasingly smaller away from the point of base excitation. This is in agreement with our remarks regarding the near-field motions that typically occur inside the ABs. We conclude that, contrary to the previous simulation, in this case the intrinsic dynamics of the granular chain does not enable the transmission of disturbances through the granular medium. In addition, from the snapshot plots of Figure 2.23b we conclude that with increasing time the motion inside the AB settles into a near-linear spatial decaying configuration where the beads nearest to the excitation have the greatest offsets from the trivial equilibrium, whereas the ones farthest have negligible offsets (this is also confirmed by the waveforms of Figure 2.23a). This indicates that there is an effective pre-compression in the granular chain away from the excitation point. So the dynamics in the AB can be studied by adopting a weakly nonlinear approach. The analytical study of the dynamics in the AB is dealt with in Section 2.2.2.

Comparing the temporal evolutions of the total energy in the system for the two previous cases (i.e., Figures 2.22c and 2.23c) we note the for excitation frequency inside the AB the energy decays with time and reaches a near-zero steady state value, whereas for excitation frequency inside the PB the energy reaches a steady state where it fluctuates about a nonzero mean value (actually, the computation of this mean value can help us represent approximately the response depicted in Figure 2.22 in the FEP of Figure 2.21a). This is a clear demonstration of the influence of the intrinsic dynamics of the granular medium on energy propagation or attenuation in this medium.

We conclude that the results presented in this section indicate that the topological structure of the PB and AB of the frequency-energy plot affects significantly the narrowband forced dynamics of the granular chain. Indeed, depending on the frequency-energy content of the excitation, the intrinsic dynamics of the medium either facilitates or hinders the spatial propagation of disturbances within the granular

medium, allowing the propagation or dissipating certain frequency components. To extend this study to broadband (shock) excitation it will be necessary to add dissipative effects such as dry friction or plasticity to the Hertzian law interaction considered herein. We expect that such dissipative effects will reveal clearly the effect of the intrinsic dynamics on the broadband response of the granular medium. Moreover, it should be possible to identify transitions in the dissipative dynamics in the FEP, in an exact similar way performed for transient smooth nonlinear dynamics of dissipative coupled oscillators [138]. Such studies can be used in formulating predictive design of this type of granular media as passive mitigators of shocks or other types of unwanted transient disturbances.

With the previous theoretical and numerical study in view, a series of experiments were set out to demonstrate this behavior experimentally in a harmonically forced system of 2 beads. The experiments were carried out by the group of Prof. Chiara Daraio of the California Institute of Technology, and in the next section we include a brief description of the obtained results.

2.2.1.1 Experimental Setup and Numerical Model

Daraio et al. considered a system of two beads placed between a dynamic sensor (PCB 208C01) and a piezoelectric actuator (PST 150/5/7 VS10) [146] (Figure 2.24). The actuator was used to harmonically excite bead 1. The piezoactive material of the actuator is much stiffer than the actuator cap so they considered the system to be displacement-driven, i.e. the excitation was realized in the base of the Hertzian interaction of equation (2.19) and acted as a moving wall. A dynamic force sensor measured transmitted force at the other fixed boundary and was used to infer the dynamics and state of the system, i.e., strongly or weakly nonlinear. Two polycarbonate support rods were used to align

the beads, actuator, and dynamic sensor along a common axis. Finally the offset bias of the actuator was adjusted to achieve dynamics at near zero pre-compression.

We model the setup described above and shown in Figure 2.24 by considering all bead interactions to be Hertzian and purely elastic. To obtain the coefficient in the Hertzian contact law, we consider the following material properties of the beads, actuator and dynamic sensor. The beads are made of stainless steel 316 and have a Young's modulus $E_s = 193$ GPa, Poisson's ratio $\mu_s = 0.3$, mass $m = 28.84$ g, and radius $R = 9.525$ mm. The Young's modulus and Poisson ratio for the actuator and dynamic sensor are $E_{PA} = 193$ GPa, $\mu_{PA} = 0.3$ and $E_D = 197$ GPa, $\mu_D = 0.272$ respectively [147]. The equations of motion for the experimental setup shown in Figure 2.24 are,

$$\begin{aligned} m\frac{d^2u_1}{dt^2} &= (4/3)E_{1*}\sqrt{R}\left[(u_0-u_1)_+^{3/2} - \frac{1}{\sqrt{2}}(u_1-u_2)_+^{3/2}\right] \\ m\frac{d^2u_2}{dt^2} &= (4/3)E_{1*}\sqrt{R}\,\frac{1}{\sqrt{2}}(u_1-u_2)_+^{3/2} - (4/3)E_{2*}\sqrt{R}(u_2)_+^{3/2} \\ \frac{1}{E_{1*}} &= \frac{1-\mu_{PA}^2}{E_{PA}} + \frac{1-\mu_S^2}{E_S} = 2\frac{1-\mu_S^2}{E_S} \\ \frac{1}{E_{2*}} &= \frac{1-\mu_S^2}{E_S} + \frac{1-\mu_D^2}{E_D} = \frac{1-\mu_S^2}{E_S} + \frac{1-\mu_D^2}{E_D} \end{aligned} \tag{2.19}$$

where u_1 and u_2 are the displacements of beads 1 and 2, respectively, and E_{1*} and E_{2*} the effective Young's modulus of the different contact interactions, respectively. We vary the harmonic excitation $u_0(t) = A\sin(\omega t)$ applied to bead 1 in order to observe the intended PB and AB, where A is the amplitude and $\omega(=2\pi f)$ the frequency of excitation. To stabilize the numerical simulations, we include a small amount of artificial viscous damping. Otherwise, the above model does not include any damping or dissipative mechanism.

2.2.1.2 Numerical Results

In Figure 2.25 we present the response of the system for a low excitation frequency of 10 Hz. Note that in all numerical simulations and experiments the excitation amplitude is approximately 0.4 μm. The force profile calculated at the dynamics sensor end (opposite to the actuator) is plotted in Figure 2.25a. At this low frequency, the responses of both beads closely follow the excitation (see the temporal evolution of the particles displacement in Figure 2.25b). When the excitation displacement is positive the beads are compressed against the dynamic force sensor, and when the excitation is negative the beads relax and lose contact with the dynamic sensor, resulting in zero applied force. The beads perform strongly nonlinear, nearly in-phase and highly asymmetric oscillations about their equilibrium positions, transmitting a force in the form of well-separated pulses to the sensor. This is indicative of dynamics in a PB of the system. Similar behavior can be seen at higher excitation frequencies (500 Hz – Figure 2.26 and 1000 Hz – Figure 2.27), with the notable difference that at higher frequencies the beads displacements do not follow the motion of the actuator but instead have more complex response waveforms.

At higher frequencies, we note a qualitatively different behavior in the dynamic response of the particles. At 3000 Hz (Figure 2.28), the bead's displacement cannot keep up with the high frequency of the actuator and are dynamically compressed to a positive equilibrium position. Furthermore, separation between beads is no longer possible. In addition, the amplitude of the oscillation about the mean position of each bead is significantly reduced from bead to bead, similar to the spatial attenuation that would be observed in linear periodic media. This induces a state of permanent compression (note the nonzero average force in Figure 2.28a), and, as a result, it changes the dynamic behavior of the system from strongly nonlinear (which characterizes motions in the PB), to weakly nonlinear and attenuated (for motions in the AB). This

change is brought solely by varying the excitation frequency, keeping the excitation amplitude nearly constant.

With an increase of the excitation frequency to 5000 Hz (Figure 2.29), the mean of the force transmitted to the wall does not change, but the oscillation amplitude about the mean value reduces considerably. Hence, when the frequency increases the spatial attenuation is stronger and the motion becomes increasingly more localized. Figure 2.30 shows the significant decrease of the amplitudes of the higher harmonics of the transmitted force when the dynamics transitions from being strongly nonlinear in the PB (Fig. 2.30a) to weakly nonlinear in the AB (Fig 2.30b). In addition, the compressed state in the AB allows us to linearize the system for a more comprehensive analytical study, as described in Section 2.2.2.

In order to carefully examine the transition between the AB to the PB, we fix the amplitude of excitation ($A = 0.375$ μm) and sweep through the frequency in the range $f = 10$ Hz to 5000 Hz. For the case of dynamics in the PB we consider the maximum force exerted on the fixed end (cf. Figure 2.25a), whereas for dynamics in the AB we consider the average of the transmitted force (cf. Figure 2.28a). This duality is due to the contrasting behavior of the dynamics in the PB and AB. In Figure 2.31 the transmitted force is plotted as function of the excitation frequency. As we sweep the frequency from lower frequency to higher, we observe that the magnitude of force increases until about $f = 1440$ Hz, and further increase in frequency decreases the transmitted force monotonically. The dynamics in this phase is still propagatory. The frequency corresponding to the maximum transmitted force is the nonlinear resonance frequency. Although this behavior is observable in the numerical simulations, its experimental verification is hardly possible, since as the resonance frequency is approached, the responses are no longer repeatable in experiments, but rather they show tendency towards chaotic behavior. Hence, the experimental response of the system near resonance is not shown in the succeeding discussion. With further increase in the

excitation frequency, we observe that the dynamics changes from PB to AB. The transition from PB to AB can be ascertained once the separation between the second bead and the fixed wall ceases to happen and the fixed wall starts experiencing an oscillatory positive average force (Figure 2.31). An interesting observation is that the average force in the AB is almost constant and independent of the excitation frequency. Again, this will be evident from the analytical study of the dynamics in the AB presented in a subsequent section.

2.2.1.3 Experimental Results

The experimental tests were carried out using the setup shown in Figure 2.24. The beads were excited harmonically with amplitude of approximately 0.4 μm and varying frequency. Small deviations (± 0.05 μm) from this excitation value occur due to inherent nonlinear behavior of the actuator. The force exerted to the dynamic sensor was measured and showed the existence of a high-amplitude strongly nonlinear state at low frequencies, and a low-amplitude weakly nonlinear state at high frequencies.

In Figure 2.32a and b, the experimental time series of the force measured by the sensor at 10 Hz and 500 Hz, respectively, are depicted. These are qualitatively similar to the numerical simulations for dynamics in the PZ at the same frequencies. We note a series of transmitted compressive force pulses, similar to the dynamics observed in simulation. The Fourier transform of the force at 500 Hz presented in Figure 2.34a shows numerous higher harmonics, another characteristic of this strongly nonlinear response. The maximum transmitted force is higher at 500 Hz, also in qualitative agreement to the simulations. However, in numerical simulations we observed resonance phenomena where the maximum force recorded was much higher at 1000Hz.

The presence of resonances was not observed in the experiments, due to experimental instabilities observed in this frequency regime.

The weakly nonlinear regime is found at higher frequencies (Figure 2.33), with the nonzero mean force indicating a state of compression. The small-amplitude oscillations of the force about this mean value is an indication of weakly nonlinear interactions in the dynamics. Increasing the frequency decreases the transmitted force amplitude for these oscillations. The Fourier spectrum shown in Figure 2.34b emphasizes that much fewer harmonics are excited in the weakly nonlinear phase, in agreement with the simulations. It should be noted that although the experimental results do not match the numerical results quantitatively, we have good qualitative agreement between the two responses. The mismatch can be attributed to the dry friction, material damping, and other uncertainties present in the experimental setup.

2.2.2 Analytical Study of the Dynamics in Attenuation Zone

In this section we analytically study the weakly nonlinear dynamics in the AB. The induced permanent compression (Figure 2.28, 2.29 and 2.33) leads to a linearizable system suitable for the application of analytical techniques. Moreover, we extend the previous results by considering a homogeneous chain of N beads. Similar to the setup of Section 2.2.1 for two beads, the first bead is harmonically driven and the N^{th} bead is constrained by a fixed wall. We incorporate linear viscous damping (coefficient d) between interacting beads to simulate dissipative effects in the experimental system and to suppress transient dynamics.

Hence, the equations of motion of the theoretical model are as follows,

$$
\begin{gathered}
m_1 \frac{d^2 u_1}{dt^2} = (4/3) E_{1*} \sqrt{R} (u_0 - u_1)_+^{3/2} - (4/3) E_* \sqrt{\frac{R}{2}} (u_1 - u_2)_+^{3/2} + \\
d\left(\dot{f}(t) - \dot{u}_1\right) \Theta\left[u_0 - u_1\right] - d\left(\dot{u}_1 - \dot{u}_2\right) \Theta\left[u_1 - u_2\right] \\
\bullet\bullet\bullet \\
m_i \frac{d^2 u_i}{dt^2} = (4/3) E_* \sqrt{\frac{R}{2}} \left\{ (u_{i-1} - u_i)_+^{3/2} - (u_i - u_{i+1})_+^{3/2} \right\} + \\
d\left(\dot{u}_{i-1} - \dot{u}_i\right) \Theta\left[u_{i-1} - u_i\right] - d\left(\dot{u}_i - \dot{u}_{i+1}\right) \Theta\left[u_i - u_{i+1}\right] \\
\bullet\bullet\bullet \\
m_N \frac{d^2 u_N}{dt^2} = (4/3) E_* \sqrt{\frac{R}{2}} (u_{N-1} - u_N)_+^{3/2} - (4/3) E_{2*} \sqrt{R} (u_N)_+^{3/2} + \\
d\left(\dot{u}_{N-1} - \dot{u}_N\right) \Theta\left[u_{N-1} - u_N\right] - d\left(\dot{u}_N\right) \Theta\left[u_N\right]
\end{gathered}
\tag{2.20}
$$

where $i = 2,3,\ldots,(N-1)$ are the bead subscripts, $u_0(t) = A\sin(\omega t)$ is the harmonic base excitation as defined in Section 2.2.1 and $\Theta[\cdot]$ is the Heaviside function. Incorporating appropriate non-dimensionalization leads to the set of normalized, non-dimensional equations of motion,

$$
\begin{gathered}
\frac{d^2 x_1}{d\tau^2} = \eta \left[\sin(\beta\tau) - x_1 \right]_+^{3/2} - \frac{1}{\sqrt{2}} (x_1 - x_2)_+^{3/2} + \\
\xi\left(\beta\cos(\beta\tau) - x_1'\right) \Theta\left[\sin(\beta\tau) - x_1\right] - \xi\left(x_1' - x_2'\right) \Theta\left[x_1 - x_2\right] \\
\bullet\bullet\bullet \\
\frac{d^2 x_i}{d\tau^2} = \frac{1}{\sqrt{2}} \left\{ (x_{i-1} - x_i)_+^{3/2} - (x_i - x_{i+1})_+^{3/2} \right\} + \\
\xi\left(x_{i-1}' - x_i'\right) \Theta\left[x_{i-1} - x_i\right] - \xi\left(x_i' - x_{i+1}'\right) \Theta\left[x_i - x_{i+1}\right] \\
\bullet\bullet\bullet \\
\frac{d^2 x_N}{d\tau^2} = \frac{1}{\sqrt{2}} (x_{N-1} - x_N)_+^{3/2} - \alpha (x_N)_+^{3/2} + \\
\xi\left(x_{N-1}' - x_N'\right) \Theta\left[x_{N-1} - x_N\right] - \xi\left(x_N'\right) \Theta\left[x_N\right]
\end{gathered}
\tag{2.21}
$$

where E_* is the effective stiffness between the interacting beads, displacement $x_i = u_i/A$, time $\tau = t(4E_*\sqrt{AR}/3m)^{1/2} \equiv \psi t$, $\eta = E_{1*}/E_*$, $\alpha = E_{2*}/E_*$, frequency $\beta = \omega/\psi$, and damping $\xi = d/m\psi$ are the non-dimensional quantities relating equation (2.20) and (2.21). Without loss of generality, we consider $\eta = 1$ and $\alpha = 1$ denoting that the

dynamic sensor, actuator and beads are made of the same material. This does not affect the validity of the resulting dynamics. Recalling the material and experimental data from the previous section, $E_* = E_s/[2(1-\mu_s^2)]$, $A = 0.35$ μm, and $\omega = 8500$ Hz; the non-dimensional quantities are calculated to be $\beta = 3.1742$, $\psi = 1.6825 \times 10^4$ and $\xi = 0.5$.

For high frequency excitations in the AB, experiments and numerical simulations show small amplitude oscillations about a permanent compressed state. This inspires us to introduce new translated coordinates $x_j(\tau) = \delta_j + y_j(\tau)$, where the $j-$th bead displacement is expressed as a combination of its static, $\delta_j > 0$, and dynamic, $y_j(\tau)$, components. In simulations we observed that $\delta_j > \delta_{j+1}$, i.e., the permanent compression for each bead decreases as we move away from the actuator (Figure 2.35). From the previously shown results it can be deduced that no separation occurs between beads once the dynamics enters the AB, i.e., the dynamics is smooth between any interacting beads. Therefore the subscript '+' can be eliminated from the bead to bead interactions in the equations of motion (2.21). The only exception is the contact between the actuator and first bead where the separation still persists.

When the dynamics is deep inside the attenuation band it holds that $|\sin(\beta\tau) - \delta_1| \gg y_1(\tau)$, except in the close neighborhood of points 'a' and 'b' as shown in Figure 2.36. Hence, it can be assumed that $[\sin(\beta\tau) - \delta_1 - y_1(\tau)] > 0$ in the region between points 'a' and 'b' where the actuator displacement exceeds the permanent compression of the first bead δ_1, and $[\sin(\beta\tau) - \delta_1 - y_1(\tau)] < 0$ when the actuator displacement is less than δ_1. To this end, we can modify (2.21) to the following form by decomposing the coordinates and incorporating the observations mentioned above,

$$\frac{d^2y_1}{d\tau^2} = \eta\left[\sin(\beta\tau)-\delta_1\right]_+^{3/2} - \frac{3}{2}\eta\left[\sin(\beta\tau)-\delta_1\right]_+^{1/2} y_1 - \frac{1}{\sqrt{2}}(\delta_1-\delta_2)^{3/2}$$

$$-\frac{3}{2\sqrt{2}}(\delta_1-\delta_2)^{1/2}(y_1-y_2) + \xi\left(\beta\cos(\beta\tau)-y_1'\right)\Theta\left[\sin(\beta\tau)-\delta_1\right] - \xi\left(y_1'-y_2'\right) + O(y_1^p y_2^q)$$

•••

$$\frac{d^2y_i}{d\tau^2} = \frac{1}{\sqrt{2}}\left\{(\delta_{i-1}-\delta_i)^{3/2} + \frac{3}{2}(\delta_{i-1}-\delta_i)^{1/2}(y_{i-1}-y_i) - (\delta_i-\delta_{i+1})^{3/2} - \frac{3}{2}(\delta_i-\delta_{i+1})^{1/2}(y_i-y_{i+1})\right\}$$

$$+\xi\left(y_{i-1}'-2y_i'+y_{i+1}'\right) + O(y_{i-1}^p y_i^q) + O(y_i^r y_{i+1}^s)$$

•••

$$\frac{d^2y_N}{d\tau^2} = \frac{1}{\sqrt{2}}(\delta_{N-1}-\delta_N)^{3/2} + \frac{3}{2\sqrt{2}}(\delta_{N-1}-\delta_N)^{1/2}(y_{N-1}-y_N)$$

$$-\alpha(\delta_N)^{3/2} - \frac{3}{2}\alpha(\delta_N)^{1/2} y_N + \xi\left(y_{N-1}'-2y_N'\right) + O(y_{N-1}^p y_N^q) + O(y_N^z) \qquad (2.22)$$

$$p+q \geq 2, \quad r+s \geq 2,\ z \geq 2$$

As in the previous discussion, the only non-smooth component is in the first equation of (2.22), modeling the separation of the actuator and first bead. We observe that there are two types of force components on the right hand side of (2.22) corresponding to the interaction between beads, (i) static components dependent only on δ_j, and (ii) dynamic components involving $y_j(\tau)$. We account for the non-smooth terms in (2.22) by expanding the harmonic excitation term $[\sin(\beta\tau)-\delta_1]_+^{3/2}$ in Fourier series to obtain 'static' and 'dynamic' components,

$$\left[\sin(\beta\tau)-\delta_1\right]_+^{3/2} = a_0 + \sum_{n=1}^{\infty} a_n\cos(n\beta\tau) + \sum_{n=1}^{\infty} b_n\sin(n\beta\tau) \qquad (2.23)$$

with the coefficients are defined as:

$$a_0 = \frac{\beta}{2\pi}\int_{-\pi/\beta}^{\pi/\beta}\left[\sin(\beta\tau)-\delta_1\right]_+^{3/2}d\tau$$

$$a_n = \frac{\beta}{\pi}\int_{-\pi/\beta}^{\pi/\beta}\left[\sin(\beta\tau)-\delta_1\right]_+^{3/2}\cos(n\beta\tau)d\tau$$

$$b_n = \frac{\beta}{\pi}\int_{-\pi/\beta}^{\pi/\beta}\left[\sin(\beta\tau)-\delta_1\right]_+^{3/2}\sin(n\beta\tau)d\tau$$

Now by balancing the static forces in all the (smooth) equations (2.22), we obtain the following recursive relation for the permanent compression of the beads,

$$\begin{aligned}&(\delta_{j-1}-\delta_j)^{3/2}-(\delta_j-\delta_{j+1})^{3/2}=0\\&\bullet\bullet\bullet\\&\frac{1}{\sqrt{2}}(\delta_{N-1}-\delta_N)^{3/2}-\alpha(\delta_N)^{3/2}=0\end{aligned} \qquad (2.24a)$$

where $j = 2,3,\ldots,(N-1)$. A trivial algebraic manipulation yields,

$$\delta_i = \frac{\delta_{i-1}\left[1+(N-i)\gamma\right]}{\left[1+(N-i+1)\gamma\right]}, \qquad 1 < i \le N \qquad (2.24b)$$

where $\gamma = 2^{1/3}\alpha^{2/3}$. The only unknown in the above set of equations is the permanent compression of the first bead δ_1. Once this is evaluated the compression of all the other beads can be expressed in terms of δ_1. The compression δ_1 can be obtained by balancing the static force components in the first equation of (2.22), i.e., balancing the constant term from the Fourier series (2.23) with the constant force interaction between the first and the second beads. This leads to the following implicit relation:

$$\frac{\eta\beta}{2\pi}\int_{-\pi/\beta}^{\pi/\beta}\left[\sin(\beta\tau)-\delta_1\right]_+^{3/2}d\tau-\frac{1}{\sqrt{2}}(\delta_1-\delta_2)^{3/2}=0 \tag{2.25a}$$

Substituting for δ_2 in terms of δ_1 and rescaling time $\tilde{\tau}=\beta\tau$, we derive the final form for the equation governing the compression of the first bead,

$$\left\{\frac{\eta}{\pi}\int_{\sin^{-1}(\delta_1)}^{\pi/2}\left(\sin(\tilde{\tau})-\delta_1\right)^{3/2}d\tilde{\tau}\right\}^{2/3}=\delta_1\left[\frac{1}{1+(N-1)\gamma}\right] \tag{2.25b}$$

where the '+' sign is removed from (2.25b) since $(\sin(\tilde{\tau})-\delta_1)^{3/2}\geq 0$ within the limits of above integration.

Equation (2.25b) is evaluated numerically to obtain δ_1. This analysis predicts that the static compression δ_1 of the first bead (and therefore of any other bead) is independent of the excitation frequency when the dynamics is in the attenuation band. This is verified through numerical simulations (Figure 2.37), where we depict the response of the first bead for a homogeneous chain with $N=10$ at various excitation frequencies (β) inside the AB. The static component of the response is independent of the excitation frequency. This analysis assumes weakly nonlinear behavior, and these predictions are not valid at lower frequencies as the dynamics makes the transition from the propagation to the attenuation band.

The static offset of each bead in the granular chain is evaluated using equations (2.24) and (2.25) and compared to the results derived from numerical simulation for a chain with $N=20$ (Figure 2.38). The numerical simulations show good correspondence with the analytical estimates and confirm that the spatial variation of the static offset is linear. As the length of the chain is increased the static component of the first bead's displacement reaches unity asymptotically, whereas the static offset of the last bead

approaches zero. In essence, for a sufficiently large number of beads, the chain detaches from the exciter and the energy input to the chain approaches zero asymptotically.

Finally, considering the dynamic components of the bead displacements in (2.22) we can obtain analytical estimates of the oscillatory responses of the beads. We arrive at reduced dynamical equations for the response $y_j(\tau)$, by removing the static components of (2.22). These reduced equations depend on the dynamic components of the Fourier series expansion (2.23). We then find analytical approximations for the oscillatory components of the bead responses, from the resulting system in the form of an N degree of freedom linear damped oscillator system with periodically varying forcing frequency. The presence of damping terms leads to steady state periodic responses. Due to the presence of damping, the amplitude of oscillations about the static offset of the response of each of the beads decreases with increasing frequency. For a particular fixed frequency the amplitude of oscillations decrease as we move away from the site of the actuator, i.e., $y_j(\tau) > y_{j+1}(\tau)$, confirming the attenuation behavior described above.

The agreement between numerical and analytical response for the forced 2-bead system is presented in Figure 2.39. The analytical responses closely match the numerical ones, and both $y_1(\tau) > y_2(\tau)$ and $\delta_1 > \delta_2$. Although the transient dynamics is not captured in our analytic study, the steady state response shows good correspondence.

2.2.3 Conclusions

Considering harmonically forced granular chains we found that for fixed amplitude of excitation, the low-frequency dynamics is strongly nonlinear; beads separate and lead to collisions resulting in propagating pulses. This represents the propagation band of the dynamics. Indeed, frequency components inside the PB propagate spatially. With an

increase in the excitation frequency, the system enters into a state of permanent compression which results in weakly nonlinear and smooth dynamics. The response is localized close to the excitation and attenuates away from it. In the event of application of a high frequency excitation, the frequency components in the PB are transmitted along the chain, whereas the frequency components in the AB are attenuated. When the system is harmonically excited at high frequency, the system settles to a localized mode and the high frequency signals are completely attenuated. This final result, which is confirmed by direct numerical simulations and experiments reported in this section have considerable practical significance in designing this type of strongly nonlinear granular media as passive mitigators of unwanted disturbances. In the transition between these two frequency bands, nonlinear resonance phenomena occur, but due to the high sensitivity of the experimental setup, results were not repeatable and resonance was not experimentally verified, but numerical results evidence the occurrence of resonance.

The dynamics inside the AB is analytically tractable and it is deduced that the permanent compression is independent of the excitation frequency. An increase in the length of the chain results in an increase in the static offset of the first bead, and in turn increases the permanent compression of the other beads. With the first bead having a substantial permanent offset, the interaction time between the first bead and the actuator decreases and less energy is transferred to the granular chain.

2.3 Classification of NNMs in Finite Homogeneous Granular Chains

In Section 2.1 we explored the oscillatory dynamics of homogeneous finite granular chains. It is interesting to note that some of the oscillatory modes did not conform to the classical definition of nonlinear normal modes (NNMs). In fact such modes were

realized for the first time in such non-cohesive systems. This necessitated the extension of the definition of NNMs to include such modes. Further to that, it is but obvious that the existing methodology to classify the normal modes either in linear or nonlinear systems fail to account for such motions. To this end, we develop a new systematic methodology for classifying the periodic orbits of homogeneous ordered granular chains with no dissipation, under the assumption that all beads oscillate with the same frequency. The analysis is based on the idea of balancing linear momentum for sets of auxiliary models consisting of *'effective particles.'* The auxiliary models may be defined for any given finite, ordered granular chain composed of n identical beads that interact with each other through strongly nonlinear Hertzian interaction law. In turn, the auxiliary models may be effectively used for theoretically predicting the total number of periodic orbits and the corresponding amplitude ratios of the beads. The derived analytical models can be utilized to predict the response of the effective particles, and based on that, to predict primary pulse transmission in periodic layered media with granular interfaces. Moreover, our analysis can be extended to the general class of nonlinear chains of particles with smooth interacting potentials and possible separations between particles during the motion.

2.3.1 Introduction

The characterization and modeling of the periodic orbits (normal modes) of Hamiltonian dynamical systems is a matter of importance from both fundamental and practical points of view and thus an area of intensive study. The considered Hamiltonian systems can be divided into two main categories. The first category is composed of systems with smooth potentials; prototypical dynamical systems in this category are smooth linear or nonlinear lattices (e.g., Fermi-Pasta-Ulam – FPU models).

The second category includes Hamiltonian systems with non-cohesive, non-smooth interacting potentials (e.g., uncompressed granular media) allowing for complete separation between interacting particles during the dynamics. The physical models admitting the first category are those frequently considered in solid state physics where methods based on normal modes are widely applied. In this section we focus our attention on systems belonging to the second category namely, one-dimensional granular chains. This class of dynamical systems has not been studied extensively in the literature, the main reason being the absence of widely applicable analytical (perturbation or asymptotic) techniques for analyzing their dynamics.

The main hurdle in developing a systematic theoretical approach to comprehensively describe the dynamics of homogeneous and heterogeneous granular systems lies in the possibility of separation between the beads of the granular medium. This property, which is intrinsic to any granular system with no pre-compression, results in complete breakdown of regular analytical techniques for analyzing their dynamics. For example, as shown by Kadanoff et al. [148, 149] the hydrodynamic equations usually applied for the description of granular flows may not be proper for these systems when a small dissipation is introduced; this is because many-particle granular systems may reach "extraordinary" states where local equilibrium is destroyed. As this happens the hydrodynamic approach fails to correctly describe the global system dynamics. In these states the dynamics can be hardly approached using regular analytical techniques, which renders these media very challenging for theoretical studies.

Interestingly enough, however, under some external loading conditions these non-smooth dynamical systems may exhibit periodic or near periodic dynamical response, but their analytical treatment is a formidable task. For example, near-periodic patterns have been observed in the dynamical responses of one dimensional granular gas [149], whereas some other works have indicated the existence of chaotic and

periodic motions in a one dimensional inelastic and elastic granular systems [85, 150]. Additional works [151-153] discussed this type of dynamical systems from the perspective of the hydrodynamic approach. However, the proper characterization of the periodic and near periodic dynamical behavior of these systems wherever the hydrodynamic formulation fails (i.e., in dynamical states where the discrete nature of the dynamics prevails and cannot be overlooked or approximated by smooth potentials) is very important for the global understanding of the complex behavior of granular materials. Moreover it constitutes the basis for understanding pattern formation in the higher dimensional granular systems [154, 155]. Therefore, special approaches should be developed to address the dynamics of this class of non-smooth dynamical systems, taking into account the discrete nature of bead interactions and capable of properly characterizing the periodic patterns exhibited by these systems. The NNMs of finite one-dimensional ordered granular chains with no pre-compression were numerically studied for fixed-fixed boundary conditions in Section 2.1 [85] and for periodic boundary conditions [63]. Moreover, different families of spatially extended traveling waves exist in these systems [63].

The previously described results highlight the distinct challenges that the study of the dynamics of this type of ordered granular media with no pre-compression entail, dictating the application of new techniques. Focusing on time-periodic responses, the definition of NNM has been extended in order to include a broad range of smooth and non-smooth responses. Such responses even include the case when separation between beads leads to regimes of 'free flight' in the granular responses and prevents synchronicity of the ensuing oscillation. It will be assumed, however, that all beads of the chain oscillate with the same frequency, in order to preclude the countable infinity of subharmornic oscillations in these systems [85].

Towards this aim, the principal goal of this section is to provide a systematic classification of a certain type of periodic orbits (or nonlinear normal modes – NNMs)

existing in general ordered one-dimensional homogeneous granular chains with no pre-compression and no dissipation. The approach developed herein is intended for complete classification and prediction of a certain kind of nonlinear normal modes (NNMs) (balanced by linear momentum) of general finite homogeneous, granular chains with no pre-compression effectively reducing the original system of uncompressed beads to an auxiliary system by introducing the concept and methodology of 'effective particles'. The concept of effective particles has been introduced in the FPU chain for studying strong energy exchanges between different parts of the chain [156]. It is important to emphasize that it is incorrect to claim that there are no other possible nonlinear modes than the ones classified in this work and the NNMs predicted here are all exhaustive since this claim cannot be proven rigorously, although this is conjectured. However, using the proposed classification we can predict the existence of a special family of NNMs (balanced by linear momentum) all of which are fully confirmed computationally and in good correspondence with theoretical prediction. Moreover, it is shown that an analytical model can be derived to depict the response of the effective particles, and that the proposed approach can be successfully applied to the prediction of primary stress wave transmission in a layered elastic system with granular interfaces. The study will be carried out under the assumptions of absence of dissipative effects (e.g., of dry friction or plasticity).

It is important to emphasize at this point that the proposed methodology is by no means restricted to chains with Hertzian interaction laws, but holds also for a more general class of nonlinear interaction potentials (i.e. $\tilde{F} \propto \delta^r, r > 1$) wherever separation between the moving beads is possible resulting in non-smooth dynamical motions. Hence, the results of this work can be generalized beyond chains of interacting spherical beads.

2.3.2 Auxiliary and Vibro-Impact Models Based on the Concept of Effective Particles

In this section we formulate the preliminary concepts for classifying time-periodic orbits in one-dimensional homogeneous granular chains with no dissipation or pre-compression, under the assumption that all beads oscillate with *identical* frequencies; hence, we will exclude subharmonic motions from our discussion. For the purpose of our discussion we will consider the most general definition of a NNM, as a general free (that is, unforced) time-periodic oscillation of a discrete dynamical system where all particles oscillate with the same frequency. As discussed previously finite granular chains are strongly nonlinear dynamical systems, not only due to the essentially nonlinear Hertzian interaction law governing interactions between neighboring beads, but also due to possible non-smooth effects when neighboring beads separate and subsequently undergo collisions; hence, they constitute a very peculiar class of dynamical systems.

Moreover, one may consider the qualitative similarity of the dynamics of these systems to their vibro-impact analogs, i.e., of systems with rigid beads where dynamical interactions occur solely due to momentum exchange between colliding beads. To address this issue we note that in granular systems the time scale governing the interaction between adjacent beads is finite, whereas in the vibro-impact limit this interaction time is infinitesimally small so no characteristic time scale exists. This makes the dynamics of granular systems more complex since more than two beads may simultaneously interact, whereas this is obviously not the case for vibro - impact models where only two-bead interactions are possible at any given time instant. Nevertheless, it will be shown that the vibro-impact model may help us classify the NNMs in granular chains.

One may question the possibility of oscillatory motion for strongly nonlinear granular systems, yet it was already shown that these strongly degenerate systems do

possess numerous time-periodic stable motions in the form of NNMs in previous section [85] or traveling waves [63]. However, unlike typical oscillatory models with inter-bead interactions governed by smooth interaction potentials, in the granular chains under consideration NNMs may exhibit multi-phase dynamics. For example, there might be a phase in the dynamics where two adjacent beads are in contact (and are mutually compressed), followed by a second phase where separation occurs and a bead executes 'free flight' motion, and a third phase where three (or more) simultaneous bead interactions occur. As shown in previous section and in [63, 85], such distinct phases of the dynamics may coexist during a single cycle of the free oscillation of the granular system. It follows that no existing classification, based, for example, on the relative phases of bead oscillations, applies in this case, so a new methodology for classifying the oscillations of granular chains is required.

In the following exposition we aim to develop such a general classification scheme that applies for homogeneous granular chains composed of finite number of nonlinearly interacting beads with fixed-fixed or periodic boundary conditions. The governing equations of motion of a typical homogeneous granular chain can be normalized and non-dimensionalized so that no parameters appear [63, 85],

$$\ddot{x}_i = (x_{i-1} - x_i)_+^{3/2} - (x_i - x_{i+1})_+^{3/2} \ , \quad i = 1, ..., n \tag{2.21}$$

where the notation from the previous section is preserved. Considering fixed-fixed or periodic boundary conditions at the two ends of the chain, we introduce its partition into N independent *clusters*. According to this partition, the l −th cluster G_l is composed of H_l number of beads, with $l = 1, \dots, N$ and $H_1 + \cdots + H_N = n$. To address the issue of how a cluster is defined, we regard the granular chain as a one-directional graph of beads (i.e., the beads are vertices in the graph), with the connection between any two

adjacent beads, say Q_p and Q_{p+1}, forming the *edge* $e(Q_p, Q_{p+1})$ in the graph. Then, we introduce the following definition of a cluster of beads.

Definition

A group of beads of the granular chain is denoted as a *cluster* G_l if and only if it satisfies the following conditions:

a) All beads (vertices) of the cluster form a simply connected graph (group of the neighboring beads in the chain).

b) Throughout the entire period of oscillation all beads $Q_p, p = 1, \dots, H_k$ forming the cluster satisfy the condition,

$$\left\{ \forall Q_p,\ Q_n \in G_l \Rightarrow \operatorname{sgn}\left[v_{Q_p}(\tau) \right] = \operatorname{sgn}\left[v_{Q_n}(\tau) \right] \quad or \quad v_{Q_p}(\tau) = 0 \quad or \quad v_{Q_n}(\tau) = 0 \right\}$$

where $v_{Q_p}(\tau)$ denotes the normalized velocity of bead Q_p.

c) No additional bead of the chain can be added to the cluster without violating condition (a).

We note that in this definition no stationary beads are assumed to exist, i.e., no beads that remain permanently immovable throughout the phase of free oscillation (NNM). The issue of stationary beads is considered in a later section to demonstrate the broad applicability of the proposed classification scheme.

Based on this definition we show that we can proceed to a complete classification of the free periodic oscillations of any one-dimensional finite homogeneous granular chain with fixed-fixed or periodic boundaries. Towards this task we need to introduce new effective coordinates for the displacement $x_i^{(AM)}(\tau)$ and velocity $\dot{x}_i^{(AM)}(\tau)$ of a cluster G_i of the auxiliary model, defined as follows:

$$x_i^{(AM)}(\tau) = \sum_{\forall j, Q_j \in G_i} x_{Q_j}(\tau)$$
$$\dot{x}_i^{(AM)}(\tau) = \sum_{\forall j, Q_j \in G_i} \dot{x}_{Q_j}(\tau) \tag{2.22}$$

where $x_{Q_j}, \dot{x}_{Q_j}$ denote the displacement and velocity, respectively, of the bead Q_j in the considered cluster of the original granular chain (2.21).

To illustrate the algorithm for the classification scheme we consider fixed-fixed boundary conditions, and refer to Figure 2.40 where we depict schematically the partition of a granular chain of n beads into N clusters. It is apparent, however, that granular chains with periodic boundary conditions fit in the same scheme of classification developed for the fixed-fixed ones, so the classification scheme developed herein for standing wave oscillations can be extended to the case of traveling waves as well [63]. Then, we regard each of the N clusters G_i, $i = 1, \dots, N$ as an independent effective particle with mass equal to H_i (the number of beads composing that cluster), defining an *auxiliary oscillatory chain* of N effective particles with corresponding masses $m_1 = H_1, \dots, m_i = H_i, \dots, m_N = H_N$. *From now on we focus on the motion of the center of mass of each of these effective particles (clusters) rather than the motion of each single bead of each cluster.* It is important to note that based on our previous definition, each effective particle (cluster) of the auxiliary oscillatory chain oscillates in out-of-phase fashion with respect to its neighboring effective particles. It is also convenient to view the auxiliary chain as a *vibro-impact model* of effective particles of non-uniform masses, with the motion of each effective particle being determined by linear momentum exchanges between all effective particles. Clearly, in the absence of dissipation the combined linear momentum of all effective particles should be conserved.

The resulting vibro-impact auxiliary chain of effective particle greatly simplifies the dynamics and enables the classification of the NNMs of the original granular chain

(2.21). This approach is somewhat related to the method of effective particles developed in the theory of solitons, where a propagating soliton may be viewed as a moving particle with its own mass (effective mass of the soliton) and linear velocity (phase velocity of the soliton). Following similar arguments, we may state that the auxiliary system of effective particles is constructed in a way to reflect the interaction of pulses propagating back and forth in the granular chain. In Figure 2.41a we depict the auxiliary oscillatory model (original granular chain partitioned to clusters) of effective particles interacting through a Hertzian like contact law, corresponding to the fixed-fixed granular chain of Figure 2.40. Note that we use the term 'Hertzian like contact law' since we are dealing with effective particles rather than the originally interacting identical spherical beads. Intuitively enough, each configuration of an auxiliary model generated from the original chain (i.e. the particular partition of the original granular chain into clusters) will correspond to the particular NNM of the original chain under consideration.

It is convenient at this point to introduce an analogous *vibro-impact model* (depicted in Figure 2.41b), where the masses of the effective particles (clusters) are the same as of the constructed auxiliary model, and the velocities of any two neighboring particles have opposite signs. The ratios of these velocities can be determined by imposing a balance of linear momentum, since otherwise no time-periodic motions where all effective particles have the same frequency would be possible in this system. It is important to note that according to the definition of the vibro-impact model *only single point interaction between effective particles is possible*. In other words, at any given instant of time, each of the effective particles of the auxiliary chain may interact with only one of its neighbors so that no multiple simultaneous interactions between effective particles are allowed in our model; this is different from the original granular chain where due to finite duration of elastic interaction between beads, more than two beads may interact at any given instant of time, which greatly complicates the nonlinear

dynamics and precludes analytical treatment of the dynamics. This does not hold in the vibro-impact chain, where there is immediate momentum exchange between interacting effective particles, due to the infinitesimally short duration of particle interaction. It follows that for any two neighboring effective particles m_i and m_{i+1} of the vibro-impact model of Figure 2.41b the following relation holds:

$$v_i / v_{i+1} = m_{i+1} / m_i \tag{2.23}$$

This relation is due to the balance of linear momentum of two adjacent clusters and is a necessary condition so that the oscillations of each cluster are of same frequency and synchronous. In the present study we demonstrate the complete correspondence of the velocity ratios predicted theoretically from the simplified vibro – impact model (i.e., from pure balance of the linear momenta) and the corresponding ratios of the amplitudes of the velocities (i.e. the maximum values of the velocities) of the effective particles of the corresponding auxiliary model. These amplitudes are derived from direct numerical integration of the governing equations of the original granular chain. The amplitude of the velocity of the i −th effective particle (cluster) G_i of the auxiliary model will be defined as follows:

$$\max\left\{\dot{x}_i^{(AM)}(\tau)\right\} = \max\left\{\sum_{\forall j, Q_j \in G_i} \dot{x}_{Q_j}(\tau)\right\} \tag{2.24}$$

We note that the maximum value of the absolute velocity of the cluster G_i is estimated over half period of the oscillation. Hence, in the following simulations we will show the nearly exact correspondence of the following velocity amplitude ratios between the auxiliary and vibro-impact models,

$$\frac{\max\left\{\dot{x}_i^{(AM)}(\tau)\right\}}{\max\left\{\dot{x}_{i+1}^{(AM)}(\tau)\right\}} \cong \frac{v_i}{v_{i+1}} \tag{2.25}$$

this will validate the reduction of the dynamics of the original granular chain in terms of greatly simplified vibro-impact models.

In synopsis, in order to classify the NNMs in the granular chain for either fixed-fixed or periodic boundary conditions one specifies the ordered sets of integer mass values for each cluster (effective particle) and enforces the requirement that the summation of all the masses of the clusters be equal to n. It follows that the set of all possible ordered, arrangements of these masses will correspond to the total number of nonlinear normal modes (NNMs) that can be realized in the granular chain and can be classified by the proposed methodology. In the next sections we provide some examples of classification of finite granular chains composed of $n = 3$ and $n = 4$ beads for the fixed-fixed boundary conditions, and leave the corresponding discussion for the case of periodic boundary conditions to a future work.

2.3.3 Classification of NNMs

Based on the previous formulation we now proceed to demonstrate the algorithm for classifying the NNMs of finite granular chains. Initially we will be assuming that no stationary beads (nodes) exist in the NNMs examined, and then extend these results to the case when nodes exist. The proposed classification methodology is demonstrated by considering granular chains with fixed – fixed boundary conditions and n identical beads of normalized mass equal to unity. We will consider the cases $n = 3$ and $n = 4$ in detail, since the results can be generalized in a straightforward fashion. According to

the proposed classification we construct a scheme that classifies all possible NNMs in this system corresponding to different ordered arrangements of 'masses' m_i of effective particles (clusters); this is presented in Table 2.2 and 2.3.

We continue with the application of the methodology for the fixed-fixed granular chain with $n = 3$ and $n = 4$. According to the proposed classification we construct Tables 2.2 and 2.3 listing the different ordered arrangements of effective particles for the four and eight NNMs of the system with three and four beads, respectively. From this classification we conclude that all NNMs, with the exception of NNM 1 and 5, are strongly or weakly localized to one or more beads of the chain with 4 beads. In Figures 2.42 and 2.43 we depict the auxiliary models of effective particles and the corresponding vibro-impact models for some of the NNMs of the systems with $n = 3$ and $n = 4$. As in the previous case the velocity amplitudes of the effective-particles can be accurately predicted by imposing the simple momentum exchange relations (2.25) for the corresponding vibro-impact models.

The developed methodology for classification of NNMs of finite granular chains can be applied to study also nonlinear localization in these periodic systems. To this end, using the proposed classification scheme, it is of importance to identify and classify the subset of NNMs with nonlinear localization properties. *Strongly localized NNMs* correspond to modes where the energy of the oscillation is primarily confined in a single bead, whereas *weakly localized NNMs* are modes where the energy is localized in a subset of the beads of the chain. When such localized modes are excited either by the initial conditions or by external forces, there are always small parts of the chain (i.e., clusters containing one or more beads) that carry a significant amount of the entire energy supplied to the chain. Apparently the methodology of effective particles may predict fairly well the distribution of the velocities between the clusters of the chain, and thus brings about a certain measure for the energy localization on some parts of the granular chain. It has been established [150] that one dimensional granular media may

exhibit strongly non-uniform behavior where the commonly used approach of hydrodynamics applied for the description of the dynamics of granular flows of higher dimension breaks down. Therefore, it is of major importance to be able to characterize and recognize (at least qualitatively) the different patterns of oscillatory motions in various granular setups provided that the conservation of linear momentum holds.

To demonstrate how the outlined methodology can be applied to study localization in finite granular chains, we study the localization properties of the NNMs of the system with $n = 4$ listed in Table 2.3. Hence, strong localization can be attributed to modes 6 and 7, since according to relation (2.25) the corresponding ratio of maximum amplitudes of the velocities of the effective particles is equal to $3:1$, which is the maximum possible one. It follows that for these modes, energy is strongly localized to the right or left end bead of the chain, as shown in Figure 2.43e. Apart from the strongly localized modes, there are also modes which may be classified as weakly localized ones. Modes 2, 3 and 4 are of this type, corresponding to ratio of maximum amplitudes of the velocities equal to $2:1$. Modes 1 and 5 can be definitely attributed to the family of non-localized modes as the corresponding velocity ratios are equal to $1:1$. The last mode to be considered is NNM 8, which according to the previous discussion can be classified as strongly localized; this is due to the fact that the collective response of the beads resembles a solitary-like pulse, and therefore, is strongly localized in space. However, the recurrent velocity peaks (as the 'pulse' bounces back and forth between the fixed boundary conditions) reached by each of the beads are almost identical, and in this sense the resulting motion may also be viewed as oscillatory rather than propagatory.

We note that it is possible to extend the results of this section to the study and classification of localization patterns and, in general, of non-uniform spatial distributions of velocities in one dimensional granular gas [152, 157]. What makes this possible is the previously discussed vibro-impact models that can be used to accurately

predict the amplitudes of the velocities of all clusters of a granular chain during a time-periodic oscillation. This task is left for future work.

Using the outlined classification scheme it is possible to obtain an analytical prediction for the number of NNMs (balanced by linear momentum) that a granular chain with n beads possesses. Since we assume only out-of-phase oscillating effective particles (see Figure 2.41a) we need to solve the equivalent combinatorial problem of finding the number of ordered sets of N positive integers, where N is the number of effective particles (clusters) in the auxiliary granular chain with masses being equal to integers summing-up to the integer n (i.e., the total number of beads of the chain). To this end, we consider an appropriate generating function $G(\zeta)$ as follows [158],

$$G(\zeta) = \frac{\zeta}{(1-\zeta)} = \sum_{s=1}^{\infty} \zeta^s \tag{2.26}$$

Therefore, the following relation holds,

$$\left[G(\zeta)\right]^N = \left\{\frac{\zeta}{1-\zeta}\right\}^N = \left\{\sum_{s=1}^{\infty} \zeta^s\right\}^N = \sum_{s=N}^{\infty} g\left(N,s\right)\zeta^s \tag{2.27}$$

where the function $g(N,s)$ can be expressed in terms of the generating function as follows,

$$g\left(N,n\right) = \lim_{\zeta\to 0} \frac{1}{n!}\frac{d}{d\xi^n} \sum_{s=N}^{\infty} g\left(N,s\right)\xi^s = \lim_{\zeta\to 0} \frac{1}{n!}\frac{d}{d\zeta^n}\left\{\frac{\zeta}{1-\zeta}\right\}^N \tag{2.28a}$$

where, according to the original problem definition $n \geq N$ so $g(N,n)$ is defined. In fact $g(N,n)$ defines the number of all possible partitions of n beads into N clusters.

Rewriting the generating function in a more explicit form:

$$\left\{\frac{\zeta}{1-\zeta}\right\}^N = \left\{\frac{1}{1-\zeta}-1\right\}^N = \sum_{j=0}^{N} C_j^N \left(\frac{1}{1-\zeta}\right)^{N-i} (-1)^i \tag{2.28b}$$

Substituting (2.28b) into (2.28a) we obtain

$$g(N,n) = \lim_{t\to 0} \frac{1}{n!}\frac{d}{d\zeta^n}\left\{\sum_{j=0}^{N} C_j^N \left(\frac{1}{1-\zeta}\right)^{N-j} (-1)^j\right\} = \left\{\sum_{j=0}^{N} C_j^N \frac{(-1)^j (N-j)!}{n!(N-j-n-1)!}\right\} \tag{2.28c}$$

Therefore, the total number of NNMs for different partitions (clusters – effective particles) of the granular chain of *n* beads may be expressed in the closed form as:

$$N_{total} = \sum_{N=1}^{n} g(N,n) \tag{2.29}$$

As a check, for $n = 4$ we obtain $N_{total} = \sum_{N=1}^{4} g(N,4) = 8$, which exactly agrees with the results of Table 2.3.

In the procedure of classification developed so far we assumed the absence of permanently stationary beads. Yet, as shown in Section 2.1 [85], for certain NNMs there exists beads that are permanently stationary since they coincide with nodes of the spatial distribution of the time-periodic oscillation; hence, it is necessary to extend the previous classification to account for this scenario. Using the similar idea of creating an effective oscillatory chain (i.e., a chain of effective particles oscillating out-of-phase fashion with respect to each other) one may proceed to add intermediate, permanently stationary particles of unit mass in between any two oscillating effective particles. In fact the oscillating effective particles are already balanced by the condition of

conservation of linear momentum in the auxiliary chain, so the insertion of a permanently stationary bead in between them does not violate momentum conservation. The scheme for inserting a permanently stationary bead (node) in an auxiliary chain of effective particles is illustrated in Figure 2.44.

It is clear that we can realize different ordered configurations where more than one node (stationary beads) are inserted and placed at certain positions in an auxiliary chain. However, to account for all possible arrangements with nodes added, we should first compute the number of ordered arrangements that occupy all available places between each of two oscillating effective-particles in the auxiliary model consisting of N effective-particles; we need to take into account that no nodes can be added between the end oscillating effective-particles and the fixed boundaries, since, otherwise, the balance of linear momentum on both sides of the inserted node would be violated. Moreover, it should be clear that only one node is allowed to be inserted in between any pair of oscillating clusters. Therefore, the enumeration of all possible positions of nodes in between the N oscillating effective-particles of an auxiliary chain may be computed as:

$$M_{insertions}(N)=\sum_{j=0}^{N-1} C_j^{N-1}, \quad C_j^{N-1}=\frac{(N-1)!}{j!(N-j-1)!}, \quad N\geq 2 \tag{2.30}$$

Combining the results of the previous section for the case of complete absence of nodes with (2.30), we are able to enumerate all possible NNMs ∂, which can be realized in a granular chain of n beads, including NNMs that may possess stationary beads (nodes):

$$\partial = g(1,n)+\sum_{N=2}^{n} g(N,n)\, M_{insertions}(N) \tag{2.31}$$

In Figure 2.45 we provide an example of a NNM with a stationary bead (node). This NNM is a variation of the out-of-phase NNM 1 of Table 2.3 with the immovable bead 2 being inserted between beads 1 and 3. It is important to note that for the NNM illustrated in Figure 2.45 all the effective particles are single beads (i.e., $\forall\, i, H_i = 1$), therefore there will be no difference between the auxiliary model and the original granular chain.

2.3.4 Theoretical Modeling of the Dynamics of Effective Particles

The methodology for classification of NNMs using auxiliary chains of effective particles derived thus far greatly helps in identifying certain patterns of motion occurring in more complicated one-dimensional granular setups, and in predicting possible localization phenomena in granular chains. However, as discussed in the next section one of the most interesting practical applications of the methodology of effective particles is in the area of shock wave transmission in layered elastic media with granular interfaces.

In order to build predictive capacity for implementing the methodology of effective particles to applied problems it is necessary to derive analytical approximations for the dynamics governing the reduced order auxiliary systems of effective particles; namely, to describe analytically the motion of effective particles in the auxiliary model corresponding to a particular NNM. This task is addressed in this section by considering the in-phase NNM mode of finite granular chains with fixed-fixed boundaries, (i.e., NNM 8 for the fixed-fixed chain with $n = 4$).

As discussed in the previous section, the corresponding auxiliary model of the in-phase NNM possesses a single effective particle bouncing between rigid boundaries (see Figure 2.46). The most natural way to model the dynamics of this effective particle

is by relating its frequency with that of the in-phase NNM, which due to the nonlinear nature of the system is directly proportional to the total energy. In order to obtain an approximate analytical frequency-energy relation for the in-phase NNM we resort to curve fitting of a numerically obtained frequency (f) – energy (h) plot [85] with an approximate analytical function in the form $f = f(h) = \Psi h^{\gamma}$, where γ is a universal constant independent of the number of beads in the chain and is found to be ~ 0.1. The value of $\Psi = \Psi(n)$ varies with the number of beads n in the granular chain. The numerical frequency-energy curves of granular chains with $n = 2, \ldots, 7$ and the corresponding curve-fit approximations are depicted in Figure 2.47, where good correspondence is noted.

Returning to the auxiliary model of a single effective particle for the in-phase mode (e.g., NNM 4 for the chain with $n = 3$ and NNM 8 for the chain with $n = 4$ – see Figure 2.42c and 2.43f respectively), we note that as the effective particle bounces repeatedly between the fixed boundaries there exist two qualitatively different dynamical regimes during each cycle of oscillation: (i) A regime of interaction of the effective particle with each of the fixed boundaries through a Hertzian interaction law, and (ii) a regime of 'free flight' during the transition from one wall to the other. Hence, the periodic oscillation of the effective particle can be described by the following non-dimensional equation of motion (where the normalizations of the previous sections were imposed),

$$\ddot{x} = \left(-\frac{D}{2} - x \right)_{+}^{3/2} - \left(-\frac{D}{2} + x \right)_{+}^{3/2} \tag{2.32}$$

with initial conditions $x(0) = (D/2) + (5h/2)^{2/5}$ and $\dot{x}(0) = 0$; D denotes the distance

between the fixed walls (a parameter of the auxiliary model that needs to be determined).

Considering the first regime of interaction of the effective particle with the fixed boundary and assuming that at $\tau = 0$ there is maximum compression of the effective particle, the time of its interaction with the boundary can be analytically computed in terms of hyper-geometric function as $\tau_1^* = 2^{-1/2}\left(5/2\right)^{2/5}\,{}_2F_1\left(1/2, 2/5; 7/5; 1\right)h^{-1/10}$. In fact, similar scaling of kinetic energy versus time has been already derived in [159]. Hence, denoting the period of oscillation of the in-phase NNM for a chain composed of n beads as $T(n) = 2\pi/f(n)$, the time of 'free flight' of the effective particle during a cycle of oscillation can be evaluated as $\tilde{\tau} = T - 4\tau_1^*$. It follows that during the regime of 'free flight' the effective particle traverses a total distance of $2D = \tilde{\tau}\sqrt{2h}$, which is a relation that can be used to analytically estimate the distance in the auxiliary model. Moreover, as discussed previously, it is possible to analytically approximate the period of oscillation of the in-phase NNM at any energy level h and for any number of beads n. Finally, once the effective particle detaches from the boundary and enters the regime of 'free flight,' all the energy of the chain is purely kinetic, which allows the computation of the velocity of the effective particle in between the boundaries as $V_p = \sqrt{2h}$.

In Figure 2.48 we depict a comparison between the response of the single effective particle corresponding to the in-phase NNM and the response of the beads of chains with $n = 4$ and $n = 5$ beads obtained by direct numerical integration. We note that according to the classification derived previously, the velocity of the single effective particle modeling the in-phase NNM is just the summation of the velocities of all the beads of the chain. The same agreement is also observed for the displacement time series of the exact and auxiliary models of effective particles. Therefore, the dynamics of homogeneous granular chains with fixed-fixed boundary conditions, when oscillating in their in-phase NNMs can be completely captured using the corresponding auxiliary

models consisting of a single effective particle bouncing between the two boundaries. Moreover, the analysis of this section can be extended to higher-frequency NNMs consisting of more than one effective particle.

The results of this section have important implications in applications of homogeneous granular media when the dynamics is dominated by one or more NNMs. For instance, considering the bead interactions realized in certain modes of coupled granular chains, one might be interested in identifying important nonlinear resonance conditions [91] under which energy from a propagating pulse gets scattered efficiently and gets transferred to the far field of the chain through traveling waves; or, considering coupled granular chains it is possible to formulate resonance conditions under which energy flows from one chain to another in a near-irreversible fashion (i.e., under which targeted energy transfer occurs) or conditions for strong energy exchanges through nonlinear beat phenomena [122]. Knowledge of the nonlinear modes that participate in such strongly nonlinear interactions leads to analytical estimates of the characteristic times for these energetic excursions, and, hence, of the rate of realization of this dynamics.

Apparently it would be a formidable task to consider the very complicated dynamics of entire granular chains, accounting for the motion of every particular particle (bead). Therefore, it would be much more convenient to study the collective behavior of these chains using the concept of effective particles, thus effectively reducing the problem to a reduced system of a few coupled, nonlinear oscillators whose analysis is straightforward. This reduction can be efficiently performed by applying the modeling proposed in this section, and is by no means restricted to the lowest mode (which was considered herein just as an example to demonstrate the approach). In fact, the outlined approach can be easily extended to any arbitrary mode of interest which will be effectively transformed to a *reduced binary model* of interacting effective particles with the analytically approximated interaction laws. Moreover, the developed

methodology of replacing the original granular chain by the binary model of effective particles can also be extended to higher dimensional granular systems, which, in turn, can be reduced to granular gasses (i.e. 2D, 3D systems) composed of effective particles. We are convinced that the proposed methodology will highly facilitate the ongoing research in this field in topics such as, pattern formation in granular systems, periodic motions of density waves in vibrating granular layers, internal resonant interactions in granular materials and wave propagation through the multi-layered granular structures.

As an example of application of the proposed methodology, in the next section we consider a layered elastic medium with homogeneous granular interfaces and forced by a short-duration applied shock is considered. As shown in a previous work [125], at least in the leading layers of this system the dynamics of the granular interfaces is dominated by the lowest frequency in-phase mode, so the reduction of the dynamics in terms of auxiliary models of effective particles should be applicable.

2.3.5 Application of Effective Particles to Study Primary Pulse Propagation in Layered Media

From the previous analysis it is apparent that a significant reduction of the dynamics of one-dimensional homogeneous ordered granular media can be achieved by decomposing the oscillatory regimes of these media into auxiliary models of effective particles oscillating in out-of-phase fashion with respect to each other. Although this modeling looks promising, its basic deficiency is that it neglects the internal dynamics between the granular particles, instead considering them as clusters or effective particles. It follows that an effective particle models only the momentum transfer occurring between subsets of beads in a granular medium (which is the most significant

piece of information in most of the practical applications dealing with shock transmission dynamics), but neglects all other internal (local) modes that are excited during the dynamics. It is quite intuitive, however, that momentum transfer in a granular medium can be primarily attributed to the in-phase motion of the subsets of the particles. Therefore we anticipate that to first order, the auxiliary model of effective particles constructed in the previous section for the 'pseudo-wave' in-phase NNM should efficiently model pulse propagation induced by a significantly short shock in a granular chain. Indeed, it was shown in [125] that for applied shocks of sufficiently short durations (compared to a characteristic time scale of the intrinsic dynamics) *primary pulse transmission* in a one-dimensional granular chain takes place through the excitation of its lowest-frequency 'pseudo-wave' in-phase mode, whereas the excitation of other modes are nearly negligible. By primary pulse transmission we mean the transmission of the main pulse through the medium (i.e., the 'front pulse'), disregarding secondary waves resulting from reflections at boundaries.

From this discussion, we conjecture that in the first approximation we should be able to study primary pulse transmission in a granular chain with fixed-fixed boundaries excited by short-duration applied shocks, by replacing it with the auxiliary model of a single effective particle modeling its 'pseudo-wave' in-phase NNM. The following study aims to verify this conjecture.

To this end we consider the layered system depicted in Figure 2.49, composed of one-dimensional linearly elastic layers (longitudinal bars executing axial oscillations) with granular interfaces of homogeneous chains of n beads. To the ends of each bar are attached rigid plates in order to suppress three-dimensional end effects, so that the granular interfaces are excited by longitudinal shock excitations. The dynamics of this periodic system has been studied in detail in [125] and it was shown that the granular interfaces can lead to drastic reduction of the transmitted primary pulse through the layered medium.

Following the analysis of [125] and omitting details, each elastic bar is modeled as linear homogeneous continuum governed by the hyperbolic wave equation and assumes the standard D'Alembert solution [36, 160]. Once the propagating wave encounters the granular interface, transmitted and reflected pulses are generated that propagate in the granular layer and back to the bar, respectively. As mentioned previously, our study is solely concerned with the primary transmitted pulse through the layered medium. To study the dynamics of primary pulse transmission we consider granular interfaces with $n = 5$ beads and excite the left boundary of the first elastic layer of the system with the shock excitation of short time duration compared to the characteristic time scale of the intrinsic dynamics of the granular interfaces.

The resulting responses of the boundaries of the two leading layers and the leading two granular interfaces of the medium are depicted in Figure 2.50. It can be observed from the displacement response of the beads and the layers, that in the initial (highly energetic) phase of the dynamics a localized pulse propagates through the layered medium; it is precisely this initial transmitted primary pulse that is the focus of our study (once the primary pulse reaches successive granular interfaces and scatters, secondary pulses are generated that complicate further the dynamics, but these will not be considered here). We note that most of the energy of the external pulse is transmitted through the layered medium by the propagating primary pulse, so that from a practical point of view, shock transmission through the medium should be mostly captured by our analysis. We also note that the granular interfaces seem to exhibit complex dynamics (especially at later times), which are caused by the nonlinear Hertzian-law interactions and the separations and ensuing between beads during wave transmission.

This complex picture of the dynamics, however, can be significantly simplified if we plot the sum of velocities of all the beads of each granular interface; this amounts to an effective particle coordinate transformation, since as mentioned in the previous section the resulting summation provides the velocity of the center of mass of the

interface and is strongly correlated to the dynamics of the single effective particle of the auxiliary model corresponding to the in-phase ('pseudo-wave') NNM of the granular interface. Clearly, this computation completely disregards the dynamics of the other higher-frequency NNMs of the granular interface, but as mentioned previously, we anticipate that most of the transmitted shock energy, at least during the initial phase of the motion, is due to the excitation of the in-phase NNM. Observation of collective motion of the beads on the edge of primary pulse transmission, as well as the analysis reported in [125] lead us to the conclusion that during the initial short duration of the excitation of the layered system by the shock a significant part of the induced shock energy excites the lowest frequency in-phase NNMs of the granular interfaces, while the remaining part of this energy is scattered to the other higher frequency NNMs and is negligible in comparison to the first. This observation, which has been verified in [125] via numerical wavelet transform analysis of bead responses, provides us with the rationale to apply the concept of effective particles to model the primary pulse propagation in the layered system, by *replacing each granular interface by an auxiliary model composed of a single effective particle* (corresponding to in-phase motion of all five beads of the interface); this is equivalent to assuming that, to a first approximation, only the lowest frequency in-phase NNMs of the granular interfaces are excited and the effects of higher NNMs are negligible.

To initiate the analysis of the reduction of the dynamics of the layered system through the introduction of effective particles, we consider the equations of motion of the beads of the 1st granular interface between the elastic layers 1 and 2 that can be expressed in normalized form as follows [125],

$$
\begin{aligned}
\varepsilon\ddot{x}_1 &= (2)^{3/2}\left[w_1(\tau,1)-x_1(\tau)\right]_+^{3/2}-\left[x_1(\tau)-x_2(\tau)\right]_+^{3/2}\\
&\bullet\bullet\bullet\\
\varepsilon\ddot{x}_p &= \left[x_{p-1}(\tau)-x_p(\tau)\right]_+^{3/2}-\left[x_p(\tau)-x_{p+1}(\tau)\right]_+^{3/2}\\
&\bullet\bullet\bullet\\
\varepsilon\ddot{x}_n &= \left[x_{n-1}(\tau)-x_n(\tau)\right]_+^{3/2}-(2)^{3/2}\left[x_n(\tau)-w_2(\tau,0)\right]_+^{3/2}
\end{aligned}
\qquad (2.33a)
$$

$$
x_p(0)=\dot{x}_p(0)=0,\quad p=1,\ldots,n
$$

where n denotes the number of beads of each interface (in this case $n=5$); $0 \le (\zeta = z/L) \le 1$ the normalized spatial variable (where L is the length of each elastic layer); $\tau = ct/L$ the normalized time variable (where c is the speed of sound in each elastic layer); $\varepsilon = M/mL$ a mass ratio (where M is the mass of each bead and mL the mass of each of the elastic layers); and $x_p(\tau) = (EA_C/LK)^{-2}u_p(t), p = 1,\ldots,n$ the normalized displacements of the beads of the interface (where $u_p(\tau)$ denotes the displacement of the $p-$th bead), where E is the Young's modulus, A_C is the area of cross section of the elastic layer and K is the stiffness coefficient of the Hertzian interaction. Moreover, the displacements of material points of the elastic layers on the left and right of the granular interface are normalized according to $v_1(t,z) = (EA_C/LK)^2 w_1(\tau,\zeta)$, $v_2(t,z) = (EA_C/LK)^2 w_2(\tau,\zeta)$, respectively. The equations of motion (2.33a) are complemented by the following equations of motion of the normalized displacements of the ends of the rods 1 and 2,

$$
\begin{aligned}
\dot{w}_1(\tau,1) &= -2F(\tau)-(2)^{3/2}\left[w_1(\tau,1)-x_1(\tau)\right]_+^{3/2}\\
\dot{w}_2(\tau,1) &= (2)^{3/2}\left[x_n(\tau)-w_2(\tau,0)\right]_+^{3/2}
\end{aligned}
\qquad (2.33b)
$$

where $w_1(\tau,1)$ denotes the normalized displacement of the right end point of the 1st rod, $w_2(\tau,0)$ the normalized displacement of the left end point of the 2nd rod, $F(\tau) = (L^3K^2/E^3A_C^3)P(t)$ the normalized force applied at the left boundary of the 1st elastic

layer (with $P(t)$ denoting the corresponding non-normalized axial force). As in [150] our analysis assumes that $\varepsilon \ll 1$, i.e., the mass of a single bead is much smaller in comparison to the mass of the elastic layer. This allows us to model approximately each granular interface as an uncompressed granular chain confined by nearly rigid and slowly moving boundaries, so that the NNMs of the corresponding fixed-fixed granular chain is expected to play a dominant role in the dynamics of primary pulse transmission in this system (for a detailed discussion on the validity of this approximation we refer to [125]).

The auxiliary model of effective particles that models primary pulse transmission in the layered system of Figure 2.49 is presented in Figure 2.51. Each granular interface is replaced by a single effective particle that is initially in contact with its left elastic layer; as discussed previously this approximation models the in-phase NNM of each interface by a single effective particle that replaces all five beads of the interface. The distances D_1 and D_2 of 'free flight' of the effective particles in the first and second auxiliary models, respectively (cf. Figure 2.51), will be evaluated below by energy considerations, taking into account the energy induced in the medium by the excitation pulse. We now describe the modeling of the effective particle for the in-phase NNM of the homogeneous granular interfaces.

Considering the first two layers, the equations of motion of the system of Figure 2.51 are given by,

$$\varepsilon \ddot{X}_1 = 2^{3/2}\left\{\left[W_1(\tau,1)-\frac{D_1}{2}-X_1(\tau)\right]_+^{3/2}-\left[X_1(\tau)-\frac{D_1}{2}-W_2(\tau,0)\right]_+^{3/2}\right\}$$

$$\varepsilon \ddot{X}_2 = 2^{3/2}\left\{\left[W_2(\tau,1)-\frac{D_2}{2}-X_2(\tau)\right]_+^{3/2}-\left[X_2(\tau)-\frac{D_2}{2}-W_3(\tau,0)\right]_+^{3/2}\right\}$$

$$\dot{W}_1(\tau,1) = -2F(\tau)-2^{3/2}\left[W_1(\tau,1)-\frac{D_1}{2}-X_1(\tau)\right]_+^{3/2},\ \dot{W}_2(\tau,0) = 2^{3/2}\left[X_1(\tau)-\frac{D_1}{2}-W_2(\tau,0)\right]_+^{3/2}$$

$$\dot{W}_2(\tau,1) = -2^{3/2}\left[W_2(\tau,1) - \frac{D_1}{2} - X_2(\tau)\right]_+^{3/2},\ \dot{W}_3(\tau,0) = 2^{3/2}\left[X_2(\tau) - \frac{D_1}{2} - W_3(\tau,0)\right]_+^{3/2}$$
$$X_1(0) = -\frac{D_1}{2},\ X_2(0) = -\frac{D_2}{2},\ \dot{X}_j(0) = 0,\ W_p(0,\zeta) = \dot{W}_p(0,\zeta) = 0 \tag{2.34}$$

where the distances of 'free flight' D_1 and D_2 enter explicitly in the equations of motion, the indexes $j = 1, 2$, $p = 1, 2, 3$ and upper cases for displacement variables are used to indicate the effective particle model. Based on the time series of the effective particle modeling the in-phase NNM (see Figure 2.42c and 2.43f) we anticipate an (approximately constant) velocity of free flight, Vel_1, of the effective particle in the first granular interface; this forms the basis for evaluating the distance D_1. Considering the mass of each effective particle equal to unity, we deduce that the energy in the first effective particle is equal to $h = Vel_1^2/2$. This estimation holds by assuming that there is the same forcing for the effective particle as in the actual layered granular system. It is worth noting that we have only considered kinetic energy and neglected the elastic potential energy attributed to the internal dynamics of actual bead interaction; so this energy estimation is approximate, but still consistent with the effective particle approach. Assuming Hertzian-law elastic interaction between the first layer and the first effective particle we compute the time of interaction of the effective particle with the left (slowly moving) boundary as [85],

$$\tau_1^* = \frac{h_1^{-1/10}}{\sqrt{2}}\left(\frac{5}{2}\right)^{2/5} {}_2F_1\left(\frac{1}{2}, \frac{2}{5}; \frac{7}{5}; 1\right) \tag{2.35}$$

For the energy level h_1, we can obtain the period of oscillation T of the in-phase NNM of the granular interface from the plot of Figure 2.47 corresponding to $n = 5$. Then, the time of free flight of the first effective particle can be evaluated as $\tilde{\tau} = T - 4\tau_1^*$, where we took into account the Hertzian interaction of the effective particle with both boundaries

during a full cycle of oscillation. It follows that during 'free flight' the effective particle traverses a total distance equal to $2D_1 = \tilde{\tau}\sqrt{2h_1}$, which evaluates the distance between the two leading layers in the auxiliary model of Figure 2.51. A similar approach can be used to evaluating the distance D_2.

In Figure 2.52 we present the correspondence between the responses of the auxiliary model based on effective particles (cf. Figure 2.51) and of the actual layered medium (cf. Figure 2.49). In this simulation the applied shock on the left boundary of the first elastic layer was taken as,

$$F(\tau) = \begin{cases} -G\sin\left(\pi\tau / \tau_s\right), & 0 < \tau \le \tau_s \\ 0\,, & \tau_s < \tau \end{cases} \tag{2.36}$$

with $G = 25$ and $\tau_s = \pi/50$; moreover, the mass ratio was chosen as $\varepsilon = 0.005$. From the numerical plots of the velocities of the centers of mass of the first two granular interfaces it is verified that in the initial phase of the motion (that is, until the primary transmitted pulse scatters at the right boundary of each granular interface), the dynamics is dominated by the single effective particle modeling the in-phase NNM. This can be deduced by comparing the initial waveforms of the plots of Figure 2.52 with the velocity waveforms of the effective particle modeling the in-phase NNMs in Figures 2.42c and 2.43f for the system with $n = 3$ and $n = 4$. Moreover, from the plots of Figure 2.52 we deduce that indeed there is an initial phase of constant velocity of the center of mass of the leading granular interfaces, which signifies that the single effective particle (cluster) formed by the five beads of each interface traverse at constant velocity without being affected by local interactions between beads.

From the comparisons of Figure 2.52 we conclude that primary pulse transmission is well predicted by the effective particle approach. This satisfactory correspondence holds for both the first and second layers of the medium. Discrepancies

arise only when secondary reflections of the primary pulse occur at the boundaries of the layers, and higher frequency NNMs are excited in the granular interfaces. As was described earlier, the effective particle model used in Figure 2.51 represents well only the lowest frequency in-phase NNM which is responsible for the major part of the initial momentum transfer through the layered medium. Once scattering of the pulse at interfaces occur at later times and higher NNMs are excited, the validity of the single effective particle model is not expected to hold. Moreover, the application of the effective particle approach for the study of shock dynamics of multi-layered repetitive structure requires certain modifications when applied to the systems with the number of layers higher than two. Indeed, we expect that modeling of primary shock transmission based on the effective particle approach is accurate only up to the second granular layer, since as the pulse penetrates further into the periodic medium the primary shock broadens due to dispersion and, hence, it ceases of being of short-time duration. In turn, violation of the assumption of short-time duration of the propagating pulse, restricts the applicability of the effective particles approach, since modes with higher frequency are excited during the initial phase of shock transmission through the layered medium [125].

Summarizing, from the results of Figure 2.52 we conclude that the methodology based on effective particles can be effectively applied for predicting primary pulse transmission in the leading layers of the periodic medium of Figure 2.49. Another valuable prediction obtained from the reduced model concerns the force transmitted in the elastic layers due to propagation of the primary pulse. The normalized force can be calculated through the Hertzian interaction law of the effective particles with the elastic layers, and the results are depicted in Figure 2.53. In the same plot we also depict the normalized transmitted force computed by direct numerical simulations of the equations of motion (2.33a, b) for comparison purposes. From these results we conclude that the theoretical prediction based on the effective particles approach satisfactorily

models the transmitted force due to the primary pulse in the second elastic layer, but it deviates from the numerical simulation in the third elastic layer. There is a simple physical explanation for this result. As mentioned previously, the effective particles approach is only valid as long as the applied force on the elastic layer is of sufficiently short duration. Although this assumption holds in the second layer of the medium, it is violated in the third layer since the transmitted primary pulse at its left boundary (after scattering at the second granular interface) broadens due to dispersion and is not of short duration anymore.

2.3.6 Conclusions

A new methodology for systematic classification of the families of time periodic solutions of one-dimensional, homogeneous granular chains, under the condition that all beads oscillate with similar frequencies is presented in this section. This methodology is applied to finite granular chains with fixed-fixed boundary conditions, and showed that NNMs of homogeneous granular chains with no pre-compression can be effectively classified by introducing auxiliary models of effective-particles (clusters) oscillating out-of-phase with respect to each other (i.e. balanced by the translational momentum), and with or without stationary beads (nodes) in between them. In addition, vibro-impact models of effective-particles are introduced that allows analytical estimation of the maximum velocities of the oscillating effective-particles. Direct numerical simulations verify the predictive capacity of the auxiliary models.

In addition, the effective particles approach has proved to be a useful tool for modeling primary shock propagation in layered media with granular interfaces excited by short time duration shocks. In such a case, primary pulse propagation is primarily due to the excitation of the lowest-frequency, i.e. in-phase mode of the granular

interfaces, which, in turn, can be modeled by simple auxiliary model, composed of a single effective particle. Indeed, it is demonstrated that the reduced model of effective particles can efficiently capture the primary impulse propagation as well as the force transmitted to the second elastic layer of the system. This example indicates that the methodology of effective particles might be useful in modeling theoretically primary pulse transmission in more complex granular media, such as dimer systems or periodic setups of higher dimensions. It is reiterated once again that the proposed classification is by no means restricted to Hertzian interaction law between interacting granular particles, but rather holds for any-type of nonlinear interaction potential (of the general form $\tilde{F} \propto \delta^r, r > 1$) wherever separation between the moving beads is allowed. This is owing to the fact that the oscillating clusters will support the propagating solitary-like pulses (that are generated due to the strong nonlinearity of the system), which, in turn, can be effectively modeled and 'replaced' by oscillating effective particles with appropriate masses and velocities. The resulting reduced system of effective particles can be used to study momentum transfer in granular media. Finally, the oscillating granular chain can be effectively reduced to a vibro-impact chain (binary model) of effective particles balanced by linear momentum.

2.4 Figures

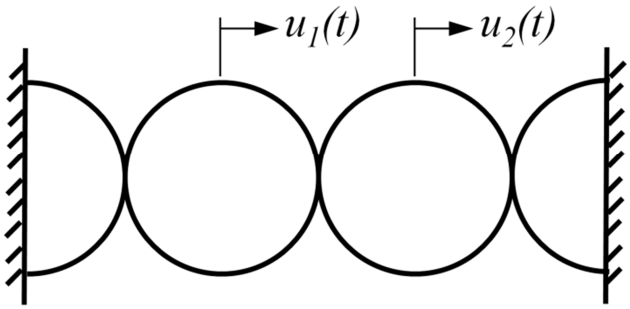

Figure 2.1: The two-bead system.

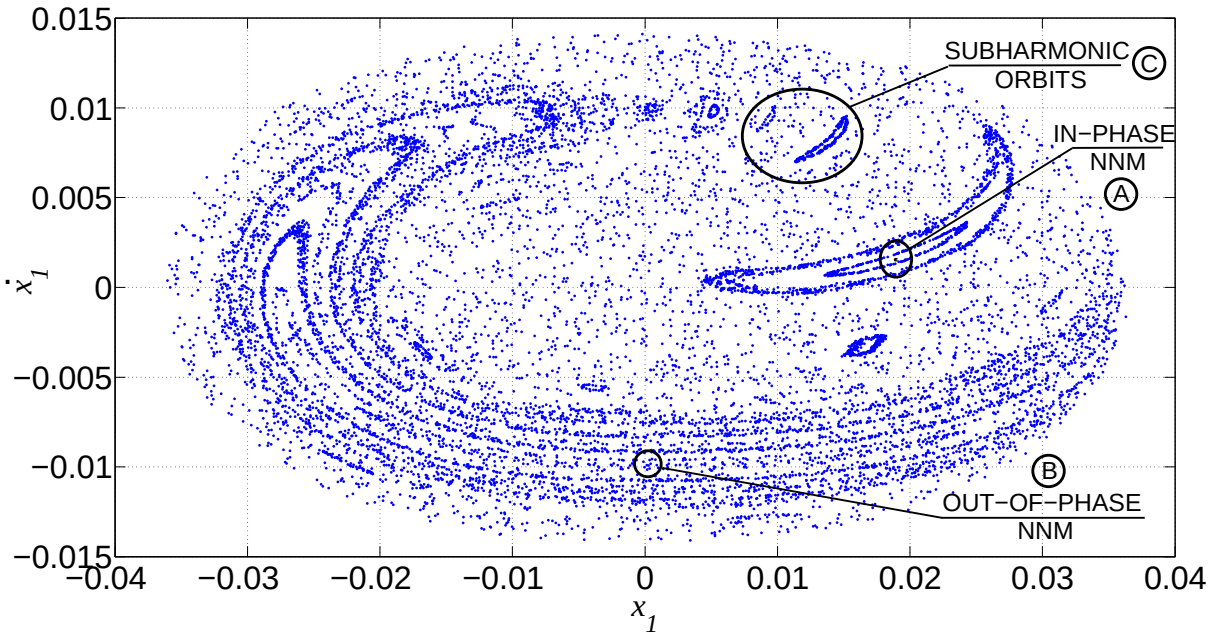

Figure 2.2: Poincaré map of the global dynamics of the two-bead system for $h = 0.0001$.

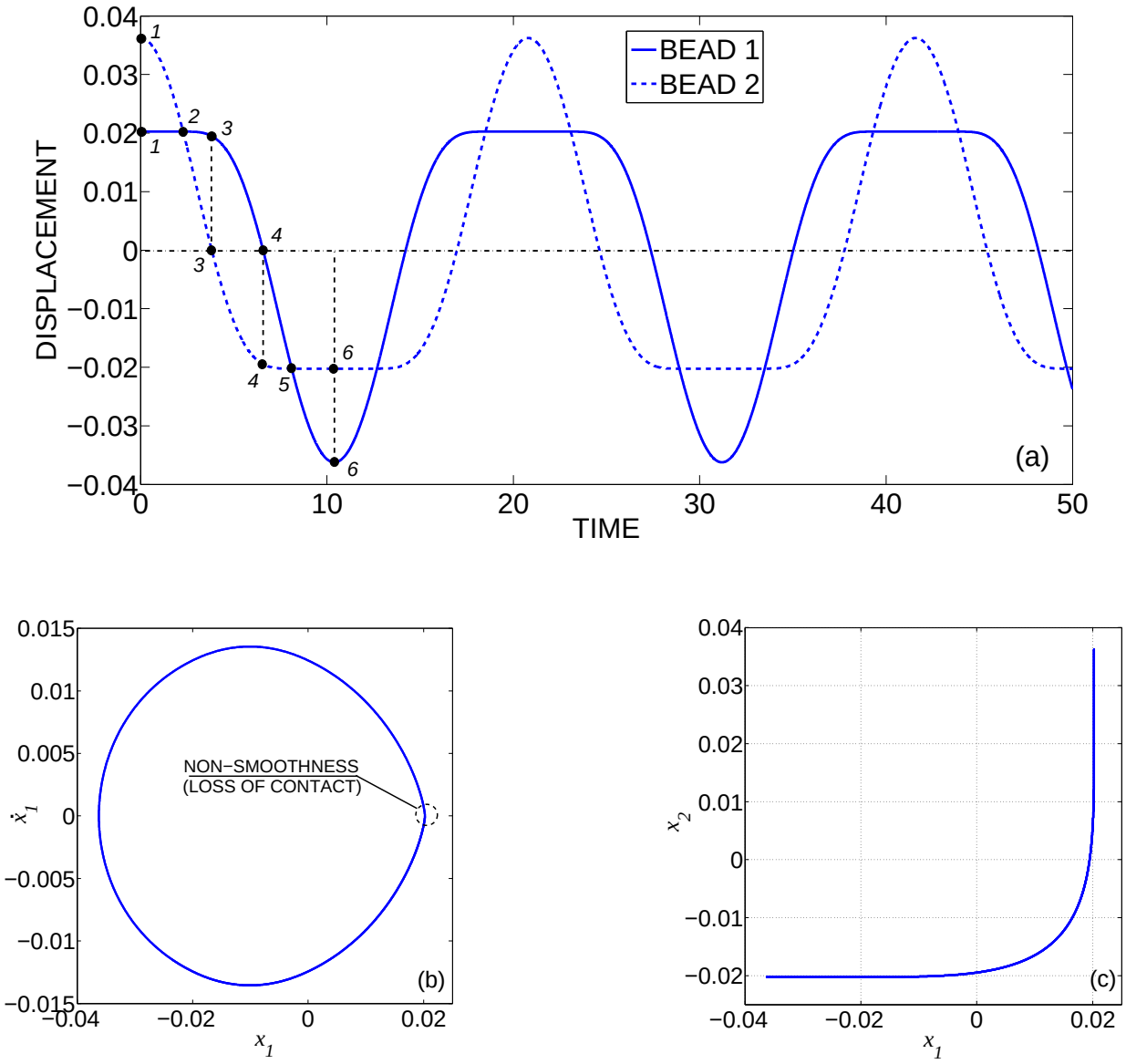

Figure 2.3: The in-phase NNM for the two-bead granular system for $h = 0.0001$, (a) time series; (b) depiction in a projection of the phase plane; (c) modal curve in the configuration plane.

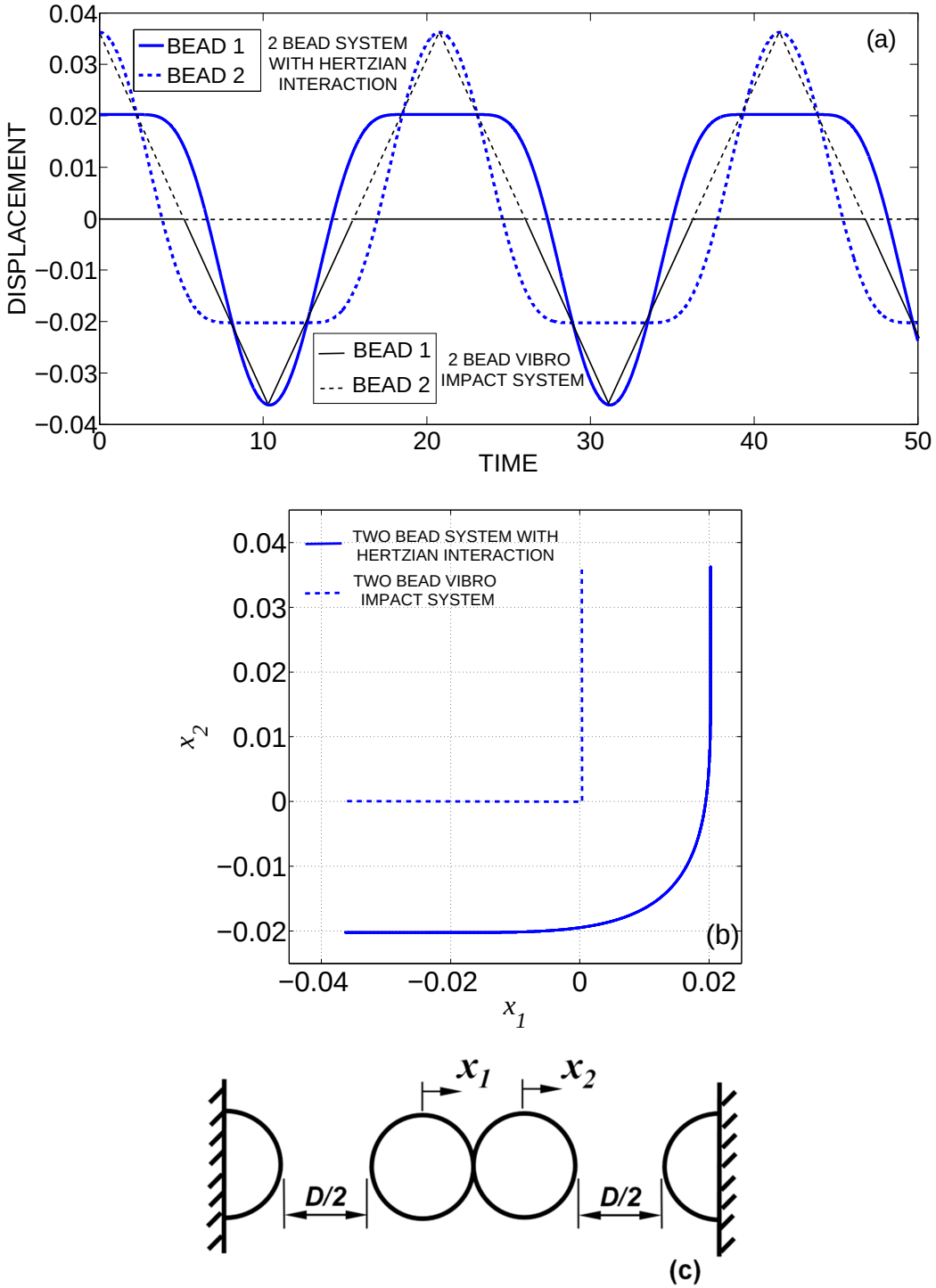

Figure 2.4: Comparing the dynamics of the two-bead granular system to the dynamics of the corresponding vibro-impacting one, (a) time series; (b) modal curve in the configuration plane; (c) two bead vibro-impact system.

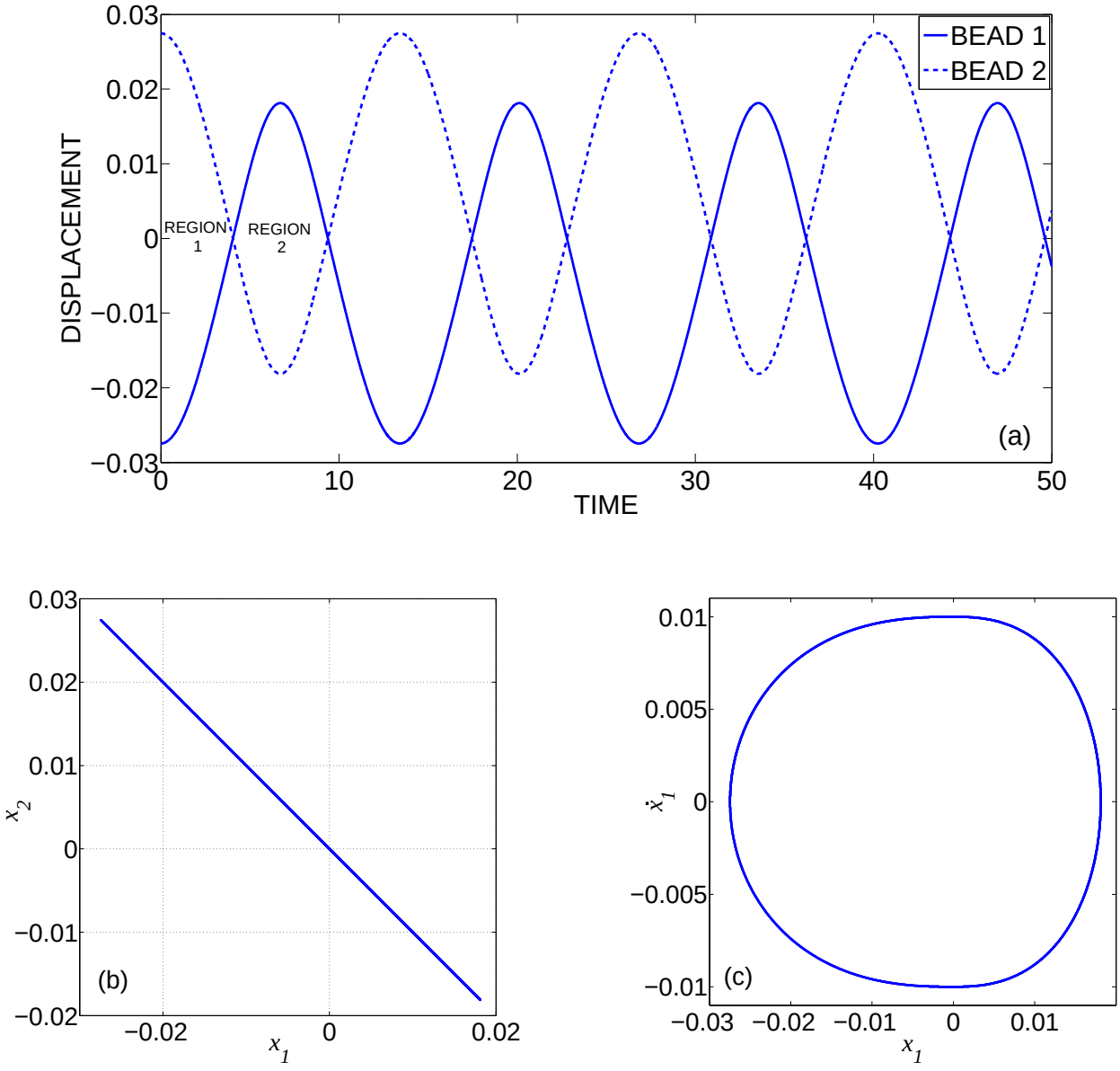

Figure 2.5: The out-of-phase NNM for the two-bead granular system for $h = 0.0001$, (a) time series; (b) modal curve in the configuration plane; (c) depiction in a projection of the phase plane.

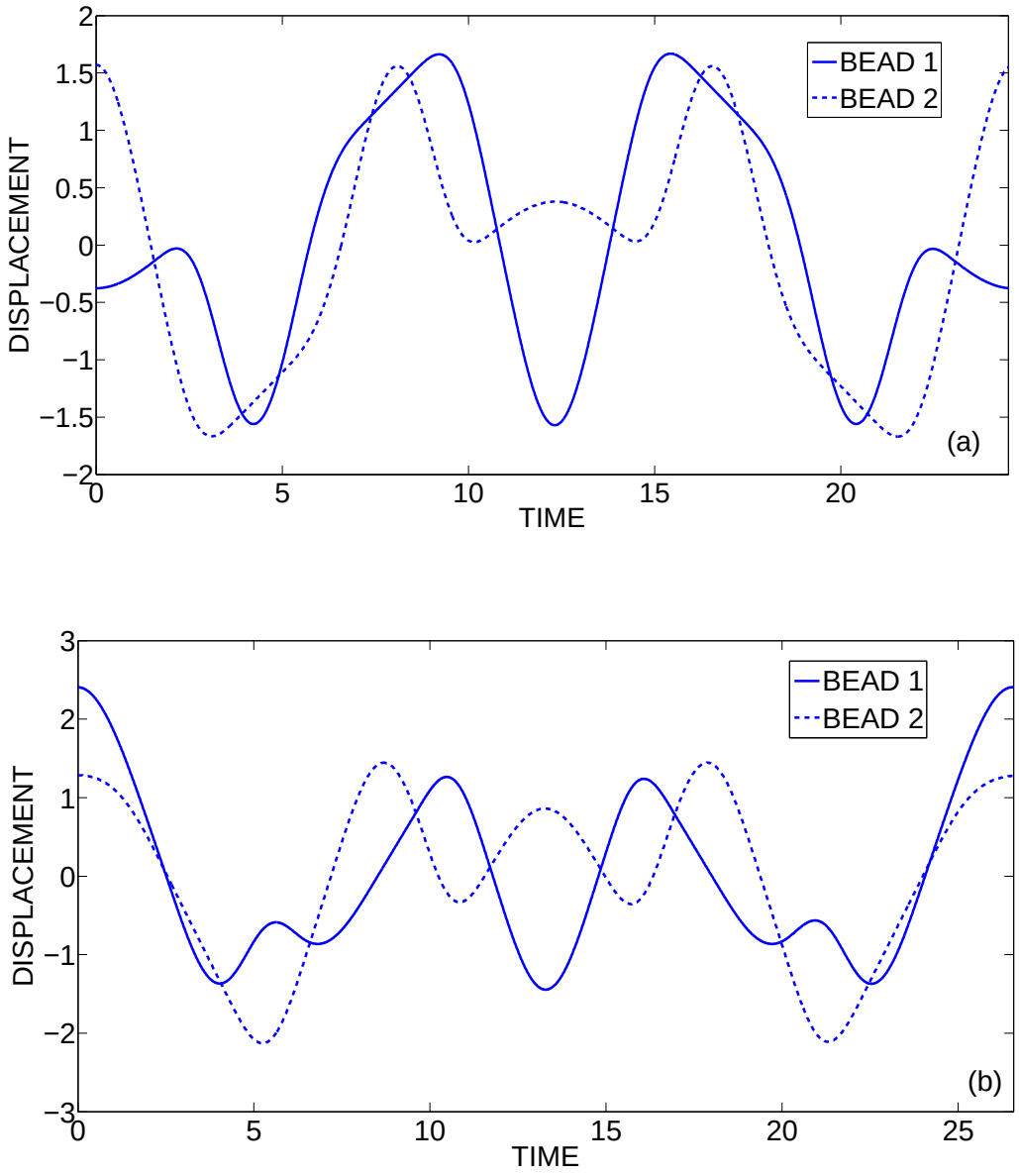

Figure 2.6: Subharmonic orbits of the two-bead system for $h = 0.0001$: (a) 1: 3; (b) 2: 3 ratios between the frequencies of the beads.

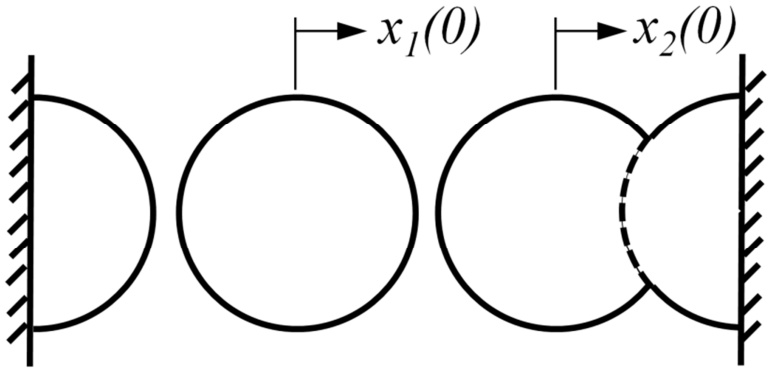

Figure 2.7: Initial conditions for applying the shooting method for the in-phase NNM (two-bead system).

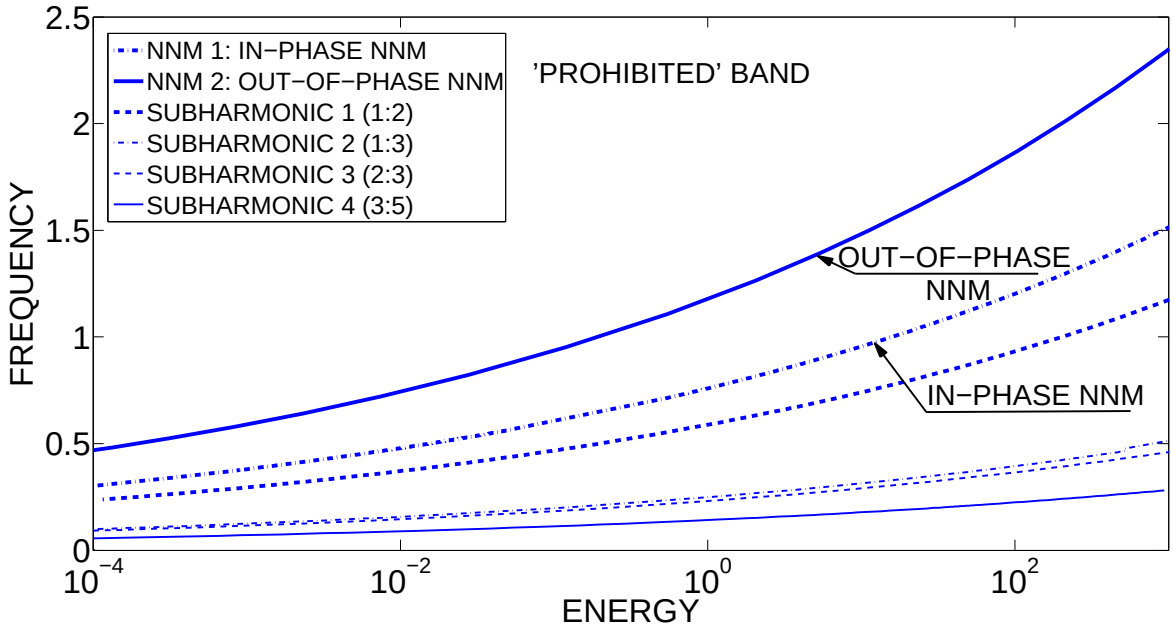

Figure 2.8: Representation of the modes of the two-bead system in the frequency – energy plot (FEP).

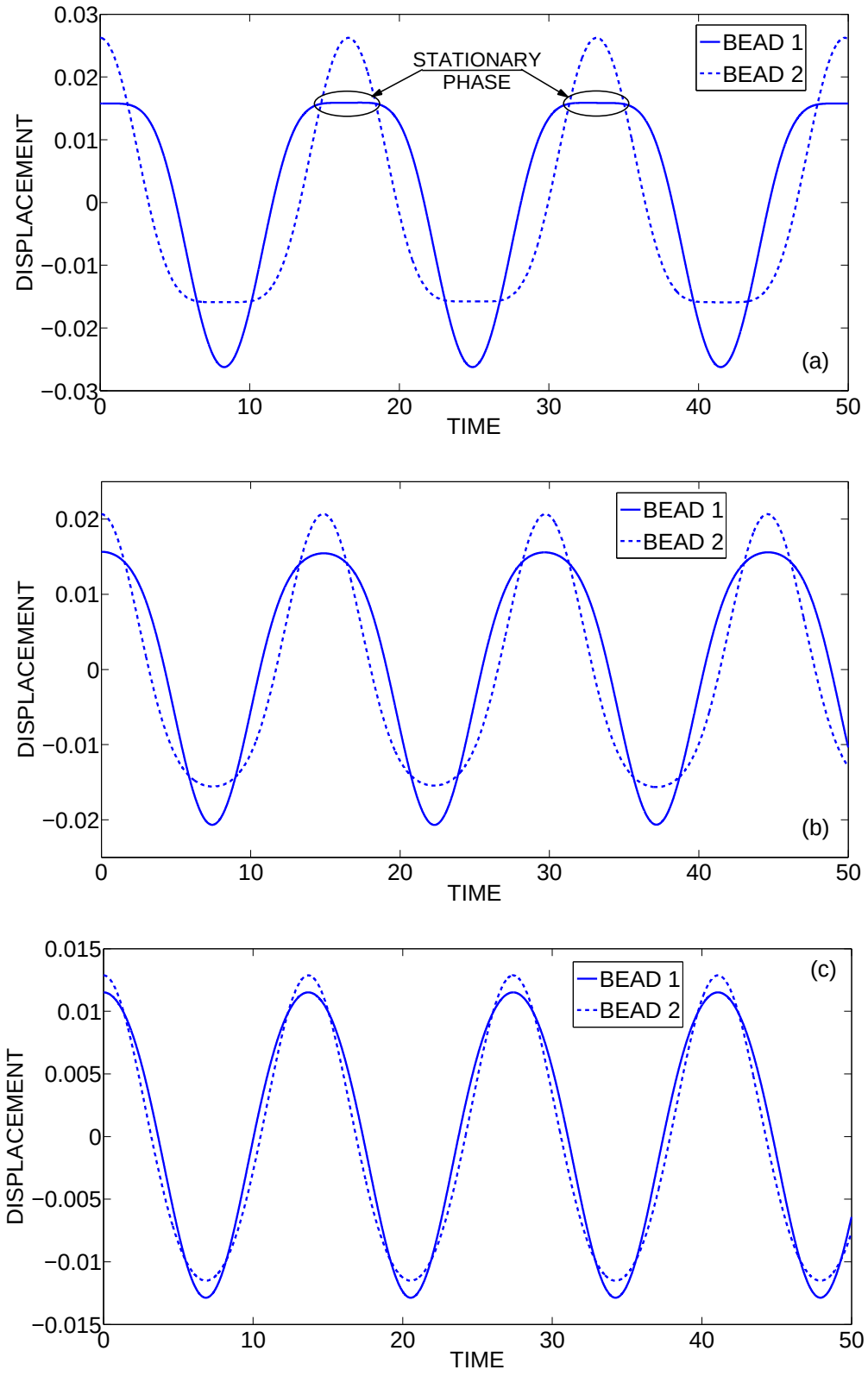

Figure 2.9: The in-phase NNM for the two-bead pre-compressed granular system for $h = 0.0001$, (a) pre-compression $\Delta = 0.01$; (b) $\Delta = 0.015$; (c) $\Delta = 0.02$.

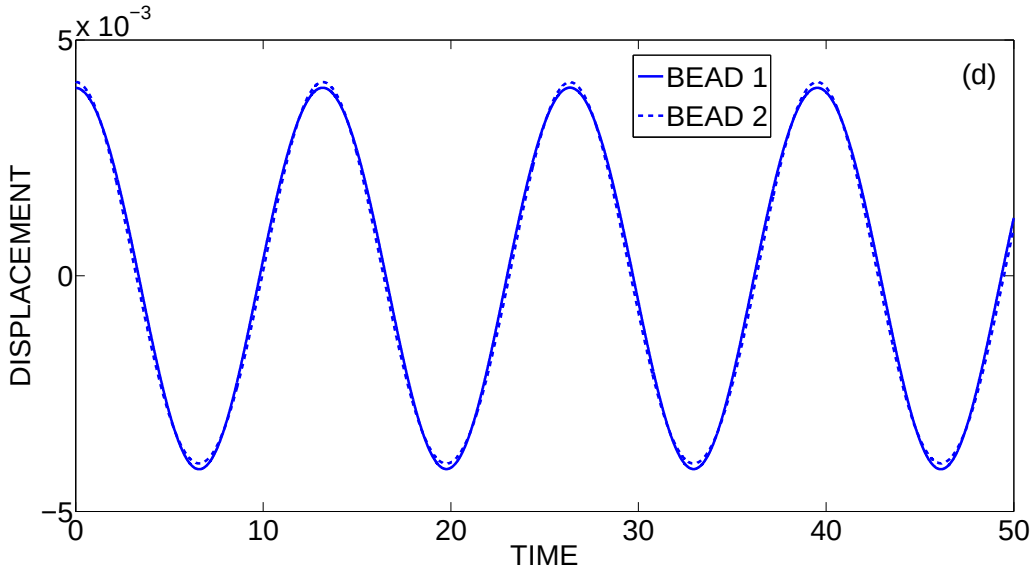

Figure 2.9 (cont'd): The in-phase NNM for the two-bead pre-compressed granular system for $h = 0.0001$, (d) pre-compression $\Delta = 0.023$.

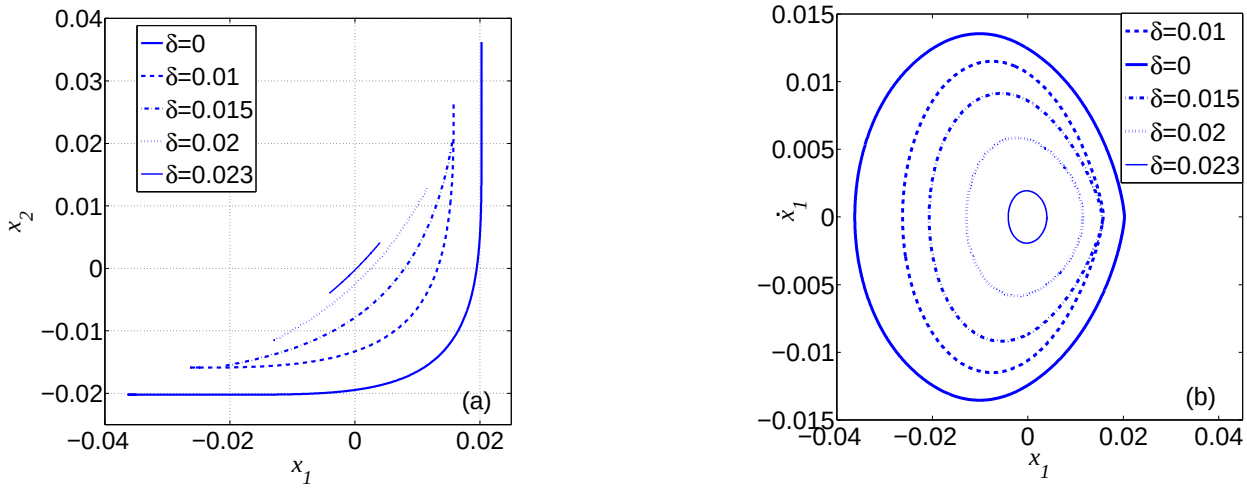

Figure 2.10: The in-phase NNM for the two-bead pre-compressed granular system for $h = 0.0001$, (a) model curves in configuration plane; (b) depiction in a projection of the phase plane for varying pre-compression.

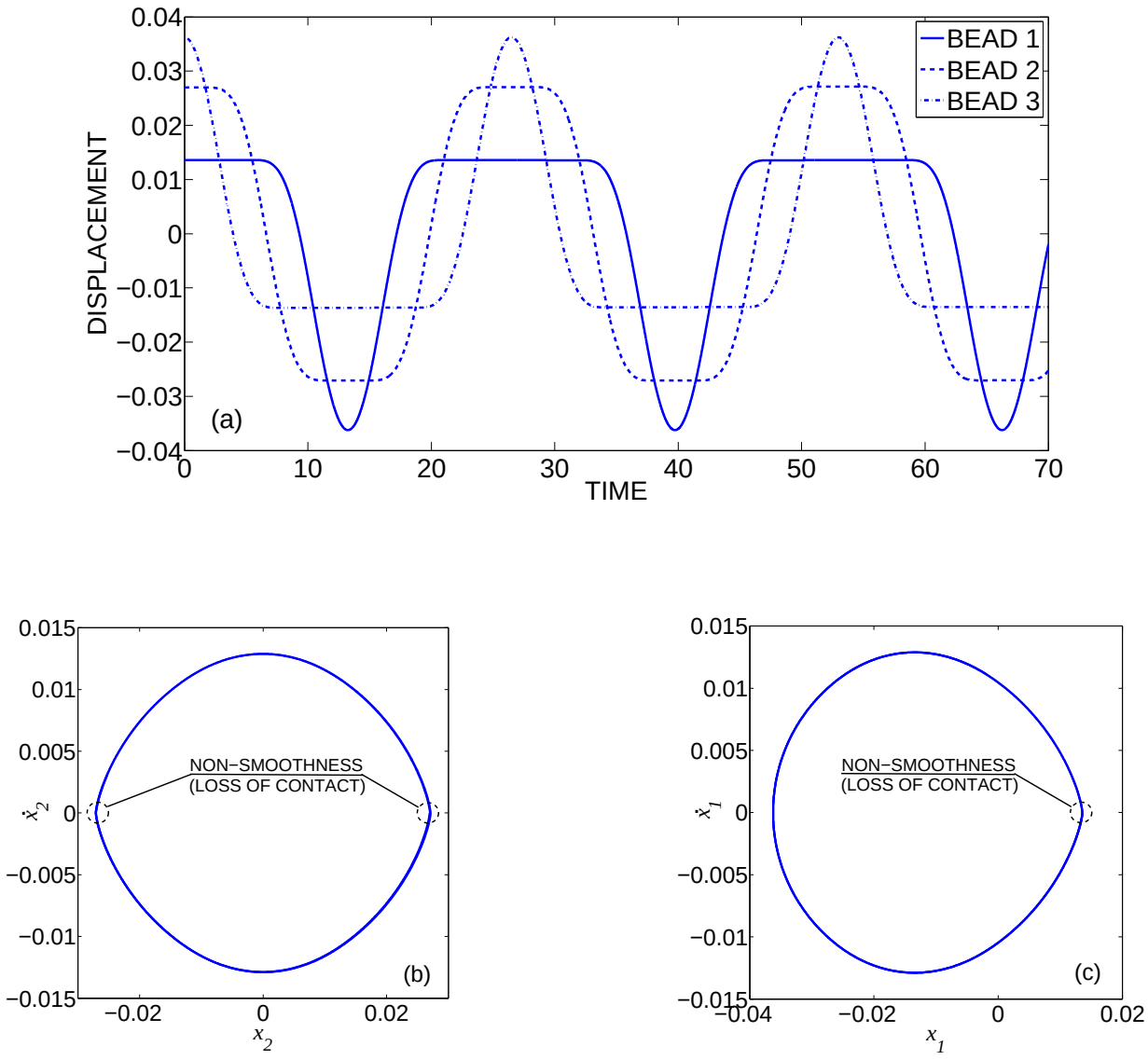

Figure 2.11: The in-phase NNM (pseudo-traveling wave) for the three-bead granular system for $h = 0.0001$, (a) time series; (b, c) depiction in projections of the phase plane.

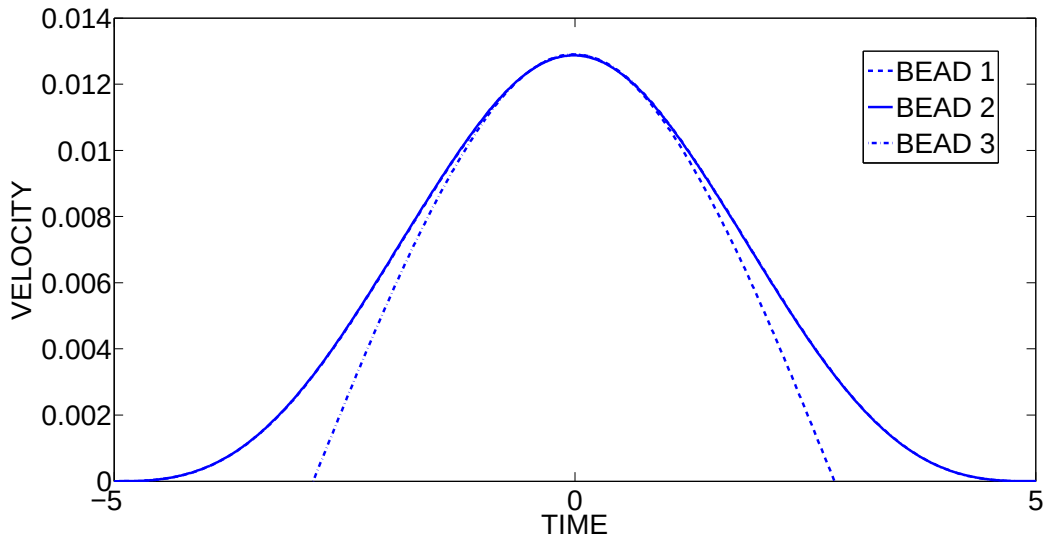

Figure 2.12: Velocity profiles for the in-phase NNM (pseudo-traveling wave) of the three-bead granular system for $h = 0.0001$.

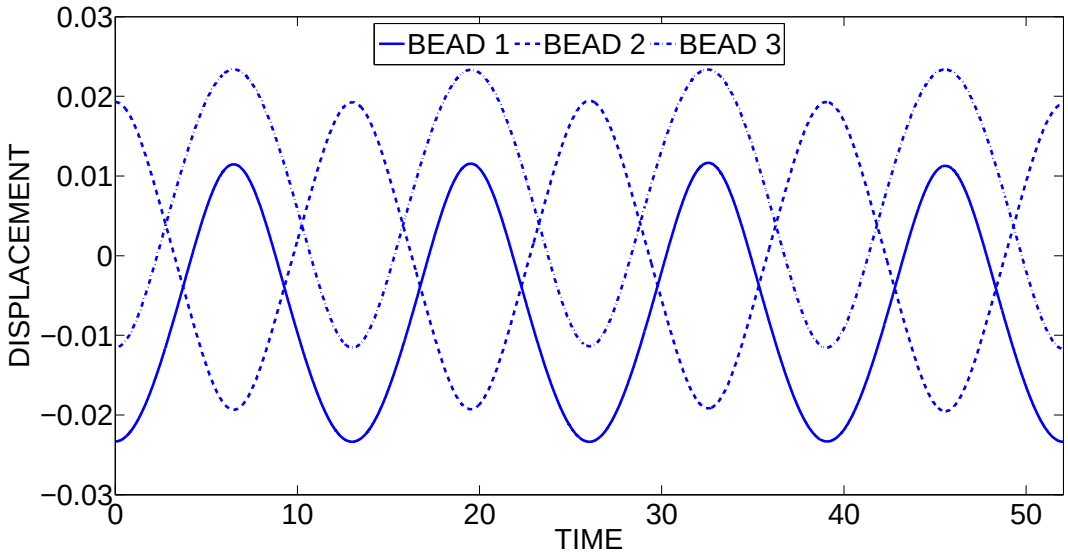

Figure 2.13: The out-of-phase NNM for the three-bead granular system for $h = 0.0001$.

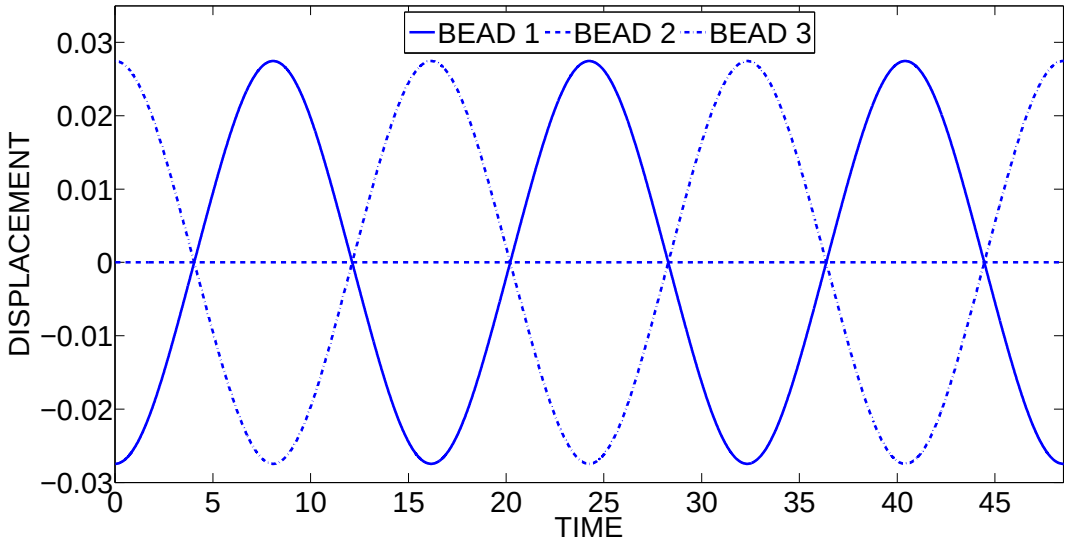

Figure 2.14: The NNM with stationarity of the central bead for the three-bead granular system for $h = 0.0001$.

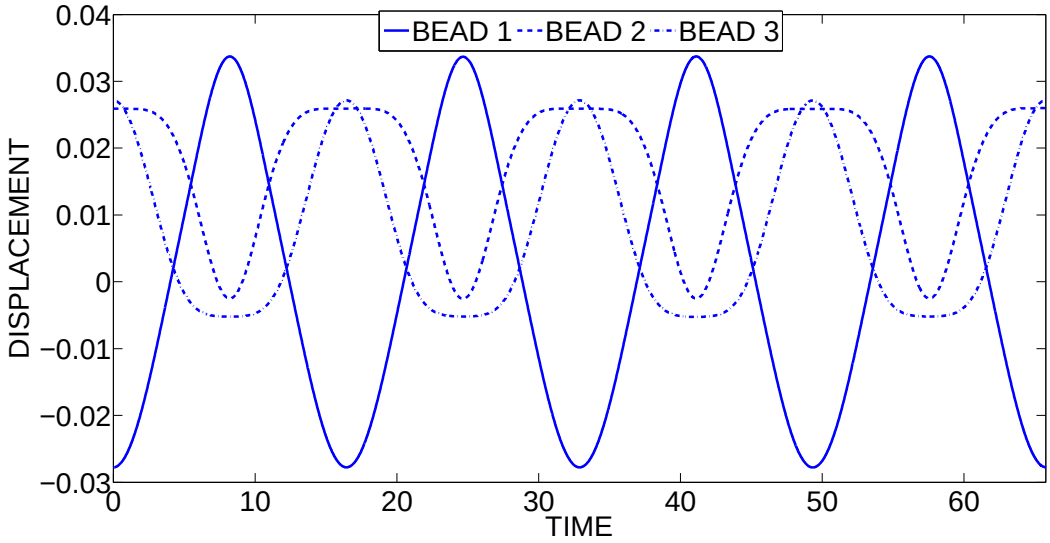

Figure 2.15: The localized NNM for the three-bead granular system for $h = 0.0001$.

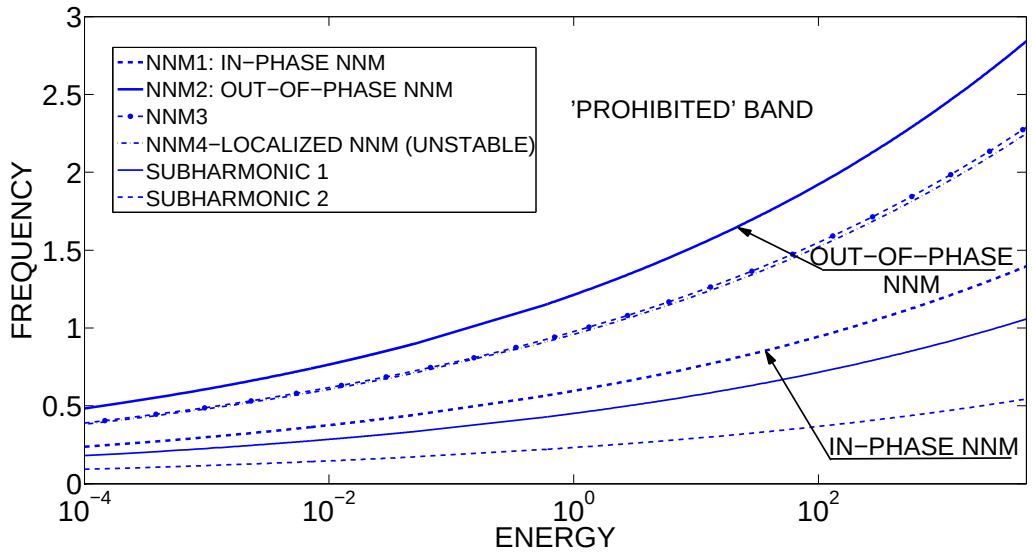

Figure 2.16: Representation of different modes of the three-bead system in the frequency – energy plot (FEP).

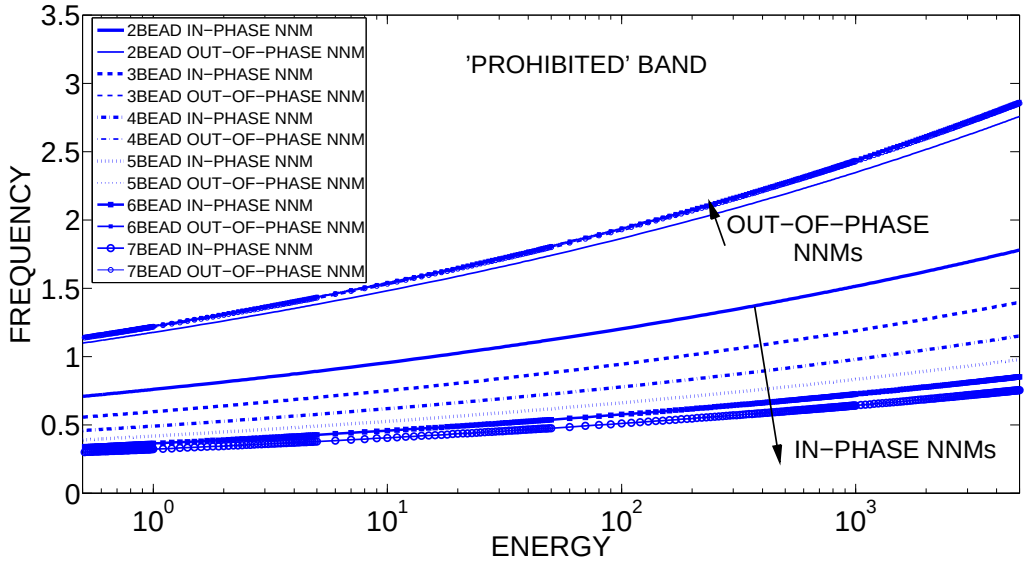

Figure 2.17: Representation of the in-phase and out-of-phase NNMs in the frequency – energy plot (FEP) for granular systems from two to seven beads; in the limit of infinite number of beads the FEP is partitioned into a propagation and an attenuation band.

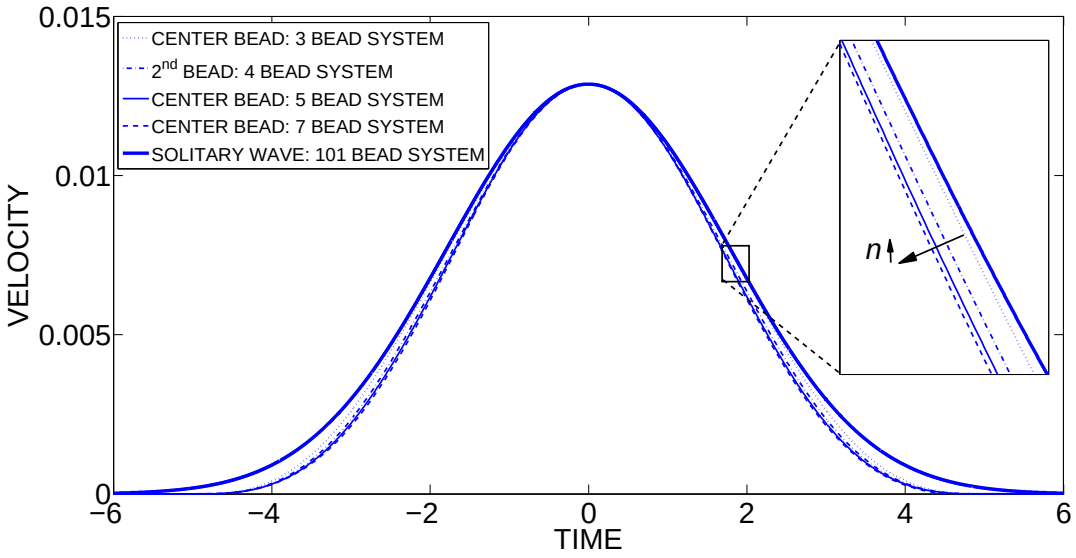

Figure 2.18: Comparison of the velocity profiles of the in-phase NNMs of fixed-fixed n −bead granular systems to the velocity profile of the solitary wave studied by Nesterenko [41].

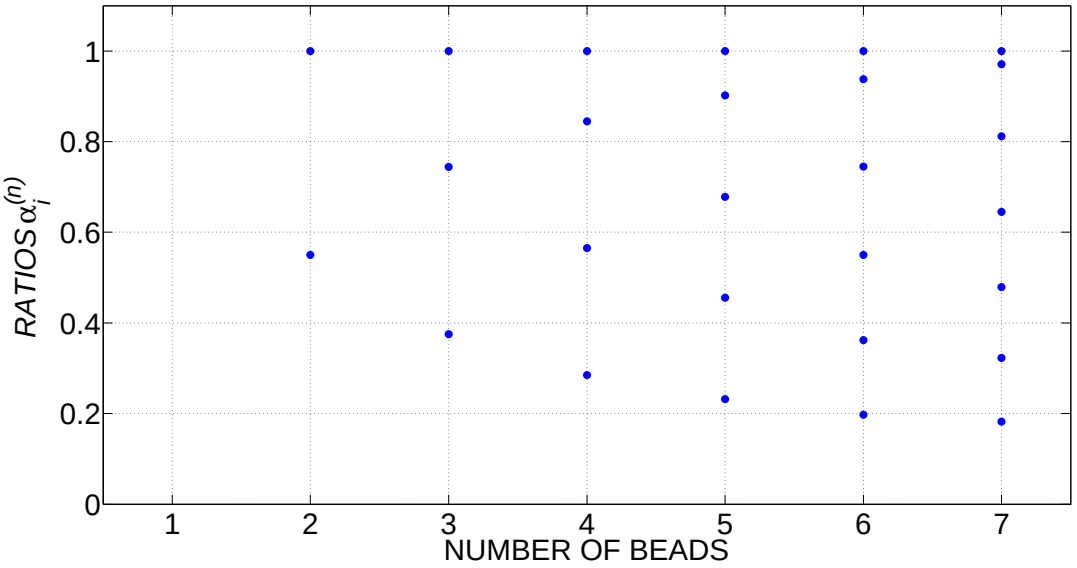

Figure 2.19: Coefficients $\alpha_i^{(n)}$, $i = 1, \dots, n-1$ for systems with $n = 2, \dots, 7$ for the in-phase NNMs of the fixed-fixed granular system, with $\alpha_n^{(n)} = 1$.

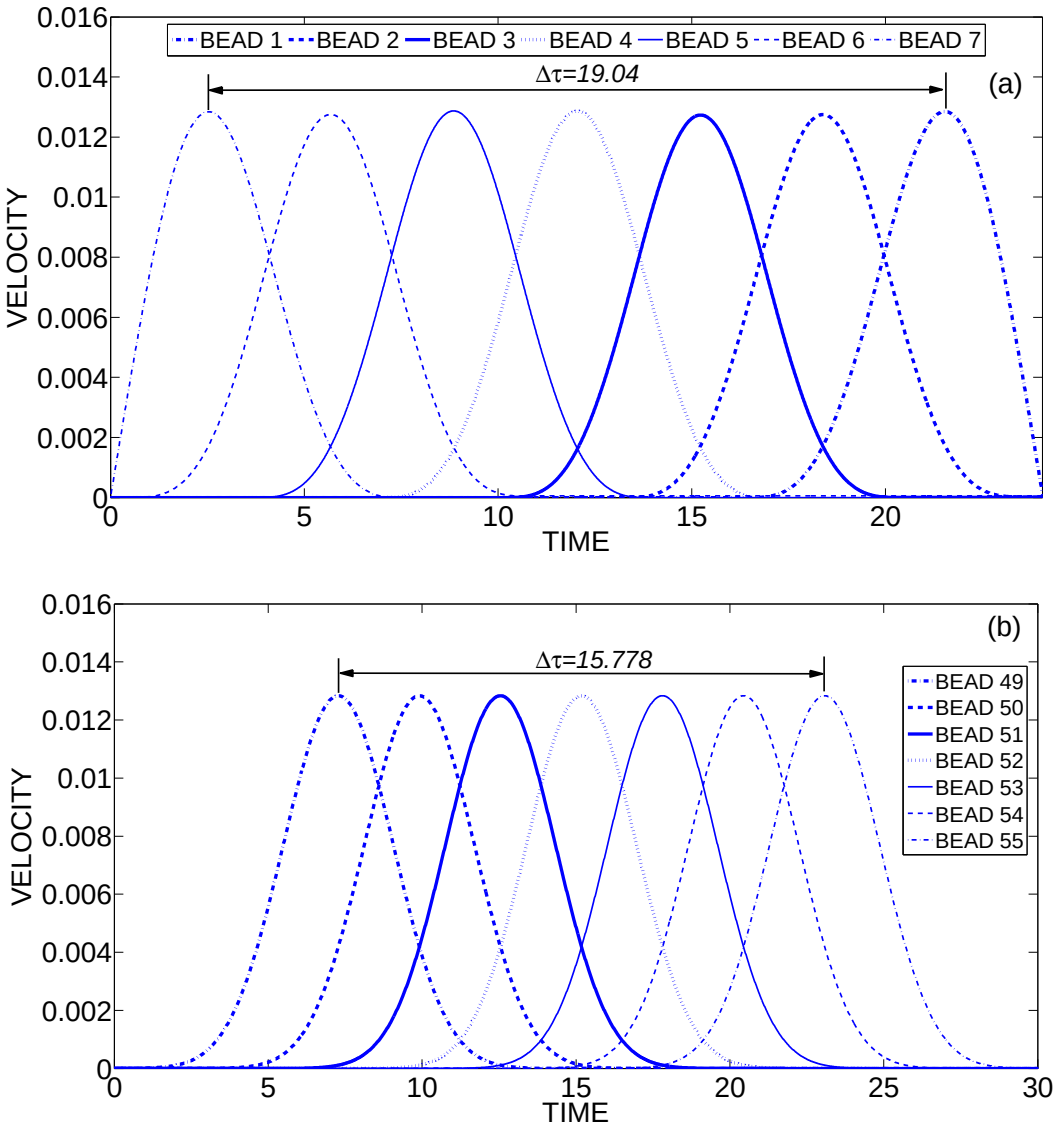

Figure 2.20: Velocity profiles of seven adjacent beads: (a) in-phase NNM; (b) the solitary wave [41]; time delays in terms of normalized time τ.

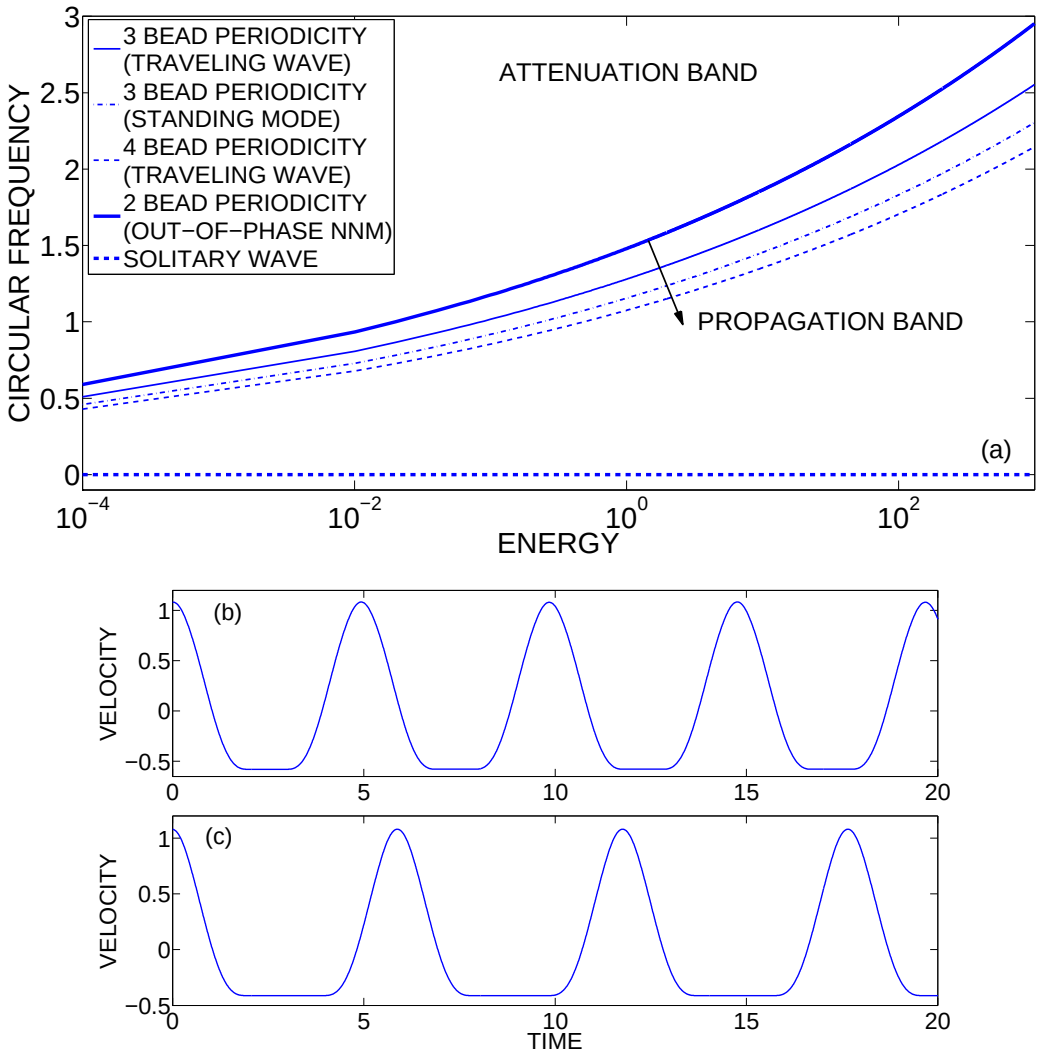

Figure 2.21: Traveling waves inside the propagation band (PB) of the FEP of the infinite granular chain [63], the attenuation band (AB) is also indicated, (a) Frequency – energy curves; (b) velocity profile of a bead of 3 bead periodicity traveling wave inside the PB for energy $h = 1$; (c) velocity profile of a bead of 4 bead periodicity traveling wave inside the PB for energy $h = 1$.

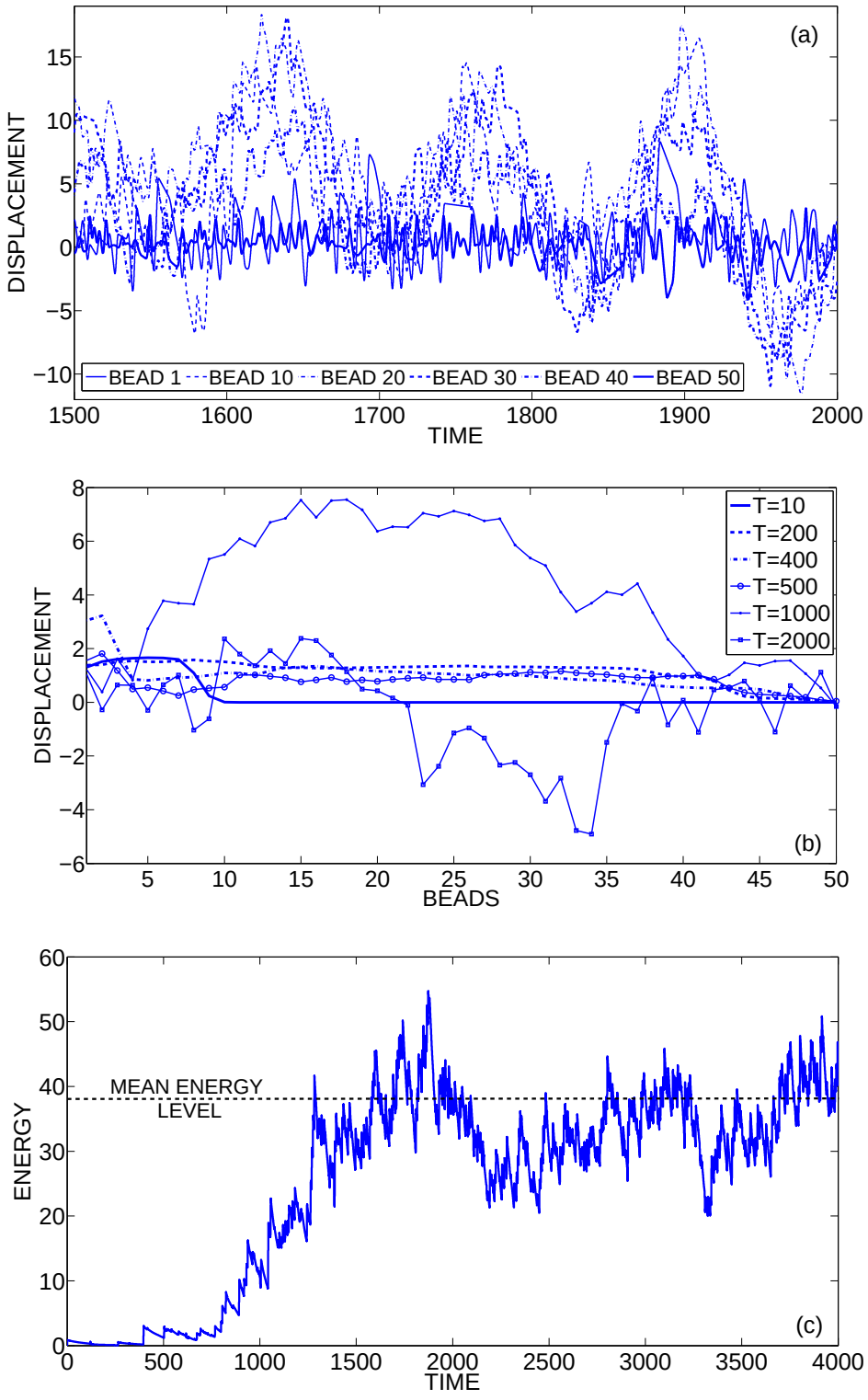

Figure 2.22: Forced response of the 50-bead granular chain for harmonic wall excitation $x_0 = 1.5\sin(\tau)$, (a) Transient responses of selected beads for $1500 < \tau < 2000$; (b) snapshots of chain deformation at selected time instants; (c) evolution of total energy in the chain.

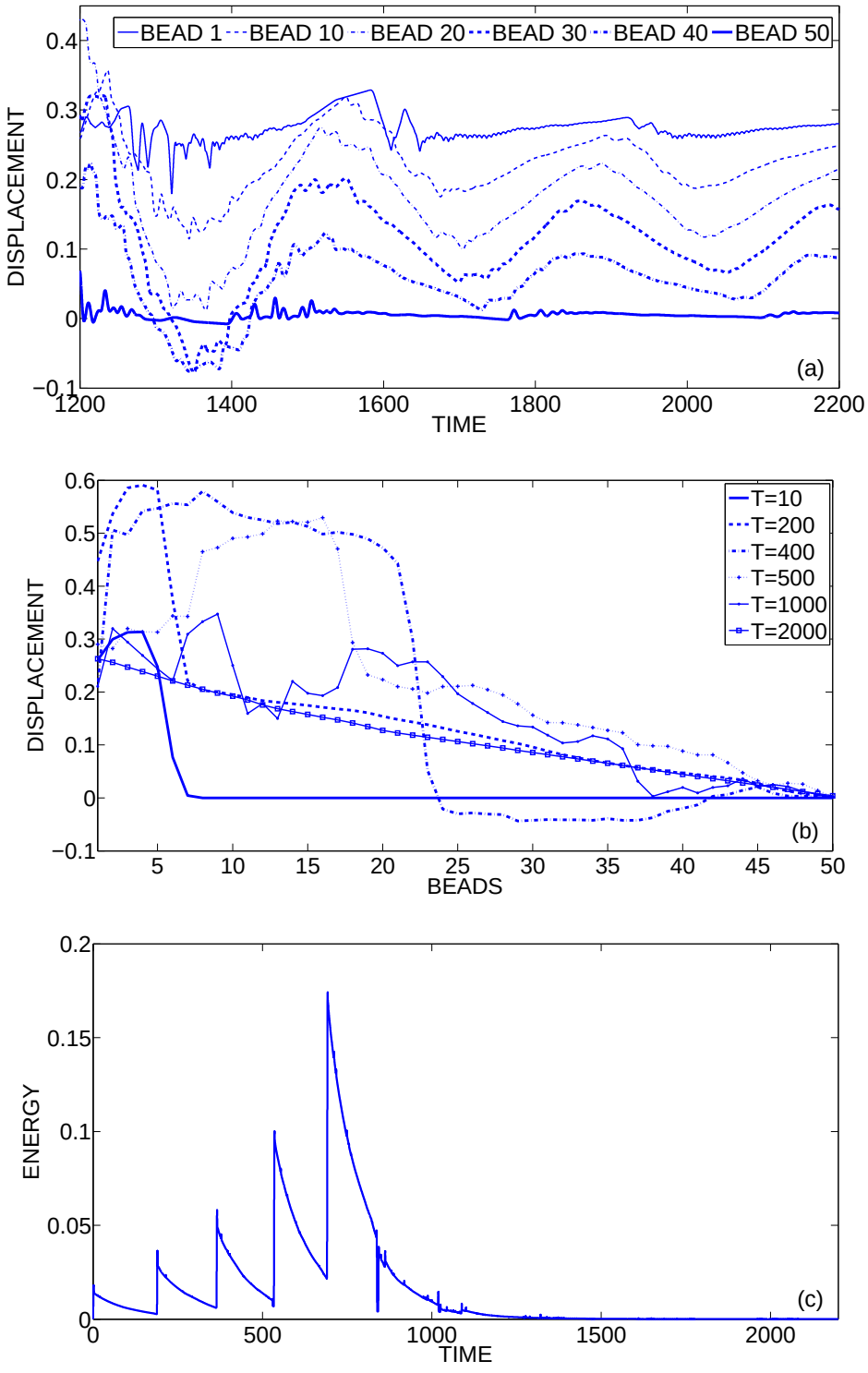

Figure 2.23: Forced response of the 50-bead granular chain for harmonic wall excitation $x_0 = 0.3\sin(\tau)$, (a) Transient responses of selected beads for $1000 < \tau < 2000$; (b) snapshots of chain deformation at selected time instants; (c) evolution of total energy in the chain.

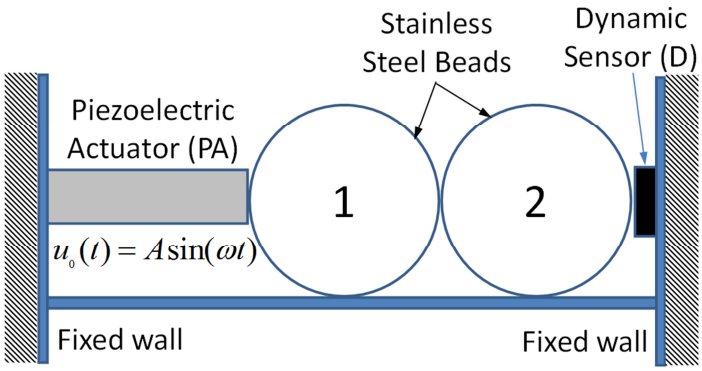

Figure 2.24: Experimental setup realized by Prof. C. Daraio's group at the California Institute of Technology.

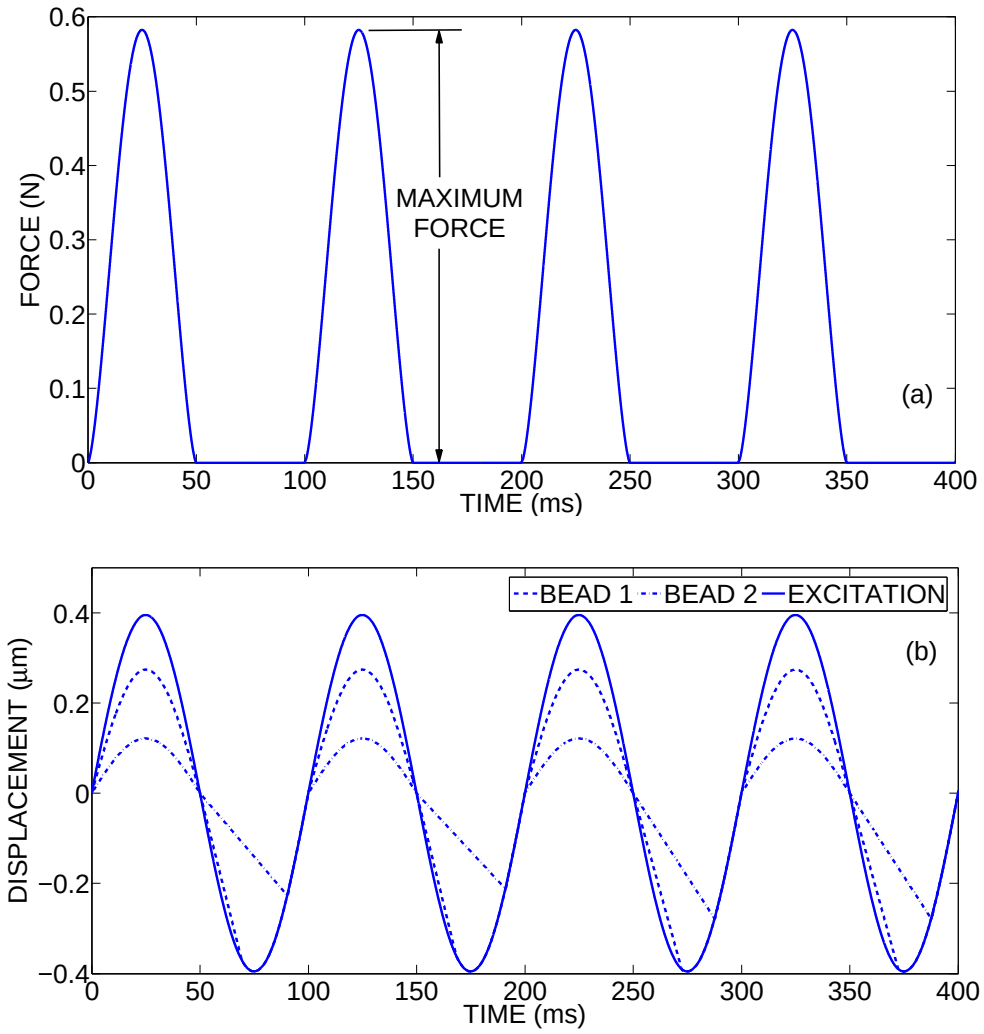

Figure 2.25: Response of the two-bead system for excitation frequency equaling $f = 10$ Hz and amplitude $A = 0.3951$ μm, (a) Transmitted force on the boundary (the site of the dynamic sensor); (b) bead displacements.

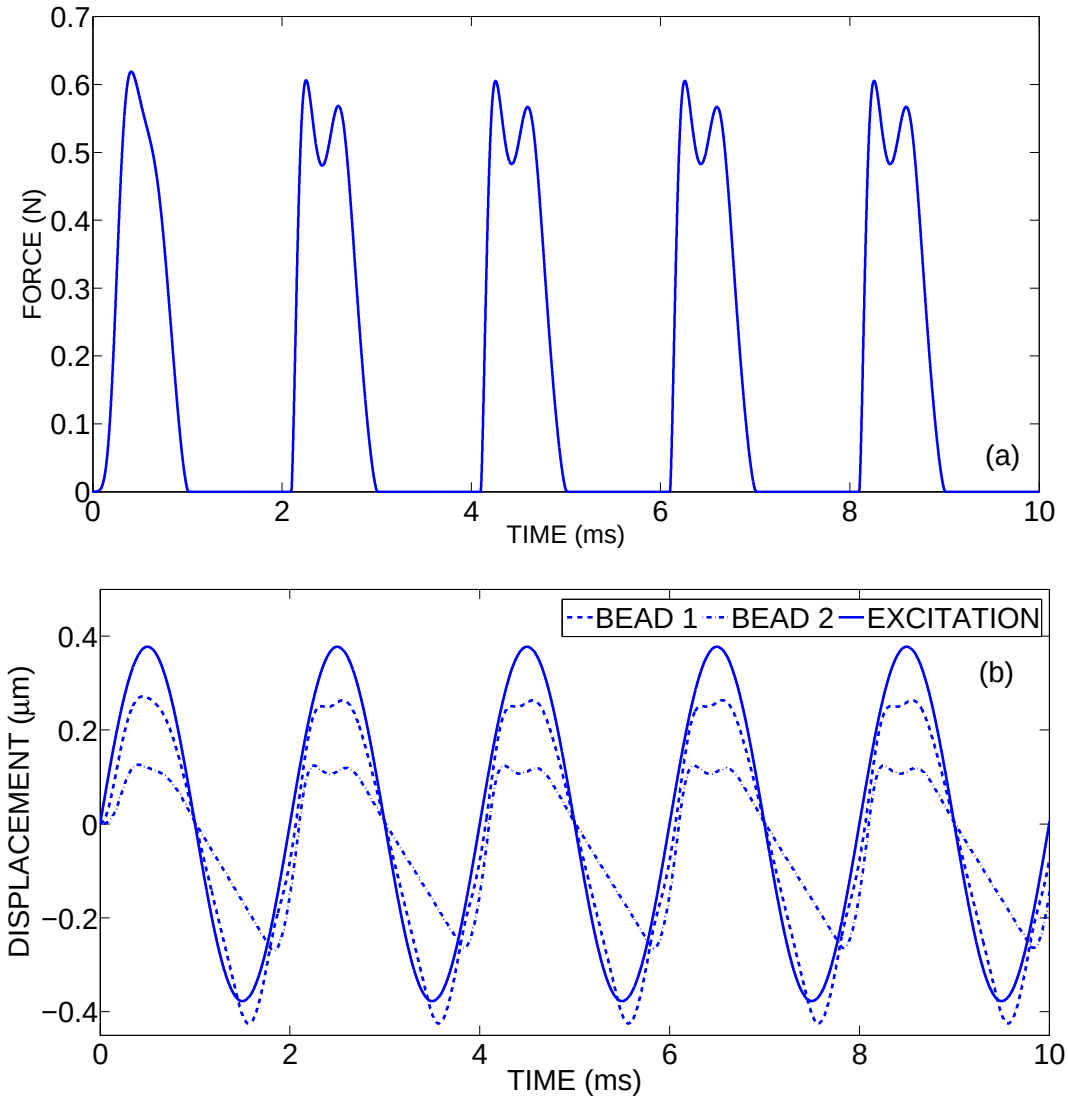

Figure 2.26: Response of the two-bead system for excitation frequency equaling $f = 500$ Hz and amplitude $A = 0.3775$ μm, (a) Transmitted force on the boundary (the site of the dynamic sensor); (b) bead displacements.

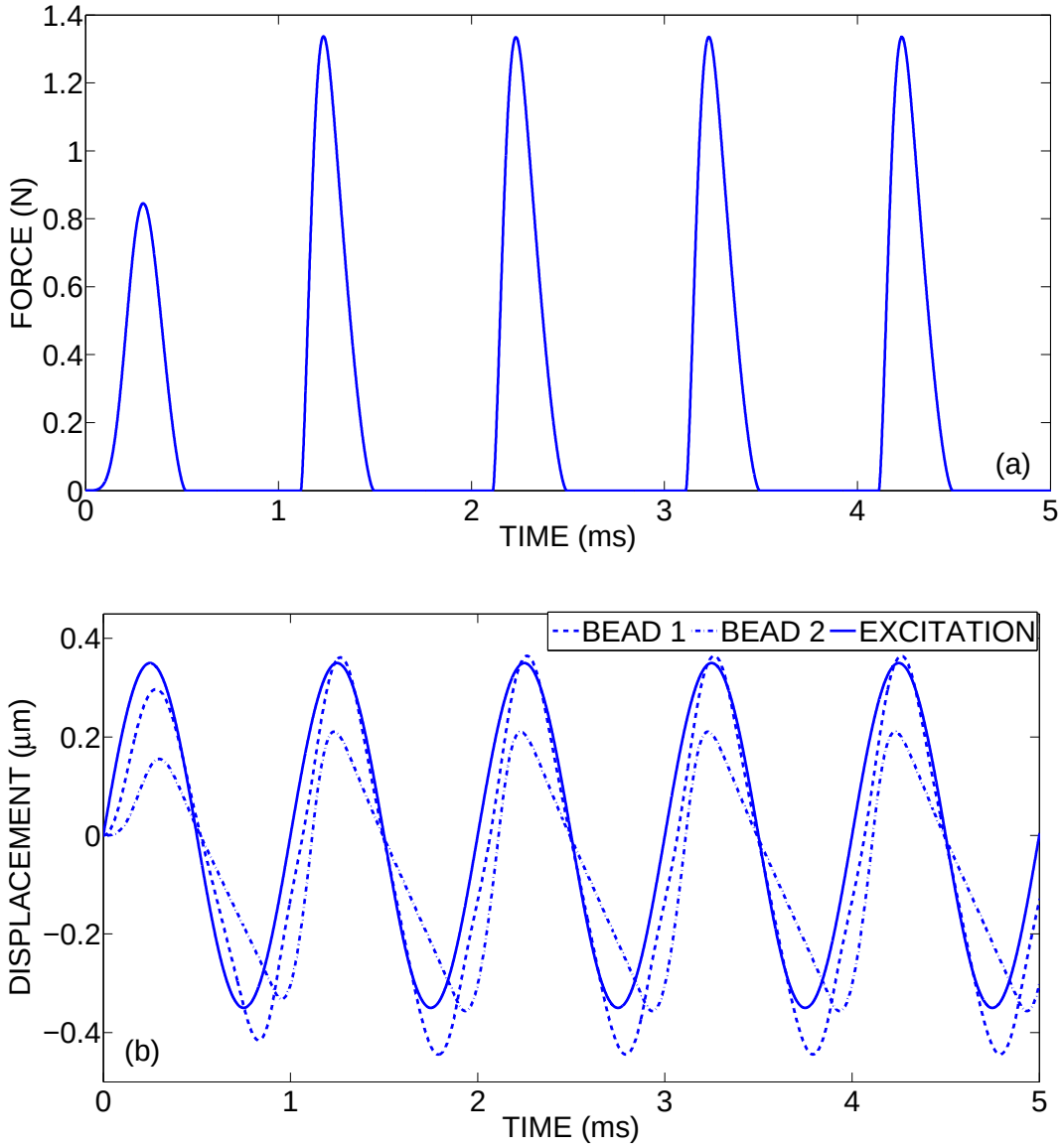

Figure 2.27: Response of the two-bead system for excitation frequency equaling $f = 1000$ Hz and amplitude $A = 0.35$ μm, (a) Transmitted force on the boundary (the site of the dynamic sensor); (b) bead displacements.

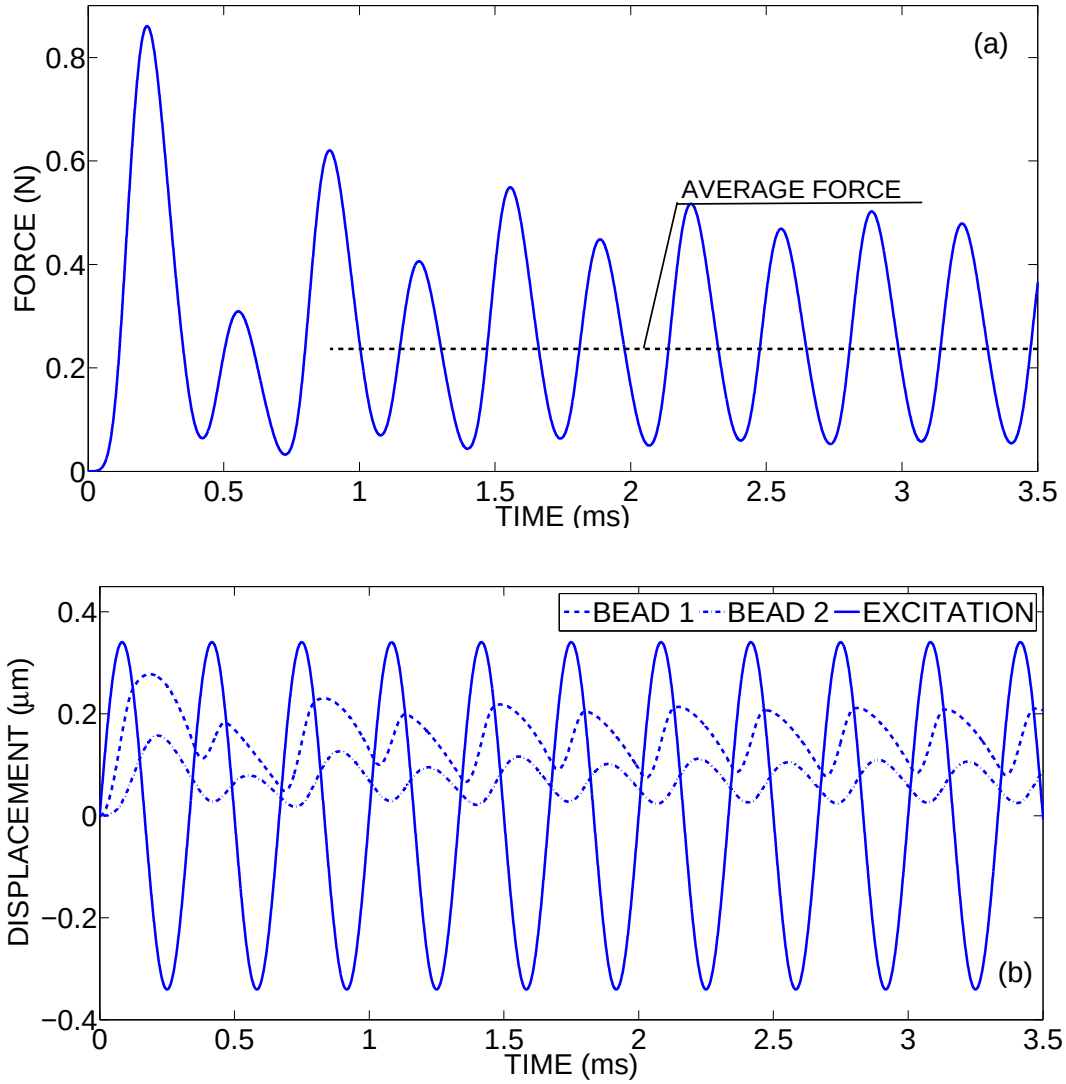

Figure 2.28: Response of the two-bead system for excitation frequency equaling $f = 3000$ Hz and amplitude $A = 0.3408$ μm, (a) Transmitted force on the boundary (the site of the dynamic sensor); (b) bead displacements.

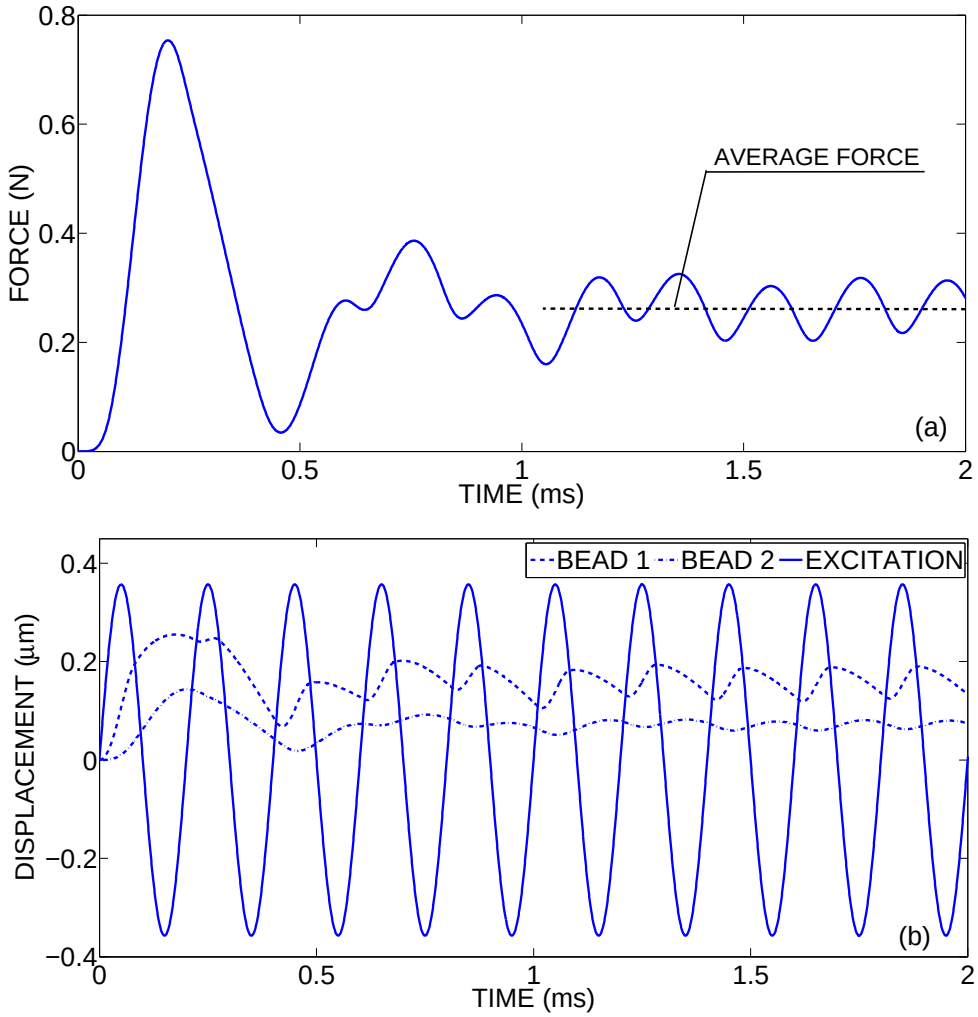

Figure 2.29: Response of the two-bead system for excitation frequency equaling $f = 5000$ Hz and amplitude $A = 0.357$ μm, (a) Transmitted force on the boundary (the site of the dynamic sensor); (b) bead displacements.

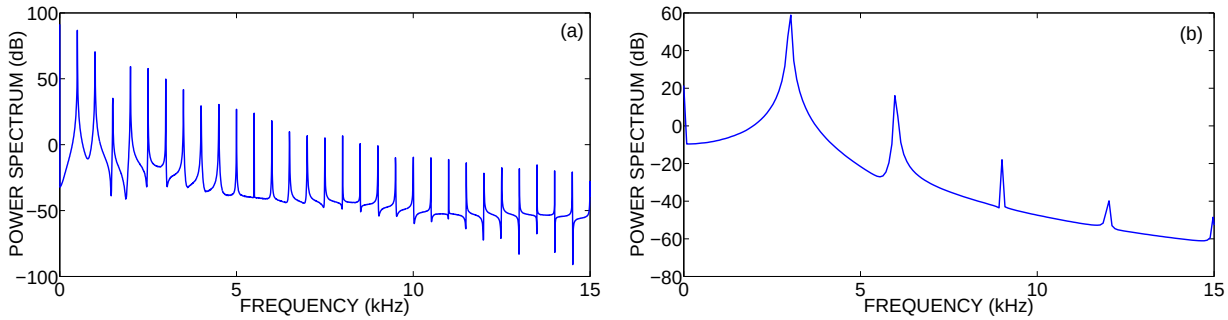

Figure 2.30: Fourier transform of the transmitted force to the dynamic sensor at forcing frequency equaling (a) $f = 500$ Hz; (b) $f = 3000$ Hz.

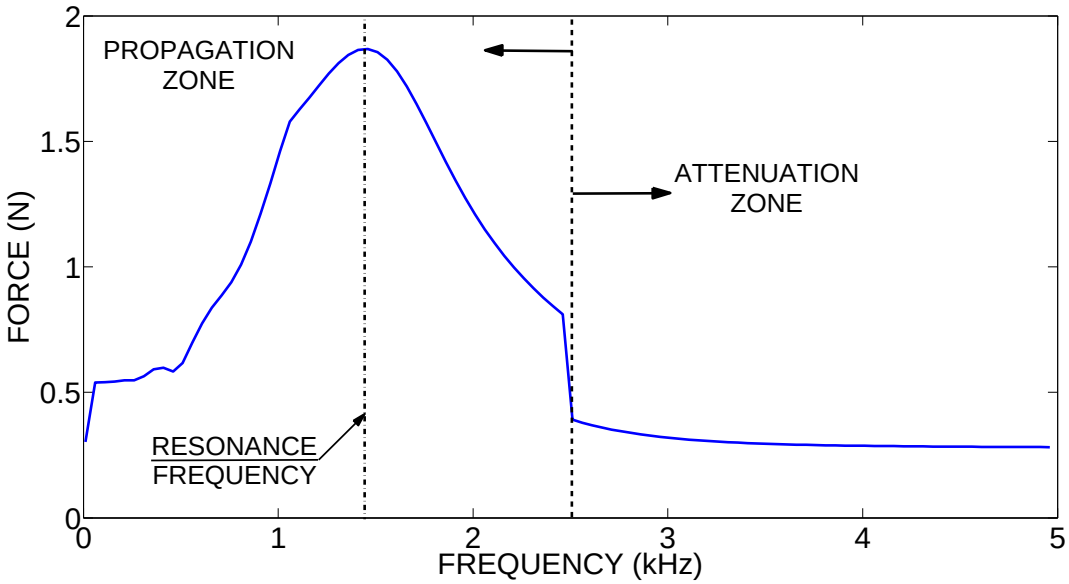

Figure 2.31: Frequency response of the 2 bead system for amplitude of $A = 0.375$ μm.

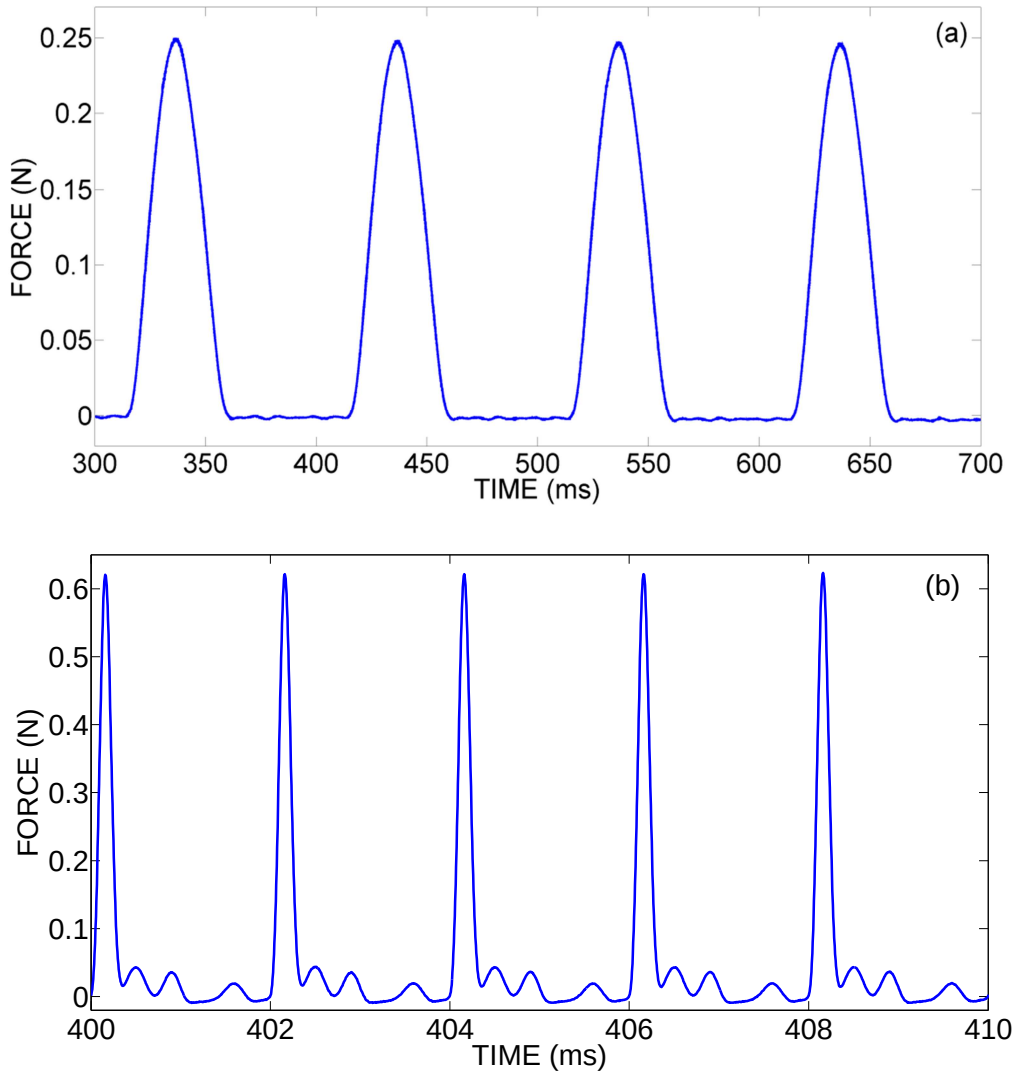

Figure 2.32: Experimental time series of the force at the dynamic sensor at (a) $f = 10$ Hz and $A = 0.3951$ μm; (b) $f = 500$ Hz and $A = 0.3775$ μm.

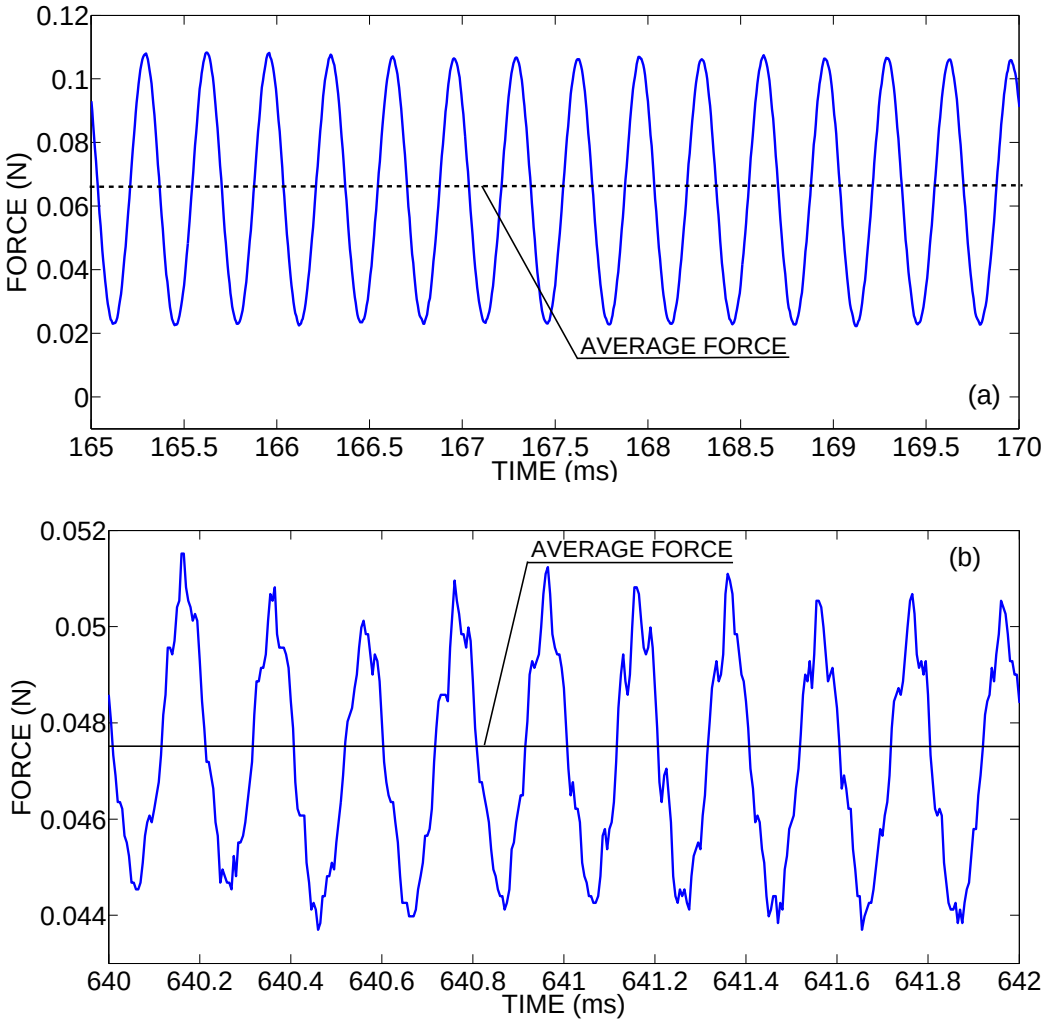

Figure 2.33: Experimental time series of the force at the dynamic sensor at (a) $f = 3000$ Hz and $A = 0.3408$ μm; (b) $f = 5000$ Hz and $A = 0.357$ μm.

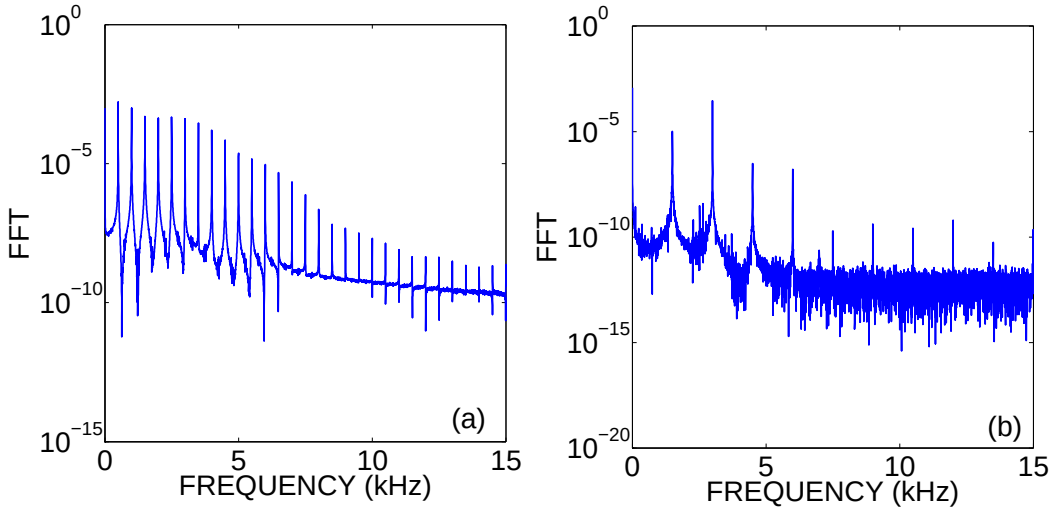

Figure 2.34: Experimental Power Spectral Densities of the force time series of (a) Figure 2.32b: $f = 500$ Hz; (b) Figure 2.33a: $f = 3000$ Hz.

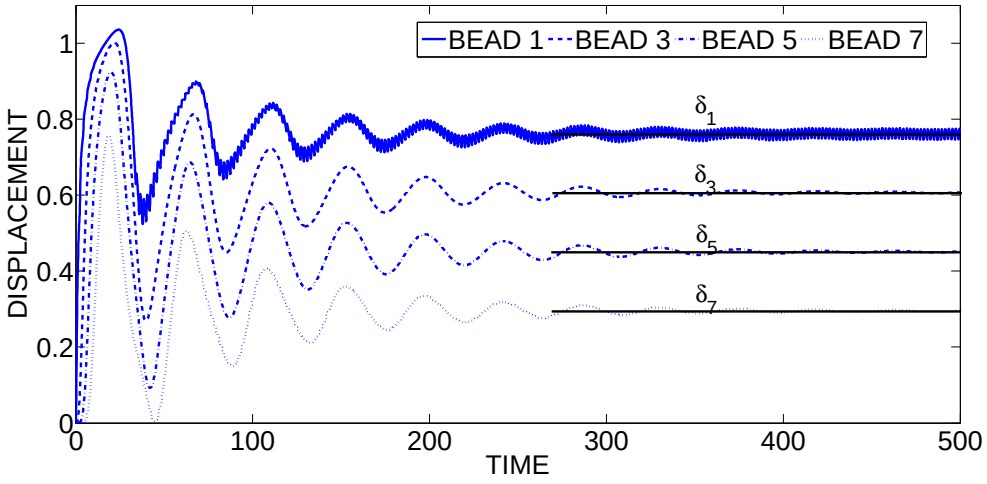

Figure 2.35: Response of 1st, 3rd, 5th and 7th beads of a 10 bead homogeneous chain under harmonic excitation with frequency in the attenuation band.

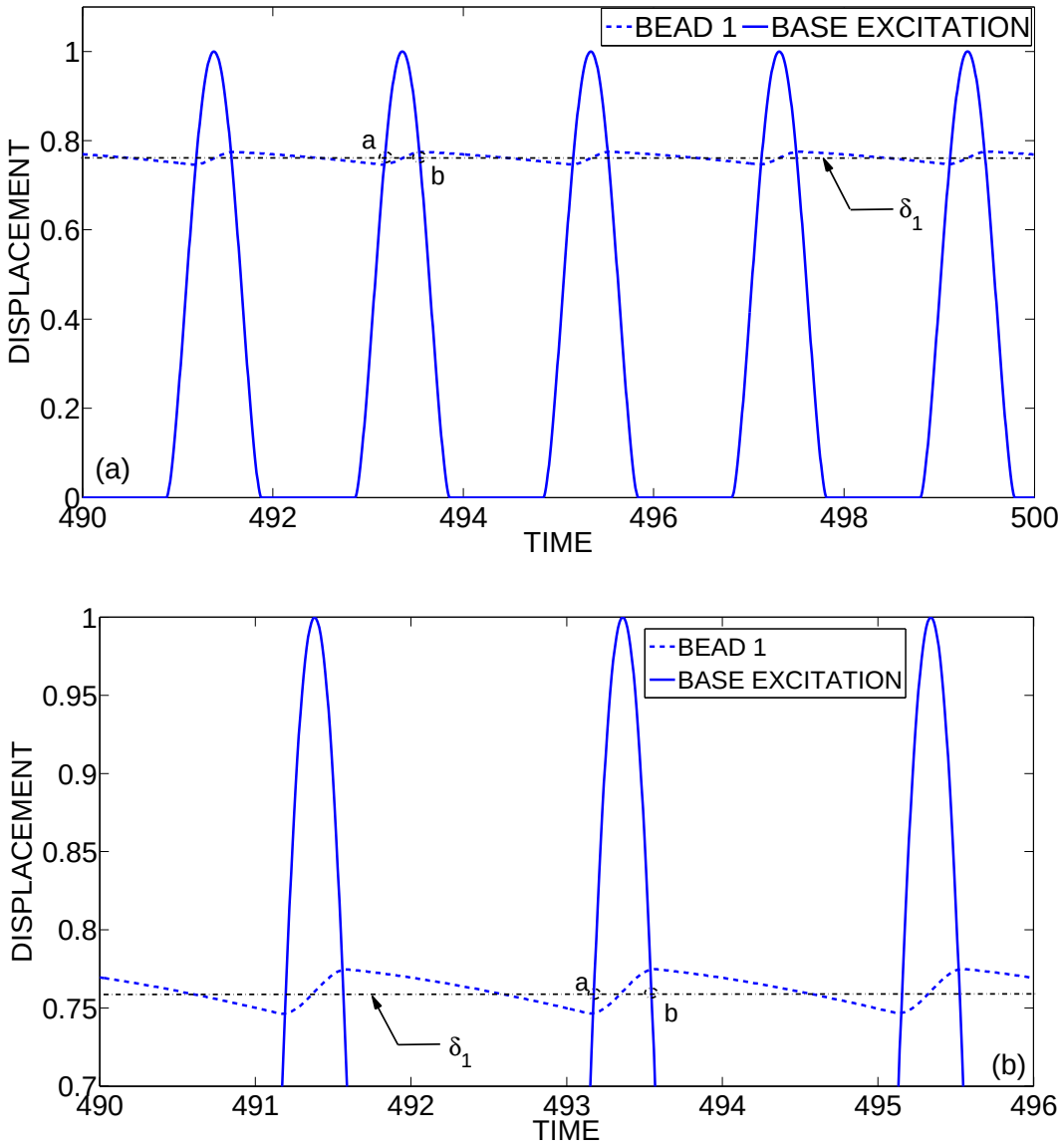

Figure 2.36: Dynamics of the 10-bead homogeneous chain under harmonic excitation with frequency in the attenuation band, (a) Response of the first bead superimposed to the excitation; (b) detail of (a).

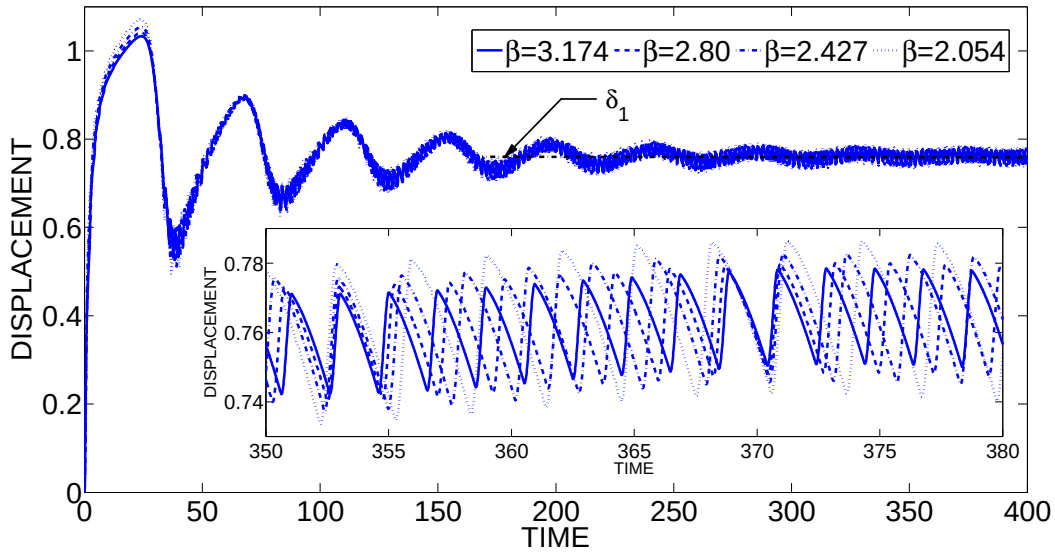

Figure 2.37: Response of first bead of a 10-bead homogeneous chain with varying normalized excitation frequency and fixed normalized excitation amplitude equaling unity (dynamics deep inside the attenuation band).

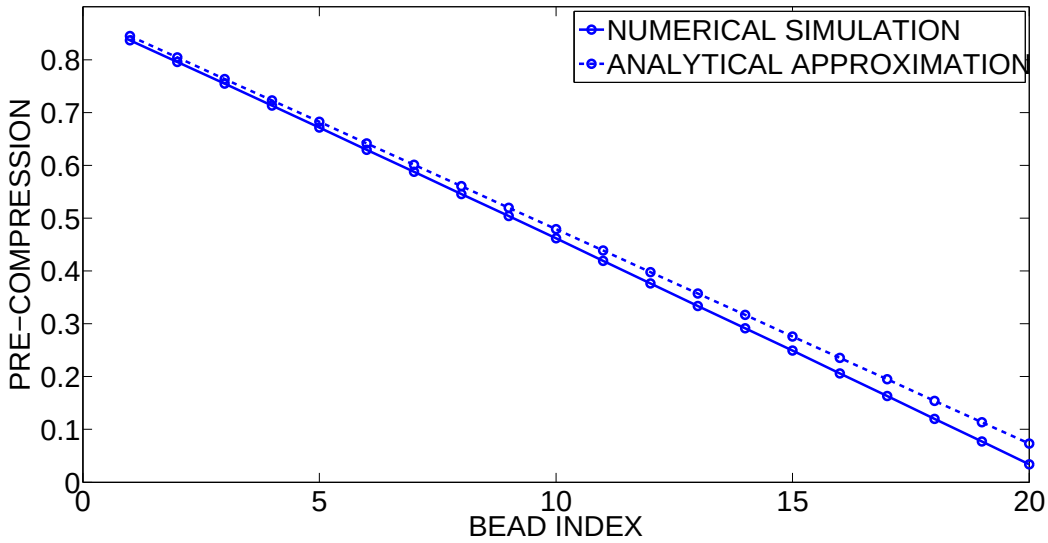

Figure 2.38: Spatial variation of permanent pre-compression (δ_i) in a 20 bead chain when the dynamics is deep in the attenuation band.

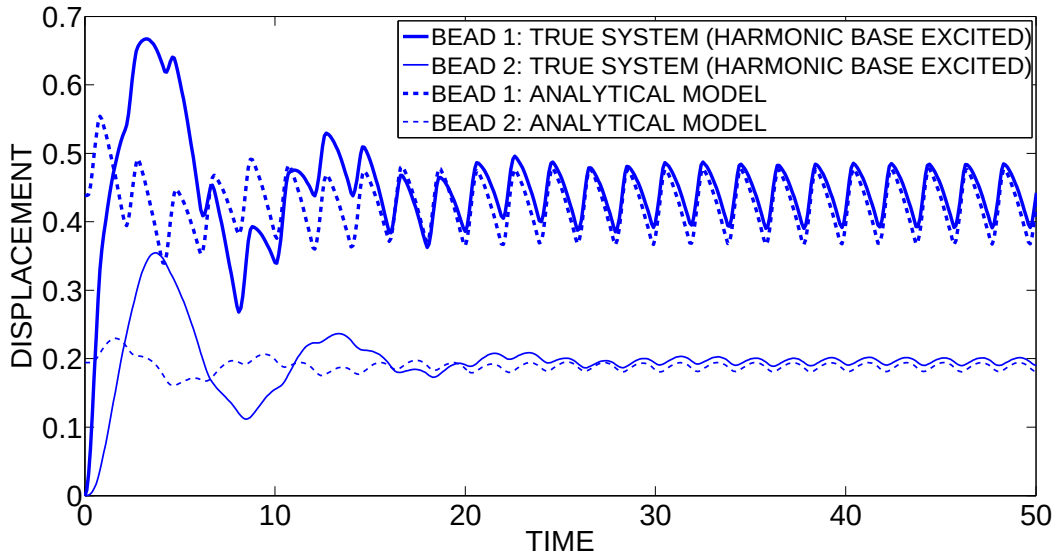

Figure 2.39: Correspondence between analytical and numerical response of the 2-bead system when the dynamics is in the attenuation band.

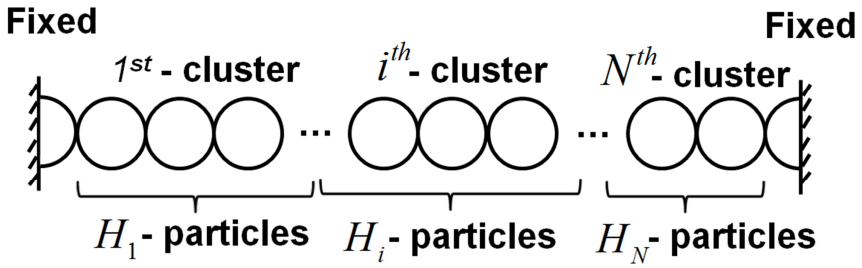

Figure 2.40: Schematic partition of a granular chain of n beads with fixed-fixed boundary conditions into N clusters – effective particles.

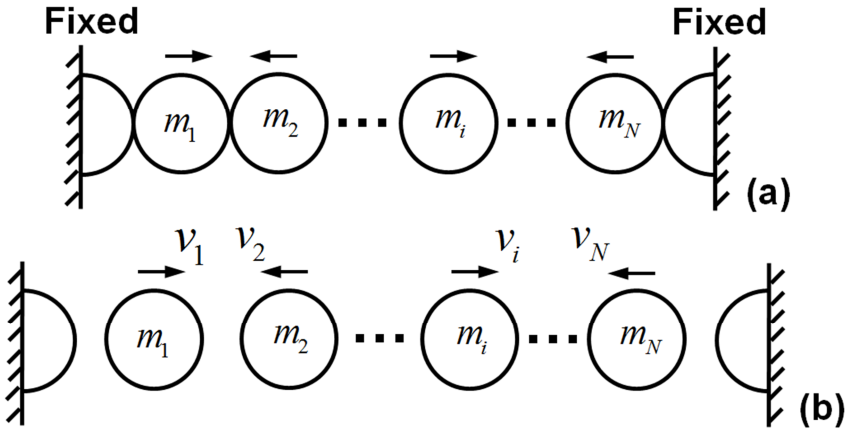

Figure 2.41: Reduced models of the granular chain of Figure 2.40, (a) Auxiliary model of effective particles; (b) vibro-impact model based on (a).

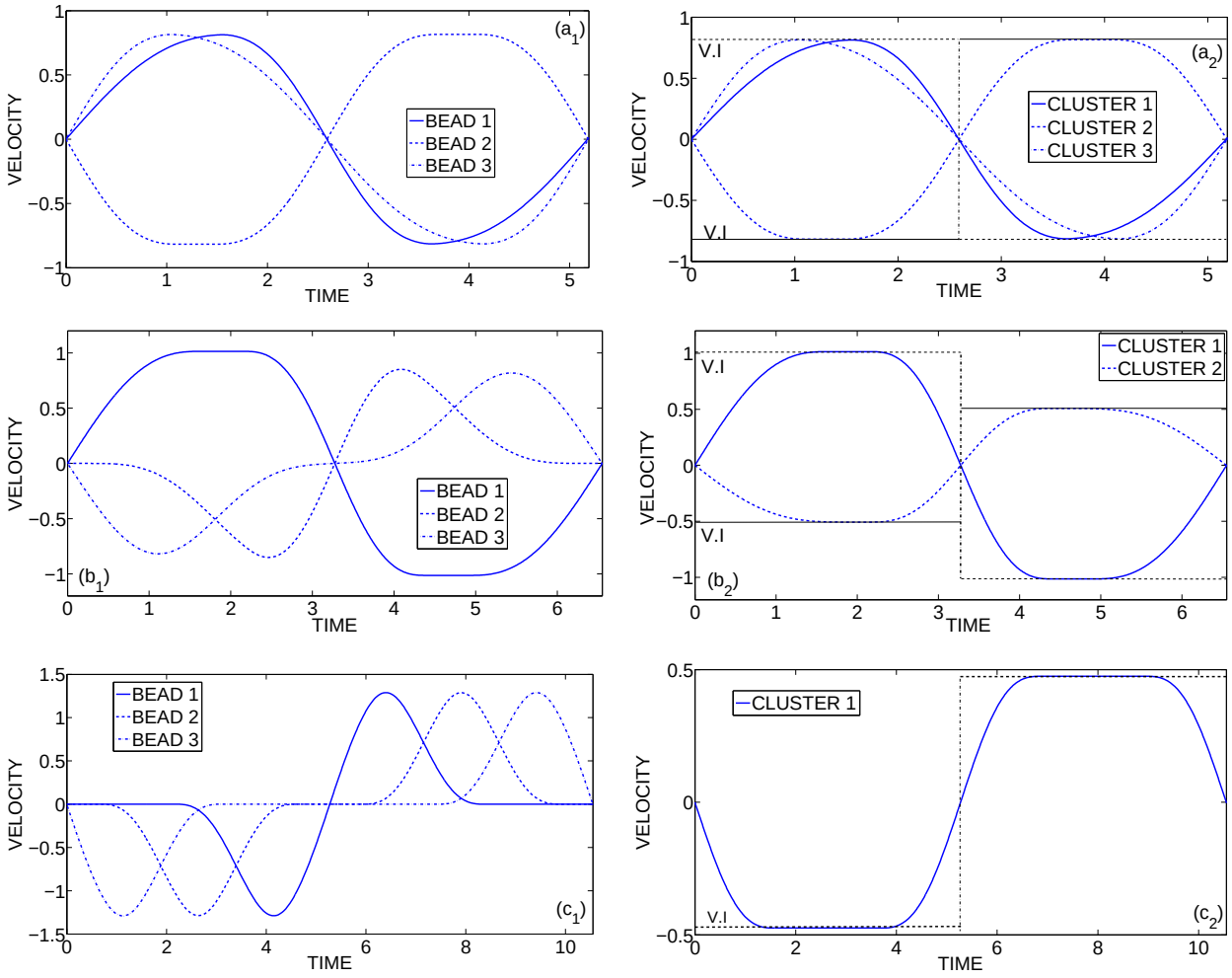

Figure 2.42: Velocity time series for the NNMs of the granular chain with $n = 3$ beads, (a) NNM1; (b) NNM2; (c) NNM4; for each mode the plots (1) depict the individual responses of the beads of the granular chain and the plots (2) the time series of effective particles of the corresponding auxiliary model (Cluster 1 to 3) and vibro-impact model (V.I).

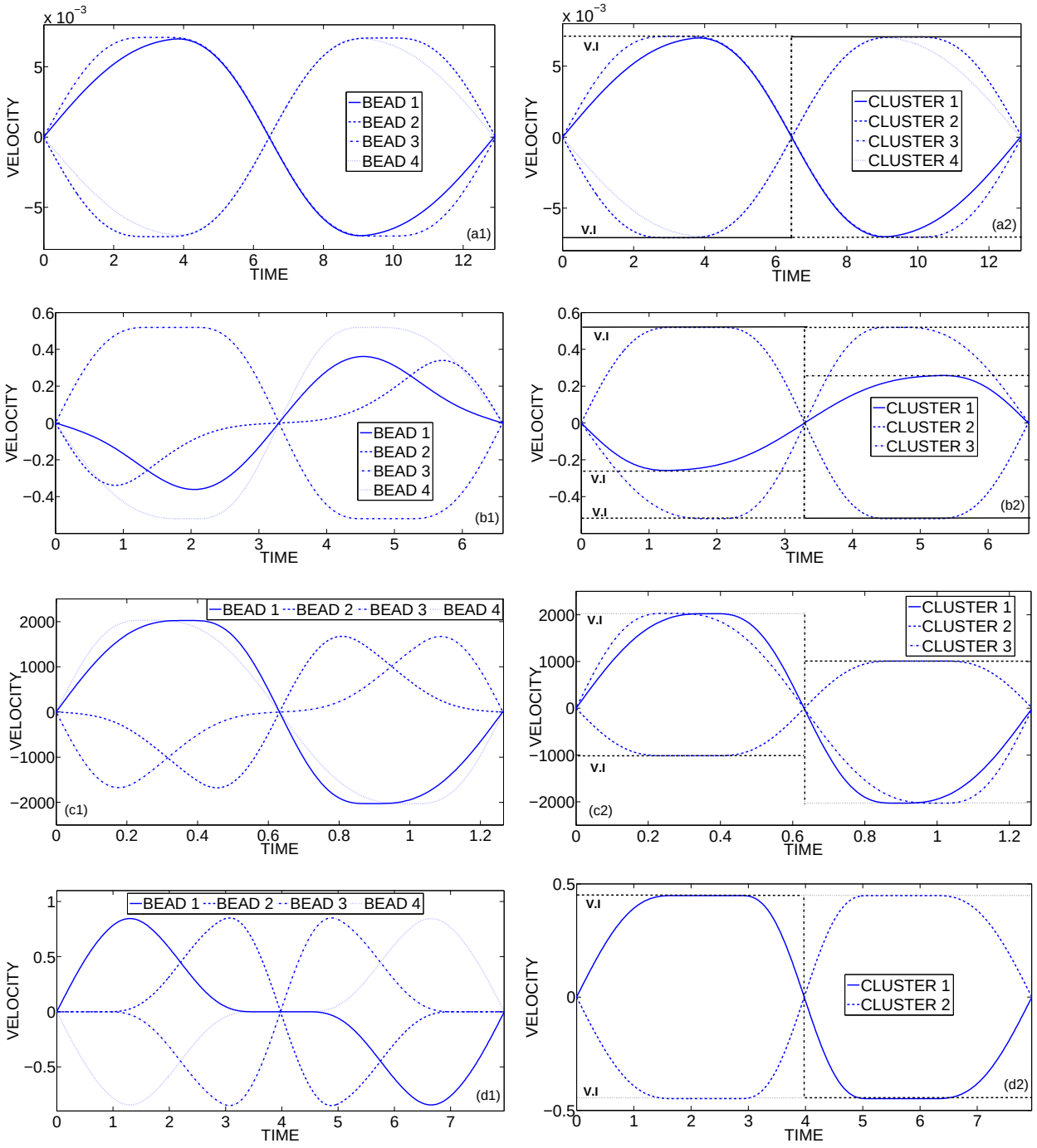

Figure 2.43: Velocity time series for the NNMs of the granular chain with $n = 4$ beads, (a) NNM1; (b) NNM2; (c) NNM3; (d) NNM5; for each mode the plots (1) depict the individual responses of the beads of the granular chain and the plots (2) the time series of effective particles of the corresponding auxiliary model (Cluster 1 to 4) and vibro-impact model (V.I).

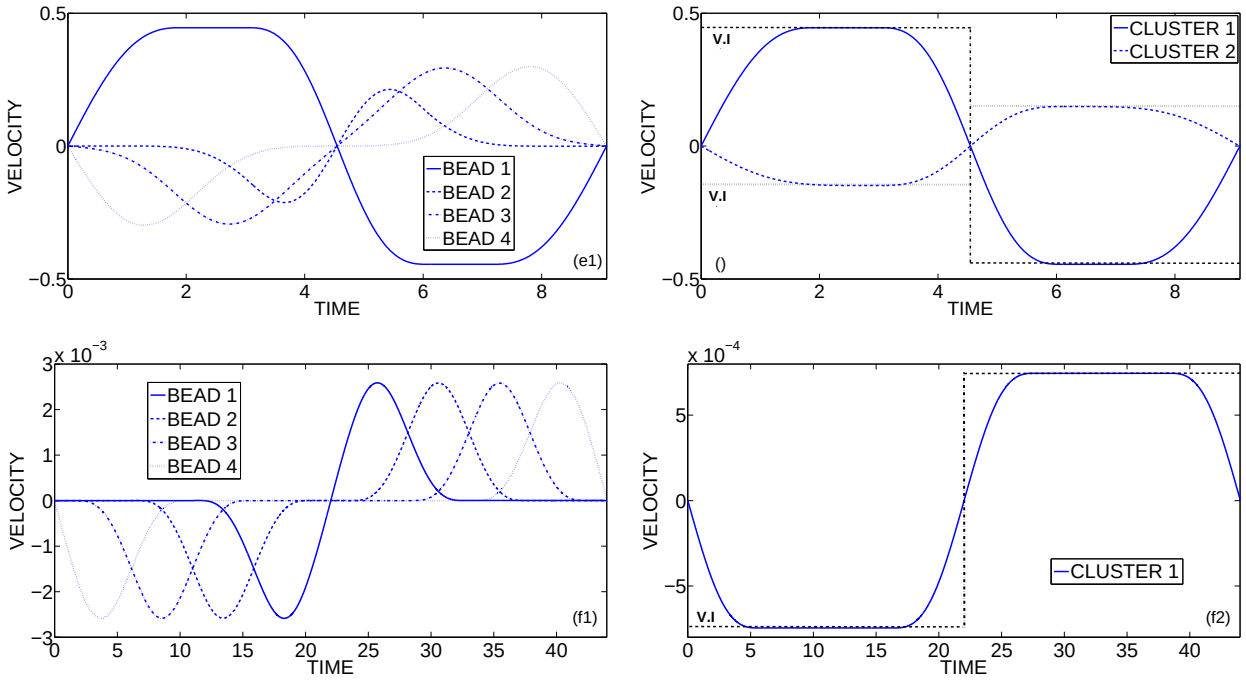

Figure 2.43 (cont'd): Velocity time series for the NNMs of the granular chain with $n = 4$ beads, (e) NNM6; (f) NNM8; for each mode the plots (1) depict the individual responses of the beads of the granular chain and the plots (2) the time series of effective particles of the corresponding auxiliary model (Cluster 1 to 4) and vibro-impact model (V.I).

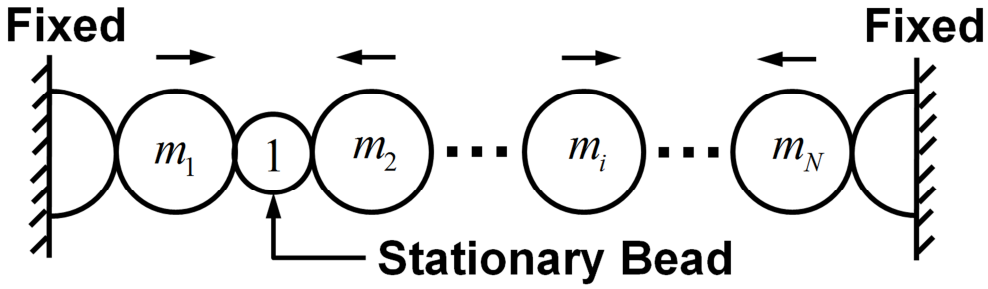

Figure 2.44: Auxiliary model of N oscillating effective particles with a permanently stationary bead (node) of unit mass.

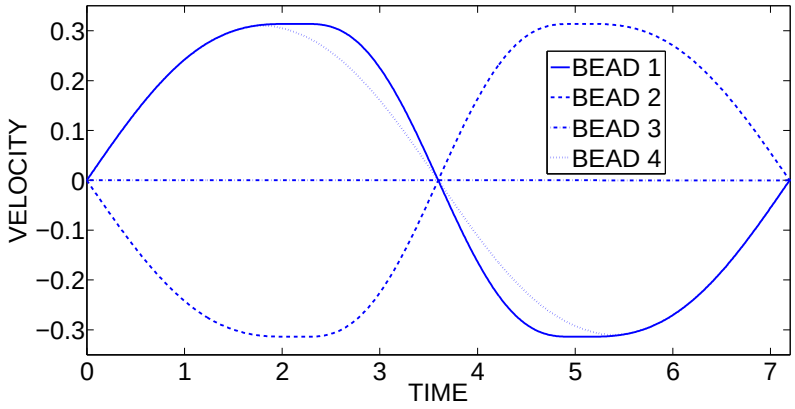

Figure 2.45: Time series of bead oscillations for a NNM of a chain with $n = 4$ possessing an immovable bead; this mode can be considered as variation of NNM1 of Table 2.3 of the chain with $n = 3$.

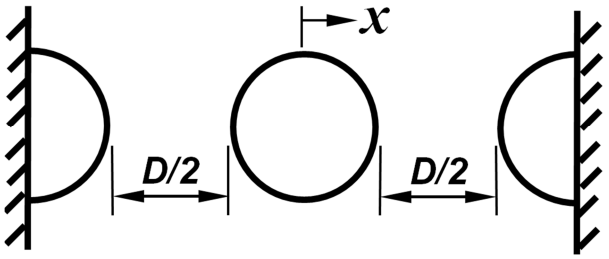

Figure 2.46: Auxiliary model of effective particle for the in-phase NNM.

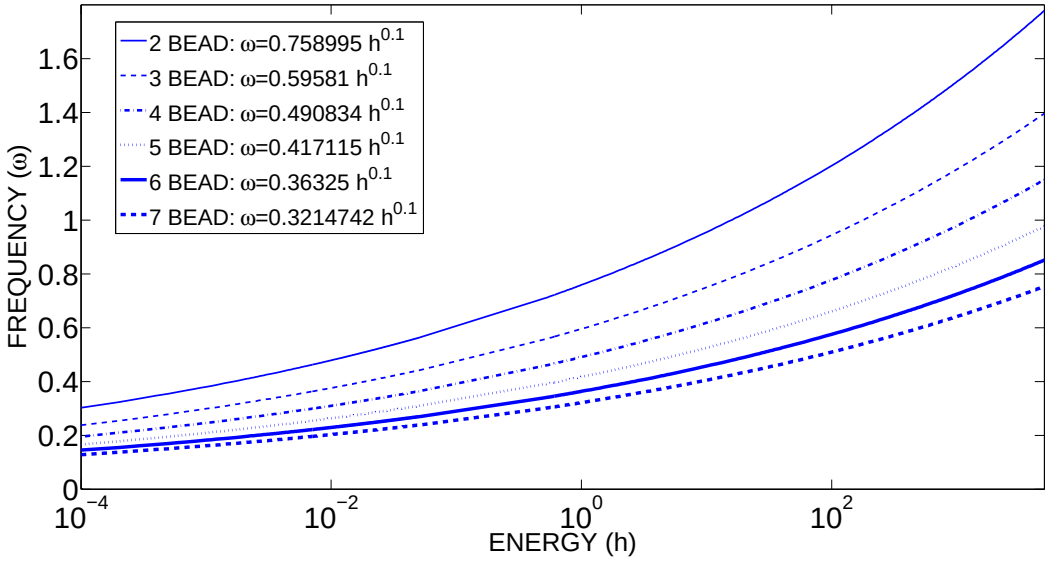

Figure 2.47: Frequency – energy curves for in-phase NNMs of granular chains with $n = 2 - 7$ beads.

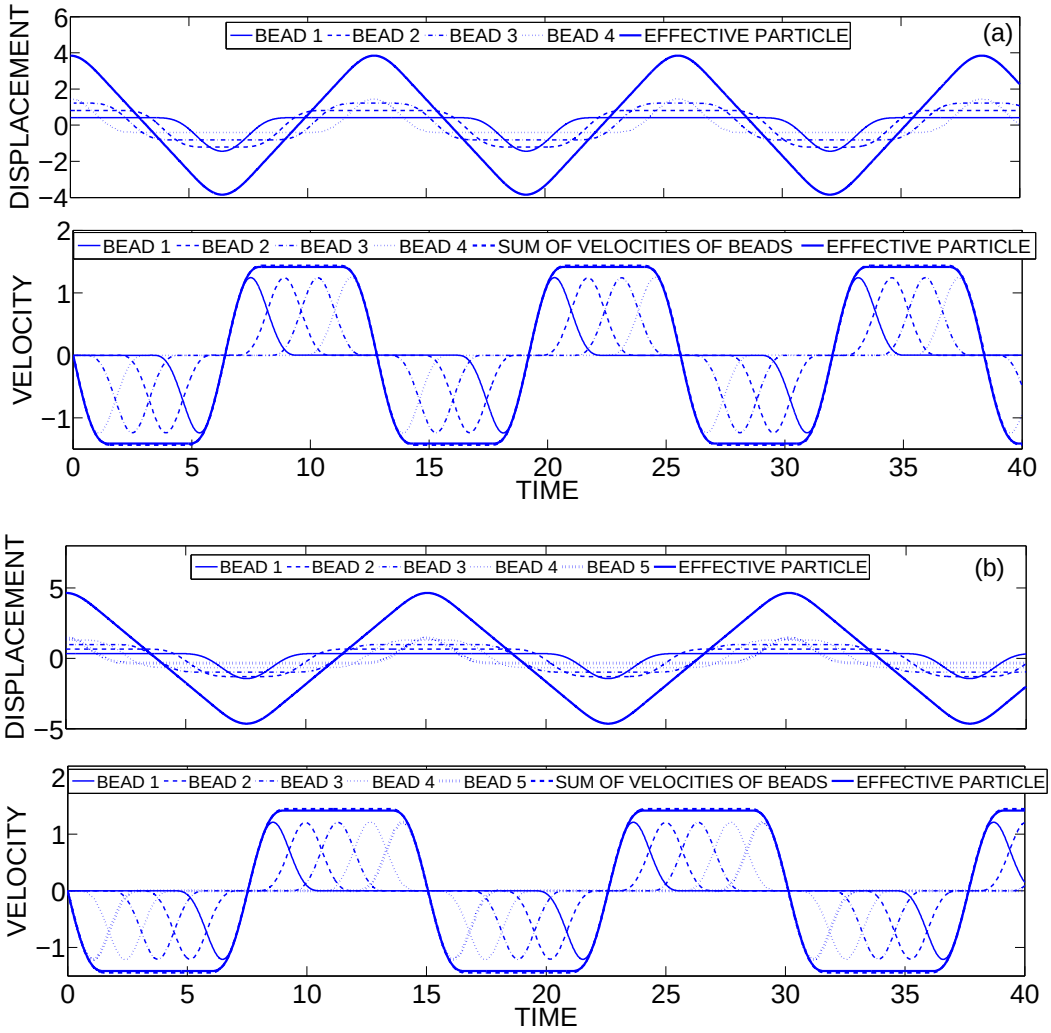

Figure 2.48: Responses of the auxiliary model and of the actual granular for the in-phase NNM of granular chains with (a) $n = 4$; (b) $n = 5$ beads.

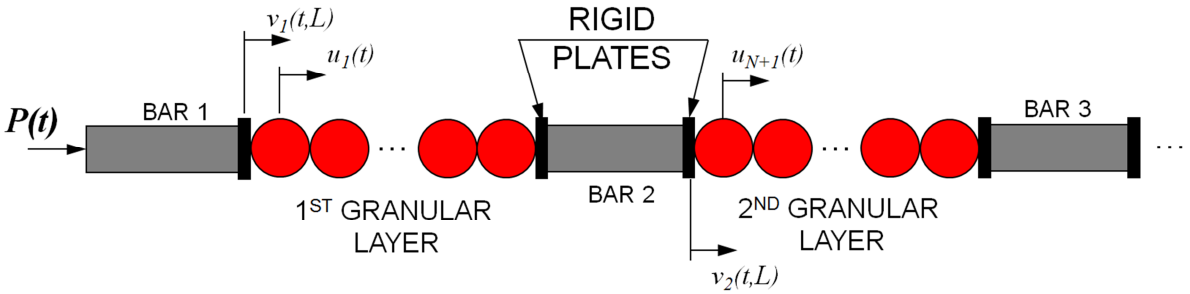

Figure 2.49: One dimensional layered elastic system with granular interfaces [125].

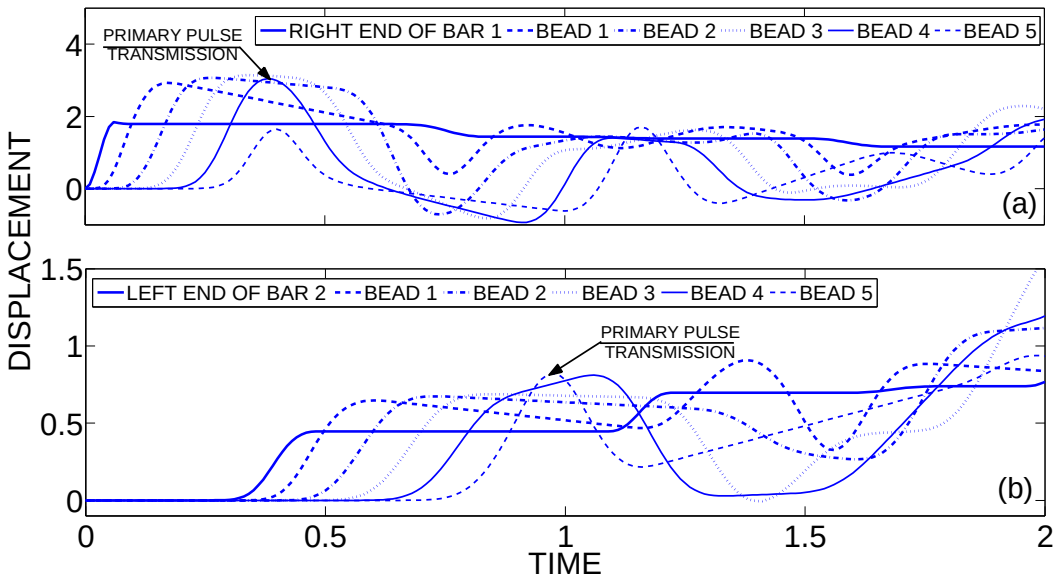

Figure 2.50: Displacements of the right boundaries of the first two layers and the first two granular interfaces ($n = 5$) of the layered medium, (a) first layer; (b) second layer.

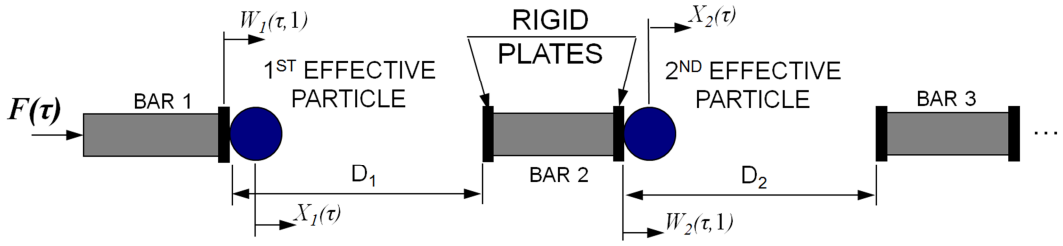

Figure 2.51: Layered medium with granular interfaces modeled as auxiliary models.

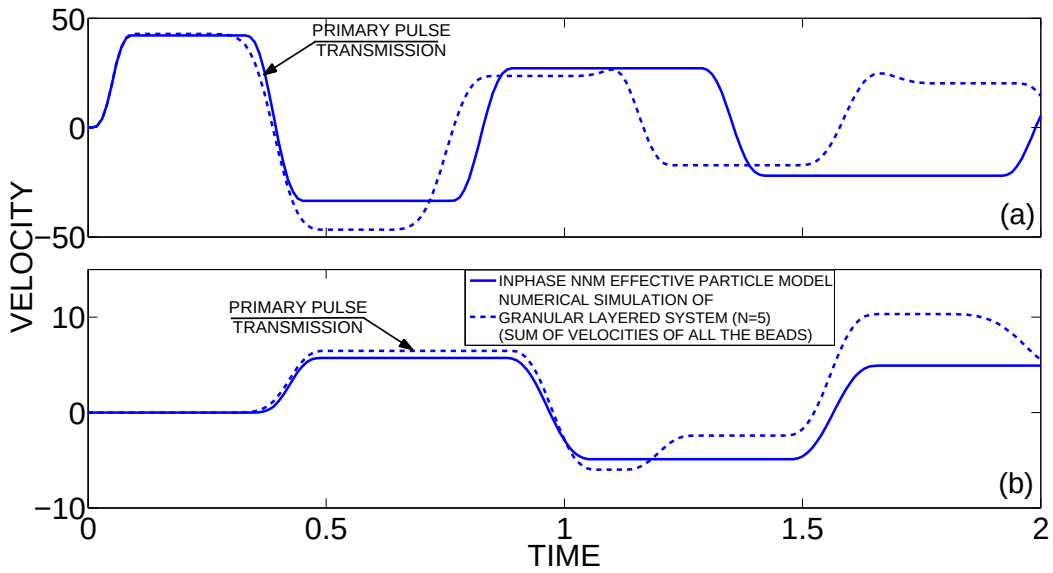

Figure 2.52: Comparison of the responses of the center of mass (in-phase NNM) of the first two granular interfaces (------), and the responses of the effective particles (——) modeling the in-phase NNMs, (a) first layer ($N = 5$); (b) second layer ($N = 5$).

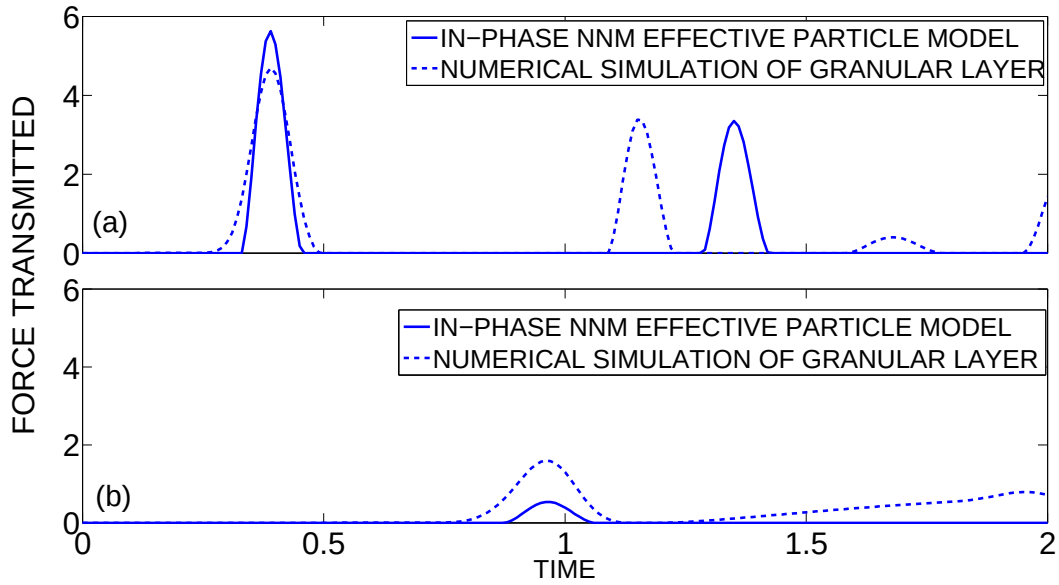

Figure 2.53: Normalized transmitted force in the leading layers of the medium, (a) left end of bar 2; (b) left end of bar 3.

2.5 Tables

Table 2.1: Normalized time delays for velocity pulse propagation

n	100-bead chain (Solitary wave [41])	n −bead system (In-phase NNM)
3	5.248	7.67
4	7.858	10.62
5	10.528	13.45
6	13.168	16.25
7	15.778	19.04

Table 2.2: Classification of NNMs of the granular chain with $n = 3$

Cluster 1 – m_1	Cluster 2 – m_2	Cluster 3 – m_3	NNM
1	1	1	1
2	1		2
1	2		3
3			4

Table 2.3: Classification of NNMs of the granular chain with $n = 4$

Cluster 1 – m_1	Cluster 2 – m_2	Cluster 3 – m_3	Cluster 4 – m_4	NNM
1	1	1	1	1
2	1	1		2
1	2	1		3
1	1	2		4
2	2			5
3	1			6
1	3			7
4				8

3. DYNAMICS OF DIATOMIC (DIMER) GRANULAR CHAINS

The propagatory dynamics in one-dimensional granular systems has been well studied theoretically [41, 42, 44, 47, 58, 59, 62], numerically and experimentally [41, 42, 51, 52, 56, 57]. Moreover, it was shown that one-dimensional monodisperse systems support solitary waves which has attracted great interest and has been studied extensively. Indeed, in homogeneous granular chains spatially localized waves may propagate without distortion. Such waves are denoted as *solitary waves*. A solitary wave is defined rigorously as in Chapter 1 [17]. An arbitrary disturbance in a homogeneous granular chain disintegrates into train of solitary waves of varying amplitudes.

As a further step in the study of granular chains, periodic diatomic chains have been considered [42, 89, 90, 92]. These are chains consisting of two different types of beads. These beads may be of different masses and or stiffness. Periodic dimer chains have been studied employing continuum limit approximation [89, 90, 93-95], but due to the mass or stiffness disparity this approach has limitations, like the disparity has to be either very large or very small. The intermediate range of mass or stiffness disparity falls outside the purview of the applied continuum limit approximation. Furthermore, there is no comprehensive study (neither analytically/numerically nor experimentally) exhausting all the parameter range of mass and stiffness disparity between the beads. Moreover, there are certain phenomena that are completely obscured when the system is not considered in the discrete limit.

In this chapter we focus exclusively on periodic dimer chains, i.e., periodic arrangements of beads of type 2 in a chain of beads of type 1. A dimer chain of similar alternating beads is denoted as 1: 1 dimer (each bead of type 1 is followed and preceded by a bead of type 2) and in such chains only periodic variation of masses can be realized, whereas a general $1: N$ $(N \geq 2)$ dimer chain can support both mass and stiffness periodicities. Our study considers these dimer chains in their discrete limit. We

begin our study by considering the propagatory dynamics in the simplest dimer chain, i.e., 1:1 dimer chain in Section 3.1. The dynamics of these dimer chains is governed by a single parameter scaling the masses of the two types of beads in the chain. We show the existence of solitary waves which are an outcome of the anti-resonance phenomenon and the realization of resonances which leads to substantial pulse attenuation. These anti-resonances and resonances are realized in un-compressed dimer chains at discrete set of mass ratios. The application of pre-compression on these chains imposes a linear term in the force interaction law between the beads and thereby lowers both the dispersive and nonlinear effects. The study of the effect of pre-compression on the anti-resonances and resonances is of primary importance in designing engineering systems incorporating dimers as it is really hard to realize un-compressed granular chains. A 1:1 dimer chain supports not only solitary waves but can also support periodic traveling waves of varying periodicities. These waves are the only mode of energy transfer to the far field of the dimer chain during pulse attenuation, an effect of the nonlinear resonance. The realization of these waves is a function of the mass ratio between the beads and can exhibit interesting bifurcations with mass ratio as the bifurcation parameter. This is of importance in understanding of the resonance and its effect on the propagatory dynamics of the dimer chain. The final part of this section is devoted to the experimental verification of the phenomena of resonance and anti-resonance in dimer chains.

In Section 3.2 we focus on the propagatory dynamics of a general class of $1:N$ dimers (a bead of type 1 preceded and followed by N beads of type 2). In contrast to 1:1 dimers where the dynamics was governed by a single parameter, the dynamics of $1:N$ dimer is governed by two parameters, mass ratio and stiffness ratio scaling the masses and stiffness characteristics respectively of the two types of beads. Initially we consider the particular case of 1:2 dimer chains and the realization of anti-resonances and nonlinear resonances. In fact we show that solitary waves can be realized only in 1:1

and $1:2$ dimer chains. Analogously, resonances can be realized only in $1:1$ and $1:2$ dimer chains. A general $1:N$ $(N \geq 2)$ dimer chain cannot support solitary waves or nonlinear resonances. This is elaborated by considering a simple case of $1:3$ dimer chain and it is shown that near solitary wave and resonances can be realized by considering the first mode of the linearized oscillatory dynamics of the light beads squeezed between the heavy beads during primary pulse propagation. An interesting particular case of degeneracy of a general $1:N$ dimer chain with very high stiffness ratio to a $1:1$ dimer chain is explored. This result can be applied in simplifying the complicated study of a general $1:N$ dimer chain with large stiffness ratio.

The last part of this chapter is concerned with the study of validity of the asymptotic approach developed and applied in this chapter. Although it may seem that the asymptotic approach is valid whenever the asymptotic parameter is small enough, we show that for a general $1:N$ dimer chain a combined parameter involving both the number of light beads N and the mass ratio governs the validity of asymptotic methodology devised herein.

3.1 Dynamics of 1:1 Dimers

3.1.1 Introduction

Polydisperse systems typically exhibit waves that radiate energy to the far field as they travel, and thus distort their initial waveforms due to continuous energy 'leakage'. In the context of one-dimensional granular media, much emphasis has been given to a $1:1$ dimer systems [89, 90, 92], i.e., in systems composed of pairs of dissimilar beads. The dynamics of these systems have been studied both theoretically in the continuum approximation [93] and experimentally [90, 93]. There has been no much progress,

however, in studying the dynamics of these systems analytically taking into account the actual discrete nature of the bead interactions; this perhaps is due to the complexity of the nonlinear dynamical interactions occurring in these media, including the possibility of bead separation in the absence of pre-compression. Theocharis et al. [96] studied localized breathers in dimers under pre-compression taking into account the linear component in the dynamics that pre-compression introduces, but no similar results exist in the strongly nonlinear case dealt with here, in the absence of pre-compression.

In this section we focus on a particular feature of the dynamics of general one-dimensional elastic dimer chains with no pre-compression, and report on the existence of a new family of localized solitary waves in these systems. As mentioned previously, this type of waves are not typical in polydisperse systems, such as the dimer chains considered herein. Solitary waves in dimers were observed and analyzed [42] for large mass mismatch and in the limit of long wave approximation. The derived expression happens to be a rescaled version of the expression for solitary wave in homogeneous chain of similar beads derived in [41, 42]. We denote this limiting system with large mass mismatch as 'auxiliary system' and use the analytical expression derived in [44, 62] as the $O(1)$ approximation in our asymptotic analysis. Furthermore, we consider higher order approximations in the limit of small mass mismatch and show the existence of a class of solitary waves in the dimer. We show that this class of perfectly localized solitary waves (as defined above) is the direct result of special symmetries or anti-resonances in the strongly (essentially) nonlinear dynamics of the un-compressed dimers. Moreover, we conjecture that there exists a countable infinity of members in this new family of solitary waves, corresponding to discrete values of a mass ratio parameter. This leads us to the interesting conjecture that *nonlinear anti-resonances may give rise to localized solitary waves in a more general class of periodic polydisperse granular media*, e.g., involving more complex spatial periodicities than the dimers considered in this section. An additional interesting feature of the reported family of solitary waves is

that they propagate faster than the corresponding solitary waves in the homogeneous system obtained in the limit of no mass mismatch (i.e., in a homogeneous chain of identical beads). This observation very much applies to the normalized system under consideration in our work, and indicates that nonlinear anti-resonances in granular media may speed up the propagation of disturbances within them. We present extensive numerical evidence of the presence of localized solitary waves in dimer chains with no pre-compression, and provide a general mathematical condition for the realization of this family of waves in these systems.

3.1.2 Anti-resonances and Solitary Waves

3.1.2.1 Numerical Evidence of Solitary Waves in the Dimer

We consider a one-dimensional 1:1 dimer chain of spherical elastic beads in Hertzian contact with no pre-compression. Denoting the materials of two neighboring beads by the labels 1 and 2, and by u_i the displacement of the i −th bead, the governing equations of motion are strongly nonlinear and given by,

$$\begin{aligned} m_i \frac{d^2 u_i}{dt^2} &= (4/3) E_* \sqrt{R} \left[(u_{i-1} - u_i)_+^{3/2} - (u_i - u_{i+1})_+^{3/2} \right] \\ m_{i+1} \frac{d^2 u_{i+1}}{dt^2} &= (4/3) E_* \sqrt{R} \left[(u_i - u_{i+1})_+^{3/2} - (u_{i+1} - u_{i+2})_+^{3/2} \right] \\ & i = \pm 1, \pm 3, \pm 5, \ldots \end{aligned} \tag{3.1}$$

where $R_i = R_1$ and $R_{i+1} = R_2$; $m_i = m_1 = (4/3)\pi R_1^3 \rho_1$ and $m_{i+1} = m_2 = (4/3)\pi R_2^3 \rho_2$; $E_* = E_1 E_2 / [E_2(1-\mu_1^2) + E_1(1-\mu_2^2)]$; $E_1(E_2)$ is the elastic modulus, $R_1(R_2)$ the radius and $\mu_1(\mu_2)$ the Poisson's ratio of bead 1 (2). We note that the interaction force between

neighboring beads is given by $\tilde{F} = (4/3)E_*\sqrt{R}\Delta^{3/2}$, where $R = R_1R_2/(R_1 + R_2)$ and Δ is the relative displacement between neighboring beads.

Introducing the non-dimensionalizations,

$$x_i = \frac{u_i}{R_1}, \quad \tau = \left[\frac{E_*}{\pi R_1^2 \rho_1}\left(\frac{R_2}{R_1 + R_2}\right)^{1/2}\right]^{1/2} t \equiv \phi t \tag{3.2}$$

we obtain the system of non-dimensional equations,

$$\begin{aligned} \ddot{x}_i &= (x_{i-1} - x_i)_+^{3/2} - (x_i - x_{i+1})_+^{3/2} \\ \varepsilon\ddot{x}_{i+1} &= (x_i - x_{i+1})_+^{3/2} - (x_{i+1} - x_{i+2})_+^{3/2} \end{aligned} \tag{3.3}$$

where overdots denote differentiation with respect to non-dimensional time τ and the only non-dimensional parameter is $\varepsilon = \rho_2 R_2^3/\rho_1 R_1^3$ scaling one of the pair of beads of the dimer system (cf. Figure 3.1). We note that if $R_1 = R_2$ the parameter ε is the ratio of the mass densities of the two materials of the dimer. In the following asymptotic analysis we will use ε as the small parameter of the problem by assuming that $0 < \varepsilon \ll 1$. Hence, we will be assuming that the dimer system is composed of 'heavy' and 'light' beads corresponding to normalized mass ratio equal to unity and ε respectively. In the notation of the original system (3.1) bead 1 is the 'heavy' bead and bead 2 is the 'light' one. The clear advantage of studying the normalized dimer (3.3) is that our results will have broad applicability to general dimer systems after appropriate rescaling. In addition to the asymptotic analysis we will explore numerically solitary waves realized for larger values of ε where the asymptotic analysis is not valid.

It will be shown that the normalized dimer system (3.3) has a special family of solitary waves (parameterized by energy) whose members are realized at a

monotonically decreasing sequence of (discrete) values of ε. Since this dimer system is non-integrable, asymptotic analysis of these solitary waves can be performed only in the limit of small ε, so initially we resort to direct numerical simulations to demonstrate their existence. For the numerical simulations we employ the setup shown in Figure 3.2 and consider the parameter in the range $\varepsilon \in (0,1]$. In the system shown in Figure 3.2 we apply an impulsive excitation equal to $F\delta(\tau)$ at the left end of a dimer chain composed of a total of 251 beads. The right end of the chain has a fixed light bead (i.e., its center of mass is immovable) so that the non-dimensionalization and rescaling employed in (3.3) are valid. To demonstrate the existence of solitary waves in this system we consider a few pairs of beads (51 to 59) in the middle of the chain and examine only primary pulse propagation, omitting reflections from the boundaries. Due to the inhomogeneity of the dimer system, intuitively one would expect a slow disintegration of the applied impulse, leading to small-amplitude oscillating 'tails' in the corresponding responses of the light and heavy beads. This has been observed in previous experimental and numerical works (e.g., [89]). However, as shown in the following numerical simulations, at specific discrete values of ε (normalized mass ratio) the applied impulse gives rise to propagation of solitary waves which travel un-deformed (i.e., their waveforms remain un-distorted during propagation) instead of disintegrating due to scattering at the interfaces between dissimilar beads.

In Figure 3.3 (unless stated all units are non-dimensional) we depict the velocities of four dimer pairs (beads 51 to 59 of the dimer) of the system of Figure 3.2 for an arbitrary value of the mass ratio $\varepsilon = 0.4$, with an applied impulse of unity. In all the numerical simulations considered hereon, unless otherwise stated, the applied impulse is unity. In this case it is observed that following the propagation of the main pulse, both light and the heavy beads of the dimer execute oscillations caused by residual energy left behind by the pulse, and appearing as oscillatory tails in the trail of the propagating pulse. Clearly, these tails are due to scattering of the main propagating

pulse at the interfaces between beads. We note that this response is typical in the dynamics of the dimer, and demonstrates the (slow) disintegration of a propagating pulse. In fact, the oscillating tails are composed of *nonlinear traveling waves* that propagate behind the main pulse, and are similar to traveling waves in homogeneous granular chains studied in an earlier work [63]. The continuous radiation of traveling waves leads to a monotonic reduction of the amplitude of the main pulse as it propagates through the dimer. The discussion on traveling waves in dimers is presented in Section 3.1.5.

Perhaps counter intuitively, at certain discrete values of the normalized mass ratio ε, localized solitary waves are formed in the dimer having the shape of traveling localized pulses with no residual oscillating 'tails' in their trails. Due to the absence of energy radiation these solitary waves propagate un-attenuated in the dimer and can be considered as analogs of the well-studied solitary pulse of the homogeneous granular chain [41]. In the case of the dimer, however, pulses with distinct waveforms are realized for the heavy and light beads. A similar observation of distinct propagating pulses in heavy and light beads in a dimer has been reported in [42]. These solitary waves are realized for a discrete set of values of the small parameter ε of the dimer, as demonstrated in the following section. Before proceeding with the numerical evidence of the solitary waves in the dimer, it is worthwhile to comment on the two limiting configurations of the dimer system (3.3), namely in the limits of the interval $0 < \varepsilon \leq 1$. In the lower limit of $\varepsilon \to 0$ the dimer degenerates to a homogeneous chain with a normalized stiffness coefficient smaller than unity; this system will be designated as the 'auxiliary system' [cf. (3.8b) below]. It should be noted that the auxiliary system does not imply that there are gaps between heavy beads, but rather it indicates that the inertial effects of the light beads are negligible so that they act effectively as pure elastic springs. In the upper limit of $\varepsilon \to 1$ the dimer degenerates again to a homogeneous

chain with normalized stiffness coefficient equal to unity; this is a homogeneous chain composed only of heavy beads.

In Figure 3.4a we present the localized solitary wave (on beads 51 to 59) realized in the dimer with $\varepsilon = 0.3428$, excited with unit impulse. In this case there are no oscillating tails following the propagation of the primary pulse. The velocity profiles of the heavy beads are in the form of a single hump and those of the light beads are double humps (that is, a slow-scale single hump superimposed with fast-scale oscillations possessing significant amplitude). Although the heavy bead waveforms of these waves are localized single humps similar to the solitary wave discussed by Nesterenko [41, 42], they have some very distinct differences. This is evidenced by the waveform of the heavy beads which is significantly affected by the fast-scale oscillations of the light beads, and also by the corresponding waveform of the light beads. However, in similarity to the Nesterenko solitary wave in the homogeneous chain, both velocity profiles of heavy and light beads decay to zero with increasing time and remain undistorted as the solitary wave propagates through the dimer. The Figure 3.4b depicts localized humps of both heavy and the light beads in the phase plane (depicting relative velocity versus relative displacement for alternating heavy or light beads) and shows them in comparison with the solitary wave that is supported in a homogeneous chain (excited by an impulse of magnitude 1.4) of heavy beads (obtained in the limit $\varepsilon \to 1$) with identical maximum displacement amplitude. It is clear that the two solitary humps of the dimer can be regarded as a disintegration of the solitary wave of the limiting homogeneous system due to scattering; yet, the fact that there is no disintegration of the main pulse to oscillatory tails implies that a special symmetry (or anti-resonance) condition is realized at this special value of ε preventing the complete disintegration of the pulse (as it occurs for arbitrary values of ε – cf. Figure 3.3). In Figure 3.4c displacement wave profile of the solitary wave is shown. As can be observed, after the passage of the solitary wave, both heavy and the light beads experience a rigid body

translation in the direction of the applied impulse. Although light beads execute oscillations, they attain zero velocity towards the end of the squeeze mode. This condition will be invoked in the next section to derive a spectrum of mass ratios where solitary waves can be realized.

Additional solitary waves realized in the dimer have been numerically detected for $\varepsilon = 0.1548$ (see Figure 3.5), $\varepsilon = 0.0901$ (see Figure 3.6), and $\varepsilon \approx 0.0615, 0.04537, 0.03448, \ldots, 0.00868$. Similar to the solitary wave for $\varepsilon = 0.3428$ these additional solitary waves have no oscillating tails but rather have velocity profiles that decay to zero with increasing time. With decreasing ε (i.e., increasing normalized mass mismatch) the light beads execute high frequency oscillations while they are being compressed in between adjacent heavy beads; this phase is denoted as the 'squeeze mode'. Generally, the frequency of oscillation of the light beads during the squeeze mode increases with decreasing ε. For a general value of ε, typically the light bead loses contact with its left neighboring heavy bead at the end of its compression phase (i.e., at the end of the squeeze mode), and retains a small portion (residual) of the energy of the propagating pulse. This residual energy manifests as oscillation of the light beads even after the propagation of the primary pulse, which in turn leads to the formation of traveling waves in oscillating tails appearing in the wake of the propagation of the primary pulse. These tails radiate energy to the far field in the opposite direction to that of the propagating pulse, and cause a continuous decrease of the amplitude (energy) of the primary pulse as it propagates through the dimer. Hence, for an arbitrary value of ε no solitary wave can be formed.

In contrast, at the aforementioned discrete values of ε, solitary waves are formed once the light beads stay in continuous contact with adjacent heavy beads (that is, no separation between light and heavy beads occurs), and the entire energy of the main pulse is conserved and transferred without loss from each heavy bead to the next heavy bead, after which each heavy bead reaches a stationary position at the end of the

squeeze mode. As a result, no residual oscillating tails are formed in this case, there is no energy radiated to the far field, and the primary pulse propagates un-attenuated through the dimer. Clearly, this lossless transfer of energy through the dimer occurs only if certain symmetry conditions are satisfied. These conditions are formulated asymptotically in the next section where it is proved that a discrete set of solitary waves exists in the dimer accumulating to a definite limit as $\varepsilon \to 0$. It is also important to point out the formation of secondary solitary waves (cf. Figure 3.5b) belonging to the same class of solitary waves discussed so far. These secondary waves are generated due to separations of the initial beads of the system following the application of the impulse, and the fact that they have the exact form of the solitary wave provides additional numerical evidence that *at the mentioned discrete values of ε, these solitary waves provide the principal (fundamental) mechanism for transferring energy in the dimer*. Thus it is concluded that this family of solitary waves constitutes the most natural type of localized traveling pulses in the dimer system for the mentioned special discrete values of ε, in similarity to the solitary waves studied by Nesterenko [41, 42] which provide the principal mechanism for transferring energy in homogeneous granular chains.

A particularly interesting feature of solitary waves in the dimer chain is that their phase velocities are higher than the phase velocity of the solitary wave in the homogeneous system obtained in the limit $\varepsilon \to 1$; in fact the solitary waves become faster as the normalized mass ratio ε decreases. Indeed, in Figure 3.7 we depict the time shift (labeled as τ_s in Figure 3.5a) of a solitary wave in the dimer (defined as the time difference between velocity peaks of successive heavy beads) plot against the velocity amplitude of the solitary wave. In essence, this plot represents the energy – speed relations for the different families of solitary waves in the dimer. Due to the discrete nature and the normalized form of the considered system, defining phase velocity as in continuum systems is not possible. An analogous quantity which can be attributed to the velocity of propagation of the solitary waves is the time shift which is presented in

Figure 3.7. The lower bounding curve corresponds to the auxiliary system obtained in the limit $\varepsilon \to 0$, and corresponds to the fastest class of solitary waves. As shown in the asymptotic analysis that follows, every point in the lower bounding curve represents an accumulation point of solitary waves as $\varepsilon \to 0$ (that is, fixing the peak velocity amplitude of the solitary wave and letting $\varepsilon \to 0$). Moreover, there is an upper bounding curve corresponding to the solitary wave of the homogeneous chain corresponding to $\varepsilon = 1$, which demonstrates that every solitary wave propagating in the dimer is faster than the solitary wave propagating in the corresponding homogeneous system composed only of heavy beads. We also note that due to the homogeneous nonlinear potential of the Hertzian law interaction [8, 48], the dimer system is fully re-scalable in the sense that for any input impulse the time shifts for the solitary waves bear a constant ratio compared to that of the solitary wave realized in the limiting homogeneous chain with $\varepsilon = 1$.

From the above discussion it is clear that the time shifts of the solitary waves in dimer converges towards that in the homogeneous chain with the increase in ε. But it is interesting to observe the convergence of the waveform of these solitary waves to the Nesterenko solitary wave in homogeneous chain. In Figure 3.8 we depict the solitary wave velocity profile on the heavy bead (51^{st} bead) in comparison with the velocity profile of the same bead in homogeneous chain. The amplitudes are matched exactly by exciting the dimer chains with appropriate impulses ($\{\varepsilon = 0.3428, F = 1.237\}, \{\varepsilon = 0.1548, F = 1.012\}; \{\varepsilon = 0.0901, F = 1.006\}; \{\varepsilon = 1, F = 1\}$). From the above discussion it is intuitive to expect that the solitary wave velocity profile of the dimer chain converge towards that in homogenous chain with increase in ε, but the response in Figure 3.8 depicts a contrastingly different scenario. In fact the solitary wave corresponding to $\varepsilon = 0.3428$ (the last mass ratio of the dimer where solitary wave is realized) shows maximal deviation from the solitary wave in homogeneous chain. In fact this can be attributed to the large high frequency oscillations that are observed in the velocity

profile of the light beads (Figure 3.4a). This strong oscillation of the light beads during the squeeze mode considerably influences the wave profile of the heavy beads. In contrast, for lower values of mass ratio the amplitude of high frequency oscillation in the velocity profile of light beads are substantially lower and have very mild/no influence on the heavy beads (cf. Figure 3.5, 3.6).

To demonstrate the effect that the solitary waves can have on the response of the dimer chain to shock excitations we reconsider the system of Figure 3.2 with a total of 85 heavy and light beads, with the last heavy bead of the dimer being in contact with a fixed light bead (such a setup has been previously employed in the context of homogeneous chains by Coste et al. [53]). Again, no pre-compression in the chain exists. A unit impulse excitation is applied to the first bead on the left end of the dimer chain. As described previously this system is fully re-scalable, and thus for any applied impulse the ratio of the maximum force transmitted $\left[F_t(\varepsilon, F) = (x_n)_{max}^{3/2}\right]$ to the fixed light bead over the corresponding force in the limiting homogeneous chain with $\varepsilon = 1$ is constant for any value of ε, i.e., $\Lambda(\varepsilon) = F_t(\varepsilon, F)/F_t(1, F)$ is constant for a particular value of ε for any arbitrary value of applied impulse strength F. This argument is valid also for the time delay τ_d between the application of the pulse on the first bead at the left end of the dimer chain (Figure 3.2) and its arrival to the right fixed bead, i.e. $\Upsilon(\varepsilon) = \tau_d(\varepsilon, F)/\tau_d(1, F)$ is constant for a particular value of ε for any arbitrary value of applied impulse strength. It follows that *we only need to consider the dynamics of the dimer subject to a unit impulse, with our results being valid at different energies (or applied pulses)*. Again, this result originates from the 'homogeneous' nature of the nonlinear interaction potential between beads, leading to dynamics that are fully re-scalable with energy. It should be noted that this result is valid only for dimer chain length less than 85 beads. With further increase in the number of beads, the propagatory dynamics exhibits a different

phenomenon and the above discussed normalization is no longer valid. This phenomenon is discussed in Section 3.1.3.2 [91].

In Figure 3.9a we depict the force transmitted to the fixed light bead normalized with respect to the corresponding force transmitted in the homogeneous system. From these results it is clear that the force transmitted is always smaller for the case of the dimer compared to the homogenous chain. The intermediate local peaks of normalized transmitted force (occurring at $\varepsilon = 0.3428, 0.1548, 0.0901, ...$) are realized at the specific values of ε for which solitary waves are realized, since only then the energy is transferred un-attenuated through the dimer. On the contrary, in between the local peaks of normalized transmitted force where no solitary waves are formed and the propagating pulse disintegrates due to scattering at bead interfaces, the normalized transmitted force decreases, with maximum reduction of the order of 75% of the normalized transmitted force occurring for $\varepsilon \approx 0.59$. These results indicate that the solitary waves represent an efficient mechanism for transferring energy through the dimer system. The normalized time delay [110] (with respect to the corresponding time delay for the homogeneous system with $\varepsilon = 1$) for the dimer is presented in Figure 3.9b, from which we infer that for an arbitrary value $0 < \varepsilon \leq 1$ the normalized time delay is smaller than unity. This leads us to the claim that solitary waves in the dimer propagate faster than the Nesterenko solitary wave in the homogeneous system of heavy beads. It is worth noting that the number of beads and the loading conditions are identical for each dimer system considered in Figure 3.9, while the only parameter being varied is the normalized mass ε. Clearly, the time delay described here is more applicable for practical/experimental applications instead of theoretical analysis since it does not provide a rigorous measure of the speed of the solitary wave in the dimer. From a theoretical perspective, the time shift (Figure 3.7) is a valid measure to describe the speed of solitary waves and Figure 3.7 rigorously evidences our claim of faster propagation of solitary waves in dimer when compared to that in a homogeneous chain

of heavy beads. Moreover, the previous observations are valid only for the normalized system under consideration, wherein the mass of the heavy bead is fixed to unity, and only the normalized mass of the light bead is varied in the range $\varepsilon \in (0,1]$.

The previous numerical results show that a granular chain with periodic inhomogeneities can support different classes of solitary waves. The solitary waves with perfect localization (i.e., with no oscillating tails following the propagation of the main pulse) considered here differ from traveling waves observed by previous researchers [42, 89, 90] in these systems that can at best be described as either quasistationary primary pulses or solitary-like pulses, but are not solitary waves as per the rigorous definition of [17]. In the context of our discussion the propagating solitary waves conserve their energy, do not radiate energy to the far field and retain their waveforms intact.

In the family of solitary waves considered herein, the light beads execute relatively high-frequency oscillations (in their squeeze mode) but they do not loose contact with their neighboring heavy beads even towards the end of the squeeze mode. Such a behavior can occur under special conditions, that is, only if the velocity (displacement) waveform of each light bead possesses special symmetric (anti-symmetric) properties. For the velocity waveform to be symmetric a light bead should end its high-frequency oscillation with precisely *zero velocity*, i.e., with precisely the initial velocity with which it begins its motion during the squeeze mode. This exactly conforms to the solitary wave definition [17] given above. Such synchronization between the motion of the light and heavy beads can only imply that a certain *anti-resonance condition* is satisfied when a solitary wave is formed; this will be confirmed in the theoretical study of the next section. For smaller values of ε (i.e., for large mass mismatch in the dimer) the oscillation of the light bead does not affect the motion of its neighboring heavy beads. It follows that in the limit of small ε we may introduce multiple time scales to describe the dynamics of the solitary waves: a *fast time scale* that

governs the relatively high-frequency oscillations of the light beads, and a *slow time scale* that governs the slowly varying localized pulse in the heavy beads. However, as the normalized mass ratio increases and we progress towards the region of upper bound ($\varepsilon = 0.3428$) of realization of these solitary waves, it is clearly seen that the amplitude of oscillations of the light beads become comparable to the solitary pulse in the heavy beads. At this stage the time scale separation breaks down and one may no longer partition the dynamics of the heavy and light beads in terms of slow and fast components (that is, the time scales become entangled). Hence, the normalized mass ratio $\varepsilon = 0.3428$ represents an upper bound for the existence of solitary waves in the dimer, in the sense that beyond this point no solitary waves can be formed, with the exception, of course, of the well-studied solitary wave in the limiting homogeneous system with $\varepsilon = 1$ studied by Nesterenko [41, 42].

The fact that the solitary waves in the dimer propagate faster than the solitary wave in the limiting system with $\varepsilon = 1$ might seem counterintuitive. Taking into account, however, that solitary waves in the dimer are formed under conditions of anti-resonance, it implies that *anti-resonance phenomena may be responsible for the higher phase velocities of the solitary waves in the dimer*. As shown in the numerical results of Figure 3.9, the existence of solitary waves in granular chains with periodicity facilitates the transmission of energy and increases the speed of disturbance transmission in these media. This implies that anti-resonance phenomena in granular chains represent an important dynamical mechanism which significantly affects the capacity of these media to transmit disturbances.

In the next section we will be concerned with the analytical study of realization of families of solitary waves in the dimer system in the limit of small ε, and the study of the anti-resonance conditions that lead to the formation of solitary waves in the dimer for specific values of normalized mass ratio ε.

3.1.2.2 Analytical Study of Anti-Resonances in Dimers

Considering again the non-dimensional governing equations for the dimer,

$$\begin{aligned} \ddot{x}_i &= (x_{i-1} - x_i)_+^{3/2} - (x_i - x_{i+1})_+^{3/2} \\ \varepsilon \ddot{x}_{i+1} &= (x_i - x_{i+1})_+^{3/2} - (x_{i+1} - x_{i+2})_+^{3/2} \\ i &= \pm 1, \pm 3, \pm 5, \ldots \end{aligned} \tag{3.3}$$

we assume that $0 < \varepsilon \ll 1$, i.e., study the dynamics in the limit of large normalized mass mismatch. The index notation in (3.3) indicates that odd indices correspond to heavy beads, and even indices to light beads. The subscripts (+) will be dropped from hereon as we will be concerned only with primary pulse transmission in the dimer, that is, we will be concerned only with the phase of the squeeze mode during which the light beads are under continuous compression from their neighboring heavy beads so that no separation between beads occurs.

Clearly, for sufficiently small values of ε, system (3.3) is in the form of a singularly perturbed problem which calls for a slow-fast time scale separation. We will be interested only in primary pulse transmission in the dimer, omitting secondary waves. Within this context we may study solitary wave transmission in the dimer since this corresponds particularly to primary pulse transmission with no separation between beads. Hence, the dynamics of solitary wave formation can be described by introducing the following asymptotic approximation for the bead displacements of the dimer,

$$\begin{aligned} x_i &= x_{i0}(t_0) + \varepsilon^a x_{i1}(t_1) + \ldots \\ x_{i+1} &= x_{(i+1)0}(t_0) + \varepsilon^c x_{(i+1)1}(t_1) + \ldots \end{aligned} \tag{3.4}$$

where t_0 and t_1 are distinct time scales of the dynamics defined as follows,

$$t_0 = \tau, \;\; t_1 = \varepsilon^b t_0 \tag{3.5}$$

and the real exponents a, b, c are to be determined by balancing terms at various orders of approximation of the asymptotic analysis. Substituting (3.4) and (3.5) into (3.3), and expanding the rational powers in power series with respect to ε we obtain the following set of governing equations valid in the limit of sufficiently small ε:

$$\begin{aligned}\ddot{x}_{i0} + \varepsilon^{a+2b} x_{i1}'' = &\left(x_{(i-1)0} - x_{i0}\right)^{3/2} - \left(x_{i0} - x_{(i+1)0}\right)^{3/2} + (3/2)\left(x_{(i-1)0} - x_{i0}\right)^{1/2}\left(\varepsilon^c x_{(i-1)1} - \varepsilon^a x_{i1}\right) \\ &-(3/2)\left(x_{i0} - x_{(i+1)0}\right)^{1/2}\left(\varepsilon^a x_{i1} - \varepsilon^c x_{(i+1)1}\right) + O\left(\left\|\varepsilon^a x_{i1} - \varepsilon^c x_{(i+1)1}\right\|^2\right)\end{aligned} \tag{3.6}$$

$$\begin{aligned}\varepsilon(\ddot{x}_{(i+1)0} + \varepsilon^{c+2b} x_{(i+1)0}'') = &\left(x_{i0} - x_{(i+1)0}\right)^{3/2} - \left(x_{(i+1)0} - x_{(i+2)0}\right)^{3/2} + (3/2)\left(x_{i0} - x_{(i+1)0}\right)^{1/2}\left(\varepsilon^a x_{i1} - \varepsilon^c x_{(i+1)1}\right) \\ &-(3/2)\left(x_{(i+1)0} - x_{(i+2)0}\right)^{1/2}\left(\varepsilon^c x_{(i+1)1} - \varepsilon^a x_{(i+2)1}\right) + O\left(\left\|\varepsilon^a x_{i1} - \varepsilon^c x_{(i+1)1}\right\|^2\right)\end{aligned} \tag{3.7}$$

In the equations above overdots indicate differentiation with respect to the time scale $t_0 = \tau$ and primes represent differentiation with respect to the time scale t_1. By considering the order of magnitude of the various terms in (3.6) and (3.7), the exponents in the asymptotic analysis are chosen as $a = 2, b = -1/2, c = 1$, since this leads to appropriate balancing of terms at successive orders of approximation. It follows that $t_0 = \tau$ is the slow time scale, whereas $t_1 = \varepsilon^{-1/2}\tau$ the fast time scale of the dynamics.

To provide a demonstration of the range of validity of the above asymptotic expansions, Figure 3.3 presents the distinct dynamical regimes that are realized during primary pulse propagation in a 1:1 dimer chain (similar results hold for general 1:N dimers with $N > 1$). To this end we consider a semi-infinite 1:1 dimer chain excited by a normalized impulse with intensity equal to unity applied to its free left boundary (i.e., the first heavy bead corresponding to $i = 1$), and depict the responses of beads 51 to 59. The resulting pulse propagation through the dimer can be classified into two distinct

regimes: (i) a primary pulse or squeeze mode, and (ii) an oscillating tail developing in the trail of the primary pulse. During primary pulse transmission (squeeze mode), the light beads are squeezed between their neighboring heavy beads and thus no bead separation is possible. Thus the dynamics is weakly nonlinear due to the strong local compression between beads associated with the first arrival of the pulse, and the asymptotic analysis formulated herein is valid. In the oscillating tail, however, there is bead separation and collision between beads, so the dynamics is strongly nonlinear. Indeed, towards the end of the squeeze mode the compression of the light beads by their neighboring heavy beads relaxes gradually (as the primary pulse passes), leading to non-smooth dynamics so that the asymptotic methodology of this section ceases to be valid. Typically, this phase is noted in the trail of the propagating primary pulse for arbitrary values of the normalized parameter ε, and is associated with radiation of energy from the primary pulse to the far field of the medium in the form of strongly nonlinear traveling waves (discussed in Section 3.1.5); this is the principal mechanism of pulse dispersion as the primary pulse gradually loses its energy as it penetrates further through this heterogeneous medium. Interestingly enough, it will be proved that for certain values of the normalized parameter ε it is possible that the oscillatory tail completely disappears (so that only the squeeze mode is realized), leading to the formation of localized solitary waves propagating with no distortion or attenuation. This corresponds to realization of *anti-resonances* (as opposed to *resonances* that lead to maximum primary pulse attenuation [91]) in the dimer.

Considering the zero-th order approximation in (3.6) and (3.7) respectively, the following set of equations that govern the *slow dynamics* of the dimer are obtained:

$$\ddot{x}_{i0} = \left(x_{(i-1)0} - x_{i0}\right)^{3/2} - \left(x_{i0} - x_{(i+1)0}\right)^{3/2}$$
$$x_{(i+1)0} = \frac{x_{i0} + x_{(i+2)0}}{2} \tag{3.8a}$$

The first set of nonlinear ordinary differential equations in (3.8a) provides the first-order approximation of the dynamics of the heavy beads, whereas the second set of linear algebraic equations provides the first-order approximation of the dynamics of the light beads. It is clear that system (3.8a) is expressed exclusively in terms of the slow time scale t_0, so the leading-order approximations of the responses of both the heavy and light mass beads of the dimer are slow dynamical motions.

By simple algebraic manipulations, (3.8a) may be rewritten in the following form:

$$\ddot{x}_{i0} = (1/2)^{3/2}\left[\left(x_{(i-2)0} - x_{i0}\right)^{3/2} - \left(x_{i0} - x_{(i+2)0}\right)^{3/2}\right]$$
$$x_{(i+1)0} = \frac{x_{i0} + x_{(i+2)0}}{2} \tag{3.8b}$$

It follows that the first-order approximation of the (slowly-varying) motion of the heavy beads is identical to the response of a homogeneous granular chain [i.e., the first set of nonlinear ordinary differential equations in (3.8b) which is in terms only of the responses of the heavy beads], whereas the first-order approximation of the response of the light beads is expressed in terms of the (slowly-varying) responses of the heavy beads [i.e., the second set of linear algebraic relations in (3.8b)]. In fact the homogeneous granular chain in (3.8b) corresponds to the auxiliary system defined in the previous section derived in the limit $\varepsilon \to 0$ of the dimer.

Hence, in the first-order of approximation *the slow dynamics of the light beads is determined in terms of the slow dynamics of the heavy beads*. At this point it is emphasized that we are interested only in the analytical description of the primary pulse propagating in the dimer. Therefore, we select the solution of the first set of equations in (3.8b) to be the solitary wave of the homogenous system for which analytical approximations have been derived in the literature [41, 47, 62, 63]. Following [62] the

analytical approximation of the slowly varying motion of the heavy beads is expressed as,

$$x_{i0}(t_0) = S_i(\varphi t_0), \quad \varphi = (1/2)^{3/4} \tag{3.9a}$$

where,

$$\begin{gathered} S_i(\varphi t_0) = S[\varphi(t_0 - i\mathrm{T})], \\ S(\xi) = \mathrm{A} + (\mathrm{A}/2)\left\{\tanh\left[\left(c_1(\xi/\mathrm{T}) + c_3(\xi/\mathrm{T})^3 + c_5(\xi/\mathrm{T})^5\right)/2\right] - 1\right\}, \\ c_1 = 2.39536,\ c_3 = 0.268529,\ c_5 = 0.0061347 \end{gathered} \tag{3.9b}$$

In (3.9b) A is the amplitude of the solitary wave and T is the time shift in the response between the maxima of two successive heavy beads (or the peak-peak delay for velocity pulse transmission between successive heavy beads). Accordingly, the slowly varying component of the motion of the light beads is expressed as:

$$x_{(i+1)0}(t_0) \equiv s_{(i+1)}(\varphi t_0) = \frac{S_i(\varphi t_0) + S_{i+2}(\varphi t_0)}{2} \tag{3.9c}$$

Thus it is observed that the $O(1)$ approximation of the responses of both the heavy and light beads always decay to zero. Such an approximation is valid only in the limit of very small ε. Such a solution was previously derived by employing the long wave approximation by Nesterenko [41, 42]. This long wave approximation and the solitary wave approximation used in this thesis are compared in [62]. Although such approximations well predict the dynamics of the heavy beads for smaller ε, the responses of the light beads need not necessarily decay to zero for arbitrary values of ε. It follows that in order to realize solitary waves it is necessary to find the discrete values

of ε for which higher order asymptotic corrections of the dynamics of the light bead decay to zero.

Proceeding to the next order approximation, at $O(\varepsilon)$ the following equations governing the *fast dynamics* of the heavy and light beads can be derived,

$$x''_{i1}(t_1) = (3/2)\left[S_{(i-1)}(\varphi t_0) - S_i(\varphi t_0)\right]^{1/2} x_{(i-1)1}(t_1) + (3/2)\left[S_i(\varphi t_0) - S_{(i+1)}(\varphi t_0)\right]^{1/2} x_{(i+1)1}(t_1)$$
$$x''_{(i+1)1}(t_1) + \Omega^2_{i+1}(t_0)\, x_{(i+1)1}(t_1) = f_{i+1}(t_0)$$

(3.10a)

where,

$$\Omega^2_{i+1}(t_0) = 3\left[\frac{S_i(\varphi t_0) - S_{(i+2)}(\varphi t_0)}{2}\right]^{1/2}, \qquad f_{i+1}(t_0) = -\ddot{s}_{(i+1)}(\varphi t_0) \tag{3.10b}$$

are the square of a slowly varying natural frequency and the slow varying excitation, respectively. These equations provide the leading-order approximation to the fast dynamics of the dimer for primary pulse propagation. We note that the second set of equations (3.10a) is uncoupled from the first set and governs the fast oscillations of the light beads. It is interesting to point out that this is in the form of uncoupled linear oscillators with slowly varying frequencies and excitations. Once analytical approximations for the fast oscillations of these oscillators are derived, the fast oscillations of the heavy beads can be approximated by integrating twice the first set of equations (3.10a). Hence, it is interesting to note that in this order of approximation of, *the fast dynamics of the heavy beads is determined in terms of the fast dynamics of the light beads*, which is the reverse of what occurred in the slow dynamics at the leading order of approximation.

From the previous discussion it is clear that we only need to focus on the second set of slowly varying linear oscillators (3.10a) since these determine completely the fast dynamics of the dimer for solitary wave propagation. Once an analytical approximation of the fast oscillation of an arbitrary light bead, say the $2p$ −th light bead, $p \in \mathbb{Z}$, is computed, the responses of the other light beads can be determined by imposing appropriate time shifts (i.e., multiples of T) to the solution. Hence, in the remainder of this section we focus mainly on the analysis of the following linear oscillator with slowly varying frequency and forcing,

$$x''_{(2p)1}(t_1) + \Omega^2_{2p}(t_0)\, x_{(2p)1}(t_1) = f_{2p}(t_0) \tag{3.11}$$

this governs the fast oscillation of the $2p$ −th light bead of the dimer for solitary wave propagation. Clearly, localized solutions in terms of the slow time scale of (3.11) correspond to solitary waves in the dimer through appropriate time shifts.

Before proceeding to the analytic approximations of the localized solutions of (3.11) it is important to discuss the symmetry conditions that these solutions should satisfy according to the numerical results of the previous section. From the velocity profiles of the three localized solitary waves depicted in Figures 3.4, 3.5 and 3.6 it is noticed that they have reflectional symmetry with respect to the time instant where the two neighboring heavy beads attain equal (but non-zero) velocities. Based on this observation we formulate a *symmetry condition* for the solitary waves of the dimer. Indeed, for the $(i+1)$ −th light bead a *reference time instant* $\tau = \mathrm{T}_{s(2p)}$ is defined as the time instant at which its velocity profile attains a local extreme and the i −th and $(i+2)$ −th neighboring heavy beads [which compress the $(i+1)$ −th light bead in the squeeze mode] attain identical but non-zero velocities. The symmetry condition states that the velocity profile of the $(i+1)$ −th light bead has reflectional symmetry with

respect to the reference time instant $\tau = \mathrm{T}_{s(2p)}$. In fact this time instant may also be regarded as the point of maximum compression of the light bead by its neighboring heavy beads. Therefore, for the velocity profile v_{i+1} of $(i+1)-$th light bead we formulate the following symmetry condition:

$$\begin{gathered} v_{i+1}(\mathrm{T}_{s(i+1)} - \chi) = v_{i+1}(\mathrm{T}_{s(i+1)} + \chi), \quad \forall\ \chi \in \mathbb{R} \\ v_i(\mathrm{T}_{s(i+1)}) = v_{i+2}(\mathrm{T}_{s(i+1)}) \end{gathered} \tag{3.12}$$

Note that if the symmetry condition (3.12) is satisfied, it automatically prevents the appearance of oscillatory tail in the velocity profile of the light intruder (as in Figure 3.3) resulting from secondary reflections in the trail of the propagation of the primary pulse. Hence, the symmetry condition (3.12) provides the necessary condition for the formation of a localized solitary wave in the dimer by preventing scattering of the main pulse at the interfaces between beads.

The symmetry condition for the velocity profile of the $(i+1)-$th light bead implies that the corresponding displacement profile is *anti-symmetric* with respect to the reference time instant $\tau = \mathrm{T}_{s(i+1)}$. Recalling that the asymptotic approximation of the response of the light bead is given by,

$$x_{i+1}(t_0, t_1, \ldots) = s_{i+1}(t_0) + \varepsilon x_{(i+1)1}(t_1) + \ldots$$

where $t_0 = \tau, t_1 = \varepsilon^{-1/2}\tau$ and that the slow part $s_{i+1}(t_0)$ is already anti-symmetric with respect to the reference time instant, condition (3.12) implies that the fast part of the dynamics, $x_{(i+1)1}(t_1)$, should also be anti-symmetric with respect to the reference time instant. It follows that *a necessary condition for the existence of the solitary wave in the dimer*

is that the fast dynamics (3.11) *of the* $(i+1)-$ *th light bead is anti-symmetric with respect to the reference time instant*.

Returning to the fast dynamics (3.11) of the $2p-$th light bead, without loss of generality we assume that its reference time instant is equal to zero, i.e. $T_{s(2p)}=0$. We recognize that by construction the excitation $f_{2p}(t_0)$ is anti-symmetric, and the natural frequency squared $\Omega_{2p}^2(t_0)$ is symmetric with respect to the reference time instant $\tau=0$. It follows that in order to satisfy the anti-symmetry condition of the fast dynamics (3.11) with respect to $\tau=0$ we require that:

$$x_{(2p)1}(t_1=0)=0 \tag{3.13}$$

This provides a *necessary condition* for the formation of the solitary wave in the dimer.

A second condition that needs to be imposed on the asymptotic solution of the $2p-$th light bead is that it is localized in time and decays as $\tau\to\pm\infty$. Recalling the asymptotic approximation of the dynamics of the light bead, $x_{2p}(t_0,t_1,\dots)=s_{2p}(t_0)+\varepsilon x_{(2p)1}(t_1)+\cdots$, and taking into account that the slow part of the dynamics already satisfies this asymptotic requirement in the far field, we impose the condition that $\lim_{t_1\to\pm\infty}x_{(2p)1}(t_1)=0$. Taking into account the anti-symmetry condition for the fast dynamics it suffices to impose the condition:

$$\lim_{t_1\to+\infty}x_{(2p)1}(t_1)=0 \tag{3.14}$$

The combined relations (3.13) and (3.14) formulate *necessary and sufficient conditions* at $O(\varepsilon)$ approximation for the formation of solitary waves in the dimer and provide the appropriate boundary conditions for the asymptotic approximation of the fast dynamics of the $2p-$th light bead.

The next goal in this regard is to find the discrete values of ε for which conditions (3.13) and (3.14) are satisfied. Recalling that a small parameter ε enters into the problem (3.11) through the differentiation with respect to the fast time scale, it is convenient to rewrite (3.11) in terms of the slow time scale $t_0 = \tau$ as follows,

$$\ddot{x}_{(2p)1}(\tau)+\frac{\Omega_{2p}^2(\tau)}{\varepsilon}x_{(2p)1}(\tau)=\frac{f_{2p}(\tau)}{\varepsilon} \tag{3.15}$$

and seek the initial conditions $x_{(2p)1}(0) = 0$, $\dot{x}_{(2p)1}(0) = V$ and the specific values of ε for (3.14) to be satisfied. This task is performed numerically and the discrete set of values $\{\varepsilon_n\}$ and initial velocities $\{V_n\}$ required for the formation of solitary waves in the dimer are computed.

Before reviewing the numerical solutions of this problem, however, it is interesting to explore the possibility of constructing analytical approximations of the solitary wave solutions of (3.15). To this end we apply the Wentzel–Kramers–Brillouin (WKB) approximation [136, 161] under the assumption of ε sufficiently small. It is well known that the WKB approach ceases to be valid in the vicinity of turning points (i.e., at points of nullification) of $\Omega_{2p}(\tau)$, and in our case we are interested in finding an approximation of the solutions of (3.15) in the semi-infinite time interval $\tau \in [0, +\infty)$. However, $\Omega_{2p}(\tau)$ is an exponentially decaying function of time so there exists a *turning point at infinity*. It follows that for relatively small values of $\Omega_{2p}(\tau)$ the proposed methodology may become invalid. According to the WKB approximation we seek the solution of (3.15) subject to the aforementioned initial conditions in the form,

$$x_{(2p)1}(\tau) \sim \exp\left[\frac{1}{\varepsilon^{1/2}}\sum_{n=0}^{\infty}\varepsilon^{n/2}G_n(\tau)\right]+\frac{f(\tau)}{\Omega_{2p}(\tau)^2}, \quad \varepsilon \to 0 \tag{3.16}$$

where the first term represents the homogeneous solution of (3.15), whereas the second term is a particular solution of the problem. Although this approximation is valid in a finite interval $\tau \in [0, \mathrm{T}^*], \mathrm{T}^* < +\infty$, as shown below this interval provides the main contribution to the sought solitary wave. Inserting (3.16) into (3.15), and considering the zeroth-order terms we obtain the following results [where $j = (-1)^{1/2}$]:

$$
\begin{gathered}
G_0(\tau) = \pm j \int_0^\tau \Omega_{2p}(\zeta) d\zeta \;\Rightarrow \\
x_{(2p)1}(\tau) \cong \frac{C_1}{\sqrt{\Omega_{2p}}} \exp\left[\frac{j}{\sqrt{\varepsilon}} \int_0^\tau \Omega_{2p}(\zeta) d\zeta\right] + \frac{C_2}{\sqrt{\Omega_{2p}}} \exp\left[\frac{-j}{\sqrt{\varepsilon}} \int_0^\tau \Omega_{2p}(\zeta) d\zeta\right] + \frac{f(\tau)}{\Omega_{2p}(\tau)^2} \\
\equiv \frac{\tilde{C}_1}{\sqrt{\Omega_{2p}}} \cos\left[\frac{1}{\sqrt{\varepsilon}} \int_0^\tau \Omega_{2p}(\zeta) d\zeta\right] + \frac{\tilde{C}_2}{\sqrt{\Omega_{2p}}} \sin\left[\frac{1}{\sqrt{\varepsilon}} \int_0^\tau \Omega_{2p}(\zeta) d\zeta\right] + \frac{f(\tau)}{\Omega_{2p}(\tau)^2}, \\
\varepsilon \to 0
\end{gathered}
\tag{3.17}
$$

The anti-symmetry condition $x_{(2p)1}(0) = 0$ yields $\tilde{C}_1 = 0$. Imposing the second initial condition $\dot{x}_{(2p)1}(0) = V$ we determine the second constant $\tilde{C}_2$ as follows,

$$
\tilde{C}_2(\varepsilon, \mathrm{V}) = \left[\frac{\varepsilon}{\Omega_{2p}(0)}\right]^{1/2} \left[\mathrm{V} - \frac{\dot{f}(0)}{\Omega_{2p}^2(0)}\right] \tag{3.18}
$$

where it holds that $\dot{\Omega}_{2p}(0) = 0, \dot{f}(0) \neq 0$ owing to the symmetric and anti-symmetric nature of these functions, respectively. Therefore, the WKB asymptotical approximation in the finite interval $\tau \in [0, \mathrm{T}^*]$ reads:

$$
x_{(2p)1}(\tau) \cong \frac{\tilde{C}_2(\varepsilon, V)}{\sqrt{\Omega_{2p}}} \sin\left[\frac{1}{\sqrt{\varepsilon}} \int_0^\tau \Omega_{2p}(\zeta) d\zeta\right] + \frac{f(\tau)}{\Omega_{2p}(\tau)^2}, \quad \varepsilon \to 0 \tag{3.19}
$$

We can find sets of values $\{\varepsilon_n, \mathrm{V}_n\}$ for which the condition $\lim_{\tau\to+\infty} x_{(2p)1}(\tau) = 0$ is satisfied for (3.19), and solitary waves are formed in the dimer. Moreover, the analytical expression (3.19) compares favorably well with the direct numerical solution of problem (3.15) that satisfies (3.14). Hence, the WKB approximation (3.19) can be regarded as an *adhoc* analytical approximation of the solitary wave over the semi-infinite interval $\tau \in [0, +\infty]$. This is demonstrated in Figure 3.10, where the numerical solution of (3.15) for $\varepsilon_n = 0.062913$ and the analytical solution (3.19) for $\varepsilon_n = 0.062748$ are compared. We note that the solutions are in good agreement, especially in the finite interval of rapid oscillations of the response where the WKB approximation is valid.

Considering the WKB approximation (3.19) and imposing the condition of anti-resonance such that the displacement $x_{(2p)1}(\tau) \to 0$ as $\tau \to \infty$. It should be noted that $f(\tau)/\Omega_{2p}(\tau)^2 \to 0$ as $\tau \to \infty$. With these conditions imposed, we obtain a spectrum of mass ratios predicted by the WKB approximation in the form,

$$\lim_{\tau\to+\infty} \sin\left[\frac{1}{\sqrt{\varepsilon}}\int_0^{\tau}\Omega_{2p}(\zeta)d\zeta\right]=0 \Rightarrow \frac{1}{\sqrt{\varepsilon}}\int_0^{\infty}\Omega_{2p}(\zeta)d\zeta=\frac{4.7219}{\sqrt{\varepsilon}}=n\pi \Rightarrow \widehat{\varepsilon}_n=\left[\frac{4.7219}{n\pi}\right]^2,\quad m=1,2,... \tag{3.20}$$

For the WKB approximation in this and the next sections, we consider amplitude $\mathrm{A} = 3$ and time shift $\mathrm{T} = 1.937$ for the solitary wave (3.9b) in the auxiliary system. From the derived spectrum of mass ratios (3.20) it can be stated that there is a countable infinity of families of solitary waves that can be realized in a typical elastic dimer system.

In Table 3.1 we provide a comparison of the set of discrete values $\{\varepsilon_n\}$ where solitary waves are realized in the dimer, computed in three different ways: (i) by direct numerical simulations of the normalized system (3.3) – exact results in the center

column; (ii) by the numerical solutions of the asymptotic model (3.11) [or equivalently (3.15)] describing the fast dynamics of the light beads – approximate results in the left column; and (iii) mass ratio spectrum (3.20) predicted by WKB approximation. As stated previously the results predicted by the asymptotic model (3.11) and (3.20) have physical meaning only for sufficiently small values of ε, so it is expected that better convergence of the two sets of results for decreasing values of ε_n (or for increasing order n). This is confirmed in the results listed in Table 3.1, where we note that the approximate results converge to the corresponding exact results for increasing order n. Although the asymptotic analysis predicts the existence of a solitary wave for $\varepsilon_2 = 0.82835$ (for $n = 2$), this corresponds to the solitary wave in the homogeneous chain ($\varepsilon = 1$). Here it is remarked that for this relatively large value of normalized mass ratio the slow-fast partition of the dynamics is not valid for describing the solitary wave in the dimer, so the asymptotic analysis is not expected to be valid in that range of values of ε.

This analysis is concluded by commenting that the anti-symmetry conditions formulated for the solitary wave in the dimer may also be viewed in the context of imposing anti-resonance conditions in the bead dynamics. In fact, the absence of a 'tail' in the solitary wave is due to the anti-symmetry conditions (3.13) and (3.14), resulting in an *anti-resonance condition* in the dynamics of the dimer. This contrasts to a *resonance condition* in the dimer dynamics which occurs when a phase difference of $\pi/2$ exists at $\tau = 0$ between the response $x_{(2p)1}(\tau)$ and the (slow) excitation $f_{2p}(\tau)/\varepsilon$ of the fast oscillator (3.15). It is worth noting that such a nonlinear resonance leads to the drastic reduction of the transmitted normalized force in the plot of Figure 3.9a, through the magnification of the amplitudes of the traveling waves in the 'tail' of the propagating pulse and corresponding maximum radiation of a significant part of the energy of the pulse as it scatters at the interfaces between heavy and light beads; we note that this is

the exact opposite of the 'zero tail' situation of the solitary wave corresponding to the condition of anti-resonance. The resonance mechanism will be dealt in greater detail in the next section.

In this context, the formation of the solitary wave in the dimer for the eigenvalue $\varepsilon = \varepsilon_n$ determines the order of anti-resonance satisfied by the velocity profile of the solitary wave. Since the characteristic frequency $\Omega_{2p}(\tau)$ of the linearized system (3.15) is slowly varying we must resort to a non-standard definition of anti-resonance in this case. Hence, we will refer to the number of peaks exhibited in the fast oscillations of a light bead compared to the one peak of the applied force $f_{2p}(\tau)$ [cf. Figure 3.11 where numerical solitary waves of the asymptotic model (3.11) or (3.15) are depicted]. Considering the first value $\varepsilon = \varepsilon_2$ predicted by the asymptotic model (3.11), we note that the fast oscillations of the light bead possesses one peak, so this would correspond to a condition of $1:1$ anti-resonance between the applied force and the light bead response; however, as discussed previously this value of ε corresponds to solitary wave in homogeneous chain. At this value of mass ratio the slow fast decomposition of the dynamics is no longer valid and it should be noted that the forcing is no longer slow in comparison to the dynamics of the beads. Proceeding to the next eigenvalue $\varepsilon = \varepsilon_3$ the fast oscillation response of the light bead possesses two peaks (cf. Figure 3.11), so this would be a condition of $1:2$ anti-resonance which indeed corresponds to a class of physically realizable solitary waves parameterized by energy. Extending this argument, the class of solitary waves corresponding to the eigenvalue $\varepsilon = \varepsilon_n$ corresponds to an $1:(n-1)$ anti-resonance, with the fast oscillation response of the light bead possessing $(n-1)$ peaks compared to a single peak of the forcing function $f_{2p}(\tau)$. Hence, as the order n increases (and the eigenvalue ε_n decreases), the fast frequency of the light bead response also increases. It follows that each solitary wave solution in the dimer

corresponds to a precise anti-resonance condition which is equivalent to the anti-symmetry conditions posed previously.

Again, it is emphasized that the asymptotic analysis is valid only as long as the slow-fast time scale separation exists. Although it is not expected that the asymptotically predicted value of $\varepsilon_2 = 0.829$ will correspond to the formation of a solitary wave in the dimer, since that would imply an exact $1:1$ anti-resonance between the slow and fast dynamics, a fact that contradicts the slow-fast time scale partition upon which the asymptotic analysis is based. However, the rest of the asymptotically predicted anti-resonance conditions do correspond to physically realizable solitary waves in the dimer starting from $\varepsilon_3 = 0.2781$ which corresponds to $(1:2)$ anti-resonance between the slow and fast dynamics and indeed was numerically detected in the dimer chain (see Figure 3.4).

3.1.2.3 Conclusions

Summarizing the findings of this section, we demonstrated the existence of a new family of solitary waves in one-dimensional granular dimer chains with elastic interactions between beads according to the Hertzian interaction law and in the absence of pre-compression. The governing equations of motion was considered in normalized form, and thus the system dynamics was governed by a single parameter ε, defined as the ratio of normalized masses between the light and heavy beads of the dimer. It should be noted that these results are applicable to a general class of $1:1$ dimers of different materials and geometric properties.

The solitary waves in the dimer explored herein can be considered analogous to the solitary wave supported by the homogeneous granular chains discovered by Nesterenko [41, 42], in the sense that these localized solitary pulses do not involve

separations between beads; rather they satisfy special symmetries/anti-symmetries, or equivalently anti-resonances in the dynamics. We may conjecture therefore that these solitary waves are the direct products of a countable infinity of anti-resonances in the dimer. Moreover, it is found that the solitary waves in the normalized dimer propagate faster than the solitary wave in the normalized homogeneous granular chain obtained in the limit of no mass mismatch and composed of only heavy beads. This seemingly counter intuitive result indicates that under certain conditions nonlinear anti-resonances can increase the speed of wave propagation in periodic granular media, by providing new ways of transferring energy to the far field of this media. At the exact mass ratio where solitary waves are realized, any arbitrary disturbance disintegrates into a train of solitary waves and this indicates that solitary waves are the only mode of energy transfer in this media. This result is very much anologous to the homogeneous chain.

The asymptotic analysis of this section was based on slow-fast partitions of the dynamics, and can be applied to a more general class of granular media with periodic disorders. Such studies would identify efficient nonlinear mechanisms for effectively propagating energy through periodic granular media.

An additional interesting topic of application of the presented methodologies is to employ the reverse mechanism of resonances for efficiently attenuating propagating pulses in granular media. An initial indication of such a phenomenon can be observed in Figure 3.9a. It is interesting to note that the force transmitted for any arbitrary mass ratio is lower than that in the homogeneous chain. Lower transmitted force indicates the attenuation of the propagating pulse. Moreover, it is evident that there are peaks and valleys in the force transmitted curve and peaks indicate local maximum transmitted force, whereas valleys indicate local minimum transmitted force. The global minimum of this curve happens to be at a mass ratio of about 0.59 and from the practical point of view of shock mitigation this is of utmost importance. In view of this, the next section is

devoted exclusively for the study of the mechanism of resonance and its effect on the pulse attenuation.

3.1.3 Resonances Leading to Pulse Attenuation in Dimers

In this section we study nonlinear resonances in granular periodic one-dimensional chains. Specifically, we consider a dimer chain composed of alternating 'heavy' and 'light' spherical beads with no pre-compression. In the previous section we discussed the existence of families of solitary waves [97] that propagate without distortion of their waveforms. In these systems we attributed this dynamical feature to 'anti-resonance' in the dimer that led to the complete annihilation of radiating waves in the trail of the propagating solitary wave. Anti-resonances were associated with certain symmetries of the velocity waveforms of the beads of the dimer. In this section we consider the exact opposite phenomenon that is of the break of all waveform symmetries, leading to drastic attenuation of traveling pulses due to radiation of traveling waves to the far field. We use the connotation of 'resonance' to describe this dynamical phenomenon resulting in maximum amplification of the amplitudes of radiated waves that emanate from the propagating pulse. Each anti-resonance can be related to a corresponding resonance in the appropriate parameter plane. We study numerically and analytically the nonlinear resonance mechanism and show that it can lead to drastic attenuation of pulses propagating in the dimer. Furthermore, we estimate the discrete values of the normalized mass ratio between the light and heavy beads of the dimer for which resonances are realized. It is worth noting that all these phenomena considered herein are in dimer chains without pre-compression or dissipation.

The present section builds on the mathematical methodology developed in Section 3.1.2. The main focus in this section is to study the capacity of a 1: 1 dimer chain

to attenuate propagating pulses through maximization of radiated energy from the pulse to the far field. This will lead us to the study of *resonances* in general dimer chains, having the opposite effect of anti-resonances and resulting in maximum dispersion of propagating pulses due to the inherent (intrinsic) dynamics. Indeed, resonance or anti-resonance phenomena in dimers correspond to maximum amplification (hence maximum radiated energy to the far field) or complete elimination (hence formation of solitary waves) of oscillating tails in the trail of propagating pulses, respectively. These are opposite nonlinear dynamical mechanisms that are realized in $1:1$ granular dimer chains with appropriate parameters. The methodology developed herein can be generalized to general $1:N$ granular dimer chains and the corresponding study is presented in Section 3.2.

3.1.3.1 Numerical Evidence of Pulse Attenuation and Resonances in Dimers

Motivated by the results reported in Section 3.1.2 where anti-resonance phenomena in the dimer (3.3) were studied leading to families of solitary waves, we anticipate that (3.3) should support the reverse phenomenon of resonance, where traveling waves [98] radiating from a propagating pulse are significantly amplified for specific values of ε. This should not be counter intuitive given that the dimer typically scatters energy to the far field through oscillating 'tails' in the trail of propagating primary pulses. Thus, it is expected that when a resonance is realized, a traveling pulse is drastically distorted and attenuated as it propagates through the dimer. In Section 3.1.2 numerical experiments were performed to study pulse attenuation in the system of Figure 3.2 with 85 beads (excluding the fixed light bead at the right boundary), by applying a unit impulse excitation at the left end, and recording the maximum force transmitted to the right fixed boundary. Since the dimer system (3.3) is re-scalable with respect to the

magnitude of the applied impulse (energy), there is no loss of generality by considering unit impulse excitation and the results are applicable to arbitrary other excitation levels. Clearly, lower the force transmitted to the right end, higher is the capacity of the dimer to attenuate propagating pulses through scattering of the pulse by its inherent dynamics.

The plot of transmitted force versus normalized mass ratio ε is presented in Figure 3.9a [97]. At the discrete values $\varepsilon_{AR} = 0.3428, 0.1548, 0.0901, \ldots$ solitary waves (anti-resonances) are realized, evidenced as peaks (local maxima) of the plot. This indicates that formation of solitary waves is a mechanism for effective transmission of energy through the dimer. On the contrary, at the discrete values $\varepsilon_R \approx 0.59, 0.24, 0.12, 0.075 \ldots$ valleys (local minima) exist, corresponding to locally optimal scattering of the energy of the pulse by the dimer (with the exception of the first valley at $\varepsilon_R \approx 0.59$ which represents the global minimum). This hints at the realization of resonances at these values of the normalized mass ratio. Moreover, each anti-resonance is preceded and followed by a resonance and vice versa. As in the case of anti-resonances [97], it is conjectured that there exists a countable infinity of resonances in the dimer system (3.3) and this conjecture is proven true in the subsequent section.

We initiate our study of the dynamics of resonance in the dimer by examining the waveforms of the light and heavy bead responses at the discrete values $\varepsilon = \varepsilon_R$. In Figure 3.12a we present the velocity waveforms of a light bead and its adjacent heavy beads for the valley of the plot corresponding to $\varepsilon_R = 0.075$; the waveforms were shifted so that $\tau = 0$ lies at the center of the combined plot. In contrast to the anti-resonance case, the velocity waveforms are not symmetric, but instead exhibits maximum break of symmetry; that is, the fast component of the velocity waveform of the light bead has a phase difference approximately equal to $\pi/2$ compared to the corresponding waveforms of its adjacent heavy beads. The fast component of the dynamics corresponds to the high-frequency small-amplitude oscillations that are

superimposed to the slowly varying (averaged) dynamics. Furthermore, the velocity of the light bead does not decay to zero, but rather attains a finite non-zero velocity towards the end of the *'squeeze mode'* (Figure 3.3) [97]. Similarly, the velocities of the heavy beads decay to nonzero values, which is an indication that the primary pulse has lost a part of its energy as it propagated through the beads under consideration. In addition, contrary to anti-resonances where the light bead has zero displacement and nonzero velocity at the axis of symmetry ($\tau = 0$) [97], in resonances the light bead has nonzero displacement and zero velocity at the same time instant (cf. Figure 3.12b, c). For the numerical simulations we consider beads 51, 53 (heavy beads) and 52 (light bead) of the dimer chain excited by a unit impulse.

At the end of squeeze mode the response of the light bead does not decay to zero as in the case of anti-resonance [97] (Figure 3.13, 3.15, 3.17), but rather the light bead executes strongly nonlinear oscillations involving separation from its adjacent heavy beads. This mode generates the oscillating 'tails' that appear in the trail of the primary pulse transmission in the dimer. These are strongly nonlinear waves that propagate in the direction of the primary pulse and continuously radiate energy from the pulse to the far field. During resonance there is locally maximum (with respect to ε) amplification of these radiating waves, resulting in effective dispersion and attenuation of the propagating pulse. In fact, during resonance the primary pulse loses a part of its energy due to scattering at each interface between heavy and light beads, and significantly attenuates as it propagates through the dimer. It follows that *resonance not only represents a very effective dynamical mechanism for pulse attenuation in the dimer, but also, it is conjectured that this is the principal mechanism for pulse attenuation in a more general class of spatially periodic one dimensional dimer granular systems* [100]. In Figure 3.14 and 3.16 we depict representative bead waveforms for resonances realized at $\varepsilon_R \approx 0.12$ and 0.24, from which similar conclusions are drawn.

As described previously about the occurrence of resonance in between anti-resonances (Figure 3.9a), it can be seen that between any two anti-resonances there exists a specific mass ratio where the oscillatory tail maximizes. This is further evidenced by the series of responses shown in Figure 3.12 to 3.17. At a mass ratio of $\varepsilon_R \approx 0.075$, we observe maximization of the oscillatory tail as shown in Figure 3.12, but with slight increase in mass ratio to $\varepsilon_{AR} = 0.0901$ we observe complete annihilation of the tails. But surprisingly enough, with further increase in mass ratio to $\varepsilon_R \approx 0.12$, the oscillatory tail reappears with maximum amplitude. This transitions observed in Figure 3.12 to 3.17 corresponds to the discussion of phase difference between the fast velocity response of the light bead with respect to the forcing. It should be noted that the phase difference for the case of resonance is $\pi/2$, whereas that for the anti-resonance it is 0.

Focusing on the oscillating tail formed in the trail of the propagating pulse, it is noted that the entire granular chain gains momentum and traverses in the direction of the applied impulse. This traversing is similar to the rigid body motion, but with an internal degree of freedom where the light beads execute oscillations between the neighboring heavy beads. This rigid body type mode is depicted in Figure 3.18 in terms of the velocity profile of the heavy bead (bead 51). It is worth mentioning that periodic traveling waves (which bear resemblance to cnoidal waves [21], which are localized periodic traveling waves) are superimposed to the rigid body type motion. From the results of Figure 3.18 we note that the velocity of the rigid body type motion of the chain increases with increasing values of ε_R. For the numerical simulation we have considered varying impulses $(\{\varepsilon = 0.075, F = 0.5525\}, \{\varepsilon = 0.12, F = 0.56\}; \{\varepsilon = 0.24, F = 0.605\}; \{\varepsilon = 0.59, F = 1\})$ in order to match the amplitude of the propagating primary pulse. As discussed below, for smaller values of ε_R one can analytically predict the amplitudes of the oscillating tails and obtain estimates for pulse attenuation. However, since pulse attenuation for smaller values of ε_R is not substantial, these energy estimates are not of much practical significance. On the contrary, for the highest

value of $\varepsilon_R \approx 0.59$ it is noted that the velocity of the rigid body type motion is significant but the analytical estimate of energy loses accuracy. An energy estimate approach is presented in this section, but it is valid for a short length of the dimer chain.

The waveforms of the oscillating tails (radiated traveling waves) for a light and a heavy bead are depicted in Figure 3.19. We note that the motion of the heavy bead is not oscillatory like that of the light bead, but has small periodic depressions which correspond to the previously mentioned cnoidal like waves. These waves possess spatially periodic waveforms with sharp crests separated by wide flat troughs. Solitary waves are found in the limit of infinite wavelength of a family of cnoidal waves. The nearly constant levels of the waveforms of the heavy beads indicate a rigid body type velocity of the granular chain in the trail of the traveling pulse. Contrary to the motion of the heavy bead, the light bead executes periodic oscillations between the neighboring beads. The motion of the light bead is strongly nonlinear since it undergoes collisions between its neighboring heavy beads after separation.

As described previously, for the discrete set of values $\{\varepsilon_R\}$, resonances occur which are characterized by maximum amplitude tail oscillations. As for all nonlinear resonances, this should correspond to integral relationships between two or more characteristic frequencies of the dynamics. Indeed, this is exactly what happens during resonance in the granular dimer, when one considers the characteristic frequencies of the light beads in each of the two phases of their motion; that is, in the initial squeeze mode during the arrival of the primary pulse when the light beads are in a state of continuous compression from their neighboring heavy beads, and in the later collision mode (after the primary pulse has propagated) when the light beads collide with their neighboring heavy beads. These two characteristic frequencies, although attributed to two different dynamical behaviors determine the type of nonlinear resonance realized. During the squeeze mode the dynamics is linearized and the corresponding characteristic frequency can be asymptotically approximated [65], whereas during the

collision mode the dynamics is strongly nonlinear and the characteristic frequency of the bead collisions can only be estimated numerically. Nonlinear resonance occurs whenever these two frequencies become commensurate, and in the case of the dimer this frequency ratio is equal to $1:n$ where n is the integer that determines the order of the resonance. Hence, we conjecture that a countable infinity of nonlinear resonances can be realized in the elastic dimer chain.

In Figure 3.20 we depict the wavelet spectra of the fast components of the oscillations of the light bead (bead 52 of the dimer chain excited by unit impulse) for four specific resonances in the dimer. For $\varepsilon_R \approx 0.075$ the ratio of characteristic frequencies is approximately equal to 4 signifying $1:4$ resonance, whereas for $\varepsilon_R \approx 0.12$ and $\varepsilon_R \approx 0.24$ this ratio is about 3 and 2 and corresponds to $1:3$ and $1:2$ resonance respectively. In these cases a multi-scale partition of the dynamics can be performed, since the time scale of the squeeze mode is well separated from the time-scale of the collision mode. However, most important from a practical point of view is the case of $\varepsilon_R \approx 0.59$, with a frequency ratio of about 1 and thus $1:1$ resonance. Thus, the time scale separation between the squeeze mode and the oscillating tail that existed for smaller values of ε is completely lost.

As discussed later, the lack of time scale separation prevents the analytical treatment of the dynamics of the dimer in $1:1$ resonance. From a physical point of view, for this large value of ε the dynamics of the light beads cannot be regarded as being driven by the dynamics of their neighboring heavy beads anymore, but rather there is strongly nonlinear interaction between them. Yet, as the plot of Figure 3.9a indicates, $1:1$ resonance corresponds to the strongest possible pulse attenuation in the dimer (of about 75%) compared to the homogeneous chain composed only of heavy beads. The previous numerical results enable a classification of resonances in the dimer according to their order, for example, $\varepsilon_R^{(1:4)} \approx 0.075$, $\varepsilon_R^{(1:3)} \approx 0.12$, $\varepsilon_R^{(1:2)} \approx 0.24$ and $\varepsilon_R^{(1:1)} \approx 0.59$.

It is interesting that in the limit of small normalized mass ratio ε, one may derive analytical approximations for the amplitudes of the strongly nonlinear traveling waves that are radiated from the propagating pulse. Moreover, based on these estimates one will be able to analytically estimate pulse attenuation in the dimer chain. Considering the case of $1:4$ resonance corresponding to $\varepsilon_R^{(1:4)} \approx 0.075$ there is clear time scale separation between the two phases of the dynamics of the light beads. In the squeeze mode the frequency of oscillation is well modeled by linearized dynamics and can be analytically approximated [65]. Then, by imposing the resonance condition we can estimate the frequency of the traveling wave as four times lower than the linearized frequency of the squeeze mode. The amplitude of oscillation of the traveling wave is then estimated by regarding the displacements of the heavy beads adjacent to the light bead as being approximately zero (this is consistent with our earlier observation that the rigid body type mode of the chain is nearly negligible for small values of ε), so the equation of motion for the light bead as it collides with the nearly motionless heavy beads approximately reduces to,

$$\varepsilon\ddot{x} \approx (-x)_+^{3/2} - (x)_+^{3/2}, \quad x(0) = \Delta,\ \dot{x}(0) = 0 \tag{3.21}$$

for nearly conserved energy $h = (2/5)\Delta^{5/2}$ where Δ is the amplitude of oscillation and for $1:n$ resonance, $n > 1$. Solving the above strongly nonlinear oscillator (in terms of Hypergeometric functions) with the specified initial conditions, and matching the resulting oscillating tail frequency ($\omega_T \approx 1.5$) we predict the amplitude of the traveling wave as $\Delta_{est}^{(1:4)} \approx 0.0343$ compared to the numerical value of $\Delta_{num}^{(1:4)} \approx 0.03$ (cf. Figure 3.21a) for $\varepsilon_R^{(1:4)} \approx 0.075$. The responses shown in Figure 3.21 correspond to beads 51 to 53 of the dimer chain excited by a unit impulse. We note that an analytical solution of the model (3.21) is possible in spite of bead separation, since the dynamics involve at

most two-bead interactions at any given time. The frequency of oscillation is related to the amplitude in the form $\omega_T = 2\pi/(6.005092h^{-0.1}\sqrt{\varepsilon})$, where $h = (2/5)\Delta^{5/2}$ is the energy of the oscillator (3.21). Similar analysis for $1:3$ resonance corresponding to $\varepsilon_R^{(1:3)} \approx 0.12$ yields $\Delta_{est}^{(1:3)} \approx 0.0766$ corresponds to a tail frequency of $\omega_T \approx 1.45$. It differs considerably from the numerical value $\Delta_{num}^{(1:3)} \approx 0.057$ (cf. Figure 3.21b). This discrepancy should be expected since for increasing values of ε the rigid body type motion of the granular chain during propagation of the traveling wave is far from being negligible so that the model (3.21) is not valid.

Clearly, the previous analytical methodology cannot be applied for the case of $1:1$ resonance since it corresponds to a high value of mass ratio $\varepsilon_R^{(1:1)} \approx 0.59$. Given, however, the significant practical importance of $1:1$ resonance in pulse attenuation, we apply a different methodology for estimating the amplitude of the traveling wave, taking into account (to first order) the rigid body type motion of the chain. In this case, due to strongly nonlinear interactions and mixing of the time scales the dynamics is highly non-stationary. Nevertheless, as we show below if the aim is to predict the amplitude of the traveling waves just after the completion of the squeeze mode, an analytical approximation is still possible.

Considering the numerical simulations of Figure 3.21c we note that for $1:1$ resonance the amplitude of the tail oscillation is nearly equal to the pre-compression (Δ) experienced by the light beads from their neighboring heavy beads. Further we observe that the relative displacement between the left heavy bead and the light bead is minimum (zero in this case), whereas the relative displacement between the light bead and the right heavy bead is maximum at the same instant of time. In order to analytically study such a scenario, we create a reduced order model under the assumption that the light bead is compressed between its neighboring heavy beads with constant pre-compression Δ. It is worth noting that although the light bead is pre-

compressed, it still executes oscillations whose amplitude is approximately equal to the pre-compression, so the reduced order model for 1: 1 resonance is:

$$\varepsilon\ddot{x} \approx (\Delta - x)_+^{3/2} - (\Delta + x)_+^{3/2}, \quad x(0) = \Delta,\ \dot{x}(0) = 0 \tag{3.22a}$$

It is worth noting that in (3.22a) the motion of the neighboring heavy beads is neglected and the initial conditions are dictated by the previous scenario. Indeed, we assume that the light bead loses contact with the right heavy bead and at the same instant it is in maximum compression with the left heavy bead. Further we assume that the velocity of the light bead is zero at this instant of time and with appropriate rescaling,

$$\frac{d^2y}{d\hat{\tau}^2} \approx (1-y)_+^{3/2} - (1+y)_+^{3/2};\ y(0) = 1, \frac{dy(0)}{d\hat{\tau}} = 0 \tag{3.22b}$$

where the rescaled time $\hat{\tau} = \tau\sqrt{(\Delta^{1/2}/\varepsilon)}$ and $y = x/\Delta$.

No analytical solution of (3.22a) exists due to the presence of pre-compression, but by rescaling (3.22a) to the normalized form (3.22b) we can numerically estimate the frequency of oscillation. The period of oscillation of the oscillator (3.22b) for the specified initial condition is $\hat{\tau}_P \approx 3.71$. Imposing the condition of 1: 1 resonance between the frequencies of the strongly nonlinear oscillator (3.22a) and the squeeze mode frequency, the pre-compression can be analytically estimated to be $\Delta_{est}^{(1:1)} = \varepsilon^2(\omega_T\hat{\tau}_P/2\pi)^4$. For the response shown in Figure 3.21c we derive the analytical estimate of $\Delta_{est}^{(1:1)} \approx 0.12$ compared to the exact numerical solution of $\Delta_{num}^{(1:1)} \approx 0.1278$ (Figure 3.21c) for a tail frequency of $\omega_T \approx 1.3$. Hence, an accurate amplitude estimation of the oscillating tail in the trail of the primary pulse is achieved.

In addition, we can estimate the energy retained in each light bead once the primary pulse has propagated. To this end we consider a dimer chain excited by a

higher impulse of magnitude 4.7 and the corresponding estimate of the pre-compression is $\Delta_{est}^{(1:1)} \approx 0.397$. The total potential energy in the light bead when its velocity is zero can be estimated to be $h = (2/5)(2\Delta)^{5/2}$ or $h_{est} = 0.2247$, corresponding to a $\Delta_{est}^{(1:1)} \approx 0.397$; this is the energy retained by a single light bead. The motivation behind the reduced order model (3.22) and the energy estimations is to predict the rate of attenuation of the propagating primary pulse due to scattering at the interfaces between the heavy and light beads. Based on the previous estimation of the energy retained by each light bead after the pulse has been transmitted, we can develop an iterative procedure whereby we subtract the energy retained by each light bead from the energy of the propagating pulse. For this estimation we take into account that in the regime of 1: 1 resonance the propagating primary pulse spans about 9 beads in space. In our model the central of these 9 beads has maximum velocity and the velocities of the neighboring beads decrease gradually. When we consider the energy contained in the primary pulse, we actually consider the kinetic energy of each of these 9 beads and their elastic energy due to their mutual interactions. Similarly, we evaluate the total energy contained in the beads in the trail of the primary pulse and designate it as the energy of the oscillating tail. Since each light bead retains a portion of the energy of the pulse, the energy in the primary pulse diminishes gradually due to scattering. For the numerical simulation, we evaluate the instantaneous energies of the primary pulse and of the oscillating tail for a small time window $t_1 < t < t_2$ when the primary pulse propagates through 13 beads (bead 49 to 61). It is clear that the energy in the tail should be increasing with time, whereas the energy of the primary pulse should be decreasing at an equal rate.

Although a purely analytical prediction of the energy loss of the primary pulse due to scattering is not possible, we resort to numerically computing the total energy $h_{num}(t_1)$ of the primary pulse at time instant t_1 and build our analytical estimates

keeping this as the reference point. As the pulse propagates through a light bead, the light bead retains a part of its energy which was estimated previously as $h_{est} = 0.2247$. In the considered short time window $t_1 < t < t_2$ the primary pulse propagates through 12 beads, so if we assume that an equal amount of energy is retained by each of the six light beads we can estimate the energy of the pulse $h_{num}(t_2)$ at $t = t_2$ as $h_{num}(t_2) \approx h_{num}(t_2) - 6h_{est}$. In Figure 3.22a we depict the analytical estimate for the energy loss of the pulse in the regime of 1: 1 resonance and compare it to direct numerical simulation. We further depict the total energy in the system in order to verify that it remains constant in the time window considered. We note that the previous energy estimate provides an accurate description of pulse attenuation in this strongly nonlinear resonance regime.

At this point a comment should be made regarding the effect of the rigid body type motion of the dimer on the previous energy estimates. As shown in Figure 3.18, in the regime of 1: 1 resonance this motion can be quite significant, caused by the applied impulse at the left end of the dimer with the entire dimer drifting in the direction of the applied impulse. This rigid body motion, however, can be disregarded in the considered small time interval $t_1 < t < t_2$ as seen from the plot of Figure 3.22b, where the rigid body velocities of two heavy beads (the ones with maximum velocities at times t_1 and t_2, respectively) just after the time instants t_1 and t_2 are depicted. However, the contribution of the rigid body type motion in pulse attenuation cannot be neglected if we consider larger time windows than the one considered herein.

3.1.3.2 Beating Wave-packets following 1: 1 Resonance

In the previous section we explored the strongly nonlinear resonance phenomena giving rise to strong pulse attenuation in the dimer. It is interesting to note that the

effect of $1:1$ resonance in the upstream and downstream of the dimer chain is not similar. In fact in the upstream, vigorous energy radiation is observed in the trail of propagating pulse, whereas in the downstream the wave dynamics is contrastingly different. We now study numerically some interesting beating wave-trains that arise in the downstream of the dimer following $1:1$ resonance. Indeed, from the previous numerical simulations, the non-stationary nature of the oscillating tail for $1:1$ resonance should be evident. We note that in this case the dynamics of the dimer is qualitatively different in the vicinity and downstream of the primary propagating pulse. This qualitatively different behavior can be inferred when the system responses are viewed in the space-time plane. In what follows we provide a sequence of plots that illustrate the gradual change in the dynamics of pulse propagation as the normalized mass ratio ε varies.

In Figure 3.23 we depict pulse propagation in a free-free dimer with $\varepsilon = 0.3428$, composed of 301 beads and an applied impulse of unity at its left end. Moreover, we have normalized the velocity of each bead with respect to the applied impulse (this is owing to the rescalable character of the dimer chain). The selected value of ε corresponds to anti-resonance in the dimer and solitary wave formation, as confirmed by the spatio-temporal plot of Figure 3.23a. The secondary and tertiary solitary pulses following the primary solitary wave are generated by the initial transients during the formation of the solitary wave immediately after the application of the impulse. In Figure 3.23b we present velocity time series at spatial points of the dimer, and it can be seen that the solitary waves leave no oscillating tails (since solitary wave energy is conserved during propagation). In this case the solitary pulse spans about 7 beads of the dimer chain.

For an arbitrary value of ε away from the discrete set of anti-resonances, there occurs radiation of energy from the propagating pulse which reduces in amplitude as it propagates through the dimer. This is particularly evident in the neighborhood of the

global minimum of the plot of transmitted force of Figure 3.9a. In Figure 3.24a we depict the normalized velocity of the beads of the dimer in space-time plane for $\varepsilon = 0.5$. Although the general shape of the primary propagating pulse is still preserved, its energy content is considerably reduced due to energy radiation. In fact a train of traveling waves forming the oscillating tail of the pulse can be clearly discerned in that plot and in the plot of Figure 3.24b where the velocity time series of four heavy beads are presented.

Now we consider the most important resonance condition from the perspective of pulse attenuation, $1:1$ resonance. In the last simulation we observed that although there was attenuation, the shape of the primary pulse is preserved. In contrast, for $\varepsilon = 0.59$, there exist two distinct phases of the dynamics of the dimer. In the initial phase the propagating pulse is strongly attenuated but still preserves its localized shape as it propagates through the dimer. This is followed by the second phase where due to severe energy radiation, the primary pulse eventually splits into a wave-train of interacting secondary solitary waves that propagate through the dimer as a localized beating wave packet. Within this wave-packet we note nonlinear beat phenomena between nonlinearly interacting stationary pulses. This can be clearly visualized from the plot of Figure 3.25a.

The realization of the beating wave-packet after the disintegration of the initial primary pulse is realized when the faster- and higher-amplitude trailing secondary pulses of the wave-train coalesce, and eventually overcome the leading primary pulse. This phenomenon repeats itself to form a type of nonlinear beat (pulsation) as the wave packet propagates through the dimer. Perhaps the most interesting feature of the localized beating wave packet is that it radiates very small amount of energy as it propagates through the dimer, so it appears to be approximately preserved downstream. This is in contrast to the initial phase of the dynamics where substantial attenuation of the primary pulse occurs due to $1:1$ resonance. We note that the beating

wave-packet appears only after a relatively large number of beads (> 85), since a prerequisite for its formation is the complete disintegration of the initially formed primary pulse due to $1:1$ resonance. Indeed, the appearance of this wave-packet signifies the elimination of $1:1$ resonance in the dimer.

We observed similar formation of beating wave-packets in a small neighborhood of $1:1$ resonance (i.e., in the vicinity of $\varepsilon = 0.59$), which confirms that this type of wave-packets can only be realized after severe attenuation of primary pulse attenuation due to $1:1$ resonance. The resulting beating wave-packets appear to be formed due to local compression of a limited number of beads of the dimers propagating downstream. This prevents bead separation and collisions between beads, which leads us to conjecture that the beating wave-packet can be studied using techniques from nonlinear modulation theory [36]. A final note concerns the simulations used to generate the transmitted force plot of Figure 3.9a. These simulations were carried out for dimers composed of a total of 85 beads, that is, before the formation of the beating wave-packet. We selected this number of beads in order to ensure that the computation of the transmitted force was within the regime of $1:1$ resonance.

The previous results demonstrate the important role of nonlinear resonances in the dynamics of elastic granular dimers. In the following section we give an analytical study of the resonance mechanism. Specifically, we develop an asymptotic approximation for the leading edge of propagating primary pulses (wave fronts) and formulate a linear eigenvalue problem whose eigensolutions provide analytical approximations to the discrete set of values of the normalized mass ratio, $\varepsilon_R^{(1:l)}, l = 1,2, \ldots$ corresponding to nonlinear resonances in the dimer.

3.1.3.3 Analytical Study of Nonlinear Resonances in Dimers

Our approach is similar to the methodology in Section 3.1.2 where anti-resonances in the dimer system were studied. The analysis presented herein provides full analytical description of resonance in the dimer and proves that there is a countable infinity of values of ε for which resonances are realized. Reconsidering WKB solution to the $O(\varepsilon)$ equation (3.15),

$$x_{(2p)1}(\tau) \equiv \frac{\tilde{C}_1}{\sqrt{\Omega_{2p}}}\cos\left[\frac{1}{\sqrt{\varepsilon}}\int_0^\tau \Omega_{2p}(\zeta)d\zeta\right] + \frac{\tilde{C}_2}{\sqrt{\Omega_{2p}}}\sin\left[\frac{1}{\sqrt{\varepsilon}}\int_0^\tau \Omega_{2p}(\zeta)d\zeta\right] + \frac{f(\tau)}{\Omega_{2p}(\tau)^2} \qquad (3.23)$$

Theoretically, the decay of the slow frequency of (3.15) should be superexponentional, although this is not the case in the analytical result (3.23) since the first order approximations (3.9a-c) are based on Pade' approximations [44, 62] of the solitary wave (instead of the exact solution which is not available analytically). Then, we can make the argument that the rapidly varying oscillatory part of the solution that includes nearly all of the energy of the propagating pulse should decay to zero as time increases. The resulting solution can then be justified on physical grounds.

It is important to emphasize again that in the present study we are primarily interested in finding the special discrete set of parameter values $\left\{\varepsilon_R^{(1:l)}\right\}$ for resonance. In order to obtain this discrete set we formulate a boundary value problem – BVP for (3.23) by imposing the appropriate conditions for resonance (see discussion of Section 3.1.3.1):

$$\dot{x}_{(2p)1}(0)=0\ ,\ x_{(2p)1}(\tau \to -\infty)=0 \qquad (3.24)$$

Then, noting that,

$$\begin{aligned} f(0)=0;\ \Omega(0)\neq 0 \\ \dot{f}(0)\neq 0;\ \dot{\Omega}(0)=0 \\ f(\tau\to-\infty)=0;\ \Omega(\tau\to-\infty)=0 \end{aligned} \tag{3.25}$$

Applying the velocity boundary condition of (3.24) in (3.23), by considering (3.25) and in view of the fact that $\dot{f}(0)/\Omega_{2p}^2(t_0)\approx 0$, we have $\tilde{C}_2=0$. By applying the displacement boundary condition as $\tau\to\infty$ we formulate the following analytical condition for the resonance values:

$$\begin{aligned} &\lim_{\tau\to-\infty}\cos\left[\frac{1}{\sqrt{\varepsilon}}\int_0^{\tau}\Omega_{2p}(\zeta)d\zeta\right]=0\ \Rightarrow \\ &\frac{1}{\sqrt{\varepsilon}}\int_0^{-\infty}\Omega_{2p}(\zeta)d\zeta=\frac{4.7219}{\sqrt{\varepsilon}}=\frac{(2l-1)\pi}{2}\ \Rightarrow \\ &\varepsilon_R^{(1:l)}=\left[\frac{9.4438}{(2l-1)\pi}\right]^2,\ \ l=1,2,... \end{aligned} \tag{3.26}$$

This result (3.26) proves that there exists a countable infinity of nonlinear resonances in the dimer (3.3) in the range $0<\varepsilon\leq 1$. In between these two limits a countable infinity of nonlinear resonances is realized, with the most interesting from a practical point of view being the 1: 1 resonance since as discussed in previous sections it leads to strong pulse attenuation.

In Figure 3.26 we depict the WKB solution (3.23) for 1: 4 resonance realized for $\tilde{\varepsilon}_R^{(1:4)}\approx 0.07468$, and compare it to the numerical solution derived by numerically integrating system (3.15) subject to the boundary conditions (3.24) and for $\hat{\varepsilon}_R^{(1:4)}\approx 0.078$.

We note good agreement in the phase of the squeeze mode, but divergence in the regime of the collision mode. This is expected since our analysis does not account for bead separation occuring after the end of the squeeze mode. This result validates the WKB solution. We note, however, that the asymptotic model (3.15, 3.23, 3.24), as well as the WKB solution are valid only for higher order resonances since they are based on the separation of time scales of the dynamics of the squeeze and collision modes. As discussed in Section 3.1.3.1 this does not hold for the case of $1:1$ resonance where mixing of time scales occurs.

In Table 3.2 we provide a comparison of the resonance values $\varepsilon = \varepsilon_R$ predicted by the asymptotic model (3.15, 3.23, 3.24) and those derived by direct numerical simulations of the dimer system (3.3). We use the terminology ω_s for the fast frequency of the light bead during the squeeze mode and ω_T for the frequency of the oscillating tail during the collison mode [hats indicate estimates based on the asymptotic model (3.15)]. From these results the orders of the different resonances are identified, and the validity of the asymptotic model is validated in the limit of small ε. As mentioned previously, $1:1$ resonance represents the most important dynamical mechansism for passive pulse attanuation in the dimer (3.3). Yet, due to the fact that there occurs mixing of the time scales of the governing dynamics of the squeeze and collission modes, it is not possible to introduce slow-fast time scale decompositions in order to perform asymptotic analysis. This is also evidenced by the poor matching of the asymptotic and numerical results for $1:1$ resonance in Table 3.2. In the next section we focus exclusively on this important resonance and provide a simplified and alternative mathematical analysis based on the binary collision approximation.

3.1.3.4 Binary Collision Approximation for $1:1$ Resonance

In order to elucidate the dynamics of $1:1$ resonance, in Figure 3.27 we depict the relative displacements of four adjacent pairs of heavy and light beads (beads 51 to 58) in the dimer system (3.3) for a value of ε (≈ 0.625) close to $1:1$ resonance and excited by unit impulse. Moreover, we consider the initial phase of the dynamics where strong pulse attenuation occurs, prior to the formation of the beating wave-packet discussed in Section 3.1.3.2. This plot reveals a very interesting feature associated with this resonance, namely, that maximum compression between a pair of heavy and light beads occurs in approximate synchronicity with a secondary (smaller) peak of compression between the previous pair of beads. As detailed previously, the asymptotic analysis of the previous section cannot account for this behavior due to the lack of time scale separation for this resonance. This near-synchronization phenomenon will enable the analytical estimation of the value of the normalized mass ratio for $1:1$ resonance, without assuming time scale separation, but rather by resorting to the binary collision model [39, 104].

To this end, we consider a slightly modified model of the normalized dimer chain (3.3) (with odd numbered beads being 'heavy' with normalized mass equal to unity, and even numbered ones being 'light' with normalized mass equal to $0 < \varepsilon \leq 1$), by introducing identical fixed clearances (gaps) between adjacent beads. Motivated by the numerical results of Figure 3.27, we aim to reproduce the bead interaction scenario shown there. Assuming that an impulse is applied to the left boundary of this system, this scenario requires that after some initial transients, at the reference normalized time $\tau = 0$ a heavy bead (labeled 'bead H1') travels with constant positive velocity V_0 (in the direction of the applied impulse) and collides with the adjacent light bead (labeled 'bead L1') in a strongly nonlinear interaction with the time of interaction being a function of their relative velocity (if this relative velocity is small, the time of interaction is large and vice versa – see equations below). Once bead H1 transfers a part of its energy to bead L1 both beads continue to travel in the same direction, until bead L1

interacts with the next heavy bead (labeled 'bead H2'). Owing to momentum and energy conservation, the velocity of the light bead L1 changes sign becoming negative and that of the heavy bead H2 becomes positive. For realization of 1:1 resonance, we need to synchronize the time taken for the heavy bead H2 to interact with the next light bead (labeled 'Bead L2') with the time taken by the light bead L1 (which now has negative velocity) to interact with heavy bead H1 (which now has positive velocity).

To reproduce this scenario mathematically, we consider constant gaps (D) between neighboring beads and impose conservation of energy and momentum during binary bead interactions and realize the bead velocities listed in Table 3.3. Moreover, Based on these velocity values we can synchronize the time taken by the pairs of beads H1-L1 and H2-L2 to reach their maximum relative displacements, which in effect amounts to realization of 1:1 resonance. The interaction time between the beads is neglected in this approximation for the sake of simplicity. The time taken by L1 to interact with H2 is $D(1+\varepsilon)/(2V_0)$. During this time duration, H1 (with velocity $(1-\varepsilon)V_0/(1+\varepsilon)$) would have traversed a distance of $D(1-\varepsilon)/2$. Further, the time duration for H2 to interact with L2 is $D(1+\varepsilon)^2/(4V_0\varepsilon)$. The time synchronization for the second interaction of H1-L1 and first interaction of H2-L2 can be denoted as below,

$$\frac{\left(D-\frac{D(1-\varepsilon)}{2}\right)}{V_0\left(\frac{1-\varepsilon}{1+\varepsilon}+\frac{2(1-\varepsilon)}{(1+\varepsilon)^2}\right)}=\frac{D(1+\varepsilon)^2}{4V_0\varepsilon} \tag{3.27}$$

This leads to the following quadratic equation in ε,

$$3\varepsilon^2+4\varepsilon-3=0 \tag{3.28}$$

this has only one acceptable real root $\bar{\varepsilon}_R^{(1:1)} = 0.537$ in the interval $(0, 1]$. This provides the analytical estimate for the normalized mass ratio corresponding to $1:1$ resonance, and compares favorably well to the exact numerical value of $\varepsilon_R^{(1:1)} \approx 0.59$. In Figure 3.28 we depict the relative displacements for the pairs of beads discussed in the previous binary collision scenario with the imposed synchronicity for $1:1$ resonance. It is clear that the binary collision model correctly predicts the significant attenuation of the pulse caused by $1:1$ resonance, although it over predicts this attenuation. This is concluded by comparing the plots of Figure 3.28 and the exact numerical plots depicted in Figure 3.27.

3.1.3.5 Conclusions

In this section we explored resonance phenomena in dimer chains with no pre-compression. Resonances are a feature of the intrinsic dynamics of these systems and can lead to strong dispersion and attenuation of propagating pulses. In that context, $1:1$ resonance was found to provide the most optimal results. In this study no dissipative mechanism of any form is incorporated, so pulse attenuation is attributed solely to redistribution of the energy of the propagating pulse to strongly nonlinear modes of the dimer and to traveling waves radiating energy to the far field. Under condition (or near condition) of $1:1$ resonance we detected two distinct phases of pulse propagation in the dimer: An initial regime of strong pulse attenuation due to pulse scattering, followed by a regime where the pulse disintegrates to strongly pre-compressed modulated wave packet of nonlinearly interacting solitary waves that propagates without radiating energy. Hence, when $1:1$ resonance is realized in the dimer, there exists an initial strongly nonlinear regime of strong pulse attenuation, followed by a regime where a

beating wave-packet (involving a limited number of beads in compression) propagates nearly un-attenuated in the dimer. This is one more indication of the complexity of the nonlinear dynamics of this granular medium.

The methodologies developed in this section can be applied to more general classes of periodic polydisperse granular media with or without pre-compression. For example, similar analysis can be applied for the case of periodically varying granular media composed of periodic sets with varying numbers of heavy and light beads. It is interesting to note that although these systems (as well as the dimers considered herein) are non-integrable dynamical systems [162], one can still apply asymptotic analysis based on slow/fast time scale partitions or binary collision approximations in order to formulate and predict the conditions for realization of strongly nonlinear resonances. It would be interesting to relate resonance phenomena to the capacity of periodic polydisperse granular media for pulse attenuation, and to study the effects of pre-compression on the resonance dynamics of these systems. As discussed previously, the results presented herein are for the 1: 1 dimer chains without pre-compression. Whereas the realization of practical granular chains without pre-compression is far from reality. Thus it is of practical significance to study the effect of pre-compression on the resonance and anti-resonance dynamics. The next section is concerned with this study.

3.1.4 Effect of Pre-compression on Resonances and Anti-resonances in Dimers

In the previous sections we considered the dimer system (3.3) without pre-compression. In practical situations, however, realization of systems without pre-compression is seldom possible, so it is of interest to study its effect on the resonance dynamics. It is well known [42] that pre-compression in ordered granular chains adds a linear component in the dynamics by making separation between beads less possible;

moreover, in the limit of high pre-compression, the strong nonlinearity is eliminated and the dynamics becomes linearized. In the context of this work, it is of interest to investigate how pre-compression affects the strongly nonlinear resonance dynamics discussed in the previous sections, since this has obvious practical implications as it relates to the capacity of the dimer to passively attenuate propagating pulses.

Considering a dimer system with set pre-compression Δ_0 the equations of motion are given by,

$$\begin{gathered} m_i \frac{d^2 u_i}{dt^2} = (4/3) E_* \sqrt{R} \left[(\Delta_0 + u_{i-1} - u_i)_+^{3/2} - (\Delta_0 + u_i - u_{i+1})_+^{3/2} \right] \\ m_{i+1} \frac{d^2 u_{i+1}}{dt^2} = (4/3) E_* \sqrt{R} \left[(\Delta_0 + u_i - u_{i+1})_+^{3/2} - (\Delta_0 + u_{i+1} - u_{i+2})_+^{3/2} \right] \\ i = 1, 3, 5, ..., 2N\text{-}1 \\ u_0(t) = 0,\ u_{2N+1}(t) = 0 \end{gathered} \tag{3.29}$$

where we use the notation and the parameter definitions of Section 3.1.2. We non-dimensionalize the bead displacements with respect to the fixed pre-compression Δ_0 by introducing the new variables,

$$x = \frac{u}{\Delta_0},\ \ \tau = t \sqrt{\frac{E_* \Delta_0 \sqrt{R}}{\pi R_i^3 \rho_i}} \tag{3.30}$$

and expressing (3.29) in the following normalized form,

$$\begin{gathered} \ddot{x}_i = (1 - x_i + x_{i-1})_+^{3/2} - (1 - x_{i+1} + x_i)_+^{3/2} \\ \varepsilon \ddot{x}_{i+1} = (1 - x_{i+1} + x_i)_+^{3/2} - (1 - x_{i+2} + x_{i+1})_+^{3/2} \\ x_0(\tau) = 0,\ x_{2N+1}(\tau) = 0 \end{gathered} \tag{3.31}$$

We observe that the dynamics is again governed by the parameter ε but also by the energy level since it is not rescalable any more with respect to the applied impulse (as it was for the case of system with no pre-compression). We conclude that the dynamics of the pre-compressed dimer is governed by two parameters, and the results depend on the specific energy level considered. Moreover, *depending on the magnitude of the applied impulse, system* (3.31) *can be characterized as strongly or weakly pre-compressed*. For very strong applied impulses and fixed pre-compression, the system is strongly nonlinear since it approaches the state of zero pre-compression. On the contrary, for very weak applied impulses (again keeping the pre-compression fixed) the system is weakly nonlinear or almost linear reaching the state of strong pre-compression. In fact, for the normalized pre-compressed dimer (3.31) we ascertain the level of pre-compression by invoking the following criterion:

$$(1+x_{i-1}-x_i)=\begin{cases}<0, \text{ Beads detached}\\ \geq 0, \text{ Weak precompression}\\ \gg 0, \text{ Strong precompression}\end{cases} \tag{3.32}$$

We wish to study how the capacity of the dimer for pulse attenuation is affected by pre-compression. As shown previously the pulse attenuation capacity of the dimer is closely tied to the realization of resonances and, in particular, of $1:1$ resonance. Hence, our study is directed to the effect of pre-compression on the strongly nonlinear resonances realized in the dimer with no pre-compression. To this end, we consider a system similar to the one shown in Figure 3.2 but with constant pre-compression, forced by an impulse $F\delta(\tau)$ at its left boundary, and compute the force transmitted to the right boundary. Further, we normalize this force with respect to the corresponding force transmitted in the homogeneous granular chain with only of heavy beads (i.e., with $\varepsilon = 1$). Since the pre-compressed dimer is governed by two parameters, namely the

normalized mass ratio ε and the magnitude of the applied impulse F, we need to study the force transmission in a two dimensional parameter plane. This is performed in the plot of Figure 3.29a for parameter ranges $\varepsilon \in (0,1]$ and $F \in [1,100]$, with resolution equal to 0.01 units for the mass ratio, and 4 units for the magnitude of applied impulse.

It should be clear that for weak impulses the system is nearly linear and non-dispersive as evidenced by the fact that the variation of the normalized mass ratio has no effect on the transmitted force. However, for moderate applied impulses the dynamics is weakly nonlinear and dispersion of the pulse becomes more evident. In the limit of strong applied impulses, the dynamics approaches the strongly nonlinear regime of no pre-compression and exhibits strong pulse dispersion and attenuation; then we converge towards the result of Figure 3.9a for the dimer with zero pre-compression. We note that in the regimes of weakly or strongly nonlinear dynamics the nonlinearity may balance the dispersion leading to families of solitary waves which propagate undistorted and un-attenuated in the dimer [97]. Clearly, no solitary waves exist in the limit of weak applied impulses where the response is nearly linear. But in the limit of strong pre-compression, the chain is both linear and approximately non-dispersive and thus a pulse can propagate without dispersion or scattering for any arbitrary mass ratio.

At stronger levels of pre-compression, the plot of transmitted force flattens out so that peaks and valleys are eliminated. In this case no global minimum for the transmitted force exists and better pulse attenuation is achieved for low normalized mass ratios. This behavior is explained when one considers that for strong pre-compression the dynamics is nearly linear so pulse transmission and attenuation between the pairs of heavy and light beads is governed by linear interactions. In this case, large linearized impedance mismatches between beads lead to relatively stronger pulse dispersion and attenuation. Based on these results we can state that *pre-compression in the dimer is detrimental to the objective of passive pulse mitigation*.

From these results we note that for relatively weak pre-compression (i.e., in the regime of strongly nonlinear response) we can still discern local minima and maxima in the plot of the transmitted force, indicating the preservation of resonances and anti-resonances (solitary waves), respectively. We conclude that *the strongly nonlinear resonance dynamics of the dimer cannot be destroyed by weak pre-compression*. However, it is also clear that the capacity of the dimer for pulse attenuation due to resonance is diminished by pre-compression. In summary, when a linear component is added to the dynamics due to weak pre-compression, pulse attenuation deteriorates but is still realized in the pre-compressed dimer.

It has been proved that with proper tuning of the parameter of mass ratio, the dimer can either support families of anti-resonances/solitary waves or resonances. The principal distinguishing feature of this phenomenon is the complete elimination or the maximization of the oscillating tail in the trail of the propagating primary pulse. From a practical point of view of utilizing the granular dimer in shock mitigation/attenuation applications, resonance is of great importance. As described previously, the oscillatory tail in the trail of the primary pulse governs the attenuation of the propagating pulse. It is interesting to note that the oscillating tails exhibit the form of periodic traveling waves (cf. Figure 3.21a, b). The maximization of the amplitude of these waves leads to substantial energy loss from the propagating pulse and eventually leads to its attenuation. Thus it is of primary interest to study the effect of these traveling waves on the efficacy of the dimer chain in attenuating propagating pulse and the effect of mass ratio on the excitation of such periodic traveling waves. Furthermore, it is of interest to compare their inherent dynamics and their excitation in relation to the global propagatory dynamics in this system. In view of these observations, the next section will deal with the study of periodic traveling waves and their dynamics in 1:1 dimer chains.

3.1.5 Periodic Traveling Waves and Bifurcations

In contrast to the special set of solitary waves that are realized for a discrete set of the mass ratio ε, for arbitrary values of ε, a primary pulse propagating in the dimer continuously radiates energy in the form of oscillatory tails in its trail [91]. Surprisingly enough, at certain values of ε these oscillatory tails take the form of spatially periodic traveling waves with different spatial periodicities (wavenumbers). This was the first instance of realization of traveling waves in dimer chains.

This section is concerned with the dynamics of spatially periodic traveling waves supported by strongly nonlinear granular dimer chains with no pre-compression. In particular, the dynamical responses of semi-infinite dimer chains subject to impulsive excitation has revealed very peculiar, spatially periodic patterns of traveling waves, excited in the trail of propagating wavefronts. Moreover, it is interesting to note that these spatially periodic traveling waves exhibit similar characteristics to the waves observed in homogeneous chains [63] with periodic boundary conditions. These traveling waves depend on a single system parameter, the mass ratio of the two beads forming each dimer pair of the chain. It is conjectured that the formation of these waves in semi-infinite dimer chains is not accidental, but rather it is indicative of special internal symmetries hidden in the structures of these complex dynamical systems. Another interesting observation from recent studies is that the variation of the mass ratio of the heavy and light beads of the dimer may lead to complete loss of stability of traveling waves. In fact, it is conjectured that strong attenuation of propagating pulses in these dimers is highly correlated with the stability of spatially periodic waves supported by the dimer chain. Currently there is an absence of theoretical models that are capable of adequately explaining the exact mechanism responsible for the efficient

attenuation of propagating pulses in heterogeneous granular structures; the correlation of the loss of stability and of bifurcations of traveling waves to pulse attenuation may provide this mechanism. The theoretical understanding of the mechanism of strong pulse attenuation is of high scientific and practical importance when designing ordered granular media as efficient shock mitigators.

The dynamics of these families of traveling waves is systematically studied by considering finite dimer chains (termed as the 'reduced systems') subject to periodic boundary conditions. In this section we demonstrate that these waves may exhibit interesting bifurcations and or loss of stability as the system parameter varies. In turn, these bifurcations and stability exchanges in infinite dimer chains are correlated to previous studies of pulse attenuation in finite dimer chains through efficient energy radiation from the propagating pulse to the far field, mainly in the form of traveling waves. Motivated by these observations, in this section we pursue a numerical study of the dynamics of spatially periodic traveling and standing waves in finite dimer granular chains subject to periodic boundary conditions. We demonstrate the existence of bifurcations of these waves as the mass ratio between the heavy and light beads vary. In addition, these bifurcations are correlated with wave propagation in semi-infinite dimer chains. Based on these findings a new formulation of attenuation and propagation zones (stop and pass bands) of semi-infinite granular dimer chains is proposed.

3.1.5.1 Excitation of Families of Traveling Waves in Semi-Infinite Dimer Chains

In the following numerical simulations we consider a semi-infinite dimer chain with a free left boundary where an impulsive force is applied, and numerically study the resulting propagating pulse in the chain. As a first demonstration of the excitation of

spatially periodic traveling waves in the dimer chain, in Figure 3.30 we depict the velocity responses of beads 49 to 54 of the semi-infinite dimer for the system with $\varepsilon = 0.303$. In this and the following simulations of this section the semi-infinite dimer is excited by an impulsive excitation $F(\tau) = F\delta(\tau)$ applied to the left free end where $F = 0.95$. It should be noted that there is a propagating primary pulse leaving an 'oscillating tail' in its trail. This trail is due to the energy radiation from the primary pulse to the dimer and eventually causes continuous attenuation of the amplitude of the pulse and the maximization of this tail is denoted as resonance and the mechanism of annihilation of tails is called the anti-resonance. Moreover, careful consideration of the oscillating tail reveals that it is composed of a nearly exact traveling wave of a 6-bead spatial periodicity, in the sense that it repeats itself every other 6 beads, or every 3 periodic sets. This periodicity can be ascertained by the time period shown in the inset of Figure 3.30. Indeed, the time period of the wave is equal to T and the constant time shift between the response profiles of any two adjacent heavy and light beads is equal to $T/3$. As we are concerned only with $1:1$ periodic traveling waves, i.e., with time-periodic oscillations where the frequencies of the heavy or light beads are identical, the mentioned time period and time shifts are identical for both the heavy and light beads. Since the time shift between any two adjacent heavy or light beads is equal to $T/3$, we designate such a wave as a 6-bead periodic traveling wave.

Surprisingly enough, such traveling waves in the trail of propagating pulses in the dimer can only be realized at special discrete values of the mass ratio ε, and their spatial periodicities vary with ε. To highlight this point, in Figures 3.31 we depict the formation of traveling waves with 8- bead periodicity by considering the velocity responses of beads 49 to 56. Indeed, the corresponding time shift can be computed as $T/4$, where, as in the previous example, T denotes the corresponding time periods of these waves. Clearly, the time period T is a function of the energy of the dynamics, i.e., of the applied external impulsive excitation, so that higher impulses produce traveling

waves of smaller time periods and vice versa. Furthermore, traveling waves of other periodicities can be realized in an impulsively excited semi-infinite dimer chain. However, the periodicity (not to be confused with time period T) and the waveform of these traveling waves are only functions of mass ratio ε, and do not depend on energy (within the assumed elastic limit of the bead interactions). An interesting feature to be noticed is that at the lower value of $\varepsilon = 0.017$ we observe a standing wave with 4-bead periodicity; that is, in this case a stationary time-periodic oscillation (ringing mode) forms in the trail of the propagating pulse in the dimer, as depicted in the velocity response of beads 49 to 52 shown in Figure 3.32. This special mode is characterized by constant rigid body velocity of the heavy beads and out-of-phase oscillation of the light beads superimposed over the rigid body motion. The rigid body velocity observed in this case is negligibly small due to the smallness of ε. Once the rigid body motion is decomposed from the response, we observe that the heavy beads stand stationary whereas the light beads execute out-of-phase oscillations. In fact, the standing wave in this degenerate, non-smooth system is realized due to perfect balance of momentum between successive light beads, which leaves the intermediate heavy beads completely stationary at all times. In the next section we illustrate a very interesting bifurcation undergone by the traveling wave with 4-bead periodicity to such a standing wave.

We note that the dimer granular system under consideration is rescalable with respect to the applied impulse, hence, the only parameter governing the system dynamics is the normalized mass ratio ε. Our primary aim in this study is to explore the traveling waves in different periodic dimer chains and ascertain their stability and possible bifurcations with changing mass ratio ε. Further, we conjecture that the existence and stability of these waves influence the capacity of the dimer to passively attenuate propagating pulses due to its intrinsic dynamics. Finally, we make the remark that due to the previously mentioned rescaling with respect to energy, our results are quite general and apply to general elastic dimer chains with different spherical bead

configurations and under varying applied impulsive excitations, as long as the assumptions associated with the construction of the models (3.1) and (3.3) are satisfied as described in Chapter 1.

3.1.5.2 Dynamics of Periodic Traveling Waves in Dimer Chains

In a previous work [63], traveling waves in homogeneous granular chains were explored. The system considered in [63] contained a finite number of identical beads and possessed periodic boundary conditions to accommodate the sought spatial periodicity of the traveling waves. By periodic boundary conditions it is meant that the first and the last beads are in mutual interaction. For example, considering a finite chain composed of n beads, the first bead is in interaction with both the second and $n-$ th beads, whereas the $n-$ th bead is in interaction with the first and the $(n-1)$ $-$th bead. Using this scheme, traveling waves with different spatial periodicities could be studied, and, further led to the conjecture that the family of solitary waves studied by Nesterenko [41, 42] was the limit of a countable infinity of families of these traveling waves as the spatial periodicity of the waves tend to infinity.

In an effort to systematically study traveling waves in the dimer system and to correlate them with the numerical results reported in the previous section for the impulsively excited semi-infinite dimer chain, in the spirit of [63] we will study the realization of traveling waves in a finite dimer chain with periodic boundary conditions; we will denote these finite dimers as 'reduced systems'. Similar to [63] the infinite repetition of the reduced chains due to the periodic boundary conditions produces dimer chains of infinite extent. Given that the dimer consists of series of pairs of beads, the total number of beads in the finite chain should always be an even number.

The equations of motion for the reduced chain are given below, considering the first bead to be heavy with normalized mass equal to unity and the last bead to be light with normalized mass equal to ε (defined previously in Section 3.1.2):

$$\begin{aligned}
\ddot{x}_1 &= (x_n - x_1)_+^{3/2} - (x_1 - x_2)_+^{3/2} \\
\varepsilon\ddot{x}_2 &= (x_1 - x_2)_+^{3/2} - (x_2 - x_3)_+^{3/2} \\
&\cdots \\
\ddot{x}_i &= (x_{i-1} - x_i)_+^{3/2} - (x_i - x_{i+1})_+^{3/2} \\
\varepsilon\ddot{x}_{i+1} &= (x_i - x_{i+1})_+^{3/2} - (x_{i+1} - x_{i+2})_+^{3/2} \\
&\cdots \\
\ddot{x}_{n-1} &= (x_{n-2} - x_{n-1})_+^{3/2} - (x_{n-1} - x_n)_+^{3/2} \\
\varepsilon\ddot{x}_n &= (x_{n-1} - x_n)_+^{3/2} - (x_n - x_1)_+^{3/2}
\end{aligned} \tag{3.33}$$

where $i = 1,3,\ldots,n-1$, and n $(n > 2)$ is an even number as discussed previously. In particular, for $n = 2$, we obtain the two-dimensional reduced system:

$$\begin{aligned}
\ddot{x}_1 &= (x_2 - x_1)_+^{3/2} - (x_1 - x_2)_+^{3/2} \\
\varepsilon\ddot{x}_2 &= (x_1 - x_2)_+^{3/2} - (x_2 - x_1)_+^{3/2}
\end{aligned} \tag{3.34}$$

Introducing the change of coordinates, $\eta = (x_1 + \varepsilon x_2)/(1 + \varepsilon)$ (denoting the motion of the center of mass of the periodic set consisting of a pair of heavy and light beads) and $\sigma = x_1 - x_2$ (denoting the relative motion between the heavy and light beads of the periodic set) the equations (3.34) are transformed to,

$$\begin{aligned}
\ddot{\eta} &= 0 \\
\sigma'' &= (-\sigma)_+^{3/2} - (\sigma)_+^{3/2}
\end{aligned} \tag{3.35}$$

where prime denotes differentiation with respect to the 'fast' time scale $\tilde{\tau} = \tau[(1 + \varepsilon)/\varepsilon]^{1/2}$. In this coordinate system the center of mass would have a simple solution of the form $\eta = C_1 + C_2\tau$, where C_1 and C_2 are integration constants determined from the initial conditions. This solution would lead to a rigid body motion of the periodic set if $C_2 \neq 0$; otherwise, if $C_2 = 0$, the center of mass of the periodic set is displaced by a constant amplitude equal to C_1. Furthermore, the consideration of the equation governing the relative displacement $\sigma(\tilde{\tau})$ would lead us to a standing wave wherein the pair of heavy and light beads executes out-of-phase oscillations [63]. In Figure 3.33 we depict this mode realized for an arbitrary value of $\varepsilon = 0.75$ and $C_1 = C_2 = 0$ (i.e. the center of mass of the two beads remains stationary). In essence, the only time-periodic solution that can be realized in a reduced system with $n = 2$ is this standing wave (or nonlinear normal mode in the notation of Chapter 2 [12, 85]). As we are concerned primarily with traveling waves in periodic dimer chains, this system would not be of particular interest in our study. Hence, we proceed to consider the 4-bead reduced system with periodic boundary conditions, seeking traveling waves with 4-bead spatial periodicity.

Before embarking on exploring the dynamics of these traveling waves, it is worth noting some of their salient features. In Figure 3.34 we present the traveling wave in a 4-bead reduced system with periodic boundary conditions for mass ratio $\varepsilon = 1$ (homogeneous chain) [63]. These waves are qualitatively different from traveling solitary waves in homogeneous [41] and dimer chains [97]. Indeed, traveling solitary waves are special solutions with no bead separation either in the wavefront of the propagating pulse or in its trail, whereas propagation of traveling waves exhibit separation between adjacent beads, and, hence, are strongly nonlinear and non-smooth motions. This can be deduced even from the traveling waves in the impulsively forced semi-infinite dimer chains depicted in Figures 3.30 and 3.31. Separations between beads give rise to collisions, add high complexity in the dynamics, and prevent direct

analytical treatment of the resulting strongly nonlinear oscillations of the dimer by means of available analytical techniques. It follows that these traveling waves can only be studied numerically, although attempts have been made to study these waves analytically [99].

We also note that due to the nonlinear nature of the Hertzian interaction law between beads, the dynamics of the system is expected to depend on the intensity of the applied excitation (or energy). As shown in the previous section traveling waves realized in the impulsively excited semi-infinite Hertzian chain are realized at specific discrete values of the mass ratio ε at a given energy level. Hence, one of the objectives of this section is to study the effect of the mass ratio and the periodicity n on the dynamics of traveling waves in dimer systems. To this end, we will resort to a numerical continuation technique. The basic philosophy of the numerical continuation will be, (a) to compute traveling wave solutions realized in homogenous reduced systems consisting of even number of beads and with periodic boundary conditions, and (b) to invoke a numerical continuation procedure by varying the masses of the even-numbered (light) beads incrementally, and study the traveling wave solutions that are realized at every decrement of the mass ratio. This procedure proves to be very effective when the decrement in the mass ratio is sufficiently small. In what follows, we provide results of the outlined continuation technique corresponding to three different dimer periodicities, and discuss their subtle features.

Fixing the normalized energy of the reduced system to unity, we decrease the value of ε, and compute numerically the corresponding traveling wave solutions that result as numerical continuations of the solution depicted in Figure 3.34. In Figure 3.35 we depict the traveling wave in the system with $\varepsilon = 0.75, n = 4$ and unit normalized energy of the reduced system. We note that for decreasing ε, the amplitudes of the light beads increase, while those of the heavy beads decrease. It is to be noted that in this traveling wave solution (as in each of those that follow) the initial conditions of the

beads are rescaled in order to preserve the normalized total energy of the reduced system to unity. As a result, the frequencies of the traveling wave solutions increase with decreasing ε.

By further decrease of the value of ε (and fixed normalized energy of the reduced system equal to unity), the amplitudes of the heavy beads in the traveling wave solution decreases continuously and monotonically until they reach zero at $\hat{\varepsilon} \approx 0.53$. Then the standing wave solution is realized, as discussed in the previous section; in this stationary mode all light beads execute out-of-phase oscillations with identical amplitudes, whereas all heavy beads remain stationary. This result is quite counter intuitive in the sense that a traveling wave transforms itself into a standing wave by just the change in the value of the mass ratio ε. Interestingly enough, we observe that no traveling wave solutions are realized for $\varepsilon \leq \hat{\varepsilon}$. In Figure 3.36 we depict the standing wave solution realized at $\varepsilon = \hat{\varepsilon}$, for $n = 4$, and unit total energy of the reduced system. It is worth noting that the standing wave can be realized for any arbitrary value of ε by providing appropriate initial conditions so that the two light beads of the reduced system oscillate out-of-phase with respect to each other while the heavy beads stand stationary, balanced by the light beads. On the contrary, the traveling wave solution for $n = 4$ can be realized only for $\varepsilon > \hat{\varepsilon}$. This interesting feature is clearly depicted in the bifurcation diagram of Figure 3.37, where we deduce that at the bifurcation point $\varepsilon = \hat{\varepsilon}$, the traveling and standing wave solutions coalesce, signifying the elimination of the traveling wave solution for smaller mass ratios ($\varepsilon \leq \hat{\varepsilon}$). It is to be noted that the standing wave is unstable for all values of ε. Furthermore, the traveling wave in this system loses stability at $\varepsilon \approx 0.74$ and the traveling waves realized for $\varepsilon < 0.74$ are unstable. It is worth noting that we have two families of traveling waves in the range $\hat{\varepsilon} < \varepsilon \leq 1$, i.e. a positive traveling and a negative traveling wave, but these two waves share the same frequency for a particular value of ε and energy. Thus the bifurcation at $\varepsilon = \hat{\varepsilon}$ is that of two unstable traveling waves and an unstable standing wave coalescing and leading to

an unstable standing wave for $\varepsilon \leq \hat{\varepsilon}$. This is described as pitchfork bifurcation in [99]. This result should be viewed in close conjunction with the results reported in the previous section concerning pulse propagation in the impulsively excited semi-infinite dimer granular chain.

An alternative way to depict these waves is on the frequency (ω) – wavenumber (κ) plane [37]. The wavenumber (κ) is defined as the inverse of the distance between two successive points of constant phase. As the system under consideration is discrete and the equations of motion are in normalized form, the distance in this context can be inferred as the number of beads. Thus an n-bead spatially periodic traveling wave would imply a wavenumber of $\kappa = 1/n$. The time period (T) is defined as the time duration for a point to reach the same phase and thus the frequency (ω) would be equal to $2\pi/T$. The definition of the time period (T) for traveling waves with spatial periodicity is denoted in Figures 3.30 and 3.31. In Figure 3.38 we consider two specific dimer chains with $\varepsilon = \hat{\varepsilon} \approx 0.53$ and $\varepsilon = 0.9$. On this plane we can recognize the existence of two families of standing waves in the infinite dimer chain for varying bead periodicity (represented by the wavenumber κ). Different traveling waves realized in the dimer for varying mass ratios can be depicted in this universal plot. The origin of the plot represents the in-unison rigid body motion of all beads of the homogeneous granular chain. Also, for zero wavenumber ($\kappa = 0$ and uniform waveform of the traveling wave with no spatial periodicity) an out-of-phase standing wave can be realized wherein any two adjacent beads execute time-periodic out-of-phase oscillations at each of the particular values of ε considered in Figure 3.38. This standing wave (nonlinear normal mode) represents the highest frequency mode in the dimer for a particular value of ε and at particular energy level.

Furthermore, at $\kappa = 1$ two standing waves are realized for each value of ε; the higher (lower) mode corresponds to a time-periodic motion where the heavy (light) beads remain stationary and adjacent light (heavy) beads execute out-of-phase

oscillations. It is worth noting that the frequency of the lower mode for $\kappa = 1$ is independent of the value of ε. The line connecting the lower frequency mode realized for $\kappa = 1$ with the origin represents approximately the *acoustic branch* of the infinite dimer chain for each of the two mass ratios ε considered, whereas the line connecting the upper frequency mode realized for $\kappa = 1$ and the out-of-phase standing waves realized for $\kappa = 0$ represent approximately the *optical branch* of the infinite dimer chain. The optical and the acoustic branches shown in here are schematic and are drawn to show the optical and acoustic zones. They are just shown as indicative curves and not the true branches. For each mass ratio $0 < \varepsilon \leq 1$, the frequency range between the upper frequencies of the standing waves at $\kappa = 0$ and the lower frequencies of the standing waves at $\kappa = 1$ for each of the acoustic and optical branches define two *propagation zones (pass bands)* for the corresponding infinite dimer chain, whereas the frequency complements of the propagation zones define attenuation zones of these dimers. For the homogeneous granular chain corresponding to $\varepsilon = 1$ the two propagation zones merge into one (cf. Figure 3.38). As discussed in the previous chapter where such zones [85] were first introduced in infinite homogeneous granular chains, in propagation zones strongly nonlinear traveling waves may exist that are capable of propagating energy to the far field of these media. On the contrary, in attenuation zones weakly nonlinear, near-field standing wave solutions are realized (under a state of permanent compression) that are incapable of radiating energy to the far field. These zones can significantly influence the propagation of pulses in ordered granular media and has been experimentally evidenced in Section 2.2 [87].

In Figure 3.38 we present a schematic (non-exact) representation of the boundaries of the acoustic and optical bands by connecting through straight lines the exact boundaries at wavenumbers $\kappa = 0$ and $\kappa = 1$. By doing this we aim to provide an indication of the frequency ranges of the optical and acoustic zones for varying κ. Referring to the frequency – wavenumber plot of Figure 3.38, for the dimer with $\varepsilon = 0.9$

the upper propagation zone (related to the optical branch) is in the range $1.026 < \omega < 1.418$ for unit energy. As expected, the traveling wave solution realized for this chain falls within this upper propagation zone. For decreasing ε, the bounding frequencies of the upper propagation zone and the frequency of the traveling wave solution increase monotonically. But an interesting phenomenon occurs at the critical value $\varepsilon = \hat{\varepsilon} \approx 0.53$, when the traveling wave solution encounters the lower boundary of the upper propagation zone. As explained previously, at precisely this value of ε the traveling wave solution bifurcates to a standing wave (cf. Figure 3.37), so we are able to show that the bifurcation of the traveling wave solution coincides with its transition from a propagation zone to an attenuation zone of the infinite dimer chain. This result further highlights that a primary pulse propagating in a semi-infinite dimer chain cannot radiate energy in the form of 4-bead spatially periodic traveling waves for normalized mass ratios below the critical value $\hat{\varepsilon} = 0.53$.

Traveling wave represents one of the classes of time-periodic solutions supported by infinite dimer granular chains; whereas standing waves (or nonlinear normal modes – NNMs) represent another class. Unlike linear systems, the number of NNMs may exceed the number of degrees of freedom of a nonlinear system [12, 85] due to mode bifurcations which introduce symmetry-breaking and localization phenomena in the dynamics. In Figure 3.39 we present two of the NNMs with 4-bead periodicity realized in the reduced system with periodic boundary conditions. These are just representative modes and the presentation is not exhaustive. As reported in [12, 63, 85] nonlinear periodic systems (such as the dimer chains considered herein) can exhibit localization phenomena wherein the amplitude of oscillation of one or more of the beads of the reduced system exceeds those of the other beads In the NNM shown in Figure 3.39a, the heavy beads oscillate, while the responses of the light beads resemble cnoidal waves [21, 22]; in addition, the light beads stand stationary for a certain time duration during every period of oscillation. In the NNM shown in Figure 3.39b the

localization is on one of the light beads whose amplitude of oscillation exceeds the amplitudes of the other beads. In contrast to the previous NNM, in this case both the heavy beads execute motions resembling cnoidal waves. Moreover, despite the symmetry of the reduced system with 4-bead periodicity both presented NNMs possess asymmetric waveforms.

We now explore if similar bifurcations can be realized in higher dimensional reduced systems, i.e., for traveling waves with bead periodicities $n > 4$. To this end we consider the 6-bead reduced system, and examine if the standing wave described previously with the light beads performing out-of-phase oscillations and stationary heavy beads can be realized in this case. Such a mode can be realized only when the momentum between adjacent light beads is uniformly balanced when they oscillate in out-of-phase fashion with respect to each other. It follows that, due to symmetry, such standing waves can only be realized in periodic chains with number of beads that are multiples of 4. It follows that no such mode can exist in the 6-bead reduced system. Instead, we consider the 12-bead reduced system which happens to be the least common multiple of 4 and 6.

Again we resort to the same procedure followed for the 4-bead periodicity and numerically continue the traveling wave solution by varying the mass ratio ε. Initially we realize the traveling wave solution with 6-bead periodicity for the homogeneous chain with $\varepsilon = 1$, and this solution is used as an initial guess for the numerical continuation of the solution for small decrements in ε. It is clear that the traveling wave with 6-bead periodicity will also trivially possess 12-bead periodicity, so we resort to computing traveling waves with 6-bead periodicity only. The resulting traveling wave solutions with 6- and 12-bead periodicity realized for $\varepsilon = 0.9$ and $\varepsilon = 0.2$ are shown in Figures 3.40 and 3.41, respectively. Similar to the case of 4-bead periodicity, the amplitude of traveling wave at the heavy beads decreases with decreasing ε. For fixed energy of the reduced system with 6-bead (and 12-bead) periodicity the frequency of

the traveling wave solution is presented in Figure 3.42 as function of ε. In the same plot we depict the frequency of the standing wave corresponding to stationary heavy beads and out-of-phase motion of adjacent light beads for the 12-bead reduced system. As described previously, due to symmetry this standing wave can be realized for 12-bead reduced system but not for the 6-bead reduced system, so to provide a fair comparison with the previously computed traveling wave solutions for 6-bead periodicity, the (fixed) energy of the traveling wave with 12-bead periodicity was taken as twice the (fixed) energy for the traveling waves with 6-bead periodicity depicted in Figures 3.40 and 3.41. Surprisingly and in contrast to the bifurcation plot of Figure 3.38 for the 4-bead periodicity, in this case traveling wave solutions are realized for all values of the mass ratio ε, and their frequencies never coincide with the frequencies of the corresponding standing wave mode. It follows that no traveling wave bifurcations exist for this spatial periodicity.

Extending these results for the case of 8-bead periodicity, in Figures 3.43 and 3.44 we depict the traveling wave solutions for total energy of the reduced system fixed to unity and different mass ratios. In similarity to the case of 12-bead periodicity (but not to the case of 4-bead periodicity) traveling wave solutions with 8-bead periodicity can be realized in the entire range $0 < \varepsilon \leq 1$; this is confirmed by the frequency-mass ratio plot of Figure 3.45 where the frequencies of the traveling waves are compared to the corresponding frequencies of the standing wave with stationary heavy beads and out-of-phase oscillations of adjacent light beads. Interestingly, for the case $\varepsilon = 0.02$ (cf. Figure 3.44) the traveling wave realized corresponds to relatively small amplitudes of the heavy beads, but the wave pattern of the traveling wave is still preserved; the inset in the plot of Figure 3.44 depicts the wave pattern of the heavy beads in more detail.

3.1.5.3 Correlation of the Stability of Traveling Waves to the Dynamics of Finite Dimer Chains

This section primarily attempts to relate the previous traveling wave solutions realized in infinite dimer chain to the dynamics of finite periodic dimer chains. The dynamics of finite dimer chains were explored in Sections 3.1.2 and 3.1.3 [91, 97]. One of the main findings of these works was the realization of countable infinities of families of solitary waves parameterized by energy, caused by nonlinear anti-resonance [97], and of similar countable infinities of nonlinear resonances also parameterized by energy [91]. Moreover, it was shown that nonlinear resonances can lead to strong passive attenuation of propagating pulses in these systems [91]. Given the complete absence of linearized acoustics in these systems (hence their designation as 'sonic vacua' [42]) the phenomenon of nonlinear resonance was attributed to maximum break of symmetry of the waveforms of the propagating pulses.

The contrasting phenomena of anti-resonance and resonance in finite dimers were depicted in a plot (Figure 3.9a) where a normalized transmitted force at the fixed right boundary of the finite dimer is plotted against the normalized mass ratio ε for a fixed intensity applied impulse on the free left boundary of the dimer. It was observed that the peaks on this curve corresponded to the anti-resonances or solitary waves, and the valleys to the resonances. The most important point observed here was that maximum pulse attenuation due to the inherent dynamics of the dimer occurs at the global minimum of the curve at $\varepsilon = 0.59$; this point corresponded to $1:1$ nonlinear resonance. From the practical perspective of pulse attenuation, this mass ratio is of most importance. In the following exposition we discuss the possibility that the dynamics of traveling wave solutions in the infinite dimer chain can influence the capacity for passive pulse attenuation in the finite-dimensional dimer chain. To this end, we consider the normalized force transmitted curve studied in Section 3.1.2 and 3.1.3 [91,

97] for finite dimer chains, and attempt to correlate it with our previous findings concerning traveling wave solutions with different bead periodicities in infinite dimer chains. It should be noted that although the traveling waves in semi-infinite dimer chain were observed only at discrete mass ratios, a continuous family of traveling waves as a function of ε are realized in the periodic dimer chains. Thus finding a one to one correlation between these systems is not possible. The primary objective of this study is to correlate the existence and possible bifurcation of the traveling waves in periodic dimer chains with the global dynamics of a finite dimer chain. Thus we concentrate on the normalized force transmitted curve, Figure 3.9a [91, 97].

In Figure 3.46 we superimpose the force transmitted plot of the finite dimer chain presented in Section 3.1.2.1 [91, 97] to the bifurcation diagram of the traveling waves with 4-bead periodicity presented in Figure 3.37 for the dimer chain of infinite extent. It is interesting to observe that the bifurcation point nearly coincides with the global minimum of the normalized force transmitted curve which represents 1:1 nonlinear resonance and maximum pulse attenuation [91]. This indicates that the energy radiated by the primary pulse for $\varepsilon < \hat{\varepsilon}$ cannot be realized in the form of traveling waves with 4-bead periodicity. This correlates with the fact that traveling waves with 4-bead periodicity were not observed in the oscillating tails of propagating pulses in a semi-infinite dimer chain.

Considering now traveling waves with 6-bead (12-bead) periodicity, no bifurcation of the traveling wave solution for varying mass ratio occurs. In this case, however, we note that traveling waves with this periodicity can be stable only in certain ranges of ε and are found to be unstable or modulationally unstable [163] in other ranges of this parameter. By modulationally unstable we mean that the waveform of this wave is distorted as time increases. Note that the distorted waveform may still preserve the basic features (albeit slowly modulated) of the traveling wave, but the wave is still modulationally unstable. An example of a modulationally unstable

traveling wave with 6-bead periodicity for $\varepsilon = 0.9$ is shown in Figure 3.47a. As can be observed, the traveling wave seems to be quite stable for the initial time period (this initial stable waveform is depicted in Figure 3.40), but as time elapses the wave becomes modulated. Surprisingly the waveform doesn't become irregular, but rather stays close to the initial stable traveling wave response as can be deduced from Figure 3.47b where the modulated waveform is presented over a small time window. Such traveling wave behavior is observed over certain ranges of mass ratio. For certain other ranges of mass ratio, the traveling waves become unstable, i.e. their long time waveform loses all characteristics of a traveling wave solution.

In Figure 3.48 we superimpose the frequency – mass ratio plot of the traveling wave solution with 6-bead periodicity realized in the infinite dimer chain to the force transmitted diagram of the finite dimer chain reported in [91, 97]. It is interesting to note that although there is no traveling wave bifurcation associated with the region of maximum pulse attenuation, still, there is a marked change in the stability behavior of the traveling wave in the parameter region where maximum passive attenuation of transmitted force occurs. This should not be surprising since the global minimum of the transmitted force plot is associated with maximum radiation of energy from the propagating primary pulse to the far field of the medium in the form of traveling waves [91]. With the observed change in stability of the traveling waves with 6-bead periodicity near the global minimum of the force transmitted curve, it can be conjectured that the instability of this type of traveling waves contributes in a more effective energy radiation from the propagating primary pulse which results in drastic attenuation of the transmitted force at the right fixed boundary of the finite dimer chain. Although, no such claims can be made for the general class (that is, with arbitrary bead-periodicities) of traveling waves, the correlation studies presented in Figures 3.46 and 3.48 strongly suggest that the stability of the different classes of nonlinear traveling

waves in the dimer chain plays an important role in the capacity of this system for passive attenuation of propagating pulses by its intrinsic dynamics.

3.1.5.4 Conclusions

In this section we have explored traveling waves in periodic dimer chains with varying bead periodicities. This is the first exposition of the periodic traveling waves in heterogeneous ordered granular chains reported in the literature [98], and extends the results reported in [63] on traveling waves in homogeneous ordered granular chains. In close conjunction to this work is the research work by Pelinovsky et al. [99]. In previous works such traveling waves were observed in oscillating tails in the trails of propagating pulses in semi-infinite dimer chains, and played an important role in radiating energy from the propagating pulse to the far field of these media. We systematically studied traveling waves with different bead periodicities by considering reduced systems composed of a finite number of dimer pairs and imposing periodic boundary conditions. This technique first introduced in [63] to study traveling waves in homogeneous granular media, proved to be quite effective for analyzing these strongly nonlinear motions and studying their dependencies on energy and on the mass ratio of the dimer.

It is found that traveling waves with 4-bead periodicity exhibits an interesting bifurcation wherein, for fixed energy and decreasing mass ratio from unity the traveling wave coincides with a standing wave, after which it ceases to exist for further decrease in the mass ratio. It is interesting to note that the point of bifurcation lies very close to the global minimum of the transmitted force plot in the corresponding finite dimensional dimer chain discussed in Section 3.1.2 and 3.1.3 [91, 97]. The global minimum of this plot indicates maximum radiation of energy to the far field in the form

of traveling waves from a propagating pulse. Hence, it is conjectured that the reported traveling wave bifurcation plays a role in the capacity of the dimer chain to passively attenuate propagating pulses by its intrinsic dynamics.

Even though no such traveling wave bifurcations were observed for the cases of 6- (12-) and 8-bead periodicities, it is found that for the case of 6-bead periodicity traveling waves exhibit a change of stability in the parameter region where maximum pulse attenuation in the finite dimer chain occurs. This provides a further indication of the influence of traveling waves and their stability on the capacity of the dimer to passively attenuate propagating pulses. However, more work is needed in order to prove this conjecture by considering the bifurcations and the stability changes of traveling waves with different bead periodicities and at varying energy and parameter ranges.

The dynamical study of 1:1 dimers in Section 3.1.2 to 3.1.5 is from the theoretical/analytical and numerical perspective. The ultimate goal of these studies is the design and realization of a practical system incorporating the granular media. Although the theoretical findings and results are convincing, the dynamics of these systems in practice may exhibit contrastingly different behaviors. For example, in all systems considered herein, the dissipative effects (like material damping, contact friction), plasticity of the beads, rotation of the interacting beads, surface characteristics of the beads have been completely neglected. In fact this is owing to the assumptions underlying the Hertzian interaction model presented in Chapter 1. These factors are invariably present in the designed practical granular systems. Even in the most carefully designed and devised systems the above described features creep in due to manufacturing limitations, handling etc. Thus it necessitates an experimental study of the dynamics in these granular chains. The effect of these subtle features on the anti-resonance and resonance dynamics will lead to better predictive design. The next

section is a step towards the experimental study of propagatory dynamics in 1:1 dimer chain.

3.1.6 Experimental Verification of Resonances and Anti-resonances in 1:1 Dimers

In the context of experimental study of one-dimensional polydisperse media, much impetus has been given to 1:1 dimer chains [89, 90, 92]. In fact the considered dimer chains in these works are pre-compressed. Moreover, the beads of the dimer chain were of the same radii and the materials of these beads were altered to obtain appropriate mass ratio. The inherent difficulty in realizing chains with dissimilar radii beads is due to the placement of these chains in a planar track and such a setup may lead to misaligned beads and/or beads dislocating completely from their designated position. With this limitation, study of uncompressed dimer chains with dissimilar radii beads and realization of resonances and anti-resonances have not been considered till of late. The current experimental study in this section will primarily dwell upon these issues [100].

The aim of the study in this section is to experimentally verify the existence of strongly nonlinear dynamical phenomena of anti-resonance and resonance in 1:1 dimer chains explored previously only analytically/numerically. This is achieved through a series of experiments involving granular dimer chains. By supporting dimer chains through carefully designed flexures, the stiff dynamics of the bead to bead interactions is considerably elevated from the soft dynamics of the flexures. With such a setup, it is intended to overcome a basic limitation for the experimental realization of such dimer systems, namely the construction of one-dimensional dimer chains with beads of different radii. One way to study resonances is by examining the transmitted force to a fixed light bead at the right boundary of a finite dimer chain which is excited by a an

impulse at its left free boundary, for varying mass ratios as described in the previous sections [91, 97]. Depending on the value of the mass ratio, a granular dimer, either may facilitate energy transmission (at anti-resonances through excitation of solitary waves), or may strongly restrict it (at resonances due to strong wave scattering and energy radiation to the far field). Thus transmitted force is a measure of the pulse attenuation in the dimer chain. In this context the maximum force transmission is observed for the case of the homogeneous chain (mass ratio of unity), whereas minimum force transmission is realized for 1:1 resonance, i.e., when the characteristic frequency of the propagating pulse equals the frequency of the radiated wave in its trail (cf. Figure 3.20d) [91]. To this end, we study the dimer chain considering three different mass ratios, a mass ratio close to an anti-resonance, a mass ratio at resonance and a mass ratio of unity (homogeneous chain). The results presented herein confirm experimentally the occurrence of nonlinear resonances and anti-resonances in dimer chains, and conclusively prove the capacity of appropriately designed granular dimers for passive strong attenuation of propagating pulses due to nonlinear resonance. Moreover, we validate the theoretical prediction that within the elastic range of bead to bead dynamical interactions the results are fully re-scalable with respect to energy. The experimental study in this section provides the first experimental evidence of strongly nonlinear resonances and anti-resonances in essentially nonlinear periodic granular media.

3.1.6.1 Experimental Fixture

The experimental setup is shown in Figure 3.49. It consists of two sturdy pillars that are connected through threaded shafts. Stainless steel holders with slots are placed on these shafts to host the flexures. The granular chain is composed of horizontally and

vertically aligned spherical beads, each rigidly attached to the one end of a thin steel flexure. The other end of the flexure is placed in a slot of the holders assembled on the threaded shafts. Once the beads are perfectly aligned, the holders are firmly bolted and rigidly fastened to the support structure. The thin flexures (made of Spring Steel grade 1095) are used in order to construct dimer assemblies composed of beads with dissimilar radii; as discussed below, by designing the flexures to be much 'softer' than the 'stiff' beads, it is feasible to separate the time scales of the dynamics of the flexure responses and the dynamics of the bead-to-bead interactions, so that the dynamics of the flexures do not affect the granular dynamics.

Considering first the homogeneous granular chain, it is composed of 21 chrome steel beads (bearing-quality aircraft-grade E52100 alloy Steel) of radius $R = 12.7$ mm, modulus of elasticity $E = 210$ GPa, density $\rho = 7850$ Kg/m^3, and Poisson's ratio $\mu = 0.3$. Each bead is fabricated with a thin slit to a depth of about 1/8th of its diameter where the supporting flexure is inserted and fastened permanently. The right end of the chain is in contact with a dynamic force sensor that is firmly mounted on an L-angled pedestal and rigidly fixed onto the surface table as shown in Figure 3.49. The left (free) end of the chain is excited by an impulse applied with a pendulum whose mass is equal to the mass of the first bead of the chain. Using energy conservation (disregarding the mass of the pendulum rod) we can approximately estimate the impact velocity (or the intensity of the applied impulse). The initial drop angle of the pendulum is measured using a protractor mounted along the pivotal axis of the pendulum (cf. Figure 3.49). A measure of transmitted force is then utilized to ascertain the dynamics of the granular chain. The transmitted force pulse through the granular chain is measured using a piezoelectric dynamic force sensor (PCB 208 C02) in contact with the last (furthest right) bead; the sensitivity of the force sensor is 11,241 mV/kN and the force signal is fed to a 24-bit m+p International VibPilot data acquisition system, allowing for direct visualization of the transmitted force. The experimental raw data is then post processed using Matlab.

Two different dimer chains will be considered composed of a total of 21 beads, with the first and last beads being heavy beads; hence, each dimer chain consists of 11 heavy beads and 10 light beads. Both heavy and light beads are made of the same material (bearing-quality aircraft-grade E52100 alloy Steel), and the heavy-light bead pairs differ only in radius. For the first dimer chain (denoted as 'dimer 1') the radii of the heavy and light beads are given by $R_1 = 12.7$ mm and $R_2 = 10.08$ mm, whereas for the second dimer chain (denoted as 'dimer 2') these radii $R_1 = 12.7$ mm and $R_2 = 6.35$ mm. As discussed below the values of the radii are selected in order to induce conditions of resonance in dimer 1, and conditions of near anti-resonance in dimer 2. The realization of nonlinear resonance and anti-resonance in these dimers will be inferred indirectly by examining the transmitted force measured by the force sensor at the right boundary of each of the granular chains. Indeed, under condition of $1:1$ resonance (realized in dimer 1) maximum scattering of the propagating force pulse occurs due to strong energy radiation in the form of traveling waves in the trail of the pulse; this results in a drastically reduced transmitted force at the site of the force sensor. On the contrary, under conditions of near anti-resonance (realized in dimer 2) a pulse propagates without substantial distortion or dispersion, facilitating force transmission through the dimer; this results in increased transmitted force at the site of the force sensor. These issues are explained in the next section and provide the basis for experimental proof of these nonlinear phenomena in the dimer chains.

3.1.6.2 Theoretical Modeling

The dimer configuration is as described previously in Section 3.1.2.1, but in here we have an additional onsite linear grounded spring at each bead modeling the supporting flexure. It is assumed that the granular chains under consideration have no pre-

compression, so the dynamics is strongly nonlinear. Furthermore, the considered dimer chain is of finite length with its left end free and the last bead at the right end in contact with a fixed planar surface (modeling the force sensor). These considerations are very much commensurate with the experimental setup which is elaborated in the previous section. Denoting the displacement of the $i-$th bead by $u_i(t)$ and the properties of the alternating heavy and light beads by subscripts 1 and 2, respectively, the governing equations of motion is given by (note that both the first and last beads are heavy):

$$
\begin{gathered}
m_1 \frac{d^2 u_1}{dt^2} + k_f u_1 = (4/3) E_* \sqrt{R} \left[-(u_1 - u_2)_+^{3/2} \right] \\
\bullet \quad \bullet \quad \bullet \\
m_i \frac{d^2 u_i}{dt^2} + k_f u_i = (4/3) E_* \sqrt{R} \left[(u_{i-1} - u_i)_+^{3/2} - (u_i - u_{i+1})_+^{3/2} \right] \\
m_{i+1} \frac{d^2 u_{i+1}}{dt^2} + k_f u_{i+1} = (4/3) E_* \sqrt{R} \left[(u_i - u_{i+1})_+^{3/2} - (u_{i+1} - u_{i+2})_+^{3/2} \right] \\
\bullet \quad \bullet \quad \bullet \\
m_n \frac{d^2 u_n}{dt^2} + k_f u_n = (4/3) E_* \sqrt{R} \left[(u_{n-1} - u_n)_+^{3/2} \right] - (4/3) E_{P*} \sqrt{R_P} \left[(u_n)_+^{3/2} \right] \\
i = 1, 3, 5, \ldots, n-2
\end{gathered}
\tag{3.36}
$$

In (3.36) k represents the stiffness of the flexures; $\tilde{R}_P$ is the radius of curvature of the surface with which the last bead is in contact. The other notations are as elaborated in Section 3.1.2. The force transducer considered has properties similar to the beads and thus we have its Young's modulus $E_{P*} = E_*$. In the numerical simulations and the following experimental study, we consider the last bead to be in contact with a planar surface [53] (force transducer with a planar cap) and, hence, it holds that $\tilde{R}_P \to \infty$, so that $R_P \cong R_1$. We assume strictly horizontal motion of the beads and model each flexure as a cantilever beam so that the stiffness is given by $k_f = (3E_f I)/L^3$, where $E_f = 200$ GPa is the elastic modulus of the flexure, $I = (bh^3)/12$ its cross-section moment of inertia, its length $L = 302$ mm, width $b = 25.4$ mm and thickness $h = 0.233$ mm.

At this point we introduce the normalizations (3.2) and express (3.36) in the following normalized form:

$$
\begin{aligned}
\ddot{x}_1 &= -(x_1 - x_2)_+^{3/2} - \frac{k_f}{(4/3)E_*\left(R_2/(R_1+R_2)\right)^{1/2}R_1}x_1 \\
&\bullet\bullet\bullet \\
\ddot{x}_i &= (x_{i-1} - x_i)_+^{3/2} - (x_i - x_{i+1})_+^{3/2} - \frac{k_f}{(4/3)E_*\left(R_2/(R_1+R_2)\right)^{1/2}R_1}x_i \\
\varepsilon\ddot{x}_{i+1} &= (x_i - x_{i+1})_+^{3/2} - (x_{i+1} - x_{i+2})_+^{3/2} - \frac{k_f}{(4/3)E_*\left(R_2/(R_1+R_2)\right)^{1/2}R_1}x_{i+1} \\
&\bullet\bullet\bullet \\
\ddot{x}_n &= (x_{n-1} - x_n)_+^{3/2} - \sqrt{1+\frac{R_1}{R_2}}(x_n)_+^{3/2} - \frac{k_f}{(4/3)E_*\left(R_2/(R_1+R_2)\right)^{1/2}R_1}x_n
\end{aligned}
\tag{3.37}
$$

Taking into account the previous numerical values for the geometric and material parameters of the system, we estimate the following upper bound for the normalized flexure stiffness parameter, $k_f/\{(4/3)E_*[R_2/(R_1+R_2)]^{1/2}R_1\} \leq 5.17\times10^{-10} \ll 1$, hence, the dynamics of the flexures are much 'softer' compared to the bead-to-bead interaction dynamics and thus can be neglected from further consideration. Equivalently, there is clear time-scale (or frequency-scale) separation in the corresponding dynamics and so the presence of the flexures does not affect the granular chain dynamics. This finding which will be validated experimentally in the next section, and further validates the design of the experimental fixture and provides a new way for experimentally studying the dynamics of heterogeneous ordered granular media. Hence, the normalized equations (3.37) can be further approximated as,

$$
\begin{aligned}
\ddot{x}_1 &= -(x_1 - x_2)_+^{3/2} \\
&\bullet\bullet\bullet \\
\ddot{x}_i &= (x_{i-1} - x_i)_+^{3/2} - (x_i - x_{i+1})_+^{3/2} \\
\varepsilon\ddot{x}_{i+1} &= (x_i - x_{i+1})_+^{3/2} - (x_{i+1} - x_{i+2})_+^{3/2} \\
&\bullet\bullet\bullet \\
\ddot{x}_n &= (x_{n-1} - x_n)_+^{3/2} - \sqrt{1+\varepsilon^{-1/3}}\,(x_n)_+^{3/2}
\end{aligned}
\tag{3.38}
$$

The only parameter governing the dynamics is the normalized mass ratio ε. Note that this normalization indicates that the results are fully re-scalable with respect to energy (i.e., magnitude of the applied shock) provided that the assumptions of the model hold, that is, for sufficiently small deformations so that the bead-to-bead interactions are elastic with no plasticity effects. In addition, no dissipative effects resulting from internal structural damping within the material of the beads or dry friction effects are taken into account in model (3.38), although later we will introduce viscous damping dissipation in order to match the results of the model and the experimental measurements. We also note that the flexure construction minimizes dry friction effects as no sliding of the beads with any supporting guides exists in the experimental fixture. Considering now the normalized equations (3.38), since both heavy and light beads are composed of the same material this parameter is expressed only in terms of the corresponding radii, $\varepsilon = R_2^3/R_1^3$, and lies in the range $0 < \varepsilon \leq 1$. Considering the aforementioned values of the radii selected for the light beads, the dimer 1 corresponds to $\varepsilon = 0.5$, whereas the dimer 2 to $\varepsilon = 0.125$.

The normalized equations (3.38) govern the dynamics of the general finite dimer chain in contact with a fixed planar surface at one end [53]. A similar setup for a finite dimer chain in contact with a fixed light bead at its right boundary was considered previously in Section 3.1.2 in order to study the efficacy of pulse transmission in the general dimer chain with varying mass ratio. From a practical point of view of effective

pulse attenuation, 1: 1 resonance is of great importance. For the particular 21-bead chain considered in this experimental work this resonance occurs at normalized mass ratio $\varepsilon = 0.5$. It is worth noting that this global minimum of the force transmitted curve is a function of the number of beads in the chain. Interestingly, with a decrease in the number beads this global minimum is realized at a lower value of ε. In Figure 3.50 we present the maximum normalized transmitted force at the right end of the 21 bead dimer chain considered in this section as function of the normalized mass ratio; a unit impulse is applied on the left free boundary of the dimer and the transmitted force is normalized with respect to the force transmitted in the homogeneous chain composed only of heavy beads. As can be observed the global minimum occurs at $\varepsilon \approx 0.5$, which coincides with the regime of 1: 1 resonance in the dimer. Furthermore, the normalized transmitted force increases with decreasing mass ratio ε as a series of anti-resonances and higher order resonances are realized [91, 97]. The global maximum of the force transmitted plot is realized for the homogeneous chain ($\varepsilon = 1$) where the solitary wave studied by Nesterenko [41, 42] is realized. It follows that by studying the plot of normalized transmitted force for varying normalized mass ratio, we can infer the presence of resonance or anti-resonance in the dimer chain. In the next section we report on a series of experimental tests designed to validate the theoretical plot of Figure 3.50.

3.1.6.3 Experimental Results

Previous experiments with dimer chains [42, 89-92, 96, 101] considered alternating beads of two different materials sliding in guides in order to explore the existence of frequency bands in these systems. To realize these experiments the beads were constructed of the same radius so that they could be assembled on a planar track and

loaded. However, the contact friction between the beads and the track presented a clear limitation. The problem of frictional contact between the beads and the track is quite an important consideration. Additionally, each material might have different material damping characteristics. To address this issue, in our flexure-based setup we consider beads composed of the same material and vary only the radius of every other bead in order to obtain the required normalized mass ratio. Since in this case the internal material damping characteristic is similar for all the beads, we conjecture that the comparison between different dimer setups is valid. Moreover, as the beads are attached through flexures and are hung down from a rigid support, it is intended to eliminate all the frictional contacts from the experiments. But it should be noted that complete elimination of friction and damping in these experiments is seldom possible. Furthermore, friction contacts still exist due to the rotation of the beads due to the very flexible flexures through which they are suspended.

As mentioned previously we consider three different cases corresponding to normalized mass ratios $\varepsilon = 1$ (homogeneous chain), $\varepsilon = 0.5$ (dimer 1) and $\varepsilon = 0.125$ (dimer 2) (indicated on Figure 3.50). Moreover, we consider three different levels of excitation for each of these dimer setups corresponding to initial drop angles of the excitation pendulum equal to $\theta_0 = 7^0$ (level 1 – providing an initial velocity – impulse – of the first bead of the chain equal to $\dot{x}_1(0) = 0.2102$ m/s), $\theta_0 = 10^0$ (level 2 – $\dot{x}_1(0) = 0.3$ m/s) and $\theta_0 = 14^0$ (level 3 – $\dot{x}_1(0) = 0.4195$ m/s), where θ_0 is the initial drop angle of the pendulum (the length of the pendulum is chosen equal to 302 mm). To test repeatability of the results there were 10 trials conducted at each excitation level for each of the three considered granular chains.

In Figure 3.51 we depict the transmitted force to the right boundary for the homogeneous chain excited by the highest excitation, i.e. level 3. The numerical result shown here corresponds to the theoretical model (3.39) without any dissipative effects incorporated. We observe that the transmitted force is in the form of a single primary

pulse followed by a train of much smaller secondary force pulses. The primary pulse represents the propagation of the Nesterenko solitary wave, whereas the secondary pulses are created due to the loss of contact (separation) between the leading beads at the left end of the chain once the chain is impacted by the pendulum.

The difference in the peaks of the primary pulse observed between the numerical and experimental data is caused by the lack of dissipative effects in the theoretical model (3.38), which, in fact, is Hamiltonian [26]. Yet, in the experiment there exist dissipative effects due to inherent internal structural damping of the material of the beads and other effects, such as plastic deformations or dry friction at the point of contact. To account for these effects we model the damping effects by introducing *ad hoc* viscous damping term [70-72, 164] in the theoretical model (3.39), and express the modified theoretical model incorporating viscous damping as follows,

$$
\begin{aligned}
\ddot{x}_1 &= -(x_1 - x_2)_+^{3/2} + \xi\left\{-\left(\dot{x}_1 - \dot{x}_2\right)\Theta\left[x_1 - x_2\right]\right\} \\
&\bullet\bullet\bullet \\
\ddot{x}_i &= (x_{i-1} - x_i)_+^{3/2} - (x_i - x_{i+1})_+^{3/2} + \xi\left\{\left(\dot{x}_{i-1} - \dot{x}_i\right)\Theta\left[x_{i-1} - x_i\right] - \left(\dot{x}_i - \dot{x}_{i+1}\right)\Theta\left[x_i - x_{i+1}\right]\right\} \\
\varepsilon\ddot{x}_{i+1} &= (x_i - x_{i+1})_+^{3/2} - (x_{i+1} - x_{i+2})_+^{3/2} + \xi\left\{\left(\dot{x}_i - \dot{x}_{i+1}\right)\Theta\left[x_i - x_{i+1}\right] - \left(\dot{x}_{i+1} - \dot{x}_{i+2}\right)\Theta\left[x_{i+1} - x_{i+2}\right]\right\} \\
&\bullet\bullet\bullet \\
\ddot{x}_n &= (x_{n-1} - x_n)_+^{3/2} - \sqrt{1+\varepsilon^{-1/3}}\,(x_n)_+^{3/2} + \xi\left\{\left(\dot{x}_{n-1} - \dot{x}_n\right)\Theta\left[x_{n-1} - x_n\right] - \dot{x}_n\Theta\left[x_n\right]\right\}
\end{aligned}
\tag{3.39}
$$

where $\xi = d/(m_1\phi)$ is the non-dimensional viscous damping coefficient, d the dimensional viscous damping coefficient, ϕ is defined in (3.2), and $\Theta[\cdot]$ the Heaviside function. We use this representation to account for the fact that damping forces are activated only during compression between beads and are absent when bead separation occurs.

As described in the previous section, we consider three experimental setups corresponding to normalized mass ratios equaling $\varepsilon = 1, 0.5$ and 0.125. We quantify the

damping coefficient in (3.39) by considering the response of the homogeneous chain ($\varepsilon = 1$). This is performed by matching the viscous damping coefficient ξ in order to match the maximum amplitude of the transmitted force obtained from the numerical computation and the experimental measurement. Since in the experimental tests we have considered 10 trials at each impact level we obtain 10 values for c following this process, so we compute the average of these estimates for each excitation level. Transforming into non-dimensional coefficients, for excitation level 1 the average value of the damping coefficient was estimated as $\xi_1 = 0.003475$, for excitation level 2 as $\xi_2 = 0.00353$, and for level 3 as $\xi_3 = 0.004025$. Taking the mean of these three averaged values we obtain the final estimate of the damping coefficient as $\xi = 0.00367$. Since the coefficient ξ is dependent on ϕ (refer (3.37)), which in turn is dependent on the radii R_1 and R_2, the dimensional damping coefficient $d = \xi m_1 \phi$) varies for each of the experimental setups. Hence, for the homogeneous chain we estimate $d \approx 35.4$ Ns/m, for dimer 1, $d \approx 34.33$ Ns/m, whereas for dimer 2, $d \approx 32$ Ns/m. These coefficients values are in good agreement with that reported in [70].

In Figure 3.52 we depict the comparison between the numerical and experimental results for the three granular chains at the lowest excitation level 1. The numerical results were obtained using the modified theoretical model (3.39) that incorporates viscous damping and, hence, accounts for dissipative effects; moreover in these plots (as in the following plots) we depict all 10 experimental trials for each excitation level. In each case we note good repeatability of the 10 experimental trials, and also good agreement with the corresponding numerical prediction. At mass ratio $\varepsilon = 0.125$ (Figure 3.52a) dimer 2 is near anti-resonance and thus it facilitates transmission of energy; in this case the force transmitted is lower than the homogeneous case (Figure 3.52c), but not significantly lower.

In contrast, for $\varepsilon = 0.5$ (Figure 3.52b) dimer 1 is in $1:1$ resonance (refer Figure 3.50), leading to strong attenuation of the pulse; in accordance, we note that in this case

the transmitted force is significantly lower compared not only to the homogeneous case but also to dimer 2. Furthermore, in this case we observe that the transmitted force does not reach zero immediately after the primary pulse. Instead, the nonzero transmitted force in the immediate trail of the primary pulse shows significant fluctuations which are attributed to the excitation of traveling waves in the trail of the primary pulse as described in Section 3.1.5 [91, 98]. These waves are responsible for strong energy radiation from the primary pulse to the far field of the dimer and to the resulting strong attenuation of the transmitted force pulse. These features are very much in contrast with what is observed for the chains with $\varepsilon = 1$ and $\varepsilon = 0.125$. A zero force level after the arrival of the primary force pulse implies that the last bead of the chain is just in contact or has lost contact with the force sensor; such a phenomenon is observed in the trail of the primary pulse in Figures 3.52a and c. On the other hand, a constant or oscillating transmitted force after the arrival of the primary force pulse signifies continuing contact of the last bead of the chain with the force sensor, as observed in Figure 3.52b. Table 3.4 provides the experimental force transmitted for varying ε and excitations levels.

Interestingly enough, the numerical results agree closely and follow the same trends with the experimental results. The mismatch between the two results is attributed to the approximation in the viscous damping model used in the numerical model (3.39), and to possible misalignment, bead rotation and loss of contact that could affect the experiments. Similar good agreement between experimental results and numerical simulations is noted for the highest excitation (level 3), as depicted in Figure 3.53. A similar correspondence is observed even in the case of excitation level 2, but we do not present them here as the results are similar and do not reveal anything new. All the experimental and numerical responses are time shifted to zero so as to have a fair comparison of the pulse widths.

As a final step we normalize the maximum transmitted force with respect to the maximum transmitted force realized in the homogeneous chain at a particular excitation level. In Figure 3.54 these normalized results are superimposed on the theoretical plot of Figure 3.50, with the error bars showing the variability of the results due to the numerous trials considered (10 trials at each excitation level). We note that the normalized results match well with the numerical plot; the error bounds show that the experimental results vary over a small range, and, hence they are consistent and repeatable. The drastic reduction of the transmitted force in the $1:1$ resonance region is fully verified, as is the amplification of the transmitted force in the near anti-resonance region. Moreover, given the agreement between the experimental and numerical normalized data for all excitation levels, we verify the theoretical prediction that the force transmitted plot of Figure 3.50 is fully re-scalable with energy (level of force excitation). It is interesting to note that the experimental results for $1:1$ resonance (at $\varepsilon = 0.5$) are slightly higher than the numerical results, whereas for near anti-resonance (at $\varepsilon = 0.125$) are lower. We conjecture that this reflects the presence of small pre-compression in the experimental system. Although every care is taken in the experiment to reduce or eliminate pre-compression, this cannot be achieved completely, and a small residual pre compression is invariably present in the system. The effect of pre-compression has been explored in detail in Section 3.1.4 and the trends reported there (Figure 3.29b) are consistent with the results depicted in Figure 3.54.

3.1.6.4 Conclusions

Motivated by the theoretical and numerical results of Section 3.1.2 [97], 3.1.3 [91] we experimentally investigated resonance and anti-resonance (solitary wave) phenomena in granular dimer chains. Our experimental study was based on granular chains

supported by thin flexures in order to minimize friction effects and to accommodate beads with dissimilar radii. By appropriately designing the supporting flexures we ensured time-scale separation of their dynamics from the dynamics of bead-to-bead interactions. To obtain a fair comparison between the different dimer setups used in this study, we have considered the same material for all beads and changed only their radii to obtain the required normalized mass ratios. It is conclusively shown that when this mass ratio is either equal to unity (i.e., for the homogeneous chain) or low ($\varepsilon = 0.125$) so that near anti-resonance conditions are realized, the pulse attenuation is not substantial. In contrast, strong pulse attenuation is realized under condition of $1:1$ resonance (when the normalized mass ratio is $\varepsilon = 0.5$), fully confirming the theoretical prediction. Moreover, by superimposing the experimental results on the plot of maximum transmitted force versus mass ratio, and by the coincidence of the results for the three considered force levels, we verified the theoretical prediction that the resonance and anti-resonance phenomena are fully re-scalable with energy, so they are independent of the level of the applied shock – provided, of course, that the assumptions of the theoretical model hold.

From the results obtained with the experimental granular chains corresponding to three mass ratios, we ascertain that the theoretically predicted resonance and anti-resonance phenomena can be observed experimentally. This provides the first such result for dimer chains from an experimental perspective, and paves the way for the implementation of nonlinear resonances in dimer chains with appropriately chosen normalized mass ratios, in order to use them as stress wave mitigators in practical material systems excited by shock excitations.

3.2 Dynamics of 1:N Dimers

3.2.1 Introduction

In Section 3.1 we studied extensively the propagatory dynamics of the 1:1 dimer chain. It revealed whole new phenomena of anti-resonances and resonances, and subsequently their existence has been verified experimentally. It should be noted that 1:1 dimer chain is a particular case of a general periodic dimer chain. Although the most general case of such chains is the randomly decorated dimer chain, but they are seldom analytically tractable. Thus research focus is primarily concentrated on periodic dimer chains. As discussed in Section 3.1 and the references cited therein, the dynamics of 1:1 dimer chain has attracted immense interest from the granular media research community. The research focus on 1:1 dimer from the analytical, numerical and experimental perspective is quite overwhelming. In contrast very limited interest has been shown in the study of general 1:N ($N \geq 2$) dimer chains. From the perspective of experiments, pre-compressed 1:2 dimer chain has been explored leading to the realization of band gaps [101]. A more general 1:N dimer chain with N ranging up to 22 has been considered in [90]. One of the most recent studies concerned with pre-compressed 1:2 dimers and explored breathers in these chains [165]. Interestingly enough, none of these studies have considered a 1:N ($N \geq 2$) dimer chain in its strongly nonlinear limit. Even the consideration of 1:1 dimers in Section 3.1 in their strongly nonlinear limit and the realization of solitary waves and resonances was the first of its kind [91, 97]. The main challenge in considering granular chains in this limit is the absence of cohesiveness between beads that can lead to separation. This motivated us to employ the idea of studying the dynamics only in the phase of primary pulse propagation when bead separation seldom happens and thus the evolution of the asymptotic methodology described in the previous section. The dynamics of the 1:1 dimer was primarily

governed by the parameter of mass ratio scaling the masses of the two types of beads and we considered it to be less than unity and thus all possible cases of periodic variation of masses were considered. It should be noted that even though the two types of beads are made of different materials with disparity in elastic modulus, the dynamics would still be governed only by the mass ratio. The system normalizes in such a way that the disparate elastic properties of the two types of beads seldom affect the dynamics. In fact this is true because any particular bead (say type 1) is in contact only with bead of the other type (type 2). Thus any interaction is only between these two types of beads and the temporal variable can be appropriately rescaled to eliminate the elastic properties from the normalized system. Depending on the elastic properties, only the temporal attributes (like pulse width, propagation velocity, time shifts) of the dynamics would change. With this in view, only mass periodic chains can be realized with $1:1$ dimers, whereas stiffness periodicity is not possible. This can be considered as one of the limitations of $1:1$ dimer chains. To overcome this limitation, consideration of a general $1:N$ dimer is a necessity since both stiffness and mass periodic chains can be realized. To this end we set out to explore a general $1:N$ dimer chain from both analytical and numerical perspective.

The present section builds on the mathematical framework developed in Section 3.1 [91, 97] to study propagatory dynamics in a more general class of $1:N$ ($N \geq 2$) granular dimer chains. These chains are composed of a number of periodic sets composed of one 'heavy' bead (type 1) followed by (and being in contact with) N 'light' beads (type 2). As assumed previously, we consider beads to be linearly elastic spheres that interact with each other through Hertzian contact forces, with no dissipation or any pre-compression being considered. Hence, the dynamics of these systems is strongly nonlinear and highly non-smooth, dictating the application of special asymptotic methodology developed in Section 3.1 [91, 97]. Moreover, unlike the case of $1:1$ dimers whose dynamics is governed by a single parameter (the normalized mass ratio [91, 97]),

the dynamics of $1:N$ $(N \geq 2)$ dimers is governed by two parameters, namely a normalized mass ratio and a normalized stiffness ratio. This is due to the fact that the heavy beads interact only with light beads, but a light bead interacts with both heavy and light beads. This leads to an additional parameter of stiffness ratio scaling the elastic properties of the two types of beads in addition to the mass ratio. Thus we can realize both mass and stiffness periodic granular chains. Although this is an advantage, the parameter addition imposes additional complexity in the analysis. We begin our study by providing a general asymptotic formulation for the dynamics of $1:N$ $(N \geq 2)$ dimer chains. Then, we study in detail the solitary wave formation in $1:2$ dimers and prove the existence of a countable infinity of this type of solutions, realized at different discrete values of the normalized mass and stiffness parameters. These periodic variations are in general more appropriate and attractive to attenuate propagating disturbances. As described in Section 3.1.3, nonlinear resonances are the mechanisms that lead to substantial attenuation. With this in view we study both analytically and numerically the mechanism of resonances and realize families of countable infinity of resonances at discrete set of mass and stiffness parameters. In contrast to $1:1$ and $1:2$ dimers, realization of solitary waves and resonances in general $1:N$ $(N \geq 3)$ granular chain is not possible, unless special symmetries are realized in the system. In that context, realization of solitary waves and resonances in homogeneous and heterogeneous $1:1$ and $1:2$ dimer granular systems represent special cases that cannot be extended to the more general class of $1:N$ $(N \geq 3)$ granular dimers. Further, we consider the degeneracy of a $1:N$ dimer chain with large stiffness coefficient to a $1:1$ dimer chain. The last part of this section is concerned with the study of validity of the asymptotic approach developed and applied in this section. Although it may generally seem that the asymptotic approach is valid whenever the asymptotic parameter is small enough, it is seldom so in this context. We show that for a general $1:N$ dimer chain a

combined parameter involving both the number of light beads (N) and the mass ratio governs the validity of asymptotic methodology devised herein.

3.2.2 General Asymptotic Formulation for Primary Pulse Propagation in 1: N Dimer Chains

We consider a one-dimensional 1: N dimer chain of spherical elastic beads in Hertzian contact with no pre-compression (cf. Figure 3.55). We assume that this system consists of two types of beads designated as 'heavy' (or type 1) and 'light' (or type 2) depending on their relative masses. We define a 1: N dimer as a chain composed of an infinite number of periodic sets, with each set composed of a single heavy bead followed by N light ones.

Denoting by u_i the displacement of the i −th bead of the dimer, the governing equations of motion of the system are expressed as:

$$
\begin{gathered}
m_i \frac{d^2 u_i}{dt^2} = (4/3) E_{1^*} \sqrt{R_{1^*}} \left[(u_{i-1} - u_i)_+^{3/2} - (u_i - u_{i+1})_+^{3/2} \right] \\
m_{i+1} \frac{d^2 u_{i+1}}{dt^2} = (4/3) E_{1^*} \sqrt{R_{1^*}} (u_i - u_{i+1})_+^{3/2} - (4/3) E_{2^*} \sqrt{R_{2^*}} (u_{i+1} - u_{i+2})_+^{3/2} \\
\bullet \quad \bullet \quad \bullet \\
m_{i+j} \frac{d^2 u_{i+j}}{dt^2} = (4/3) E_{2^*} \sqrt{R_{2^*}} \left[(u_{i+j-1} - u_{i+j})_+^{3/2} - (u_{i+j} - u_{i+j+1})_+^{3/2} \right] \\
\bullet \quad \bullet \quad \bullet \\
m_{i+N} \frac{d^2 u_{i+N}}{dt^2} = (4/3) E_{2^*} \sqrt{R_{2^*}} (u_{i+N-1} - u_{i+N})_+^{3/2} - (4/3) E_{1^*} \sqrt{R_{1^*}} (u_{i+N} - u_{i+N+1})_+^{3/2} \\
i = 1 + n(1+N), \; 1 < j < N, \; n = 0, 1, 2, \ldots
\end{gathered}
\tag{3.40}
$$

At this point we introduce the normalizations (3.2) and consider $\tilde{\tau} = \phi t$ where $\tilde{\tau}$ is the non-dimensional time, ϕ is as defined in (3.2) and express the equations of motion in the following non-dimensional form,

$$
\begin{aligned}
\frac{d^2x_i}{d\tilde{\tau}^2} &= (x_{i-1}-x_i)_+^{3/2} - (x_i - x_{i+1})_+^{3/2} \\
\varepsilon\frac{d^2x_{i+1}}{d\tilde{\tau}^2} &= (x_i - x_{i+1})_+^{3/2} - \alpha(x_{i+1} - x_{i+2})_+^{3/2} \\
&\bullet\ \bullet\ \bullet \\
\varepsilon\frac{d^2x_{i+j}}{d\tilde{\tau}^2} &= \alpha\left\{(x_{i+j-1} - x_{i+j})_+^{3/2} - (x_{i+j} - x_{i+j+1})_+^{3/2}\right\} \\
&\bullet\ \bullet\ \bullet \\
\varepsilon\frac{d^2x_{i+N}}{d\tilde{\tau}^2} &= \alpha(x_{i+N-1} - x_{i+N})_+^{3/2} - (x_{i+N} - x_{i+N+1})_+^{3/2}
\end{aligned}
\tag{3.41}
$$

We note that there are two non-dimensional parameters, namely, a non-dimensional stiffness parameter (α) and a non-dimensional mass parameter (ε), defined as:

$$
\alpha = \frac{1}{2\sqrt{2}}\left\{\frac{E_2(1-\mu_1^2)}{E_1(1-\mu_2^2)} + 1\right\}\sqrt{1+\frac{R_2}{R_1}}\ , \quad \varepsilon = \frac{\rho_2 R_2^3}{\rho_1 R_1^3} \tag{3.42}
$$

As described in the previous sections, in the following asymptotic analysis we will consider ε as the small parameter of the problem by assuming that $0 < \varepsilon \ll 1$; that is, we will develop our asymptotics in the limit of large mass mismatch between the heavy and light beads. Alternatively, we will be assuming that the dimer system is composed of heavy and light beads with normalized mass ratios equal to unity and ε, respectively (in the notation of system (3.41) beads with indices $i = 1 + (N+1)n, n = 0,1,2$ ... are heavy, whereas those with indices $i + j, 1 \le j \le N$ are light). The parameter α scales the relative stiffness of the two types of beads. It is worth noting that the minimum value of this parameter is equal to $1/(2\sqrt{2})$, whereas the limiting values $\varepsilon = \alpha = 1$ correspond to the homogeneous granular chain. The other limit $\varepsilon = 0$ corresponds to the so-called 'auxiliary system,'(cf. Section 3.1.2.2 [97]) wherein the masses of the light beads are neglected and only their stiffness is taken into account.

The asymptotic analysis of the normalized system (3.41) will be performed in the regime of *primary pulse propagation (squeeze mode)*, i.e. the phase during which there are no bead separations. Of course, after the passage of the primary pulse and the gradual relaxation of the compressive forces, bead separations are possible (and indeed do occur); this influences primarily the radiation of the energy of the pulse to the far field through the propagation of nonlinear (and highly non-smooth) traveling waves (cf. Section 3.1 [63, 91, 97, 98]), but it does not affect primary pulse transmission. Hence, the subscripts (+) will be dropped from (3.41) from here on.

For primary pulse propagation we consider the following asymptotic expansions of the responses of the heavy and light beads,

$$\begin{aligned} x_i &= x_{i0}(t_0) + \varepsilon^a x_{i1}(t_1) + \dots \\ x_{i+j} &= x_{(i+j)0}(t_0) + \varepsilon^c x_{(i+j)1}(t_1) + \dots \end{aligned} \tag{3.43}$$

where t_0 and t_1 are two distinct time scales of the dynamics defined as follows, $t_0 = \tilde{\tau}(k/(N-1+2k))^{3/4} = \psi\tilde{\tau}$, $t_1 = \varepsilon^b t_0$, $k = \alpha^{2/3}$ and from the previous section we have $a = 2, b = -1/2, c = 1$. Expanding the rational powers in power series with respect to ε, we obtain the following set of governing equations at the first order approximation, valid in the limit of sufficiently small ε:

$$\begin{aligned} \psi^2\left(\ddot{x}_{i0} + \varepsilon^{a+2b} x_{i1}''\right) = {} & \left(x_{(i-1)0} - x_{i0}\right)^{3/2} - \left(x_{i0} - x_{(i+1)0}\right)^{3/2} + \left(\frac{3}{2}\right)\left(x_{(i-1)0} - x_{i0}\right)^{1/2}\left(\varepsilon^c x_{(i-1)1} - \varepsilon^a x_{i1}\right) \\ & - \left(\frac{3}{2}\right)\left(x_{i0} - x_{(i+1)0}\right)^{1/2}\left(\varepsilon^a x_{i1} - \varepsilon^c x_{(i+1)1}\right) + O\left(\left\|\varepsilon^a x_{i1} - \varepsilon^c x_{(i+1)1}\right\|^2\right) \end{aligned} \tag{3.44a}$$

$$\varepsilon\psi^2(\ddot{x}_{(i+1)0}+\varepsilon^{c+2b}x''_{(i+1)0}) = \left(x_{i0}-x_{(i+1)0}\right)^{3/2} - \alpha\left(x_{(i+1)0}-x_{(i+2)0}\right)^{3/2}$$
$$+\left(\frac{3}{2}\right)\left(x_{i0}-x_{(i+1)0}\right)^{1/2}\left(\varepsilon^a x_{i1}-\varepsilon^c x_{(i+1)1}\right) - \alpha\left(\frac{3}{2}\right)\left(x_{(i+1)0}-x_{(i+2)0}\right)^{1/2}\left(\varepsilon^c x_{(i+1)1}-\varepsilon^c x_{(i+2)1}\right) \qquad (3.44b)$$
$$+O\left(\left\|\varepsilon^a x_{i1}-\varepsilon^c x_{(i+1)1}\right\|^2\right)+O\left(\left\|\varepsilon^c x_{(i+1)1}-\varepsilon^c x_{(i+2)1}\right\|^2\right)$$

$$\varepsilon\psi^2(\ddot{x}_{(i+j)0}+\varepsilon^{c+2b}x''_{(i+j)1}) = \alpha\left\{\left(x_{(i+j-1)0}-x_{(i+j)0}\right)^{3/2}-\left(x_{(i+j)0}-x_{(i+j+1)0}\right)^{3/2}\right\}+$$
$$\alpha\varepsilon^\gamma\left(\frac{3}{2}\right)\left(x_{(i+j-1)0}-x_{(i+j)0}\right)^{1/2}\left(x_{(i+j-1)1}-x_{(i+j)1}\right)-\alpha\varepsilon^\gamma\left(\frac{3}{2}\right)\left(x_{(i+j)0}-x_{(i+j+1)0}\right)^{1/2}\left(x_{(i+j)1}-x_{(i+j+1)1}\right)$$
$$+O\left(\left\|\varepsilon^c x_{(i+j-1)1}-\varepsilon^c x_{(i+j)1}\right\|^2\right)+O\left(\left\|\varepsilon^c x_{(i+j)1}-\varepsilon^c x_{(i+j+1)1}\right\|^2\right)$$

(3.44c)

$$\varepsilon\psi^2(\ddot{x}_{(i+N)0}+\varepsilon^{c+2b}x''_{(i+N)1}) = \alpha\left(x_{(i+N-1)0}-x_{(i+N)0}\right)^{3/2}-\left(x_{(i+N)0}-x_{(i+N+1)0}\right)^{3/2}+$$
$$\alpha\varepsilon^\gamma\left(\frac{3}{2}\right)\left(x_{(i+N-1)0}-x_{(i+N)0}\right)^{1/2}\left(x_{(i+N-1)1}-x_{(i+N)1}\right)-\left(\frac{3}{2}\right)\left(\varepsilon^c x_{(i+N)0}-\varepsilon^a x_{(i+N+1)0}\right)^{1/2}\left(x_{(i+N)1}-x_{(i+N+1)1}\right)$$
$$+O\left(\left\|\varepsilon^c x_{(i+N-1)1}-\varepsilon^c x_{(i+N)1}\right\|^2\right)+O\left(\left\|\varepsilon^c x_{(i+N)1}-\varepsilon^a x_{(i+N+1)1}\right\|^2\right)$$

(3.44d)

In these equations overdots indicate differentiation with respect to the slow time scale t_0 and primes denote differentiation with respect to fast time scale t_1.

Considering system (3.44) at the $O(1)$ approximation, and applying simple algebraic manipulations we obtain the relations,

$$\ddot{x}_{i0} = (x_{(i-(N+1))0}-x_{i0})_+^{3/2}-(x_{i0}-x_{(i+N+1)0})_+^{3/2} \qquad (3.45)$$

$$x_{(i+j)0} = \frac{(N-j+k)x_{i0}+(k+j-1)x_{(i+N+1)0}}{N-1+2k} \qquad (3.46a)$$

where $k=\alpha^{2/3}$. The set of *nonlinear* ordinary differential equations (3.45) provides the first-order approximation of the dynamics of the heavy beads, whereas the set of *linear*

algebraic equations (3.46a) provides the first-order approximation of the dynamics of the light beads. It is worth noting that the $O(1)$ approximation of the responses of the light beads is the weighted average of the $O(1)$ approximation of the response of the bounding heavy beads. Moreover, since systems (3.45, 3.46) are expressed only in terms of the slow time scale t_0, the $O(1)$ approximations of the responses of both the heavy and light beads of the dimer are governed solely by the slow time scale.

The $O(1)$ approximation of the slowly-varying motion of the heavy beads is identical to the response of a homogeneous auxiliary system composed of weakly coupled heavy beads, realized in the limit $\varepsilon \to 0$; whereas the $O(1)$ approximation of the response of the light beads is expressed entirely in terms of the corresponding responses of the heavy beads. As we are interested only in studying solitary wave transmission in the dimer, we select as solution of the set of equations (3.45) the well-known Nesterenko's solitary wave. This is very much similar to the considered solutions in Section 3.1.2.2. To this end, the slow motion of the heavy beads is approximated as (3.9a, b). Accordingly, the slow component of the dynamics of the light beads is expressed as:

$$x_{(i+j)0}(t_0) \equiv s_{(i+j)}(\varphi t_0) = \frac{(N-j+k)S_i(\varphi t_0) + (k+j-1)S_{i+N+1}(\varphi t_0)}{N-1+2k} \tag{3.46b}$$

It is interesting to note that the $O(1)$ approximations of the responses of both the heavy and light beads invariably decay to zero for increasing or decreasing t_0. Hence, they are denoted as *compactons* [42, 46] as they decay to zero in finite time, and need finite compact support from the media for their propagation. Although these approximations predict quite well the dynamics of the heavy beads for sufficiently small ε, this does not guarantee that the responses of the light beads in the actual system would decay to zero even for small values of ε, owing to the fact that bead

separation can occur towards the end of the squeeze mode for arbitrary values of ε (cf. Figure 3.3), and this bead separation can be ascertained only from the $O(\varepsilon)$ approximation of the response of the light beads. Once there is bead separation, solitary waves cannot be realized. It is noted at this point that the propagation of solitary waves in homogeneous [35, 41, 52, 58] or 1:1 dimer granular chains [97] does not involve separation between beads. Hence, in order to realize solitary waves in a general $1:N$ dimer we need to determine the specific values of the normalized parameters α and ε for which the higher order asymptotic corrections of the dynamics of the light beads also decay to zero. By requiring that the higher order oscillations also decay to zero towards the end of the squeeze mode, we ascertain that the light beads do not separate (at least correct to the order of approximation considered) and all the energy of the propagating pulse is transmitted without any loss through each periodic set in the form of a localized solitary pulse. In that case the dynamical state of the chain would be the same before and after the propagation of the solitary wave except for a rigid body translation (assuming no boundaries) in the direction of the propagation of the solitary wave.

From the above discussion it should be clear that there is a need to consider the equations of motion at the $O(\varepsilon)$ approximation, leading to the following equations governing the *fast dynamics* of the heavy and light beads,

$$x_{i1}(t_1) = \frac{(3/2)}{\psi^{4/3}}\left\{\left[S_{(i-(N+1))}(\varphi t_0) - S_i(\varphi t_0)\right]^{1/2} x_{(i-(N+1))1}(t_1) + \left[S_i(\varphi t_0) - S_{(i+N+1)}(\varphi t_0)\right]^{1/2} x_{(i+N+1)1}(t_1)\right\} \tag{3.47a}$$

$$\begin{Bmatrix} x''_{(i+1)1} \\ x''_{(i+2)1} \\ \dots \\ x''_{(i+N-1)1} \\ x''_{(i+N)1} \end{Bmatrix} = -\Omega_i^2(t_0) \begin{bmatrix} 1+k & -k & 0 & \dots & 0 \\ -k & 2k & -k & \dots & 0 \\ \dots & \dots & \dots & \dots & \dots \\ 0 & \dots & -k & 2k & -k \\ 0 & \dots & 0 & -k & 1+k \end{bmatrix} \begin{Bmatrix} x_{(i+1)1} \\ x_{(i+2)1} \\ \dots \\ x_{(i+N-1)1} \\ x_{(i+N)1} \end{Bmatrix} - \begin{Bmatrix} \ddot{x}_{(i+1)0} \\ \ddot{x}_{(i+2)0} \\ \dots \\ \ddot{x}_{(i+N-1)0} \\ \ddot{x}_{(i+N)0} \end{Bmatrix} \tag{3.47b}$$

where,

$$\Omega_i^2(t_0) = \frac{3}{2}\frac{N-1+2k}{k}\left(S_i\left(\varphi t_0\right) - S_{i+N+1}\left(\varphi t_0\right)\right)^{1/2}$$

$$\ddot{x}_{(i+j)0}(t_0) \equiv \ddot{s}_{(i+j)}(\varphi t_0) = \frac{(N-j+k)\ddot{S}_i\left(\varphi t_0\right) + (k+j-1)\ddot{S}_{i+N+1}\left(\varphi t_0\right)}{N-1+2k} \tag{3.47c}$$

It can be observed that the $O(\varepsilon)$ approximation of the fast response of the light beads lead to a $N-$degree of freedom linear system of coupled oscillators with slowly varying frequencies and forces. Once analytical approximations for the fast oscillations of the light beads are derived, the $O(\varepsilon)$ fast oscillations of the heavy beads can be approximated by means of relations (3.47a). Higher order corrections are not needed, since in the limit of small ε they are expected to be insignificant compared to the previous leading order expressions.

From the previous discussion it is clear that we only need to focus on the second set of slowly varying linear oscillators (3.47b) since these determine completely the fast dynamics of the dimer for primary pulse propagation. Hence, for the realization of anti-resonances (resonances) in the general $1:N$ dimer chain we simply require that the responses of all N light beads at this order of approximation decay to zero (maximize) at the end of the squeeze mode. Viewed from another perspective, since the system (3.47b) is linear, the equations can be decoupled with respect to the fast time scale to obtain equations of motion in modal coordinates corresponding to N normal modes. It follows that for solitary wave propagation (resonance) we should require that the response of

each mode decays to zero (maximizes) at the end of the squeeze mode. Up till now we have formulated a very general asymptotic model for the propagatory dynamics of a general $1:N$ dimer chain. It is interesting to note that either for the realization of anti-resonances or resonances, the corresponding conditions needs to be imposed on these N equations. Interestingly, the dynamics of these chains are governed by only two parameters (ε and α), whereas N equations are required to be satisfied. As a result and as shown in the next section, this is only possible for the case of $N = 2$, since for $N > 2$ this decay or maximization condition cannot be realized with just two parameters unless special symmetries are satisfied. To this end we consider the propagatory dynamics of the particular case of $1:2$ dimer chains in the next couple of sections.

3.2.3 Anti-Resonances and Solitary Waves in $1:2$ Dimer Chains

In this section we consider the particular case of $1:2$ dimer chains. We prove numerically and asymptotically the existence of a countable infinity of traveling solitary waves in $1:2$ dimer chain. These solitary waves, which can be regarded as anti-resonances in these strongly nonlinear media, are found to be qualitatively different than those previously studied in homogeneous [35, 41, 52, 58] and $1:1$ dimer chains [97] which possess symmetric velocity waveforms. In contrast, for traveling solitary waves in $1:2$ dimers the velocity waveforms of the responses of the heavy beads are symmetric, whereas those of the light beads are non-symmetric. In this context we employ the asymptotic model developed in the previous section.

For the particular case of $1:2$ dimer chain, the $O(\varepsilon)$ equation (3.47b) governing the fast dynamics of the light beads during primary pulse propagation reduces to a two degree of freedom system, with in-phase and out-of-phase modes. Motivated by this observation, we introduce new coordinates for the dynamics of the two light beads of

each periodic set, namely, the response of their center of mass $\eta_i = x_{i+1} + x_{i+2}$ (for the in-phase mode) and their relative displacement $\sigma_i = x_{i+1} - x_{i+2}$ (for the out-of-phase mode) where $i = 3n + 1, n = 0, \pm 1, \pm 2, ...$ According to the previous general asymptotic we define the two time scales $t_0 = \tilde{\tau}(k/(1+2k))^{3/4} = \psi\tilde{\tau},\ t_1 = \varepsilon^{-1/2} t_0$ and introduce the asymptotic expansions,

$$\begin{aligned} x_i &= x_{i0}(t_0) + \varepsilon^2 x_{i1}(t_1) + ... \\ \sigma_i &= \sigma_{i0}(t_0) + \varepsilon\sigma_{i1}(t_1) + ... \\ \eta_i &= \eta_{i0}(t_0) + \varepsilon\eta_{i1}(t_1) + ... \end{aligned} \tag{3.48}$$

At the $O(1)$ approximation we obtain the following slow dynamics for the heavy and light beads,

$$\ddot{x}_{i0} = \left(x_{(i-3)0} - x_{i0}\right)_+^{3/2} - \left(x_{i0} - x_{(i+3)0}\right)_+^{3/2} \qquad \text{(Heavy beads)} \tag{3.49}$$

$$\begin{aligned} \sigma_{i0} &= \frac{x_{i0} - x_{(i+3)0}}{1+2k} = \frac{S_i(\varphi t_0) - S_{i+3}(\varphi t_0)}{1+2k} \\ \eta_{i0} &= x_{i0} + x_{(i+3)0} = S_i(\varphi t_0) + S_{i+3}(\varphi t_0) \end{aligned} \qquad \text{(Light beads)} \tag{3.50}$$

The notation of the previous section for Nesterenko's solitary wave in the auxiliary system (3.49) is retained.

Proceeding to the next order approximation, we study the $O(\varepsilon)$ fast dynamics of the lights beads of each periodic set. In view of the previous coordinate transformations, the system (3.47b) takes the form of a set of two coupled oscillators:

$$\begin{aligned} \eta_{i1}'' &= -\frac{3}{2\psi^2}\left(\frac{k}{1+2k}\right)^{1/2} \left(S_i(\varphi t_0) - S_{i+3}(\varphi t_0)\right)^{1/2} \eta_{i1} - \ddot{\eta}_{i0} \\ \sigma_{i1}'' &= -\frac{3}{2\psi^2}\left(k^{1/2}\left(1+2k\right)\right)\left(S_i(\varphi t_0) - S_{i+3}(\varphi t_0)\right)^{1/2} \sigma_{i1} - \ddot{\sigma}_{i0} \end{aligned} \tag{3.51}$$

Hence, the $O(\varepsilon)$ approximations for the motion of the center of mass and the relative displacement between the two light beads are governed by decoupled linear oscillators with slowly varying frequencies and excitations. It can be observed that the frequency of the oscillator modeling the motion of the center of mass of the light beads is smaller compared to the one of the oscillator governing the relative displacement between light beads. This can be seen in light of classical linear theory wherein the in-phase mode typically possesses the lowest frequency and captures the highest energy.

From the previous discussion and the asymptotic methodology of the previous section, it is clear that we need to focus only on the slowly varying linear oscillators (3.51) since they determine completely the fast dynamics of the light beads of the 1: 2 dimer during primary pulse propagation. Once an analytical approximation of the fast oscillation of an arbitrary pair of light beads, say beads $3p+2$ and $3p+3$ for some $p \in \mathbb{Z}$, is determined, the responses of the other light beads can be determined by imposing appropriate time shifts (i.e., multiples of T) to the solution. Moreover, the fast oscillation of the heavy bead $3p+1$ is also determined from this solution [cf. relation (3.47a)]. From here on we denote the center of mass and relative displacement of light beads $3p+2$ and $3p+3$ by $\eta_{(3p+1)}$ and $\delta_{(3p+1)}$, respectively. Hence, in the remainder of this section we focus exclusively on the analysis of the following linear oscillator with slowly varying frequency and forcing,

$$\begin{aligned} \eta''_{(3p+1)1} &= -\Omega^2_{(3p+1)1}(t_0)\eta_{(3p+1)1} + f_{(3p+1)1}(t_0) \\ \sigma''_{(3p+1)1} &= -\Omega^2_{(3p+1)2}(t_0)\sigma_{(3p+1)1} + f_{(3p+1)2}(t_0) \end{aligned} \tag{3.52a}$$

where,

$$\begin{aligned} \Omega^2_{(3p+1)1}(t_0) &= \frac{3}{2\psi^2}\left(\frac{k}{1+2k}\right)^{1/2}\left(S_{(3p+1)}(\varphi t_0) - S_{(3p+1)+3}(\varphi t_0)\right)^{1/2} \\ \Omega^2_{(3p+1)2}(t_0) &= \frac{3}{2\psi^2}\left(k^{1/2}\left(1+2k\right)\right)\left(S_{(3p+1)}(\varphi t_0) - S_{(3p+1)+3}(\varphi t_0)\right)^{1/2} \end{aligned} \tag{3.52b}$$

and slow time varying excitations $f_{(3p+1)1}(t_0) = -\ddot{\eta}_{(3p+1)0}$ and $f_{(3p+1)2}(t_0) = -\ddot{\sigma}_{(3p+1)0}$. Since we selected Nesterenko's solitary wave as solution of the $O(1)$ auxiliary homogeneous system (3.49), taking into account relations (3.52), we conclude that both these forces decay to zero as $t_0 \to \pm\infty$. Moreover, it can be shown that at $t_0 = 0$, it holds that $f_{(3p+1)1}(0) = 0$ and $f_{(3p+1)2}(0)$ is maximum. These features will be of importance when formulating the appropriate boundary conditions in the following asymptotic analysis.

As discussed previously, to realize solitary waves in these systems we need to impose appropriate boundary conditions such that the $O(\varepsilon)$ fast oscillations of the light beads decay to zero. Before we formulate these boundary conditions we provide numerical evidence of realization of solitary waves in the $1:2$ dimer chains. In Figure 3.56 we depict velocity profiles for two light beads of a periodic set (numbered 44 and 45 of the semi-infinite $1:2$ dimer numerical model with an applied impulse of intensity 1.5 applied to its free left boundary) and the corresponding bounding heavy beads (numbered 43 and 46 in the numerical model) for normalized parameters $\varepsilon = 0.05616$ and $\alpha = 2.78$. We note that all velocities decay to zero with increasing or decreasing normalized time. This implies that the propagating primary pulse does not radiate energy, and, hence, propagates without distortion. Interestingly, the individual responses of the light beads possess reflectional symmetry about a middle point of the velocity profile (cf. Figure 3.56a), whereas the velocity of their center of mass is symmetric and their relative velocity is anti-symmetric with respect to the middle point (cf. Figure 3.56b). Moreover, decomposing the fast and slow dynamics of these velocity profiles (cf. Figure 3.56c) we can ascertain the appropriate boundary conditions that need to be imposed on the $O(\varepsilon)$ equations (3.52a) for solitary wave formation. Moreover, based on these decompositions we can numerically compute the slow excitations on the right-hand-sides of these equations (cf. Figure 3.56d).

Indeed, for the periodic set composed of the $(3p+2)-$th and $(3p+3)-$th light beads we define the reference time instant $\tau = T_{s(3p+1)}$ as the time instant when the bounding heavy beads $(3p+1)$ and $(3p+4)$ attain identical non-zero velocities (cf. Figure 3.56a); in fact this time instant represents the point of maximum compression of the light beads by their neighboring heavy beads. Then, we impose the symmetry conditions that the velocity profile of, (a) the center of mass of the light beads has reflectional symmetry, and (b) the relative velocity of the light beads is anti-symmetric with respect to the reference time instant. It follows that the following symmetry conditions should be imposed for the velocity profiles $\eta'_{(3p+1)}$ and $\sigma'_{(3p+1)}$ of the pair of light beads and of the bounding heavy beads:

$$\begin{aligned} &\eta'_{(3p+1)}(T_{s(3p+1)} - \chi) = \eta'_{(3p+1)}(T_{s(3p+1)} + \chi), \\ &\sigma'_{(3p+1)}(T_{s(3p+1)} - \chi) = -\sigma'_{(3p+1)}(T_{s(3p+1)} + \chi), \quad \forall\ \chi \in \mathbb{R}, \\ &\dot{x}_{3p+1}(T_{s(3p+1)}) = \dot{x}_{3(p+1)+1}(T_{s(3p+1)}), \quad p = 0, \pm 1, \pm 2, \ldots \end{aligned} \tag{3.53}$$

These symmetry conditions ensure the annihilation of the oscillatory tail in the response of the center of mass and relative displacement of the light beads, so they represent *necessary conditions* for absence of radiation from the propagating primary pulse, and, hence, the realization of propagating solitary wave in the 1:2 dimer. Moreover, the symmetry condition for the velocity profile of the center of mass of the $(3p+2)-$th and $(3p+3)-$th light beads implies that the corresponding displacement profile is *anti-symmetric* with respect to the reference time instant $\tau = T_{s(3p+1)}$. This can be observed from the decomposed fast oscillation of the response of the center of mass shown in Figure 3.56c.

Considering now the equations for the fast dynamics (3.52a), without loss of generality we shift the reference time to $T_{s(3p+1)} = 0$. Taking into account that the slow excitation $f_{(3p+1)1}(t_0)$ ($f_{(3p+1)2}(t_0)$) is anti-symmetric (symmetric) (cf. Figure 3.56d), and

the slow frequencies squared $\Omega^2_{(3p+1)1}(t_0)$ and $\Omega^2_{(3p+1)2}(t_0)$ are symmetric with respect to $T_{s(3p+1)} = 0$, in order to satisfy the previous symmetry conditions we impose the boundary conditions:

$$\begin{aligned} \eta_{(3p+1)1}(t_1{=}0) &= 0 \\ \sigma'_{(3p+1)1}(t_1{=}0) &= 0 \end{aligned} \tag{3.54}$$

As discussed previously, these provide the *necessary conditions* for solitary wave formation. A second set of conditions that needs to be imposed concerns the asymptotic behavior of the solutions as $\tau \to \pm\infty$ [17], but in view of the previous symmetry conditions we only need to consider the solutions in the semi-infinite interval $\tau \in [0, +\infty)$. We are seeking localized (simple-hump) solitary pulses, and noting that by construction the $O(1)$ (slow) approximations of the bead responses decay to zero as $\tau \to +\infty$ (since they are based on Nesterenko's solitary wave of the auxiliary system (3.49)), we only need to consider the behavior at infinity of the $O(\varepsilon)$ (fast) components. Hence, we need to impose the following additional limiting conditions,

$$\begin{aligned} \lim_{t_1 \to +\infty} \eta_{(3p+1)1}(t_1) &= 0 \\ \lim_{t_1 \to +\infty} \sigma_{(3p+1)1}(t_1) &= 0 \end{aligned} \tag{3.55}$$

which together with (3.54) form *necessary and sufficient conditions* at the $O(\varepsilon)$ approximation for the formation of solitary waves in 1:2 dimers.

In summary, solitary wave propagation in the 1:2 dimer is governed by the following linear boundary value problems (LBVPs) governing the fast components of the response of the center of mass (CM), and of the relative displacement (RD) between the two light beads of an arbitrary periodic set,

$$\varepsilon\,\ddot{\eta}_{(3p+1)1}(\tau)+\Omega^2_{(3p+1)1}(\tau)\,\eta_{(3p+1)1}(\tau)=f_{(3p+1)1}(\tau)$$
$$\eta_{(3p+1)1}(\tau=0)=0 \tag{3.56}$$
$$\lim_{\tau\to+\infty}\eta_{(3p+1)1}(\tau)=0$$

$$\varepsilon\,\ddot{\sigma}_{(3p+1)1}(\tau)+\Omega^2_{(3p+1)2}(\tau)\,\sigma_{(3p+1)1}(\tau)=f_{(3p+1)2}(\tau)$$
$$\dot{\sigma}_{(3p+1)1}(\tau=0)=0 \tag{3.57}$$
$$\lim_{\tau\to+\infty}\sigma_{(3p+1)1}(\tau)=0$$

where $p=0,\pm1,\pm2,\ldots$ and we have re-introduced the normalized time through the transformation $t_1=\varepsilon^{-1/2}t_0=\varepsilon^{-1/2}\tau$. In these LBVPs the normalized parameters ε and α enter explicitly (since the slowly varying frequencies and nonhomogeneous terms depend on the parameter $k=\alpha^{2/3}$). Commenting on the symmetric boundary conditions in relations (3.56) and (3.57), these correspond to the formation of an *anti-resonance* in the dimer chain. As discussed in Section 3.1.2 and 3.1.3 [91, 97], depending on the form of the boundary conditions in the reduced problems governing the higher-order fast frequency oscillations of the light beads, one can study the formation of either *anti-resonances* corresponding to absence of oscillating tails in the trails of propagating pulses [97], or of *resonances* corresponding to maximization of the amplitudes of the oscillating tails and resulting in maximum distortion or attenuation of propagating pulses [91]. This section focuses on the formation of anti-resonances (and solitary waves) in the 1:2 dimers, whereas the study of resonances in the same system will be considered in the next section.

To solve the boundary value problems (3.56) and (3.57) we follow the following methodology. For fixed parameter α we seek the initial conditions $\eta_{(3p+1)1}(0)=0$, $\dot{\eta}_{(3p+1)1}=V_q(\alpha)$ at the discrete values $\varepsilon=\varepsilon_q^{CM}(\alpha), q=1,2,\ldots$ (spectrum) that solve the LBVP (3.56). Similarly, we seek the initial conditions $\sigma_{(3p+1)1}(0)=A_r(\alpha)$, $\dot{\sigma}_{(3p+1)1}=0$ at the discrete values $\varepsilon=\varepsilon_r^{RD}(\alpha), r=1,2,\ldots$ that solve the LBVP (3.57). Hence, we derive

two separate discrete spectra $\{\varepsilon_q^{CM}(\alpha)\}$ and $\{\varepsilon_r^{RD}(\alpha)\}$ corresponding to each of the problems (3.56) and (3.57). Clearly, *for the realization of a solitary wave both LBVPs should be satisfied simultaneously*, and this is achieved by requiring that:

$$\varepsilon_Q^{CM}(\alpha_{QR}) = \varepsilon_R^{RD}(\alpha_{QR}) \text{ for some } (Q,R) \in \mathbb{N}^+ \times \mathbb{N}^+ \tag{3.58}$$

This condition provides the discrete pairs (spectra) of the normalized parameters for which solitary waves are realized. In the following analysis we apply the outlined methodology in two different ways, namely, either by developing asymptotic solutions of (3.56) and (3.57) in the limit of small ε, or, alternatively by computing direct numerical solutions of the same problems.

We initiate our study by applying the Wentzel–Kramers–Brillouin (WKB) approximation [136] to construct the analytical approximations of the solutions of the LBVP (3.60) in the limit of sufficiently small ε. We emphasize at this point that the WKB method ceases to be valid in the vicinity of turning points (i.e., at the points of nullification) of the frequency $\Omega_{(3p+1)1}(\tau)$. In this case we are interested in finding asymptotic approximation to the solutions of (3.56) in the semi-infinite time interval $\tau \in [0,+\infty)$, but since this frequency is exponentially decaying as $\tau \to \infty$ and thus it possesses a turning point at infinity. It follows that for sufficiently small values of the frequency, the WKB approximation may cease to be valid, so our asymptotic approximations are restricted to finite values of the normalized time τ. We then seek the asymptotic solution of (3.56) in the form (3.16) and substitute it back into (3.56) to have:

$$\eta_{(3p+1)1}(\tau) \equiv \frac{\tilde{C}_1}{\sqrt{\Omega_{(3p+1)1}}}\cos\left[\frac{1}{\sqrt{\varepsilon}}\int_0^\tau \Omega_{(3p+1)1}(\zeta)d\zeta\right] + \frac{\tilde{C}_2}{\sqrt{\Omega_{(3p+1)1}}}\sin\left[\frac{1}{\sqrt{\varepsilon}}\int_0^\tau \Omega_{(3p+1)1}(\zeta)d\zeta\right] + \frac{f_{(3p+1)1}(\tau)}{\Omega^2_{(3p+1)1}(\tau)} \tag{3.59}$$

Imposing the first boundary condition $\eta_{(3p+1)1}(0) = 0$ yields $\tilde{C}_1 = 0$, whereas imposing the limiting boundary condition $\lim_{t_1\to\infty} \eta_{(3p+1)1}(t_1) = 0$ (and taking into account that it must hold that $\tilde{C}_2 \neq 0$) we derive an asymptotic approximation for the spectrum (eigenvalues) of the LBVP (3.56):

$$\lim_{\tau\to\infty} \sin\left[\frac{1}{\sqrt{\varepsilon}}\int_0^{\tau} \Omega_{(3p+1)1}(\zeta)d\zeta\right] = 0 \Rightarrow$$
$$\frac{1}{\sqrt{\varepsilon}}\int_0^{\infty} \Omega_{(3p+1)1}(\zeta)d\zeta = \left[\frac{3(1+2k)}{2k}\right]^{1/2} \frac{(3.8744/2)}{\sqrt{\varepsilon}} = q\pi \Rightarrow \tag{3.60}$$
$$\varepsilon = \varepsilon_q^{CM}(\alpha) = \left[\frac{3(1+2\alpha^{2/3})}{2\alpha^{2/3}}\right]\left[\frac{3.8744/2}{q\pi}\right]^2, \quad q = 1,2,...$$

Note that it holds that $\dot{\Omega}_{(3p+1)1}(0) = 0$ and $\dot{f}_{(3p+1)1}(0) \neq 0$, oweing to the symmetric and anti-symmetric nature of these functions, respectively. To each eigenvalue $\varepsilon_q^{CM}(\alpha)$ corresponds the following eigenfunction valid in the finite interval $\tau \in [0, \mathrm{T}^*]$,

$$\eta^{CM}_{(3p+1)1_q}(\tau;\alpha) \cong \frac{\tilde{C}_2}{\sqrt{\Omega_{(3p+1)1}(\tau;\alpha)}} \sin\left[\frac{1}{\sqrt{\varepsilon_q^{COM}(\alpha)}}\int_0^{\tau} \Omega_{(3p+1)1}(\zeta;\alpha)d\zeta\right] + \frac{f_{(3p+1)1}(\tau;\alpha)}{\Omega^2_{(3p+1)1}(\tau;\alpha)} \tag{3.61}$$

where $\tilde{C}_2$ is a free parameter that can be chosen arbitrarily [since (3.56) is a linear BVP], and the explicit dependence of the eigensolution on the slow time and α has been indicated. Hence, the spectrum (3.60) of (3.59) consists of a countable infinity of one-dimensional curves of eigenvalues parametrised by the normalized stiffness parameter α. It should be noted that these do not correspond to solitary wave solutions since they only satisfy the LBVP (3.56) governing the fast oscillations of the center of mass of the pair of light beads of an arbitrary periodic set, and not necessarely the LBVP (3.57) governing the fast relative oscillations between the same pair of light beads.

In Figure 3.57 we provide a comparison of the WKB approximations (3.59) and (3.60), and the direct numerical solution of (3.60) for the eigenfunction $\eta^{CM}_{(3p+1)1_5}(\tau;3)$ of a $1:2$ dimer chain with $\varepsilon^{CM}_5 \approx 0.056597$ and $\alpha = 3$; for the WKB approximation a solitary wave solution with amplitude $\mathrm{A} = 3$ and time shift $\mathrm{T} = 1.937$ is considered. This representative result validates the asymptotic analysis. Extending this comparison, in Table 3.5 we provide a similar comparison for the spectrum $\{\varepsilon^{CM}_q(3)\}, q = 2,\dots,6$. Again, we note satisfactory agreement between the direct numerical solutions and the WKB approximations, especially for higher order eigenvalues, i.e., for decreasing eigenvalues, in accordance to the assumptions of the asymptotic analysis. We note, however, that this spectrum corresponds only to the center of mass of the light beads of a periodic set, and is not related to the oscillations of their relative displacement. This implies that it may so happen that the fast oscillations of the centre of mass decays to zero whereas that of the relative displacement does not. This calls for the study of the complementary LBVP (3.57).

Following a similar analysis in the limit of small ε, we asymptotically approximate the eigensolution of (3.57) as,

$$\sigma_{(3p+1)1}(\tau) \cong \frac{\tilde{C}_3}{\sqrt{\Omega_{(3p+1)2}}}\cos\left[\frac{1}{\sqrt{\varepsilon}}\int_0^\tau \Omega_{(3p+1)2}(\zeta)d\zeta\right] + \frac{\tilde{C}_4}{\sqrt{\Omega_{(3p+1)2}}}\sin\left[\frac{1}{\sqrt{\varepsilon}}\int_0^\tau \Omega_{(3p+1)2}(\zeta)d\zeta\right] + \frac{f_{(3p+1)2}(\tau)}{\Omega^2_{(3p+1)2}(\tau)} \tag{3.62}$$

where due to the first boundary condition we set $\tilde{C}_4 = 0$. Then, to obtain the spectrum of ε values where the relative displacement decays to zero, we impose the second limiting boundary condition, which in view of the fact that $\tilde{C}_3 \neq 0$, leads to:

$$\lim_{\tau\to\infty}\cos\left[\frac{1}{\sqrt{\varepsilon}}\int_0^{\tau}\Omega_{(3p+1)2}(\zeta)\,d\zeta\right]=0\ \Rightarrow$$

$$\frac{1}{\sqrt{\varepsilon}}\int_0^{\infty}\Omega_{(3p+1)2}(\zeta)\,d\zeta=\left[\frac{3(1+2k)^2}{2k}\right]^{1/2}\frac{(3.8744/2)}{\sqrt{\varepsilon}}=(2r+1)\frac{\pi}{2}\ \Rightarrow$$

$$\varepsilon_r^{RD}=\left[\frac{3(1+2k)^2}{2k}\right]\left[\frac{3.8744}{(2r+1)\pi}\right]^2,\quad r=1,2,... \tag{3.63}$$

To each eigenvalue $\varepsilon_r^{RD}(\alpha)$ corresponds the following eigenfunction valid in the finite interval $\tau\in[0,\mathrm{T}^*]$,

$$\sigma_{(3p+1)1_r}^{RD}(\tau;\alpha)\cong\frac{\tilde{C}_3}{\sqrt{\Omega_{(3p+1)2}(\tau;\alpha)}}\cos\left[\frac{\int_0^{\tau}\Omega_{(3p+1)2}(\zeta;\alpha)d\zeta}{\sqrt{\varepsilon_r^{RD}(\alpha)}}\right]+\frac{f_{(3p+1)2}(\tau;\alpha)}{\Omega_{(3p+1)2}^2(\tau;\alpha)} \tag{3.64}$$

where again $\tilde{C}_3$ is a free parameter that can be chosen arbitrarily. Hence, similar to the spectrun of (3.60), the eigenvalue spectrum $\{\varepsilon_r^{RD}(\alpha)\}, r=1,2,...$ of (3.57) consists of a countable infinity of one-dimensional eigenvalue curves parametrised by the normalized stiffness parameter α. These, however, do not correspond to solitary wave solutions of the dimer since they only govern the fast oscillations of the relative displacement of the pair of light beads of an arbitrary periodic set, and not necessarely the LBVP (3.56) governing the fast oscillations of the center of mass of the same pair of light beads.

In Figure 3.58 we provide a comparison of the WKB approximations (3.62) and (3.63), and the direct numerical solution of (3.57) for the eigenfunction $\sigma_{(3p+1)1_5}^{RD}(\tau;3)$ of a 1:2 dimer chain with $\varepsilon_6^{RD}\approx 0.17$ and $\alpha=3$, and in Table 3.6 we provide a similar comparison for the spectrum $\{\varepsilon_r^{RD}(3)\}, r=3,4,...,13$. Again, we note satisfactory agreement between the direct numerical solutions and the WKB approximations, especially for higher order eigenvalues.

According to the previous discussion for the realization of a solitary wave the two eigenvalue spectra should intersect in accordance with the condition (3.58). In Figure 3.59 we depict the asymptotic spectra $\{\varepsilon_q^{CM}(\alpha)\}$ and $\{\varepsilon_r^{RD}(\alpha)\}$ for a range of values of α. Each crossing between these two families of spectral curves corresponds to a solitary wave in the $1:2$ dimers, since at these points both problems (3.56) and (3.57) are satisfied. In fact, this topology indicates that there exists a double countable infinity of families of solitary waves parameterized by energy. This is due to the fact that, as the previous mathematical construction reveals, the wave profiles and speed of propagation of these solitary waves depend on their amplitudes (energies). Indeed, the Nesterenko solitary wave [41], upon which the entire asymptotic approximation of the solitary waves of the dimer is based, is highly dependent on energy [42, 97].

To verify the existence of the analytically predicted solitary waves we perform direct numerical simulations of the governing equations of motion of semi-infinite $1:2$ dimer chains forced by impulses at their free boundaries. In Figure 3.60a we depict the solitary wave realized in the $1:2$ dimer with parameters $\alpha = 0.4935$ and $\varepsilon = 0.082$. For this and the additional numerical simulations depicted in Figures 3.61 and 3.62 we have considered two heavy beads (the 43-rd and 46-th beads) and the corresponding enclosed pair of light beads (the 44-th and 45-th beads) of a long (for practical purposes, semi-infinite) $1:2$ dimer chain with a free left boundary forced by an impulse of intensity 1.5 at its left free end. The plot in Figure 3.60 shows the velocity time series of these light and heavy beads. We note that all responses decay to zero, which verifies the realization of an exact solitary waves in this $1:2$ dimer chain. An important feature to note is the symmetric waveforms of the heavy beads, and the non-symmetric waveforms of the light beads. In this case the number of waves in the fast oscillations of the CM of the pair of light beads is equal to 4, while that on their RD is equal to 6, hence this particular solitary wave can be assigned the index notation $(4:6)$. For this solitary

wave the previous WKB analysis predicts the parameter values $\alpha = 0.5$ and $\varepsilon = 0.0822$ (see Table 3.7 and the discussion below).

Furthermore, we consider the formation of solitary waves in $1:2$ dimer chains with other parameter values. In Table 3.7 we tabulate the numerical and theoretically predicted values (derived by the WKB approximation, corresponding to the crossing points of the spectral lines depicted in Figure 3.59) of the parameters corresponding to these solitary waves. These results prove that the WKB approximation is capable of accurately predicting the formation of solitary waves in this system, and confirm numerically the existence of multiple such solutions in the highly inhomogeneous but ordered system considered. In the same Table 3.7 we also provide details regarding the number of oscillations in the fast component of the response of CM and of RD of a pair of light beads of an arbitrary periodic set. In all cases listed, the wavenumber (the number of peaks in the fast oscillation) of the fast oscillation of CM is equal to 4 (Figure 3.60a_2 to d_2), whereas the corresponding wavenumber for RD varies from 6 (Figure 3.60a_2) to 10 (Figure 3.60d_2) as the normalized stiffness parameter α increases. In this context, the normalized parameter values for the realization of the solitary wave depicted in Figure 3.60a would be denoted as $(\tilde{\varepsilon}, \tilde{\alpha})^{(4:6)} = (0.082, 0.4935)$, where the tildes are used to denote that they were derived by direct numerical simulations. Moreover, we may consider all solitary waves listed in Table 3.7 as members of the same family of solitary waves of the $1:2$ dimers with fixed wavenumber of the fast oscillation of the CM of the pair of light beads, and parameterized by the wavenumber of the fast oscillation of the corresponding RD of the same pair, and by energy. From this point of view, the $1:2$ dimers possesses a double infinity of families of solitary waves parameterized by the two mentioned wavenumbers and energy.

An additional numerical confirmation of the previous theoretical prediction that multiple (in fact, a double countable infinity of) solitary waves can be realized in general 1:2 dimer granular chain is provided by the solitary waves depicted in Figure

3.61. These are realized in dimers with vastly dissimilar values of normalized parameters, hinting on the existence of solitary waves in a broad range of parameters. Indeed, as the mass and stiffness properties change, so does the profile of the solitary wave since the wavenumber of the fast oscillations of the CM and RD of the pairs of light beads depend strongly on these properties. In the limit $\varepsilon = \alpha = 1$ we recover the Nesterenko solitary wave [41] realized in the homogeneous granular chain as depicted in Figure 3.62. In this case there are no high-order (fast frequency) corrections for the bead responses and the waveforms of the CM and the RD between adjacent beads are composed of purely slow motion.

It is well known that solitary waves in nonlinear media propagate with constant velocity and without change in their waveforms. This was confirmed for the solitary waves propagating in the $1:2$ granular dimers depicted in Figures 3.60 and 3.61. A quantity that can be associated to the propagation velocity of the solitary waves in this normalized discrete lattice is the normalized time shift τ_s (defined in Figure 3.5a) between the responses of adjacent heavy beads; this is discussed in detail in Section 3.1.2. We define such a time shift in order to study the propagation speed of the family of solitary waves listed in Table 3.7, corresponding to fixed wavenumber (equal to 4) of the fast oscillations of the CM of the light beads of a periodic set and varying wavenumber of the corresponding RD. To this end, the amplitudes of the velocities of the solitary waves of the heavy beads are set equal to unity and the normalized time shift τ_s is studied as a function of the normalized parameter α (note that the normalized parameter ε also varies for these solitary waves – see the numerical results of Table 3.7). The results are depicted in Figure 3.63. We note that the time shift decreases with increasing wavenumber of the fast oscillations of the RD of the light beads (i.e., with increasing α and decreasing ε), indicating a corresponding increase in the speed of the solitary wave. As discussed in [97], solitary waves are effective mechanisms for transferring energy through the dimer chain, so these results indicate that energy

propagates faster in 1:2 dimer chains with high wavenumber of fast oscillations of their light beads. Similar studies can be performed for other families of solitary waves and similar results can be deduced. It should be noted here that these results are very particular to the normalized system under consideration.

In the next section we will attempt to relate the realization of solitary waves to effective pulse transmission in semi-infinite 1:2 dimers forced by an external impulse. This study is motivated by previous results of Section 3.1.2 [91, 97], where realization of a solitary wave (characterized as *anti-resonance*) and resonances were associated with effective shock propagation in the 1:1 dimer. The contrasting dynamic phenomenon of *resonance* in the 1:1 dimer [91] was associated with maximum dispersion of a propagating pulse due to strong energy radiation to the far field of the medium through excitation of strongly nonlinear traveling waves; resonances in 1:2 dimers will be studied in a subsequent Section 3.2.4.

3.2.3.1 Pulse Transmission in Finite 1:2 Dimer Chains

Until now we examined formation of solitary waves in the 1:2 dimer chains by formulating necessary and sufficient conditions for the realization of such localized pulses. In Section 3.1.2, it was shown that 1:1 dimers are capable of supporting solitary waves and facilitate the transmission of shock-induced pulses. This was studied by considering a finite 1:1 dimer chain with free left and fixed right boundary and with an impulsive excitation applied to its free boundary. By studying the transmitted force to the fixed boundary for varying normalized mass ratio of the dimer chain (which indicates the relative mass ratio between adjacent light and heavy beads, and which is the only parameter for the normalized 1:1 dimer), it was found that local maxima of transmitted force occur for normalized mass ratios where solitary waves are realized.

Hence, a direct correlation between occurrence of solitary waves and local maximization of transmitted force was established. We aim to perform a similar study in this section, by considering impulsively forced finite $1:2$ dimer chains, and taking into account that in the present case, there exist two normalized parameters to consider, namely the normalized mass ε and stiffness α.

To this end we consider a similar series of numerical simulations and the transmitted force measure. The system we consider is a finite normalized $1:2$ dimer chain composed of 71 beads and is depicted in Figure 3.64. The first bead of the chain is a heavy bead and so is the 70-th bead which is followed by a fixed light bead (the 71-st bead). We measure the force transmitted at the right fixed boundary of the system and normalize this force by the corresponding force transmitted in the homogeneous granular chain with $\varepsilon = \alpha = 1$. As we have two design parameters, we sweep the complete parameter space (ε, α) and construct a two-dimensional surface of normalized transmitted force. This is presented in Figure 3.65, where it should be noted that from a physical point of view the minimum value of the normalized stiffness parameter is $\alpha_{min} = 1/(2\sqrt{2})$.

From the force transmitted surface (cf. Figure 3.65a) we can deduce that the force transmitted is maximum for the homogeneous granular chain with $\varepsilon = 1$ and $\alpha = 1$. The peaks observed in the surface plot correspond to local maxima of the normalized transmitted force, whereas valleys of the plot correspond to local minima of force transmission. In Figure 3.65b we present 'slices' of the surface plot by examining the normalized transmitted force for fixed values of α. We conclude that the global minimum of transmitted force occurs is the $1:2$ dimer with $\alpha = 0.4$ and $\varepsilon = 0.78$. Moreover, it is noted that the transmitted force is much higher in dimers with higher values of α for the fixed value of $\varepsilon = 0.78$. Hence, it appears that the stiffness parameter α plays a major role in pulse propagation in $1:2$ dimer chains.

Another important feature worth noting is that for any particular value of α the force transmitted curve has peaks and valleys. To elaborate more on this issue, we choose an arbitrary value for the normalized stiffness parameter, $\alpha = 3$, and depict the corresponding normalized transmitted force plot for varying normalized mass parameter ε, as shown in Figure 3.66. In the case of $1:1$ dimers, the peaks in the force transmitted plot are realized at values of ε where solitary waves are realized [91, 97]. This agrees with physical intuition, since dimers supporting solitary waves are expected to facilitate transmission of energy applied by external shock excitations. But in general $1:N$ dimer chains, such peaks in force transmitted curves need not necessarily correspond to the formation of solitary waves that are realized at the intersection of the two eigenvalue spectra described by relation (3.58). Rather, these peaks appear to correspond to the spectrum ε_q^{CM} resulting as solution of problem (3.56) and corresponding to decay of the fast oscillations of the center of mass of the light beads of a periodic set of the $1:2$ dimers. This is concluded by comparing the values of ε corresponding to the local maxima of the plot of Figure 3.66 and the corresponding eigenvalues $\tilde{\varepsilon}_q^{CM}(3), q = 2,\ldots,6$ listed in Table 3.5. This is surprising in the sense that we have two spectra governed by the LBVPs (3.56) and (3.57), yet it appears that only one of these spectra appear to affect the local maxima of the transmitted force curve. Similar correspondence was obtained for other values of the normalized parameters, verifying the correlation of the spectra of the fast oscillations of the CM of the light beads and peaks of transmitted force in the $1:2$ dimers.

3.2.3.2 Conclusions

This section considered the formation of solitary waves in an ordered but highly inhomogeneous 1:2 granular dimers, composed of an infinite set of 'heavy' beads separated by two 'light' beads. It is found that in similarity to 1:1 dimers considered in Section 3.1.2 [97], 1:2 dimers support a countable infinity of solitary waves parameterized by energy. These are localized pulses (in space and time) that propagate undistorted and with speeds that depend on their amplitudes in these inhomogeneous media. However, in these solitary waves the waveforms of the responses of the heavy and light beads are markedly different; indeed, although both waveforms decay to zero with increasing (or decreasing) time, the velocity waveforms of the heavy beads are symmetric with respect to appropriately defined reference points, whereas those of the light beads are asymmetric with respect to the same reference points. This is a new finding since until now only solitary waves with symmetric velocity waveforms were known to exist in 1:1 dimers and homogeneous.

Asymptotic analysis of solitary waves in 1:2 dimer chains was performed by slow/fast partition of the nonlinear dynamics in the weakly nonlinear regime of primary pulse. The aforementioned symmetry and anti-symmetry conditions for the solitary wave profiles were imposed as boundary conditions in appropriately defined linear (with slowly varying frequency and excitation) boundary value problems that govern the fast frequency approximations of the responses of the light beads of the dimer during solitary wave propagation. Then, necessary and sufficient conditions for the formation of solitary waves in the 1:2 dimer are formulated. The results of the asymptotic analysis are found to agree with the results of direct numerical simulations of solitary waves formed in semi-infinite 1:2 dimers forced by impulses applied to their boundaries. As the systems under consideration are fully rescalable with respect to the applied impulses, the theoretically predicted solitary waves can be realized for

arbitrarily applied impulses, provided that the assumptions of the analysis are satisfied. Furthermore, any arbitrary shaped transmitted pulse in a 1:2 dimer supporting a solitary wave (i.e., for a dimer with the specific values of the normalized parameters ε and α required for realization of a solitary wave) would eventually disintegrate into a train of solitary waves of varying amplitudes. This is similar to what is observed in homogeneous [41, 45] and 1:1 dimer granular chains [97]. Hence, *once a granular* 1:2 *dimer chain is 'tuned' to support a specific family of solitary waves, solitary pulse propagation becomes the fundamental mechanism for transmission of energy in this medium*. This result highlights the high passive adaptability of this class of highly non-smooth and inhomogeneous media to different modes of energy transmission.

Although we proved the existence of families of solitary waves in 1:2 dimer chains, they can be realized only at certain specific discrete ordered pairs of parameters (ε and α). But for arbitrary parameter values, the dimer chain exhibits scattering and more so, intuitively it is expected that such inhomogeneous granular chains would scatter, disperse the propagating pulses. In fact it is certainly counterintuitive that they support not a few, but a countable infinity of families of solitary waves. It the next section we set out to study the mechanism of resonances that can lead to substantial attenuation of the propagating pulses. Such mechanisms are of interest in incorporating granular media in shock and blast protection.

3.2.4 Resonances in 1:2 Dimer Chains

In this section we continue our study of 1:2 dimer chains emphasizing primarily on the nonlinear resonances in 1:2 granular dimer chains. In the previous section we proved the existence of countable infinite of families of solitary waves in these systems; these are localized pulses that propagate without distortion of their waveforms through these

highly inhomogeneous nonlinear media. We attributed these waves to nonlinear *anti-resonance* that led to complete elimination of radiating waves in the trail of the propagating localized pulse. Anti-resonances were associated with certain symmetries of the velocity waveforms of the beads of the dimer. In this section we dwell on the opposite phenomenon that is of the breakup of waveform symmetries of the bead responses leading to drastic attenuation of propagating pulses due to energy radiation to the far field by means of nonlinear traveling waves. We develop analytical approximations for the resonance dynamics in the limit of small mass ratios. Similar to the case of anti-resonance (solitary waves) [102], we realize a countable infinity of families of nonlinear resonances. We use the connotation of *resonance* to describe this dynamical phenomenon resulting in the maximum amplification of the amplitudes of radiated waves that emanate from the propagating pulse. The resonances are characterized by substantial pulse attenuation as they propagate through the chain, which, mathematically, can be related to maximization of the oscillatory tail (radiating nonlinear waves) in the trail of the propagating primary pulse. With the application of asymptotic analysis, it will be shown that countable infinity of families of nonlinear resonances can be realized in these systems. We study numerically and analytically the nonlinear resonance mechanism in this class of strongly nonlinear periodic media, and demonstrate that it can lead to drastic attenuation of shock-induced pulses propagating in the dimers.

Before embarking on the mathematical analysis of the nonlinear resonance, it would be interesting to observe how these resonances are manifested in the global dynamics of the 1: 2 dimers. Accordingly, we examine numerically the 1: 2 dimer chains for its efficacy to attenuate a propagating pulse. To this end we revisit the normalized force transmitted plots of Figure 3.65.

From the force transmitted plots we deduce that lower the force transmitted, the higher is the pulse attenuation through the dimer. On the contrary, local maxima

observed in the surface plot correspond to points where the force transmitted reaches local maxima, whereas valleys correspond to substantial pulse attenuation. In Figure 3.65b we depict 'slices' of the plot of Figure 3.65a corresponding to fixed values of α. As noted previously, the stiffness parameter has significant effect on the propagatory dynamics of the $1:2$ dimer chains. It was noted previously that for any particular value of α we observe that the normalized transmitted force possesses peaks and valleys. Here we note that in the case of $1:1$ dimers [91] (where the only parameter in the dynamics is the mass ratio ε) valleys correspond to resonances leading to local maximum primary pulse distortion, whereas peaks to anti-resonances leading to solitary wave formation. In contrast, we will establish that in $1:2$ dimer chains these valleys do not necessarily correspond to resonances.

To elucidate the system response for varying ε, we examine the plot corresponding to $\alpha = 3$ in Figure 3.66. In this case there exists a local minimum at $\varepsilon = 0.37$, with corresponding bead responses presented in Figure 3.67. For the numerical simulations we have considered a $1:2$ dimer chain composed of 77 beads wherein the 77^{th} bead (light bead) is fixed, and the responses are normalized with respect to the applied impulse. In Figure 3.67a we present the velocity contours of all bead responses in a space-time diagram, whereas in Figure 3.67b we depict velocity time series of selected heavy beads of this system. The attenuation of the propagating primary pulse is evident in these numerical simulations, as a significant portion of its energy is radiated to the far field of the medium by traveling waves in the trail of the propagating pulse.

Intuitively, we would expect that by increasing the mass ratio beyond $\varepsilon = 0.37$ the force transmitted has to further decrease due to the increase of the mass of the light beads which should enhance the scattering of the primary pulse at interfaces between heavy and light beads. However, surprisingly enough, we observe that a peak in the transmitted force occurs at $\varepsilon = 0.56$. In Figure 3.68 we present the corresponding

responses of the dimer in that case, from which we deduce that the energy radiated in the tail of the propagating pulse is at a substantially lower level compared to the case of $\varepsilon = 0.37$ (cf. Figure 3.67a). We note, however, that in contrast to what was observed in the $1:1$ dimer, in the present case the peak of transmitted force is not associated with formation of solitary waves; this is evident by the considerable oscillating tails in the trail of the propagating pulse in the plots of Figure 3.68b.

As described previously, as $\varepsilon \to 0$ we realize the auxiliary system, and an applied impulse would propagate as a solitary wave without any attenuation leading to relatively high levels of the transmitted force. In the other limit, as $\varepsilon \to 1$, a dimer system is realized composed of heavy beads but with alternating stiffness changes. Intuitively, one would expect that the applied impulse would travel without attenuation and distortion through the medium in that case. Interestingly, such a phenomenon is not observed, since when further increasing the mass ratio beyond $\varepsilon = 0.56$ we do not observe any peaks or valleys in the transmitted force plot, but rather the realization of a global minimum (for the considered range $\varepsilon \in (0, 1]$) at $\varepsilon = 1$. In this case the primary pulse is radiating substantial energy as it propagates, exclusively due to stiffness (but not mass) inhomogeneity in the granular medium. An analysis of the dynamics of this limiting system will be presented in a later section.

Returning to the $O(\varepsilon)$ equations (3.52), for the realization of nonlinear resonance we need to impose boundary conditions that guarantee that the light beads end the squeeze mode of oscillation with maximum velocity, as this will lead to maximization of the oscillatory tail (traveling waves) in the trail of the propagating primary pulse; as mentioned previously, this would mean maximization of energy radiation and consequent maximum dispersion of the propagating primary pulse. The necessary conditions for the maximization of the oscillatory tails in the $1:2$ dimer under consideration can be ascertained by examining the response of the light beads in the valleys of the force transmitted curve for an arbitrary value of α. Similarly to the case of

resonances in the 1: 1 dimer [91] a break of symmetry of the velocity waveforms should be imposed in the present case as well. To this end, we need to impose conditions for maximum asymmetry with respect to an axis passing through the time instant when the two light beads are under maximum compression from their neighboring heavy beads [91]. These conditions can be summarized as, $\eta_{(3p)1}(0) \neq 0,\ \eta'_{(3p)1} = 0,\ \eta_{(3p)1}(t_1 \to -\infty) = 0$ for the motion of the CM, and $\sigma_{(3p)1}(0) \neq 0,\ \sigma'_{(3p)1} \neq 0,\ \sigma_{(3p)1}(t_1 \to -\infty) = 0,$ for the RD of the pair of light beads of the periodic set. Combining these conditions with (3.52) we formulate the following pair of uncoupled linear boundary value problems (LBVPs) that govern the resonance dynamics in the squeeze mode,

$$\begin{gathered}\ddot{\eta}_{(3p+1)1}(\tau)+\frac{\Omega^2_{(3p+1)1}(\tau)}{\varepsilon}\eta_{(3p+1)1}(\tau)=\frac{f_{(3p+1)1}(\tau)}{\varepsilon}\\ \eta'_{(3p+1)1}(\tau=0)=0\\ \lim_{\tau\to-\infty}\eta_{(3p+1)1}(\tau)=0\end{gathered} \tag{3.65}$$

$$\begin{gathered}\ddot{\sigma}_{(3p+1)1}(\tau)+\frac{\Omega^2_{(3p+1)2}(\tau)}{\varepsilon}\sigma_{(3p+1)1}(\tau)=\frac{f_{(3p+1)2}(\tau)}{\varepsilon}\\ \sigma'_{(3p+1)1}(\tau=0)\ \neq\ 0\\ \lim_{\tau\to-\infty}\sigma_{(3p+1)1}(\tau)=0\end{gathered} \tag{3.66}$$

where $p = 0, \pm1, \pm2, \ldots$ and we re-introduced the normalized time through the transformation $t_1 = \varepsilon^{-1/2}t_0 = \varepsilon^{-1/2}\tau$.

In these LBVPs the parameters ε and α enter implicitly through the slowly varying frequencies and nonhomogeneous terms (i.e. the forcing). Our objective is to determine the values of ε and α corresponding to solutions of *both* LBVPs; accordingly, we adopt the following methodology. For a fixed value of the stiffness ratio α we seek the initial conditions $\eta_{(3p)1}(0) = A(\alpha), \dot{\eta}_{(3p)1}(0) = 0$ at the discrete values $\varepsilon = \varepsilon_q^{CM}(\alpha), q = 1,2,\ldots$ (CM-spectrum) that solve the LBVP (3.65). Similarly, we seek the initial conditions $\sigma_{(3p)1}(0) = \mathrm{B}(\alpha), \dot{\sigma}_{(3p)1}(0) = \mathrm{V}(\alpha),$ at the discrete values $\varepsilon =$

$\varepsilon_s^{RD}(\alpha), s = 1,2,...$ that solve the LBVP (3.71) (RD-spectrum). Hence, we derive two separate discrete CM- and RD-spectra $\{\varepsilon_q^{CM}(\alpha)\}$ and $\{\varepsilon_s^{RD}(\alpha)\}$, respectively, corresponding to solutions of the problems (3.65) and (3.66). Clearly, *for the realization of nonlinear resonance both LBVPs should be satisfied simultaneously*, and it is achieved by requiring that the CM- and RD-spectra intersect:

$$\varepsilon_Q^{CM}(\alpha_{QS}) = \varepsilon_S^{RD}(\alpha_{QS}) \text{ for some } (Q,S) \in \mathbb{N}^+ \times \mathbb{N}^+ \tag{3.67}$$

This condition provides the discrete pairs (spectra) of the normalized parameters for which nonlinear resonances are realized. In the following analysis we apply the outlined methodology in two different ways, namely, either by developing asymptotic solutions of (3.65) and (3.66) in the limit of small values of ε, or, alternatively by computing direct numerical solutions of the same problems.

Further, we apply the Wentzel–Kramers–Brillouin (WKB) approximation [136] to construct the analytical approximations of the solutions of LBVPs (3.65, 3.66) in the limit $0 < \varepsilon \ll 1$. The formulation is similar to the one employed in the previous section where anti-resonances in 1: 2 dimer chains were considered. It is emphasized at this point that the WKB approach ceases to be valid in the vicinity of turning points (i.e., at the points of nullification) of $\Omega_{(3p+1)1}(\tau)$, and in our case we are interested in finding an approximation of the solutions of the LBVPs in the semi-infinite time interval $\tau \in (-\infty, 0]$.

The general solution of the LBVP (3.65) is reproduced from equation (3.59) from previous section:

$$\eta_{(3p+1)1}(\tau) \equiv \frac{\tilde{C}_1}{\sqrt{\Omega_{(3p+1)1}}}\cos\left[\frac{1}{\sqrt{\varepsilon}}\int_0^\tau \Omega_{(3p+1)1}(\zeta)d\zeta\right] + \frac{\tilde{C}_2}{\sqrt{\Omega_{(3p+1)1}}}\sin\left[\frac{1}{\sqrt{\varepsilon}}\int_0^\tau \Omega_{(3p+1)1}(\zeta)d\zeta\right] + \frac{f_{(3p+1)1}(\tau)}{\Omega_{(3p+1)1}(\tau)^2} \tag{3.68}$$

It is important to emphasize again that in this study we are mostly interested in finding the special discrete set of parameter values (ε, α) for resonance. Accordingly, we impose the appropriate conditions (3.65) for resonance, $\eta'_{(3p+1)1}(0) = 0, \eta_{(3p+1)1}(\tau \to \infty) = 0$, and taking into account that,

$$\begin{aligned} f_{(3p+1)1}(0) = 0;\ \Omega_{(3p+1)1}(0) \neq 0 \\ f_{(3p+1)1}(\tau \to -\infty) = 0;\ \Omega_{(3p+1)1}(\tau \to -\infty) = 0 \end{aligned} \tag{3.69}$$

we formulate the following analytical condition for the resonance for the CM of the pair of light beads of the periodic set:

$$\begin{gathered} \lim_{\tau \to -\infty} \cos\left[\frac{1}{\sqrt{\varepsilon}} \int_0^{\tau} \Omega_{(3p+1)1}(\zeta) d\zeta \right] = 0 \ \Rightarrow \\ \frac{1}{\sqrt{\varepsilon}} \int_0^{-\infty} \Omega_{(3p+1)1}(\zeta) d\zeta = \left(\frac{3(1+2k)}{2k} \right)^{1/2} \frac{(3.8744/2)}{\sqrt{\varepsilon}} = (2q+1)\frac{\pi}{2} \Rightarrow \\ \varepsilon = \varepsilon_q^{CM}(\alpha) = \left(\frac{3(1+2\alpha^{2/3})}{2\alpha^{2/3}} \right) \left[\frac{3.8744}{(2q+1)\pi} \right]^2 \\ q = 1, 2, \ldots \end{gathered} \tag{3.70}$$

The CM-spectrum ε_q^{CM} denotes the discrete mass ratio as a function of stiffness ratio $k = \alpha^{2/3}$ where the response (3.68) after the application of the conditions (3.65) would attain maximum velocity towards the end of the squeeze mode. Hence, for any arbitrary value of α, the spectrum provides a countable infinity of discrete set of mass ratios where the CM of the two light beads complete their squeeze mode of oscillation with maximum velocity and lead to maximization of the oscillatory tail in the trail of the primary pulse (and, hence, maximization of energy radiation from the primary pulse to the far field of the dimer chain).

In Table 3.8 we provide a comparison of the truncated CM-spectrum $\{\varepsilon_q^{CM}(3)\}, q = 2, \ldots, 6$ predicted by the WKB approximation and computed by the numerical simulation of the $O(\varepsilon)$ equation of the CM (3.65) for $\alpha = 3$. Further we also tabulate the values of ε corresponding to valleys in the normalized transmitted force plot of Figure 3.66 for $\alpha = 3$. We note that for small values of the mass ratio, the mass ratios for resonance predicted by the asymptotic analysis match well with the numerical results obtained by solving the LBVP (3.65) and from direct numerical simulations of the finite 1:2 dimer chain of Figure 3.64.

A comparison of the responses from the numerical simulation of the numerical solution of the $O(\varepsilon)$ equation (3.65) and the WKB solution (3.70) is presented in Figure 3.69 for the eigenfunction $\eta_{(3p+1)1}^{CM}(\tau; 3)$ of the 1:2 dimer chain with $\varepsilon_4^{CM} \approx 0.07$ and $\alpha = 3$. These results confirm our previous assertion that reduced force transmission in the 1:2 dimer is associated with the realization of nonlinear resonances that enable enhanced attenuation of propagating pulses in this medium.

Similar analysis was performed for the LBVP (3.66) governing the RD between the two light beads of the periodic set of the 1:2 dimer. In this case we impose the boundary conditions $\sigma_{(3p+1)1}(\tau = 0) = f_{(3p+1)2}(0)/\Omega_{(3p+1)2}^2(0) \neq 0$ and $\lim_{t_1 \to -\infty} \delta_{(3p+1)1}(\tau) = 0$ to the WKB solution,

$$\sigma_{(3p+1)1}(\tau) \equiv \frac{\tilde{C}_3}{\sqrt{\Omega_{(3p+1)2}}} \cos\left[\frac{1}{\sqrt{\varepsilon}} \int_0^\tau \Omega_{(3p+1)2}(\zeta) d\zeta\right] + \frac{\tilde{C}_4}{\sqrt{\Omega_{(3p+1)2}}} \sin\left[\frac{1}{\sqrt{\varepsilon}} \int_0^\tau \Omega_{(3p+1)2}(\zeta) d\zeta\right] + \frac{f_{(3p+1)2}(\tau)}{\Omega_{(3p+1)2}(\tau)^2}$$
$$\varepsilon \to 0 \tag{3.71}$$

leading to the conditions, $\tilde{C}_3 = 0$ and (since $\tilde{C}_4 \neq 0$):

$$\lim_{\tau\to-\infty}\sin\left[\frac{1}{\sqrt{\varepsilon}}\int_0^{\tau}\Omega_{(3p+1)2}(\zeta)d\zeta\right]=0\ \Rightarrow$$

$$\frac{1}{\sqrt{\varepsilon}}\int_0^{-\infty}\Omega_{(3p+1)2}(\zeta)d\zeta=\left(\frac{3(1+2k)^2}{2k}\right)^{1/2}\frac{(3.8744/2)}{\sqrt{\varepsilon}}=s\pi\ \Rightarrow \tag{3.72}$$

$$\varepsilon_s^{RD}=\left(\frac{3(1+2\alpha^{2/3})^2}{2\alpha^{2/3}}\right)\left[\frac{3.8744/2}{s\pi}\right]^2$$

$$s=1,2,\ldots$$

The resulting truncated RD-spectrum $\{\varepsilon_s^{RD}(3)\}, s=3,\ldots,12$ predicted by the WKB approximation is presented in Table 3.9, together with the corresponding numerical values computed by solving the LBVP (3.66) for $\alpha=3$. Again, good correspondence is observed in the limit of small values of the mass ratio.

From the previous results we note that the discrete spectra $\{\varepsilon_q^{CM}(3)\}$ and $\{\varepsilon_s^{RD}(3)\}$ listed in Tables 3.8 and 3.9 do not coincide for the particular value of $\alpha=3$, and this is expected to hold for arbitrary values of α. Moreover, we do not observe a one to one correspondence between the two spectra. This indicates that maximization of the oscillatory tails in terms of the center of mass – CM response of the pair of light beads of a periodic set, does not imply maximization of the corresponding oscillatory tails in terms of their relative displacement – RD. Another notable feature is that the valleys in the normalized force transmitted plot corresponding to $\alpha=3$ in Figure 3.66 coincide with the spectrum $\varepsilon_q^{CM}(3)$ in Table 3.8; this means that the valleys in the plot primarily correspond to the maximization of the oscillatory tails in terms of the CM of the light beads. This is quite a surprising result given that we have two independent spectra for this problem, and indicates that *the motion of the CM of the light beads mainly governs the resonant propagatory dynamics in the class of dimer chains considered herein*. Moreover, since the $O(\varepsilon)$ oscillators (3.65, 3.66) that we have derived to study the fast oscillations of the light beads are linear in terms of the fast time scale (but not with respect to the slow time scale, rendering them quasi-linear in time), *the lowest frequency mode is expected to*

capture the main amount of energy of the propagating pulse and to control the resonance dynamics of the propagating primary pulse.

In synopsis, the resonance phenomenon in $1:2$ dimers is mainly influenced by the dynamics of the CM of the pair of light beads, whereas the corresponding RD is not much pronounced. However, in order to render our study of resonances compatible with that of anti-resonances developed in the previous section [102], we will follow a similar approach and designate as resonances the intersections in the (ε, α) plane of the two spectra, i.e., requiring that for resonance to occur in the $1:2$ dimer both LBVPs (3.65) and (3.66) need to be satisfied. This requirement, however, cannot be satisfied in the more general class of $1:N$ dimers and will be relaxed in the next section where only the CM-spectrum will be considered. In Figure 3.70a we present the superposition of CM- and RD-spectra as functions of α. We note that due to the introduced rescalings in the normalized system (3.41) these spectra can be characterised as *global* in the sense that they apply for the general class of $1:2$ granular dimers within the assumptions of the present theoretical formulation. There are transverse intersections between the resonance families $\{\varepsilon_q^{CM}(\alpha)\}, q = 1,2,\ldots$ and $\{\varepsilon_s^{RD}(\alpha)\}, s = 1,2,\ldots$ corresponding to different pairs of (q, s). The notion of resonance family will be elaborated subsequently.

As discussed in Section 3.1.3 [91], the phenomenon of resonance is related to rational relations between the characteristic frequencies of the squeeze mode and the traveling waves in the oscillating tail. For example, in Figure 3.70 the families of resonances corresponding to the CM-spectrum $\{\varepsilon_q^{CM}(\alpha)\}, q = 1,2,\ldots$ are denoted by $n{:}\, m_{CM}$, indicating that the ratio of characteristic frequencies of the two phases is equal to n/m where n, m are relatively prime positive integers; similar notation holds for the resonance families denoted by $m_{CM}{:}\, m_{RD}$, where m_{CM}, m_{RD} are not necessarily relatively prime (ref. Table 3.10, column 3). This was elaborated in detail in Section 3.1.3 [91] for the case of $1:1$ dimer where a single family of resonances could be realized. Although

the same theory of resonance holds for the case of $1:2$ dimers, the main difference is that in the latter case different families of resonances can be realized.

Indeed, although the CM-dynamics of the light beads has greater influence on propagating pulse attenuation, the RD-dynamics are essential in distinguishing between different resonances belonging to the same family. Moreover, as discussed previously exact resonances are achieved when the CM- and RD-spectra intersect [cf. relation (3.72)]; this provides the discrete pairs (spectra) of the normalized parameters for which exact nonlinear resonances are realized. In Table 3.10 we provide a comparison of asymptotic and exact values of the parameters (ε, α) for the family of exact resonances along the $1:4_{CM}$ curve of Figure 3.70b. What differentiates these resonances are the frequency ratios of the RD-resonances, as denoted by the transverse intersections of curves $1:m_{RD}$ with the curve $1:4_{CM}$.

This is better illustrated by considering the wavelet transforms of the fast oscillations of both CM and RD of the pairs of light beads. In the following simulations we consider the responses of the pair of light beads 44-45 of a normalized $1:2$ dimer (with varying ratios ε and α) composed of a total number of 200 beads and forced by an impulse with normalized magnitude 1.5. The wavelet transform spectra of the fast oscillation of the CM of two light beads presented in Figure 3.71a correspond to the dimer with $(\alpha, \varepsilon) = (0.8, 0.052)$ corresponding to a point on the $1:4_{CM}$ curve shown in Figure 3.70b; the two distinct phases of the oscillations are clearly discerned. In this case the ratio of the dominant frequency of the squeeze mode is about four times that of the characteristic frequency of the traveling waves in the oscillating tail, hence the designation of the dynamics as 1:4 CM resonance. The wavelet spectrum depicted in Figure 3.71b depicts the fast oscillation of the RD of the light beads at the same point, and we note that the corresponding frequency ratio is about 4, from which we discern that this is an exact 1:4 resonance as defined in the previous formulation. Resonances of order $1:4_{CM}$ are shown in Figure 3.72 and 3.73. It should be noted that the frequency

ratio for RD in these cases are 4:14 (or 1:3.5) and 4:17 (1:4.25) respectively. These two cases do not correspond to the exact resonance in the previously described notation.

Furthermore, in Figures 3.74 and 3.75, we depict the corresponding wavelet spectra for the exact $1:2$ and $1:1$ resonances, respectively. These lower-order resonances result in better pulse attenuation as can be realized from the normalized transmitted force plot of Figure 3.65a (such lower order resonances would correspond to valleys in this plot). This holds especially true for $1:1$ resonance where the requency of the squeeze mode coincides with the frequency of the traveling wave in the oscillating tail that radiates pulse energy to the far field of the medium. This coincidence of frequencies prevents the application of asymptotic techniques based on slow-fast time scale separation since mixing of time scales occurs at this resonance. However, alternative methods, e.g., based on binary collision approximations (as explored in Section 3.1.3), could be applied for analyzing the dynamics in this resonance regime [91].

3.2.4.1 Conclusions

We explored the nonlinear resonances in $1:2$ dimer granular chains with no pre-compression. The resonance phenomenon in these strongly nonlinear systems is characterized by strong energy radiation from a pulse propagating through the dimer and is associated with the creation of relatively high-amplitude traveling waves in the oscillatory tail in the trail of the propagating pulse. It is precisely these waves through which the energy of the pulse is radiated to the far field of the dimer, and their existence in $1:1$ dimers not only has been predicted theoretically, but has been shown experimentally in Section 3.1.6 [100].

The particular case of 1: 2 dimer was considered in detail and we proved that this system possessed a countable infinity of resonances. The asymptotic analysis of primary pulse transmission (the squeeze mode of the dynamics) was carried out under the assumption $\varepsilon N = O(\varepsilon) \ll 1$, and was based on the solitary wave solution of the auxiliary homogeneous system realized in the limit when the mass ratio ε (but not the stiffness ratio α) tends to zero. In that context, the leading order (slow) approximation of the motions of the heavy beads of the 1: 2 dimer was approximated by the solitary wave, whereas the corresponding slow approximation of the light beads was computed by algebraic relations in terms of the slow response of the heavy beads (i.e., the solitary solution). Hence, by construction the slow approximation of the primary pulse dynamics invariably decays to zero. In the next order the fast dynamics was considered and conditions were posed to maximize the velocity of each light bead at the end of the squeeze mode, which led to maximum radiation of energy from the propagating primary pulse. This led to two classes of linear boundary value problems in terms of the fast dynamics of the light beads, providing two independent eigenvalue spectra: The first for the motion of the CM of the pair of light beads, $\{\varepsilon_q^{CM}(\alpha)\}$, and the other for the relative motion between the two light beads, $\{\varepsilon_s^{RD}(\alpha)\}$. Realization of *exact* nonlinear resonances corresponded to transverse intersections of these two spectra, which provided the countable infinity of parameter pairs $\varepsilon_Q^{CM}(\alpha_{QS}) = \varepsilon_S^{RD}(\alpha_{QS})$, $(Q, S) \in \mathbb{N}^+ \times \mathbb{N}^+$. Asymptotic analysis of the two LBVPs was performed utilizing WKB approximations and the results compared well with the numerical simulations as long as $\varepsilon N = O(\varepsilon) \ll 1$.

The methodology discussed in this section deals directly with the discrete strongly nonlinear equations of ordered granular media and does not resort to homogenization approaches which are not valid given the realization of bead separations and collisions. Instead, we focused on primary pulse propagation (i.e., the

squeeze mode) where under conditions of (transient) strong bead compression during the arrival of the primary pulse a smooth analysis of the dynamics can be performed. It would be of interest to investigate the application of a similar methodology to study primary pulse transmission in other classes of problems such as, two-dimensional ordered granular media with or without intruders, stochastically disordered granular media and granular flows. This would provide us with predictive capacity for designing such media as effective shock mitigators of external shocks.

In the next section we intend to extend the previously discussed methodology and consider the realization of anti-resonances and resonances in general $1{:}N$ ($N \geq 3$) dimer chains. By reconsidering the system of $O(\varepsilon)$ fast oscillators (3.47a, b) with slowly varying frequencies and forcings derived in Section 3.2.2, our analysis will show that although realization of *exact* anti-resonance and resonance is not possible in this system, one can still formulate a condition for *approximate* anti-resonance and resonance based on dynamics of lowest frequency mode.

3.2.5 Resonances and Anti-Resonances in General $\mathbf{1}{:}\boldsymbol{N}$ ($\boldsymbol{N > 2}$) Dimer Chains

As noted in the previous sections, the realization of resonances and anti-resonances are primarily governed by the $O(\varepsilon)$ fast oscillators (3.47a, b). For a $1{:}N$ dimer chain it follows that the $O(\varepsilon)$ model of the dynamics of the light beads is governed by an $N-$degree-of-freedom system of *time-varying* but *linear* coupled oscillators. This is a reflection of the nearly-linear dynamics governing the squeeze mode. We note that the oscillators (3.47b) have slow time varying excitations and frequencies. Accordingly, the fast oscillations of the heavy beads (3.47a) can be approximated once the corresponding approximations for the light beads have been derived. Since the $O(\varepsilon)$ corrections of the responses of the heavy beads are much smaller than the leading order approximations

(3.45, 3.46) for small values of ε, we neglect (3.47a) from hereon and focus only on the set (3.47b) which determines completely the fast dynamics of the dimer. In addition, since the system (3.47b) is linear it can be decoupled using the modal coordinates [13], and the appropriate boundary conditions similar to the one imposed in the previous section will be imposed such that the response of each mode attains zero (for anti-resonance) or maximum (for resonance) velocity towards the end of the squeeze mode.

This appears to be a formidable task in view of the fact that we have just two parameters governing the system dynamics (α and ε) and we need to impose a set of N conditions for the N decoupled modal oscillators. This in fact indicates an ill posed problem. However, as we show, the first (lowest frequency) mode of the fast system (3.47b) is dominant in the squeeze mode (or primary pulse dynamics) of the dimer, and so the first mode plays the most important role in the anti-resonance/resonance dynamics of the dimer system. We note that the lowest frequency mode corresponds to the near-rigid translation of the center of mass – CM of the N light beads of each periodic set, and we expect that momentum transfer through the dimer chain should be dominated by this low frequency mode which is expected to carry most of the energy of the primary pulse; so our considerations are justified from the perspective of physics as well. We note that similar arguments were employed in a previous work on layered media with granular interfaces [125], and in an additional work [166] where the concept of 'effective particle' was introduced to create reduced-order models of granular media. It was shown that the effective particle corresponding to the lowest frequency mode is mainly responsible for momentum transfer in granular interfaces, and under certain assumptions [125, 166] higher order modes may be neglected.

We now consider the question of solitary wave formation in the general class of $1:N$ dimers with $N > 2$. The analysis follows the lines of the asymptotic method developed in Section 3.2.3 for the $1:2$ dimer, and is general, in the sense that it applies to general $1:N$ dimer chains with $N > 2$. To this end, we reconsider the $O(\varepsilon)$

approximations (3.47b, c) governing the fast dynamics of the light beads of a general $1:N$ dimer chain. Since there is time-scale separation between the coefficients and forcing terms depending on the slow time t_0, and the dependent variables depending on the fast time scale t_1, and since this slowly-varying dynamical system is linear, we may decouple the equations of motion (in the fast time scale) by using its corresponding matrix of eigenvectors. Hence, we may express (3.47b) in modal coordinates, and derive a set of uncoupled modal equations governing the amplitudes of the N modes of the fast oscillations of the light beads. To demonstrate this analysis and to avoid cumbersome mathematical expressions, we provide the resulting uncoupled system below for $N = 3$:

$$\begin{Bmatrix} z_{i1}''(t_1) \\ z_{i2}''(t_1) \\ z_{i3}''(t_1) \end{Bmatrix} = -\Omega_i^2(t_0) \begin{bmatrix} \frac{1+3k-\sqrt{1-2k+9k^2}}{2} & 0 & 0 \\ 0 & 1+k & 0 \\ 0 & 0 & \frac{1+3k+\sqrt{1-2k+9k^2}}{2} \end{bmatrix} \begin{Bmatrix} z_{i1}(t_1) \\ z_{i2}(t_1) \\ z_{i3}(t_1) \end{Bmatrix} - \begin{bmatrix} 1 & \frac{1-k+\sqrt{1-2k+9k^2}}{2k} & 1 \\ 1 & 0 & -1 \\ 1 & \frac{-1+k-\sqrt{1-2k+9k^2}}{2k} & 1 \end{bmatrix} \begin{Bmatrix} \ddot{x}_{(i+1)0}(t_0) \\ \ddot{x}_{(i+2)0}(t_0) \\ \ddot{x}_{(i+3)0}(t_0) \end{Bmatrix} \tag{3.73}$$

where $z_{il}, l = 1,2,3, i = 1 + 4n, n = 0,1,2, \ldots$, denotes the amplitude of the $l-$th mode of the fast oscillation of the three beads of the $i-$th periodic set.

It is now possible to apply WKB analysis to each of the three uncoupled equations in (3.73), subject to appropriate boundary conditions similar to those considered in (3.56, 3.57) (anti-resonances in $1:2$ dimers) and (3.65, 3.66) (resonances in $1:2$ dimers) in order to compute the three independent eigenvalue spectra $\varepsilon = \varepsilon_q^l(\alpha), q = 1,2,3, \ldots$, l=1,2,3, one for each of the three modes. The $l-$th spectrum $\{\varepsilon_q^l(\alpha)\}$

consists of an infinite set of eigenvalue curves in $\mathbb{R}^2$ corresponding to functional dependencies of the normalized mass parameter with respect to the normalized stiffness parameter, for which the fast oscillations of that mode of the light beads decay to zero as time tends to infinity. Moreover, the three spectral families are independent from each other. It should be clear that *realization of solitary waves in the* $1:3$ *dimer chains requires that for certain values of* α *all three eigenvalue spectra should coincide*. Therein lies the difficulty of solitary wave formation in this system (as well as in more general $1:N$ dimer with $N > 3$), since from geometrical point of view simultaneous transverse intersections of $N > 2$ one-dimensional curves at a single point in $\mathbb{R}^2$ is non-generic. We conclude that the formation of solitary waves in $1:N$ $(N > 2)$ dimers is not typical, in contrast to $1:1$ and $1:2$ dimers, which, as shown in Section 3.1.2 and 3.2.3 respectively, can support countable infinities of solitary waves.

Although imposing the exact conditions for realization of solitary waves in general $1:N$ dimers is not feasible, rather we can obtain approximations of near-solitary waves by considering only the spectra of the two lowest-frequency modes in (3.73) and computing the normalized parameters α and ε corresponding to transverse intersections of the corresponding lowest-frequency eigenfrequency curves (i.e., following the procedure developed in Section 3.2.3 for the $1:2$ dimer). The reasoning behind this approximation lies in the fact that when an external shock is applied to the general dimer, energy transmission mainly occurs through excitation of the lower frequency modes of the periodic sets; this was confirmed by previous results . Taking this argument one step further we may simplify the approximation even more by taking into account only the lowest (fundamental) mode with spectrum $\{\varepsilon_q^1(\alpha)\},\ q = 1,2,\dots,$ since predominantly the in-phase mode is expected to capture most of the energy induced by an external shock, and hence, the mode most responsible for transferring energy through the dimer; it follows that this mode is most appropriate for modeling

near-solitary waves in the general dimer. To test this approximation we consider the system of equations (3.73) with $N = 3,\ k = 1$, and study only the first mode:

$$\begin{gathered} z_{i1}''(t_1) = -6(2-\sqrt{2})\left[x_{i0}(t_0) - x_{(i+4)0}(t_0)\right]^{1/2} x_{i1}(t_1) - \\ (1/4)\left[\ddot{x}_{(i+1)0}(t_0) + \sqrt{2}\ddot{x}_{(i+2)0}(t_0) + \ddot{x}_{(i+3)0}(t_0)\right] \\ z_{i1}(t_1 = 0) = 0,\ \ z_{i1}'(t_1 = 0) \neq 0 \\ \lim_{t_1 \to \infty} z_{i1}(t_1) = 0 \end{gathered} \tag{3.74}$$

In Figure 3.76a we compare the fast oscillation computed by (3.74) to the fast component of the center-of-mass oscillations of the light beads 26-28 of the 1:3 dimer with normalized parameters $\varepsilon = 0.0207$ and $\alpha = 1$, forced by a unit impulse applied at its left end. This numerical fast oscillation was computed using the following approximate expression,

$$\tilde{z}_{i1} \approx \frac{(x_{(i+1)1} + x_{(i+2)1} + x_{(i+3)1})}{3} - \frac{(x_{i0} + x_{(i+4)0})}{2} \tag{3.75}$$

where $x_{(i+1)1}, x_{(i+2)1}, x_{(i+3)1}$ are the responses of the three light beads (26-28) and $x_{i0}, x_{(i+4)0}$ (25, 29) are the responses of the bounding heavy beads of the periodic set with $i = 25$. It is to be noted that the asymptotic approximation (3.75) is valid only in the limit when ε is sufficiently small, since only in this limit the responses of the heavy beads would be very close to the Nesterenko solitary wave of the auxiliary system obtained in the limit $\varepsilon \to 0$. In Figure 3.76b we depict the corresponding comparison regarding the velocity of the center-of-mass of the same set of light beads (i.e., the composite responses superimposing slow and fast components).

From the results of Figure 3.76 we conclude that the fast oscillation of the first mode predicted by the asymptotic model (3.74) closely matches the result of the

numerical simulation. This indicates that in the limit of small normalized mass ratios the lowest mode approximation (3.74) provides a satisfactory approximation of the near-solitary wave since it captures most of the energy of the transmitted pulse which is induced by the applied impulse. We emphasize, however, that since the exact conditions for the formation of solitary waves cannot be satisfied exactly in the $1:3$ dimer; it is only possible that near-solitary pulses are realized, with most of the energy of these pulses transferred by the lowest-frequency mode of the fast oscillations of the light beads in each periodic set. With an increase in the value of ε, however, the energy of the transmitted pulse 'spreads' to higher modes of the fast frequency oscillations of the light beads, which become more profound in the dynamics. In that case the previous asymptotic simplification is not expected to hold and no near-solitary pulses can exist. A confirmation of this conjecture is provided by the responses depicted in Figure 3.77, where plots similar to those in Figure 3.76 are depicted for the $1:3$ dimer with parameters $\varepsilon \approx 0.05275$ and $\alpha = 1$. The oscillating tail in the trail of the pulse observed in the numerical simulation signifies the lack of a near-solitary pulse in this case, in contrast to the asymptotic model (3.74) which predicts such a solution.

We now extend the analysis of resonances to the general class of $1:N$ dimers with $N \geq 3$. In order to extend the methodology developed in the previous section to the system of N decoupled $O(\varepsilon)$ fast oscillators (3.47b), we need to impose necessary and sufficient conditions so that each fast oscillator ends its squeeze mode of oscillation with maximum velocity. As discussed above, we need to satisfy N conditions with just two parameters, namely the mass ratio ε and the stiffness ratio α, which, as discussed above represents a mathematically ill-posed problem. Arguing along the same lines as for the case of $1:2$ dimers, we note that, even if we obtain the N independent spectra of ε as a function of α corresponding to these N decoupled oscillators, it is non-generic that these N spectra will transversely *simultaneously* intersect in the two-dimensional plane (ε, α),

providing the discrete ordered pairs of ε and α for *exact* nonlinear resonances. Hence, *realization of exact nonlinear resonances in* $1:N$ *dimers with* $N \geq 3$ *is non-generic*.

Interestingly enough, however, numerical simulations indicate that pulse attenuation can still occur in general $1:N$ dimer chains. As an example, we consider a $1:3$ dimer chain composed of 140 beads with $\alpha = 1$ and $\varepsilon = 0.49$. The attenuation of the propagating primary pulse can be clearly discerned from the space-time plot of bead velocities shown in Figure 3.78a, where the velocity of each bead is normalized with respect to the applied impulse. In Figure 3.78b we present the velocity response of some intermediate heavy beads, to highlight the strong primary pulse attenuation in this case. This indicates that pulse attenuation in this $1:3$ dimer chain is still possible even though the exact resonance conditions may not be satisfied.

This can be explained by recalling our previous discussion concerning the influence of the lowest frequency mode of the system of fast oscillators (3.47b) (modeling the low frequency motion of the center of mass of the N light beads of each periodic set) on primary pulse propagation and attenuation. Hence, instead of considering conditions for exact resonances (which, as mentioned previously, cannot be satisfied in the general case), one can still focus to the decoupled oscillator corresponding to the lowest frequency fast oscillations and impose the appropriate resonance condition only for this specific oscillator; this will derive a condition for approximate resonance which can be used to explain pulse attenuation in the general $1:N$ dimer case. This will be performed in the following analysis considering the case $N = 3$, however, the analysis can be generalized for $N > 3$ (although, as discussed in the next section there are some restrictions in extending the asymptotic analysis when N increases).

To this end, we consider the $O(\varepsilon)$ system of fast oscillators (3.75) and set $N = 3$ and the corresponding decoupled set of equations (3.73). Arguing along the same lines as in the case of anti-resonances in $1:3$ dimers, we formulate conditions for *approximate*

nonlinear resonances for the first mode of oscillation of the $O(\varepsilon)$ equation (3.73) and formulate the following LBVP for the lowest frequency oscillator,

$$z_{i1}''(t_1) = -6(2-\sqrt{2})\left[x_{i0}(t_0) - x_{(i+4)0}(t_0)\right]^{1/2} x_{i1}(t_1) - (1/4)\left[\ddot{x}_{(i+1)0}(t_0) + \sqrt{2}\ddot{x}_{(i+2)0}(t_0) + \ddot{x}_{(i+3)0}(t_0)\right]$$
$$z_{i1}(t_1 = 0) \neq 0, \quad z_{i1}'(t_1 = 0) = 0$$
$$\lim_{t_1 \to -\infty} z_{i1}(t_1) = 0 \tag{3.76}$$

where $t_1 = 0$ corresponds to the time instant when the adjacent heavy beads have equal non-zero velocity. This LBVP is similar to the CM-LBVP (3.65) formulated for the 1: 2 dimer in Section 3.2.4. As before, this problem can be solved either asymptotically (using the WKB approximation) or numerically to yield the discrete spectrum $\{\varepsilon_r^l(\alpha)\}, r = 1,2,\ldots$ for the approximate nonlinear resonances based on the lowest frequency (dominant) mode. This discrete set of mass ratios is seen to have one to one correspondence with the local minima (valleys) in the normalized force transmitted curve, validating our approximate approach.

Indeed, in Figure 3.79 we depict the normalized transmitted force curve for a 1: 3 dimer chain composed of 82 beads (with the 82nd bead being a fixed light bead – where the transmitted force is measured) and a unit impulse applied to the first heavy bead on the left boundary of the chain; to this plot we superimpose the discrete spectra $\{\varepsilon_r^l(\alpha)\}$ predicted by WKB analysis (ε_{Asym}) of the LBVP (3.76) and compare them to the values of ε_{Num} where valleys of the plot occur. As expected, the asymptotic solutions of the approximate model (3.76) predicts well the local minima for lower values of ε, but deviate substantially for higher values. This is consistent with the basic assumption of our asymptotic analysis which is based on time scale separation in limit of sufficiently small values of ε for fixed values of N (a discussion of this assumption is provided in the next section). However, the most important feature of the plot is that it confirms that

force attenuation in the $1:3$ dimer is associated with the nonlinear resonance of the lowest frequency mode of the triplets of light beads or, equivalently, approximate nonlinear resonance in the dimer. This approximate resonance scenario can be further extended to the more general class of $1:N$ dimers with $N > 3$.

As a concluding remark, the extension of the asymptotic analysis to a general class of $1:N$ $(N > 2)$ granular dimer chains to realize anti-resonances or resonances, although seems straightforward, possess distinct difficulties from a mathematical point of view due to the fact that the resulting set of boundary value problems cannot be simultaneously solved; hence resulting in an ill-posed mathematical problem. This is due to the fact that realization of exact solitary waves or resonances in $1:N$ $(N > 2)$ dimers requires the simultaneous transverse intersection of N one-dimensional eigenvalue curves in $\mathbb{R}^2$; whereas for $N = 2$ this can be performed, as such intersections are generic, but for $N > 2$ this is not generally possible. Hence, *it is conjectured that solitary wave or resonance realization in a general* $1:N$ $(N > 2)$ *granular dimer chain is not mathematically possible, unless special symmetries can be realized*. Even in these systems, however, the formation of near-solitary localized pulses and near resonances are still possible, since in the limit of small values of the normalized mass parameter most of the energy of a propagating pulse is captured by the lowest frequency mode of the fast oscillations of the light beads of each periodic set. In that case, one can approximately consider only the linear boundary value problem corresponding to the lowest frequency mode of the fast oscillations of the light beads, and theoretically predict the existence of near-solitary (but not exact) solitary pulses and resonances. Numerical evidences support this claim.

3.2.6 A Note on the Dynamics of 1: N Dimer Chains with Large Stiffness Ratios

In the previous discussion we considered two limiting cases of dimers corresponding to $\varepsilon \to 0$ and $\varepsilon \to 1$. The former case leads to the auxiliary system which is homogeneous in mass and stiffness, whereas the latter case denotes a mass homogeneous, but stiffness periodic dimer chain. Thus it is evident that the stiffness parameter can render the chain inhomogeneous, but still periodic. Although it may seem that as the chain is mass homogeneous and thus analytically tractable, it is hardly so. Due to the presence of this stiffness periodicity, there are no known analytical tools or approximations that can capture the dynamics of such dimer chains. Even the consideration of binary collision approximation [39, 104, 110] fails in view of the fact that this approximation cannot account for the stiffness disparity between beads. This is the scenario for a general 1: N dimer chain for an arbitrary value of stiffness ratio. Interestingly enough, dimer chains with large stiffness ratio lend themselves to certain approximations. It was noted previously that due to the physical reasoning the minimum value of stiffness ratio is $\alpha_{min} = 1/2\sqrt{2}$, but there is no specific upper bound for this parameter. In fact this is quite advantageous in applying certain approximations and in exploring the dynamics. The primary objective of this section is considering the 1: N dimer chain in the limit of large stiffness ratio and its degeneracy to a 1: 1 dimer chain.

To this end, we reconsider the normalized equations of motion (3.41) and introduce the rescaling $\tilde{\varepsilon} = \varepsilon/\alpha$ with $\tilde{\varepsilon} \ll 1$, as $\alpha \ll 1$. It will be of interest to consider the limiting case obtained when $\tilde{\varepsilon} \to 0$. Then, expressing the responses of the heavy and light beads of an arbitrary periodic set in the following asymptotic forms $x_i = x_{i0}(t_0) + \tilde{\varepsilon}^2 x_{i1}(t_1) + \ldots$, $x_{i+j} = x_{(i+j)0}(t_0) + \tilde{\varepsilon}^2 x_{(i+j)1}(t_1) + \ldots$, substituting into (3.41) and setting $\tilde{\varepsilon} = 0$ we obtain the following $O(1)$ approximation,

$$\ddot{x}_{i0} = (x_{(i-1)0} - x_{i0})^{3/2} - (x_{i0} - x_{(i+1)0})^{3/2}$$
$$x_{(i+j-1)0} = x_{(i+j)0} = x_{(i+j+1)0} \tag{3.77}$$

where $i = 1 + n(1+N), n = 0,1,2,\ldots, 1 < j < N$ and the notation of previous section is preserved. We note that at the $O(1)$ approximation the responses of all light beads are identical, i.e., the N light beads of each periodic set move in-unison; more precisely, the internal dynamics between the lights beads is completely annihilated due to the high stiffness ratio between the light and the heavy beads. This indicates that in the limit of small values of the ratio $\tilde{\varepsilon} = \varepsilon/\alpha$ the lowest frequency mode of the set of N light beads is primarily responsible for momentum transfer during primary pulse transmission. In Section 2.3 [166] such arguments were employed to construct *effective particles*, i.e., reduced order models of homogeneous granular chains, and on the same lines the asymptotic analysis in this section will be developed.

Returning to system (3.41) and substituting the previous asymptotic expansions and transforming back to the original parameters ε and α we derive the following normalized system of governing equations of $O(1)$ for an arbitrary periodic set:

$$\begin{aligned}
\ddot{x}_{i0} &= (x_{(i-1)0} - x_{i0})_+^{3/2} - (x_{i0} - x_{(i+1)0})_+^{3/2} \\
\varepsilon\ddot{x}_{(i+1)0} &= (x_{i0} - x_{(i+1)0})_+^{3/2} - \alpha(x_{(i+1)0} - x_{(i+2)0})_+^{3/2} \\
\varepsilon\ddot{x}_{(i+j)0} &= \alpha\left\{(x_{(i+j-1)0} - x_{(i+j)0})_+^{3/2} - (x_{(i+j)0} - x_{(i+j+1)0})_+^{3/2}\right\} \\
\varepsilon\ddot{x}_{(i+N)0} &= \alpha(x_{(i+N-1)0} - x_{(i+N)0})_+^{3/2} - (x_{(i+N)0} - x_{(i+N+1)0})_+^{3/2}
\end{aligned} \tag{3.78}$$

Motivated by the afore mentioned discussion concerning the effective particle in the $O(1)$ approximation, we proceed to the summation of the N intermediate equations in (3.78) governing the light beads to derive the following reduced system,

$$\begin{aligned}\ddot{x}_{i0} &= (x_{(p-1)0} - x_{i0})_+^{3/2} - (x_{i0} - x_{p0})_+^{3/2} \\ N\varepsilon\ddot{x}_{p0} &= (x_{i0} - x_{p0})_+^{3/2} - (x_{p0} - x_{(i+N+1)0})_+^{3/2} \\ \ddot{x}_{(i+N+1)0} &= (x_{p0} - x_{(i+N+1)0})_+^{3/2} - (x_{(i+N+1)0} - x_{(p+1)0})_+^{3/2}\end{aligned} \tag{3.79}$$

where $x_{p0} = (1/N)\sum_{j=1}^{N} x_{(i+j)0}$. Hence, the set of N light beads is replaced by a *cluster* or *effective particle* with effective mass equal to $N\varepsilon$, and, in essence the slow approximation (3.79) represents a $1:1$ dimer chain with heavy and light beads with normalized masses equal to unity and $N\varepsilon$, respectively; hence, *a* $1:N$ *dimer with high stiffness ratio can be effectively reduced to a* $1:1$ *effective dimer chain with effective mass ratio equaling* $1:N\varepsilon$. This represents a significant simplification (and reduction) of the problem.

We now consider the finite $1:2$ dimer chain and set $\varepsilon = 1$; thus we have a granular chain with homogeneous mass but with periodic variation in stiffness. In this case the only parameter that can be varied is the stiffness ratio, so the center of mass of the light beads can be replaced by an effective particle of normalized mass equal to $N\varepsilon = 2$ in the limit of very high α. The resulting effective normalized $1:1$ dimer corresponds to a mass ratio equal to 0.5. In Figure 3.80 we present the corresponding transmitted force curve of this system for varying α, normalized with respect to the homogeneous chain with $\alpha = \varepsilon = 1$ (this plot represents a 'slice' $\varepsilon = 1$ of the plot of Figure 3.65a). It is to be noted that the maximum force transmitted is in the homogeneous chain ($\alpha = \varepsilon = 1$) whereas force transmitted is substantially lower for higher values of α. This dynamics is quite non-intuitive given that the dimer chain considered is mass-homogeneous (since $\varepsilon = 1$) and there is only stiffness disparity. Moreover, this result indicates that this type of granular dimer is especially suitable for strong pulse attenuation due to its intrinsic dynamics.

In Figure 3.81a we present the velocity response of the CM of the two light beads (44 and 45) and their adjacent heavy beads (43 and 46) of a $1:2$ dimer with $\varepsilon = 1$ and $\alpha = 114$ composed of 200 beads and excited by an impulse of normalized magnitude 1.5

(such a high stiffness ratio is realizable for a dimer composed of steel and Teflon or PTFE beads). As described above, for such high stiffness ratios, the $1:2$ dimer chain emulates a $1:1$ dimer with an effective mass ratio of 0.5. This is confirmed by the results depicted in Figure 3.81b where the velocity response of a heavy bead (bead 51) and its adjacent light beads (beads 50 and 52) in a $1:1$ dimer chain with mass ratio 0.5 consisting 200 beads, excited by an impulse of $1:1$ are shown. As can be noted, the responses in the two plots show good qualitative agreement. It should be noted that the response of the CM of the light beads in the $1:2$ dimer chain is an analogue of the response of the heavy bead in the effective $1:1$ dimer chain; and the responses of the heavy beads of the $1:2$ dimer are analogous to the responses of the light beads in the effective $1:1$ dimer chain. It is worth noting that a mass ratio of ~ 0.59 corresponds to the global minimum of transmitted force (or maximum pulse attenuation) in the normalized $1:1$ dimer chain (cf. Figure 3.9a in Section 3.1.2). Since the $1:2$ dimer with high stiffness ratio of our example corresponds to the effective $1:1$ dimer with effective mass ratio 0.5 (i.e., close to 0.59), we expect substantial pulse attenuation in that system as well. In fact the amplification of the oscillatory tail in Figure 3.81 indicates substantial pulse attenuation.

A second example is given with a 200-bead $1:3$ dimer chain with homogeneous mass distribution $\varepsilon = 1$ and large stiffness ratio $\alpha = 114$ excited by an impulse with a unit normalized magnitude. In Figure 3.82a we present the velocity response of the CM of the light beads (beads 50-52) and their adjacent heavy beads (beads 49 and 53). In this case the effective mass of the CM of the light beads is equal to $N\varepsilon = 3$ whereas that of the heavy beads equals unity. The responses of the corresponding effective $1:1$ dimer of 200 beads with an effective mass ratio 1/3 and excited by an impulse with normalized magnitude equal to 0.5 is depicted in Figure 3.82b (we depict the velocity of the heavy bead 51 and of its adjacent light beads 50 and 52). Again the responses in the Figures 3.82a and b show good qualitative agreement, with the cluster (effective particle) of the

light beads of the $1:3$ dimer chain having a response that is analogous to that of the heavy bead of the $1:1$ dimer chain; in addition, the responses of the heavy beads of the $1:3$ dimer is observed to correspond to the responses of the light beads of the effective $1:1$ dimer chain. It is interesting to note, however, that the time durations of the pulses in the two systems are different; this is due to the fact that in a $1:3$ dimer chain any two adjacent heavy beads are separated by three light beads, and thus its responses stretch out in time when compared to the corresponding responses in the $1:1$ dimer chain (which is relatively 'stiffer').

In conclusion, the principal idea in this approximation is owing to the fact that if the stiffness ratio of a $1:N$ dimer (with mass ratio ε) is very large, the dynamics of the light beads (or their internal dynamics) loose significance, and move approximately in unison. This enables us to model them as a single effective particle or cluster with an effective mass equal to $N\varepsilon$, and to approximately reduce the $1:N$ dimer to an effective $1:1$ dimer thus simplifying substantially the analysis. This reduction can help us interpret the highly effective pulse attenuation observed in this type of $1:N$ dimers (cf. Figure 3.80) in terms of pulse attenuation in the effective $1:1$ dimer with effective ratio $N\varepsilon$ which has been studied in detail in Section 3.1.3.

3.2.7 Validity of the Asymptotic Approach for the General $1:N$ Dimer Chains

In general, the validity of asymptotic analysis is limited to the asymptotic parameter being relatively small. The smallness of this parameter is a relative term, but not absolute. Further to this, each order of asymptotic approximation has an error of higher order defined in terms of the asymptotic small parameter. Thus the asymptotic approximation becomes invalid once the error at any order of approximation becomes comparable to that order. In essence it implies that for sufficiently small asymptotic

parameter, the asymptotic approximation converges towards the exact solution. Indeed this criteria is valid for general asymptotic analysis, i.e. the asymptotic solutions are valid when the small parameter (ε) in the analysis is sufficiently small. But in contrast to this criteria, for a general $1:N$ dimer chain, the smallness of ε is a necessary condition, but not sufficient for the validity of asymptotic analysis. In this section we formulate an alternate qualitative measure for ascertaining the validity of the developed asymptotic analysis.

The asymptotic formulation developed for the general $1:N$ dimer chain leads to the N dimensional system of fast linear oscillators (3.47) in the $O(\varepsilon)$ approximation. The asymptotic analysis was carried out in the asymptotic limit of small mass ratios $\varepsilon \ll 1$ for N fixed. Although the asymptotic approximation closely agrees with direct numerical simulations for small values of the mass parameter ε and $N = O(1)$, it deviates for large values of N even though ε remains small. From the perspective of asymptotics this can be explained by considering the $O(\varepsilon)$ equations governing the fast dynamics of the N light beads of each periodic set. Due to the finite asymptotics, the error in the approximation of the response of each light bead one would expect to be of order $O(\varepsilon^2)$; yet, given that the system (3.47b) is a set of N DOF coupled oscillators, the total error in the $O(\varepsilon)$ approximation accumulates to $O(\varepsilon^2 N)$. Hence, the error in the asymptotics increases not only when ε increases, but (and perhaps counter intuitively) also when N increases. It follows that if the product $\varepsilon N = O(1)$ the total error in the asymptotic approximation is expected to be of $O(\varepsilon)$, and given that the approximation itself is of $O(\varepsilon)$ the solution becomes asymptotically invalid. Before proceeding to validate these arguments with direct numerical simulations, we discuss the asymptotic approximations of the responses of the heavy beads of the dimer chain.

In the previous sections it was noted that for sufficiently small values of ε, the solitary wave solution of the auxiliary system (corresponding to $\varepsilon = 0$) provides a good approximation to the $O(1)$ response of the heavy beads. Furthermore, it was noted that

the $O(\varepsilon)$ correction of the heavy beads depended on the $O(\varepsilon)$ approximation of the light beads (3.47b), but, the $O(\varepsilon)$ approximation of the heavy beads was seldom required because the effect of light beads on the heavy beads was found to be insignificant for lower values of ε. With an increase in ε, the influence of light beads on the response of the heavy beads also increases. With the increase in both N and ε the error in the approximation of the light beads increases, and thus the error in the $O(\varepsilon)$ correction of the response of the heavy beads becomes more significant. Moreover, when $\varepsilon N = O(1)$, the $O(\varepsilon)$ correction of the heavy beads becomes even less valid and the asymptotic approximations of the responses of the heavy beads deviate considerably from the actual numerical simulations. In that case it can be clearly inferred that the responses of the heavy beads are greatly affected by the light beads, so these responses deviate considerably from the solitary pulse of the auxiliary system which cannot be used anymore as generating solution for the asymptotic analysis. Viewed from another perspective, the quantity εN denotes the relative mass of the N light beads of the entire periodic set with respect to the mass of their neighboring heavy beads; hence, as εN increases the set of N light beads has sufficient inertia to influence the dynamics of their neighboring heavy beads instead of being just driven by them (as the asymptotic theory assumes).

The numerical evidences that substantiate the aforementioned criteria are divided into two categories, namely simulations for fixed ε and varying N, and then simulations for fixed N and varying ε. In Figure 3.83 we consider primary pulse propagation in $1{:}N$ dimer chain with $\varepsilon = 0.05$ and varying N, forced at its left end by a unit impulse. In each case we consider the velocity responses of a specific periodic set consisting of N light beads and the neighboring two heavy beads. In the plot of Figure 3.83a we consider a dimer with $N = 3$ and a total of 200 beads; we depict the velocity responses of the heavy beads 81 and 85, the velocity of their CM and the velocity of the CM of the light beads 82 to 84. We note that in this case the responses of the heavy

beads are close to the theoretical solitary pulse of the auxiliary system, which indicates that the asymptotic approximation is valid, and that the heavy beads drive (and are not influenced by) the dynamics of the light beads. Further, we observe that the CM of the light beads executes oscillations of $O(\varepsilon)$, very close to the CM of the heavy beads, as predicted by the asymptotics. In particular, the error in the asymptotic approximation is estimated to be of the order of $\varepsilon N = 0.15 \ll 1$.

In Figure 3.83b we consider a dimer with $N = 8$ and a total of 400 beads; we depict the velocity responses of the heavy beads 181 and 190, the velocity of their CM and the velocity of the CM of the light beads 182 to 189. Despite the small value of $\varepsilon = 0.05$, the response of the heavy beads deviates considerably from the previous case of the $1:3$ dimer. Furthermore, the amplitude of the CM of the light beads is seen to deviate considerably from that of the heavy beads, not being of $O(\varepsilon)$ as in the previous case. This implies that the asymptotic approximation is less valid in this case, which is consistent with the fact that $N\varepsilon = 0.40$ (i.e., not small). This indicates that even when the mass ratio is fixed to a small value, increasing N would render the asymptotic approximation based on the solitary wave generating solution invalid. This is further confirmed by the numerical simulations depicted in Figures 3.83c, d corresponding to dimer chains with $N = 14$ (total of 500 beads with the responses of the periodic set of beads 301 to 316 shown) and $N = 20$ (total of 600 beads with the responses of the periodic set of beads 421 to 442 shown), respectively. The corresponding values of the product $N\varepsilon = O(1)$ for these two cases are 0.7 and 1, respectively, invalidating the previous asymptotic approximations.

In the second series of simulations we consider a $1:10$ dimer chain composed of a total of 400 beads and varying ε. The results presented in Figure 3.84 correspond to the responses of the periodic set composed of two heavy beads (221 and 232), and ten light beads (222 to 231). Similarly to the previous numerical simulations we depict the velocity profiles of the two heavy beads, of their CM, and of the CM of the ten light

beads of the periodic set. Starting from the plot of Figure 3.84a for the $1:10$ dimer with $N\varepsilon = 0.05 \ll 1$, we note that the responses of the heavy beads are close to the asymptotically predicted solitary pulse of the corresponding auxiliary system (obtained in the limit $\varepsilon \to 0$). In addition, the oscillations of the CM of the light beads are $\varepsilon-$close to the CM response of the heavy beads, again in agreement with the asymptotic approximation. An increase of the mass ratio to $\varepsilon = 0.01$ (cf. Figure 3.84b) corresponds to $\varepsilon N = 0.1 \ll 1$, so the asymptotic approximation still maintains its validity. This is also confirmed by the numerical simulations. In both cases the asymptotics is valid since, due their small total inertia the set of light beads is driven by their neighboring heavy beads without being capable to influence their dynamics.

However, further increase of the mass ratio renders the asymptotics invalid, as the set of ten light beads gains sufficient inertia to influence the dynamics of their neighboring heavy beads instead of merely being driven by them. This is evident from the numerical simulations of Figures 3.84c and d corresponding to $\varepsilon = 0.05$ ($N\varepsilon = 0.5$) and $\varepsilon = 0.1$ ($N\varepsilon = 1$), respectively. In both cases, the errors of the corresponding asymptotic approximations are expected to be significant.

The previous discussion confirms that the asymptotic approximation is valid as long as $N\varepsilon \ll 1$, and ceases to be valid once $N\varepsilon = O(1)$ or more precisely when $N = O(1/\varepsilon)$. In the region of validity of the asymptotics the dynamics of the light beads can be approximated by (slow) algebraic equations at the $O(1)$ approximation, and by a set of N coupled linear driven (fast) oscillators at the $O(\varepsilon)$ approximation. These fast oscillators give rise to N linear vibration modes driven by the (slow) motions of the neighboring heavy beads, and the dynamics of the dimer chain that can be classified as being of *oscillatory type*. We note that although we designate such a response as oscillatory, the primary pulse propagation through the dimer is mainly governed by the $O(1)$ approximation (i.e., the solitary wave generating solution) and so is always propagatory. Once the asymptotic approximation ceases to be valid, the dynamics

inside the layer of N light beads cannot be described by the system of N fast oscillators and their dynamics are wave-like instead of vibration-like. In this case the dynamics are classified as being of *propagatory type*. The latter case of primary wave transmission in layered elastic media with granular interfaces is discussed in [125].

3.3 Figures

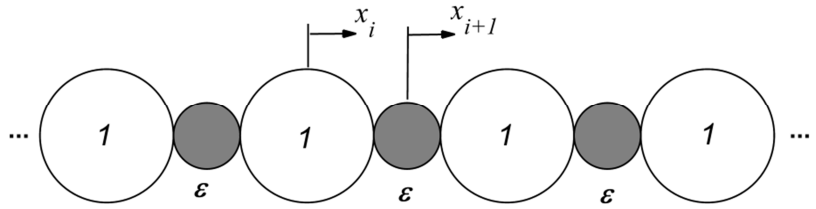

Figure 3.1: Non-dimensional dimer system composed of 'heavy' and 'light' beads.

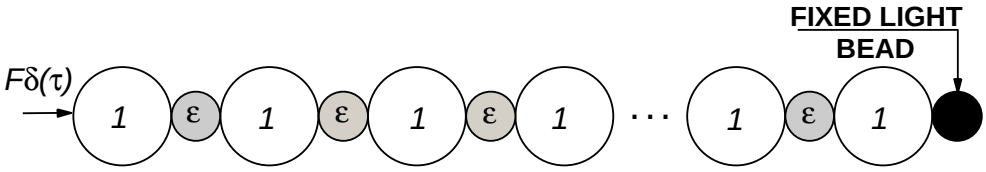

Figure 3.2: Dimer setup for numerical simulations.

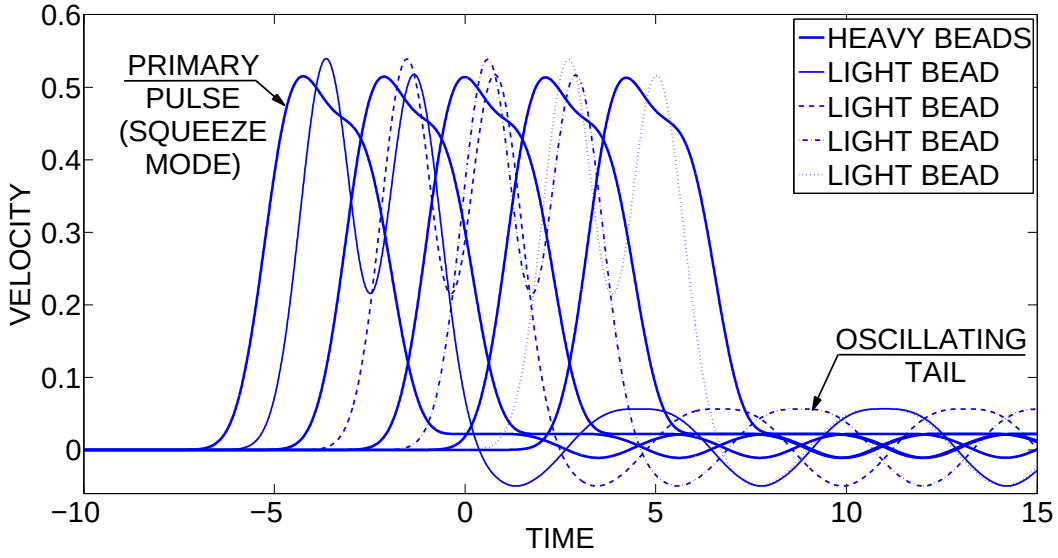

Figure 3.3: Velocity profiles of dimer pairs for $\varepsilon = 0.4$.

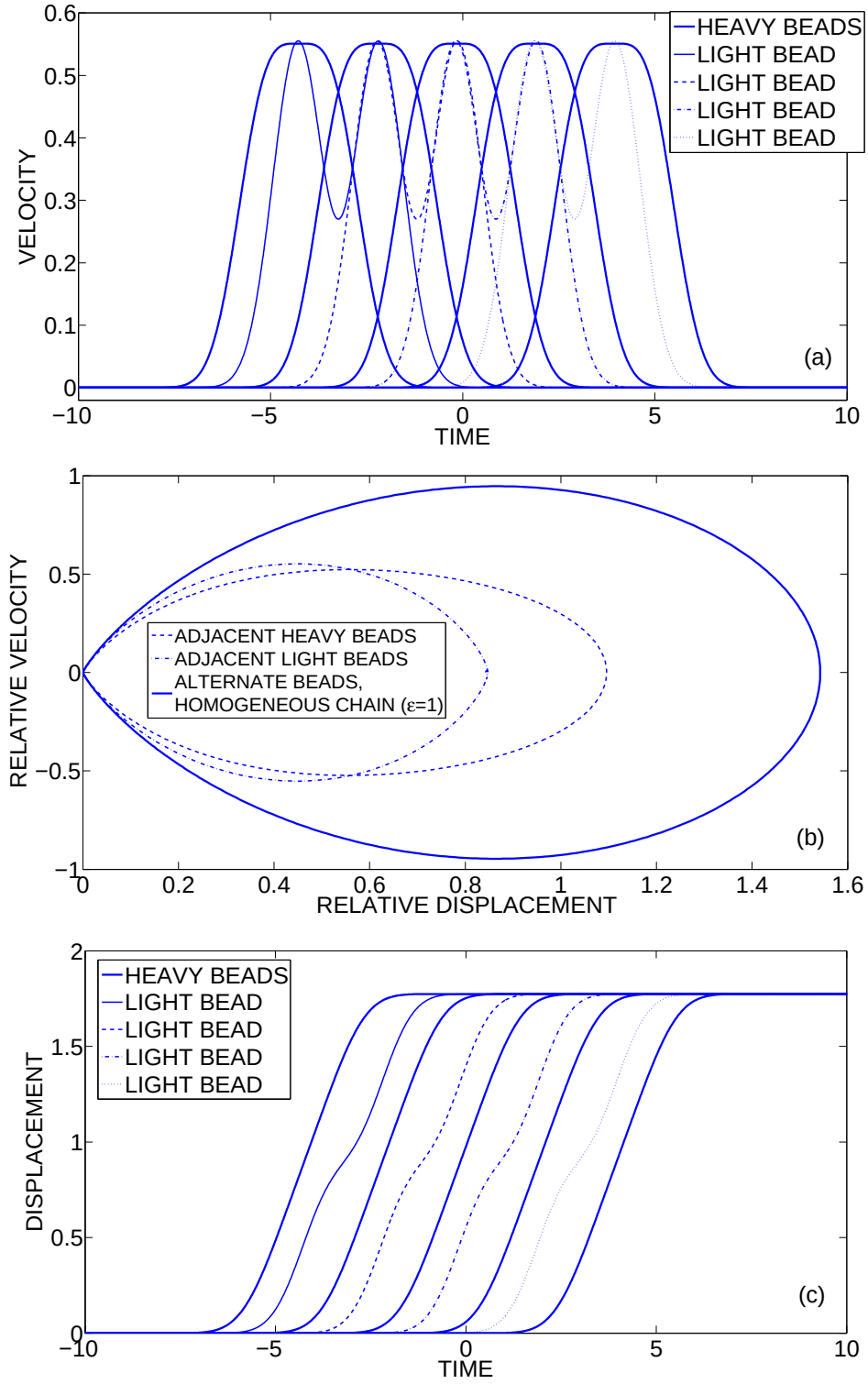

Figure 3.4: Solitary wave in the dimer with $\varepsilon = 0.3428$, (a) Velocity profiles of dimer pairs; (b) phase plot of relative velocity versus relative displacement between successive heavy and light beads compared to the solitary wave of the homogeneous chain of heavy beads ($\varepsilon = 1$); (c) displacement profiles of dimer pairs.

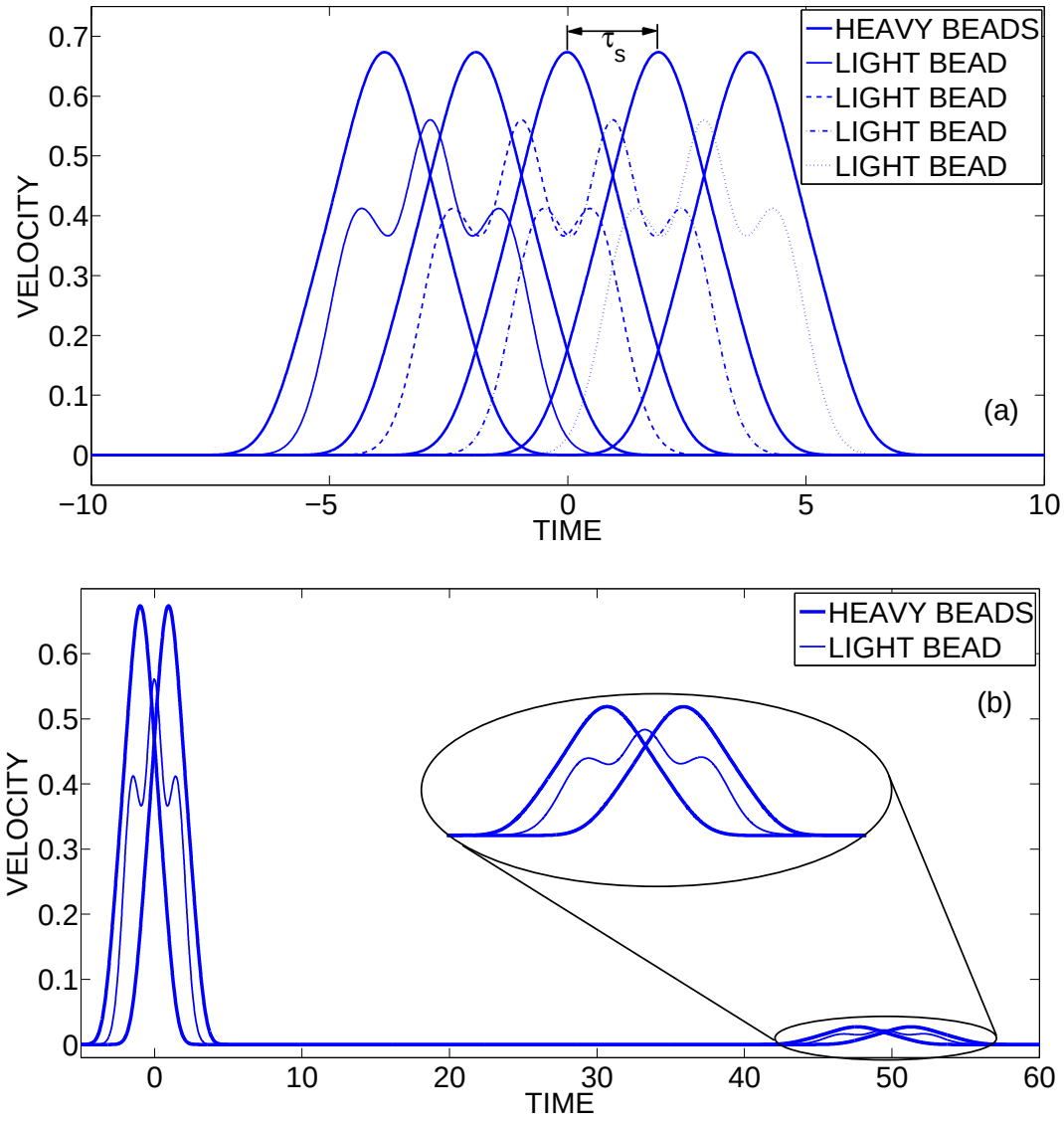

Figure 3.5: Solitary wave in the dimer with $\varepsilon = 0.1548$: (a) Velocity profiles of dimer pairs; (b) primary solitary wave followed by secondary solitary waves (on beads 51 to 53).

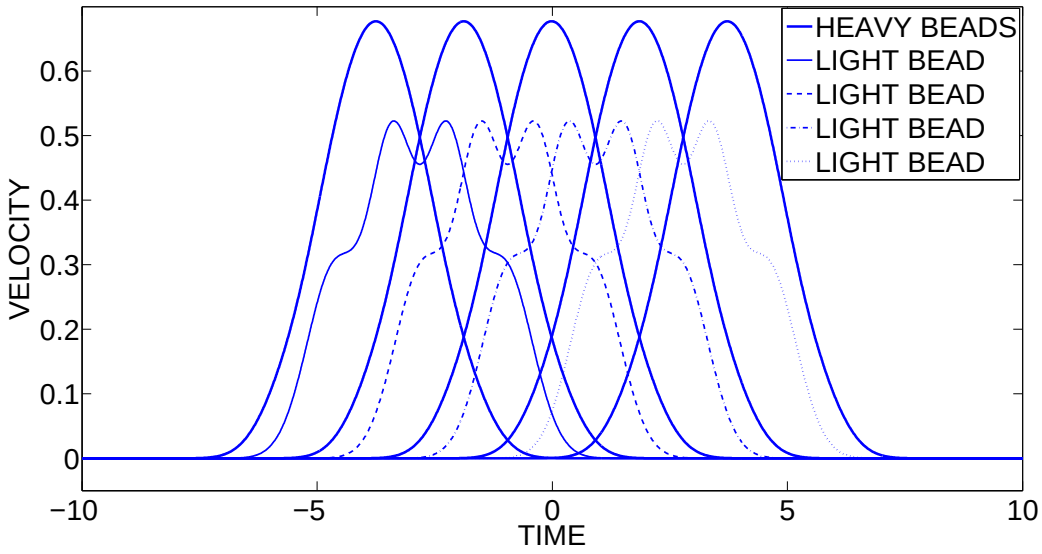

Figure 3.6: Solitary wave in the dimer with $\varepsilon = 0.0901$, velocity profiles of dimer pairs.

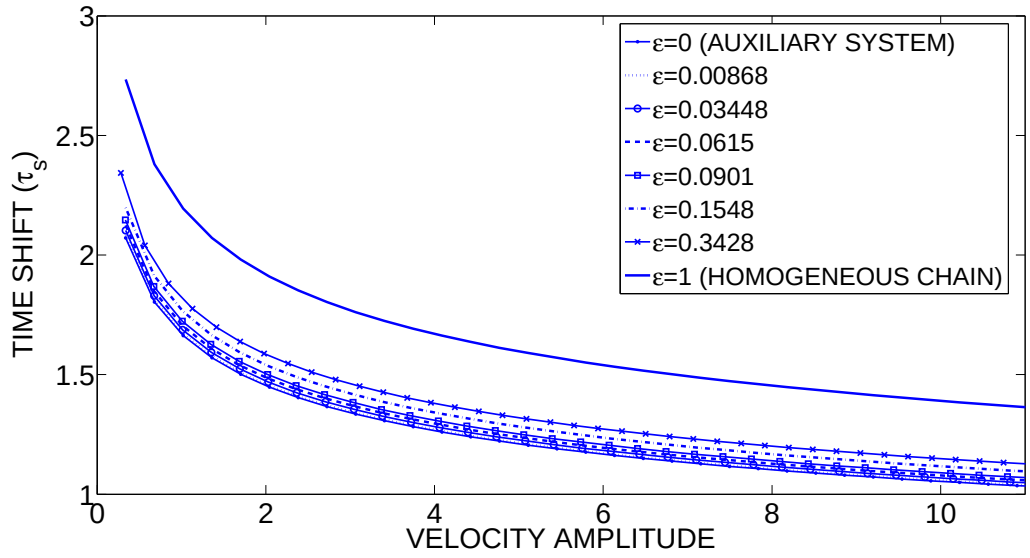

Figure 3.7: Time shifts τ_s versus peak velocities of the different families of solitary waves in the dimer.

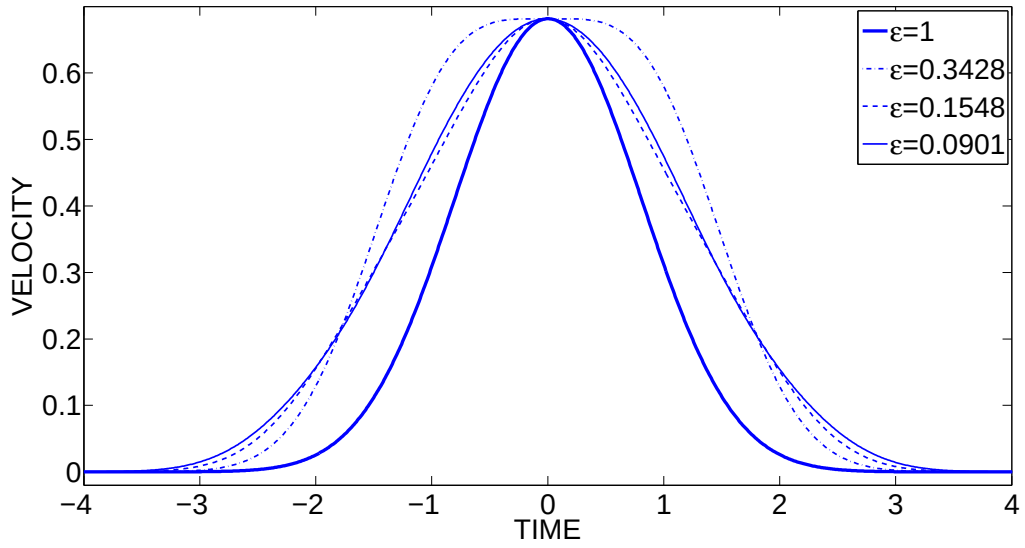

Figure 3.8: Comparison of dimer solitary wave profiles on heavy beads with Nesterenko solitary wave.

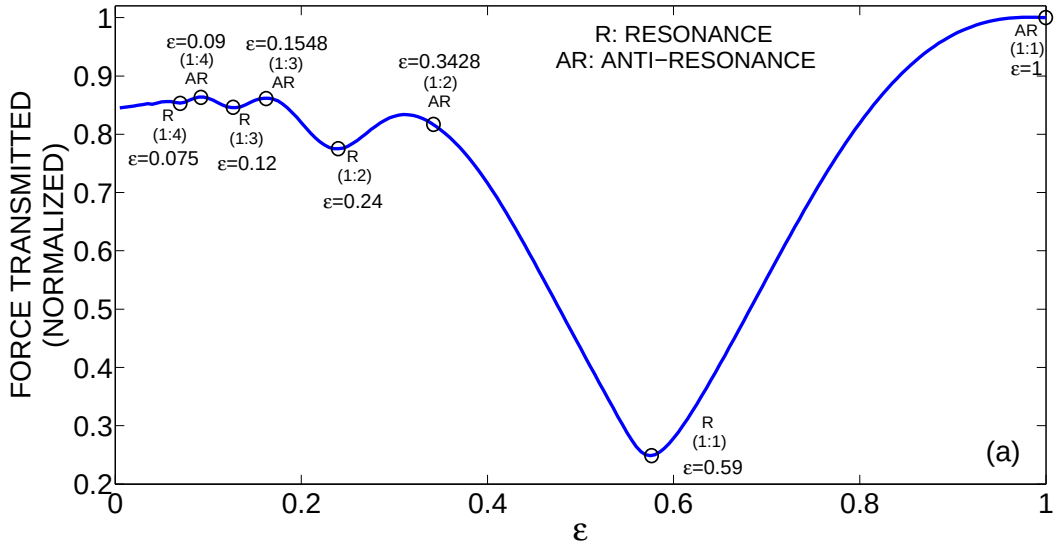

Figure 3.9: (a) Normalized transmitted force as function of the normalized mass ratio parameter ε for an impulsively excited dimer.

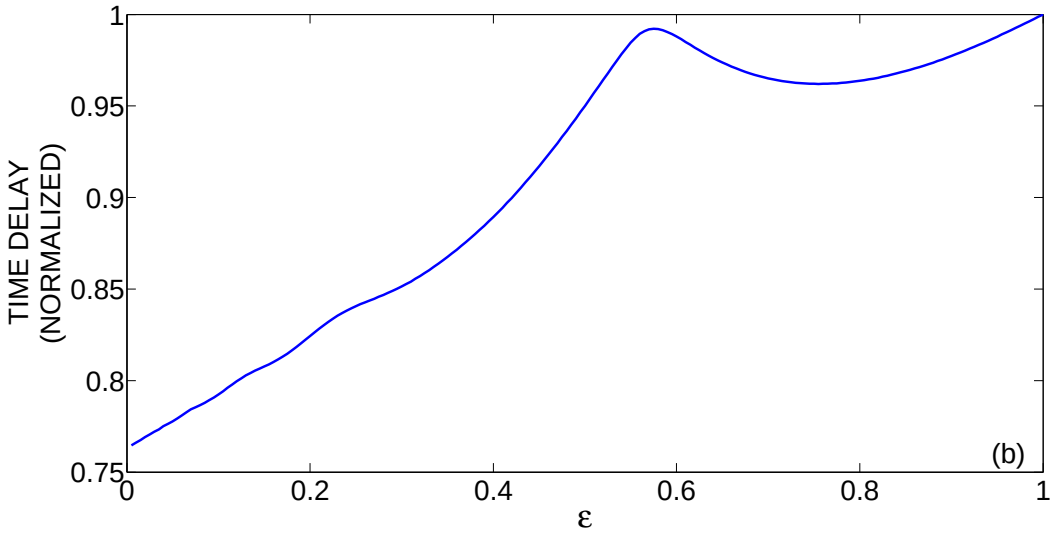

Figure 3.9 (cont'd): (b) Normalized time delay as function of the normalized mass ratio parameter ε for an impulsively excited dimer.

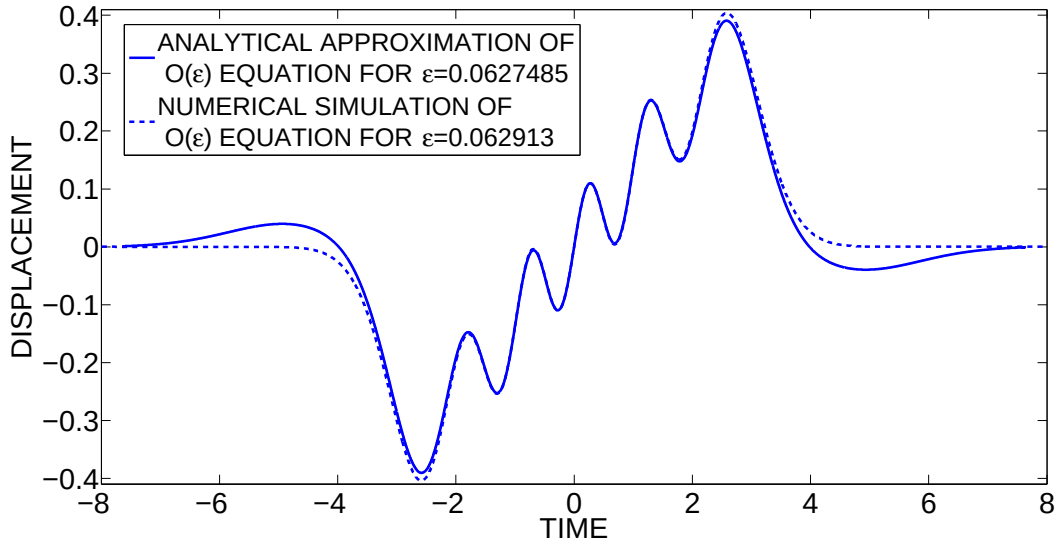

Figure 3.10: Comparison of the numerical solution of the fast dynamics (3.11) and the WKB analytical approximation (3.19).

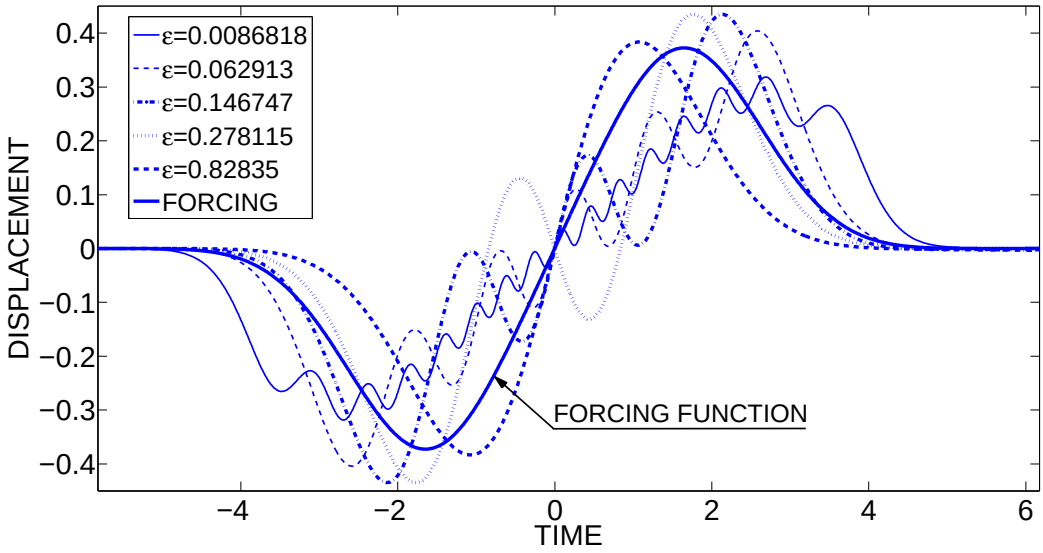

Figure 3.11: Numerical solutions of the fast dynamics (3.11) for certain values of ε_n at which solitary waves are realized in the dimer.

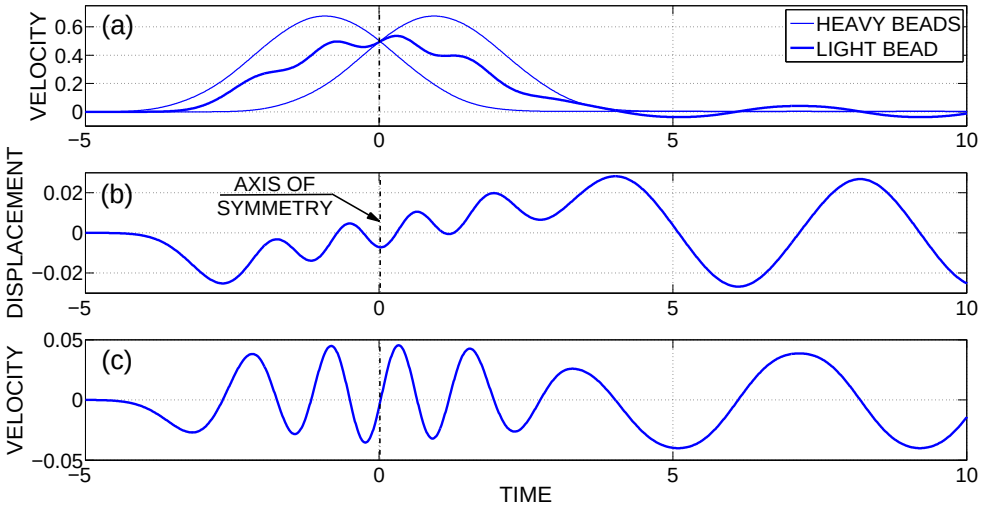

Figure 3.12: Resonance at $\varepsilon_R \approx 0.075$, (a) Velocity profiles of a light bead and its neighboring heavy beads; (b, c) fast components of the displacement and velocity, respectively, of the light bead.

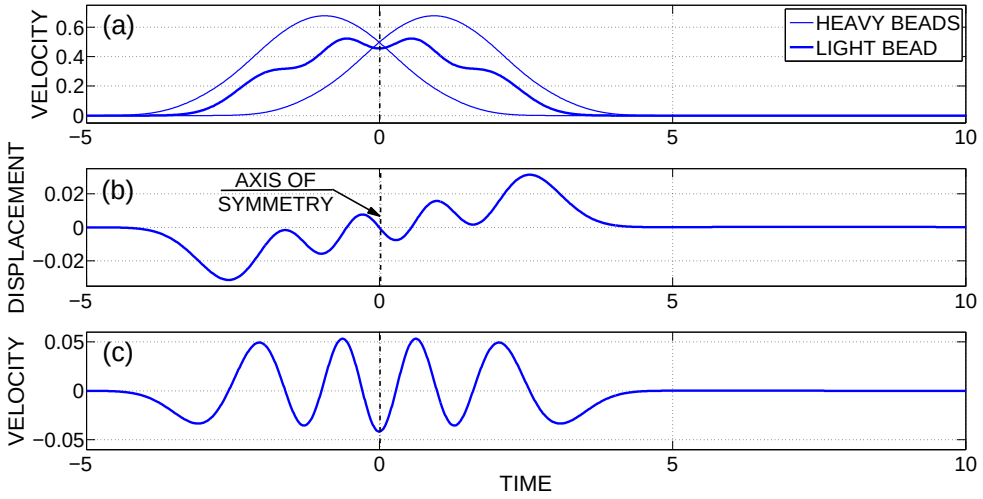

Figure 3.13: Anti-Resonance at $\varepsilon_{AR} = 0.0901$, (a) Velocity profiles of a light bead and its neighboring heavy beads; (b, c) fast components of the displacement and velocity, respectively, of the light bead.

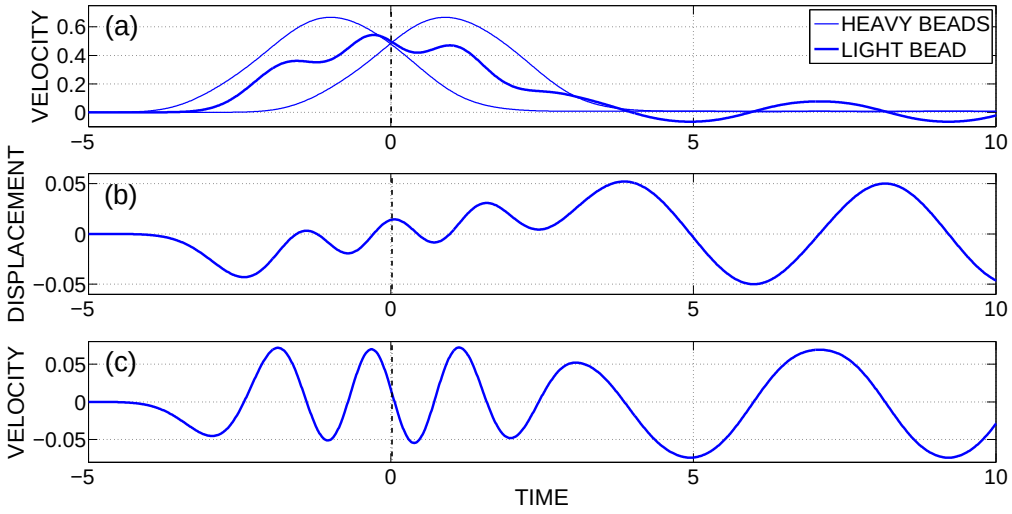

Figure 3.14: Resonance at $\varepsilon_R \approx 0.12$, (a) Velocity profiles of a light bead and its neighboring heavy beads; (b, c) fast components of the displacement and velocity, respectively, of the light bead.

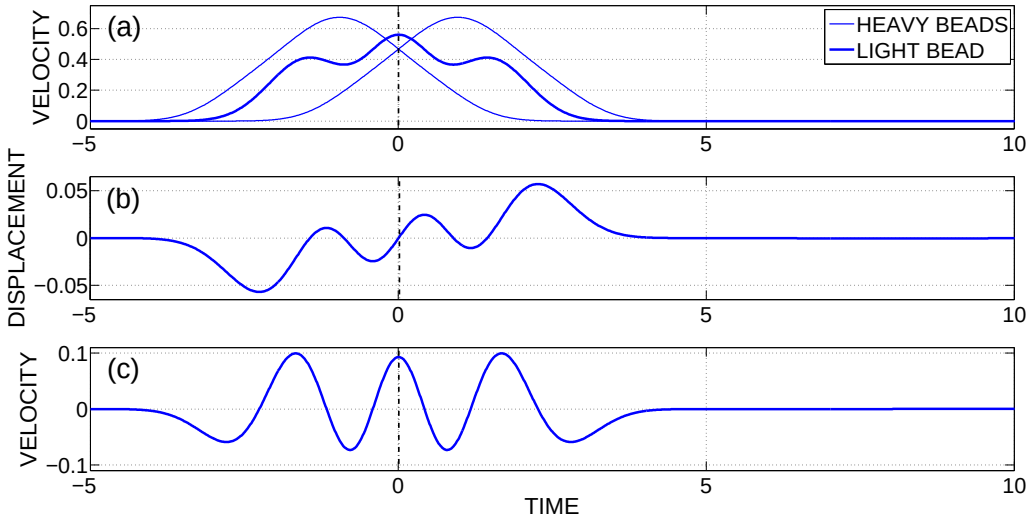

Figure 3.15: Anti-Resonance at $\varepsilon_{AR} \approx 0.1548$, (a) Velocity profiles of a light bead and its neighboring heavy beads; (b, c) fast components of the displacement and velocity, respectively, of the light bead.

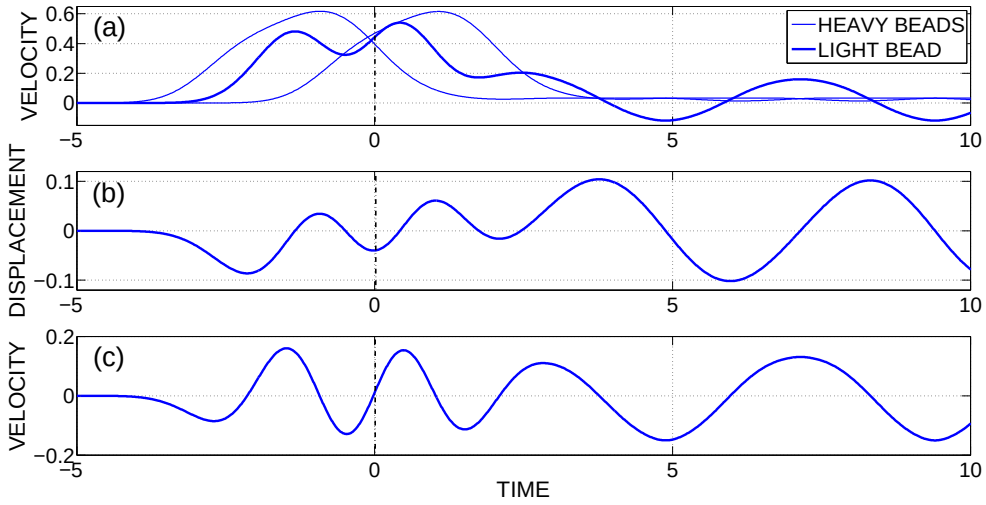

Figure 3.16: Resonance at $\varepsilon_R \approx 0.24$, (a) Velocity profiles of a light bead and its neighboring heavy beads; (b, c) fast components of the displacement and velocity, respectively, of the light bead.

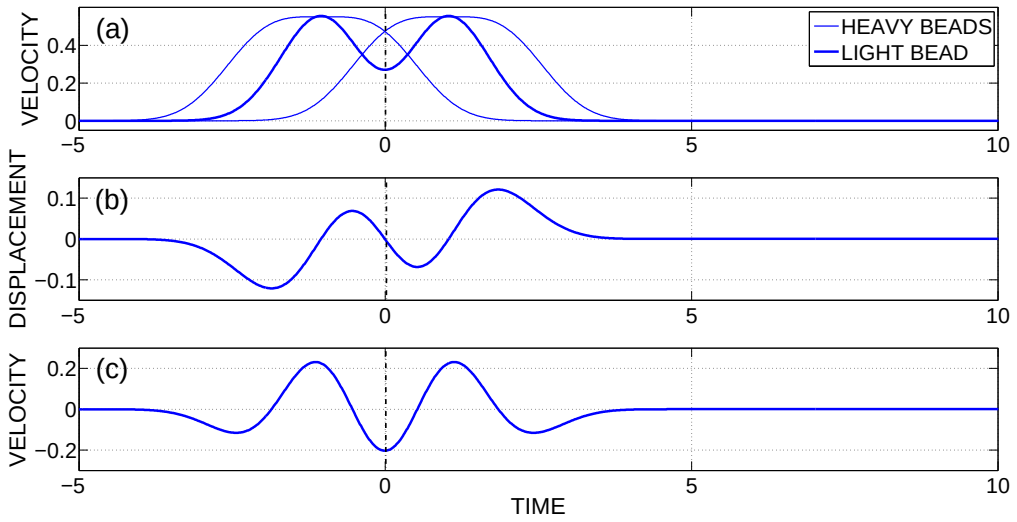

Figure 3.17: Anti-Resonance at $\varepsilon_{AR} \approx 0.3428$, (a) Velocity profiles of a light bead and its neighboring heavy beads; (b, c) fast components of the displacement and velocity, respectively, of the light bead.

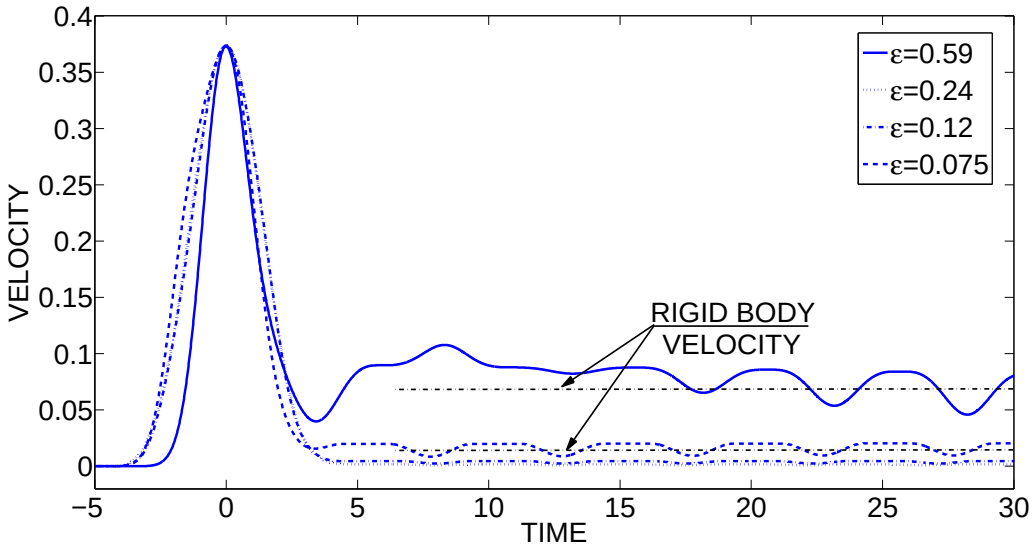

Figure 3.18: Velocity time series of heavy beads during resonance.

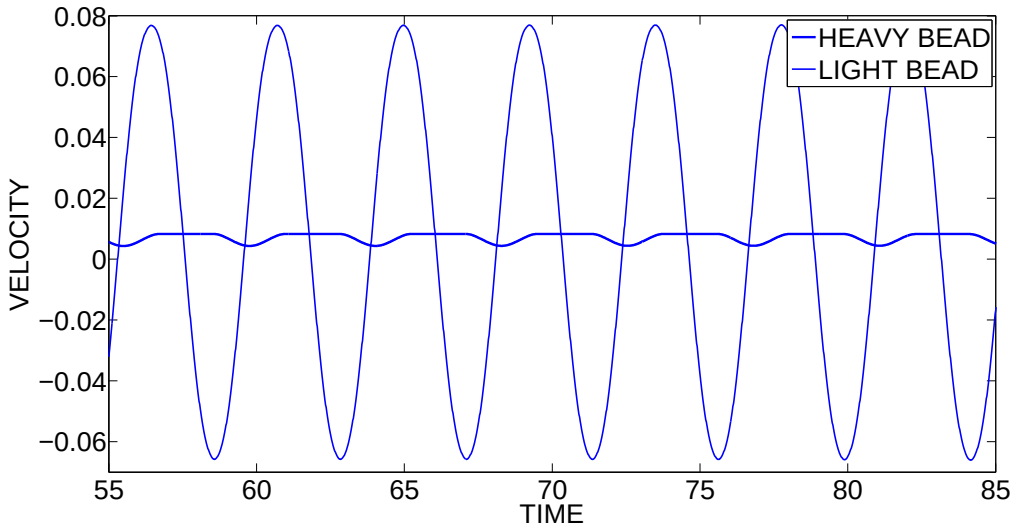

Figure 3.19: Velocity time series of heavy and light bead in the oscillating tail (radiated traveling wave) during resonance for $\varepsilon_R^{(1:3)} = 0.12$.

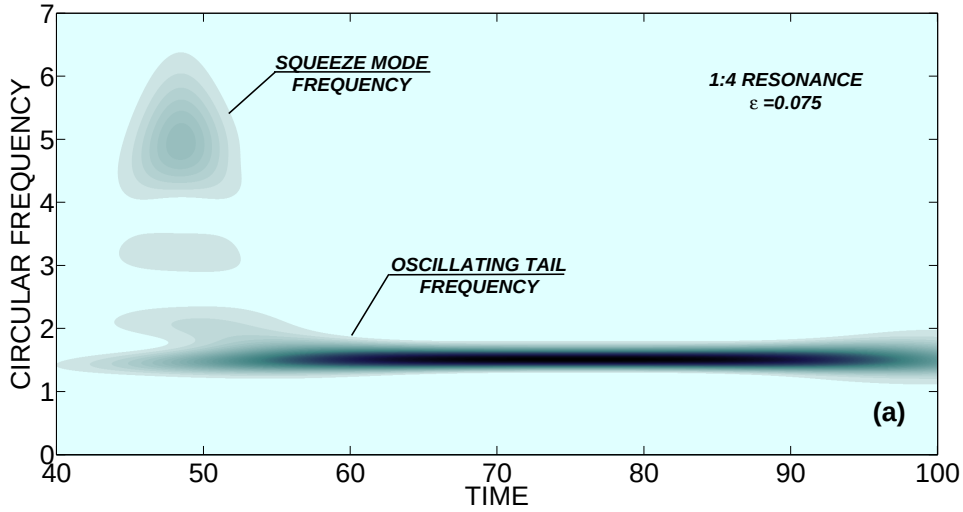

Figure 3.20: Wavelet transform spectra of the fast component of the oscillation of a light bead for (a) $\varepsilon \approx 0.075$.

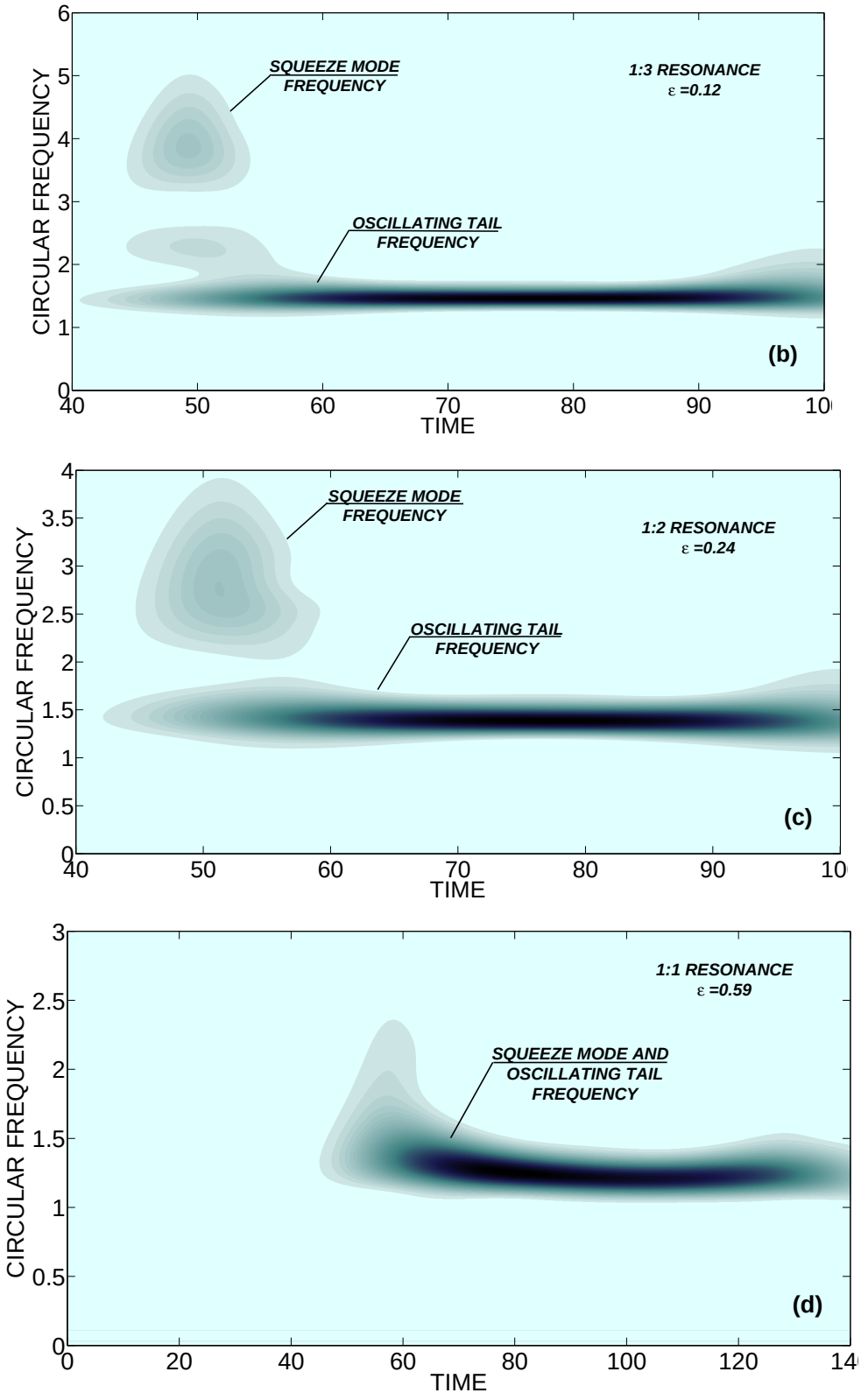

Figure 3.20 (cont'd): Wavelet transform spectra of the fast component of the oscillation of a light bead for (b) $\varepsilon \approx 0.12$; (c) $\varepsilon \approx 0.24$; (d) $\varepsilon \approx 0.59$.

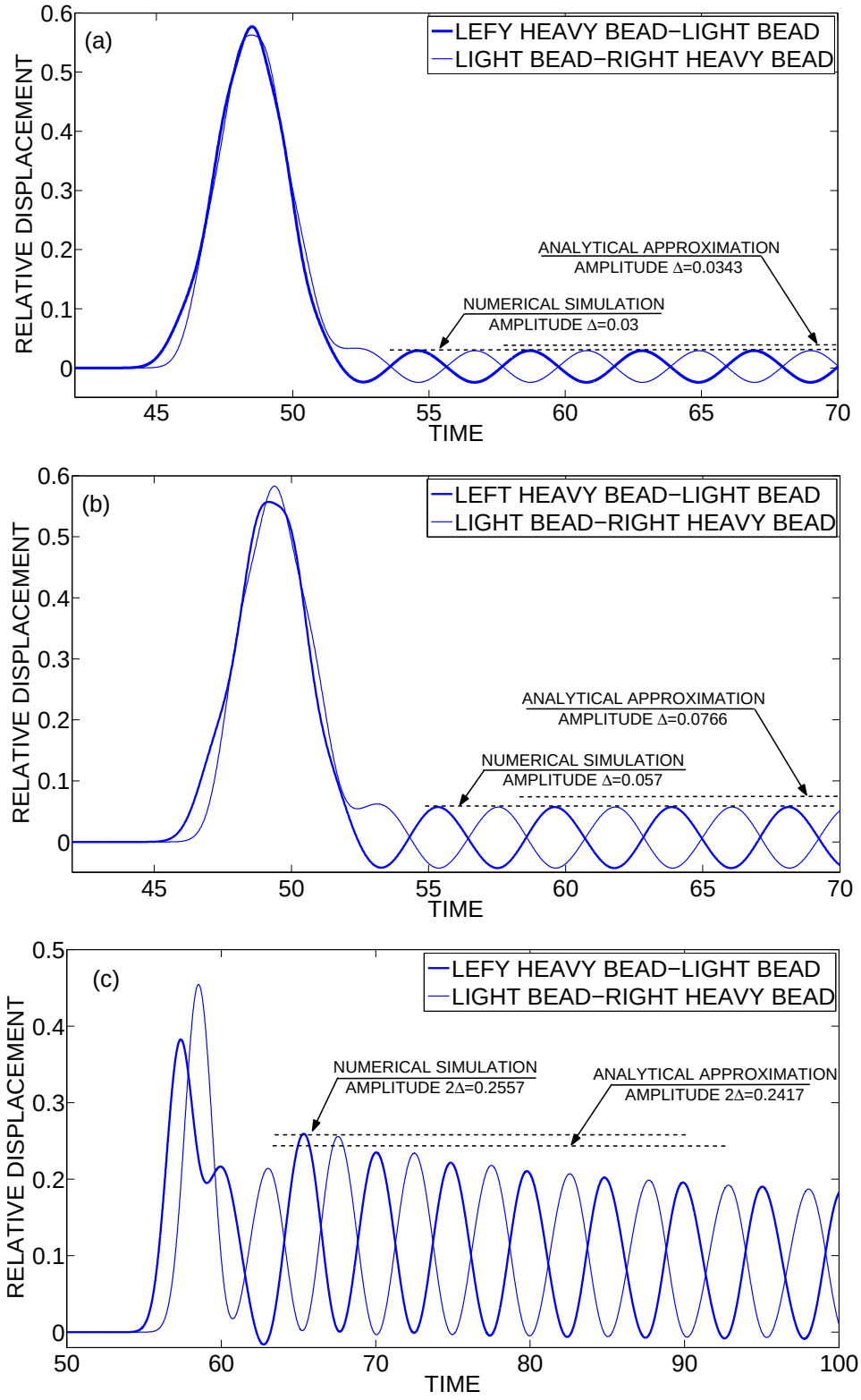

Figure 3.21: Relative displacements between adjacent light and heavy beads for (a)$\varepsilon_R^{(1:4)} \approx 0.075$; (b) $\varepsilon_R^{(1:3)} \approx 0.12$; (c) $\varepsilon_R^{(1:1)} \approx 0.59$ (for adjacent beads 51-53).

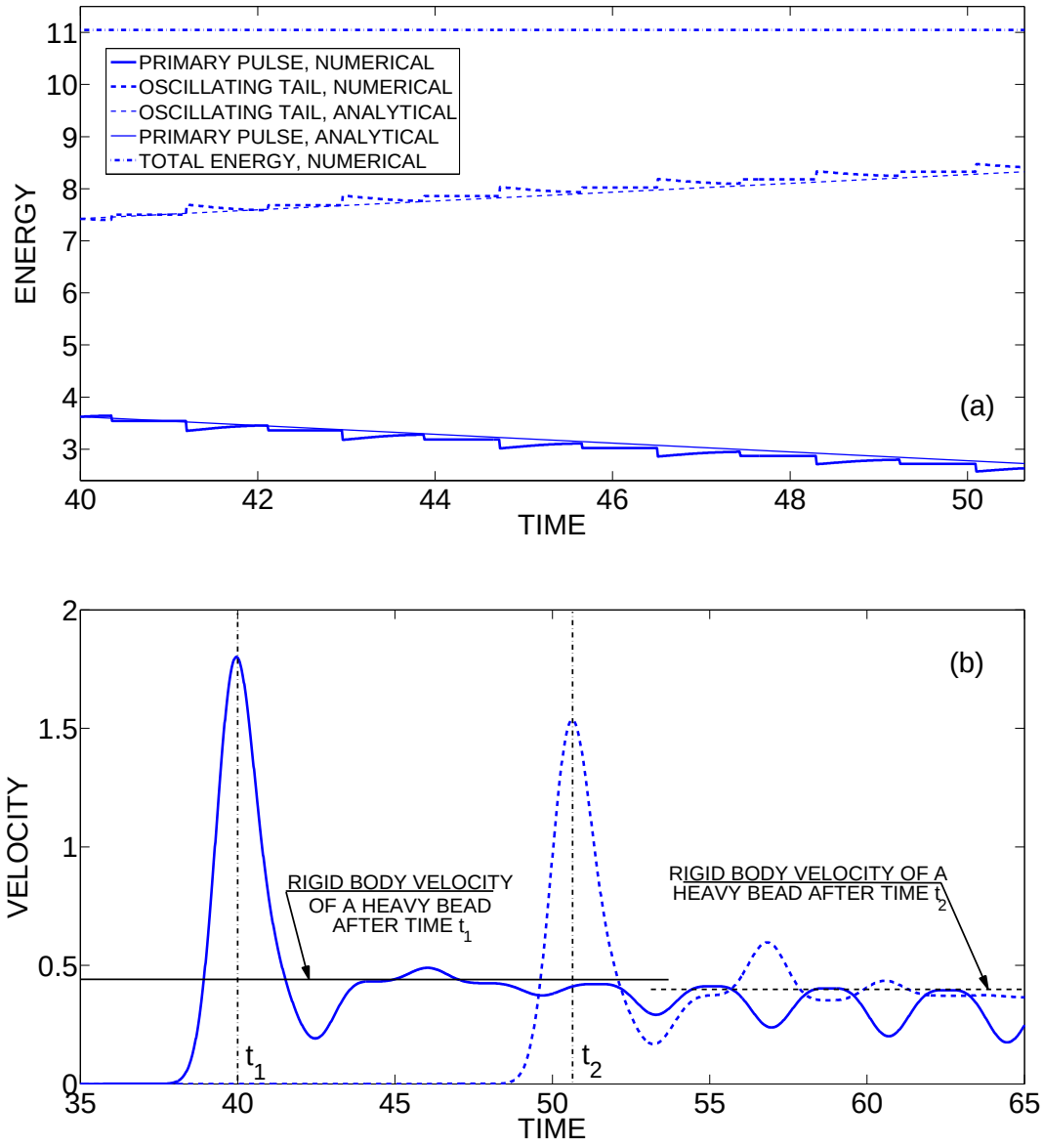

Figure 3.22: Pulse attenuation in the regime of 1: 1 resonance ($\varepsilon_R^{(1:1)} \approx 0.59$) in the short time interval $t_1 < t < t_2$, (a) Energy contained in the primary pulse and in the oscillating tail; (b) rigid body velocities of the heavy beads with maximum velocities at times t_1 and t_2.

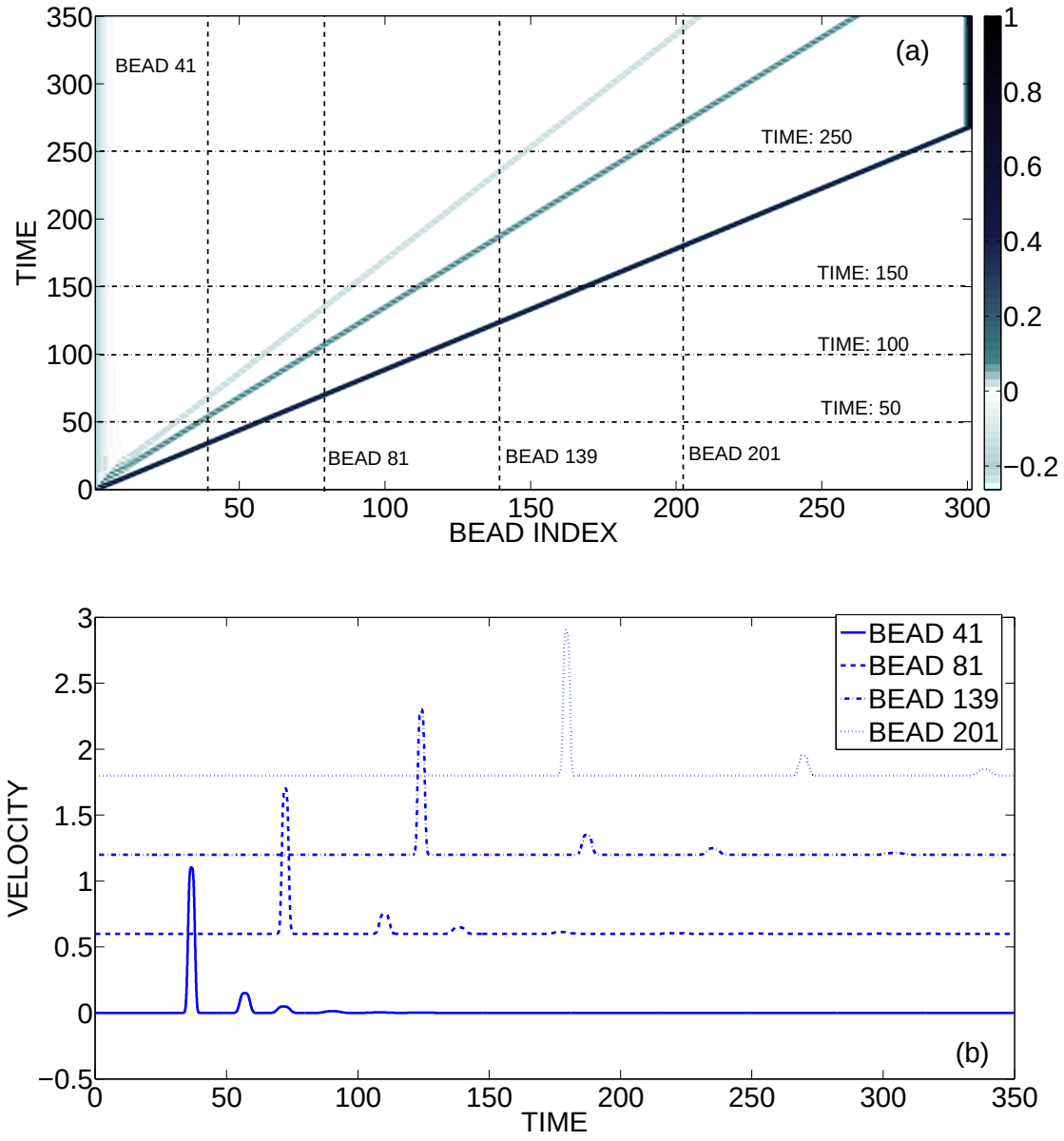

Figure 3.23: Normalized velocity of the dimer for $\varepsilon = 0.3428$, (a) solitary wave propagation in space and time; (b) time series at four spatial points.

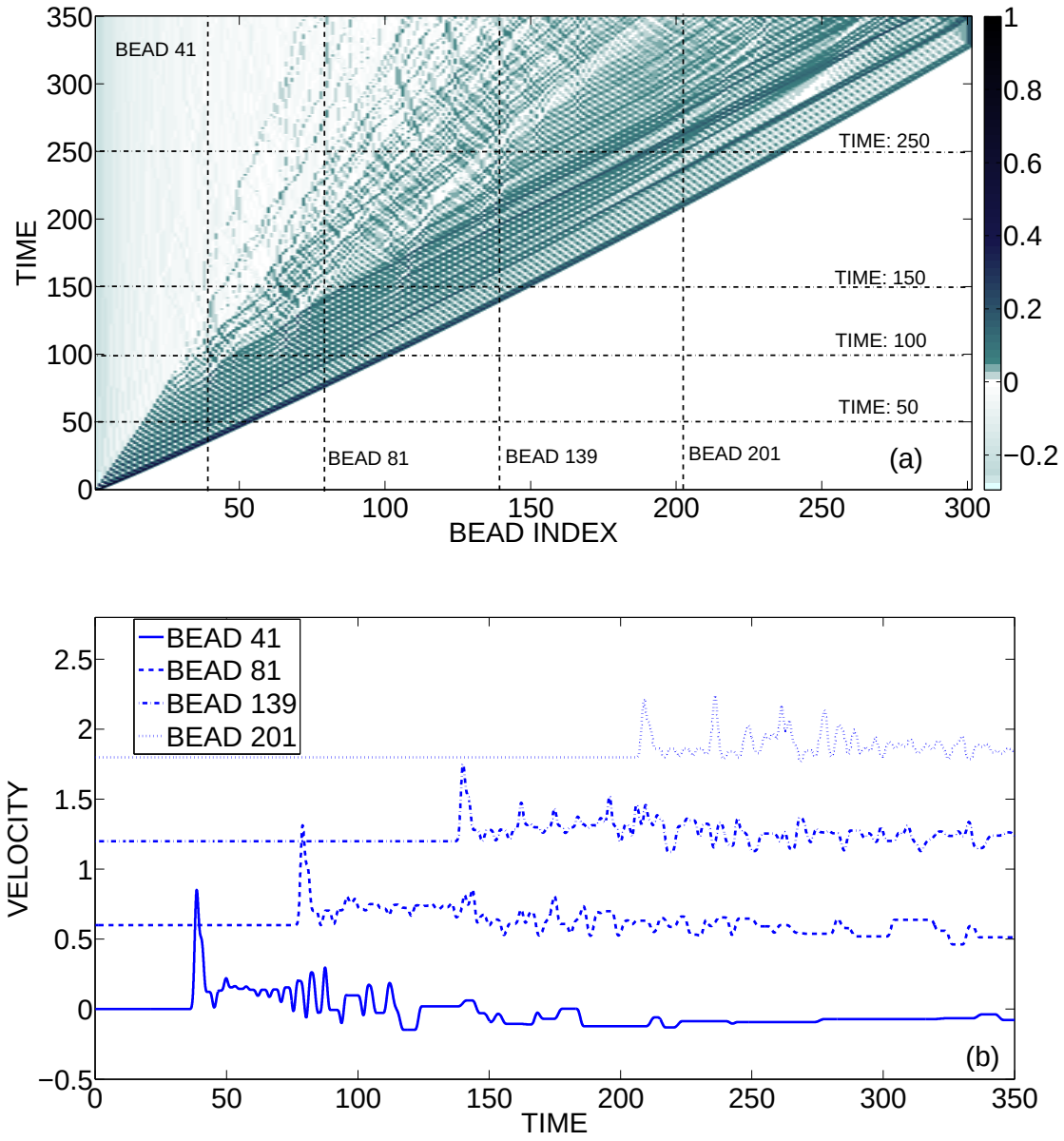

Figure 3.24: Normalized velocity of the dimer for $\varepsilon = 0.5$, (a) pulse propagation in space and time; (b) time series at four different locations.

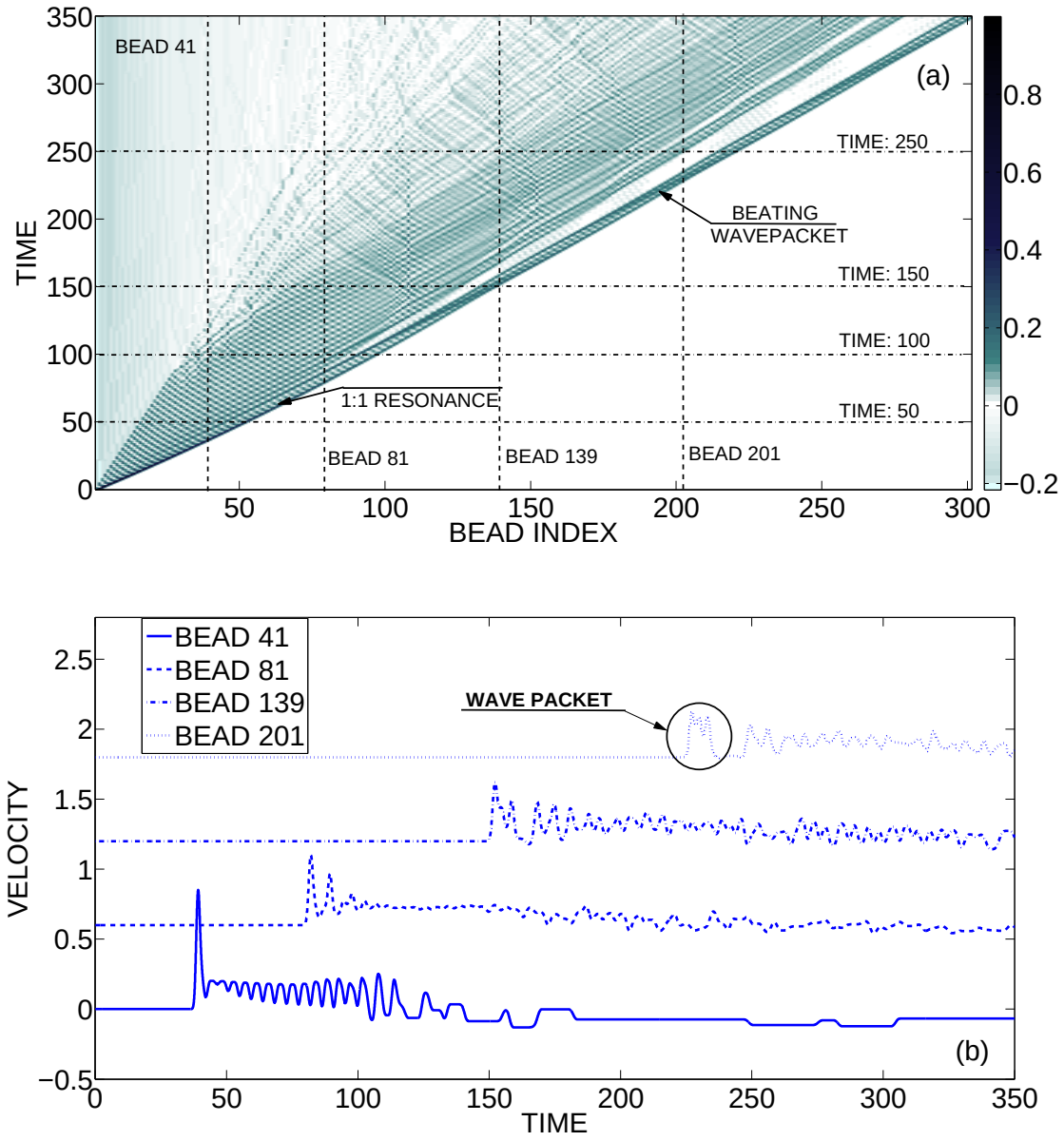

Figure 3.25: Normalized velocity of the dimer for $\varepsilon = 0.59$ (1: 1 resonance), (a) pulse propagation in space and time; (b) time series at four different locations.

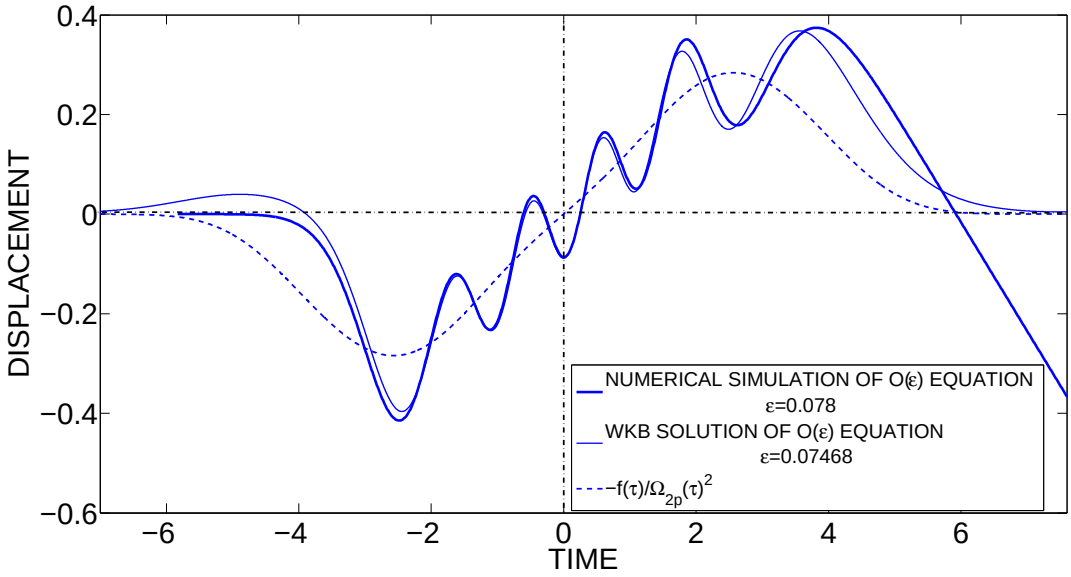

Figure 3.26: Comparison of the WKB solution (3.23) and the asymptotic model (3.15, 3.23, 3.24) for 1:4 resonance.

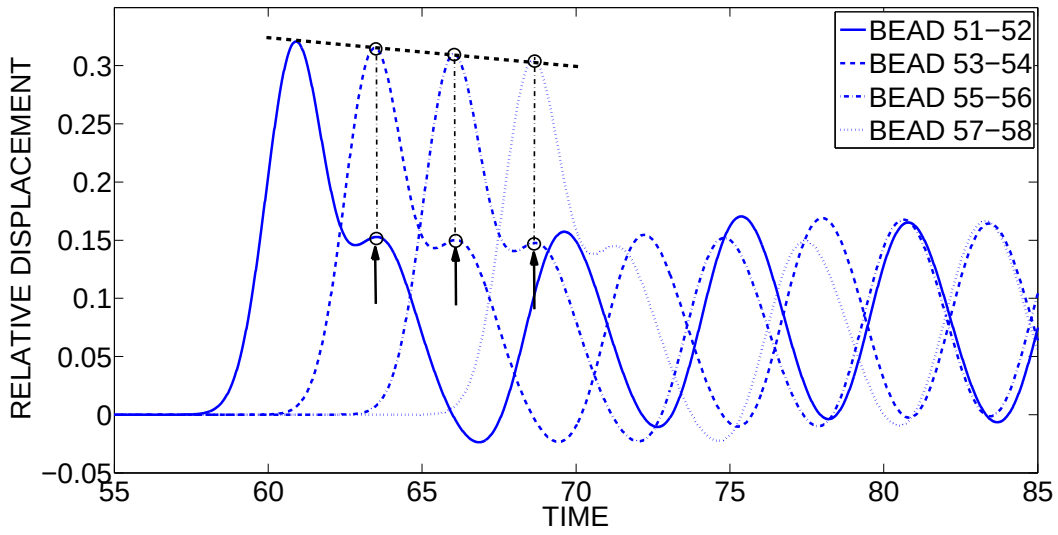

Figure 3.27: Relative displacement responses between four pairs of neighboring beads of the dimer (3.3) with $\varepsilon = 0.625$ in the regime of strong pulse attenuation due to 1: 1 resonance.

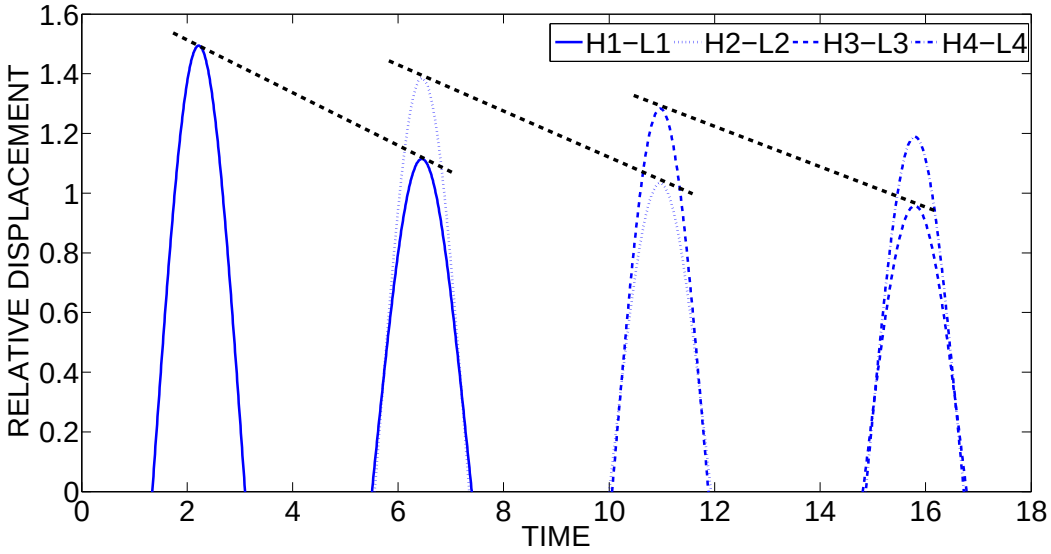

Figure 3.28: Relative displacement responses between four pairs of neighboring beads for the binary model with gap $D = 3.3489$ and $\bar{\varepsilon}_R^{(1:1)} = 0.537$.

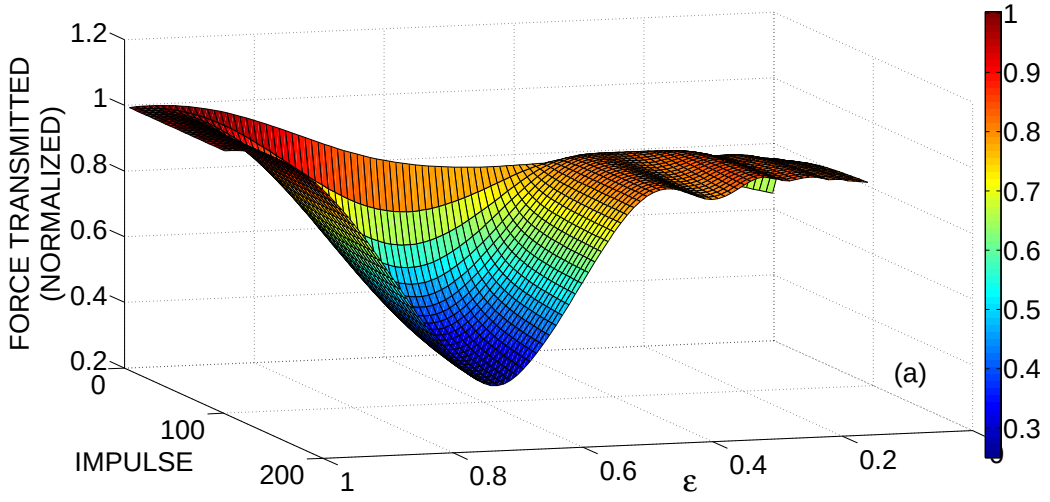

Figure 3.29: Maximum normalized force transmitted to the right boundary of the dimer for varying pre-compression as function of normalized mass ratio and applied impulse, (a) Plot in parameter space.

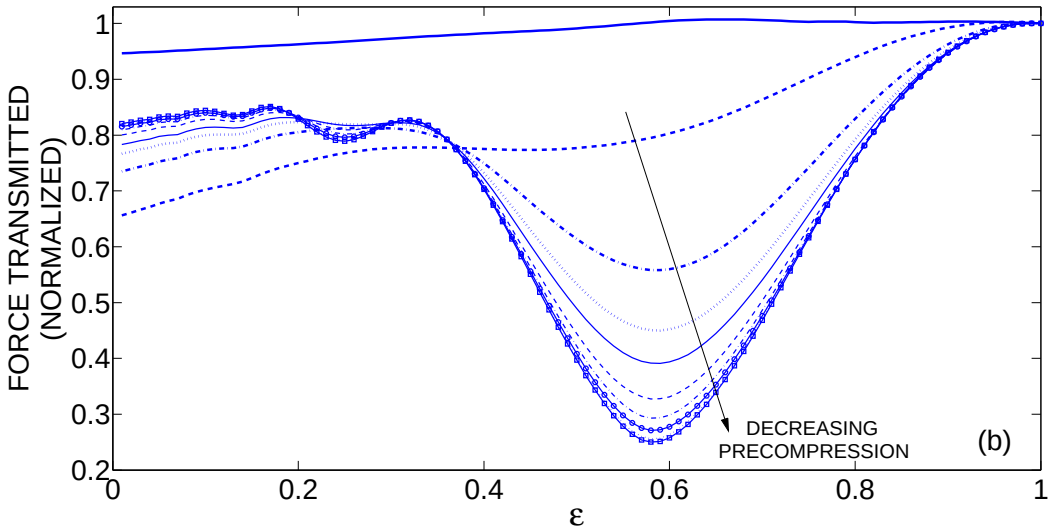

Figure 3.29 (cont'd): Maximum normalized force transmitted to the right boundary of the dimer for varying pre-compression as function of normalized mass ratio and applied impulse, (b) plots for decreasing levels of pre-compression.

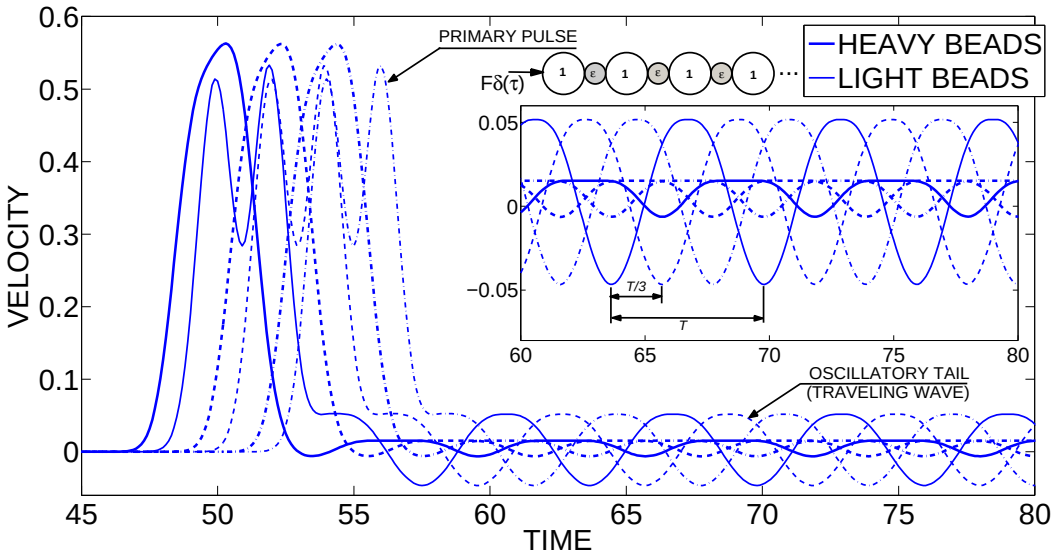

Figure 3.30: Traveling wave with 6-bead periodicity in the trail of a propagating pulse in a semi-infinite dimer chain with $\varepsilon = 0.303$; (thick lines correspond to responses of heavy beads and thin ones to responses of light beads).

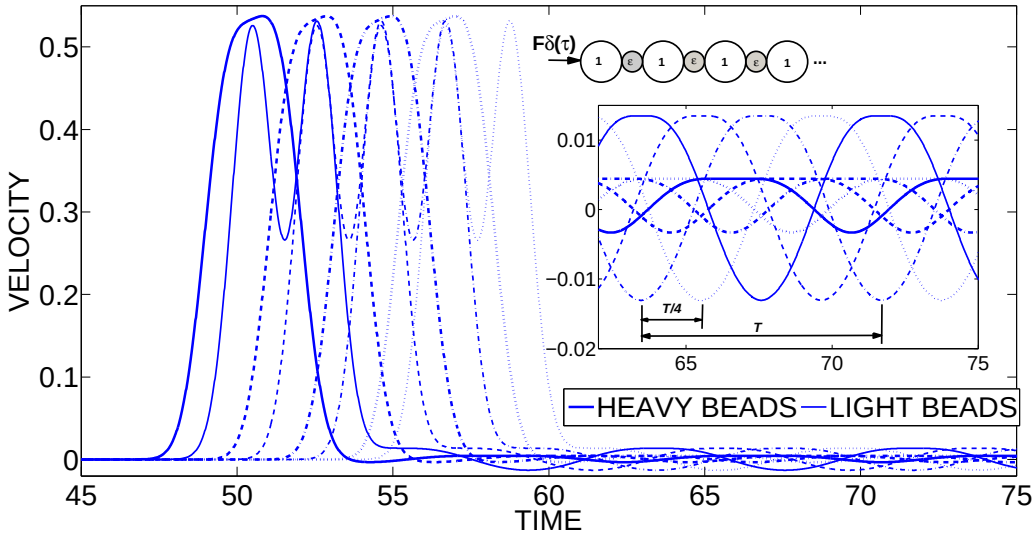

Figure 3.31: Traveling wave with 8-bead periodicity in the trail of a propagating pulse in a semi-infinite dimer chain with $\varepsilon = 0.3305$; (thick lines correspond to responses of heavy beads and thin ones to responses of light beads).

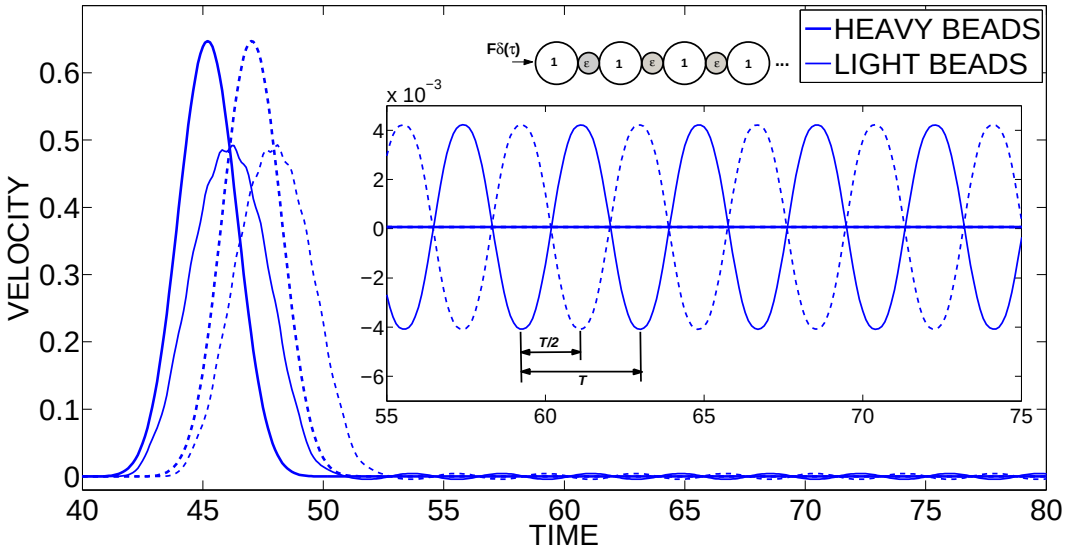

Figure 3.32: Standing wave with 4-bead periodicity in the trail of a propagating pulse in a semi-infinite dimer chain with $\varepsilon = 0.017$; (thick lines correspond to responses of heavy beads and thin ones to responses of light beads).

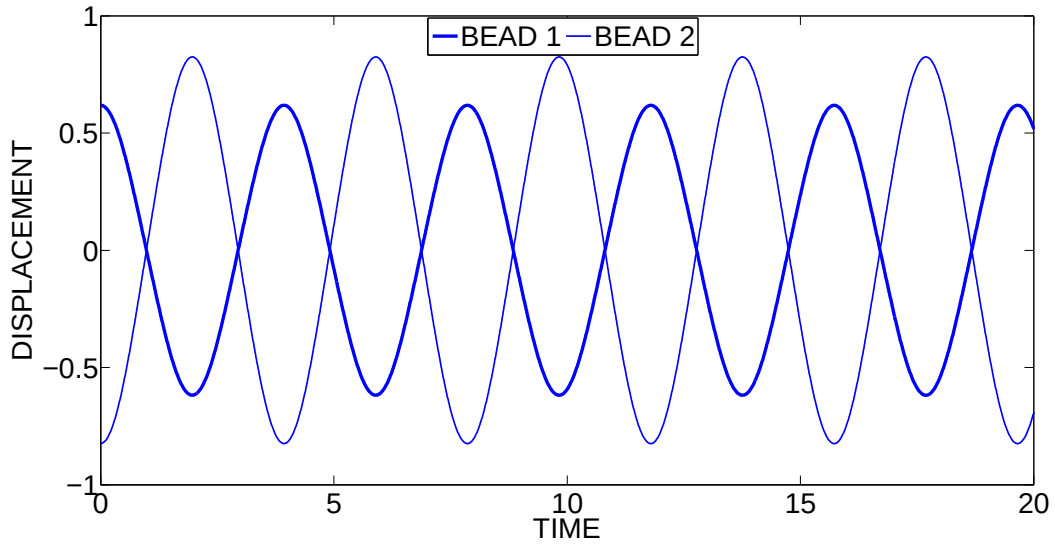

Figure 3.33: Out-of-phase standing wave in the 2-bead reduced system for $\varepsilon = 0.75$.

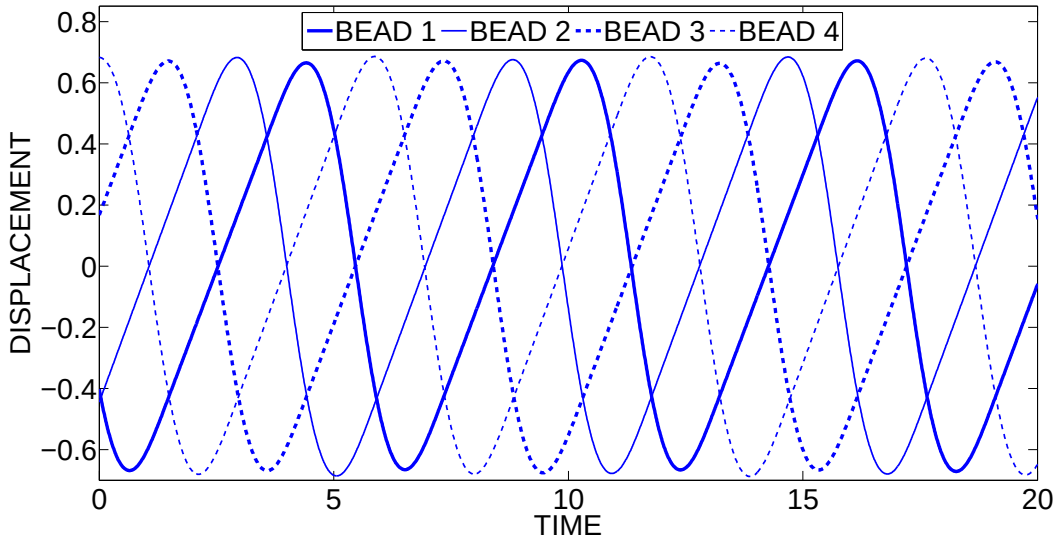

Figure 3.34: Spatially periodic traveling wave with 4-bead periodicity in the homogeneous chain ($\varepsilon = 1$) for unit normalized energy level [63].

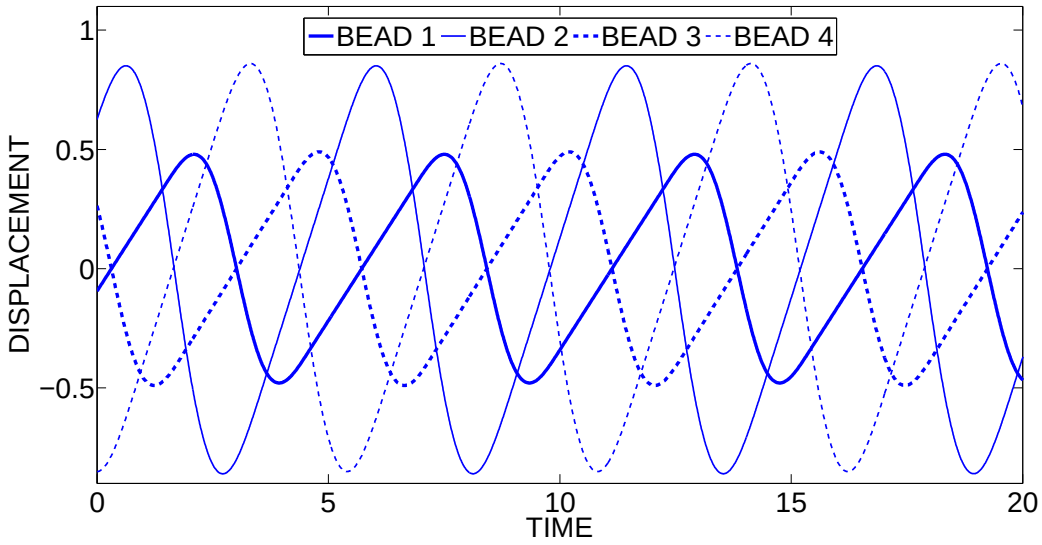

Figure 3.35: Spatially periodic traveling wave with 4-bead periodicity in the dimer chain with $\varepsilon = 0.75$ for unit normalized energy level.

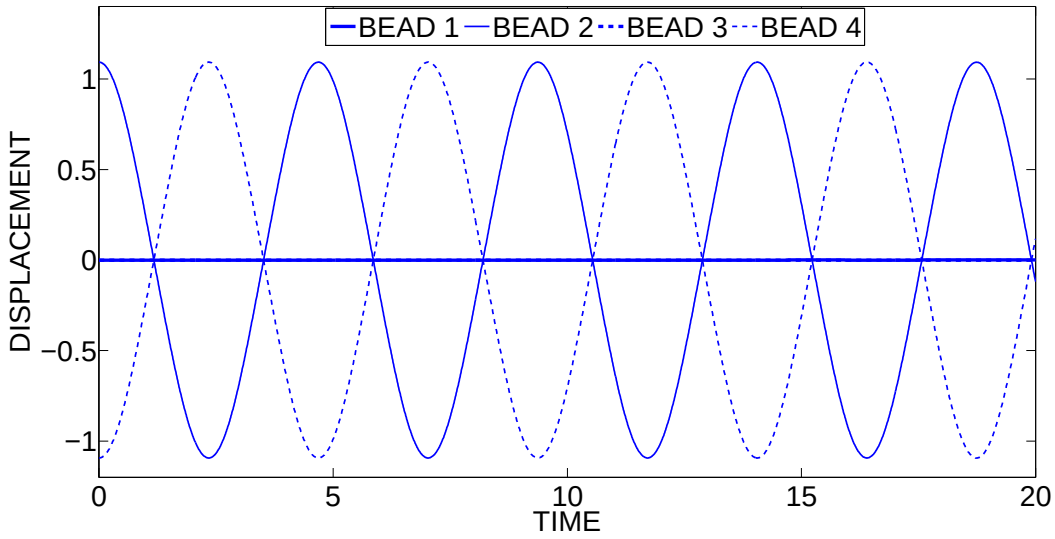

Figure 3.36: Standing wave solution with 4-bead periodicity in the dimer chain with $\hat{\varepsilon} = 0.53$ and normalized energy level equal to unity.

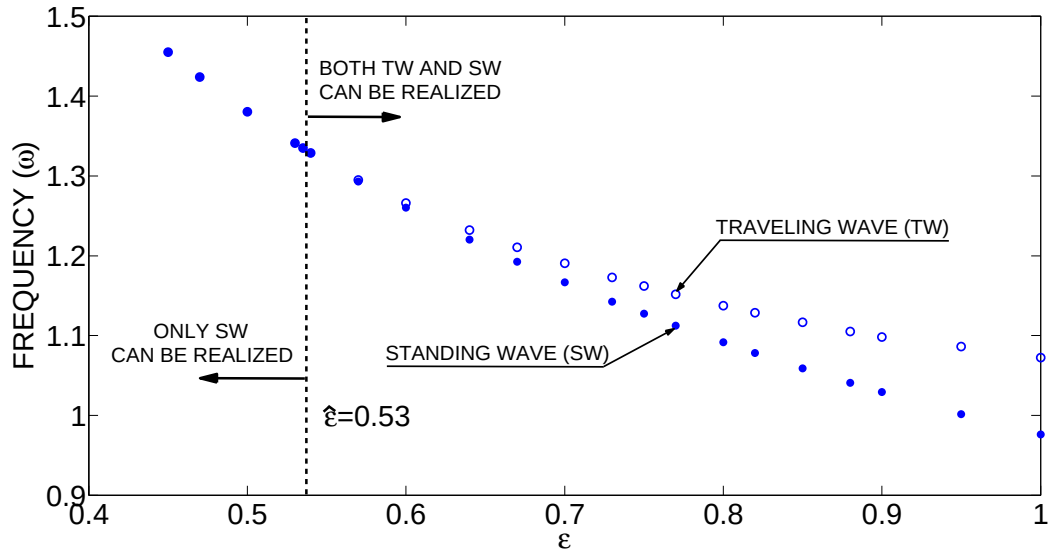

Figure 3.37: Bifurcation diagram for traveling and standing wave solutions for 4-bead periodicity ($n = 4$) and total energy of the reduced system equal to unity.

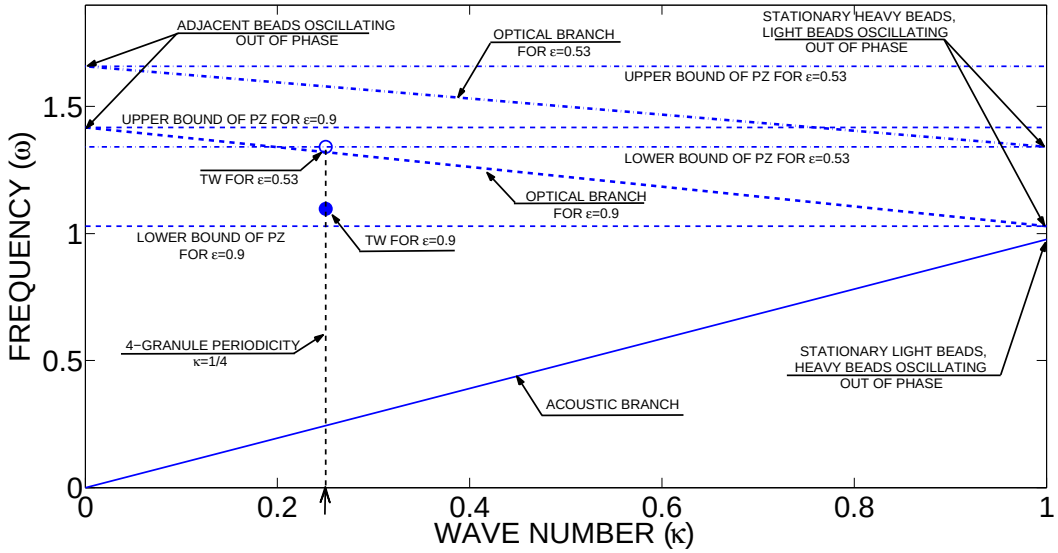

Figure 3.38: Approximate depiction of acoustic and optical branches for infinite granular dimer chain for unit energy with for $\varepsilon = 0.9$ and $\varepsilon = 0.53$; the traveling waves for 4-bead periodicity $\kappa = 1/4$ are depicted.

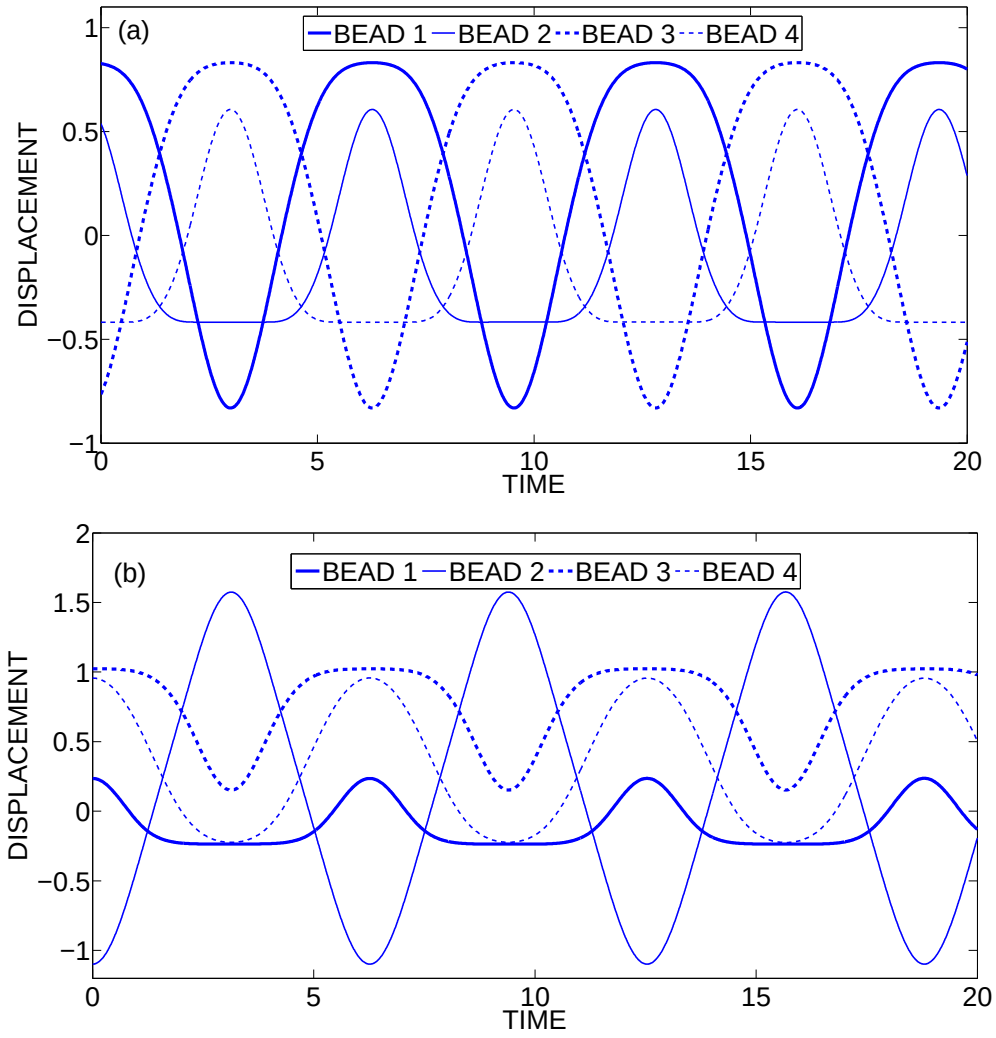

Figure 3.39: Localized standing waves with 4-bead periodicities for $\varepsilon = 0.9$ and normalized total energy of reduced systems equal to unity: (a) $\omega = 0.9601$, (b) $\omega = 1.0026$.

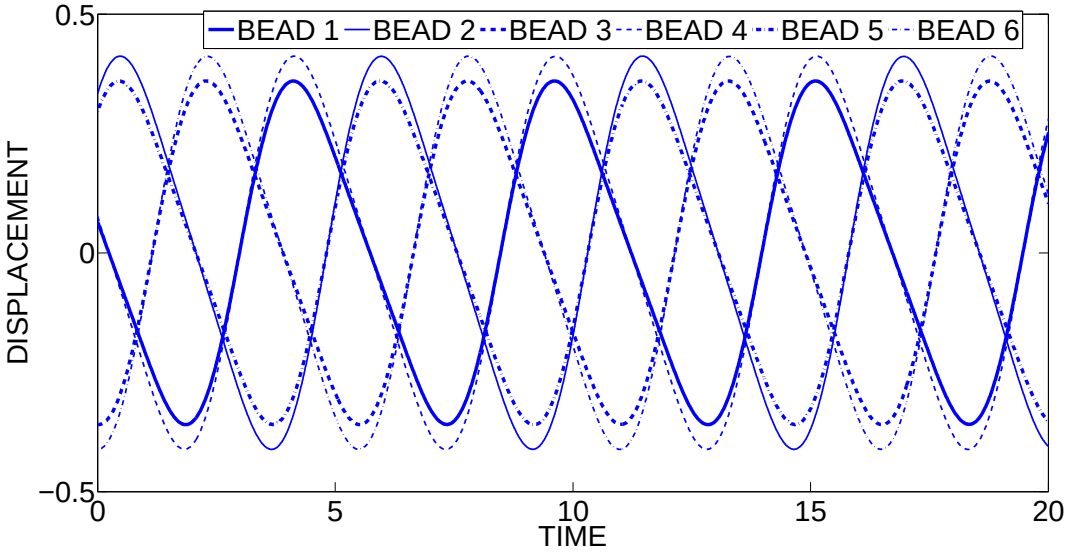

Figure 3.40: Spatially periodic traveling wave with 6-bead (and 12-bead) periodicity in the dimer chain with $\varepsilon = 0.9$ for unit normalized energy level.

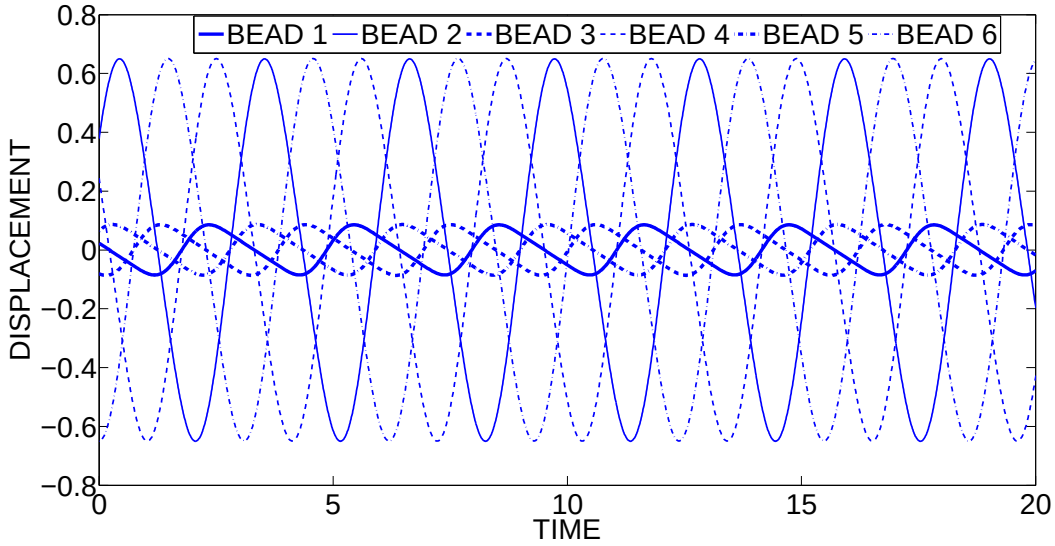

Figure 3.41: Spatially periodic traveling wave with 6-bead (and 12-bead) periodicity in the dimer chain with $\varepsilon = 0.2$ for unit normalized energy level.

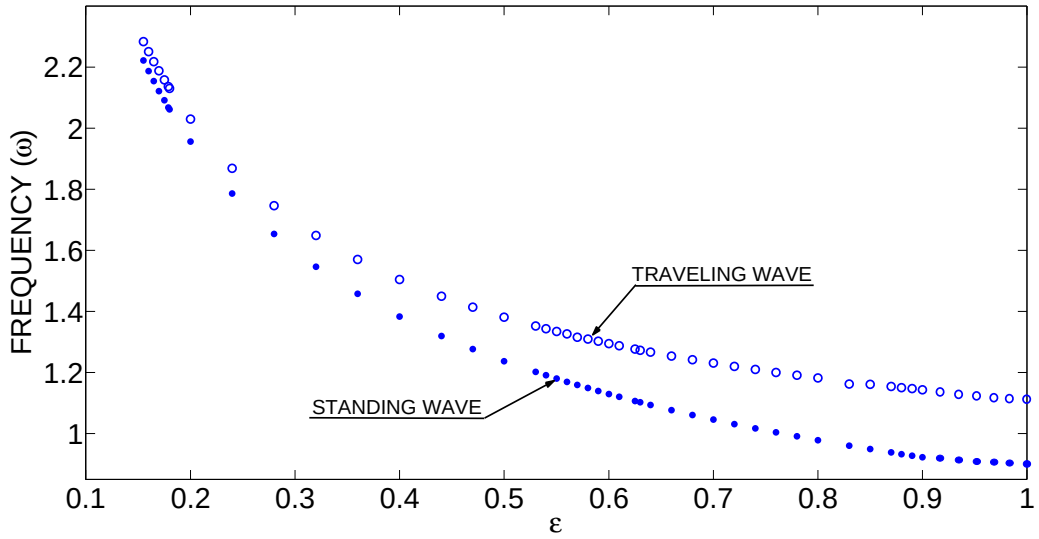

Figure 3.42: Frequencies of traveling and standing waves with 12-bead periodicities as functions of the mass ratio for the same fixed energy level; note absence of bifurcation in this case.

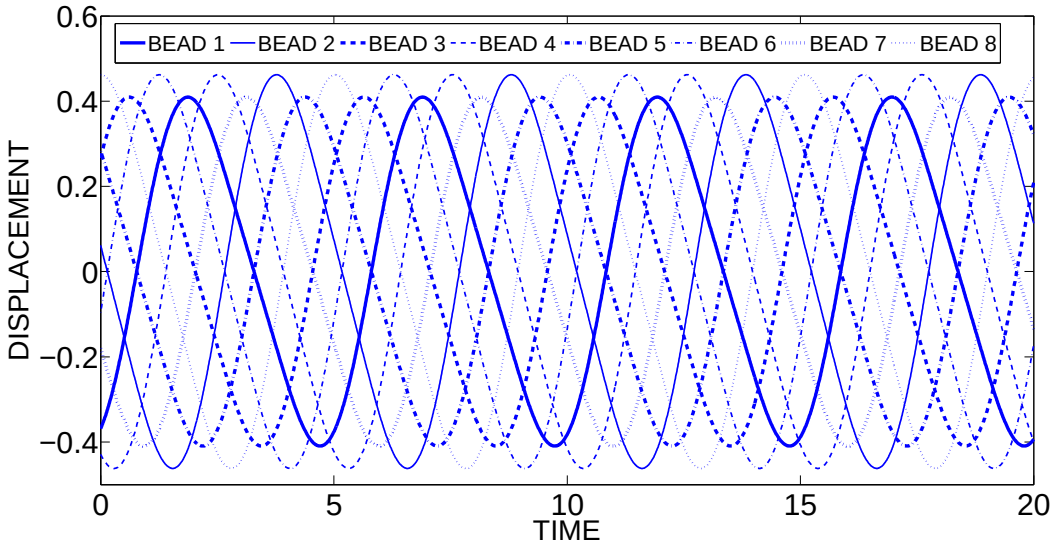

Figure 3.43: Spatially periodic traveling waves with 8-bead periodicity in the dimer chain with $\varepsilon = 0.9$ for unit normalized energy level.

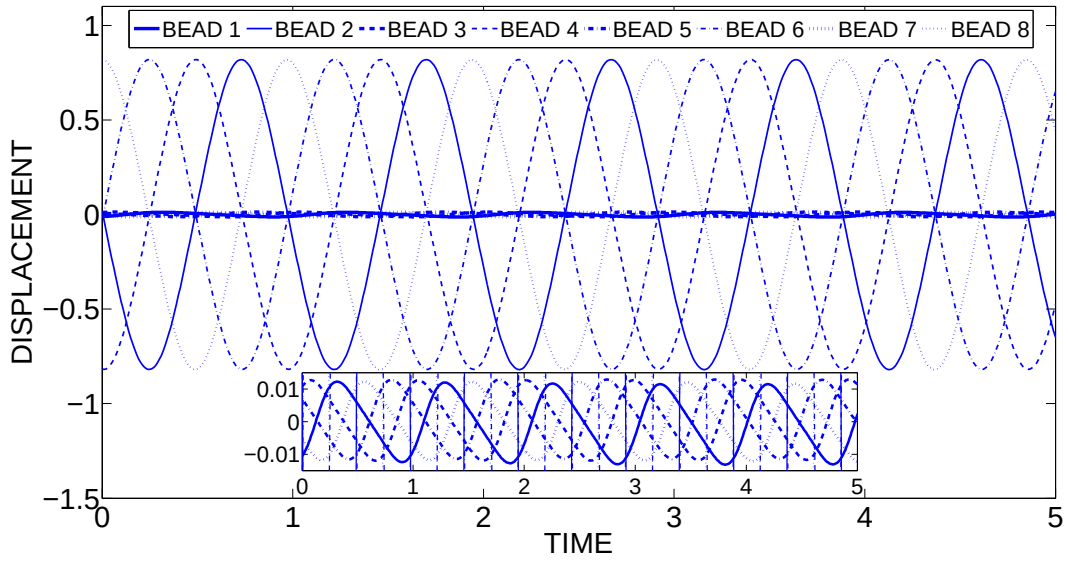

Figure 3.44: Spatially periodic traveling waves with 8-bead periodicity in the dimer chain with $\varepsilon = 0.02$ for unit normalized energy level.

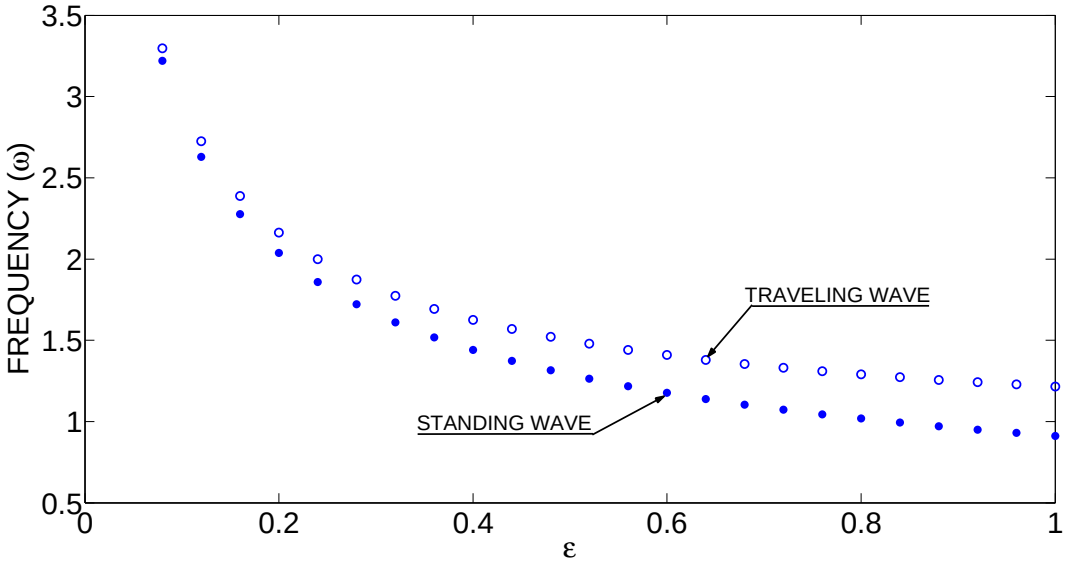

Figure 3.45: Frequencies of traveling and standing waves with 8-bead periodicities as functions of the mass ratio for the same fixed energy level; note absence of bifurcation in this case.

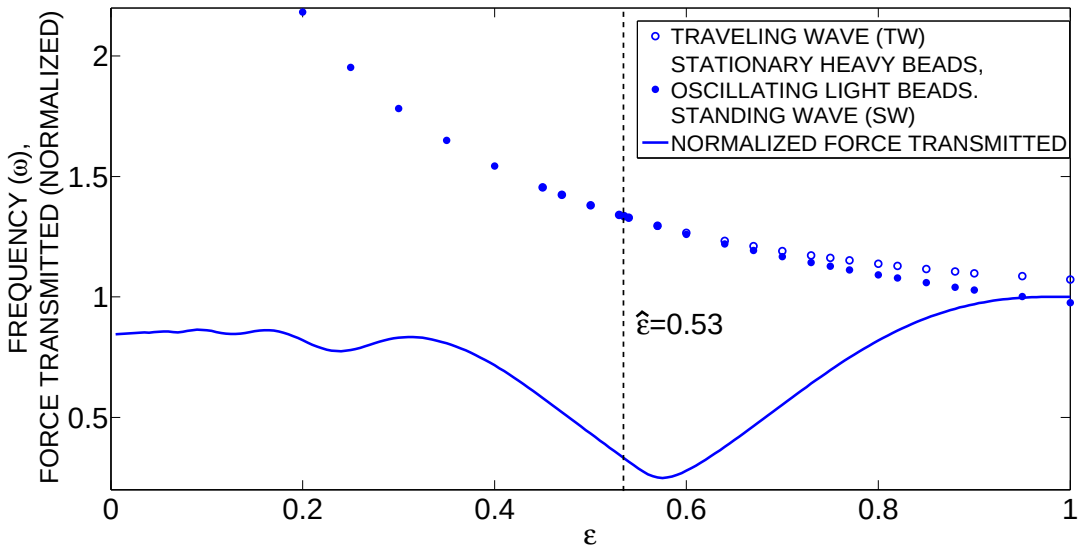

Figure 3.46: Correlation of the bifurcation diagram for traveling waves with 4-bead periodicity and the plot of normalized transmitted force in a finite dimer chain [91, 97].

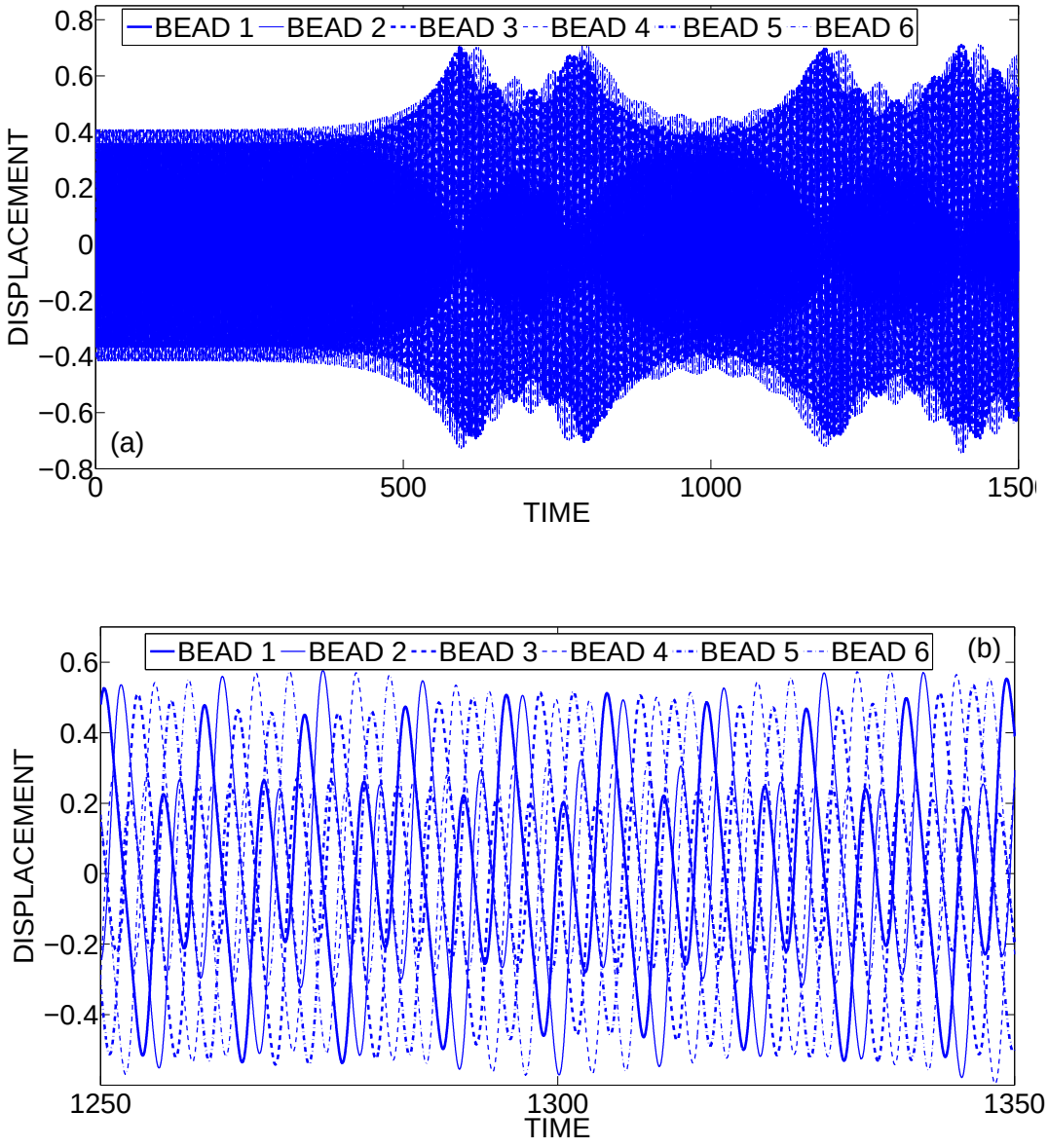

Figure 3.47: Modulationally unstable traveling wave with 6-bead periodicity for $\varepsilon = 0.9$, (a) Waveform; (b) long-time preservation of traveling wave characteristics.

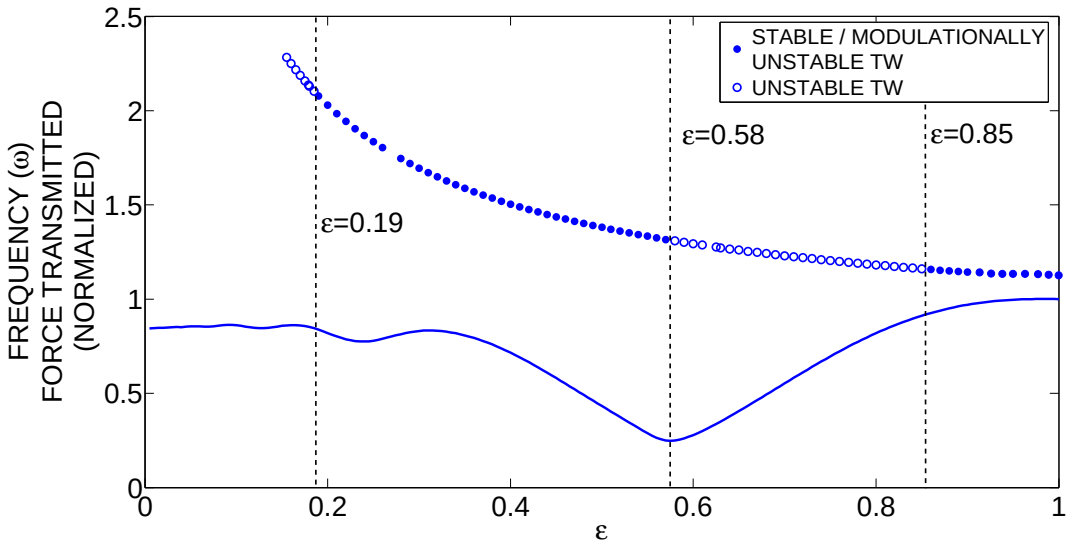

Figure 3.48: Correlation of the stability of traveling waves with 6-bead periodicity and the plot of normalized transmitted force in a finite dimer chain [91, 97]; regions of stable, modulationally unstable and unstable traveling waves are indicated.

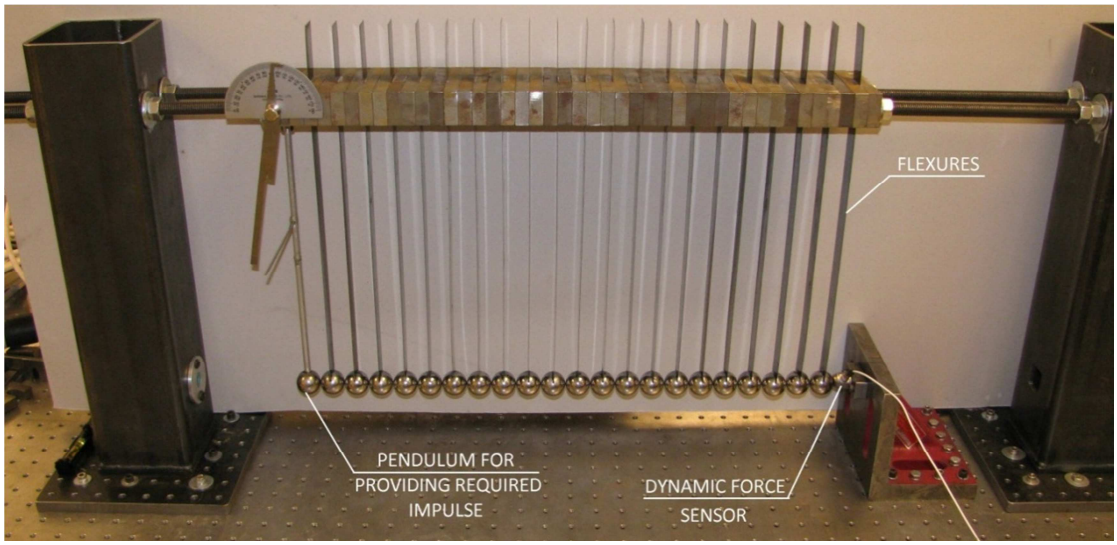

Figure 3.49: Experimental setup with a homogeneous granular chain.

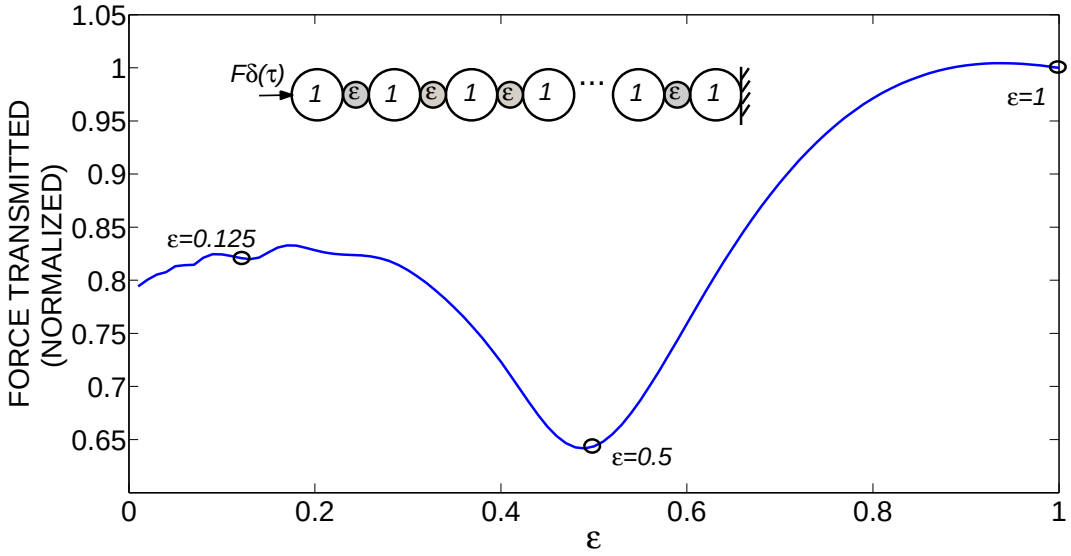

Figure 3.50: Normalized transmitted force as function of the normalized mass ratio for the general 21 bead dimer chain; the three granular chains considered in this study are indicated in the plot.

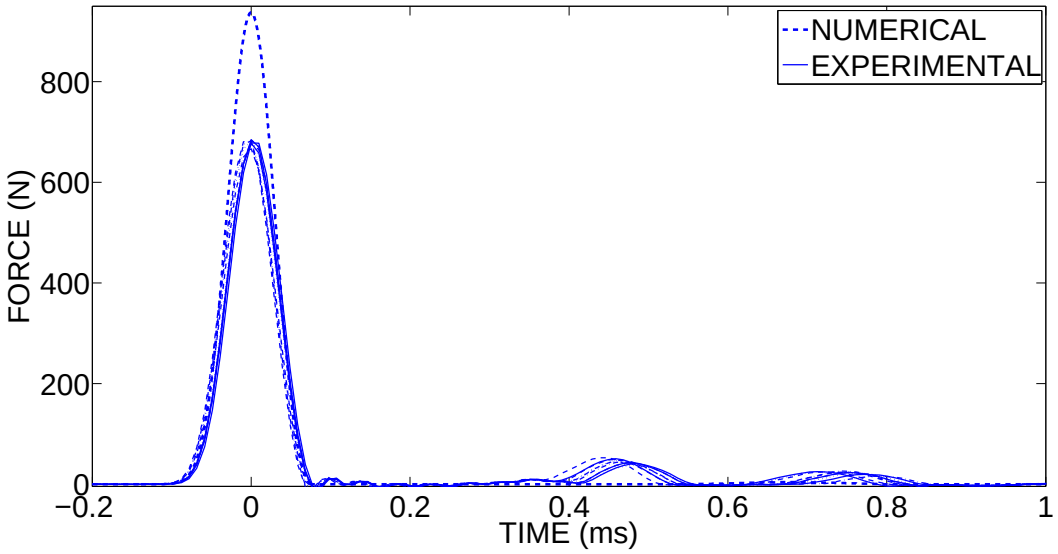

Figure 3.51: Experimental and numerical transmitted force at the force sensor for the homogeneous granular chain composed of 21 heavy beads at excitation level 1; no dissipation effects are assumed in the numerical model.

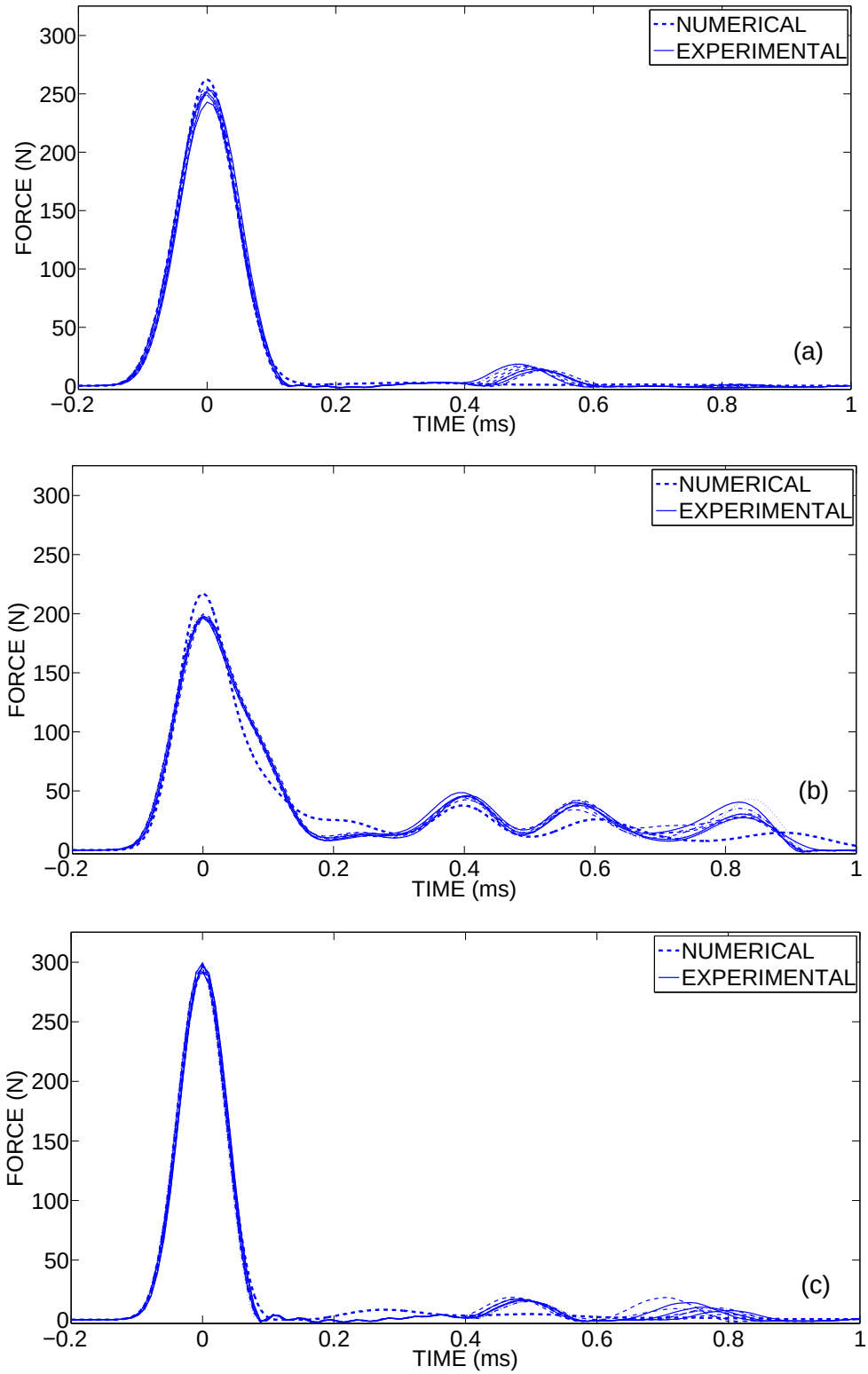

Figure 3.52: Comparison of experimental measurements and numerical simulations for excitation level 1, (a) dimer 2 ($\varepsilon = 0.125$); (b) dimer 1 ($\varepsilon = 0.5$); (c) homogeneous chain ($\varepsilon = 1$).

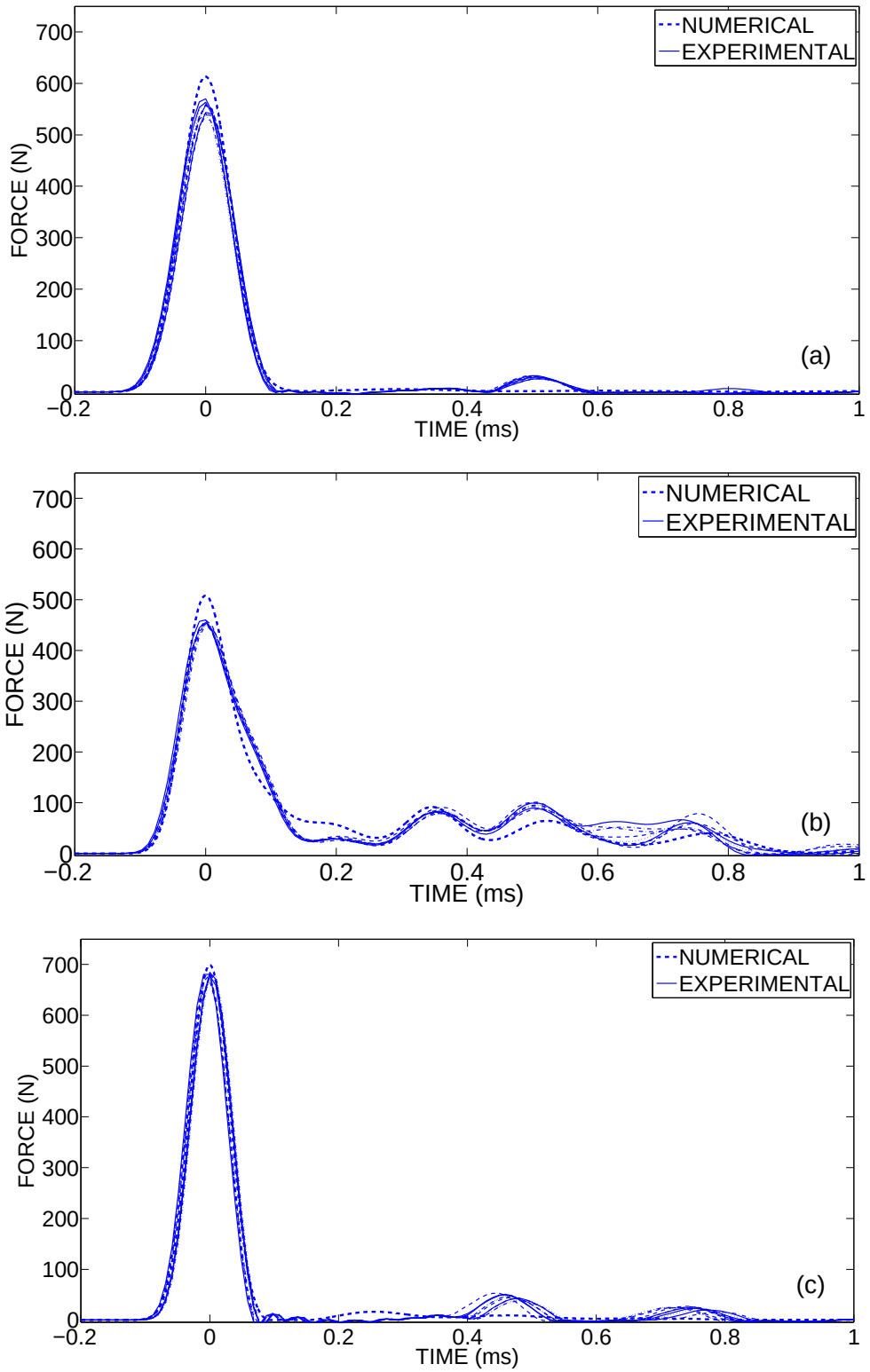

Figure 3.53: Comparison of experimental measurements and numerical simulations for excitation level 3, (a) dimer 2 ($\varepsilon = 0.125$); (b) dimer 1 ($\varepsilon = 0.5$); (c) homogeneous chain ($\varepsilon = 1$).

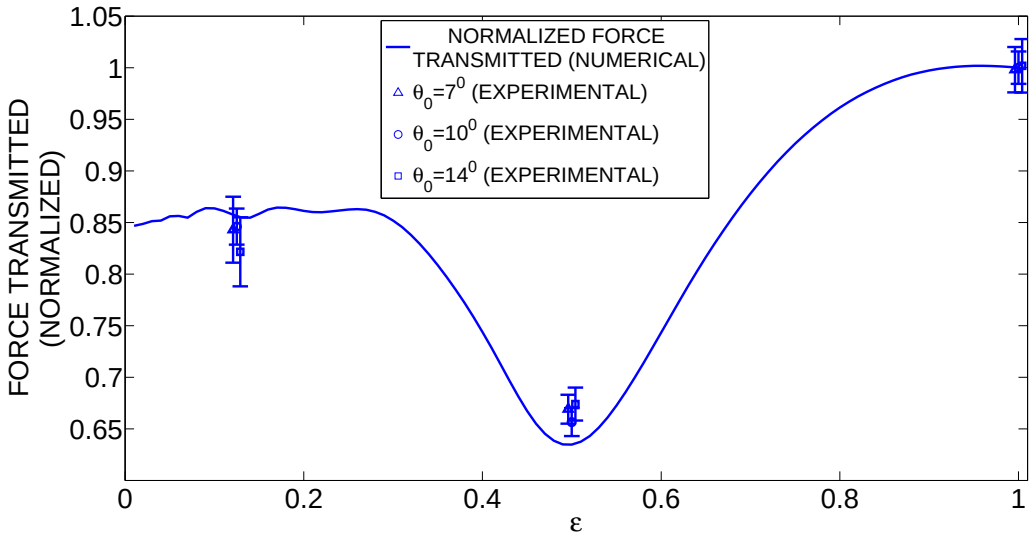

Figure 3.54: Experimental results of maximum normalized transmitted force measured at the site of the dynamical force sensor and comparison with the theoretical prediction; the three levels of force excitation are depicted.

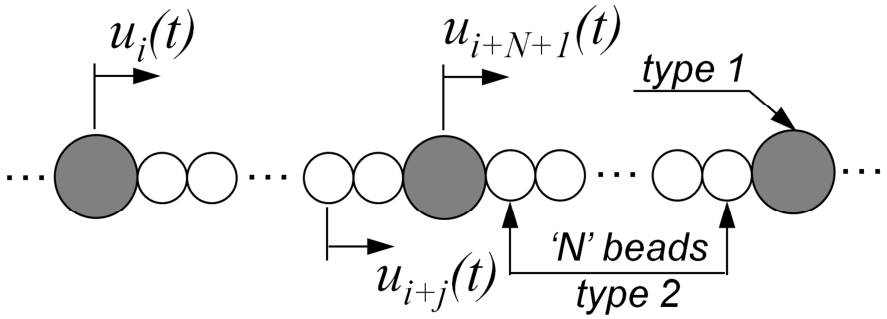

Figure 3.55: The 1: N elastic dimer chain.

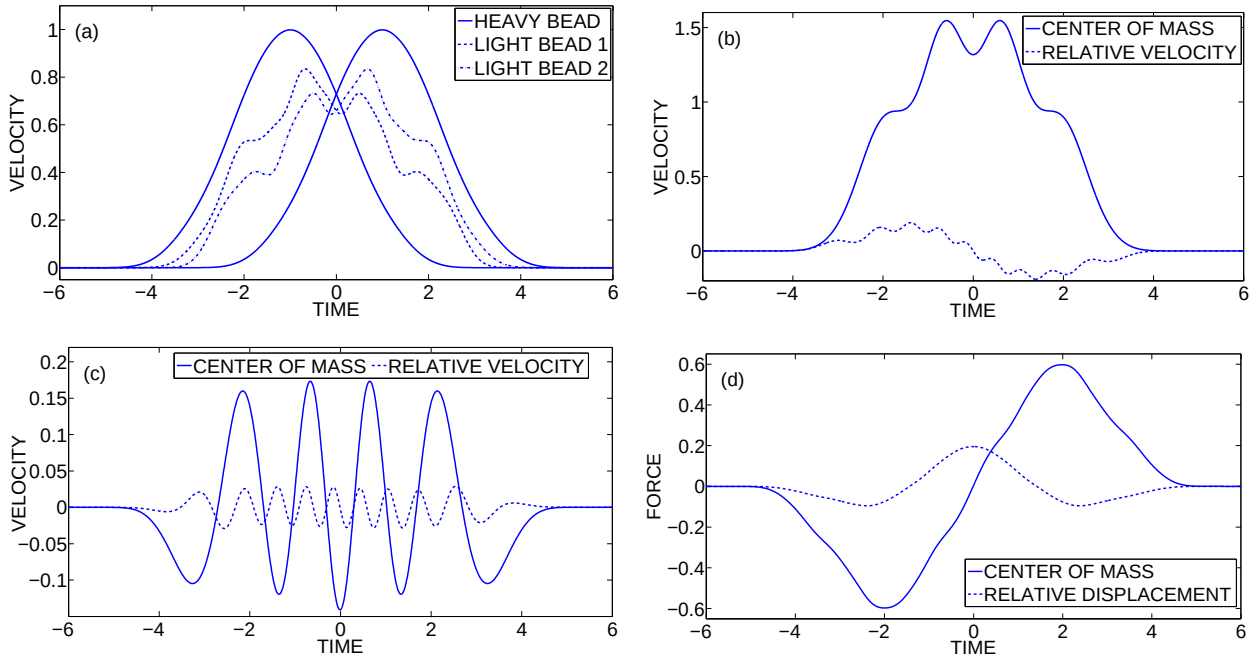

Figure 3.56: Response profiles for solitary wave formation in the 1: 2 dimer with $\varepsilon = 0.05616$ and $\alpha = 2.78$, (a) Velocities of light beads and bounding heavy beads; (b) velocity of the center of mass and relative velocity of the light beads; (c) fast dynamic components of the responses in (b); (d) corresponding slow varying forces $f_{(3p+1)1}(t_0)$ and $f_{(3p+1)2}(t_0)$ in the fast equations (3.52a).

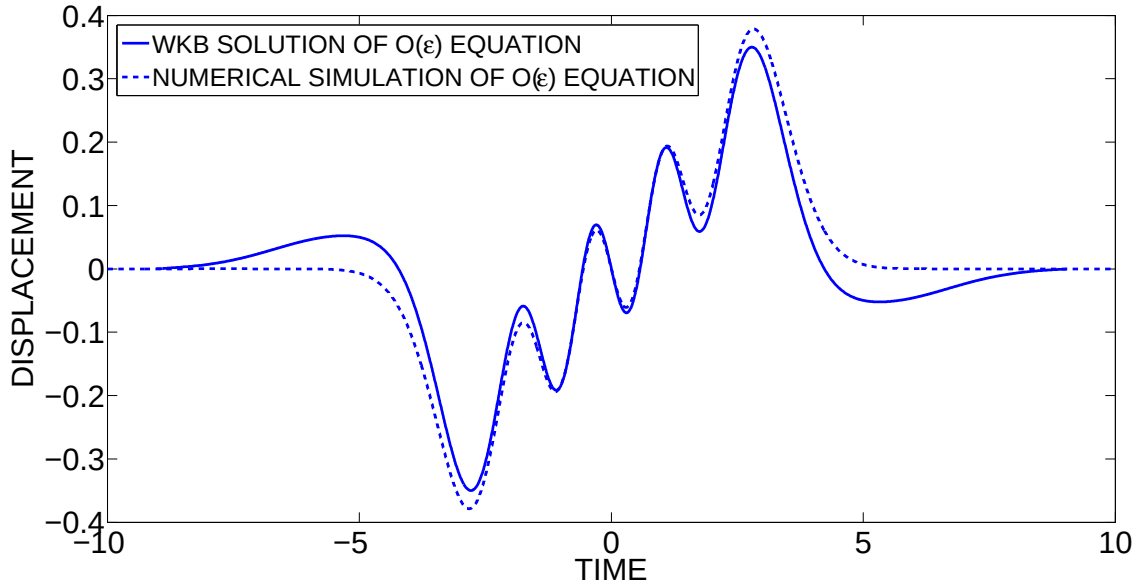

Figure 3.57: Comparison between numerical and asymptotic eigenfunctions $\eta^{CM}_{(3p+1)1_5}(\tau;3)$ for $\varepsilon^{CM}_5 \approx 0.056597$ and $\alpha = 3$.

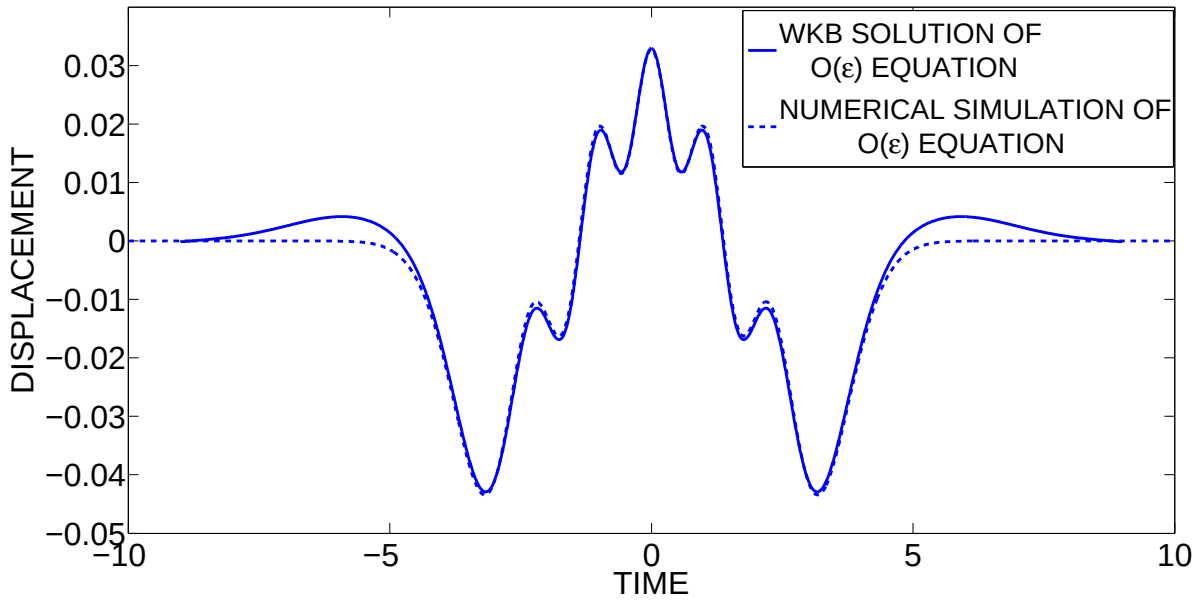

Figure 3.58: Comparison between numerical and asymptotic eigenfunctions $\sigma^{RD}_{(3p+1)1_6}(\tau;3)$ for $\varepsilon^{RD}_6 \approx 0.17$ and $\alpha = 3$.

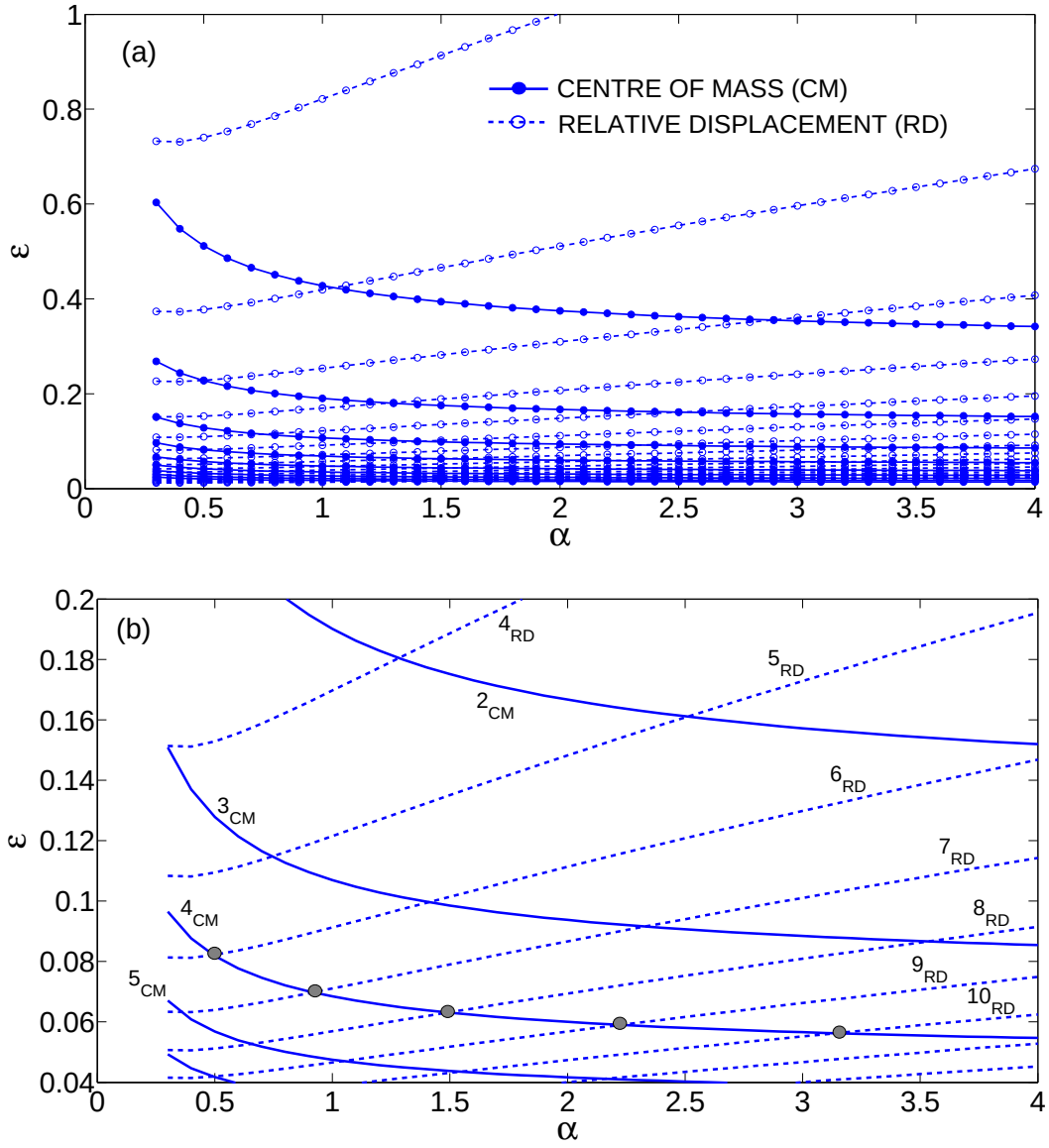

Figure 3.59: (a) Asymptotic eigenvalue spectra $\{\varepsilon_q^{CM}(\alpha)\}$ and $\{\varepsilon_r^{RD}(\alpha)\}$ of (3.56) and (3.57), respectively, derived by WKB approximation; crossings of these spectral lines correspond to realization of solitary waves in the 1: 2 dimer; (b) detail of (a) (solid lines correspond to CM spectrum and dotted to the RD spectrum).

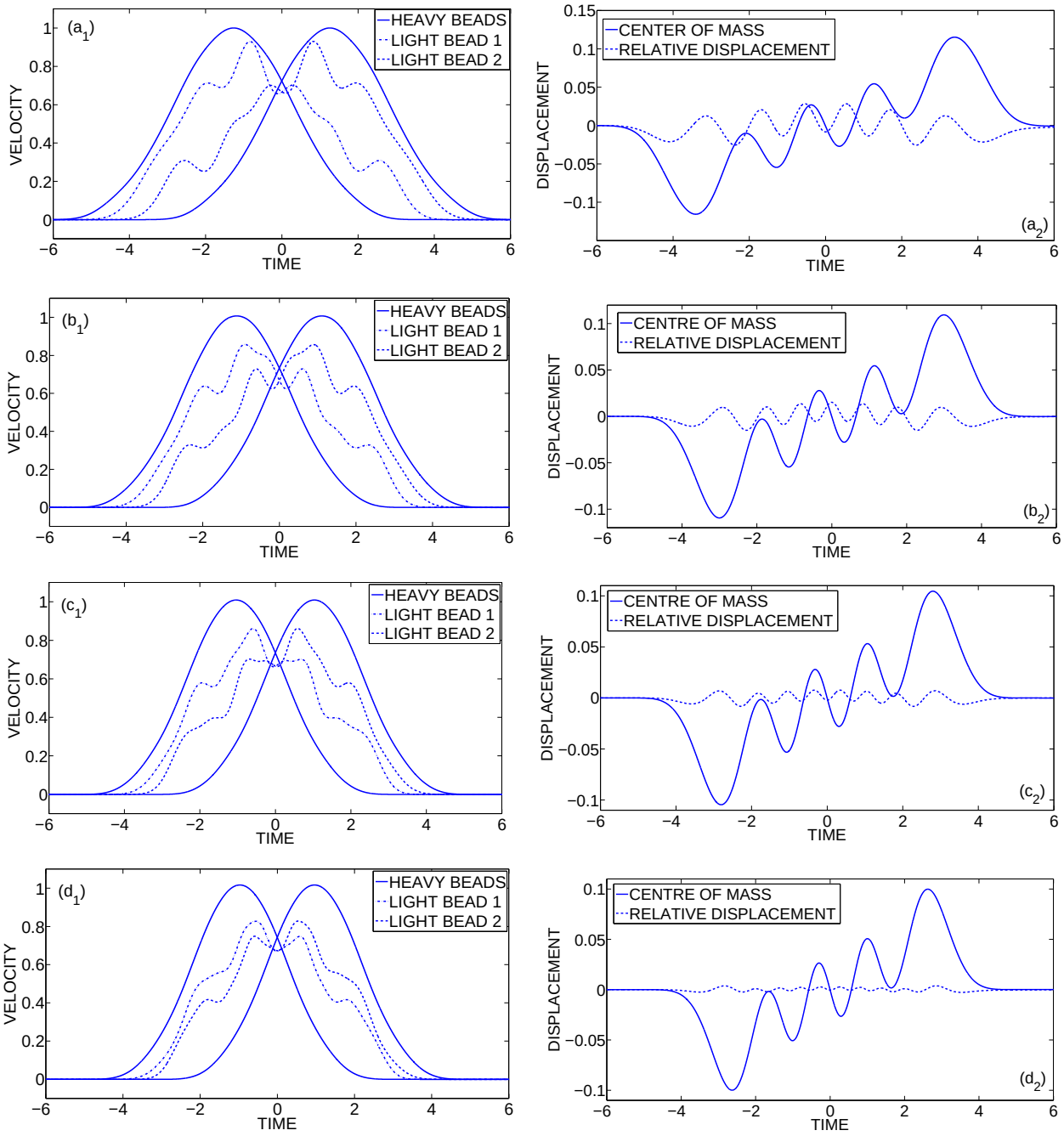

Figure 3.60: Solitary wave in the 1: 2 dimer chain with (a) $\varepsilon = 0.082$ and $\alpha = 0.4935$; (b) $\varepsilon = 0.06664$ and $\alpha = 1.037$; (c) $\varepsilon = 0.05969$ and $\alpha = 1.822$; (d) $\varepsilon = 0.05389$ and $\alpha = 3.925$, (1) Velocity profiles of heavy and light beads of an arbitrary periodic set, (2) fast oscillations of the center of mass and the relative displacement of the light beads.

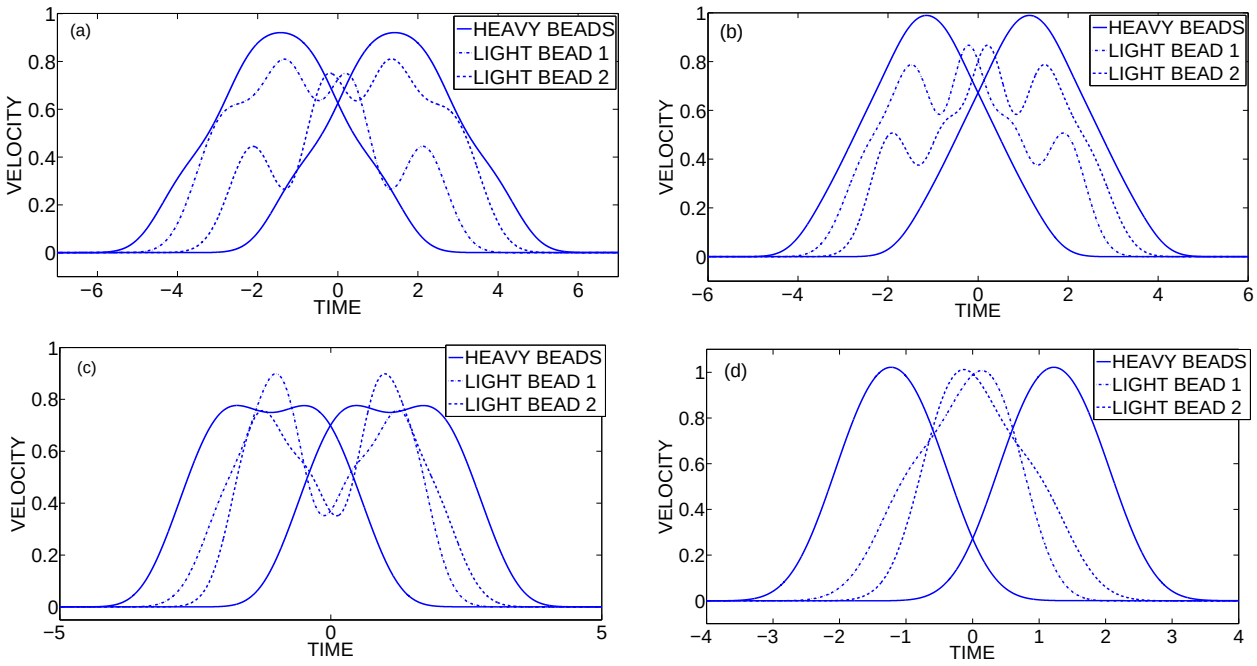

Figure 3.61: Numerically computed solitary waves in 1: 2 dimer chains with parameters, (a) $\varepsilon = 0.175$ and $\alpha = 0.3795$; (b) $\varepsilon = 0.1169$ and $\alpha = 1.122$; (c) $\varepsilon = 0.225$ and $\alpha = 3.569$; (d) $\varepsilon = 0.578$ and $\alpha = 6$; in all cases we depict the velocity profiles of heavy and light beads of an arbitrary periodic set.

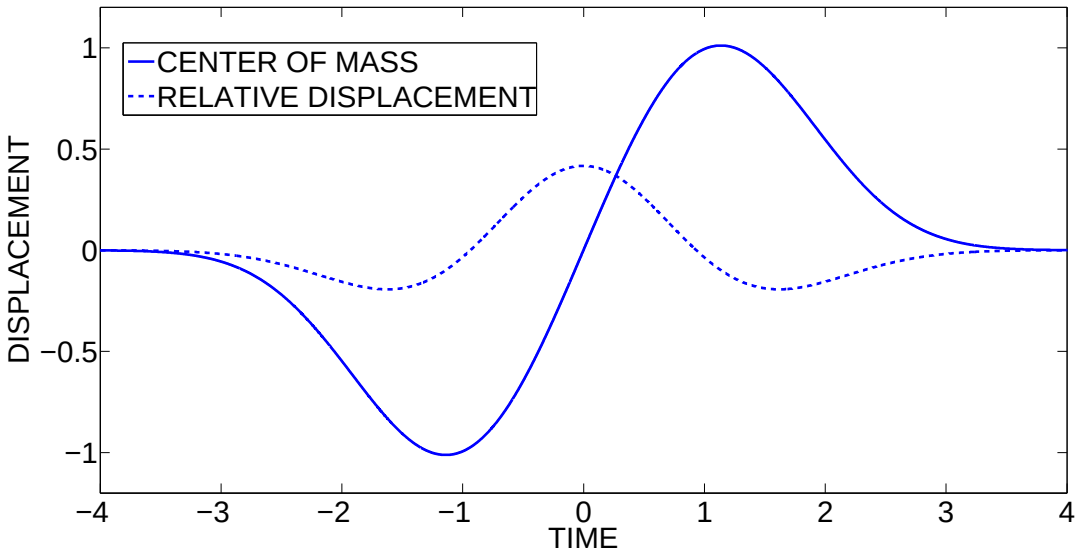

Figure 3.62: The Nesterenko solitary wave [41] in the limiting homogeneous granular chain with $\varepsilon = 1$ and $\alpha = 1$, representing pure slow oscillations.

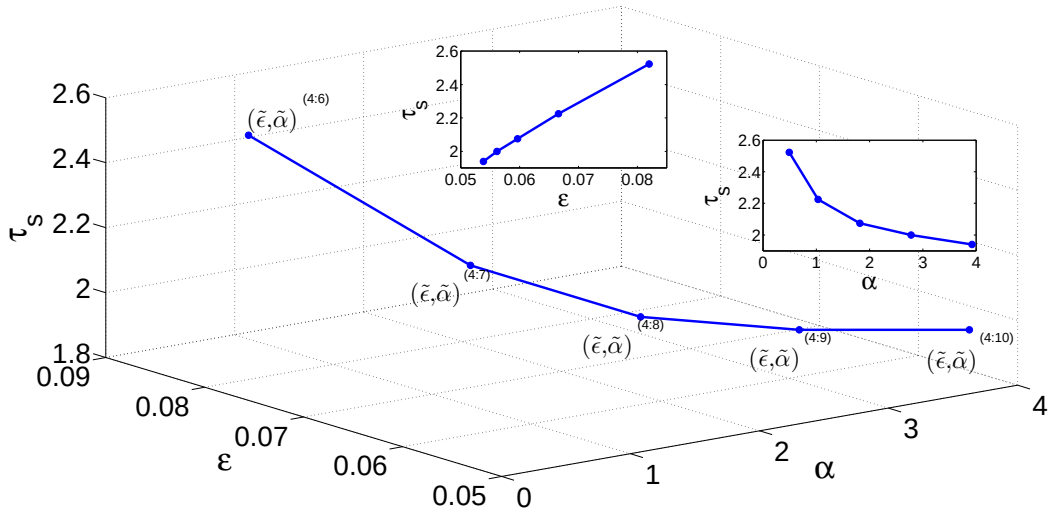

Figure 3.63: Normalized time shift for solitary wave propagation between adjacent heavy beads for the family of solitary waves listed in Table 3.7.

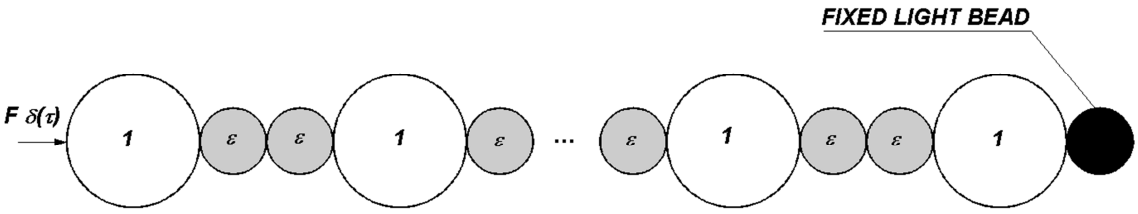

Figure 3.64: Schematic of a finite dimensional 1: 2 dimer granular chain.

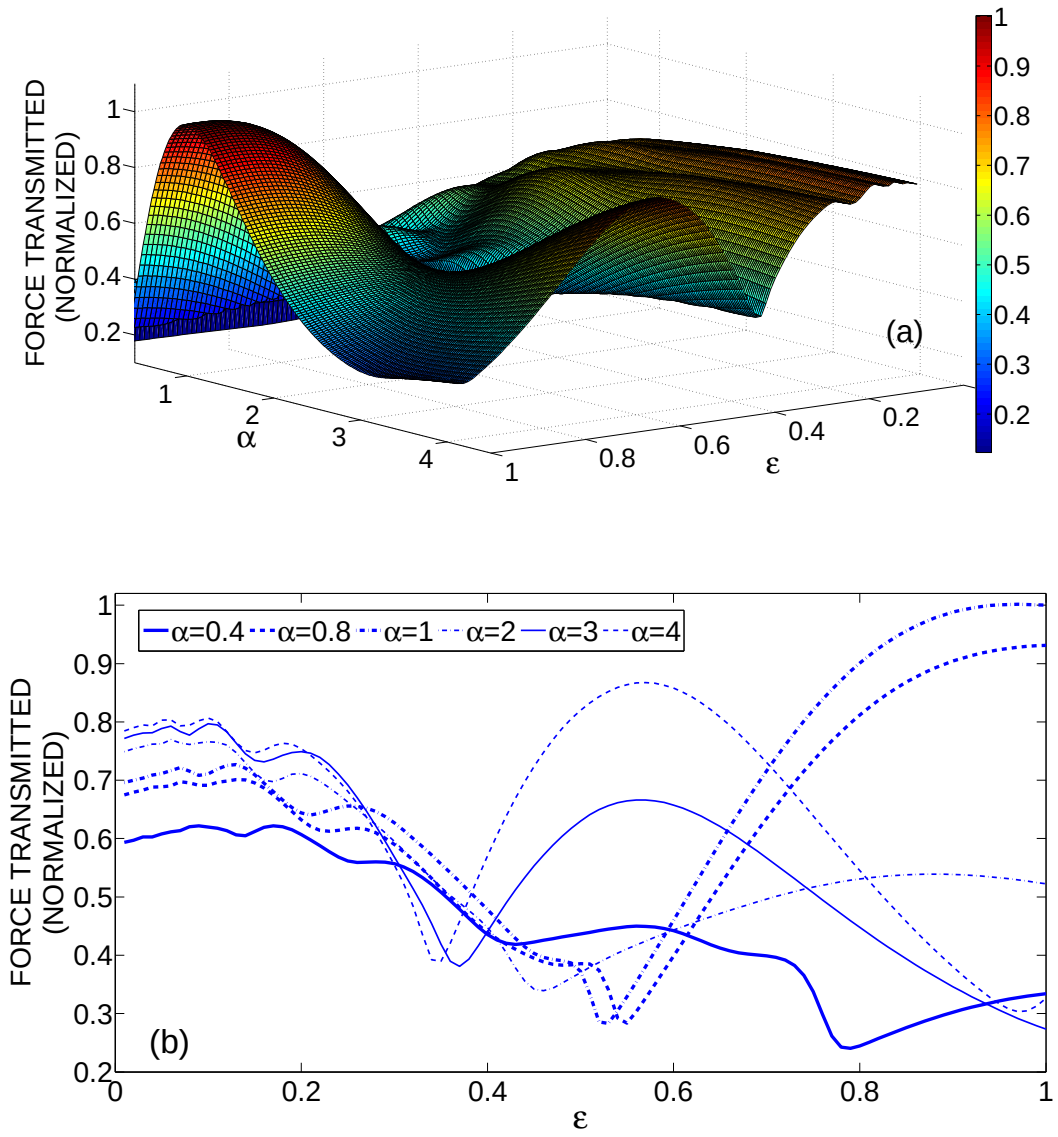

Figure 3.65: Normalized transmitted force in the finite 1: 2 dimer chain: (a) Transmitted force surface, (b) 'slices' of the surface corresponding to fixed α.

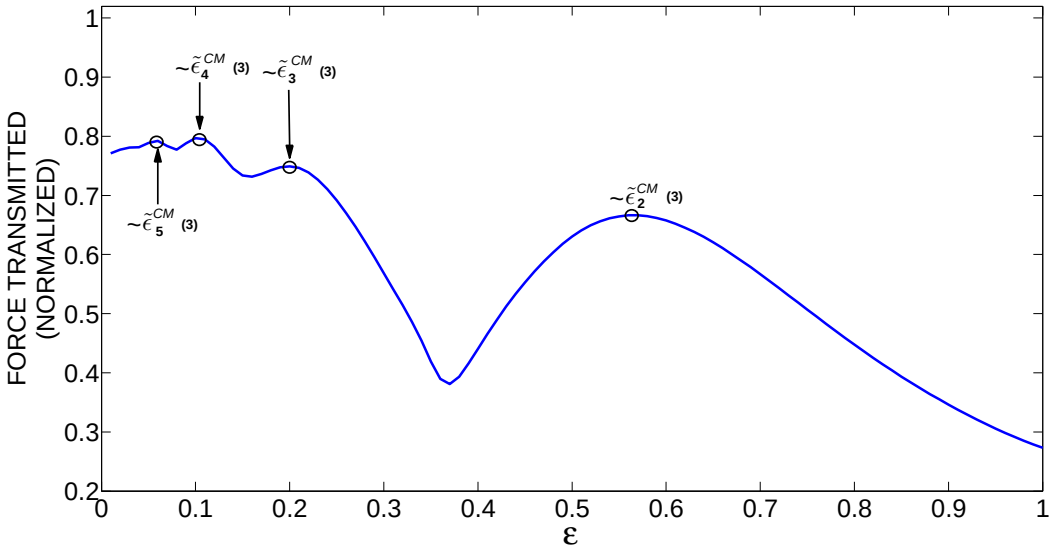

Figure 3.66: Force transmitted curve in 1: 2 dimer chain for $\alpha = 3$.

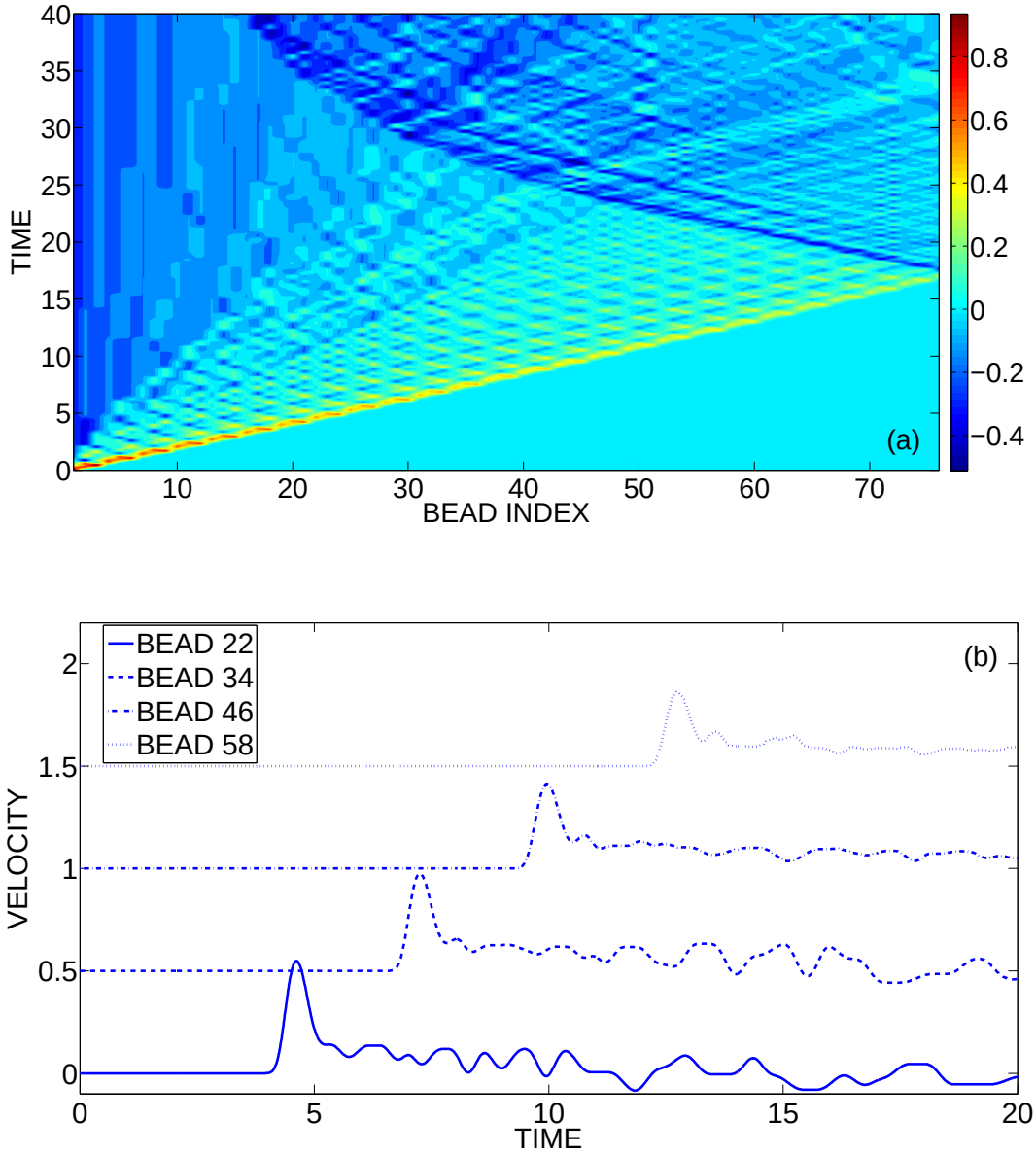

Figure 3.67: Dynamics of the 1: 2 dimer chain with $\varepsilon = 0.37$ and $\alpha = 3$, (a) Velocity contours of the system in the space-time plane; (b) velocity time series of selected heavy beads.

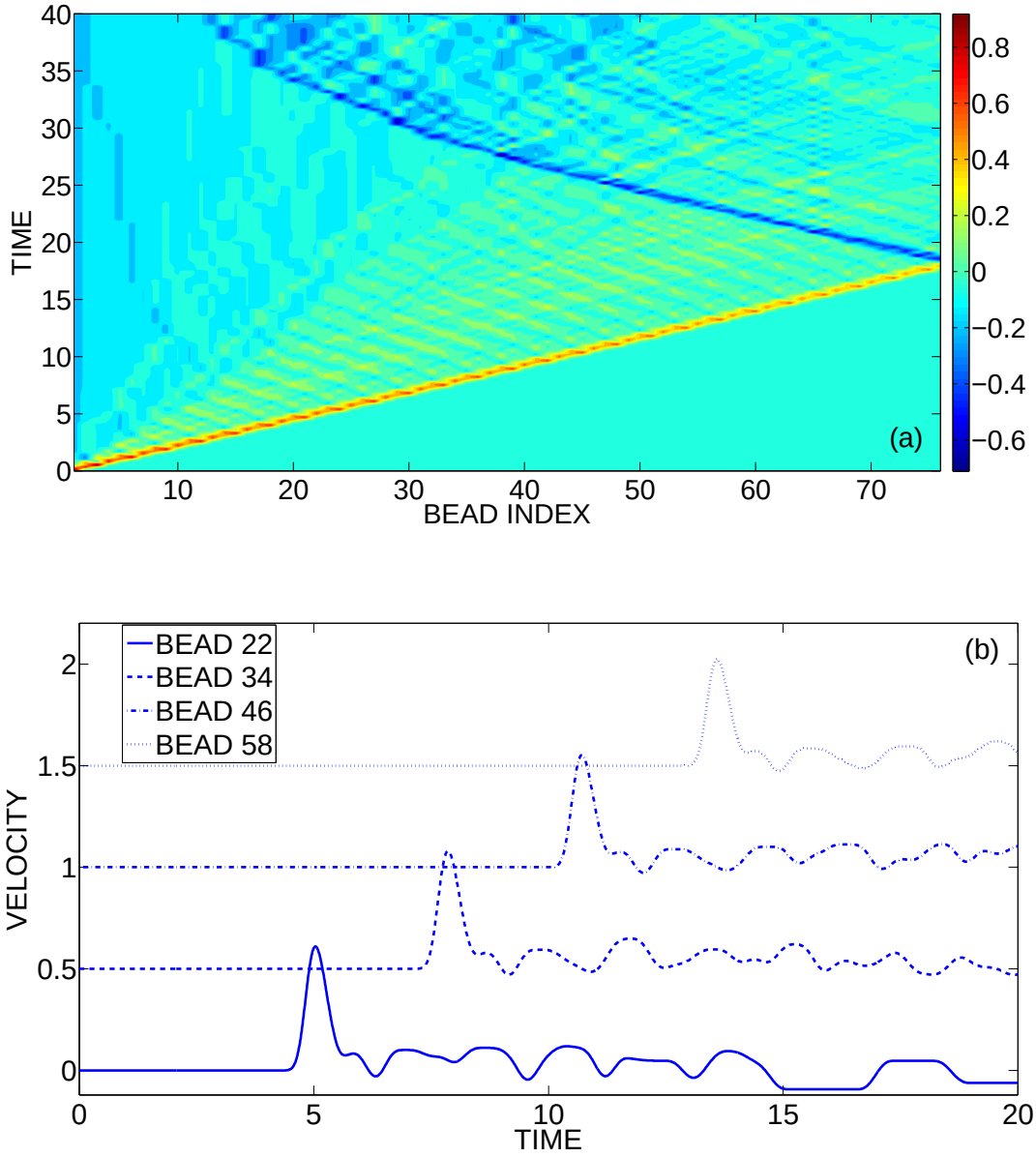

Figure 3.68: Dynamics of the 1: 2 dimer chain with for $\varepsilon = 0.5675$ and $\alpha = 3$, (a) Velocity contours of the system in the space-time plane; (b) velocity time series of selected heavy beads.

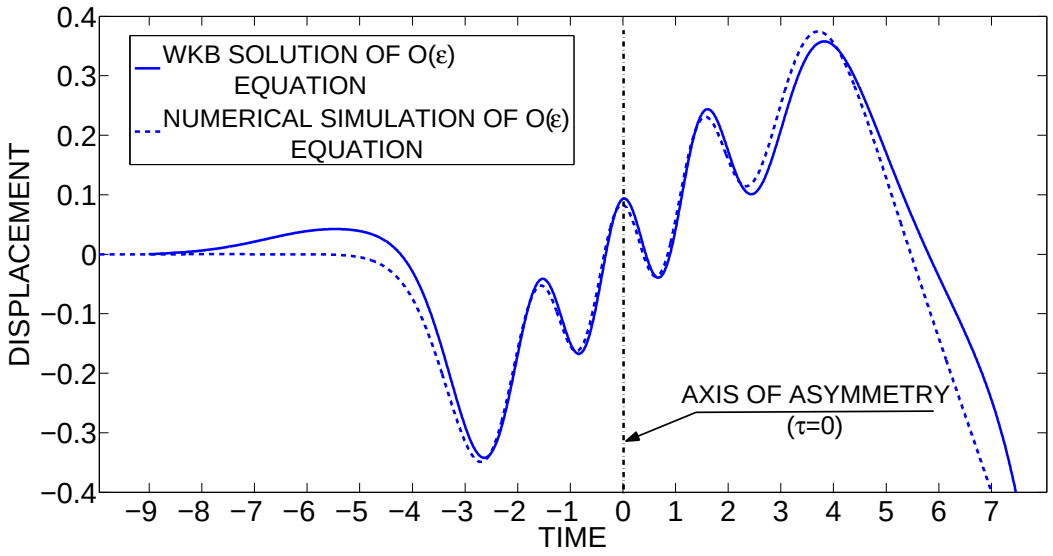

Figure 3.69: Comparison of WKB approximation (3.68) for $\tilde{\varepsilon}_4^{CM}(3) = 0.068$ and the numerical simulation of the LBVP (3.65) for $\varepsilon_4^{CM} \approx 0.0699$ and $\alpha = 3$.

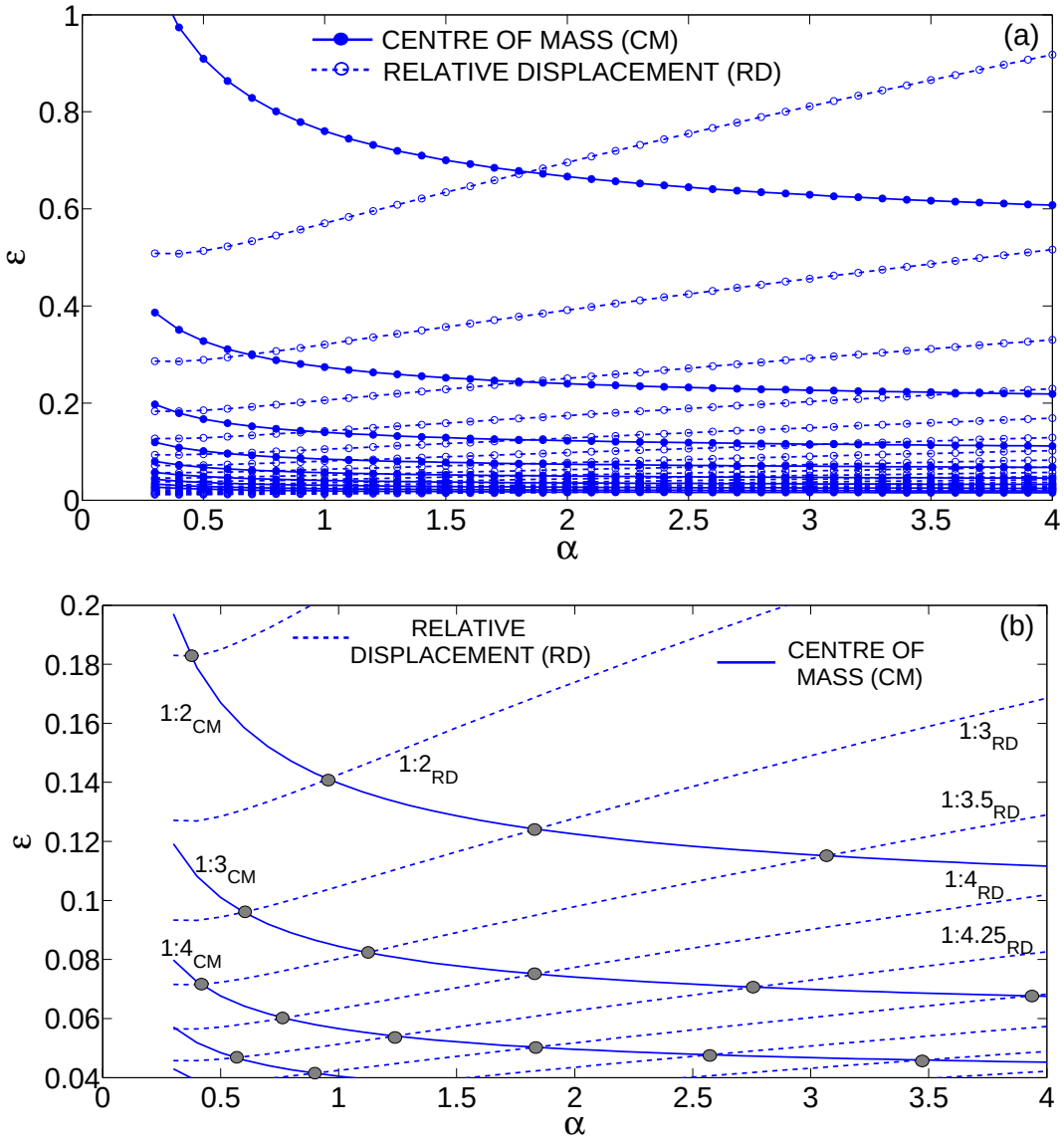

Figure 3.70: Global diagram of resonances in the 1: 2 dimer, (a) WKB asymptotic spectra $\{\varepsilon_q^{CM}(\alpha)\}$ and $\{\varepsilon_s^{RD}(\alpha)\}$ of (3.70) and (3.72), respectively, with crossings corresponding to resonances; (b) detail of (a).

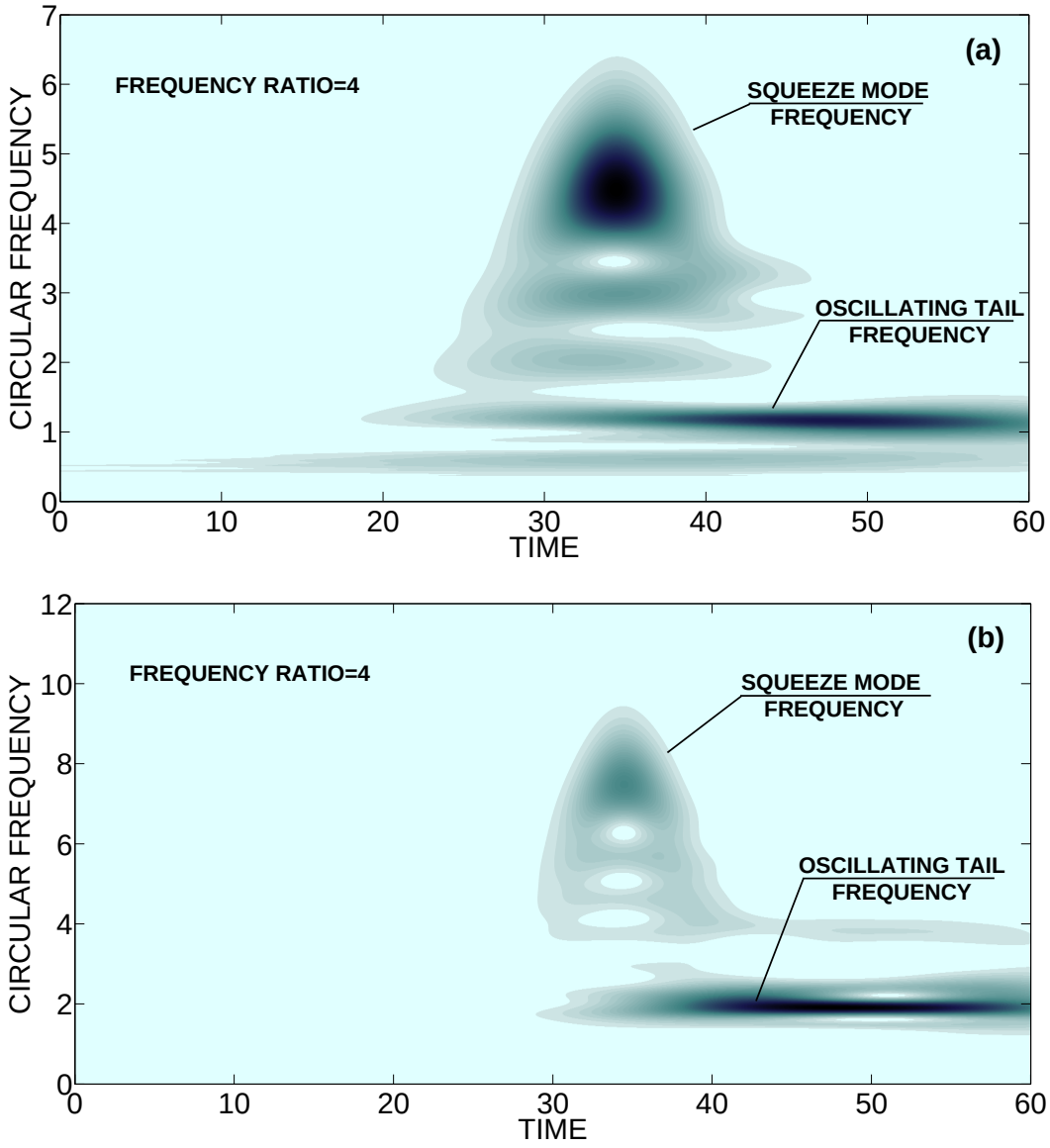

Figure 3.71: Exact 1:4 resonance for the 1: 2 dimer with $(\alpha, \varepsilon) = (0.8, 0.052)$ on the $1{:}\,4_{CM}$ curve shown in Figure 3.70b; wavelet transform spectrum of the response of (a) the CM; (b) the RD of the pair of light beads.

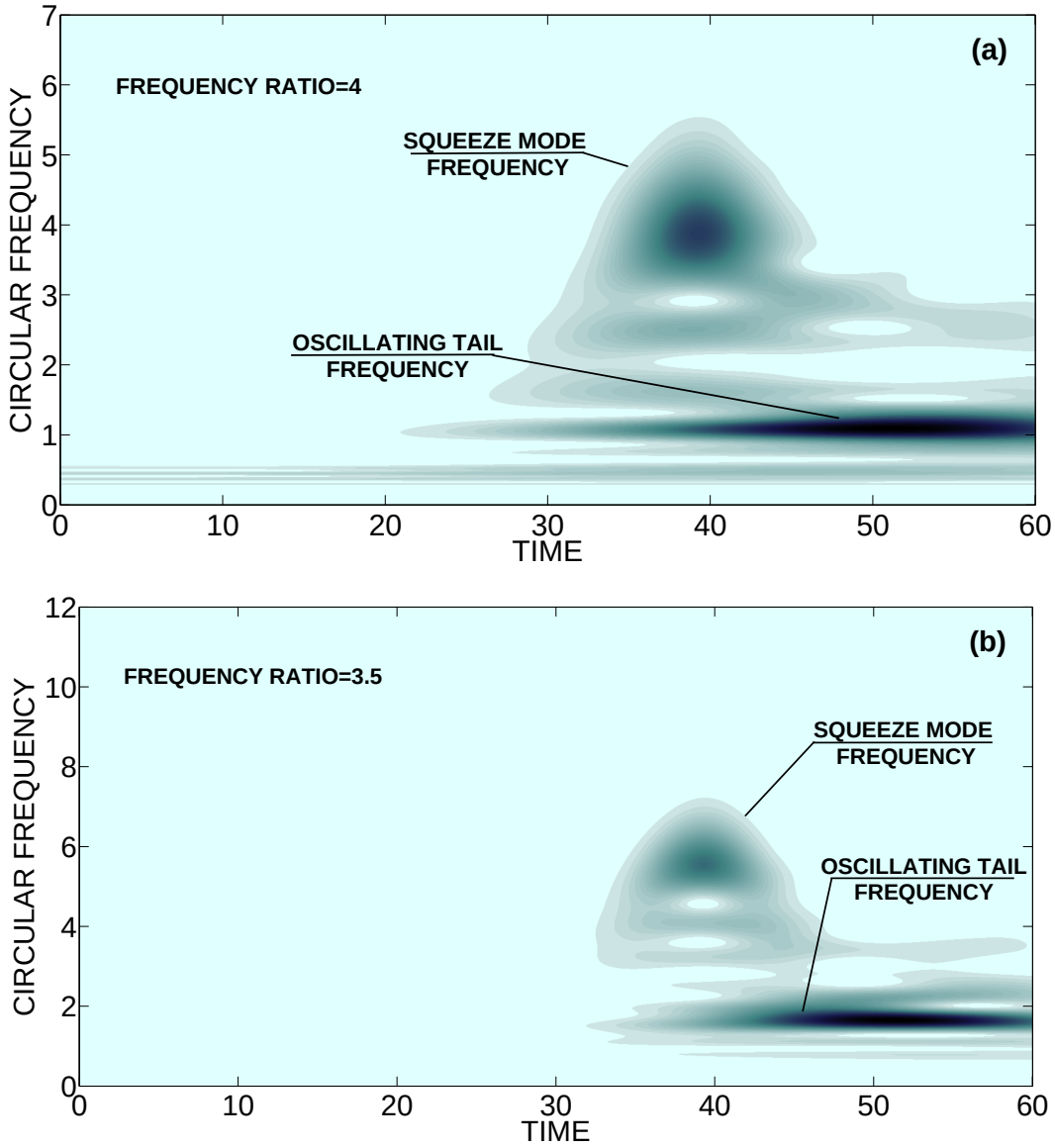

Figure 3.72: Resonance in 1: 2 dimer with $(\alpha, \varepsilon) = (0.4, 0.069)$ on the $1{:}\,4_{CM}$ curve shown in Figure 3.70b; wavelet transform spectrum of the response of (a) the CM; (b) the RD of the pair of light beads.

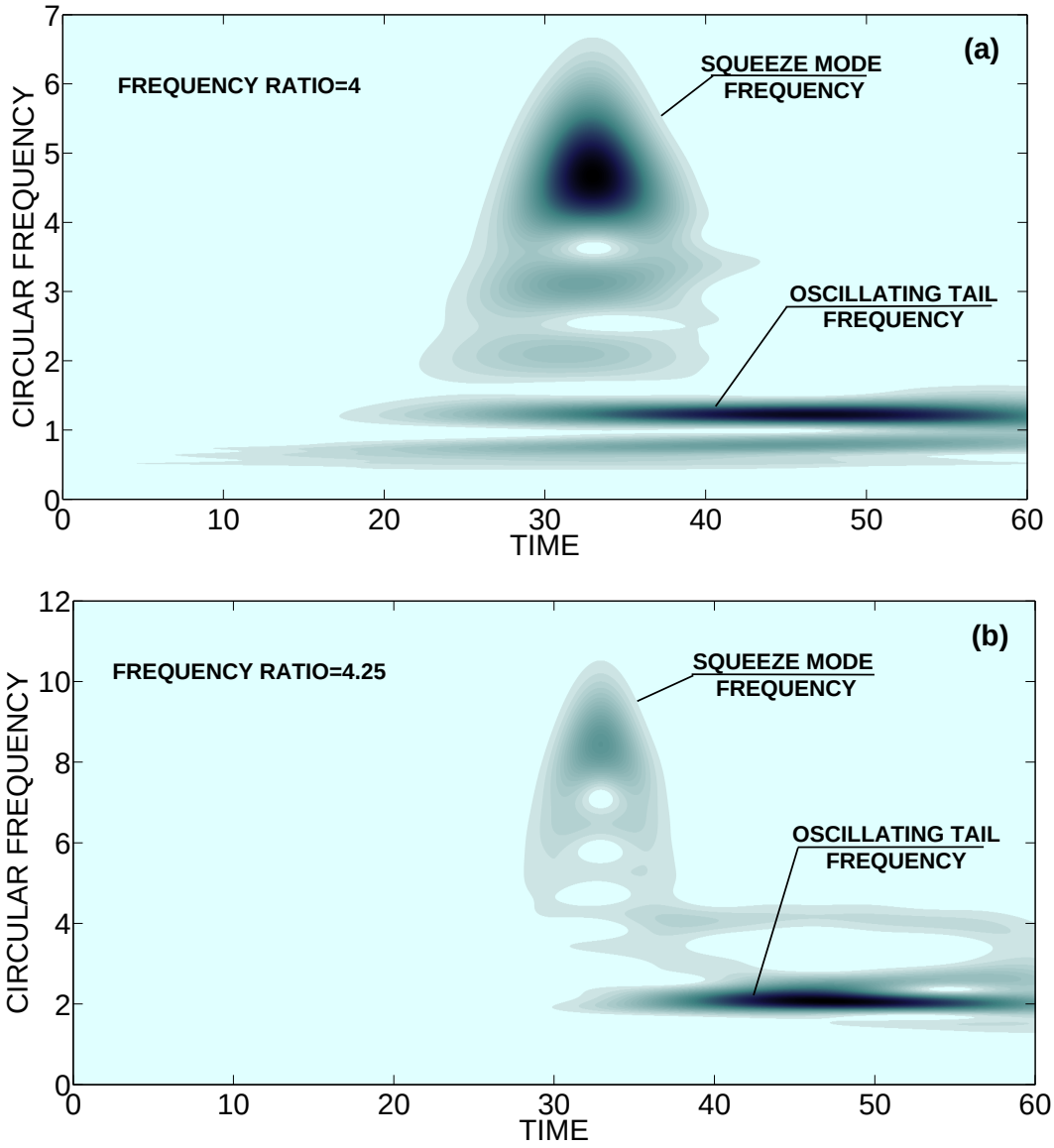

Figure 3.73: Resonance in 1: 2 dimer with $(\alpha, \varepsilon) = (1.1, 0.048)$ on the $1: 4_{CM}$ curve shown in Figure 3.70b; wavelet transform spectrum of the response of (a) the CM; (b) the RD of the pair of light beads.

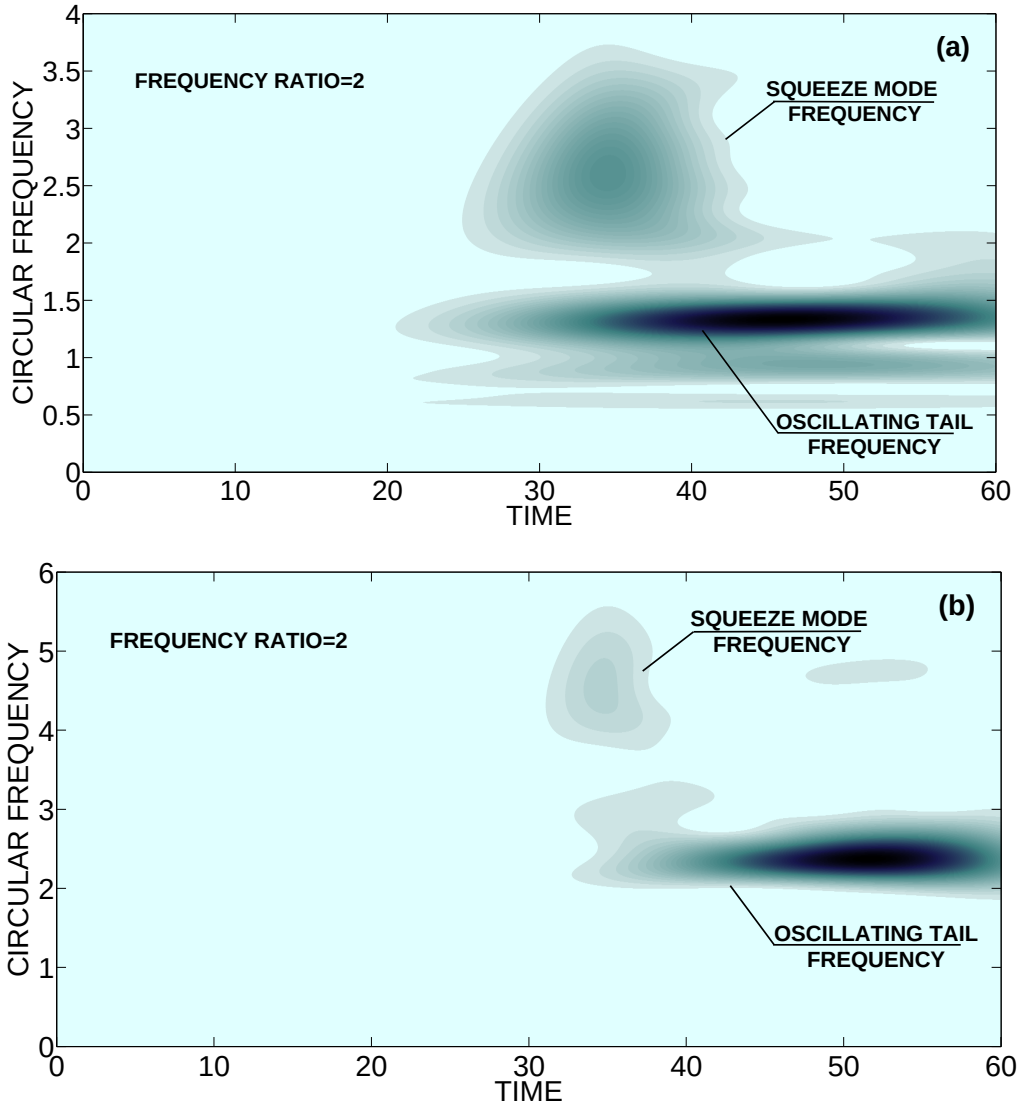

Figure 3.74: Exact 1: 2 resonance for the 1: 2 dimer with $(\alpha, \varepsilon) = (1.364, 0.1715)$; wavelet transform spectrum of the response of (a) the CM; (b) the RD of the pair of light beads.

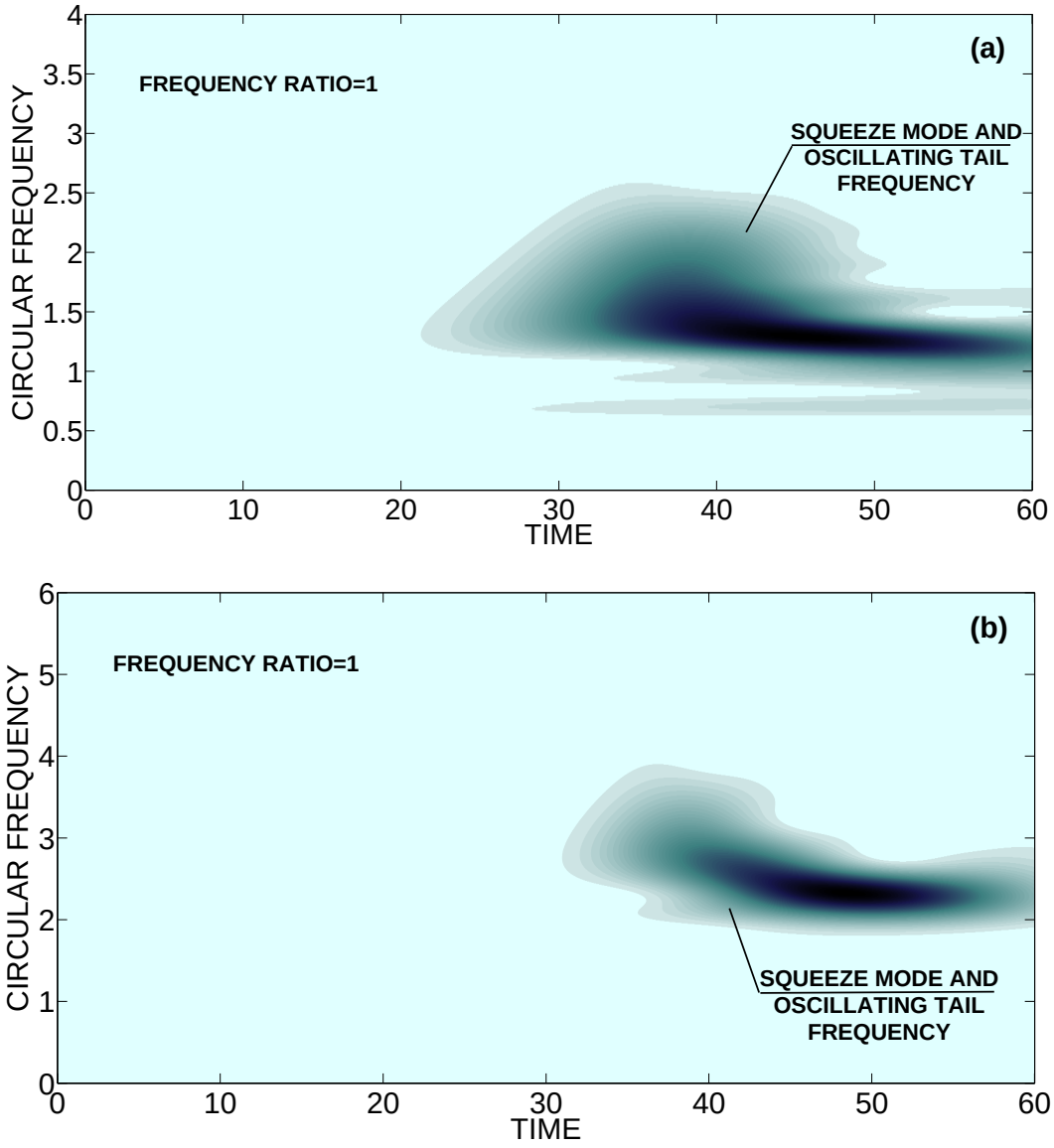

Figure 3.75: Exact 1: 1 resonance for the 1: 2 dimer with $(\alpha, \varepsilon) = (2.2, 0.42)$; wavelet transform spectrum of the response of (a) the CM; (b) the RD of the pair of light beads.

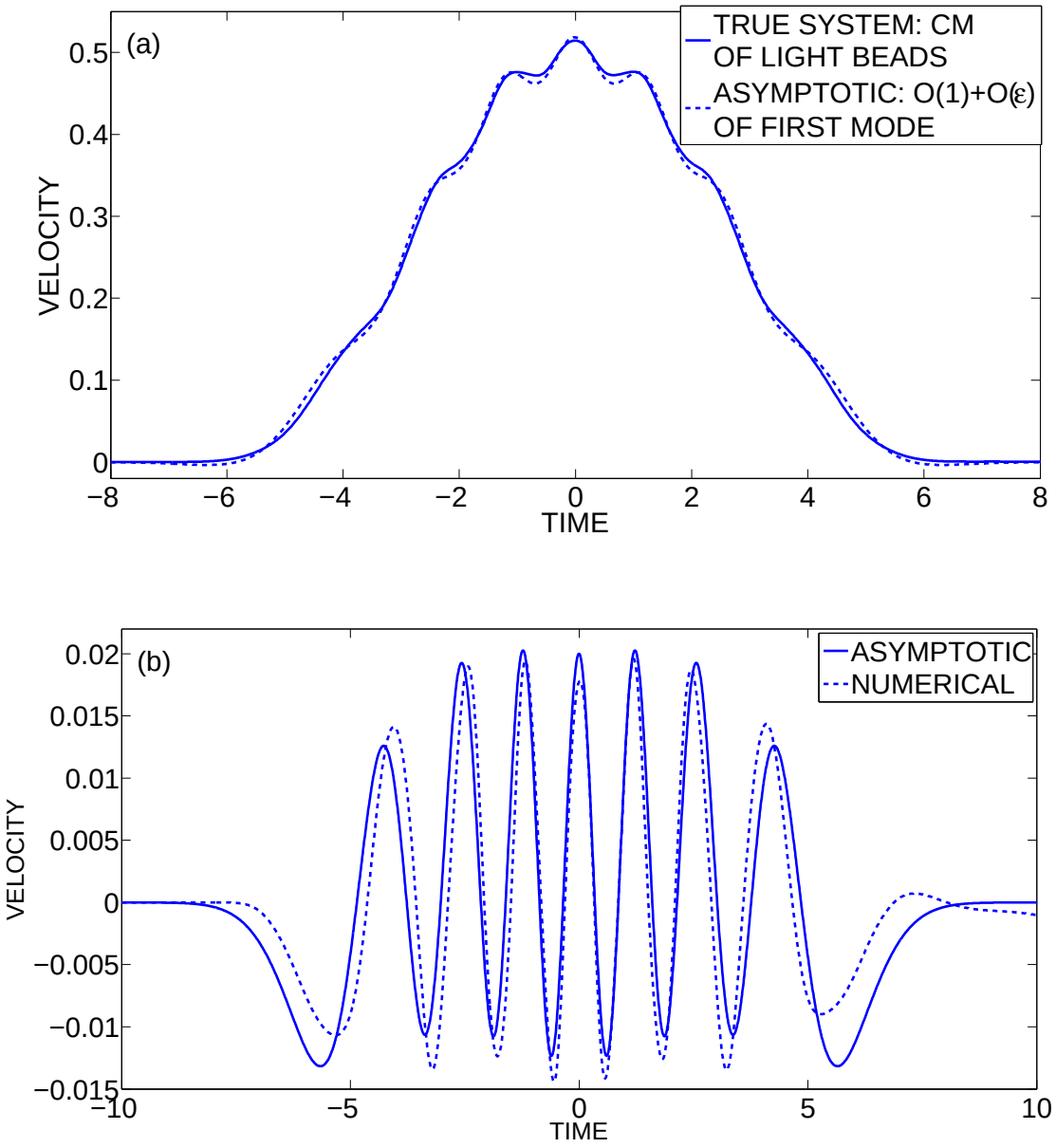

Figure 3.76: Comparison between the asymptotic model (3.74) and direct numerical simulations for the 1: 3 dimer with $\varepsilon = 0.0207$ and $\alpha = 1$, (a) Fast frequency component of the response of the center-of-mass of the light beads 26-28; (b) corresponding velocity of the center-of-mass of the same light beads.

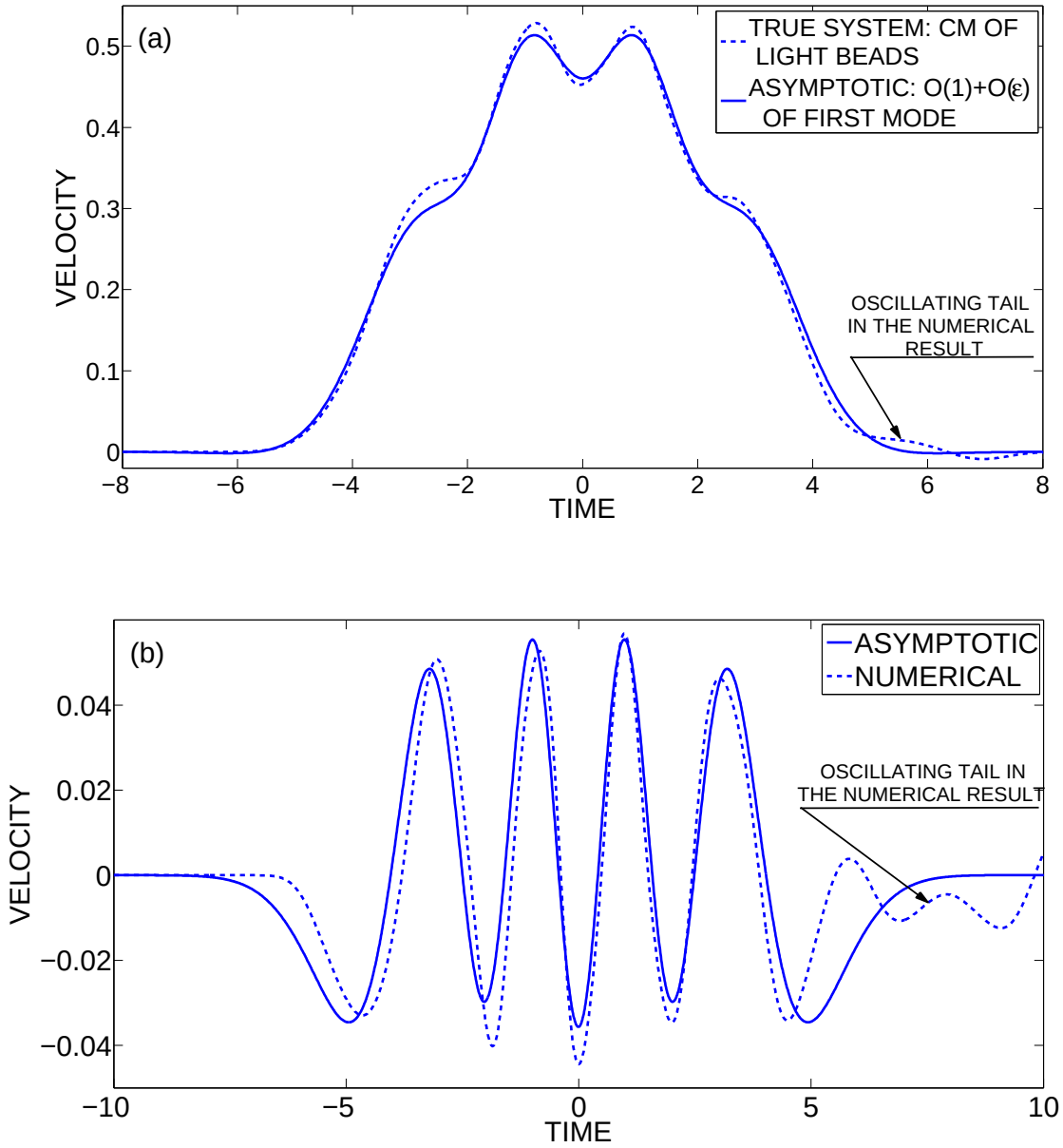

Figure 3.77: Comparison between the asymptotic model (3.74) and direct numerical simulations for the 1: 3 dimer with $\varepsilon \approx 0.05275$ and $\alpha = 1$, (a) Fast frequency component of the response of the center-of-mass of the light beads 26-28; (b) corresponding velocity of the center-of-mass of the same light beads.

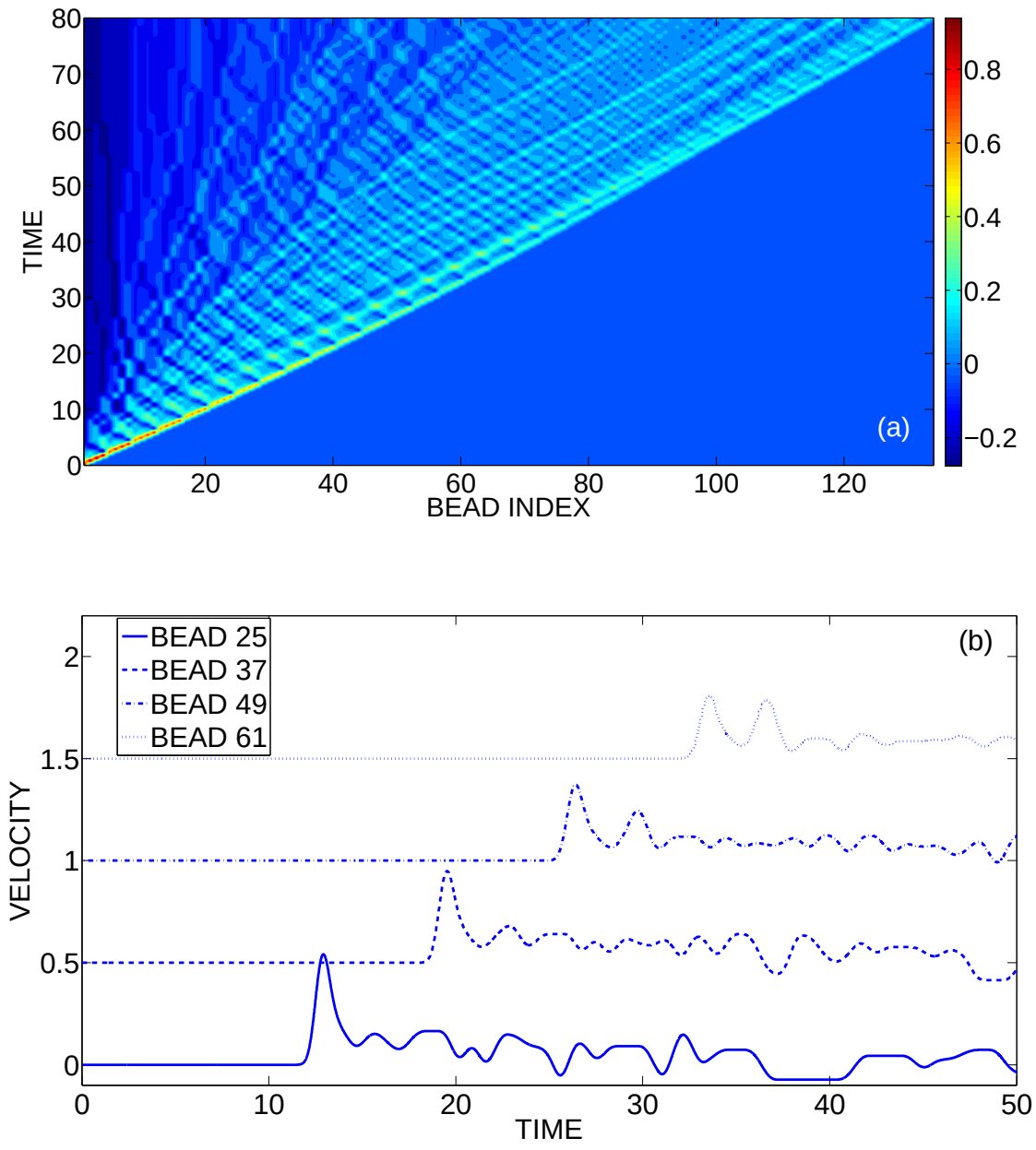

Figure 3.78: Normalized bead velocities of a 1: 3 dimer chain with $\varepsilon = 0.49$ and $\alpha = 1$, (a) Space-time plot; (b) Velocity time series of selected intermediate heavy beads (time series are vertically displaced for clarity).

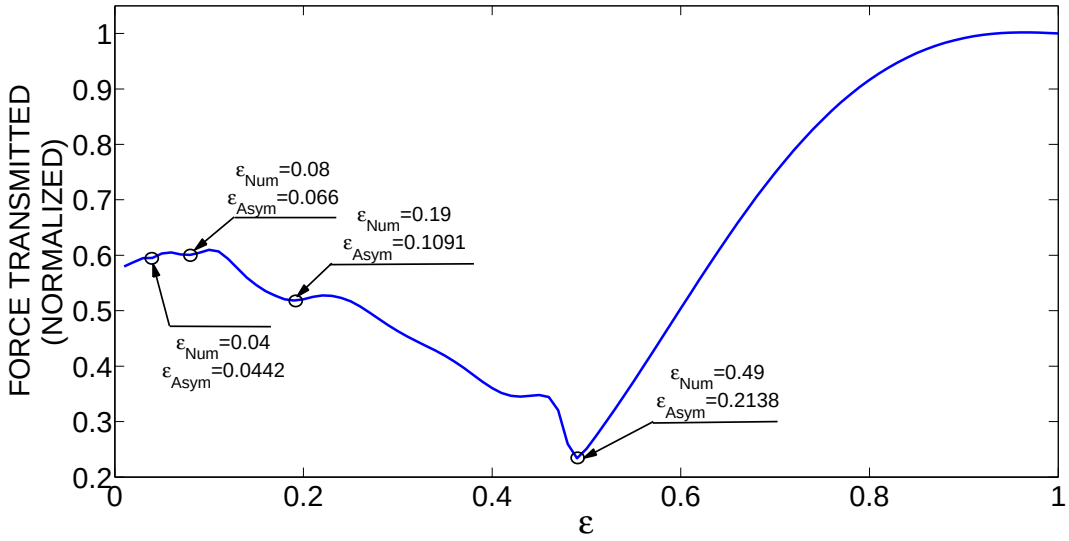

Figure 3.79: Normalized transmitted force in a finite 1: 3 dimer chain for $\alpha = 1$, with superimposed the asymptotic spectra $\{\varepsilon_r^l(1)\}$ of the LBVP (3.76); for comparison we indicate the values of the mass ratio ε where valleys of the plot occur.

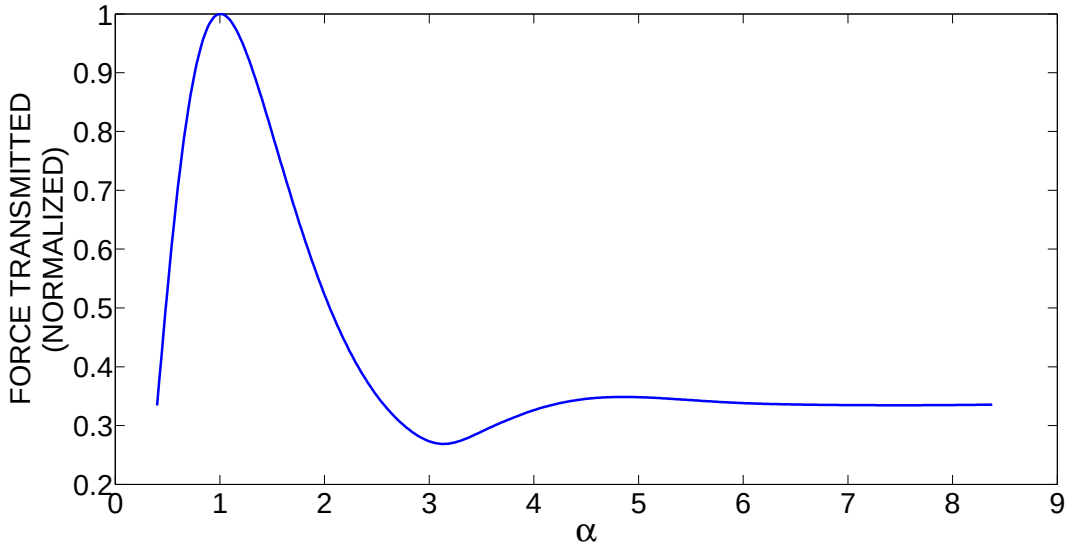

Figure 3.80: Normalized force transmitted in the 1: 2 dimer chain with $\varepsilon = 1$ and high stiffness ratio α; note the strong pulse attenuation compared to the homogeneous granular chain with $\alpha = 1$.

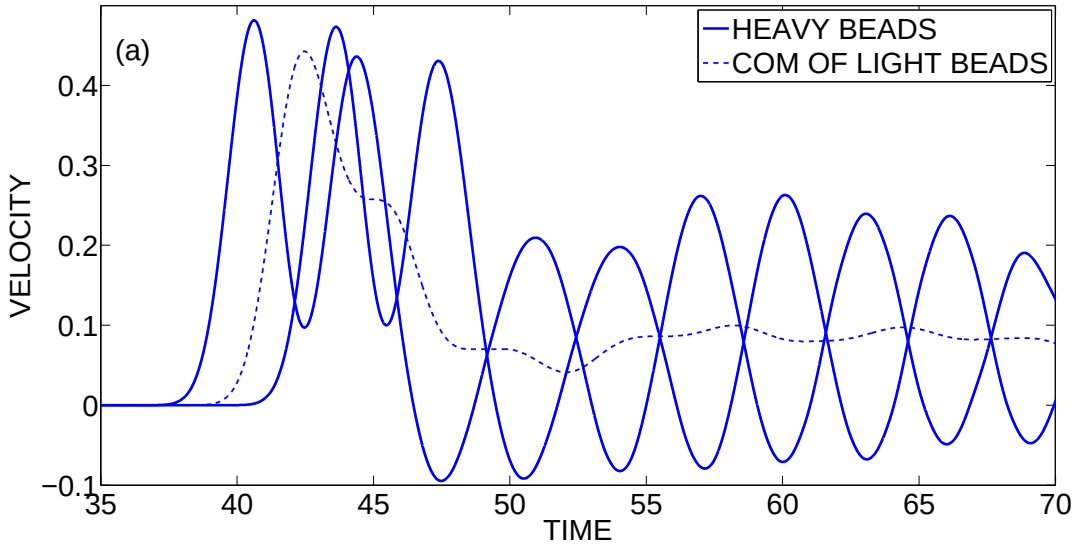

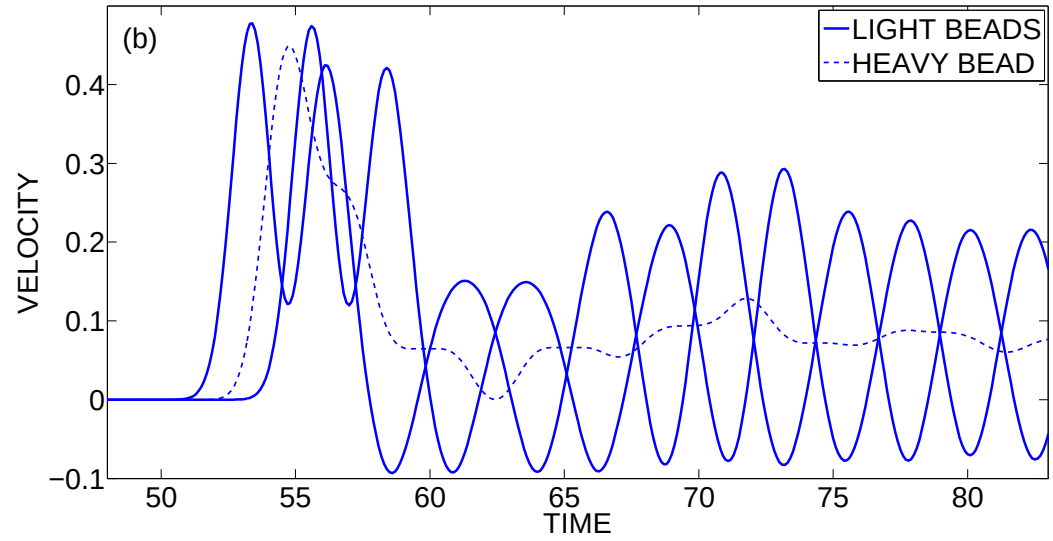

Figure 3.81: Comparison of velocity responses of, (a) a 1: 2 dimer with $\varepsilon = 1$ and $\alpha \approx 114$; (b) the corresponding effective 1: 1 dimer with effective mass ratio equal to 0.5.

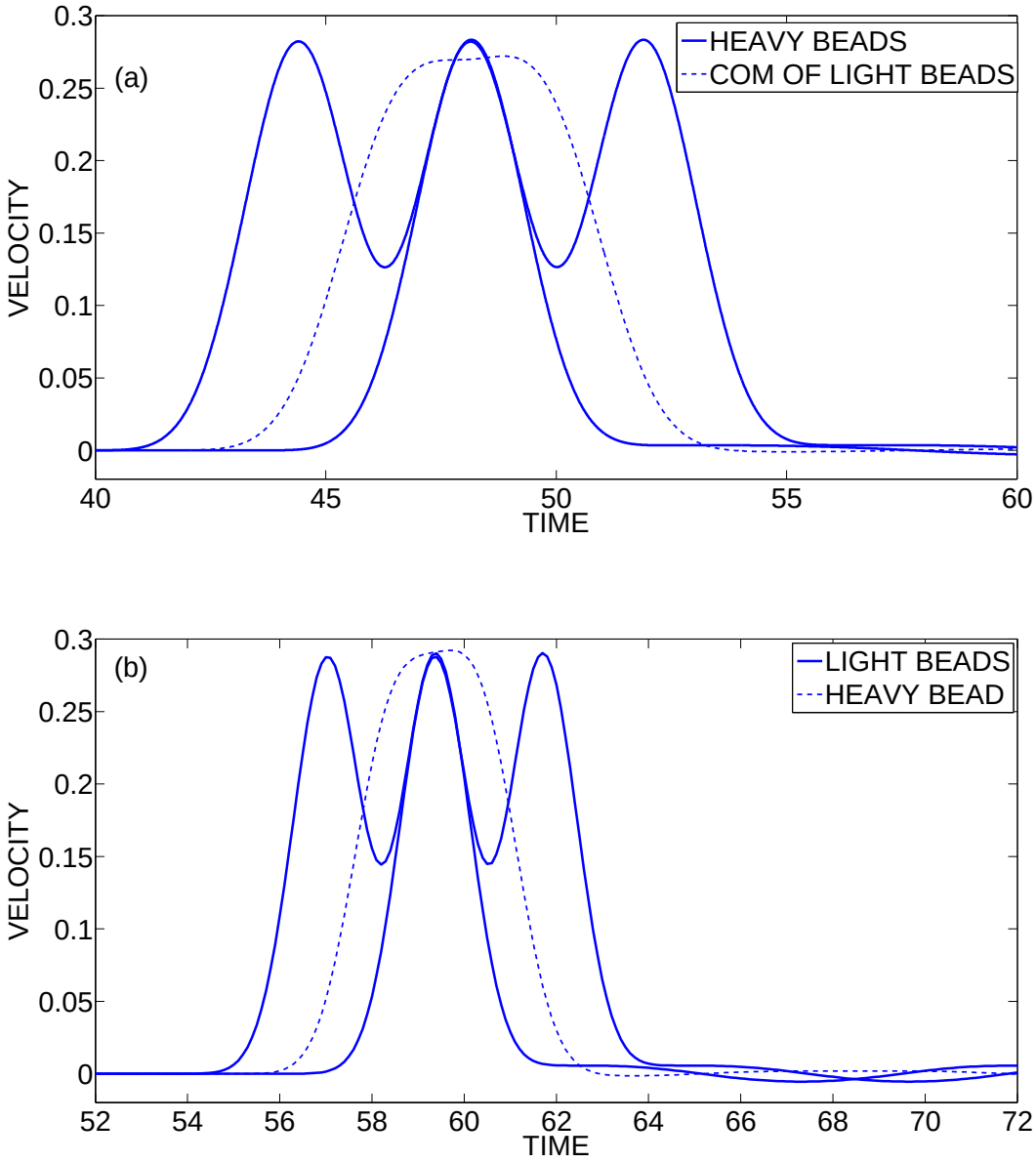

Figure 3.82: Comparison of velocity responses of, (a) a 1: 3 dimer with $\varepsilon = 1$ and $\alpha \approx 114$; (b) the corresponding effective 1: 1 dimer with mass ratio equal to 1/3.

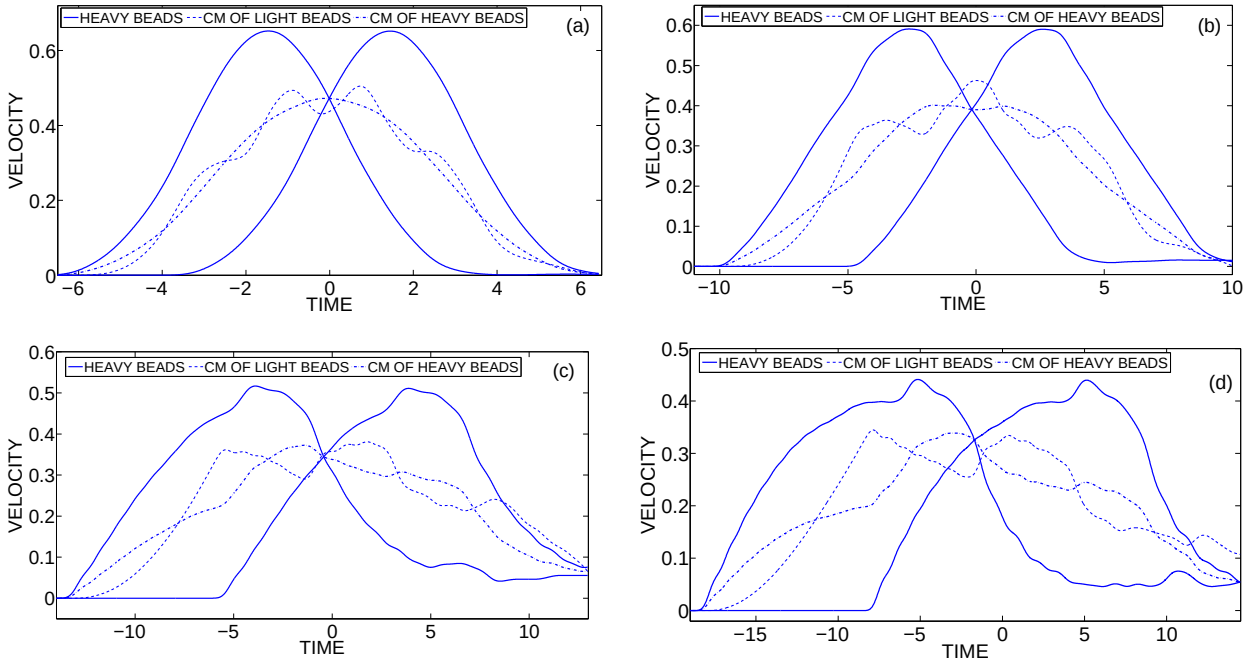

Figure 3.83: Velocity responses of periodic sets of 1: N dimers with $\varepsilon = 0.05$ and $\alpha = 1$ and (a) $N = 3$; (b) $N = 8$; (c) $N = 14$; (d) $N = 20$, note increasing inaccuracy of the asymptotics as $N\varepsilon$ increases.

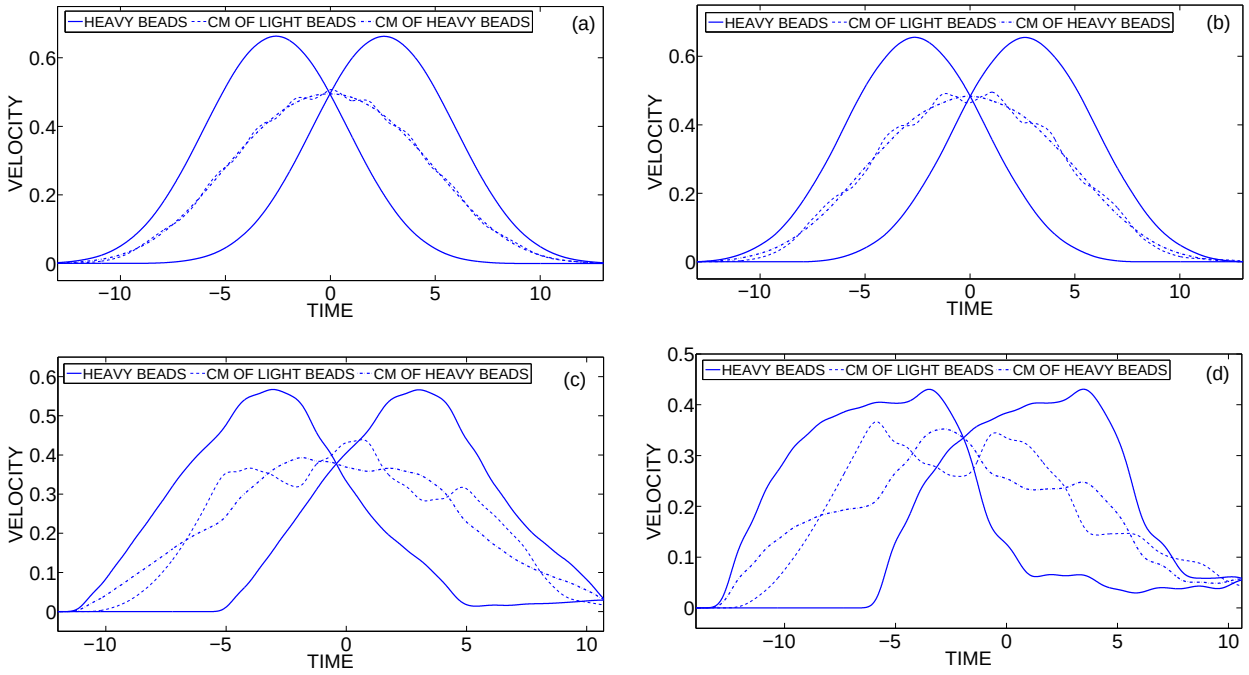

Figure 3.84: Velocity responses of a periodic set of the 1: 10 dimer with $\alpha = 1$ and (a) $\varepsilon = 0.005$; (b) $\varepsilon = 0.01$; (c) $\varepsilon = 0.05$; (d) $\varepsilon = 0.1$, note increasing inaccuracy of the asymptotics as $N\varepsilon$ increases.

3.4 Tables

Table 3.1: Parameter values ε_n for realization of solitary waves in the dimer

n	Numerical simulation of the $O(\varepsilon)$ fast dynamics (3.11) ε_n	Numerical simulation of system (3.3) ε_n	WKB approximation (3.20) $\hat{\varepsilon}_n$
2	0.82835	1.0	0.56477
3	0.278115	0.3428	0.25101
4	0.146747	0.1548	0.1412
5	0.091702	0.0901	0.09036
6	0.062913	0.0615	0.06275
16	0.0086818	0.00868	0.0088245

Table 3.2: Resonances in the dimer system (3.3).

Resonance $1:n$	Asymptotic Model (3.15)			Numerical Simulation of System (3.3)		
	$\hat{\varepsilon}_R^{(1:n)}$	$\widehat{\omega}_S$	$\widehat{\omega}_T$	$\varepsilon_R^{(1:n)}$	ω_S	ω_T
1:1	0.420	2.545	2.545	0.590	1.37	1.28
1:2	0.205	3.642	1.821	0.240	2.77	1.42
1:3	0.111	4.950	1.650	0.120	4.0	1.45
1:4	0.078	5.905	1.476	0.075	5.2	1.5
1:5	0.052	7.212	1.442			

Table 3.3: Binary Collision Model for Realization of 1: 1 Resonance in the Dimer

Event	Velocity of Heavy bead H1	Velocity of Light bead L1	Velocity of Heavy bead H2	Velocity of Light bead L2
$\tau = 0$	V_0	0	0	0
Bead H1 interacts with Bead L1	$\frac{V_0(1-\varepsilon)}{(1+\varepsilon)}$	$\frac{2V_0}{(1+\varepsilon)}$	0	0
Bead L1 interacts with Bead H2	$\frac{V_0(1-\varepsilon)}{(1+\varepsilon)}$	$-\frac{2V_0(1-\varepsilon)}{(1+\varepsilon)^2}$	$\frac{4\varepsilon V_0}{(1+\varepsilon)^2}$	0

Table 3.4: Force transmitted (in newton) and normalized force transmitted (in brackets) in different dimer chain setups for varying impact velocities

$\varepsilon \rightarrow$		$\varepsilon = 0.125$	$\varepsilon = 0.5$	$\varepsilon = 1$
$\dot{x}_1(0) = 0.2102\ m/s$	$F_{Tr}^{\max}$ ($F_{Tr\_norm}^{\max}$)	256 (0.875)	199.77 (0.683)	299.56 (1.02)
	$F_{Tr}^{\min}$ ($F_{Tr\_norm}^{\min}$)	243 (0.811)	196.37 0.655)	292.37 (0.976)
$\dot{x}_1(0) = 0.3\ m/s$	$F_{Tr}^{\max}$ ($F_{Tr\_norm}^{\max}$)	395.6 (0.864)	307 (0.67)	464.57 (1.0158)
	$F_{Tr}^{\min}$ ($F_{Tr\_norm}^{\min}$)	385 (0.829)	298.8 (0.643)	457.77 (0.9843)
$\dot{x}_1(0) = 0.4195\ m/s$	$F_{Tr}^{\max}$ ($F_{Tr\_norm}^{\max}$)	569.97 (0.855)	460.2 (0.69)	684.3 (1.026)
	$F_{Tr}^{\min}$ ($F_{Tr\_norm}^{\min}$)	539.55 (0.788)	450.3 (0.658)	666.78 (0.974)

Table 3.5: Spectrum of eigenvalues of the LBVP (3.56) for $\alpha = 3$.

$\tilde{\varepsilon}_q^{CM}(3)$ [Direct numerical simulation of (3.56)]	q	$\varepsilon_q^{CM}(3)$ [WKB approximations (3.59) and (3.60)]
0.03941	6	0.03923
0.05744	5	0.056597
0.09192	4	0.088433
0.1742	3	0.15721
0.51886	2	0.3537

Table 3.6: Spectrum of eigenvalues of the LBVP (3.57) for $\alpha = 3$.

$\tilde{\varepsilon}_r^{RD}(3)$ [Direct numerical simulation of (3.57)]	r	$\varepsilon_r^{RD}(3)$ [WKB approximations (3.62) and (3.63)]
0.039417	13	0.0401
0.04599	12	0.0467
0.05463	11	0.0552
0.06527	10	0.0662
0.07984	9	0.0809
0.09995	8	0.1011
0.12881	7	0.1298
0.17242	6	0.1728
0.24302	5	0.2414
0.36935	4	0.3606
0.6357	3	0.5960

Table 3.7: Analytical and numerical values of the normalized parameters for a family of solitary waves of the 1: 2 dimer chain

Analytical predictions (WKB approximation)	Numerical values
$(\varepsilon,\alpha)^{(4:6)} = (0.0822, 0.5)$	$(\tilde{\varepsilon},\tilde{\alpha})^{(4:6)} = (0.082, 0.4935)$ (Figure 3.60a)
$(\varepsilon,\alpha)^{(4:7)} = (0.06978, 0.9193)$	$(\tilde{\varepsilon},\tilde{\alpha})^{(4:7)} = (0.06664, 1.037)$ (Figure 3.60b)
$(\varepsilon,\alpha)^{(4:8)} = (0.06312, 1.492)$	$(\tilde{\varepsilon},\tilde{\alpha})^{(4:8)} = (0.05969, 1.822)$ (Figure 3.60c)
$(\varepsilon,\alpha)^{(4:9)} = (0.05904, 2.23)$	$(\tilde{\varepsilon},\tilde{\alpha})^{(4:9)} = (0.05616, 2.78)$ (Figure 3.56)
$(\varepsilon,\alpha)^{(4:10)} = (0.05631, 3.148)$	$(\tilde{\varepsilon},\tilde{\alpha})^{(4:10)} = (0.05389, 3.925)$ (Figure 3.60d)

Table 3.8: Truncated CM-spectrum $\{\varepsilon_q^{CM}(3)\}, q = 2, \ldots, 6$ for the 1: 2 dimer with $\alpha = 3$.

$\tilde{\varepsilon}_q^{CM}(3)$ [Direct numerical simulation of (3.65)]	$\hat{\varepsilon}_q^{CM}$ [Numerical simulation of the 1: 2 dimer system (Figure 3.64)]	q	$\varepsilon_q^{CM}(3)$ [WKB approximation (3.70)]
0.0324	0.033	6	0.0335
0.0452	0.0424	5	0.0468
0.068	0.08	4	0.0699
0.115	0.16	3	0.1155
0.2254	0.37	2	0.2264

Table 3.9: Truncated RD-spectrum $\{\varepsilon_s^{RD}(3)\}, s = 3, \ldots, 12$ for the 1: 2 dimer with $\alpha = 3$.

$\tilde{\varepsilon}_s^{RD}(3)$ [Direct numerical simulation of (3.66)]	s	$\varepsilon_s^{RD}(3)$ [WKB approximation (3.71-3.72)]
0.0497	12	0.0507
0.059	11	0.0603
0.071	10	0.073
0.088	9	0.0901
0.11	8	0.1141
0.143	7	0.149
0.196	6	0.2028
0.282	5	0.292
0.436	4	0.4563
0.79	3	0.8112

Table 3.10: Family of nonlinear resonances of the 1: 2 dimer on the $1: 4_{CM}$ curve of Figure 3.70b.

WKB approximation	Numerical simulation	CM / RD frequency ratios
$(\varepsilon, \alpha) = (0.0738, 0.422)$	$(\varepsilon, \alpha) = (0.069, 0.4)$	1:4 / 4:14 (Figure 3.72)
$(\varepsilon, \alpha) = (0.06, 0.7757)$	$(\varepsilon, \alpha) = (0.052, 0.8)$	1:4 / 4:16 (Figure 3.71)
$(\varepsilon, \alpha) = (0.054, 1.241)$	$(\varepsilon, \alpha) = (0.048, 1.1)$	1:4 / 4:17 (Figure 3.73)
$(\varepsilon, \alpha) = (0.0502, 1.844)$	$(\varepsilon, \alpha) = (0.045, 1.7)$	1:4 / 4:18
$(\varepsilon, \alpha) = (0.04778, 2.563)$	$(\varepsilon, \alpha) = (0.042, 2.3)$	1:4 / 4:19
$(\varepsilon, \alpha) = (0.0459, 3.47)$	$(\varepsilon, \alpha) = (0.04, 3.35)$	1:4 / 4:21

4. DYNAMICS OF GRANULAR CONTAINERS

In our present study we have concentrated primarily on the homogeneous granular chains (Chapter 2) and periodic granular chains (Chapter 3). In the study of homogeneous granular chains we explored frequency band zones and their effect on the forced dynamics. We discovered frequency band zones in homogeneous granular chains under zero pre-compression, which are otherwise called the sonic vacuum due to the absence of characteristic speed of sound. It is interesting to note that localization was observed in harmonically base excited homogeneous granular chains wherein only low frequency signals can propagate spatially, while the high frequency signals lead to localized motions near the excited end and results in a non-zero constant compressive force at the fixed end. Such frequency band zones can be utilized to great advantage for vibration and shock isolation, for example in precluding the unwanted high frequency components of a harmonic excitation from reaching the object being protected. Although we considered damping in the system, the purpose was to suppress the transient dynamics, whereas the localization and the band zones were an intrinsic behavior of the granular chain.

On the other hand, we considered impulsive excitation of the dimers and discovered resonance phenomena that lead to substantial attenuation of propagating pulses through these media. We emphasize that in these systems the applied shocks/impulses are attenuated by the intrinsic nonlinear dynamics of the dimer chains, and not by any dissipative mechanisms (indeed the theoretical studies were performed for systems that were dissipation-free). Other types of granular setups considered for such purposes are tapered granular chains, randomly decorated granular chains [104-109]. Again, wave attenuation in these setups happens gradually over space. The objective of all these granular setups was to protect an object from propagating unwanted disturbances.

There are other methodologies that address these issues from a different perspective. These setups are called wave arresters or granular wave containers and they entrap the wave energy to a certain spatial domain of the granular chain. Although eventually the entrapped energy leaks and trickles through the boundaries of this spatial domain, however, the intensity is considerably reduced than the initially applied shock. The motivation for such a setup came from the scattering of the solitary wave at the interface of two homogeneous granular chains [42, 45, 68]. As noted previously, solitary waves are the only mechanism for energy/disturbance propagation in homogeneous granular chains. It is observed that there is complete transmission of the solitary wave when propagating from a homogeneous chain of heavy beads to a homogeneous chain of light beads. Interestingly, although there is complete transmission, the single solitary pulse impinging on the interface disintegrates into a train of solitary waves of varying amplitudes in the chain of light beads [68]. On the other hand a solitary wave disintegrates into a transmitted and a reflected pulse when propagating from a chain of light beads to a chain of heavy beads [44, 45, 68, 69, 167]. Although different materials can be used to construct such setups, for simplicity we assume here that the beads are made of the same material. With these observations in view, granular wave containers were conceptualized [69]. For example if a chain of light beads is sandwiched in between two chains of heavy beads, the propagating solitary wave disintegrates at the first interface (heavy to light beads chain) with total transmission and in contrast, at the second interface (light to heavy beads chain) each disintegrated solitary pulse transmits only a part of its energy and reflects the rest. As can be visualized, the initial solitary pulse is disintegrated into a train of solitary pulse at the interface and then allowed to leak energy gradually at the second interface. With this scenario in place, the wave energy is eventually localized or entrapped in the center layer of light beads with slight energy leakage through the interfaces. Wave containers have been previously studied by researchers with different interaction potentials and

chain lengths [44, 69, 113]. Such phenomenon has also been experimentally studied in pre-compressed chains [167]. The primary objective of the study in this chapter is the application of binary collision approximation (BCA) [39] in predicting the number of disintegrated solitary pulses and their amplitudes. In fact BCA has been in use in granular media research and has provided surprisingly good correspondence with the exact numerical simulations [104, 110, 168]. Further we consider a harmonically base excited granular container and study the realization of PZ and AZ and explore the transitions region between these two zones.

4.1 Theoretical Model

In this study we consider a granular system wherein a homogeneous granular chain of type 2 (type 1) beads is sandwiched between two homogeneous granular chains of type 1 (type 2) beads. As described previously, under certain conditions such a setup can act as granular wave containers. The assumptions made previously are still applicable, damping is disregarded, and the considered granular chains are assumed to be uncompressed. A schematic of a typical granular container is shown in Figure 4.1. As shown, the granular chain of N light (heavy) beads is sandwiched between two granular chains of n heavy (light) beads and with an applied impulse of strength F applied at the left end of the chain.

The application of an impulse on the left end of the chain leads to the formation of solitary wave in the left homogeneous chain [41, 51, 52, 56]. It is worth noting that solitary waves in granular chains with Hertzian contact spans about 6-7 beads [42, 44, 45] and for the formation of these waves a minimum chain length of about 10 beads [42, 44] is necessary. Thus in all our numerical simulations we make sure that these

requirements are fulfilled and solitary wave is formed in the left homogeneous chain ($n \geq 30$) and impinges on the center layer (N beads).

The equations of motion of the described granular setup are expressed as,

$$
\begin{aligned}
m\ddot{u}_i &= \frac{2}{3}\frac{E_1}{(1-\mu_1^2)}\sqrt{\frac{R_1}{2}}\left[\left(u_{i-1}-u_i\right)_+^{3/2}-\left(u_i-u_{i+1}\right)_+^{3/2}\right] \\
m\ddot{u}_n &= \frac{2}{3}\frac{E_1}{(1-\mu_1^2)}\sqrt{\frac{R_1}{2}}\left(u_{n-1}-u_n\right)_+^{3/2}-\frac{4}{3}\frac{E_1E_2}{E_2(1-\mu_1^2)+E_1(1-\mu_2^2)}\sqrt{\frac{R_1R_2}{R_1+R_2}}\left(u_n-u_{n+1}\right)_+^{3/2} \\
M\ddot{u}_{n+1} &= \frac{4}{3}\frac{E_1E_2}{E_2(1-\mu_1^2)+E_1(1-\mu_2^2)}\sqrt{\frac{R_1R_2}{R_1+R_2}}\left(u_n-u_{n+1}\right)_+^{3/2}-\frac{2}{3}\frac{E_2}{(1-\mu_2^2)}\sqrt{\frac{R_2}{2}}\left(u_{n+1}-u_{n+2}\right)_+^{3/2} \\
&\bullet\bullet\bullet \\
M\ddot{u}_{n+l} &= \frac{2}{3}\frac{E_2}{(1-\mu_2^2)}\sqrt{\frac{R_2}{2}}\left[\left(u_{n+l-1}-u_{n+l}\right)_+^{3/2}-\left(u_{n+l}-u_{n+l+1}\right)_+^{3/2}\right] \\
&\bullet\bullet\bullet \\
M\ddot{u}_{n+N} &= \frac{2}{3}\frac{E_2}{(1-\mu_2^2)}\sqrt{\frac{R_2}{2}}\left(u_{n+N-1}-u_{n+N}\right)_+^{3/2}-\frac{4}{3}\frac{E_1E_2}{E_2(1-\mu_1^2)+E_1(1-\mu_2^2)}\sqrt{\frac{R_1R_2}{R_1+R_2}}\left(u_{n+N}-u_{n+N+1}\right)_+^{3/2} \\
m\ddot{u}_{n+N+1} &= \frac{4}{3}\frac{E_1E_2}{E_2(1-\mu_1^2)+E_1(1-\mu_2^2)}\sqrt{\frac{R_1R_2}{R_1+R_2}}\left(u_{n+N}-u_{n+N+1}\right)_+^{3/2}-\frac{2}{3}\frac{E_1}{(1-\mu_1^2)}\sqrt{\frac{R_1}{2}}\left(u_{n+N+1}-u_{n+N+2}\right)_+^{3/2} \\
m\ddot{u}_j &= \frac{2}{3}\frac{E_1}{(1-\mu_1^2)}\sqrt{\frac{R_1}{2}}\left[\left(u_{j-1}-u_j\right)_+^{3/2}-\left(u_j-u_{j+1}\right)_+^{3/2}\right]
\end{aligned}
\tag{4.1}
$$

It should be noted that the above equations of motion hold for $N \geq 3$. We consider the mass of each bead on the left and right chain to be equal to m, and that of the center chain equal to M; moreover, the indices are in the ranges $i < n$, $j > n + N + 1$ and $(n + 1) < l < (n + N)$. We have index 1 (2) corresponding to left and right (center) chain, E is the Young's modulus, μ is the Poisson's ratio, R is the radius of the bead and u is the dimensional displacement of the beads. The subscript (+) indicates that the bracketed terms are considered only if they are positive and are neglected otherwise. Applying the non-dimensionalizations for displacement and time,

$$x_i = \frac{u_i}{R_1}; \quad \tau = \left[\frac{2}{3}\frac{E_1}{m(1-\mu_1^2)}\frac{R_1}{\sqrt{2}}\right]^{1/2} t \tag{4.2}$$

Hence, we have the non-dimensional equations of motion for $N \geq 3$,

$$\begin{aligned}
x_i'' &= \left(x_{i-1} - x_i\right)_+^{3/2} - \left(x_i - x_{i+1}\right)_+^{3/2} \\
x_n'' &= \left(x_{n-1} - x_n\right)_+^{3/2} - \frac{2\alpha}{1+\alpha}\sqrt{\frac{2\varpi}{1+\varpi}}\left(x_n - x_{n+1}\right)_+^{3/2} \\
\varepsilon x_{n+1}'' &= \frac{2\alpha}{1+\alpha}\sqrt{\frac{2\varpi}{1+\varpi}}\left(x_n - x_{n+1}\right)_+^{3/2} - \alpha\sqrt{\varpi}\left(x_{n+1} - x_{n+2}\right)_+^{3/2} \\
&\bullet\bullet\bullet \\
\varepsilon x_{n+l}'' &= \alpha\sqrt{\varpi}\left[\left(x_{n+l-1} - x_{n+l}\right)_+^{3/2} - \left(x_{n+l} - x_{n+l+1}\right)_+^{3/2}\right] \\
&\bullet\bullet\bullet \\
\varepsilon x_{n+N}'' &= \alpha\sqrt{\beta}\left(x_{n+N-1} - x_{n+N}\right)_+^{3/2} - \frac{2\alpha}{1+\alpha}\sqrt{\frac{2\varpi}{1+\varpi}}\left(x_{n+N} - x_{n+N+1}\right)_+^{3/2} \\
x_{n+N+1}'' &= \frac{2\alpha}{1+\alpha}\sqrt{\frac{2\varpi}{1+\varpi}}\left(x_{n+N} - x_{n+N+1}\right)_+^{3/2} - \left(x_{n+N+1} - x_{n+N+2}\right)_+^{3/2} \\
x_j'' &= \left(x_{j-1} - x_j\right)_+^{3/2} - \left(x_j - x_{j+1}\right)_+^{3/2}
\end{aligned} \tag{4.3a}$$

where primes denote derivatives with respect to non-dimensional time τ and we introduce the non-dimensional parameters,

$$\alpha = \frac{E_2(1-\mu_1^2)}{E_1(1-\mu_2^2)}; \quad \varpi = \frac{R_2}{R_1}; \quad \varepsilon = \frac{\rho_2 R_2^3}{\rho_1 R_1^3} = \frac{\rho_2}{\rho_1}\varpi^3 = \gamma\varpi^3 \tag{4.4}$$

As can be seen the dynamics of the granular containers is governed by three non-dimensional parameters; namely, the stiffness ratio (α), radius ratio (ϖ) and the density ratio (γ) of the two types of beads of the chain. Although there is an additional

parameter scaling the masses of the two types of beads, the mass ratio (ε), this is dependent on ϖ and γ.

For the particular case of $N = 1$ we have,

$$
\begin{aligned}
x_i'' &= \left(x_{i-1} - x_i\right)_+^{3/2} - \left(x_i - x_{i+1}\right)_+^{3/2} \\
x_n'' &= \left(x_{n-1} - x_n\right)_+^{3/2} - \frac{2\alpha}{1+\alpha}\sqrt{\frac{2\varpi}{1+\varpi}}\left(x_n - x_{n+1}\right)_+^{3/2} \\
\varepsilon x_{n+1}'' &= \frac{2\alpha}{1+\alpha}\sqrt{\frac{2\varpi}{1+\varpi}}\left[\left(x_n - x_{n+1}\right)_+^{3/2} - \left(x_{n+1} - x_{n+2}\right)_+^{3/2}\right] \\
x_{n+2}'' &= \frac{2\alpha}{1+\alpha}\sqrt{\frac{2\varpi}{1+\varpi}}\left(x_{n+1} - x_{n+2}\right)_+^{3/2} - \left(x_{n+2} - x_{n+3}\right)_+^{3/2} \\
x_j'' &= \left(x_{j-1} - x_j\right)_+^{3/2} - \left(x_j - x_{j+1}\right)_+^{3/2}
\end{aligned}
\tag{4.3b}
$$

Similarly, for the case $N = 2$ one can deduce the equations of motion by eliminating the equations involving the index k in (4.3a).

4.2 Numerical Simulations

To explore the efficacy of the system for wave containment, we use the maximum transmitted force to the right fixed boundary as a measure (as employed in Chapter 3). We mainly consider the case of $\varepsilon \leq 1$, which implies that the left and the right chains are heavy bead chains, whereas the center chain comprises of light beads. To this end, we fix a heavy bead at the right end of the chain and measure the maximum force transmitted (first pulse) as we vary ϖ, ε and N. The measured maximum force transmitted indicates the scattering experienced by the solitary wave as it propagates through the interfaces, and subsequent attenuation as it reaches the right fixed end of

the chain. As the solitary pulse propagates from the left chain to the center chain, it encounters the first interface (if $\varepsilon \neq 1$). This interface acts as a defect and leads to the scattering of the propagating pulse.

In Figure 4.2 (unless stated all units are non-dimensional) we depict the normalized maximum force transmitted to the fixed bead for the case when the center layer is of the same material as the right and the left chains. Thus we have $\alpha = 1, \varepsilon = \varpi^3$. The normalization of the transmitted force is with respect to the force transmitted for the case of homogeneous chain, i.e., $\alpha = 1, \varpi = 1, \gamma = 1$. For the case of homogeneous chain, a solitary wave propagates without any scattering or attenuation and thus corresponds to the maximum transmitted force.

If the center chain consists of only one light bead, the impinging solitary wave encounters an interface ($\varepsilon \neq 1$) and leads to the formation of transient breathers [64] [65]. Breathers are time-periodic spatially localized high frequency oscillators and are excited in this case due to the presence of the small mass intruder in between the two (left and right) homogeneous chains. The small mass intruder retains some amount of energy from the propagating pulse and executes high frequency oscillations while squeezed between the adjacent heavy beads. It should be noted that breathers are excited only when the intruder is of sufficiently small mass ($\varepsilon \ll 1$). Once $\varepsilon \approx O(1)$, these breathers can no longer be excited. As can be seen for the case of $N = 1$, even for sufficiently small mass ratio the decrease in transmitted force is not substantial, whereas the transmitted force decreases drastically for increasing N for the same value of mass ratio. The excitation of transient breathers happens, in general, for small N and for sufficiently small ε. This is due to the fact that the (internal) nonlinear normal modes of the light beads of the center chain are excited only for small N. On the other hand, propagatory dynamics are realized when N is sufficiently large, enabling the intermediate chain to support the formation of solitary waves. Such chains come under

the class of granular containers. A brief note on the excitation of transient breathers is provided in the next section.

Another notable feature in Figure 4.2 is that for a particular mass ratio, the normalized force transmitted decreases with an increase in the number of light beads in the center layer. This is an interesting observation and an important feature of the granular containers. For sufficiently long center layer, depending on the magnitude of ε, we observe two different phenomenon. If $\varepsilon < 1$, the solitary wave from the left chain disintegrates into a train of solitary pulses at the first interface and, interestingly enough, there is complete transmission and no reflection back into the left chain. These solitary wave trains have decreasing amplitudes. As the highest amplitude pulse travels the fastest, it reaches the second interface and scatters once again into a right traveling transmitted pulse and a left traveling reflected pulse. Thus the solitary wave generated in the left chain by the initial applied impulse scatters twice and the maximum amplitude solitary pulse (the first pulse) reaching the fixed end is substantially lower than the solitary wave in the left chain generated by the applied impulse. This scenario is observed only when N is sufficiently long enough to support the solitary wave train. Thus the first pulse reaching the right fixed end is of lower amplitude and so are the subsequent pulses. The reflected solitary wave in the center chain which is a left traveling wave interacts with the first interface and again splits into a left traveling transmitted solitary pulse and a right traveling reflected solitary pulse. This phenomenon goes on until the energy of the reflected pulse in the center chain is completely spent. Thus we have wave energy entrapped in the center layer and these waves emit solitary waves to the left and the right chains whenever they interact with the first and second interfaces, respectively. This scenario is clearly depicted in Figure 4.3a where we consider a 30:70:30 granular container excited by a unit impulse and present the instantaneous velocity profiles at specific time snapshots normalized with respect to the applied impulse (unity).

As a final note we consider the case of $\varepsilon = 2$ in a 30:70:30 chain. The space-time plot is shown in Figure 4.3b. Interesetingly, there is partial transmission at the first interface and complete transmission at the second. Thus there is no effect of wave containment in this configuration.

The next section provides a brief introduction to the excitation of transient breathers excited in a homogeneous granular chain with a small mass intruder. Such a phenomenon was observed in a granular container with small N and $\varepsilon \ll 1$. We discuss in brief the subtle features of transient breathers and how the energy is entrapped in such breathers.

4.3 Excitation of Transient Breathers

It is well known that any propagating disturbance in a homogeneous granular chain disintegrates into a train of solitary pulse, which is the principal mechanism of energy propagation in this nonlinear periodic system. But whenever a solitary wave encounters a defect (small mass intruder), the interaction leads to excitation of transient breathers at the site of the defect. Although no bead separation is observed during solitary wave propagation, such separations (and ensuing bead collisions) are observed at the site of transient breathers. When separation between beads occurs, localized transient breathers are excited corresponding to repeated collisions of the small mass intruder with its heavy bead neighbors. This leads to high-frequency scattering of energy, and radiation of this energy to the far field of the granular medium in the form of low-amplitude slowly modulated oscillatory pulses. Repeated excitation of localized transient breathers by an array of periodically placed intruders can result in drastic reduction of the amplitude of the pulse propagating through the granular medium. In contrast to traveling solitary waves, transient breathers are spatially localized standing

waves that confine energy (at least at a fast time scale). It indicates that this type of granular media can be designed for effective energy entrapment. Such phenomenon has been well studied in previous works [65, 67].

Considering the uncompressed granular chain of identical beads in Hertzian contact with a single intruder studied in [67] and depicted in Figure 4.1, an initial impulse applied to the free left boundary of the chain leads to the formation of a solitary wave that propagates undispersed until it impedes on the intruder, in this case $N = 1$ and $\varepsilon \ll 1$. Then a strongly nonlinear interaction between the intruder and the solitary wave takes place leading to fast-scale oscillations of the intruder. An example of this interaction is depicted in the plot of Figure 4.4 where the displacements of the light intruder and of its left and right neighboring heavy beads are shown for a unit impulse applied to the left free end of a 100:1:100 granular container. For this simulation the mass of the intruder is chosen as 5% ($\varepsilon = 0.05$) of the mass of its neighboring beads ($\alpha = 1, \varpi = 1$). Clearly two modes of intruder-chain interaction are inferred from this plot.

The first mode of interaction corresponds to 'fast' oscillation of the light intruder under heavy compression from its left and right neighbor beads which themselves undergo 'slow' motions. There is no separation between these three beads so the dynamics is smooth and governed by the Hertzian law interaction between beads under compression. The second mode of interaction corresponds to separations and collisions between the intruder and its neighboring heavy beads and the resulting dynamics is non-smooth. The ensuing (elastic) collisions between the intruder and its left and right neighbors give rise to a localized *transient breather* [67] at the site of the intruder, in the form of a 'fast' (non-smooth) oscillation of the intruder with varying amplitude and frequency and 'slow' motions of its neighboring beads. As discussed in [65], the excitation of this breather acts in essence as 'energy trap' since it is a high-frequency energy scatterer. Under certain conditions the excitation of such transient breathers can

drastically reduce the amplitude of a pulse propagating through granular medium, e.g., by placing such intruders periodically the wave energy can be periodically trapped in these breathers and thus the pulse can be efficiently and effectively attenuated.

In the previous section we described the phenomenon of wave containment in granular containers. The dynamics of such granular systems has been well studied in the literature cited therein. In estimating the energy retained in the center chain and the energy propagated to the right chain it is important to ascertain the amplitudes of scattered solitary waves at the two interfaces. To this end, it is noted that a simplified model of binary collisions can provide very good approximations. The next section describes the application of BCA in this regard and compares it to the exact dynamics of the original system.

4.4 Binary Collision Approximation

Let's consider $x_n' = w$ and $x_{n+1}' = v$, which are the velocities of beads of mass 1 and ε at the interface between the left and the center chains, respectively. In the binary collision approximation – BCA, it is considered that at any instant of time there can be interaction between at most two beads. Further, it is assumed that the interaction is purely elastic and no dissipation occurs during this interaction so the total energy and momentum are conserved.

Applying conservation of momentum for the two particles at the interface we have,

$$w_0 + \varepsilon v_0 = w_1 + \varepsilon v_1 \tag{4.4a}$$

where w_0, v_0 are the initial velocities of the velocities of beads of mass 1 and ε at the interface between the left and the center chains, respectively. But we have that $w_0 = U$, $v_0 = 0$, i.e., we provide an impulse of magnitude U at the left end of the chain which propagates un-attenuated and impinges on the interface. Thus we have $w_1 + \varepsilon v_1 = w_0 = U$. As the interaction is purely elastic, we have the coefficient of restitution $e = 1$,

$$e = \frac{v_1 - w_1}{w_0 - v_0} \Rightarrow v_1 - w_1 = w_0 \tag{4.4b}$$

so we have that,

$$w_1 = \frac{w_0(1-\varepsilon)}{1+\varepsilon};\ v_1 = \frac{2w_0}{1+\varepsilon} \tag{4.4c}$$

From these relations we observe that if $\varepsilon < 1, w_1 > 0$ and $v_1 > 0$. As the center chain is homogeneous, the first bead (of mass ε) of the center chain interacts with the second (of mass ε), thus the conservation of momentum yields $(v_1 + p_0) = (\tilde{v}_1 + p_1)$, where $p_{0,1}$ denotes the velocity of second bead of the center chain before ($p_0 = 0$) and after collision respectively and $\tilde{v}_1$ is the velocity of first bead of the center chain after collision. Applying the relation of coefficient of restitution, we have $p_1 - \tilde{v}_1 = v_1$. Solving these two equations we have $p_1 = v_1 > 0$, $\tilde{v}_1 = 0$. This indicates that the first bead of the center chain becomes stationary after colliding with the second bead of the center chain. This transmitted pulse propagates un-attenuated in the center chain. As the heavy bead also has a positive velocity ($w_1 > 0$), it collides with the first bead of the center chain which is stationary leading to the second transmitted pulse with the heavy bead still having a positive velocity ($w_2 > 0$). In essence it so happens that the bead of mass unity (last bead of left chain) incessantly collides with the bead of mass ε (first bead of center chain) and loses its energy gradually. This leads to a series of solitary pulses being injected into the center chain. The magnitude of each subsequent solitary

pulse can be obtained by recursively considering conservation of momentum and the relation for the coefficient of restitution:

$$\begin{aligned} w_1 &= w_2 + \varepsilon v_2 \\ w_1 &= -w_2 + v_2 \end{aligned} \tag{4.5a}$$

Solving the above equations we have,

$$\begin{aligned} w_2 &= \frac{(1-\varepsilon)w_1}{(1+\varepsilon)} = \frac{(1-\varepsilon)^2}{(1+\varepsilon)^2} w_0 \\ v_2 &= \frac{2w_1}{1+\varepsilon} = \frac{2(1-\varepsilon)}{(1+\varepsilon)^2} w_0 \end{aligned} \tag{4.6a}$$

Further we can estimate the amplitude of the n −th solitary pulse as follows,

$$\begin{aligned} w_n &= \frac{(1-\varepsilon)w_{n-1}}{(1+\varepsilon)} = \frac{(1-\varepsilon)^n}{(1+\varepsilon)^n} w_0 \\ v_n &= \frac{2w_{n-1}}{1+\varepsilon} = \frac{2(1-\varepsilon)^{n-1}}{(1+\varepsilon)^n} w_0 \end{aligned} \tag{4.6b}$$

where w_n and v_n are the velocities of the beads of mass unity and ε at the first interface after n collisions, respectively. Thus the heavy bead of mass unity emits solitary pulses of monotonously decreasing amplitudes. In other words, v_n is the velocity amplitude of the n −th solitary wave generated at the interface. In the following results we have considered that the beads are made of the same material, thus $\alpha = 1, \gamma = 1, \varepsilon = \varpi^3$.

In the first set of simulations we consider $\varepsilon < 1$. As described earlier, there is complete transmission of the impeding solitary wave, which disintegrates and leads to a solitary wave train. The top plot in the Figure 4.5a ($\varepsilon = 0.216$) corresponds to the

original system, and the bottom one to the BCA model. As can be observed, the amplitude of the solitary wave in the left chain is of amplitude unity for both the original system and the BCA model. In the original system we observe that the impinging solitary wave disintegrates into to a train of solitary waves which propagates in the center chain and there are no reflected pulses at the interface. This scenario is fully captured by the BCA model presented in the bottom plot of Figure 4.5a. Moreover, the BCA model predicts quite well the number of disintegrated solitary waves in the center chain. In Figure 4.5b we provide a comparison of the amplitudes of the solitary waves in the center chain as predicted by BCA versus the corresponding amplitudes in the original system. The estimations by the BCA model closely match that in the original system.

It is worth noting that as the mass ratio increases, the number of disintegrated solitary waves decreases. Even this is very well captured by the BCA model, whereas the amplitudes predicted by BCA model correspond much better than in the previous case [as shown in Figure 4.6 ($\varepsilon = 0.512$) and Figure 4.7 ($\varepsilon = 0.729$)]. But, as expected, for $\varepsilon = 1$, there is complete transmission without disintegration of the solitary wave.

Now we consider the dynamics at the second interface with $y_0 > 0$ being the amplitude of first solitary wave reaching the second interface (in other words the velocity of the last bead of the center chain) and $z_0 = 0$ being the velocity of the first bead of the right chain. Applying again conservation of momentum at the second interface we have,

$$z_0 + \varepsilon y_0 = z_1 + \varepsilon y_1 \tag{4.4a}$$

$$e = \frac{z_1 - y_1}{y_0 - z_0} \Rightarrow z_1 - y_1 = y_0 \tag{4.4b}$$

Solving these two equations we have:

$$y_1 = -\frac{y_0(1-\varepsilon)}{1+\varepsilon};\ z_1 = \frac{2\varepsilon y_0}{1+\varepsilon} \tag{4.4c}$$

It can be observed that for $y_0 > 0$ and $\varepsilon < 1$, we have that $y_1 < 0$ and $z_1 > 0$. This implies a transmitted solitary pulse and a reflected pulse at the second interface. The transmitted pulse reaches the right far end of the granular container, whereas the reflected pulse travels left and encounters the first interface and again leads to a transmitted pulse and a reflected pulse. Thus the first solitary pulse reaching the right end of the granular container has an amplitude of $z_1 = 2\varepsilon y_0/(1+\varepsilon) = 4\varepsilon w_0/(1+\varepsilon)^2$, where we consider $y_0 = v_1 = 2w_0/(1+\varepsilon)$. For the case of $\varepsilon = 0.216$ and $w_0 = 1$, we have $z_1 = 0.5843$, whereas from the numerical simulation of the original system we have $\tilde{z}_1 = 0.679$. For the other cases shown in Figure 4.6 ($\varepsilon = 0.512$) we have $z_1 = 0.8958$ and $\tilde{z}_1 = 0.9337$; and $z_1 = 0.988$ and $\tilde{z}_1 = 0.9754$ for the case of $\varepsilon = 0.729$ (Figure 4.7). From these results it is clear that the granular containers are very efficient for smaller values of mass ratio, but the amplitudes of the solitary waves predicted by the BCA loses accuracy for lower values of the mass ratio.

Now considering the case of $\varepsilon > 1$, we observe that we have a transmitted pulse and a reflected pulse at the first interface. The beads at the first interface come into contact only once during this interaction. For $\varepsilon = 2$, the binary collision model predicts that $w_1 = -0.267$ and $v_1 = 0.7334$ for $w_0 = 1$ and thus there is no further pulse disintegration. On the other hand, for the original system the amplitude of the transmitted pulse is 0.745 and of the reflected pulse -0.208. Furthermore, the transmitted pulse experience complete transmission and disintegrates into a solitary wave train of decreasing amplitudes at the second interface. Thus there is no wave container phenomenon in this case as described previously (cf. Figure 4.3b).

Until now we considered systems with $\alpha = 1$, i.e., systems wherein all beads are made of materials having similar stiffness characteristics. It should be noted that the parameters α and ε are related due to the fact that both depend on material properties, i.e., α is a parameter dependent on Young's modulus and Poisson's ratio, whereas ε $(= \gamma\varpi^3)$ depends on the densities of the two materials. Hence, practically these two parameters cannot be independently chosen. It follows that if any two materials are chosen, α and γ will be fixed; the only parameter that still can be varied is the radius ratio ϖ leading to the variation of the mass ratio ε.

A primary drawback of the BCA model is its inability to incorporate the material parameters such as Young's modulus, Poisson's ratio in the dynamical analysis. As this model is based on pure momentum transfer considerations, it takes into account only the masses of the beads, so the stiffness of the beads is of no importance. Hence, even if one incorporates the Hertzian interaction law in the BCA, the time of interaction between the beads would change with a change in α, but the final momentum of each bead would remain the same. Thus the BCA cannot be applied for a general case of $\alpha \neq 1$. In addition, and because of the assumed instantaneous interactions between beads in the BCA, only single bead to bead interactions exist and (the more realistic) simultaneous interactions between more than two beads are excluded in the analysis. This simplifies the dynamics but it leads to the inaccuracies and mismatches described previously.

4.5 Propagation and Attenuation Zones in Granular Containers

In the previous section we particularly considered the granular containers excited by impulses and showed the phenomenon of wave containment and the corresponding applicability of BCA. Furthermore, we considered the beads in the chain made of

materials with similar elastic properties. In this section we consider a similar setup but with harmonic excitation at the left end while the right end being fixed. The primary objective of this study is the realization of PZ and AZ in this class of granular chains and study the transition zone between these phases. To this end we consider a 30:50:30 granular container with a normalized harmonic excitation of $B\sin(\beta\tau)$, where B and β are the normalized amplitude and frequency respectively. We consider a particular mass ratio and sweep the harmonic excitation frequency. The time average of the transmitted force measured at the fixed end is considered as an indication of the PZ or AZ. The average transmitted force for the case of $\varepsilon = 0.729$ for $B = 5$ is presented in Figure 4.8. The numerical simulation is considered for a total of 10000 time units and the force is averaged over the last 1000 time units. As it is expected, for lower frequencies of excitation the system is in PZ and the energy is distributed spatially in the chain. This is evidenced by the time snapshot of the displacement response of the beads in Figure 4.9a. Furthermore, Figure 4.9b depicts the transmitted force as a function of time. Thus it can be ascertained that the average transmitted force over the last 500 time units is non-zero. In contrast, for an excitation frequency in the AZ, we observe localization near the excitation end and spatial attenuation towards the fixed end (Figure 4.10a), whereas the transmitted force response (Figure 4.10b) shows almost zero force indicating that energy from the excited end no longer is reaching the fixed end. These behaviors are previously observed in homogeneous granular chains.

The most interesting feature in Figure 4.8 is the transition region between the PZ and the AZ. In fact, the transition is not a single point but happens over a range of frequencies. It is interesting to note that both AZ and PZ can be realized in this frequency range. In the following series of simulations we show the response of the granular container excited by two frequencies which are sufficiently close but exhibit propagatory and attenuatory behaviors. Consider the response of the system for $\beta = 1.568$ and 1.572 in Figure 4.11a, b respectively. Interestingly enough, although the

frequencies are sufficiently close, they exhibit contrastingly different behaviors. While response at $\beta = 1.568$ is propagatory, the response at $\beta = 1.572$ is attenuatory. Such a behavior is further evidenced by the response of the system at $\beta = 1.856$ and 1.864 in Figure 4.12a, b respectively. It is worth noting that the considered granular chain is high dimensional nonlinear system and chaotic behavior is quite expected. In fact even in the case of two degree of freedom granular system, chaos was observed on the Poincaré map (cf. Figure 2.2). Thus the contrasting behavior of PZ and AZ for sufficiently close excitation frequencies can be attributed to the sensitive dependence on initial conditions, a distinct feature of chaotic systems. In essence, both AZ and PZ can be realized in this transition region with very slight variation in excitation frequency. This result can be seen in close conjunction with the experimental results of Section 2.2.1.3 wherein the transition region could not be captured experimentally due to the nonlinear resonance and chaotic behavior.

4.6 Conclusions

In conclusion, granular containers exhibit very interesting dynamics. In the present analysis we have considered a normalized system where we have three non-dimensional material and geometric parameters. The three primary parameters governing the dynamics are the stiffness, radius and density ratios between the two different types of beads. It should be noted that the mass ratio depends both on the radius ratio and on the material properties. In our work we focus mainly on systems composed of beads of the same material; so we have stiffness, density ratio equal to unity and the mass ratio depending only on the ratio of radii.

In this case we observed two different behaviors. If the mass ratio is less than unity, the solitary wave disintegrates at the first interface between the heavy (left) and

the light (center) chains. An impinging solitary pulse disintegrates into a train of solitary waves which propagates in the center chain. Once these waves impinge on the second interface of the light (center) and the heavy (right) chain, they split into two solitary waves, one reflected wave traveling in the center chain and the other transmitted wave propagating in the right chain. The reflected wave in the center chain is entrapped and wave containment results. Although the wave energy leaks through the two interfaces gradually (at a slow time scale), the magnitudes of these 'leaked' waves are very much reduced in comparison to the initial applied impulse.

In contrast, a chain with mass ratio greater than unity exhibits no wave containment effect. To this end, we applied the Binary Collision Approximation for this system and observed that the BCA model predicts the dynamics well. This simple model predicts the number of disintegrated solitary waves and their amplitudes. For smaller mass ratios, the number of disintegrated solitary waves increases. Although the BCA predicts the number of pulses quite well, the amplitude predictions are less accurate. Whereas for higher mass ratios, BCA predicts both the amplitude and the number of solitary pulses quite well. In conclusion, BCA can be effectively employed in estimating the amplitudes of disintegrated solitary waves and the energy contained in the center chain.

Finally we have considered harmonically base excited granular containers. Previously we explored the AZs and PZs in homogeneous granular chains. Such frequency band zones are not particular to homogeneous chains, but can also be realized in granular containers. We observe that for a particular mass ratio (ε), the lower excitation frequencies are propagated spatially, whereas the higher frequencies are attenuated. The transition between these zones exhibit behavior which is sensitively dependent on the excitation frequency. In essence both propagatory and attenuatory behaviors can be realized for very close excitation frequencies.

4.7 Figures

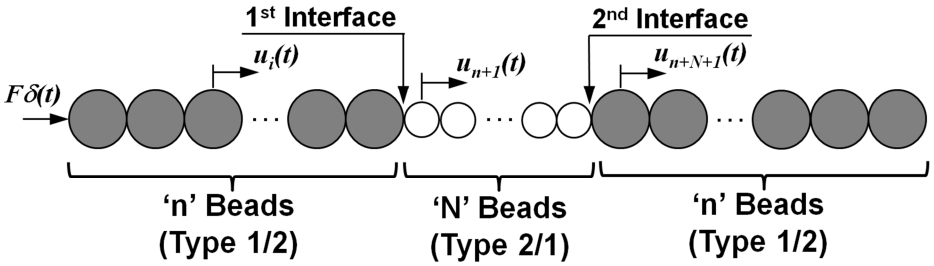

Figure 4.1: Schematic of a granular container

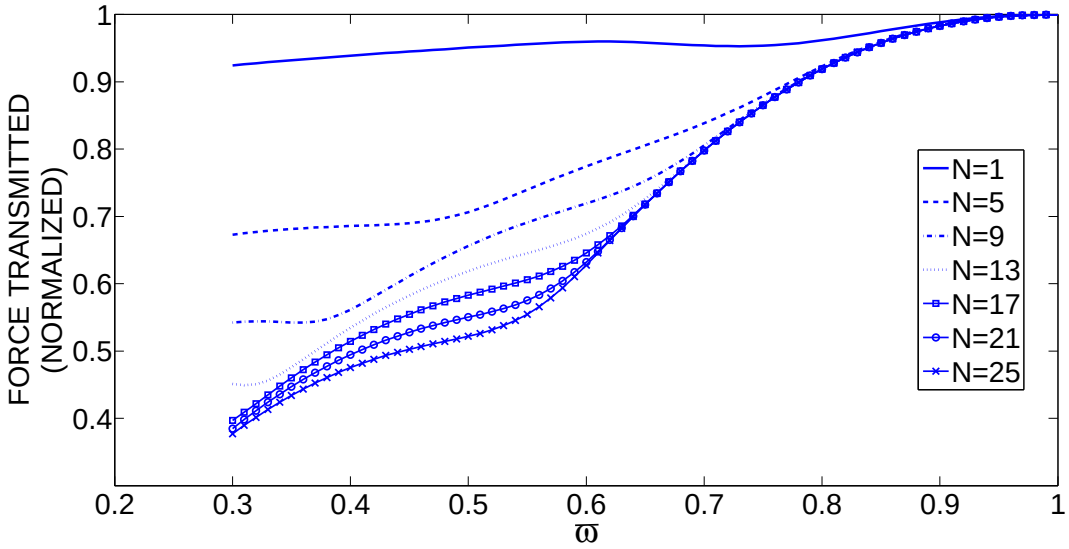

Figure 4.2: Normalized maximum transmitted force at the fixed right boundary for $\alpha = 1, \gamma = 1$.

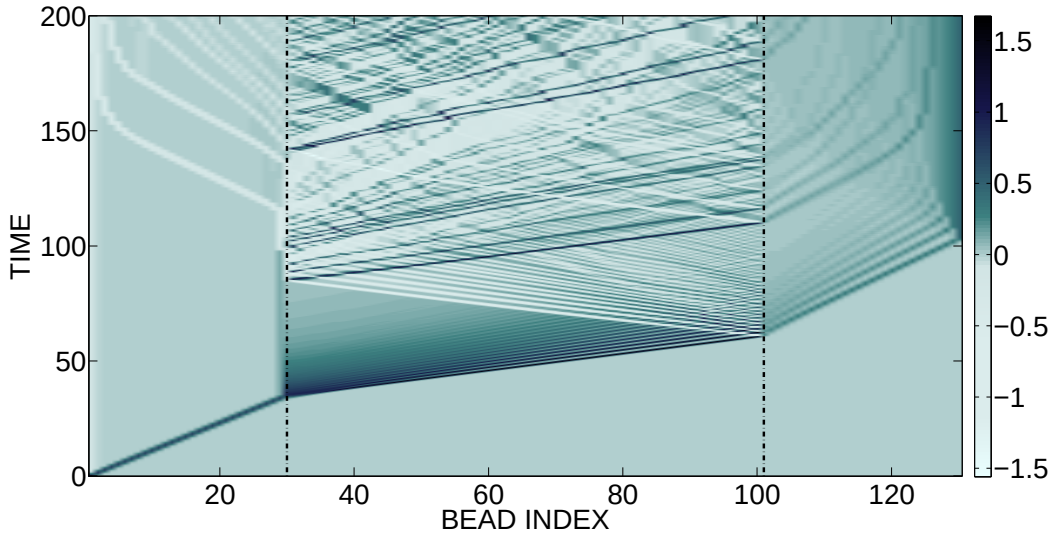

Figure 4.3a: Instantaneous normalized velocity in a granular container for $\alpha = 1$, $\gamma = 1, \varpi \approx 0.368, \varepsilon \approx 0.05$.

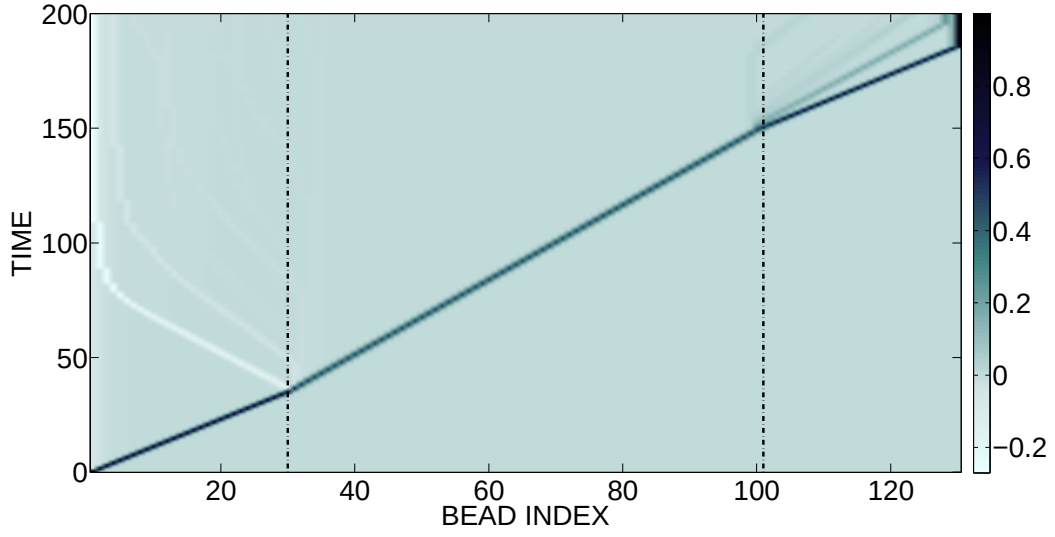

Figure 4.3b: Instantaneous normalized velocity in a granular container for $\alpha = 1$, $\gamma = 1, \varpi \approx 1.26, \varepsilon \approx 2$.

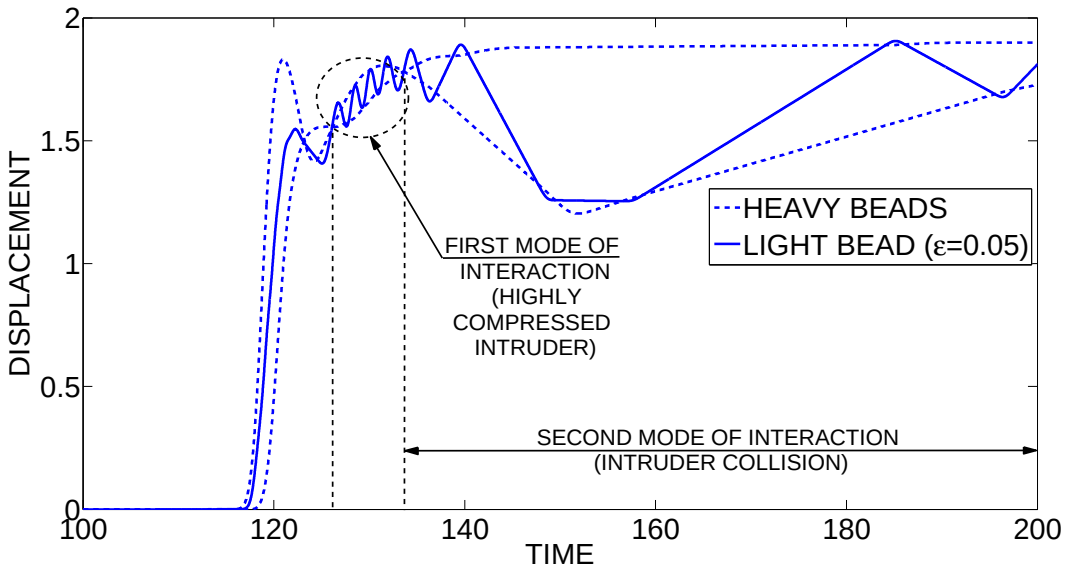

Figure 4.4: Excitation of transient breather in 100:1:100 granular container for $\varepsilon = 0.05$.

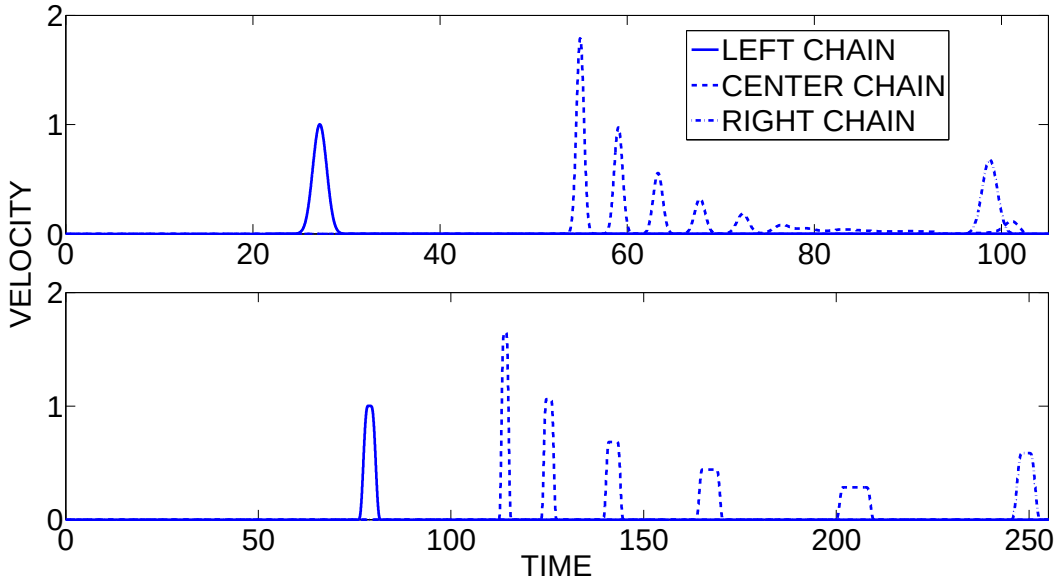

Figure 4.5a: Comparison of original system (top plot) and the BCA (bottom plot) model for $\varepsilon = 0.216$.

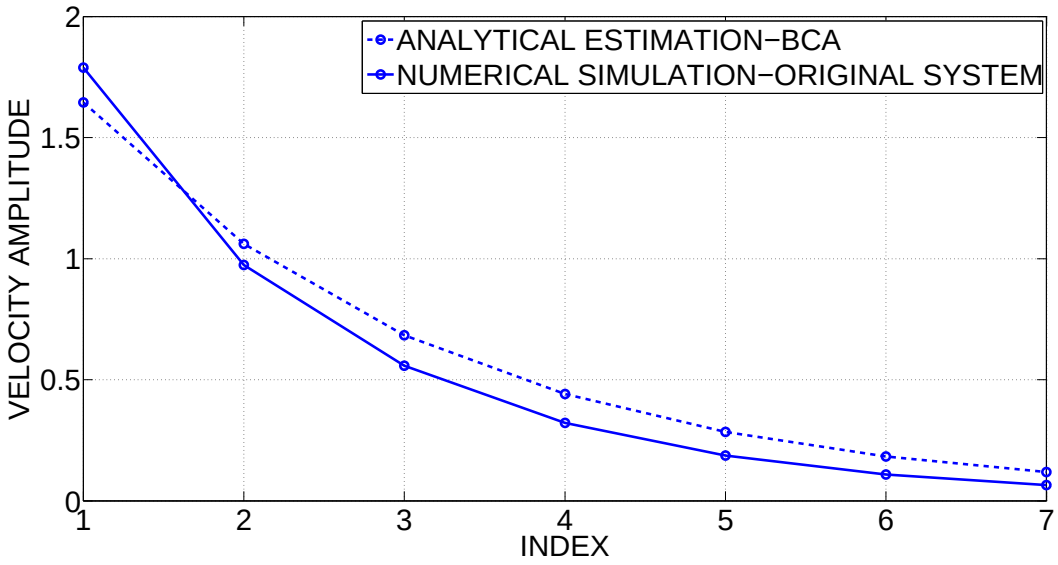

Figure 4.5b: Solitary pulse amplitude comparison of original system and the BCA model for $\varepsilon = 0.216$.

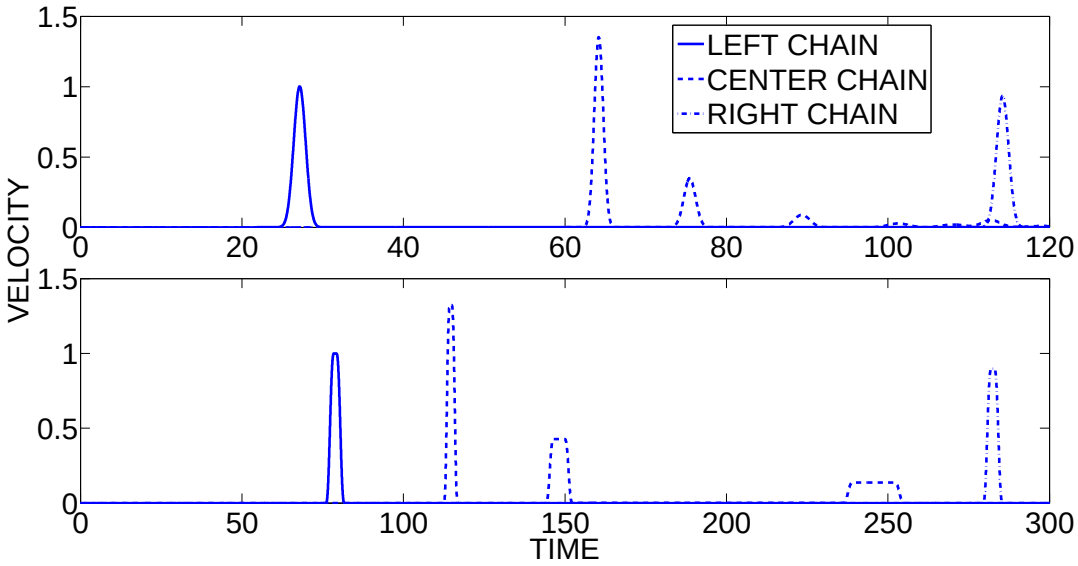

Figure 4.6a: Comparison of original system (top plot) and the BCA (bottom plot) model for $\varepsilon = 0.512$.

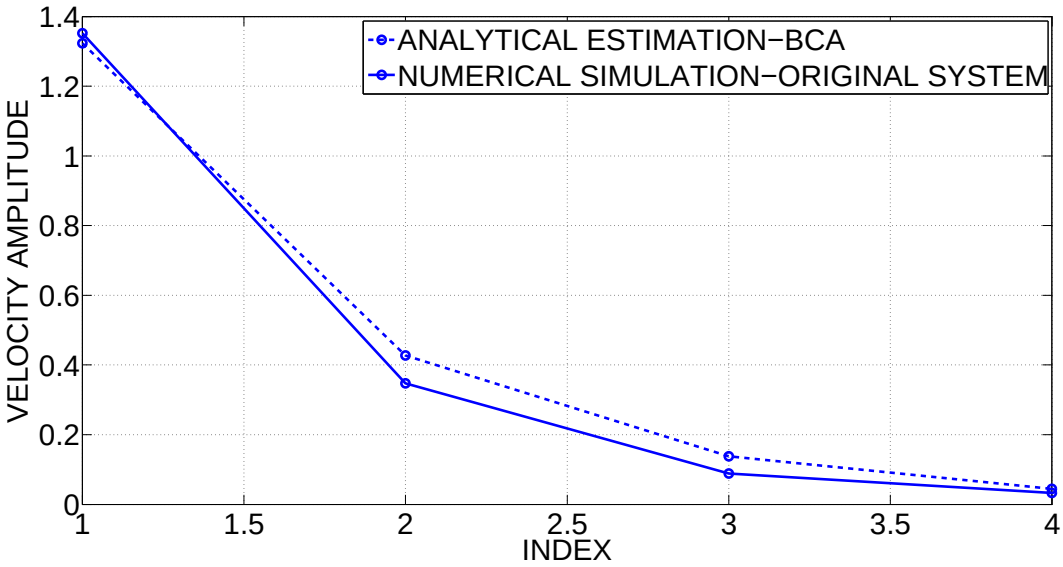

Figure 4.6b: Solitary pulse amplitude comparison of original system and the BCA model for $\varepsilon = 0.512$.

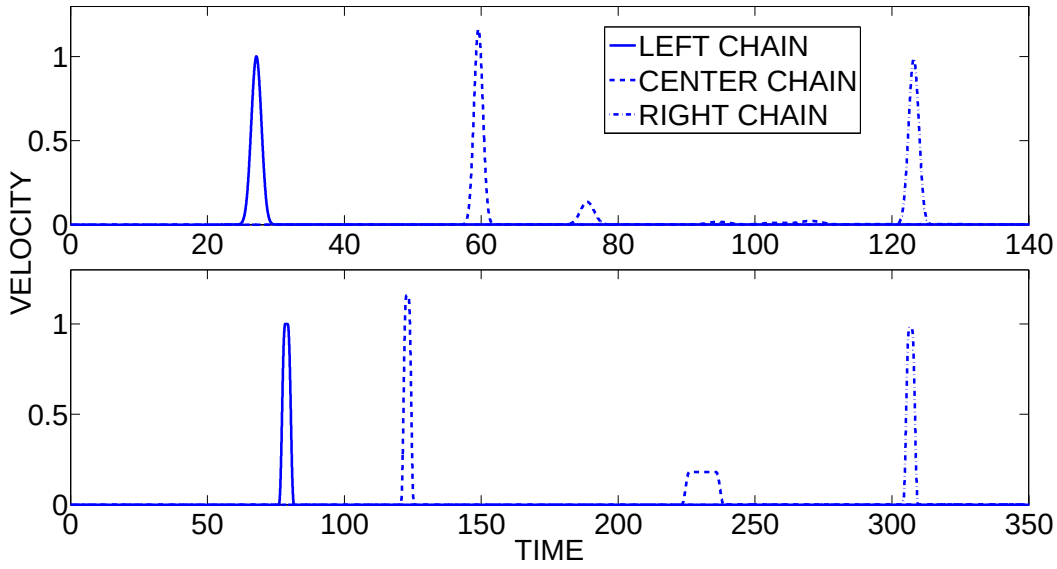

Figure 4.7a: Comparison of original system (top plot) and the BCA (bottom plot) model for $\varepsilon = 0.729$.

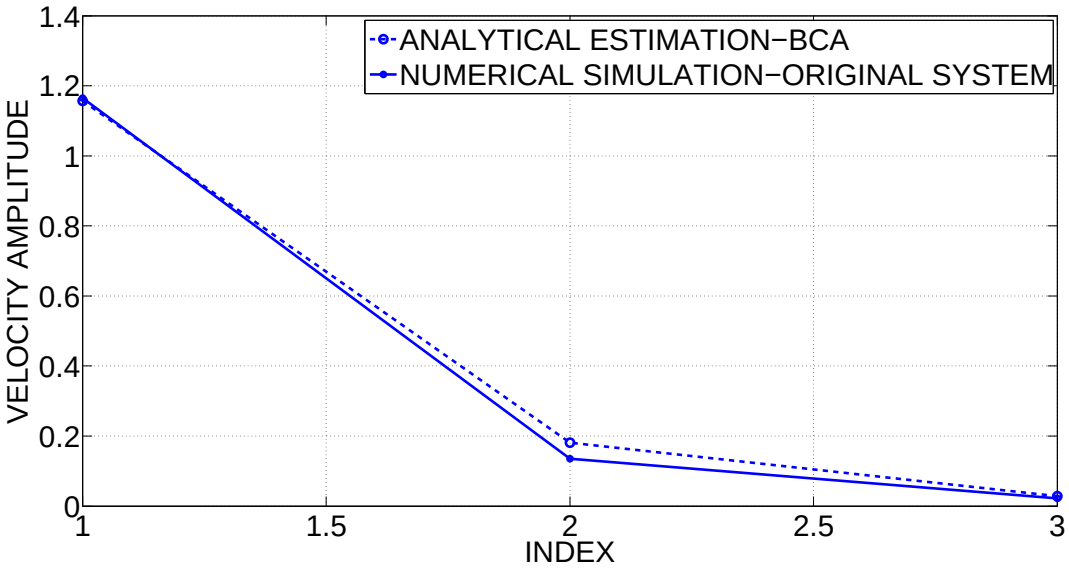

Figure 4.7b: Solitary pulse amplitude comparison of original system and the BCA model for $\varepsilon = 0.729$.

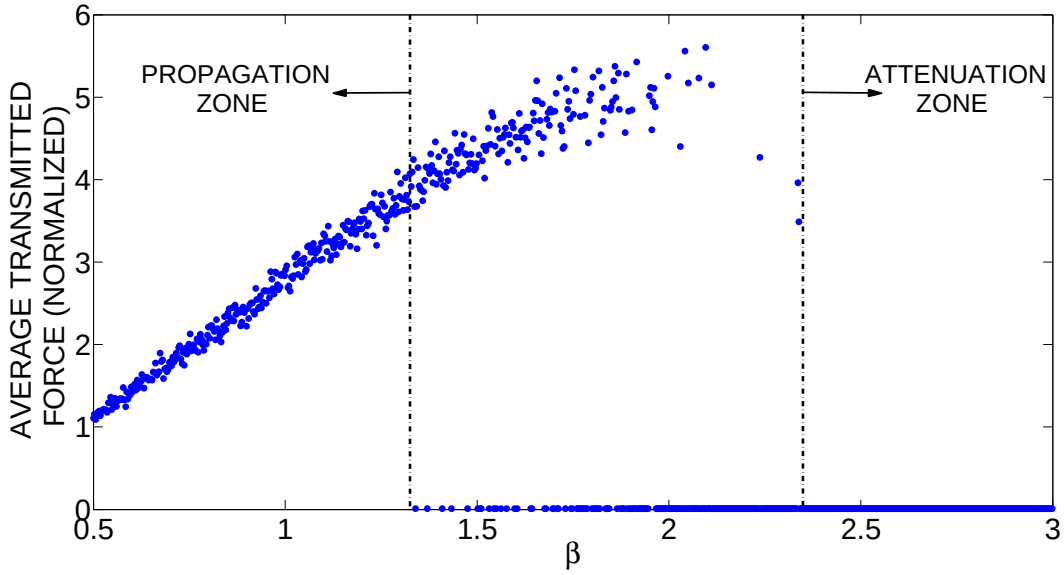

Figure 4.8: Average normalized force in a 30:50:30 granular container with $\varepsilon = 0.729$ harmonically excited with an amplitude $B = 5$.

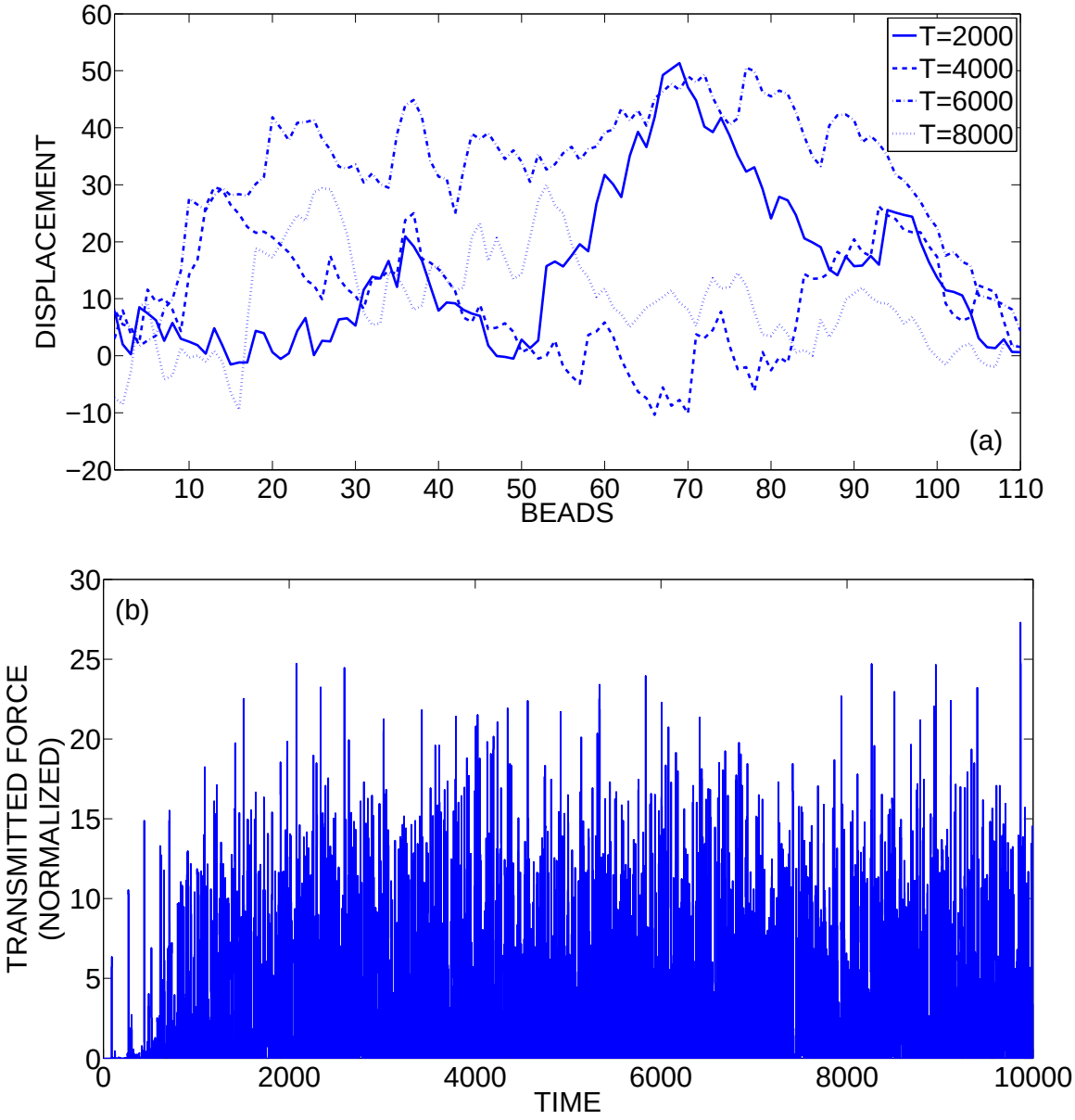

Figure 4.9: (a) Time snapshot of the displacement variation; (b) Normalized transmitted force in a 30:50:30 granular container with $\varepsilon = 0.729$ harmonically excited with an amplitude $B = 5$ and frequency $\beta = 0.94$.

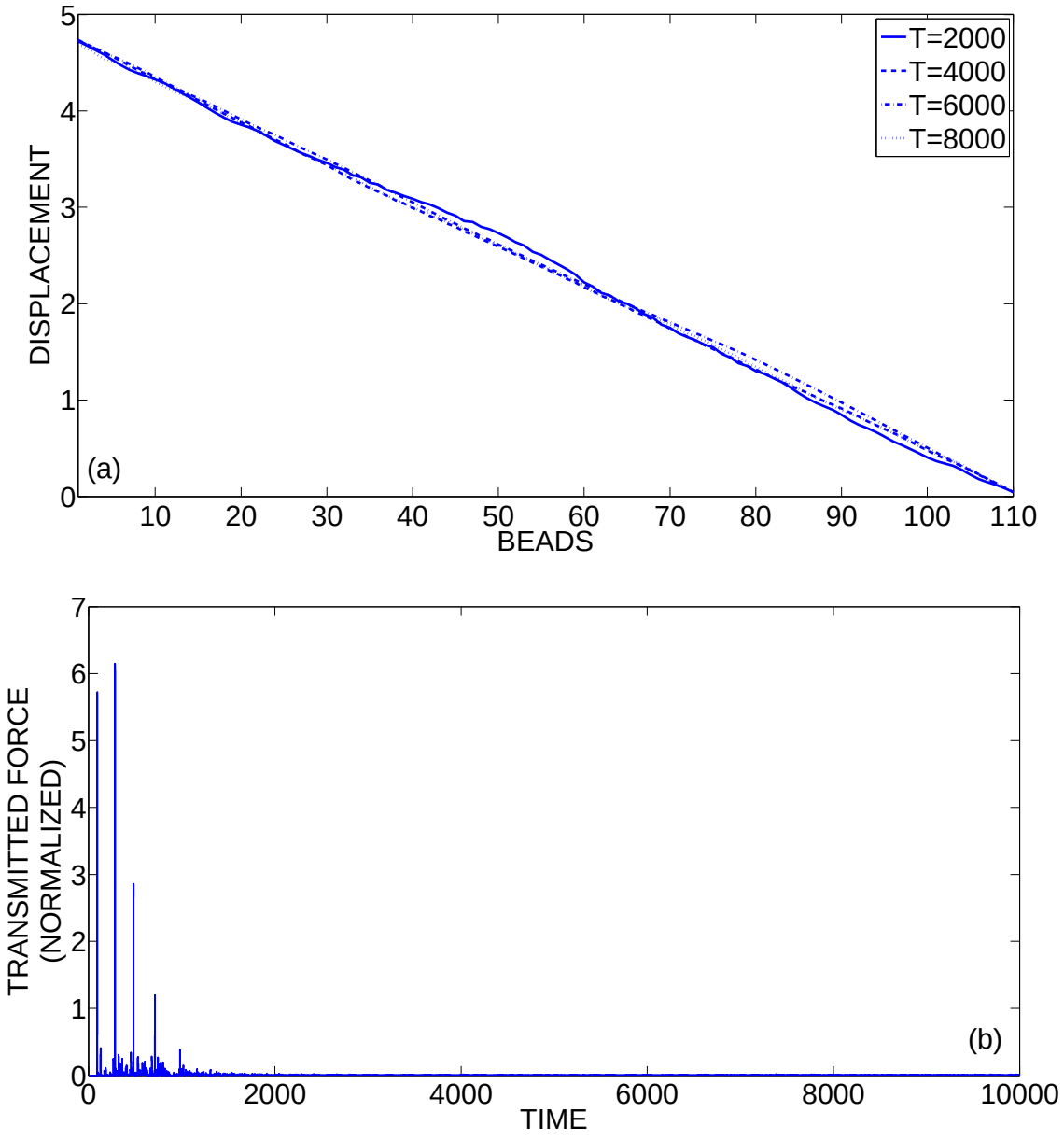

Figure 4.10: (a) Time snapshot of the displacement variation; (b) Normalized transmitted force in a 30:50:30 granular container with $\varepsilon = 0.729$ harmonically excited with an amplitude $B = 5$ and frequency $\beta = 2.65$.

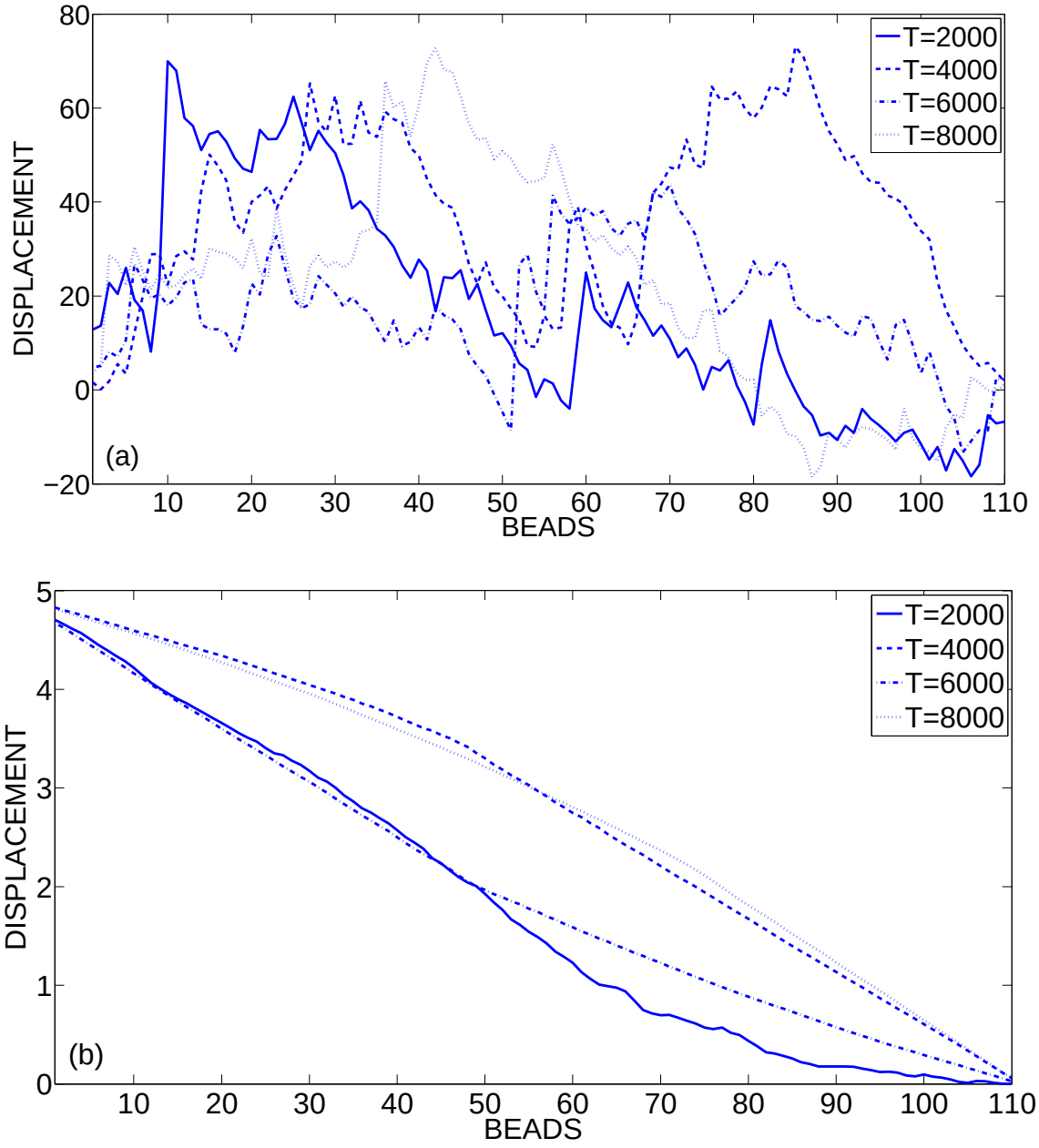

Figure 4.11: Time snapshot of the displacement variation in a 30:50:30 granular container with $\varepsilon = 0.729$ harmonically excited with an amplitude $B = 5$ for (a) $\beta = 1.568$ and (b) $\beta = 1.572$.

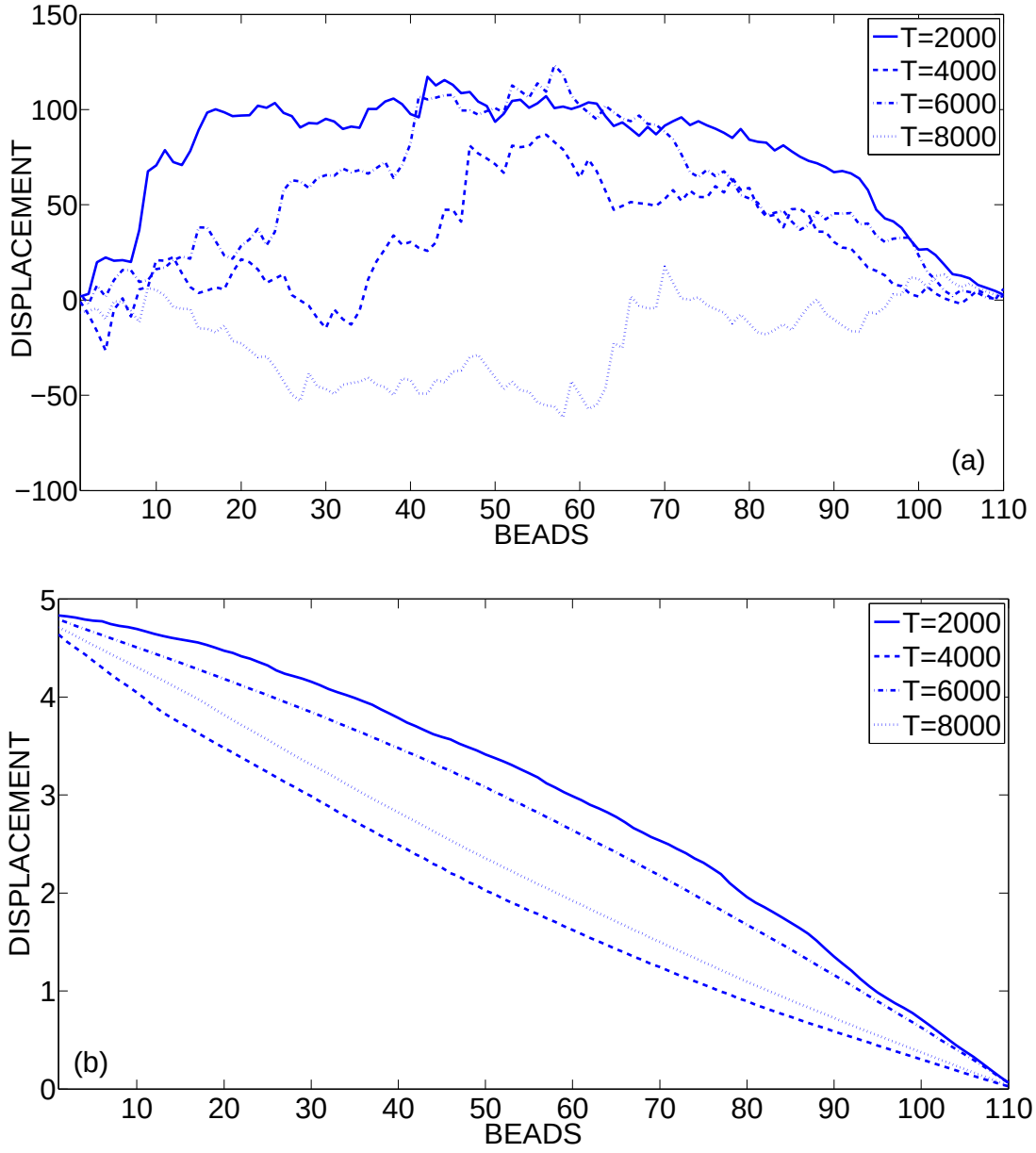

Figure 4.12: Time snapshot of the displacement variation in a 30:50:30 granular container with $\varepsilon = 0.729$ harmonically excited with an amplitude $B = 5$ for (a) $\beta = 1.856$ and (b) $\beta = 1.864$.

5. CONCLUSIONS AND DIRECTIONS FOR FUTURE RESEARCH

The primary objective of this work was the study of one dimensional granular chains. In this regard we have considered both homogeneous and dimer chains and analyzed their nonlinear dynamics and acoustics. Further, some of the most important and intriguing results have been verified experimentally. As an epilogue, in this chapter we provide a synopsis of the derived results and provide some directions for future research.

The first granular system under consideration in this work is the homogeneous chain with fixed boundary conditions. Beginning with the simplest case of two bead system and the NNMs supported by them, we progressed to higher order systems and studied the corresponding NNMs. To our knowledge, this is first such systematic study of time-periodic standing waves (nonlinear normal modes – NNMs) in this class of strongly (essentially) nonlinear dynamical systems. Owing to the non-cohesive nature of the considered granular chains, the definition of NNMs had to be broadened to include time-periodic orbits that may not necessarily be synchronous. When the realized NNMs are depicted on the frequency-energy plane, the out-of-phase NNM was found to split the plane into two zones (bands). The normal modes and the subharmonics were realized in the zone below the out-of-phase NNM, which was denoted as the propagation zone – PZ or propagation band – PB, whereas the complementary zone was denoted as the prohibited band (attenuation zone – AZ or attenuation band – AB) where only near field solutions are realized. The effect of such frequency zones is quite well pronounced when the homogeneous chain is harmonically excited in these distinct frequency zones. To this end we have observed that for fixed amplitude of excitation, the low-frequency dynamics is strongly nonlinear and the beads execute strongly nonlinear oscillations. This represents the propagation band of the dynamics. With the system excited in the attenuation zone, it was observed

that the system entered into a state of permanent compression with the response localized close to the excitation source and attenuates away from it. Thus, a homogeneous chain behaves as a low pass filter, transmitting only low frequency/energy harmonics and attenuating (or spatially localizing) high frequency/energy harmonics. Although the NNMs were realized in dissipation free systems, the harmonically excited granular chains possessed weak viscous damping to suppress the initial transients.

The first experimental study in this work comes in the form of the verification of the frequency band zones in homogeneous granular chains. To this end we have considered a simple case of two bead system excited by harmonic excitation at one end while providing fixed boundary condition at the other. The previously described frequency zones were captured according to theoretical predictions. Although in this experimental study we have considered a simple two bead system, any higher dimensional granular chains would exhibit a similar behavior and these frequency band zones should be realized in these systems as well.

Although the dynamics in the PB is strongly nonlinear and exhibits separation between beads, the dynamics inside the AB is weakly nonlinear and beads no longer separate so their dynamics is analytically tractable. From the analytical study it is deduced that the permanent compression experienced by the beads is independent of the excitation frequency and varies linearly in space. With increase in the granular chain length, the compression experienced by the first bead adjacent to the excitation end increases in the AB, and thus the time of interaction of the first bead with the exciter decreases, as does the energy input to the system. It is worth noting that due to the incessant bead separations possible in the PB, there are no known analytical techniques to study the system dynamics, so we only resort to direct numerical simulations.

The final part of the study of homogeneous granular chains is concerned with the systematic classification of the NNMs based on the concept of effective particles.

Effective particles are packets of energy accounting for the kinetic energy of a propagating pulse, or for momentum transfer in the chain. Although there are methodologies to classify NNMs in strongly nonlinear systems, these are seldom applicable in the case of interaction potentials that are non-cohesive (tension free) and, hence, non-smooth. Thus a new methodology for the classification of NNMs in these highly degenerate strongly nonlinear systems is devised. This methodology introduces auxiliary models of effective-particles (clusters) oscillating out-of-phase with respect to each other (i.e., balanced by the translational momentum). Additionally, vibro-impact models of effective-particles were introduced that allowed analytical estimation of the maximum velocities of the oscillating effective-particles. This classification methodology was applied to a granular chain with Hertzian interaction potential, but it was not certainly limited to that considered system. In fact the methodology holds for any general non-cohesive nonlinear interaction potential (i.e., of the general form $\tilde{F} \propto \delta^r, r > 1$) where separation between the interacting beads is allowed.

Although it may seem that application of effective particles is limited to the classification of the NNMs, it is seldom so. Indeed, the concept of effective particles has been successfully applied to model primary shock propagation in layered media with granular interfaces excited by short time duration shocks. Primary pulse propagation in granular layers is mainly dominated by overall momentum transfer, and, thus, by the excitation of the lowest-frequency in-phase NNM of these layers. In turn, the in-phase NNM can be effectively modeled by a single effective particle (as all the beads are moving in unison) and provides good correspondence with numerical results. In essence, the concept of effective particle can be further extended to two and three dimensional granular setups to model primary pulse transmission, and permits drastic simplification of the strongly nonlinear acoustics of many-bead granular chains.

The second class of granular systems considered in this Thesis is diatomic or dimer chains, more particularly periodic dimer chains of type 1: N. We have primarily

considered the propagatory dynamics of this class of dimer chains. It is interesting to note that no parameters were involved in the dynamical evolution of homogeneous chains, in contrast the dynamics of $1:1$ and $1:N$ $(N > 1)$ dimers is governed by one (mass ratio) and two (mass and stiffness ratio) parameters, respectively. Owing to the periodic variation in mass and or stiffness, it is quite intuitive to expect that a pulse propagating in this class of systems scatters and disperses. In fact this is true for a typical value of the system parameters. However, it was found that at special values (discrete spectrum) of system parameters a pulse can propagate without attenuation or distortion, forming a solitary wave. Although propagating primary pulses in the dimers have been observed previously [42, 89, 90] and have been denoted as solitary waves, they do not exactly conform to the solitary definition of [17], whereas the families of solitary waves presented in this work do conform to this definition. The formation of solitary waves has been attributed to the phenomenon of anti-resonance wherein the oscillatory tails formed in the trail of the propagating primary pulse is completely eliminated. The solitary waves are realized at the discrete spectrum of mass ratios in $1:1$ dimer and at the discrete ordered pairs of mass and stiffness ratios in $1:2$ dimers. In fact, it is an interesting revelation that a general $1:N$ $(N > 2)$ dimer does not support such 'exact' solitary waves, although near solitary waves can be realized in these systems, as well, based on the excitation of the in-phase NNM as the light beads of the dimer are compressed between the adjacent heavy beads.

In the case of anti-resonance (solitary wave formation), the oscillatory tail in the trail of a propagating primary pulse was completely annihilated. The contrasting effect of maximization of that oscillating tail was attributed to the reverse phenomenon of resonance. Indeed, as the oscillating tail maximizes its amplitude, the propagating primary pulse attenuates substantially due to energy radiation through traveling waves (in the oscillating tail) to the far field of the medium. Hence, resonances can lead to substantial passive attenuation of propagating pulses in heterogeneous media, such as

the dimers considered herein. Similar to the case of anti-resonances, nonlinear resonances are realized at a discrete spectrum of mass ratios in $1:1$ dimers, and at discrete ordered pairs (spectra) of mass and stiffness ratios in $1:2$ dimers. From a practical point of view and the employment of dimers in shock attenuation and mitigation, resonances play the most important role. Furthermore, although exact resonances cannot be realized in a general $1:N$ $(N > 2)$ dimer chain, still substantial pulse attenuation is observed at near-resonances that can be realized based on the first mode of oscillation of the light beads when compressed between the heavy beads.

The second experimental study reported in this work comes in the form of verification of anti-resonances and resonances in $1:1$ dimers. The experiment considers dimer chains at three different mass ratios, namely, near anti-resonance, $1:1$ resonance and $1:1$ anti-resonance ($\varepsilon = 1$). The experimental results are found to be in very good correspondence with theoretical/numerical predictions and positively verify these phenomena in dimer chains. An experimental linear viscous damping coefficient has been deduced in this process to model the observed dissipation in granular chains.

A detailed study of oscillatory tails in $1:1$ dimers at arbitrary values of their mass ratio revealed that the oscillations therein are not random, but rather consist of strongly nonlinear traveling waves with varying spatial periodicity (wavenumbers). The amplitude of these waves are functions of energy, but the excitation of traveling waves of a certain wavenumber appears to depend only on the mass ratio of the dimer. With this observation in view we have considered a detailed study of traveling waves in reduced systems which are dimer chains consisting of an even number of beads and possessing periodic boundary conditions. For a particular periodicity of the reduced system, interesting bifurcations were observed with the mass ratio being the bifurcation parameter. For the case of four bead periodicity, the traveling wave bifurcated to a standing wave and ceased to be excited below a certain value of the mass ratio. The bifurcation point was very close to the mass ratio at which maximum attenuation was

observed in the corresponding finite dimer chain, indicating that the bifurcation of traveling waves influenced the maximum attenuation of the pulse in this range of mass ratios. It is interesting to note that such bifurcation was not observed for any other periodicity, although it was found that the stability of the traveling waves changed when the mass ratio was varied. In view of these observations, it was conjectured that the excitation of traveling waves is intrinsically related to the resonance mechanism and the subsequent attenuation of the propagating pulse.

Finally, we considered the dynamics of granular wave containers. Although these systems have been explored previously, we show the applicability of the simplified binary collision approximation (BCA) model in the analysis of its dynamics. Although the BCA is a simplified model, the dynamics of granular wave containers was well captured by this approximation. The BCA not only well predicted the amplitude of scattered solitary pulses, but also predicted correctly the resulting solitary wave trains. The main drawback of this methodology is its inability to incorporate the stiffness mismatch between beads. However, if the stiffness disparity is included in the model, the interaction time changes but the final velocity of the interacting beads remains unchanged. Thus the BCA is effective only for granular chains consisting of beads made of the same or similar material properties. We have further considered the granular container excited by harmonic base excitation and numerically explored the PZ and AZ. The chaotic behavior in the transition region between these zones has been shown numerically.

Regarding suggestions for future work, there are numerous potential extensions of the topics addressed herein. In this Thesis, NNMs in one dimensional homogeneous granular chains have been explored. As a further step, such normal modes can be considered for general $1{:}N$ dimer chains. It is worth noting that, perhaps surprisingly, the NNMs of homogeneous chains did not exhibit any bifurcations with respect to energy or to any other system parameter. It would be interesting to explore possible

NNM bifurcations in granular dimers where the mass ratio for the case of $1:1$ dimer, or the mass and stiffness ratios greatly influence the dynamics. Furthermore, it would be worth exploring the frequency band zones in such dimers which may not just depend on frequency, but also on system parameters.

In addition, NNMs in two and three-dimensional matrix of beads can be explored. In fact a new classification methodology based on the concept of effective particles can be formulated to classify the different classes of modes realized. However, it should be noted that a two- or three-dimensional matrix of beads may not necessarily be rescalable with respect to energy and thus the energy will become an additional bifurcation parameter in the dynamical evolution of the realized normal modes.

The periodic dimer chains considered in this work, i.e., $1:N$ dimers is a particular subclass of the general periodic $M:N$ dimer chains. It is worth noting that the dynamics of such general $M:N$ $(M > 1, N > 1)$ dimer chains is governed by two stiffness parameters and the mass ratio, whereas if $N = 1$, the dynamics is governed by a single stiffness ratio and the mass ratio. Such general periodic dimer chains can reveal interesting internal resonance mechanisms for the attenuation of propagating primary pulses. Moreover, one can explore new families of solitary waves in these systems.

It was observed that in the case of $1:1$ dimer with mass ratio of $\varepsilon \approx 0.59$, beating wavepackets were excited once the chain length exceeded 85 beads. Although near $1:1$ resonance conditions are realized at this mass ratio, the wave packet seldom attenuates and does not radiate oscillating tails. This is an interesting dynamical phenomenon and can be studied analytically owing to the fact that the beads no longer separate during this propagatory phase.

It was noted previously that solitary waves are the main mechanism for energy propagation in homogeneous granular chains and dimer chains (at the specific discrete values of the system parameters). Thus any arbitrary signal disintegrates into a train of solitary waves with varying amplitudes and propagate with corresponding

proportional velocities. This behavior is observed only numerically, however, there are no analytical theories to model this disintegration of the signal and estimate the amplitudes of the disintegrated solitary waves. An interesting prospective research can be initiated to formulate an exact or an approximate analytical methodology in this regard.

As a further topic, it would be of interest to extend the concept of effective particles to heterogeneous granular media in one, two or three dimensions and to study reduced order models based on this concept. This would enable predictive design of these strongly nonlinear media by providing accurate estimates of primary propagating pulses. In addition, it would contribute to the design of granular interfaces in layered media and to the design of new classes of highly discontinuous acoustic metamaterials with tunable material properties and the capacity to adapt their dynamics and acoustics to different forcing environments.

In the process of experimental study of resonances and anti-resonances in 1:1 dimer chains, we have considered a velocity proportional linear viscous damping. Although this simple damping model proves quite effective, a nonlinear damping model for the bead interaction seems more appropriate. A more careful experiment with the interaction of two beads with varying radii needs to be considered to ascertain the exact damping mechanism.

The existence of solitary waves in discrete homogeneous lattices is proved by Friesecke et al. [43] and has been extended to the particular case of granular chains with Hertzian interaction by MacKay [58] and Ji et al. [60]. In this work, realization of families of solitary waves in 1:1 and 1:2 dimers has been shown numerically and approximate asymptotic methods are invoked to find the discrete spectra of mass and stiffness ratio for their realization. But there are no particular existence theorems for the realization of solitary waves in dimer chains. An interesting prospective research is to formulate an appropriate existence theorem in this regard.

6. REFERENCES

[1] K. K. Rao and P. R. Nott, An Introduction to Granular Flow, New York: Cambridge University Press, 2008.

[2] D. R. Lowe, "Grain Flow and Grain Flow Deposits," *Journal of Sedimentary Petrology,* vol. 46(1), pp. 188-199, 1976.

[3] M. G. Kleinhans, H. Markies, S. J. de Vet, A. C. in't Veld and F. N. Postema, "Static and Dynamic Angles of Repose in Loose Granular Materials Under Reduced Gravity," *Journal of Geophysical Research,* vol. 116, no. E11004, pp. 1-13, 2011.

[4] H. P. Zhu and A. B. Yu, "Averaging Method for Granular Materials," *Physical Review E,* vol. 66(2), no. 021302, pp. 1-10, 2002.

[5] I. V. Andrianov and J. Awrejcewicz, "Continuous Models for 1D Discrete Media Valid for Higher-Frequency Domain," *Physics Letters A,* vols. 345(1-3), p. 55–62, 2005.

[6] I. V. Andrianov and J. Awrejcewicz, "Continuous Models for Chain of Inertially Linked Masses," *European Journal of Mechanics A/Solids,* vol. 24(3), p. 532–536, 2005 .

[7] I. V. Andrianov, G. A. Starushenko and D. Weichert, "Numerical Investigation of 1D Continuum Dynamical Models of Discrete Chain," *ZAMM-Journal of Applied Mathematics and Mechanics,* vols. 92(11-12), pp. 945-954, 2012.

[8] K. L. Johnson, Contact Mechanics, Cambridge: Cambridge University Press, 1985.

[9] A. E. H. Love, A Treatise on the Mathematical Theory of Elasticity, New York: Dover, 1927.

[10] V. L. Popov, Contact Mechanics and Friction, Berlin: Springer-Verlag, 2010.

[11] E. Fermi, J. Pasta and S. Ulam, "Studies of Non Linear Problems," in *From Collected Papers of Enrico Fermi*, Chicago, The University of Chicago Press, 1965, pp. 978-988.

[12] A. F. Vakakis, L. I. Manevitch, Y. Mikhlin, V. Pilipchuk and A. A. Zevin, Normal Modes and Localization in Nonlinear Systems, New York: Wiley, 1996.

[13] F. S. Tse, I. E. Morse and R. T. Hinkle, Mechanical Vibrations: Theory and Applications, Boston: Allyn and Bacon, 1978.

[14] L. Meirovitch, Fundamentals of Vibrations, New York: McGraw Hill, 2001.

[15] N. J. Zabusky and M. D. Kruskal, "Interaction of "Solitons" in a Collisionless Plasm and the Recurrence of Initial States," *Physical Review Letters,* vol. 15(6), pp. 1-4, 1963.

[16] D. J. Korteweg and G. de Vries, "On the Change of Long waves Advancing in a Rectangular Canal, and on a New Type of Long Stationary Waves," *Philosophical Magazine, Series 5*, vol. 39, pp. 422-443, 1895.

[17] A. C. Scott, F. Y. F. Chu and D. W. McLaughlin, "The Soliton: A New Concept in Applied Science," *Proceedings of The IEEE,* vol. 61(10), pp. 1443-1483, 1973.

[18] M. Toda, "Studies of a Non-Linear Lattice," *Physics Reports,* vol. 18(1), pp. 1-124, 1975.

[19] M. Toda, "Nonlinear Lattice and Soliton Theory," *IEEE Transactions on Circuits and Systems,* vol. 30(8), pp. 542-553, 1983.

[20] M. Toda, Theory of Nonlinear Lattices, Berlin: Springer-Verlag, 1989.

[21] M. Remoissenet, Waves Called Solitons, Berlin: Springer-Verlag, 1999.

[22] T. Dauxois and M. Peyrard, Physics of Solitons, Cambridge: Cambridge University Press, 2006.

[23] R. K. Dodd, J. C. Eilbeck, J. D. Gibbon and H. C. Morris, Solitons and Nonlinear wave Equations, London: Academic Press Inc., 1982.

[24] D. K. Campbell, S. Flach and Y. S. Kivshar, "Localizing Energy Through Nonlinearity and Discreteness," *Physics Today,* vol. 57(1), pp. 43-49, 2004.

[25] S. Flach and A. Gorbach, "Discrete Breathers in Fermi-Pasta-Ulam Lattices," *Chaos,* vol. 15(1), no. 015112, pp. 1-10, 2005.

[26] H. Goldstein, C. Poole and J. Safko, Classical Mechanics, San Francisco: Addison Wesley, 2002.

[27] M. A. Porter, N. J. Zabusky, B. Hu and D. K. Campbell, "Fermi, Pasta, Ulam and the Birth of Experimental Mathematics: A Numerical Experiment that Enrico Fermi, John Pasta, and Stanislaw Ulam Reported 54 Years Ago Continues to Inspire Discovery," *American Scientist,* vol. 97(3), p. 214, 2009.

[28] A. Carati, L. Galgani and A. Giorgilli, "The Fermi–Pasta–Ulam Problem as a Challenge for the Foundations of Physics," *Chaos,* vol. 15(1), no. 015105, pp. 1-8, 2005.

[29] G. P. Berman and F. M. Izrailev, "The Fermi–Pasta–Ulam Problem: Fifty Years of Progress," *Chaos,* vol. 15(1), no. 015104, pp. 1-18, 2005.

[30] S. Hutzler, G. Delaney, D. Weaire and F. MacLeod, "Rocking Newton's Cradle," *American Journal of Physics,* vol. 72(12), pp. 1508-1516, 2004.

[31] D. R. Lovett, K. M. Moulding and S. Anketell-Jones, "Collisions between Elastic Bodies: Newton's Cradle," *European Journal of Physics,* vol. 9(4), pp. 323-328, 1988.

[32] K. Atkins, Physics Once Over Lightly, New York: Wiley, 1972.

[33] F. Herrmann and M. Seitz, "How does the Ball-Chain Work?," *American journal of Physics,* vol. 50(11), pp. 977-981, 1982.

[34] F. Herrmann and P. Schmalzle, "Simple Explanation of a Well-known Collision Experiment," *American Journal of Physics,* vol. 49(8), pp. 761-764, 1981.

[35] E. J. Hinch and S. Saint-Jean, "The Fragmentation of a Line of Balls by an Impact," *Proceedings of The Royal Society of London A,* vol. 455(1989), pp. 3201-3220, 1999.

[36] G. B. Whitham, Linear and Nonlinear Waves, New York: Wiley Interscience, 1999.

[37] L. Brillouin, Wave Propagation in Periodic Structures, New York: Dover, 1953.

[38] V. Ceanga and Y. Hurmuzlu, "A New Look at an Old Problem: Newton's Cradle," *Journal of Applied Mechanics,* vol. 68(4), pp. 575-583, 2001.

[39] M. T. Robinson, "The Binary Collision Approximation: Background and Introduction," *Radiation Effects and Defects in Solids,* vol. 130(1), pp. 3-20, 1994.

[40] C. M. Donahue, C. M. Hrenya, A. P. Zelinskaya and K. J. Nakagawa, "Newton's Cradle Undone: Experiments and Collision Models for the Normal Collision of Three Solid Spheres," *Physics of Fluids,* vol. 20(11), no. 113301, pp. 1-11, 2008.

[41] V. F. Nestrenko, "Propagation of Nonlinear Compression Pulses in Granular Media," *Journal of Applied Mechanics and Technical Physics,* vol. 24(5), pp. 733-743, 1983.

[42] V. F. Nesterenko, Dynamics of Heteregeneous Materials, New York: Springer-Verlag, 2001.

[43] G. Friesecke and J. A. D. Wattis, "Existence Theorem for Solitary Waves on Lattices," *Communications in Mathematical Physics,* vol. 161(2), pp. 391-418, 1994.

[44] S. Sen, J. Hong, J. Bang, E. Avalos and R. Doney, "Solitary Waves in the Granular Chain," *Physics Reports,* vol. 462, pp. 21-66, 2008.

[45] A. Sokolow, E. G. Bittle and S. Sen, "Solitary Wave Train Formation in Hertzian Chains," *Europhysics Letters,* vol. 77(2), no. 24002, pp. 1-4, 2007.

[46] P. Rosenau and J. M. Hyman, "Compactons: Solitons with Finite Wavelength," *Physical Review Letters,* vol. 70(5), pp. 564-567, 1993.

[47] A. Chatterjee, "Asymptotic Solution for Solitary Waves in a Chain of Elastic Spheres," *Physical Review E,* vol. 59(5), pp. 5912-5919, 1999.

[48] H. Hertz, "Ueber die Beruhrung fester elastischer Korper," *Journal fur die reine und angewandte Mathematik (Crelle's Journal),* vol. 1882(92), pp. 156-171, 1882.

[49] B. Bhushan, "Contact Between Solid Surfaces," in *Modern Tribology Handbook*, Boca Raton, CRC Press, 2001, pp. 121-150.

[50] L. D. Landau and E. M. Lifshitz, Course of Theoretical Physics, Vol. 7: Theory of Elasticity, London: Pergamon, 1975.

[51] A. N. Lazaridi and V. F. Nestrenko, "Observation of a New Type of Solitary Waves in a One-Dimensional Granular Medium," *Journal of Applied Mechanics and Technical Physics,* vol. 26(3), pp. 405-408, 1985.

[52] C. Coste, E. Falcon and S. Fauve, "Solitary Waves in a Chain of Beads Under Hertz Contact," *Physical Review E,* vol. 56(5), pp. 6104-6117, 1997.

[53] C. Coste and B. Gilles, "On the Validity of Hertz Contact law for Granular Material Acoustics," *The European Physical Journal B*, vol. 7(1), pp. 155-168, 1999.

[54] D. Sun, C. Daraio and S. Sen, "Nonlinear Repulsive Force Between Two Solids with Axial Symmetry," *Physical Review E,* vol. 83(6), no. 066605, pp. 1-5, 2011.

[55] C. Daraio, V. F. Nesterenko, E. B. Herbold and S. Jin, "Tunability of Solitary Wave Properties in One-Dimensional Strongly Nonlinear Phononic Crystals," *Physical Review E,* vol. 73(2), no. 026610, pp. 1-10, 2006.

[56] C. Daraio, V. F. Nesterenko, E. B. Herbold and S. Jin, "Strongly Nonlinear Waves in a Chain of Teflon Beads," *Physical Review E,* vol. 72(1), no. 016603, pp. 1-9, 2005.

[57] S. Job, F. Melo, A. Sokolow and S. Sen, "Solitary Wave Trains in Granular Chains: Experiments, Theory and Simulations," *Granular Matter,* vol. 10(1), pp. 13-20, 2007.

[58] R. S. MacKay, "Solitary Waves in a Chain of Beads under Hertz Contact," *Physics Letter A,* vol. 251(3), pp. 191-192, 1999.

[59] J. M. English and R. L. Pego, "On the Solitary Wave Pulse in a Chain of Beads," *Proceedings of the American Mathematical Society,* vol. 133(6), pp. 1763-1768, 2005.

[60] J. Y. Ji and J. Hong, "Existence Criterion of Solitary Waves in a Chain of Grains," *Physics Letters A,* vols. 260(1-2), pp. 60-61, 1999.

[61] A. Stefanov and P. Kevrekidis, "On the Existence of Solitary Traveling Waves for Generalized Hertzian Chains," *Journal of Nonlinear Science,* vol. 22(3), pp. 327-349, 2012.

[62] S. Sen and M. Manciu, "Solitary Wave Dynamics in a Generalized Hertz Chains: An Improved Solution of the Equation of Motion," *Physical Review E,* vol. 64(5), no. 056605, pp. 1-4, 2001.

[63] Y. Starosvetsky and A. F. Vakakis, "Traveling Waves and Localized Modes in One-dimensional Homogeneous Granular Chains with no Pre-compression," *Physical Review E,* vol. 82 (2), no. 026603, pp. 1-14, 2010.

[64] E. Hascoet and H. J. Herrmann, "Shocks in Non-loaded Bead Chains with Impurities," *European Physical Journal B,* vol. 14(1), pp. 183-190, 2000.

[65] Y. Starosvetsky, K. R. Jayaprakash and A. F. Vakakis, "Scattering of Solitary Waves and Excitation of Transient Breathers in Granular Media by Light Intruders," *Journal of Applied Mechanics,* vol. 79, no. 011001, pp. 1-12, 2012.

[66] S. Job, F. Melo, F. Santibanez and F. Tapia, "Nonlinear Waves in Hertzian Granular Chains: Effects of Inertial and Stiffness Heterogeneities," in *Proceedings of the International Congress on Ultrasonics*, Vienna, April 9-13, 2007.

[67] S. Job, F. Santibanez, F. Tapia and F. Melo, "Wave Localization in Strongly Nonlinear Hertzian Chains with Mass Defect," *Physical Review E,* vol. 80(2), no. 025602(R), pp. 1-4, 2009.

[68] V. F. Nesterenko, A. N. Lazaridi and E. B. Sibiryakov, "The Decay of Soliton at the Contact of Two "Acoustic Vacuums"," *Journal of Applied Mechanics and Technical Physics,* vol. 36(2), pp. 166-168, 1995.

[69] J. Hong, "Universal Power-law Decay of the Impulse Energy in Granular Protectors," *Physical Review Letters,* vol. 94(10), no. 108001, pp. 1-4, 2005.

[70] E. B. Herbold and V. F. Nestrenko, "Shock Wave Structure in a Strongly Nonlinear Lattice with Viscous Dissipation," *Physical Review E,* vol. 75(2), no. 021304, pp. 1-8, 2007.

[71] R. Carretero-Gonzalez, D. Khatri, M. A. Porter, P. G. Kevrekidis and C. Daraio, "Dissipative Solitary Waves in Granular Crystals," *Physical Review Letters,* vol. 102(2), no. 024102, pp. 1-4, 2009.

[72] L. Vergara, "Model for Dissipative Highly Nonlinear Waves in Dry Granular Systems," *Physical Review Letters,* vol. 104(11), no. 118001, pp. 1-4, 2010.

[73] S. Job, F. Santibanez, F. Tapia and F. Melo, "Nonlinear Waves in Dry and Wet Hertzian Granular Chains," *Ultrasonics,* vols. 48(6-7), pp. 506-514, 2008.

[74] A. M. Lyapunov, "Probleme General de la Stabilite du Mouvement," *Annales de la faculté des sciences de Toulouse Sér. 2,* vol. 9, pp. 203-474, 1907.

[75] C. H. Pak and R. M. Rosenberg, "On the Existence of Normal Mode Vibrations in Nonlinear Systems," *Quarterly of Applied Mathematics,* vol. 26, pp. 403-416, 1968.

[76] R. H. Rand, "Nonlinear Normal Modes in Two-Degrees-of-Freedom Systems," *Journal of Applied Mechanics,* vol. 38(2), p. 561, 1971.

[77] R. M. Rosenberg, "The Normal Modes of Nonlinear n-Degrees-of-Freedom Systems," *Journal of Applied Mechanics,* vol. 30(1), pp. 7-14, 1962.

[78] R. M. Rosenberg and J. Kuo, "Nonsimilar Normal Mode Vibrations of Nonlinear Systems having Two Degrees of Freedom," *Journal of Applied Mechanics,* vol. 31(2), pp. 283-290, 1964.

[79] R. M. Rosenberg, "On Nonlinear Vibrations of Systems with Many Degrees of Freedom," *Advances in Applied Mechanics,* vol. 9, pp. 155-242, 1966.

[80] A. F. Vakakis and R. H. Rand, "Normal Modes and Global Dynamics of a Two-Degree-of-Freedom Non-Linear System-I. Low Energies," *International Journal of Non-Linear Mechanics,* vol. 27(5), pp. 861-874, 1992.

[81] A. F. Vakakis and R. H. Rand, "Normal Modes and Global Dynamics of a Two-Degree-of-Freedom Non-Linear System-II. High Energies," *International Journal of Non-Linear Mechanics,* vol. 27(5), pp. 875-888, 1992.

[82] D. Jiang, C. Pierre and S. W. Shaw, "Large-Amplitude Nonlinear Normal Modes of Piecewise Linear Systems," *Journal of Sound and Vibration,* vols. 272(3-5), pp. 869-891, 2004.

[83] S. Chen and S. W. Shaw, "Normal Modes for Piecewise Linear Vibratory Systems," *Nonlinear Dynamics,* vol. 10(2), pp. 135-163, 1996.

[84] L. Zuo and A. Curnier, "Non-Linear Real and Complex Modes of Conewise Linear Systems," *Journal of Sound and Vibration,* vol. 174(3), pp. 289-313, 1994.

[85] K. R. Jayaprakash, Y. Starosvetsky, A. F. Vakakis, M. Peeters and G. Kerschen, "Nonlinear Normal Modes and Band Gaps in Granular Chains with no Pre-compression," *Nonlinear Dynamics,* vol. 63(3), pp. 359-385, 2011.

[86] D. J. Mead, "Wave Propagation and Natural Modes in Periodic Systems. I. Monocoupled Systems.," *Journal of Sound and Vibration,* vol. 40, pp. 1-18, 1975.

[87] J. Lydon, K. R. Jayaprakash, D. Ngo, Y. Starosvetsky, A. F. Vakakis and C. Daraio, "Frequency Bands of Strongly Nonlinear Finite Homogeneous Granular Crystals," *Physical Review E,* (under review), 2012.

[88] L. Ponson, N. Boechler, Y. M. Lai, M. A. Porter, P. G. Kevrekidis and C. Daraio, "Nonlinear Waves in Disordered Diatomic Granular Chains," *Physical Review E,* vol. 82(2), no. 021301, pp. 1-9, 2010.

[89] M. A. Porter, C. Daraio, E. B. Herbold, I. Szelengowicz and P. G. Kevrekidis, "Highly Nonlinear Solitary Waves in Periodic Dimer Granular Chains," *Physical Review E,* vol. 77(1), no. 015601(R), pp. 1-4, 2008.

[90] M. A. Porter, C. Daraio, I. Szelengowicz, E. B. Herbold and P. G. Kevrekidis, "Highly Nonlinear Solitary Waves in Heterogeneous Periodic Granular Media," *Physica D,* vol. 238(6), pp. 666-676, 2009.

[91] K. R. Jayaprakash, Y. Starosvetsky, O. V. Gendelman and A. F. Vakakis, "Nonlinear Resonances Leading to Strong Shock Attenuation in Granular Dimer Chains," *Journal of Nonlinear Science,* doi: 10.1007/s00332-012-9155-0, 2012.

[92] N. Boechler, G. Theocharis, S. Job, P. G. Kevrekidis, M. A. Porter and C. Daraio, "Discrete Breathers in One-Dimensional Diatomic Granular Crystals," *Physical Review Letters,* vol. 104(24), no. 244302, pp. 1-4, 2010.

[93] A. Molinari and C.Daraio, "Stationary Shocks in Periodic Highly Nonlinear Granular Chains," *Physical Review E,* vol. 80(5), no. 056602, pp. 1-15, 2009.

[94] St. Pnevmatikos, N. Flytzanis and M. Remoissenet, "Soliton Dynamics of Nonlinear Diatomic Lattices," *Physical Review B,* vol. 33(4), pp. 2308-2321, 1986.

[95] St. Pnevmatikos, M. Remoissenet and N. Flytzanis, "Propagation of Acoustic and Optical Solitons in Nonlinear Diatomic Chains," *Journal of Physics C: Solid State Physics,* vol. 16(11), pp. L305-L310, 1983.

[96] G. Theocharis, N. Boechler, P. G. Kevrekidis, S. Job, M. A. Porter and C. Daraio, "Intrinsic Energy localizatioan through Discrete Gap Breathers in One-Dimensional Diatomic Granular Crystals," *Physical Review E,* vol. 82(5), no. 056604, pp. 1-11, 2010.

[97] K. R. Jayaprakash, Y. Starosvetsky and A. F. Vakakis, "New Family of Solitary Waves in Granular Dimer Chains with No Pre-compression," *Physical Review E,* vol. 83(3), no. 036606, pp. 1-11, 2011.

[98] K. R. Jayaprakash, A. F. Vakakis and Y. Starosvetsky, "Strongly Nonlinear Traveling Waves in Granular Dimer Chains," *Mechanical Systems and Signal Processing,* doi: 10.1016/j.ymssp.2012.04.018, 2012.

[99] M. Betti and D. E. Pelinovsky, "Periodic Travelling Waves in Dimer Granular Chains," *Journal of Nonlinear Science,* doi: 10.1007/s00332-013-9165-6, 2012.

[100] R. Potekin, K. R. Jayaprakash, D. M. McFarland, K. Remick, L. A. Bergman and A. F. Vakakis, "Experimental Study of Strongly Nonlinear Resonances and Anti-Resonances in Granular Dimer Chains," *Experimental Mechanics,* doi: 10.1007/s11340-012-9673-6, 2012.

[101] N. Boechler, J. Yang, G. Theocharis, P. G. Kevrekidis and C. Daraio, "Tunable Vibrational Band Gaps in One-Dimensional Diatomic Granular Crystals with Three-Particle Unit Cells," *Journal of Applied Physics,* vol. 109(7), no. 074906, pp. 1-7, 2011.

[102] K. R. Jayaprakash, A. F. Vakakis and Y. Starosvetsky, "Solitary Waves in a General Class of Granular Dimer Chains," *Journal of Applied Physics,* vol. 112(3), no. 034908, pp. 1-17, 2012.

[103] K. R. Jayaprakash, A. F. Vakakis and Y. Starosvetsky, "Nonlinear Resonances in a General Class of Granular Dimers with No Pre-compression," *Granular Matter,* (under review), 2012.

[104] U. Harbola, A. Rosas, M. Esposito and K. Lindenberg, "Pulse Propagation in Tapered Granular Chains: An Analytic Study," *Physical Review E,* vol. 80(3), no. 031303, pp. 1-10, 2009.

[105] R. L. Doney and S. Sen, "Decorated, Tapered, and Highly Nonlinear Granular Chain," *Physical Review Letters,* vol. 97(15), no. 155502, pp. 1-4, 2006.

[106] R. L. Doney and S. Sen, "Impulse Absorption by Tapered Horizontal Alignments of Elastic Spheres," *Physical Review E,* vol. 72(4), no. 041304, pp. 1-11, 2005.

[107] R. L. Doney and S. Sen, "Shock Mitigation for Blast Protection using Hertzian Tapered Chains," in *22nd International Symposium on Ballistics*, Vancouver, BC, 14-18 November, 2005.

[108] R. L. Doney, J. H. Agui and S. Sen, "Energy Partitioning and Impulse Dispersion in the Decorated, Tapered, Strongly Nonlinear Granular Alignment: A System with many Potential Applications," *Journal of Applied Physics,* vol. 106, no. 064905, pp. 1-13, 2009.

[109] A. Sokolow, J. M. M. Pfannes, R. L. Doney, M. Nakagawa, J. H. Agui and S. Sen, "Absorption of Short Duration Pulses by Small, Scalable, Tapered Granular Chains," *Applied Physics Letters,* vol. 87, no. 254104, pp. 1-3, 2005.

[110] U. Harbola, A. Rosas, A. H. Romero and K. Lindenberg, "Pulse Propagation in Randomly Decorated Chains," *Physical Review E,* vol. 82(1), no. 011306, pp. 1-7, 2010.

[111] S. Sen, F. S. Manciu and M. Manciu, "Thermalizing an Impulse," *Physica A,* vols. 299(3-4), pp. 551-558, 2001.

[112] F. Melo, S. Job, F. Santibanez and F. Tapia, "Experimental Evidence of Shock Mitigation in a Hertzian Tapered Chain," *Physical Review E,* vol. 73(4), no. 041305, pp. 1-7, 2006.

[113] F. Fraternali, M. A. Porter and C. Daraio, "Optimal Design of Composite Granular Protectors," *Mechanics of Advanced Materials and Structures,* vol. 17(1), pp. 1-19, 2010.

[114] http://www.ehow.com/info_8206199_uses-sandbags.html.

[115] Daily Telegraph, "World War 2: Sandbags cover Venus de Milo," *Daily Telegraph,* September 1939.

[116] Department of the Army, "Army Tactics, Techniques, and Procedures: ATTP 3-39.32 (FM 3-19.30)," Department of the Army, Washington, DC, 2010.

[117] Secretary of the Air Force, "Guide To Fighting Positions, Obstacles, and Revetments - Air Force Handbook 10-222, Volume 14," Department of the Air Force, Washington, DC, 2000.

[118] G. Li, P. Summers, K. Clutter and D. Bonaventure, "Blast and Impact Resistant Design of Overhead Protection Structures," in *Structures Congress 2012*, Chicago, 2012.

[119] K. Hellevang, "Sandbagging for Flood Protection [AE-626 (Revised)]," North Dakota State University Extension Service, Fargo, 2011.

[120] D. Ngo, F. Fraternali and C. Daraio, "Highly Nonlinear Solitary Wave Propagation in Y-Shaped Granular Crystals with Variable Branch Angles," *Physical Review E,* vol. 85(3), no. 036602, pp. 1-10, 2012.

[121] Y. Starosvetsky, M. A. Hasan and A. F. Vakakis, "Nonlinear Pulse Equi-partition in Weakly Coupled Ordered Granular Chains with no Pre-Compression," *Journal of Computational and Nonlinear Dynamics,* (in press), 2012.

[122] Y. Starosvetsky, M. A. Hasan, A. F. Vakakis and L. I. Manevitch, "Strongly Nonlinear Beat Phenomena and Energy Exchanges in Weakly Coupled Granular Chains on Elastic Foundations," *SIAM Journal on Applied Mathematics,* vol. 72(1), pp. 337-361, 2012.

[123] A. Leonard and C. Daraio, "Stress Wave Anisotropy in Centered Square Highly Nonlinear Granular Systems," *Physical Review Letters,* vol. 108(21), no. 214301, pp. 1-4, 2012.

[124] A. Leonard, F. Fraternali and C. Daraio, "DirectionalWave Propagation in a Highly Nonlinear Square Packing of Spheres," *Experimental Mechanics,* doi: 10.1007/s11340-011-9544-6, 2011.

[125] Y. Starosvetsky and A. F. Vakakis, "Primary Wave Transmission in Systems of Elastic Rods with Granular Interfaces," *Wave Motion,* vol. 48(7), pp. 568-585, 2011.

[126] S. Job, F. Melo, A. Sokolow and S. Sen, "How Hertzian Solitary Waves Interact With Boundaries in a One Dimensional Granular Medium," *Physical Review Letters,* vol. 94(17), no. 178002, pp. 1-4, 2005.

[127] J. Yang, C. Silvestro, D. Khatri, L. D. Nardo and C. Daraio, "Interaction of highly Nonlinear Solitary Waves with Linear Elastic Media," *Physical Review E,* vol. 83(4), no. 046606, pp. 1-12, 2011.

[128] X. Ni and P. Rizzo, "Use of highly nonlinear solitary waves in NDT," *Materials Evaluation,* vol. 70(5), pp. 561-569, 2012.

[129] J. Yang, C. Silvestro, S. Sangiorgio, S. Borkowski, L. D. Nardo, E. Ebramzadeh and C. Daraio, "Nondestructive Evaluation of Orthopedic Implant Stability in THA using Highly Nonlinear Solitary Waves," *Smart Materials and Structures,* vol. 21(1), no. 012002, pp. 1-10, 2012.

[130] J. Yang, F. Restuccia and C. Daraio, "Highly Nonlinear Granular Crystal Sensor and Actuator for Delamination Detection in Composite Structures," in *Proceeding of International Workshop on Structural Health Monitoring*, Stanford, 2011.

[131] X. Ni, P. Rizzo, J. Yang, D. Khatri and C. Daraio, "Monitoring the Hydration of Cement using Highly Nonlinear Solitary Waves," *NDT & E International,* doi: 10.1016/j.ndteint.2012.05.003, 2012.

[132] X. Ni and P. Rizzo, "Highly Nonlinear Solitary Waves for the Inspection of Adhesive Joints," *Experimental Mechanics,* vol. 52(9), p. 1493–1501, 2012.

[133] D. Khatri, C. Daraio and P. Rizzo, "Highly Nonlinear Waves' Sensor Technology for Highway Infrastructures," in *Proceedings of the SPIE*, SanDiego, 2008.

[134] N. Boechler, G. Theocharis and C. Daraio, "Bifurcation-based Acoustic Switching and Rectification," *Nature Materials,* vol. 10(9), pp. 665-668, 2011.

[135] A. Spadoni and C. Daraio, "Generation and Control of Sound Bullets with a Nonlinear Acoustic Lens," *PNAS-Proceedings of the National Academy of Sciences of the United States of America,* vol. 107(16), pp. 7230-7234, 2010.

[136] C. M. Bender and S. A. Orszag, Advanced Mathematical Methods for Scientists and Engineers: Asymptotic Methods and Perturbation Theory, New York: Springer-Verlag, 1991.

[137] M. Abramowitz and I. A. Stegun, Handbook of Mathematical Functions, New York: Dover, 1972.

[138] M. Peeters, R. Viguie', F. Serandour, G. Kerschen and J. C. Golinval, "Nonlinear Normal Modes. Part II. Toward a Practical Computation using Numerical Continuation," *Mechanical Systems and Signal Processing,* vol. 23(1), pp. 195-216, 2009.

[139] G. Theocharis, M. Kavousanakis, P. G. Kevrekidis, C. Daraio, M. A. Porter and I. G. Kevrekidis, "Localized Breathing Modes in Granular Crystals with Defects," *Physical Review E,* vol. 80(6), no. 066601, pp. 1-11, 2009.

[140] N. Boechler and C. Daraio, "An Experimental Investigation of Acoustic Band Gaps and Localization in Granular Elastic Chains," in *ASME, IDETC/CIE International Design Engineering Technical Conferences and Biennial Conference on Mechanical Vibration and Noise*, San Diego, CA, 2009.

[141] A. F. Vakakis and C. Cetinkaya, "Dispersion of Stress Waves in One-dimensional Semi-infinite, Weakly Coupled Layered Systems," *International Journal of Solids and Structures,* vol. 33(28), pp. 4195-4213, 1996.

[142] A. F. Vakakis and M. E. King, "Nonlinear Wave Transmission in a Monocoupled Elastic Periodic System," *Journal of the Acoustic Society of America,* vol. 98(3), pp. 1534-1546, 1995.

[143] A. F. Vakakis and M. E. King, "Resonant Oscillations of a Weakly Coupled, Nonlinear Layered System," *Acta Mechanica,* vols. 128(1-2), pp. 59-80, 1998.

[144] A. W. Norris, "Waves in Periodically Layered Media: A Comparisona of Two Theories," *SIAM Journal of Applied Mathematics,* vol. 53(5), pp. 1195-1209, 1993.

[145] C. Cetinkaya, A. F. Vakakis and M. El-Raheb, "Axisymmetric Elastic Waves in Weakly Coupled Layered Media of Infinite Radial Extent," *Journal of Sound and Vibration,* vol. 182(2), pp. 283-302, 1995.

[146] http://www.piezomechanik.com/en/home/allcatalogs/index.html.

[147] A. M. Handbook, Metals Handbook, Materials Park, OH: ASM , 2012.

[148] L. P. Kadanoff, "Built Upon Sand: Theoretical Ideas inspired by Granular Flows," *Reviews of Modern Physics,* vol. 71(1), pp. 435-444, 1999.

[149] Y. Du, H. Li and L. P. Kadanoff, "Breakdown of Hydrodynamics in a One-Dimensional System of Inelastic Particles," *Physical Review Letters,* vol. 74(8), pp. 1268-1271, 1995.

[150] J. Yang, "Dynamics of a One-dimensional Inelastic Particle System," *Physical Review E,* vol. 61(3), pp. 2920-2923, 1999.

[151] H. M. Jaeger, S. R. Nagel and R. P. Behringer, "Granular Solids, Liquids, and Gases," *Reviews of Modern Physics,* vol. 68(4), pp. 1259-1273, 1996.

[152] F. Cecconi, F. Diotallevi, U. M. B. Marconi and A. Puglisi, "Fluid-like Behavior of a One-dimensional Granular Gas," *Journal of Chemical Physics,* vol. 120, pp. 35-42, 2004.

[153] E. L. Grossman and B. Roman, "Density Variations in a One-dimensional Granular System," *Physics of Fluids,* vol. 8(12), pp. 3218-3228, 1996.

[154] F. Melo, P. B. Umbanhowar and H. L. Swinney, "Hexagons, Kinks, and Disorder in Oscillated Granular Layers," *Physical Review Letters,* vol. 75(21), pp. 3838-3841, 1995.

[155] J. R. d. Bruyn, C. Bizon, M. D. Shattuck, D. Goldman, J. B. Swift and H. L. Swinney, "Continuum-Type Stability Balloon in Oscillated Granular Layers," *Physical Review Letters,* vol. 81(7), pp. 1421-1424, 1998.

[156] L. I. Manevitch and V. V. Smirnov, "Limiting Phase Trajectories and the Origin of Energy Localization in Nonlinear Oscillatory Chains," *Physical Review E,* vol. 82(3), no. 036602, pp. 1-9, 2010.

[157] I. L. D. Pinto, A. Rosas and K. Lindenberg, "Energy Transport in a One-dimensional Granular Gas," *Physical Review E,* vol. 79(6), no. 061307, pp. 1-6, 2009.

[158] C. Kittel and H. Kroemer, Thermal Physics, San Francisco: W. H. Freeman and Company, 1980.

[159] A. Rosas and K. Lindenberg, "Pulse Velocity in a Granular Chain," *Physical Review E,* vol. 69(3), no. 037601, pp. 1-3, 2004.

[160] K. F. Graff, Wave Motion in Elastic Solids, New York: Dover, 1991.

[161] J. D. Murray, Asymptotic Analysis, New York: Springer-Verlag, 1984.

[162] V. I. Arnold, Dynamical Systems III, Encyclopedia of Mathematical Sciences Vol. 3, Berlin: Springer-Verlag, 1988.

[163] V. E. Zakharov and l. A. Ostrovsky, "Modulation Instability: The Beginning," *Physica D,* vol. 238(5), pp. 540-548, 2009.

[164] A. Rosas, A. H. Romero, V. F. Nestrenko and K. Lindenberg, "Observation of Two-Wave Structure in Strongly Nonlinear Dissipative Granular Chains," *Physical Review Letters,* vol. 98(16), no. 164301, pp. 1-4, 2007.

[165] C. Hoogeboom and P. G. Kevrekidis, "Higher Gap Breathers In Periodic Granular Chains," http://arxiv.org/pdf/1105.6354.pdf.

[166] Y. Starosvetsky, K. R. Jayaprakash, A. F. Vakakis and L. I. Manevitch, "Effective Particles and Classification of Periodic Orbits of Homogeneous Granular Chains with No Pre-compression," *Physical Review E,* vol. 85(3), no. 036606, pp. 1-15, 2012.

[167] C. Daraio, V. F. Nesterenko, E. B. Herbold and S. Jin, "Energy Trapping and Shock Disintegration in a Composite Granular Medium," *Physical Review Letters,* vol. 96(5), no. 058002, pp. 1-4, 2006.

[168] U. Harbola, A. Rosas, A. H. Romero, M. Esposito and K. Lindenberg, "Pulse propagation in decorated granular chains: An analytical approach," *Physical Review E,* vol. 80(5), no. 051302, pp. 1-9, 2009.